Author:
Macdonald, John Hugh George

Title:
Identification of the dynamic behaviour of a cable-stayed bridge from full scale testing during and after construction

UNIVERSITY OF BRISTOL

DEPARTMENT OF CIVIL ENGINEERING

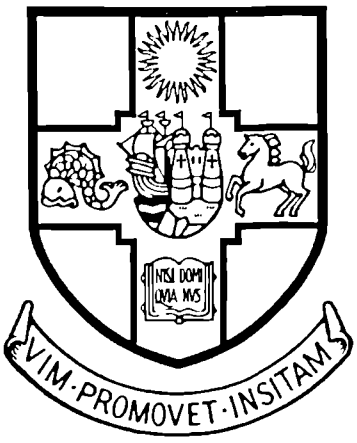

IDENTIFICATION OF THE DYNAMIC BEHAVIOUR OF A CABLE-STAYED BRIDGE FROM FULL-SCALE TESTING DURING AND AFTER CONSTRUCTION

John Hugh George Macdonald

A thesis submitted to the University of Bristol in accordance with the requirements for the degree of Doctor of Philosophy in the Faculty of Engineering

June 2000

Since God assures us

"I'll never let you down, never walk off and leave you",

we can boldly quote,

"God is there, ready to help"

Hebrews 13:5-6

Thankyou God

3

AUTHOR'S DECLARATION

NAME ... JOHN HUGH GEORGE MACDONALD
(in full, block capitals)

TITLE OF DISSERTATION ... IDENTIFICATION OF THE DYNAMIC BEHAVIOUR OF A CABLE-STAYED BRIDGE FROM FULL-SCALE TESTING DURING AND AFTER CONSTRUCTION

ADVISER ... Dr. C.A. TAYLOR

DEPARTMENT ... CIVIL ENGINEERING

I the undersigned am willing that this thesis should be made available for consultation in Bristol University Library and for inter-library lending for use in another library and may be copied in full or in part for any bona fide library or research worker, on the understanding that users are made aware of their obligations under copyright, *i.e.* that no quotation and no information derived from it may be published without the author's prior consent.

Signed ... J Macdonald

Date ... 29/6/00

ABSTRACT

With the increasing popularity and maximum spans of cable-stayed bridges, their aerodynamic performance is becoming of greater importance. In recent years there have been many advances in the analysis of these structures, considering both aerodynamic and structural issues, but there is a lack of detailed measured data from such bridges at full scale for the validation of these methods.

This thesis presents measured data from the Second Severn Crossing (SSC) cable-stayed bridge, both during construction and after completion. Short-term tests were performed to identify particular characteristics of the dynamic behaviour, and long-term tests recorded the response in different environmental conditions.

An improved method for the analysis of ambient vibration data is developed, for more accurate determination of modal parameters. This method is applied to the SSC data, and the measured natural frequencies and mode shapes are compared with results of a finite element model. Long-term records in various wind conditions are analysed, for both the finished bridge and an important construction stage. Thus, the contributions of aerodynamic and structural damping are separated and other variations in the response are considered. Also, the measured amplitudes of vibration are compared with predictions from the design buffeting analysis.

Specific vibration problems of the bridge are addressed. Measurements of vortex-induced vibrations and associated wind conditions are analysed, to improve understanding of the phenomenon on site and to evaluate the accuracy of wind tunnel tests. The causes of large cable vibrations are discussed, and the contributions of aerodynamic and structural cable damping are evaluated. Evidence of cable-deck interaction is presented.

This is believed to have been the most extensive monitoring programme on a major cable-stayed bridge during construction. The results have revealed several aspects of the dynamic behaviour, and have demonstrated that they provide useful information for the validation of analysis techniques in further studies.

DECLARATION

I declare that, except where referenced or acknowledged in the text, the work and ideas presented in this thesis are original and are entirely my own.

Any views expressed herein are not necessarily those of the University of Bristol.

This thesis has not previously been submitted for examination to any university, college or other institution.

J Macdonald 28/6/00

John Hugh George Macdonald

ACKNOWLEDGEMENTS

There are many individuals and organisations to which I am indebted for their assistance in carrying out this work. I would particularly like to thank the following:

Laing-GTM for allowing access to the Second Severn Crossing (SSC) site during construction, for facilitating and partly funding the monitoring work, and for providing construction drawings and other information;

Severn River Crossing PLC for access and funding after completion of the bridge, and for allowing use of the data for this research;

Laing Engineering Ltd. for practical assistance for access after completion;

Rowan Williams Davies & Irwin Inc. (RWDI) for the results of the wind tunnel tests and design buffeting analysis;

Halcrow-SEEE for design information;

Engineering and Physical Sciences Research Council (EPSRC) for funding of the development of the Computer Vision System and of the site monitoring during construction;

Colin Taylor for his encouragement and advice;

Nick Dobinson for creating the initial finite element model of the SSC cantilever;

Elsa Caetano for further development of the finite element model;

Richard Bridgeman for support with electrical instrumentation;

Frank Gibbs and Chris Setchell for the development of the image processing side of the Computer Vision System;

David Harvey for writing the Matlab routine to read the binary site data files;

Countless members and visitors of the Department of Civil Engineering at the University of Bristol, including Richard Bridgeman, Rafael Fernandez, Adith Gnanendran, Barny Wainwright, Nick Dobinson, Max Radcliffe, Christos Georgakis and Dave Ward, for their help on site, at all hours and in all weather conditions!

Wendy Daniell for her rigorous and valuable review of the draft of this thesis;

Richard Edwards, Pete Ettridge and Cathy Banton for proof reading the text.

Finally, I would like to thank my mother and Jane Stark for their love and support, particularly while I was writing up. I would also like to thank Jane for her patience, but now this thesis is finished, I look forward to getting married!

NOMENCLATURE

Notation and abbreviations are defined in each chapter of this thesis. The following lists are not intended to be exhaustive, but they cover the frequently used terms.

Notation

A	Cross-sectional area of cable
B	Width of bridge deck
B_e	Resolution bandwidth of spectral estimates
B_r	Half power bandwidth of resonant peak in power spectral density
C_D, C_L, C_M	Static drag, lift and moment coefficients
D	Cable diameter, depth of bridge deck
E	Young's Modulus
E_{eq}	Equivalent Young's Modulus of sagging cable
f	Frequency
f_n	Natural frequency
f_r	Natural frequency of mode r
F_D	Drag force per unit length
F_L	Lift force per unit length
g	Acceleration due to gravity
$H(f)$	Frequency Response Function
i	$\sqrt{-1}$, index of summation
I	Polar second moment of mass of the deck per unit length
I_u, I_v, I_w	Turbulence intensities of wind velocity components
L	Cable length along chord
${}^xL_u$, etc.	Integral length scale of turbulence of wind component u in direction x
m	Mass per unit length of deck or cable
M_r	Generalised mass of mode r
M_α	Pitching moment per unit length
n	Number of blocks in spectral processing

r	Index of specific mode under consideration
R_e	Reynolds number = UD/v, where D = representative dimension of the body, v = kinematic viscosity (=15mm^2/s for air)
S	Strouhal number
S_c	Scruton number = $m\zeta/\rho D^2$
$S_{yy}(f)$	Power Spectral Density of y(t) (single-sided)
$S_{xy}(f)$	Cross Spectral Density of x(t) and y(t)
${}_iS_{yy}(f)$	Contribution of mode i to S_{yy}
t	Time
T	Record length, mean cable tension
u,v,w	Fluctuating components of wind velocity in along wind, transverse and vertical directions respectively
U	Mean wind speed
U_{eq}	Equivalent normal mean wind speed
U_{norm}	Mean component of wind velocity normal to the bridge axis
$w(t)$	Window function in time domain
$W(f)$	Window function in frequency domain = Fourier transform of $w(t)$
x,y,z	Cartesian co-ordinate set, x normal to bridge, y along bridge, z vertical
$x(t)$	Input (force) time history
$y(t)$	Output (acceleration) time history
α	Vertical angle of attack of incident wind or angular displacement of deck
β	Angle of inclination of cable
$\gamma^2_{xy}(f)$	Coherence between $x(t)$ and $y(t)$
ε	Normalised error
ε_b	Bias error
ε_r	Variance error
ϕ_i	Vector of mode shape of mode i
σ^2_x	Variance of x
ζ	Viscous damping ratio

θ	Direction of the wind, measured clockwise from normal to the bridge on the south side
ρ	Density of air (=1.225kg/m^3)
χ^2	Aerodynamic admittance
ω	Circular frequency
ω_n	Circular natural frequency

Abbreviations

2-D	Two-dimensional
3-D	Three-dimensional
ADC	Analogue to Digital Converter (board)
CSD	Cross Spectral Density
CVS	Computer Vision System
DC	Direct Current (i.e. static component of instrument signal)
ESDU	Engineering Sciences Data Unit
FE	Finite Element
FFT	Fast Fourier Transform
FRF	Frequency Response Function (or pseudo-Frequency Response Function, when considering the relationship between two outputs)
HPB	Half Power Bandwidth
IWCM	Iterative Windowed Curve-fitting Method
M1	Pylon and cantilever on west (Welsh) side of SSC
M2	Pylon and cantilever on east (English) side of SSC
MDOF	Multiple-Degree-Of-Freedom
MECS	Multiple Element Cable System
OECS	One Element Cable System
PSD	Power Spectral Density (also known as Autopower Spectral Density, Autopower Spectrum, or Spectrum)
RMS	Root Mean Square
RWDI	Rowan Williams Davies & Irwin Inc.

SDOF	Single-Degree-Of-Freedom
SISO	Single Input Single Output
S/N	Signal to Noise (ratio)
SSC	Second Severn Crossing (cable-stayed bridge)
WCM	Windowed Curve-fitting Method

CONTENTS

LIST OF FIGURES

LIST OF TABLES

CHAPTER 1 INTRODUCTION

1.1 Background to research

Over the last four decades, the design of cable-stayed bridges has developed and they have become the most popular structural form for bridges of 200-600m span. The record span has reached 890m, for the Tatara Bridge in Japan, completed in 1999, and the trend towards longer spans is likely to continue.

The consequences of longer spans include greater susceptibility to large amplitude vibrations, particularly due to aerodynamic effects, and greater significance of non-linear behaviour. Some issues are shared with suspension bridges, including wind loading and aeroelastic instabilities of the deck, but there are other effects which are particular to cable-stayed bridges. These include inclined cable aerodynamics, cable-deck interaction and the sources of non-linearity, particularly cable sag.

There is a need for a thorough understanding of the dynamic behaviour of cable-stayed bridges to improve the tools available for their design. Several major bridges built in recent years have experienced large amplitude cable vibrations, and in some cases significant vibrations of the deck. Retrofitting has generally been successful for these bridges, but improved predictions of the dynamic response at the design stage would be of great benefit to avoid potential problems.

Wind tunnel tests are invaluable in the design and research of the aerodynamics of long-span bridges, but they have limitations, for example being unable to model cables fully along with a bridge deck, due to scaling problems.

There have been significant recent advances in methods of analysis, including coupled multi-mode analyses, non-linear Finite Element (FE) modelling and the development of mathematical models for cable-deck interaction. However, there remains a need for validation of these techniques from measurements on full-scale bridges, particularly when subject to ambient loading. Dynamic tests have been conducted on several cable-stayed bridges, but the majority have been of short duration, so there are limited data available for bridges in a variety of wind conditions. In particular, there have been very few dynamic tests on cable-stayed bridges during construction, although this is potentially the most vulnerable period for such a structure.

In view of the need for full-scale data, the research described in this thesis concentrated on the long-term dynamic monitoring of a typical major cable-stayed bridge, both during construction and for the first three years of service.

1.2 Objectives

The final aim of this research was to increase the understanding of cable-stayed bridge dynamic behaviour. The approach taken was through full-scale monitoring, principally in ambient conditions. The methods of analysis of the data from such tests were also addressed.

1.2.1 Full-scale monitoring

The first objective of this research was the establishment of a large database of the dynamic response, and corresponding wind conditions, for a full-scale cable-stayed bridge, to enable the validation of methods of analysis and the identification of the significance of particular issues.

The bridge considered in this study was the Second Severn Crossing (SSC) cable-stayed bridge. It was monitored at several stages of construction and after completion. Long-term records aimed to reduce errors in the results by averaging, and to provide data in a variety of different conditions. Other shorter tests were required to monitor particular aspects of the behaviour.

In parallel with the main monitoring programme, a 'Computer Vision System' for the remote measurement of displacements was developed.

It is believed that the monitoring programme undertaken for this study was the most comprehensive to have been conducted on a cable-stayed bridge during construction (§11.2).

The analysis of all of the data is beyond the scope of this thesis, since they are also intended for further research. It is proposed that new methods of theoretical response analysis be applied to the SSC and that the data collected be used for their validation.

Although this study was based on testing a single cable-stayed bridge, it aims to provide insights into the dynamic behaviour that can be applied more generally to other similar bridges.

1.2.2 Improvements in ambient vibration data processing

An important part of the study was the minimisation of errors in the analysis of site data, particularly for estimates of modal parameters, including damping. Therefore, the

shortcomings of previous techniques for the analysis of ambient vibration data were addressed.

A method was developed to improve the accuracy of modal parameter estimates (§11.3). It was validated with simulated data and was then applied to the SSC measurements.

1.2.3 Improved understanding of the dynamic behaviour of cable-stayed bridges

The monitoring of the SSC and the subsequent data analysis aimed to give a detailed description of the dynamic characteristics of the bridge for comparison with analytical predictions and to identify the significance of particular issues. Where predictions of the behaviour were available they were compared with the measured response to validate the methods that were applied.

The principal aspects of the behaviour that were of interest for this study were as follows:

i) *Global natural frequencies and mode shapes of vibration*

It was aimed to determine the natural frequencies and mode shapes of vibration of the bridge to define its basic dynamic characteristics. Such measurements allow comparison with the results of FE models to confirm the accuracy of the methods of modelling and to give confidence in the methods of monitoring and data analysis. Detailed data provide the opportunity for updating models to match the measured characteristics, which could be of use for improving predictions during the construction period or for structural health monitoring in the longer term. Of particular value were measurements at different stages of construction to give several structural variations to evaluate methods of updating.

ii) *Global damping*

The level of damping is important in determining the amplitude of response of a structure to given loading. There is no reliable analytical means of predicting the damping of real structures, so measurements from existing structures are of value. Aerodynamic damping can be estimated from theory and is believed to be significant, but it has previously been quantified on very few full-scale long-span bridges, and on none with a bluff cross-section. Application of the improved method for ambient data analysis to the long-term data from the SSC aimed to distinguish the contributions of aerodynamic and structural damping. The aerodynamic component could then be compared with theoretical values and more accurate estimates of structural damping could be made than previously obtained.

iii) *Variations in modal behaviour*

Variations of modal parameters could provide evidence of non-linear behaviour, temperature effects or changes due to the presence of traffic. Interactions between modal responses could provide evidence of modal coupling, for which there have been recent developments of methods of analysis, but with little validation from physical tests. Also, variations as construction proceeds are of interest - in particular, changes in damping and the effects of the addition of wind barriers. Evidence of any such variations was sought from the SSC data.

iv) *Amplitudes of buffeting vibrations*

The principal dynamic loading of long-span bridges in normal service conditions is from wind buffeting. Site measurements can be compared with predicted amplitudes of response from buffeting analyses and wind tunnel tests to assess the accuracy of conventional methods or to validate new methods. Such comparisons have been made for very few full-scale bridges so the amplitudes of vibrations of the SSC at full scale were of interest for this purpose.

v) *Vortex-induced vibrations and wind tunnel testing*

Large amplitude vortex-induced vibrations occurred on the SSC during the monitoring period. The opportunity was taken to establish the criteria for them to occur, to assess the accuracy of predictions from wind tunnel tests, and to identify reasons for discrepancies.

vi) *Cable damping*

The damping of bridge cables is extremely low so they are susceptible to large vibrations. These occurred on the SSC, in common with several other major cable-stayed bridges. With such low damping, aerodynamic damping is likely to be significant, but previously it has not been quantified for inclined bridge cables for an arbitrary wind velocity. This study aimed to distinguish the contributions of aerodynamic and structural damping from full-scale tests and to derive and validate theoretical expressions for the aerodynamic damping. More accurate estimates of structural damping also resulted, which were compared with previously proposed criteria for cable aerodynamic instabilities.

vii) *Cable-deck interaction*

Cable-deck interaction is a particular feature of cable-stayed bridges, caused by the natural frequencies of the cables and of the global structure being in the same frequency range. Although there has been significant theoretical and analytical research on this phenomenon, and it has been speculated that it has played a role on several bridges, there is little direct evidence of it from site measurements.

Simultaneous measurements of cable and deck vibrations in both forced and ambient vibration tests aimed to monitor this behaviour.

All of the above objectives were met through the full-scale monitoring of the SSC and analysis of the site data. The principal conclusions are presented under the same headings in §11.4.

1.3 Overview of thesis

It is hoped that this thesis will be of particular value to the practising engineer, by providing a detailed account of several aspects of the full-scale dynamic behaviour of cable-stayed bridges. Since it covers a range of disciplines, including instrumentation, signal processing, aerodynamics and structural dynamics, some detail is provided on standard issues to inform the non-specialist in each of these areas.

The principal issues of the dynamics of cable-stayed bridges are reviewed in Chapter 2, concentrating on the response to wind loading. In particular the need for full-scale measurements is demonstrated - to validate methods of response analysis and to determine the significance of certain effects that have been studied theoretically.

Chapter 3 provides background information to the site monitoring and data analysis, including a description of the SSC, details of the FE models created for this study, and an outline of the design wind tunnel tests.

The site monitoring is described in Chapter 4. This covers a description of the equipment, including the Computer Vision System, and details of the test methods. The data collected from this monitoring campaign are unique and form the basis of the analysis in later chapters.

Methods for the analysis of site data are reviewed in Chapter 5, and the calculation of spectral estimates and sources of errors are discussed, with particular reference to the SSC data.

Chapter 6 presents the results of the preliminary tests on the SSC at an early stage of construction of the cable-stayed section. Also, the wind measurements are analysed and an expression for the estimated spectrum of dynamic loading is derived.

In Chapter 7, an improved method for estimating modal parameters from spectral estimates from ambient vibration data is developed and validated. Advantages include consideration of a realistic loading spectrum, for which the estimated spectrum from Chapter 6 could be used.

The new method is applied to the SSC data in Chapter 8. The results are compared with predictions from the FE models of Chapter 3 and the design buffeting analysis. Also, variations in the measured response are used to separate the contributions of

aerodynamic and structural damping, and to identify the existence of additional modes and modal coupling.

Chapter 9 addresses the particular problem of vortex-induced vibrations, which occurred on the SSC. The wind conditions required to cause the vibrations are identified. The measurements are compared with results of the design wind tunnel study and reasons for discrepancies are discussed. The effectiveness of modifications to the deck, to inhibit the vibrations, is evaluated.

Cable vibrations and cable-deck interaction are covered in Chapter 10. An expression is derived for the aerodynamic damping of an inclined cable, which is validated from site measurements. Evidence of cable-deck interaction is presented, and the effectiveness of secondary cables in preventing large vibrations is assessed.

Finally Chapter 11 summarises the principal conclusions of the study, critically reviews the work and provides recommendations for further research.

CHAPTER 2 REVIEW OF CABLE-STAYED BRIDGE DYNAMIC BEHAVIOUR AND WIND LOADING

2.1 Introduction

This chapter reviews the principal issues in the dynamic behaviour of cable-stayed bridges, and corresponding methods of analysis, including recent developments. Particular attention is paid to wind loading and the resulting bridge response. The need for full-scale testing is demonstrated - to provide data for validating methods of analysis and for identifying the significance of effects studied theoretically. Key results from previous full-scale tests are discussed in relation to each subject, and their shortcomings are highlighted.

2.2 Trends in cable-stayed bridge design

Since 1960, cable-stayed bridges have become increasingly popular, and ever longer spans have been constructed. Fourteen cable-stayed bridges with spans over 450m have been constructed world-wide in the last ten years and in the future the number and maximum spans of such bridges are likely to continue to increase. The principal developments which have led to their rise in popularity have been the introduction of computer analysis, orthotropic steel decks, and high strength steel cables.

The recent trend for major cable-stayed bridges is for multiple cables, typically at 5-10m spacing, enabling modular construction and minimising bending moments in the deck. H-shaped pylons, with cable fans on either side of the deck in the vertical plane are common. However, A-shaped pylons are preferred for the longest spans since they provide increased torsional rigidity. Forms of deck construction include steel and concrete box girders, steel trusses and composite decks.

The main advantages of cable-stayed bridges over suspension bridges are the shorter construction period and the lack of a need for massive anchorage blocks. Some of the aerodynamic issues are similar, since the principal wind loading is often on the deck. However particular dynamic effects for cable-stayed bridges include cable vibrations, cable-deck interaction, 'less sinusoidal' mode shapes (Scanlan 1987, Gimsing 1997), and non-linearities, possibly leading to more coupling of the modes of vibration.

Further details of the history and developments of cable-stayed bridges are provided by Gimsing (1997), Walther et al. (1989), Troitsky (1988) and Billington & Nazmy (1990).

2.3 Full-scale test methods

Before considering the analysis and principal dynamic issues of cable-stayed bridges, methods of full-scale testing are introduced here. Results from such tests are quoted in later sections, under the discussion of each of the main topics.

Various methods are available for the dynamic testing of large civil engineering structures. Controlled excitation methods have been employed on cable-stayed bridges, including vertical mass exciters (Ohlsson 1987, Yoshimura et al. 1989, Narita & Yokoyama 1991), release from a static deflection (Ohlsson 1987, Murià-Vila et al. 1991) and swinging a massive pendulum beneath the bridge (Stiemer et al. 1988). However these tests are relatively difficult to perform, can be expensive and normally only cover a narrow range of excitation frequencies.

Tests can also be performed with unmeasured excitation, with assumptions being made about its characteristics. For some studies, trucks have provided the excitation, sometimes driving over a series of ramps (Persoon 1981, Casas 1995, Gentile et al. 1998). However ambient loading, from wind and traffic, has also been employed (Hay 1981,1984, Wilson & Liu 1991, Murià-Vila et al. 1991, Owen & Blakeborough 1993). Although this is the least expensive test method, it still enables the modal parameters to be estimated, although often with less accuracy. Also, by this method, the response can be measured in typical loading conditions, for comparison with predictions.

An extensive bibliography of methods and earlier tests on long-span bridges is provided by Brownjohn (1988). Methods for extracting modal parameters from test data are addressed in §5.3.

2.4 Dynamic analysis of cable-stayed bridge structures

Cable-stayed bridges are more flexible than most other bridge types, so they are more prone to large amplitude vibrations. Wyatt (1991) provides an overview of their dynamic issues. They are particularly susceptible to wind loading, and, under normal service conditions, dynamic traffic loading. These are the main forms of loading considered in this thesis. Earthquake loading can also be significant, but it is relatively unusual and is not critical in many regions, so it is not specifically addressed.

2.4.1 Structural non-linearities

Cable-stayed bridges exhibit non-linear behaviour due to three principal causes:

i) Cable sag;

ii) Interaction of the axial load and bending of the deck, causing a reduction in stiffness;

iii) Large deflections causing geometric non-linearities.

Other causes include aeroelastic loading (§2.6.5) and material non-linearities.

Cable sag is usually the most significant of these effects. As the cable tension increases, the sag is reduced, causing the cable effectively to become stiffer. The equivalent Young's Modulus of the sagging cable is often approximated by (Ernst 1965):

$$E_{eq} = \frac{E}{1 + \frac{(mgh)^2 AE}{12T^3}} \tag{2-1}$$

where: E = Young's Modulus of the material

m = mass per unit length

g = acceleration due to gravity

h = horizontal projected length

A = cross-sectional area

T = mean tension

Local cable vibrations and their interaction with the deck and pylon can also exhibit non-linear behaviour (§2.8&2.9).

For dynamic analysis, the initial equilibrium state needs to be established, so often a non-linear static analysis is conducted first (§2.4.3). For small amplitude vibrations, the dynamic behaviour is approximately linear, but for larger vibrations non-linearities may become significant.

2.4.2 Modal analysis

If linear dynamic behaviour is assumed, the response can be described by the superposition of modal responses (Ewins 1984). For low damping the modes can be considered structurally uncoupled, with each mode acting as a Single-Degree-Of-Freedom (SDOF) system according to the equation of motion:

$$M_r\left(\ddot{y}_r + 2\zeta_r\omega_r\dot{y}_r + \omega_r^2 y_r\right) = P_r(t) \tag{2-2}$$

where: y_r = generalised modal displacement

$\omega_r = 2\pi f_r$ = circular natural frequency of the mode

ζ_r = modal damping ratio to critical

t = time

the dots represent differentiation with respect to time

M_r and $P_r(t)$ are the generalised mass and load, given by:

$$M_r = \int m\phi_r(s)^2 ds \tag{2-3}$$

$$P_r(t) = \int p(s,t)\phi_r(s) ds \tag{2-4}$$

where: $\phi_r(s)$ = mode shape

m = mass per unit length

$p(s,t)$ = force per unit length

The integrals are strictly over the whole structure, but often are taken over the deck only, since its mass and applied loads are dominant. If the force per unit length is correlated over a short distance compared with changes in the mode shapes, the generalised loads can be considered uncorrelated and the modal responses uncoupled.

Wyatt (1980) provides simplified analyses to estimate the natural frequencies of various configurations of cable-stayed bridges. However they exhibit a high degree of statical indeterminacy and significant non-linearities for large displacements, so detailed analysis is usually performed by Finite Element (FE) modelling.

2.4.3 Finite element modelling

For distributed loading, including wind, the primary role of the FE dynamic analysis is to determine the natural frequencies and mode shapes, to enable the generalised masses and loads, and hence response, to be calculated.

For design purposes, usually less than ten modes are considered, but for multi-mode analyses (§2.6.6) more than 20 modes are useful (Scanlan & Jones 1990). Also, for model updating or structural health monitoring (§2.4.4), more modes are beneficial.

Kanok-Nukulchai et al. (1992) describe the principal issues and FE modelling methods for cable-stayed bridges. Three-dimensional models are usually necessary, particularly for

modelling torsional modes, although for bridges with a single plane of cables, or two closely-spaced planes, two-dimensional models can provide reasonable results (Casas 1995).

The pylons and piers are usually modelled as beam elements, but other components are more challenging to represent accurately. Typically cables are modelled as single truss elements with an equivalent elastic modulus (equation (2-1)), neglecting their mass, sag and local vibrations. Alternatively they can be modelled as curved finite elements (Jayaraman & Knudson 1981) or multiple truss elements (§2.9.2).

The deck can be modelled in a number of ways, and is similar for cable-stayed and suspension bridges. A popular approach is to define a longitudinal spine of beam elements, with equivalent properties of the full deck, linked to the cable anchorage nodes with transverse rigid links. Wilson & Gravelle (1991) detail refinements to this method, with particular attention to the mass distribution and torsional and warping stiffnesses. Kumarasena et al. (1989) used a variation of the method, with additional longitudinal elements at the edge of the deck.

Other models for bridge decks have included:

i) A single equivalent plate for each section between cable anchorages (Dumanoglu & Severn 1985);

ii) A longitudinal beam on each side of the deck, representing main physical beams, with rigid links between (Kovacs et al. 1992);

iii) A combination of shell elements for the deck slab and vertical webs of the longitudinal steel girders, with beam elements for other components (Owen 1994).

Several authors have considered the significance of non-linearities in FE analyses. For the static case, Fleming (1979) found that geometric non-linearities (§2.4.1), especially from cable sag, were important for the dead load case, but a linear approximation for the additional effects of the live load was reasonable. Seif & Dilger (1990) considered material non-linearities also, which were significant for concrete elements near failure, but not otherwise. Virlogeux (1992) found material non-linearities to be insignificant on the predominantly steel Normandy Bridge.

For dynamic behaviour, Fleming & Egeseli (1980) and Abdel-Ghaffar & Nazmy (1991) suggest that linear analysis is adequate, provided it is preceded by non-linear static analysis. However, Wilson & Gravelle (1991) and Owen (1994) have shown that purely linear analysis can result in reasonable predictions of natural frequencies and mode shapes, compared with measurements at full scale.

2.4.4 Model updating and structural health monitoring

An accurate FE model provides a tool for structural health monitoring, whereby the causes of changes in dynamic properties, such as damage or deterioration, can be identified (Brownjohn 1988). It is therefore desirable to update the initial FE model to achieve closer agreement with the measured response.

There are several model updating methods, including simply modifying a few chosen parameters. Deger et al. (1996) found, for a cable-stayed footbridge, that allowing some foundation flexibility reduced the error in natural frequencies for all identified modes from up to 40%, to below 10%. Link et al. (1996) also updated the foundation stiffness for a prestressed concrete bridge, reducing errors in natural frequencies from up to 30% to typically 10%, and achieving slight increases in Modal Assurance Criteria (MACs). The deck torsional stiffness and Young's Moduli of the deck and pylon concrete were modified by Gentile et al. (1998) for the Malpensa 2000 Airport North Bridge. For the nominally identical south bridge, a Young's Modulus 13% higher was required for the deck (Gentile & Martinez y Cabrera 1999).

Another possibility for bridges is to update the model at an early stage of construction, to improve the predictions for later stages. The potential of this approach was demonstrated on a 110m prestressed concrete bridge constructed by the balanced cantilever method (Skrinar & Strukelj 1996). An elastic block was added to model the foundation flexibility, with parameters chosen to match the first natural frequency for the first construction stage. The predicted natural frequencies of the first modes were then within 1% of the measured values for twelve subsequent stages.

This approach would be particularly valuable for cable-stayed bridges, with long erection periods, allowing time for construction modifications if necessary. However, the complex nature of cable-stayed bridges demands a systematic updating method. This is an area of research potential, but data from full-scale structures, particularly at different construction stages, is needed for validating the methods. Also, estimates of the accuracy of the measured values and their variation under normal working conditions are required.

2.5 Damping

Damping is one of the most important factors influencing the amplitude of response of a structure. Damping mechanisms are addressed by Wyatt (1977), while Brownjohn (1994) discusses sources of damping for suspension bridges, several of which are applicable to cable-stayed bridges, including strain-dependent damping, hysteresis, friction, stiction, aerodynamic damping and apparent damping due to geometric non-linearities. There are several mathematical models for damping, but in practice viscous

damping is usually assumed for bridges. All damping values in this thesis are expressed as viscous damping ratios to critical, as a percentage.

In this thesis, aerodynamic damping is treated separately, since it varies considerably (§2.6.3), but all other forms of damping are taken together under the general term 'structural damping'. It can be affected by the type of excitation or amplitude of vibration, but only values for low amplitude wind or traffic excitation are considered here. For earthquake loading the damping can be considerably higher (Narita & Yokoyama 1991, Wilson & Atkins 1999).

It has been attempted to predict structural damping, based on the distribution of strain energy (Raggett 1975). Thus a damping ratio for each mode can be estimated, which can result in an increasing or decreasing trend with frequency, depending on the structural form. Similar methods have been applied to arrays of bridge cables with secondary cables (Yamaguchi & Jayawardena 1992), and a cable-stayed bridge model (Kawashima et al. 1993). Kawashima et al. (1988) also modelled foundation radiation damping and friction at bridge end supports. However, since the mechanisms are many and complex, accurate predictions are currently not possible, so estimates are usually based on previous measurements on similar structures.

2.5.1 Full-scale measurements of damping

Unfortunately it is difficult to measure the damping of large structures accurately. For forced vibration tests, excitation is often limited to a few modes, and there is difficulty in exciting significant amplitudes, particularly if other uncontrolled loading (e.g. wind) is present. For ambient testing, the unknown loading leads to uncertainty in the results (§5.3.1), so long records are required to obtain improved accuracy, particularly for low frequencies and damping.

Many methods for extracting modal parameters from test data have been employed (§5.3), but the method chosen can significantly affect the damping estimates. Littler (1992) stresses that damping ratios estimated from frequency spectra are overestimated due to bias errors (§5.6.1), particularly for low frequency modes, while Murià-Vila et al. (1991) obtained values between 0.1% and 0.9% for the same mode from several tests, using two different processing techniques.

Eyre & Tilly (1977) present forced vibration damping measurements on 23 steel and composite box girder and plate girder bridges. Generally, lower values were found for steel rather than composite, box girder rather than plate girder, and multi-span rather than single span bridges. Many vibration tests have been conducted on suspension bridges (Brownjohn 1994, Jensen et al. 1999), which tend to have higher damping at

lower frequencies, although this may be exaggerated by the signal processing methods (Littler 1992).

A trend for higher damping at lower frequencies has been reported from some tests on cable-stayed bridges also. Values of approximately 2% for the first one or two modes, decreasing to around 1% for higher modes have been reported on the Alamillo Bridge (Casas 1995), Evripos Bridge (Lekidis et al. 1998) and Quincy Bayview Bridge (Wilson & Liu 1991). In other studies, a frequency dependence has not been found, with values of 1.0-1.6% estimated for all identified modes on the Figueira da Foz Bridge (Rodrigues & Campos-Costa 1998) and Aratsu Bridge (Yoshimura et al. 1989). Values of 0.3-0.5% have been found for the first few modes on several other cable-stayed bridges, including the Wye Bridge (Smith 1980) and Annacis and Pasco-Kennewick Bridges (Stiemer et al. 1988). Similar values were obtained for very low amplitude vibrations of the Tjörn Bridge, but with values up to 1.6% for an amplitude of 15mm (Ohlsson 1987).

Forced vibration tests were conducted on 22 cable-stayed bridges in Japan, yielding values of 0.22-1.4% with a mean of 0.83% for the first vertical bending mode (Narita & Yokoyama 1991). There was no clear trend of frequency dependence for a given bridge, but generally damping decreased with span length, and was lower for steel rather than concrete bridges, and for plate girder decks rather than trusses.

The large scatter of values from previous full-scale tests may be caused by overestimates due to aerodynamic damping (§2.6.3) or signal processing errors (§5.3).

2.6 Wind loading

Cable-stayed bridges are more flexible than most other bridge types, so they are more prone to large amplitude vibrations, particularly for longer spans. They are especially susceptible to wind loading. Gusts cause dynamic loads in the same low frequency range as the natural frequencies of the structures, while aeroelastic instabilities can occur even in steady winds.

There have been several failures of suspension bridges due to aerodynamic effects, the most famous being the first Tacoma Narrows Bridge, in moderate winds in 1940 (Farquharson et al. 1950-1954). However, wind-induced vibrations were observed on five other suspension bridges of over 200m main span built in late the 1930's, and between 1818 and 1889 ten suspension bridges failed due to wind, including the Menai Straits Bridge (Provis 1842), and a span of the Brighton Chain Pier (Scott Russell 1841).

To date, there has been no major cable-stayed bridge failure due to wind loading, but large amplitude vibrations have been observed on several. Miyata (1991) summarises wind effects and measures to counteract vibrations on cable-stayed bridges, for both the

global structure and cables, while Simiu & Scanlan (1986) detail wind loading mechanisms. Much of the basic theory in this section is taken from this reference.

2.6.1 Role of wind tunnel tests and Computational Fluid Dynamics (CFD)

Irwin (1998) discusses the role of wind tunnel testing and identifies three aims of model tests - to directly model the full-scale structure, to identify parameters for use with semi-empirical analyses, and to address vibration problems of specific components, for example cables. Different types of models and similitude requirements are discussed by Scanlan (1987), whilst Ostenfeld-Rosenthal et al. (1992) address uncertainties in applying wind tunnel results to full scale.

Compared to full scale, Reynolds number (R_e)† is not normally represented correctly. It is generally believed that for bluff sections this is not very important, but details of the effects are largely unknown. Although wind tunnel testing has proved to be valuable for design and research, there remains a need for full-scale data for validating model results and assessing their accuracy.

The main types of model for global bridge structures are deck sectional models, typically representing a 50-100m length of the deck at approximately 1:50 scale, and full aeroelastic models of the whole bridge, typically at 1:150 scale.

Methods of sectional model testing, in smooth flow, were developed by Bleich (1949) and Steinman (1950). The methods were given credence by the good agreement obtained with observations at full-scale on the Tacoma Narrows Bridge (Farquharson et al. 1950-1954) and with measurements on a full aeroelastic model of the originally proposed Severn Bridge (Frazer & Scruton 1952). Sprung supports allow the vertical and torsional natural frequencies each to be adjusted, to simulate two uncoupled modes, while offset of the mass and stiffness centres allows coupling of lateral and torsional motion, as for full bridges (Irwin 1979a). Damping of sectional models can be controlled also. Now tests are normally conducted in turbulent flow as well, but it is not generally possible to simulate the large scale turbulence.

Full aeroelastic models can allow for full mode shapes, modal coupling and distributed wind loading. Also turbulence can be modelled well at the smaller scale. However, geometric details are more difficult to reproduce accurately, so aerodynamic effects sensitive to minor changes are less well modelled. Also, there is less control over the natural frequencies and damping ratios of individual modes. Full aeroelastic models are useful for considering construction stages (§2.10), for which loading on the pylon and three-dimensional effects are more significant (Scanlan 1987).

---

† $R_e=UD/\nu$, where U = wind speed, D = representative dimension of the body, ν = kinematic viscosity.

Taut-strip models have many of the advantages of full aeroelastic models but are simpler to construct (Davenport et al. 1992). The resulting vertical and torsional modes are sinusoidal, which model suspension bridges well but are less appropriate for cable-stayed bridges.

It is not possible to create aeroelastic models with the bridge cables and deck both correctly scaled. However, tests on short cable sections are valuable for understanding mechanisms of cable excitation (§2.8).

A recent development in estimating the wind loads on bridge decks has been the use of Computational Fluid Dynamics (CFD), which has the potential of reducing the expense and time taken by wind tunnel testing. Aerodynamic parameters for bridge cross-sections can be derived (Larsen & Walther 1997), or CFD analyses can be coupled with a simple FE model of the structure (Kvamsdal et al. 1999).

2.6.2 Quasi-static wind loads

The mean wind around a section causes 'quasi-static' lift and drag forces and a pitching moment, given, per unit length, by (Simiu & Scanlan 1986):

$$F_L = \tfrac{1}{2}\rho U^2 B C_L \tag{2-5}$$

$$F_D = \tfrac{1}{2}\rho U^2 B C_D \tag{2-6}$$

$$M_\alpha = \tfrac{1}{2}\rho U^2 B^2 C_M \tag{2-7}$$

where: ρ = density of air

U = mean wind speed

B = deck width (or other representative dimension of the section)

C_L, C_D, C_M = non-dimensional force coefficients, dependent on the cross-sectional shape and the vertical angle of attack of the wind, α

'Quasi-static theory' (or 'quasi-steady theory') for dynamic loading assumes that the above relationships hold for varying relative velocity of the wind and deck, either from wind gusts or from movement of the deck. A vertical component of the wind, torsional displacement, or vertical velocity of the deck leads to an effective vertical angle of attack, causing changes to the force coefficients. Usually small angles are assumed, so

the values and the derivatives of the force coefficients at α=0 are sufficient for estimating the required values.

In practice, small scale turbulence around the body gives different dynamic forces than assumed by quasi-static theory. Nevertheless, it is generally taken to give a reasonable first estimate of the dynamic loading, using a limited number of parameters easily obtained from sectional model tests.

2.6.3 Aerodynamic damping

When a structure vibrates in the presence of wind, aeroelastic forces occur, which are approximately proportional to the velocity of the structure. This is equivalent to additional damping, termed 'aerodynamic damping'. The structure behaves in each mode as if subject to total viscous damping equal to:

$$\zeta = \zeta_{struc} + \zeta_{aero} \tag{2-8}$$

where: ζ_{struc} = structural damping

ζ_{aero} = aerodynamic damping

Davenport (1962a) showed that, based on quasi-static theory, for vertical vibrations of a uniform horizontal structure in a wind normal to its axis, the aerodynamic damping is approximately:

$$\zeta_{aero,z} = \frac{\rho BU}{8\pi f_n m}\left[\frac{dC_L}{d\alpha}\right]_{\alpha=0} \tag{2-9}$$

where: f_n = natural frequency of the mode of vibration

For pure horizontal vibrations (in the direction of the wind), it was also shown that the aerodynamic damping is approximately:

$$\zeta_{aero,x} = \frac{\rho BUC_D}{4\pi f_n m} \tag{2-10}$$

For torsional modes, the relative wind velocity varies over the cross-section, so the quasi-static approach is less applicable. However, considering the relative velocity at the windward edge, where the undisturbed flow encounters the deck, the aerodynamic damping for torsional vibrations is given by:

$$\zeta_{aero,\alpha} = \frac{\rho B^3 U}{16\pi f_n I}\left[\frac{dC_M}{d\alpha}\right]_{\alpha=0} \qquad (2\text{-}11)$$

where: I = polar second moment of mass of the deck per unit length

Thus, for vibrations in any mode, based on quasi-static theory, the aerodynamic damping is proportional to the wind speed. Also it is inversely proportional to natural frequency, so lower frequency modes have higher aerodynamic damping.

In practical cases, the aerodynamic damping for horizontal deck vibrations is very low, and often insignificant compared with the structural damping. However, the aerodynamic damping for vertical and torsional modes can be significant, and in high wind speeds it can be the dominant component of damping. Generally the horizontal and torsional vibrations are coupled (Irwin 1979a), so the aerodynamic damping depends on the relative magnitudes of the components, which must be integrated over the mode shape to estimate the net effect.

Some wind tunnel tests have suggested that the actual aerodynamic damping is considerably lower than predicted by quasi-static theory (Holmes 1975, Zan & Wardlaw 1987). Alternatively it can be estimated from the flutter derivatives (§2.6.5.1), which give a non-linear variation of damping with wind speed.

2.6.3.1 Full-scale measurements of aerodynamic damping

Damping measurements on full-scale bridges (§2.5.1) are of total damping, but for only a few tests on suspension bridges has an attempt been made to account for the contribution of aerodynamic damping, to estimate the true structural damping. Jones & Spartz (1990) estimated the aerodynamic damping from wind tunnel tests for the Deer Isle Bridge and subtracted it from the full-scale damping measurements. In independent studies on the Humber Bridge, Littler (1992) and Brownjohn (1994) both estimated the average damping for different wind speed ranges, finding higher damping in stronger winds. Tanaka et al. (1998) found variations in damping estimates for the Höga Kusten Bridge, during construction, broadly agreeing with aerodynamic damping estimates from flutter derivatives. Finally, for the Great Belt Bridge, Jensen et al. (1999) plotted measured total damping against wind speed and fitted straight lines to estimate the structural damping. The values of 0.11-1.0% obtained were generally lower than those measured on other suspension bridges, presumed to be due to the removal of the contribution of aerodynamic damping.

On the Saint-Nazaire Cable-stayed Bridge, Bietry et al. (1994) found a trend of measured damping with wind speed broadly in agreement with quasi-static theory, but this was based on a total of only six hours of data and only considered two modes. It

appears that previously no other attempt to separate the contributions of structural and aerodynamic damping has been made at full scale for a cable-stayed bridge. Furthermore, this has not been considered for any full-scale long-span bridge with a bluff cross-section. Long-term tests are needed for this purpose, to obtain measurements in a range of wind speeds.

2.6.4 Wind buffeting

Wind buffeting is the dynamic loading due to wind turbulence. Gusts vary in velocity, both temporally and spatially, leading to complex patterns of loading on structures. Conventional buffeting analyses are based on statistical methods, first applied by Liepmann (1952) to aircraft wings, and by Davenport (1961a,c,1962a,b) to long-span bridges. Alternative formulations were developed by Scanlan & Gade (1977) and Irwin (1977). For a slender structure, the basic method involves estimating the Power Spectral Density (PSD) of wind velocity, and hence loading, at a cross-section. This is then integrated over the length, considering the mode shape and cross-correlation of the wind loading, to find the generalised load of each mode. According to Davenport's (1962a) formulation, the PSD of vertical response in each mode is given by:

$$ {}_rS_{zz}(f) = \frac{4F_L^2}{U^2} |H_r(f)|^2 |J_r(f)|^2 \chi^2(f) S_{ww}(f) \qquad (2\text{-}12) $$

where: f = frequency

$H_r(f)$ = Frequency Response Function of the structure in the mode (§5.2.1)

$|J_r(f)|^2$ = joint acceptance of the mode (§2.6.4.2)

$\chi^2(f)$ = aerodynamic admittance (§2.6.4.3)

$S_{ww}(f)$ = PSD of vertical gust velocity (§2.6.4.1)

Conventional buffeting analyses assume uncoupled modal responses. In turn this is based on the assumptions of linear dynamic behaviour (§2.4.1&2.4.3), uncorrelated generalised forces (§2.6.4.2), and insignificant aeroelastic effects for the wind conditions considered (§2.6.5). However, the latter two assumptions are not required for multi-mode analyses (§2.6.6).

2.6.4.1 Wind turbulence

The characteristics of wind turbulence depend on a number of factors, including wind speed, ground roughness and height above the ground. Its sources and effects are discussed by Simiu & Scanlan (1986). The turbulence intensity is defined as:

$$I_i = \frac{\sigma_i}{U} \tag{2-13}$$

where: σ_i = Root Mean Square (RMS) of varying component of wind velocity

$i = u,v,w$ for the longitudinal, transverse and vertical directions (relative to wind direction)

Studies of turbulence have included measurements by Bailey & Vincent (1939) on the former Severn Railway Bridge (analysed by Davenport 1961a), by Harris & Deaves (1980), who made extensive measurements on tall masts, and by Teunissen (1980), who monitored the wind with an array of 15 masts.

Various wind spectra are discussed by Simiu & Scanlan (1986) and Mann et al. (1998). Hay (1984,1992) compared spectra proposed by Davenport (1961b), Irwin (1977) and Harris & Deaves (1980) with measured wind data from five major UK bridges. Above 0.1Hz the proposed spectra agreed well with the measurements, with the Irwin spectra, from the von Kármán (1948) model for homogenous isotropic turbulence, giving the closest correlation.

The von Kármán model has generally been recognised as the best description of turbulence for strong winds, giving reduced (non-dimensional) PSDs of longitudinal (with respect to wind direction) and vertical gust velocities at a point of (ESDU 1993)†:

$$\bar{S}_{uu}(f) = \frac{fS_{uu}(f)}{\sigma_u^2} = \frac{4\tilde{f}_u}{\left(1+70.8\tilde{f}_u^2\right)^{5/6}} \tag{2-14}$$

$$\bar{S}_{ww}(f) = \frac{fS_{ww}(f)}{\sigma_w^2} = \frac{4\tilde{f}_w\left(1+755.2\tilde{f}_w^2\right)}{\left(1+283.2\tilde{f}_w^2\right)^{11/6}} \tag{2-15}$$

† Note that slightly different notation is used here than by ESDU and several other wind engineering references, for consistency within this thesis. Single-sided spectra are used throughout this thesis.

where: $\tilde{f}_u = \frac{{}^xL_u f}{U}$ and $\tilde{f}_w = \frac{{}^xL_w f}{U}$ are reduced (non-dimensional) frequencies

${}^xL_u$ is an integral length scale, giving a measure of the average longitudinal size of eddies, defined as:

$$ {}^xL_u = \frac{1}{\sigma_u^2}\int_0^\infty R_{u_1u_2}(x)dx \qquad (2\text{-}16) $$

where: $R_{u_1u_2}(x)$ is the cross-correlation function of the varying component of longitudinal velocity measured at two points distance x apart in the longitudinal direction.

An equivalent definition applies for ${}^xL_w$, and indeed other length scales.

Additional turbulence may be created by the structure itself, termed 'signature turbulence', but its effects are generally ignored in buffeting analyses.

Davenport (1962a) showed that the PSD of loading for the cross-section of a line-like structure is a linear combination of the longitudinal and vertical wind PSDs and the Cross Spectral Density (CSD), the contribution of each depending on the mean wind speed and the force coefficients. The loading due to the CSD is usually insignificant, so it is generally disregarded in the analysis.

2.6.4.2 Spatial variation of wind loading

For long-span bridges, usually only the contribution of loading on the deck is considered. The distribution of wind velocity along the deck shows high correlation between closely-spaced points decreasing rapidly to very low correlation over longer distances. This is commonly represented by the relationship (Davenport 1962a):

$$ R_{y_1y_2}(y_1, y_2, f) = e^{-|y_1 - y_2|/l} \qquad (2\text{-}17) $$

where: y_1 and y_2 are two positions along the bridge

l = scale of the turbulence $\approx U/7f$

A more complex formulation, describing the CSDs of velocity components at variable spacing, is provided by Irwin (1979b), based on von Kármán's (1948) model of turbulence.

The correlation of loading over the length of the bridge is normally considered to be equal to the correlation of the wind velocity. However Kumarasena et al. (1991) found that the span-wise correlation of signature turbulence could be significant in increasing

the buffeting loading on a bluff deck, but Walshe & Wyatt (1983) estimated that signature turbulence contributed only 2% of the loading for a streamlined deck.

Assuming the loading is distributed according to the wind velocity, the PSD of the generalised load of each mode is related to the PSD of the load on a cross-section by the 'joint acceptance', given by:

$$|J_r(f)|^2 = \int_0^L \int_0^L R_{y_1 y_2}(y_1, y_2, f)\phi_r(y_1)\phi_r(y_2)dy_1 dy_2 \qquad (2\text{-}18)$$

where: L is the full length of the bridge

$\phi_r(y)$ is the mode shape, normalised such that:

$$\int_0^L \phi_r^2(y)dy = 1 \qquad (2\text{-}19)$$

The 'short correlation assumption' allows the separation of the wind correlation and mode shape factors in the double integral of equation (2-18), since on a long-span bridge the wind is highly correlated over a short length compared with variations in the mode shape. This also leads to the generalised loads being uncorrelated.

2.6.4.3 Aerodynamic admittance

The aerodynamic admittance accounts for variations in wind velocity over the cross-section. For small cross-sections it can approach unity, but for typical road bridges it can significantly reduce the loading.

The most commonly used expression for aerodynamic admittance was derived by Sears (1941) for an aerofoil, and is usually approximated by (Liepmann 1952):

$$\chi^2(f) = \frac{1}{1 + 2\pi^2 fB/U} \qquad (2\text{-}20)$$

Wind tunnel tests have shown that for bridge decks this can underestimate the actual values, so slight modifications have been proposed (Holmes 1975, Konishi et al. 1975, Walshe & Wyatt 1983). However, other tests have shown Sears' function to give reasonable approximations of measured values for a streamlined box girder bridge deck (Davenport et al. 1992).

An alternative expression was provided by Davenport (1962b) and modified by Irwin (1977), generally giving greater values for typical bridges. There remains some uncertainty over the most appropriate expression to use for bridge decks.

2.6.4.4 Long-term tests and measured relationship of amplitude to wind conditions

Surprisingly few full-scale tests have been conducted on long-span bridges over a sufficiently long period to establish the relationship between the wind conditions and the amplitude of response. The conditions for vortex-induced vibrations have been measured for some bridges (§2.6.5.3), but the buffeting response has been considered less.

Hay (1981,1984,1992) describes tests of several months duration on the Wye, Erskine, Kessock (all cable-stayed), Cleddau (box girder) and Severn (suspension) Bridges. The amplitudes of vibrations were compared with wind speed and turbulence intensity, by plotting $\ln(\sigma_z/I_u)$ (where σ_z = RMS vertical displacement) against $\ln(U)$. Approximately linear relationships were found, with gradients close to the theoretical value of 2.83 from a simplified buffeting analysis.

Owen (1994) monitored the Kessock Bridge for a few months, and attempted to correlate the relative amplitudes of response in different modes to the spatial variation of the wind loading, but with limited success. Bietry et al. (1994) present limited results of full-scale tests on the Saint-Nazaire Cable-stayed Bridge, showing reasonable agreement of measured amplitudes with quasi-static theory for the first vertical mode, but an overestimation by a factor of 2.3 for the first lateral mode.

Two suspension bridges have been the subject of extensive full-scale studies. The Deer Isle Bridge has been monitored with six pairs of accelerometers and eight anemometers since 1981 (Kumarasena et al. 1989,1990,1991). In moderate winds (11-15.5m/s), measured buffeting vibrations were up to five times the amplitudes predicted, based on the approach of Scanlan & Gade (1977). The discrepancies were attributed to additional buffeting due to signature turbulence, and Sears' function being inappropriate for the aerodynamic admittance. The Humber Bridge has also been the subject of testing over a significant period, and amplitudes of vibrations have been compared with wind conditions (Brownjohn et al. 1987,1993,1994).

Recently interest has increased in permanent dynamic monitoring of major bridges for operational and structural health monitoring purposes. For example, extensive systems have been installed on the Tsing Ma Suspension Bridge and Kap Shui Mun Cable-stayed Bridge (Lau & Wong 1994), and the Evripos Cable-stayed Bridge (Lekidis et al. 1998). However, few results have yet been published on the long-term or wind-dependent responses of cable-stayed bridges.

2.6.5 Aerodynamic and aeroelastic instabilities

Apart from buffeting, other dynamic wind loads can occur due to the disturbance of the flow by the body itself. These can be aerodynamic effects, due to the flow around a stationary body, or aeroelastic effects, which result from the interaction of the wind and the motion of the body. Generally the two-dimensional case of a deck cross-section is considered for this discussion, but the principles can be extended to three dimensions for practical cases.

Flutter is the principal aeroelastic instability which must be considered in the design of long-span bridges, since it causes divergent vibrations, potentially leading to failure. There are several types of flutter, but the two of most concern for bridge design are classical and Single-Degree-Of-Freedom (SDOF) flutter. Vortex-induced vibrations and galloping are also addressed here. Other aerodynamic and aeroelastic instabilities exist, but they are generally not important for long-span bridges (Simiu & Scanlan 1986).

2.6.5.1 Classical flutter

Classical flutter occurs due to the interaction of the vertical and torsional degrees of freedom. Scanlan & Tomko (1971) applied previous work on the flutter of aerofoils to bridge decks, and adopted semi-empirical equations for the aeroelastic lift force and pitching moment of the following form:

$$F_{Lae} = \tfrac{1}{2}\rho U^2 (2B)\left[KH_1^*(K)\frac{\dot{z}}{U} + KH_2^*(K)\frac{B\dot{\alpha}}{U} + K^2 H_3^*(K)\alpha\right] \qquad (2\text{-}21)$$

$$M_{aae} = \tfrac{1}{2}\rho U^2 (2B^2)\left[KA_1^*(K)\frac{\dot{z}}{U} + KA_2^*(K)\frac{B\dot{\alpha}}{U} + K^2 A_3^*(K)\alpha\right] \qquad (2\text{-}22)$$

where: z = vertical displacement

α = angular displacement (in radians)

$K = \dfrac{2\pi fB}{U}$

$H_1^*, H_2^*, H_3^*, A_1^*, A_2^*, A_3^*$ are 'flutter derivatives' (also known as aerodynamic derivatives or coefficients), which are non-dimensional functions of K and are dependent on the deck cross-section. They can be determined from sectional model tests.

Alternative formulations, including complex forms, are discussed by Falco et al. (1992) and Zasso (1996).

Based on the above formulation, the vertical and torsional degrees of freedom are coupled through the terms in H_2^*, H_3^* and A_1^*, resulting in a rapid onset of flutter above a critical wind speed. In design, this must be well above the maximum wind speed anticipated at the bridge location.

Classical flutter is avoided by altering the cross-section, or by increasing the ratio of the torsional and vertical natural frequencies, usually by increasing the torsional stiffness.

Considering the full length of a bridge deck, the vertical and torsional mode shapes need to be of similar form for the net effect of the interaction along the bridge length to lead to flutter. Usually only the first vertical and torsional modes need to be considered. Equations of the above forms can still be used, but based on generalised parameters from integration over the mode shapes.

There has been no confirmed case of classical flutter occurring on a full-scale long-span bridge.

2.6.5.2 Single-Degree-Of-Freedom (SDOF) flutter

Another form of flutter instability is SDOF flutter, which is more common for long-span bridges (Scanlan 1978a,1987). This occurs in pure torsion, due to the flutter derivative A_2^* (equation (2-22)) becoming positive. At low reduced velocities ($=U/fB$) it is normally negative, leading to aerodynamic damping. However, for most bridge deck sections, at higher reduced velocities it becomes positive (Scanlan & Tomko 1971), causing negative aerodynamic damping, leading to an instability.

The susceptibility of a bridge to SDOF flutter can be reduced by increasing the torsional stiffness, which causes a decrease in the reduced velocity, or by altering the cross-section.

Scanlan & Tomko (1971) showed that H-shaped sections are vulnerable to SDOF flutter, and attributed the failure of the Tacoma Narrows bridge to this cause. Fung (1993), however, explained the same incident as a consequence of 'stall flutter', due to separation of the flow with torsional motion, causing a non-linear change in the loading on the section. Such separation is only likely for large rotations, so to define the conditions for the initial instability to develop, the linearised equations (2-21)&(2-22) are generally considered adequate.

2.6.5.3 Vortex shedding

For most practical structures in typical wind speeds, as the flow passes, vortices are shed alternatively from either side, causing an oscillating force of frequency:

$$f_V = \frac{SU}{B} \tag{2-23}$$

where: S is the Strouhal number, which is a function of the cross-sectional shape. It can also vary with Reynolds number, although it is normally fairly constant over a wide range of values.

If the frequency of vortex shedding corresponds to a natural frequency of the structure, large amplitude vibrations can result. This occurs at a critical wind speed for each mode, often considerably below the critical flutter wind speed.

The emphasis in designing against vortex-induced vibrations is on limiting vibration amplitudes to an acceptable level. This can be achieved by altering the cross-section to reduce the magnitude of the force, or by providing sufficient damping.

The occurrence of vortex shedding is not dependent on the motion of the body. However, once vibrations have commenced, the vortices tend to become more correlated over the length of the structure and to 'lock-in' to the vibration frequency, even for small changes in the wind speed. This results in increased loading, and hence response, but only up to a steady-state amplitude.

Due to the complex nature of the flow separation around the body, no reliable analytical model of the behaviour has been developed. Several empirical models have been proposed (e.g. Hartlen & Currie 1970, Iwan & Blevins 1974), the simplest of which (Simiu & Scanlan 1986) gives a lift force per unit length of deck of:

$$F_{LV} = \tfrac{1}{2}\rho U^2 B\left[KH_0^*(K)\frac{\dot{z}}{U} + C_{LV}\sin 2\pi f_V t\right] \tag{2-24}$$

where: H_0^* is a coefficient of the aeroelastic lift force

C_{LV} is a coefficient of the aerodynamic lift force

The coherent formation of vortices is inhibited by turbulence, as demonstrated in aeroelastic model tests at different turbulence intensities by Zan et al. (1989). An empirical model accounting for the lack of correlation of vortex shedding along the length of a structure in turbulent wind has been proposed by Ehsan et al. (1990).

Vortex-induced vibrations have been observed on a number of cable-stayed bridges. When measured, the critical wind direction has usually been within 15° of normal to the bridge axis. On the Kessock Cable-stayed Bridge, vibrations of 200mm amplitude were measured in the first vertical bending mode, which agreed with wind tunnel tests in smooth flow (Cullen Wallace 1985). Owen et al. (1996) established that the vibrations occurred normally only when the turbulence intensity was below 6%. However in higher turbulence, vibrations occurred in the first torsional mode, believed to be due to a different category of vortex shedding. Shiraishi & Matsumoto (1983) suggest that there are three categories, involving vortices originating at the windward edge, leeward edge or both. For vortices shed at both, torsional excitation is at 1/2 or 3/2 the frequency of vertical excitation for the same wind speed.

On the Wye Bridge, Smith (1980) measured vortex-induced vibrations of amplitude 18mm, compared with 50-100mm in wind tunnel tests in smooth flow. Hay (1984) established the wind criteria on site to include longitudinal turbulence intensity below 10%, and suggested that dense traffic on the bridge reduced the amplitude, due to the additional turbulence created. The variation in wind conditions along the main span (length 235m) was also considered significant. There was a delay of approximately 3 minutes from the wind entering the critical range to the build up of significant vibrations. Measurements on the similar Erskine Bridge (Hay 1981) found no vortex-induced vibrations, although they had been predicted by wind tunnel tests. This was attributed to the higher levels of turbulence at the site (typically >8%).

Vortex-induced vibrations were also observed on the Quincy Bayview and Long's Creek Bridges (Wardlaw 1991) and the Ishikari Kako Bridge (Burden 1990), in each case being inhibited by the addition of fairings and other minor modifications. The Hawkshaw Bridge, almost identical to the Long's Creek Bridge, experienced no large vibrations, believed to be due to adjacent hills increasing the turbulence (Wardlaw 1981).

On the half-constructed Ewijk Bridge, Persoon (1981) measured vortex-induced vibrations of 56mm estimated amplitude, in agreement with wind tunnel tests for smooth flow (van Nunen & Persoon 1982).

Suspension bridges have also suffered vortex-induced vibrations, including the Deer Isle Bridge (Kumarasena et al. 1991), and the Great Belt Bridge, where they were limited by installing guide vanes (Jensen et al. 1999).

Vortex-induced vibrations can affect the pylons of cable-stayed bridges, as observed on the Sitka Harbor Bridge (Gade et al. 1976). In Japan, tuned mass dampers have been fitted to the pylons of six bridges, and wind deflectors to another, mainly to control vortex-induced vibrations during construction (Burden 1990, Miyata 1991).

2.6.5.4 Galloping

Another aeroelastic effect is galloping, arising from the effective angle of attack of the incident wind for across-wind motion of a body. Based on the quasi-static force coefficients, for small amplitude vibrations, there is a lift force equal to:

$$F_{Lgal} = -\tfrac{1}{2}\rho U^2 B\left[\frac{dC_L}{d\alpha} + C_D\right]_{\alpha=0} \frac{\dot{z}}{U} \qquad (2\text{-}25)$$

This is equivalent to additional damping, but an instability can develop if:

$$\left[\frac{dC_L}{d\alpha} + C_D\right]_{\alpha=0} < 0 \qquad (2\text{-}26)$$

Although common for transmission lines, galloping is not known to have occurred for bridge decks, since the cross-sections are wide. However, Wardlaw (1991) reports that the Aratsu and Katsushika Bridge pylons are susceptible to galloping as well as vortex shedding.

2.6.6 Multi-mode and combined buffeting and flutter analysis

The phenomena of flutter and buffeting are normally considered separately, but they can interact. Recent work, described here, has considered their interaction, which necessarily involves coupling of the modal responses through the aeroelastic forces. Coupling of modes through structural non-linearities is generally ignored, but correlated generalised forces can be included in the methods. The aim is to obtain improved estimates of the response of a complete bridge across the full range of wind speeds, based on parameters derived from sectional model tests and mode shapes from FE models. Thus the need for more time-consuming and expensive full aeroelastic models would be reduced.

Scanlan (1978a,b) first considered a unified formulation for the flutter and buffeting analyses. The aeroelastic forces on a cross-section were taken from equations (2-21) &(2-22), along with a similar equation for the drag force involving 'lateral flutter derivatives'. The buffeting equations also included quasi-static loads from wind variations, based on force coefficients.

Lin & Ariaratnam (1980) suggested that turbulence can have a destabilising effect on aeroelastic forces for SDOF torsional flutter. Simiu & Scanlan (1986) and Sarkar et al. (1994) report only minor differences between experimental values of flutter derivatives in smooth and turbulent flow, but Ostenfeld-Rosenthal et al. (1992) report an unfavourable

effect of turbulence on the aerodynamic stability of sectional models. Bucher & Lin (1988) found that turbulence could either stabilise or destabilise the coupling between vertical and torsional modes, depending on the bridge cross-section. They extended their method to allow for a lateral degree of freedom, which could have a stabilising effect in the presence of turbulence (Bucher & Lin 1989). The lack of correlation of wind velocity along the bridge length could also delay the onset of flutter (Scanlan 1987, Scanlan & Jones 1990).

Jain et al. (1996) included 18 flutter derivatives in their combined flutter and buffeting formulation, allowing for the effects of vertical displacement, horizontal displacement and horizontal velocity on the aeroelastic forces. Modal coupling leads to a slight increase in the total buffeting response compared with the amplitude for uncoupled modes. The difference was only significant for higher wind speeds but was considered more important for longer or more streamlined bridges. The method was applied to the Akashi-Kaikyo Suspension Bridge (1991m main span) by Katsuchi et al. (1999), who found that six modes contributed to the flutter response, with the lateral flutter derivatives having a significant effect. Slightly better agreement with wind tunnel tests was achieved compared with an uncoupled modal analysis. The lateral response was significantly over-estimated, which it was suggested was due to errors in the assumed lateral flutter derivatives.

Other multi-mode coupled flutter and buffeting analyses have been proposed by Lin & Yang (1983), Kovacs et al. (1992) and Namini et al. (1992). With the increasing interest in such methods, there is a need for accurate measurements of the necessary coefficients. Techniques have been developed to extract all the principal flutter derivatives from sectional model tests simultaneously (Sarkar et al. 1992,1994, Singh et al. 1996).

Although multi-mode analysis is a subject of much research interest, there remains little evidence of its accuracy in practice. There has been little comparison with measured responses on full aeroelastic models, and apparently no validation at full scale. Jones et al. (1998) and Katsuchi et al. (1998) emphasise the need for full-scale data to validate these sophisticated methods of analysis.

2.7 Traffic effects

Traffic effects on long-span bridges include loading, additional mass and changes to the aerodynamic behaviour. Also, wind effects on vehicles on exposed bridges have led to the consideration of the addition of wind barriers.

2.7.1 Traffic loading

Traffic provides the principal static live load on road bridges, but, apart from minor non-linear effects (§2.4.1&2.4.3), this is of little interest to the dynamic behaviour. Dynamic traffic loading can be significant, but for long-span bridges it is less critical than wind loading, so relatively little work has been performed on it. Often the effect of traffic loads on bridges is not considered in terms of vibrations, but rather is expressed in terms of impact factors, relating the maximum dynamic response to the response from the same load if static.

Green (1977) discusses vehicle-structure interaction, including road surface roughness, and reports measurements of vibration amplitudes for several highway bridges. Impact factors showed relatively large responses of bridges with natural frequencies of 2-5Hz, suggesting that vehicles cause larger excitation in this range. Also, the decrease in wind loading with increasing frequency (§2.6.4.1) means that traffic loading is relatively more important at higher frequencies. When vehicle loading has been used for dynamic testing of bridges (§2.3), the input force has generally been considered to have a white noise spectrum.

Traffic loading on a cable-stayed bridge was considered by Wang & Huang (1992), who created simple FE models of a truck and a bridge, and modelled the interaction between them as the truck passed over. Impact factors were estimated at around 30%. A similar study by Fertis (1987) found the vehicle speed and type to affect the frequency content of excitation, so the spectrum of typical traffic loading is not clearly defined.

2.7.2 Other traffic effects on bridges

Other traffic effects on the dynamic response of bridges include:

i) *Added mass, causing a drop in natural frequencies*

Changes of up to 18% were measured on a three span 69.1m long timber bridge by Horyna et al. (1996), but for the 1410m main span Humber Bridge, with a significantly heavier steel box girder deck, Brownjohn (1994) estimated a maximum change of 2% for heavy traffic.

ii) *Change in aerodynamic profile*

The presence of vehicles affects the wind flow around the deck, influencing the wind loading.

iii) *Quasi-static rotation due to asymmetric traffic loads*

This can also affect the wind loading, but the angles of rotation are likely to be small compared with variations in the vertical angle of attack of the wind.

iv) Turbulence from the passage of vehicles

This can inhibit vortex-induced vibrations (§2.6.5.3), for example.

2.7.3 Wind barriers

The wind on exposed bridges also has significant effects on vehicles, causing handling difficulties and potential overturning of high-sided vehicles (Baker 1991).

The increasing desire for reliable road links in all weather conditions has led to the consideration of wind barriers on major bridges. Strategies for restrictions on major bridges and the benefits of barriers are discussed by Smith & Barker (1998). Hay (1992) presents results of wind tunnel tests on overturning moments of vehicles. 3m high barriers of 50% porosity have been found to cause a 50% reduction in moments, but they have adverse effects on the drag forces and aerodynamic stability of bridge decks (Wyatt 1992).

The Second Severn Crossing (SSC) was the first long-span bridge to be fitted with wind barriers along the full length (Head et al. 1997, §3.2.5).

2.8 Cable vibrations

Whereas many of the dynamic issues discussed so far apply equally to suspension and cable-stayed bridges, the following issues of cable vibrations are particular to cable-stayed bridges. This section deals with local cable vibrations, assuming fixed ends, and the following section (§2.9) considers dynamic interaction of the cables with the rest of the structure.

Cables have very low damping, so they are susceptible to large amplitude vibrations. A useful non-dimensional parameter related to the damping is the Scruton number, based on the work of Scruton & Walshe (1957), defined as (Irwin 1997)†:

$$S_c = \frac{m\zeta}{\rho D^2} \tag{2-27}$$

where: D = cable diameter

Large cable vibrations have been observed on many cable-stayed bridges, and several excitation mechanisms have been identified.

† Note that other authors include a factor of 2π or 4π in the definition of the Scruton number. The definition presented here is used throughout this thesis.

2.8.1 Rain-wind excitation of cables

Vibrations of bridge cables under combined rain and wind were first observed on the Meiko Nishi Bridge during construction in 1984 (Hikami & Shiraishi 1988). The maximum amplitude was measured as 550mm, in wind of 14m/s at approximately 45° from normal to the bridge axis. The damping was estimated as 0.11-0.45%, and modes with natural frequencies of 1-3Hz were excited for all cables. Secondary cables were added to tie the main cables together, preventing further large amplitude vibrations. Wind tunnel tests on cable sections with artificial rain showed the presence of rivulets on the cables, particularly on the upper side, to be necessary for the instability to occur.

Similar vibrations have since been observed on several other cable-stayed bridges. Miyata (1991) found, from several Japanese bridges, that the critical wind conditions have a direction 20-60° from normal to the bridge axis, reduced velocity ($=U/fD$) approximately equal to 20, and low turbulence. Further wind tunnel studies have improved understanding of the phenomenon. Matsumoto et al. (1989) considered the behaviour to be similar to galloping, affected by the rivulets and an axial flow on the leeward side of the cable, due to the cable inclination. Further tests were conducted for a variety of configurations, in which the axial flow and upper rivulet were each found to cause vibrations independently, but protuberances on the cables could stabilise them (Matsumoto et al. 1990,1992). Various surface modifications have since been employed on the cable sheaths of several cable-stayed bridges, with some success (Virlogeux 1998, Yamaguchi & Fujino 1998).

Yamaguchi (1990) conducted wind tunnel tests with rigid bars fixed to the cable surface to model the rivulets. He concluded that the movement of the rivulet around the cable was significant in causing two-degree-of-freedom galloping. Further wind tunnel tests with artificial rain by Verwiebe (1998) identified three different configurations of rivulets causing instabilities, covering a wide range of wind speeds (5-30m/s).

The mechanisms of rain-wind excitation are still not well understood, but experience has shown that the vibrations can be inhibited by adding secondary cables or by providing additional damping. Miyata (1991) and Narita & Yokoyama (1991) suggest that damping of at least 0.3% is required to prevent the vibrations. Irwin (1997) proposes the criterion $S_c>10$, based on wind tunnel experiments by Saito et al. (1994), but he emphasises the need for further measurements of cable damping at full scale.

2.8.2 Other aerodynamic excitation mechanisms of cables

Several other mechanisms of cable excitation have been identified, including:

i) Vortex shedding (§2.6.5.3)

Vortex-induced excitation of typical bridge cables commences at very low wind speeds (typically 0.5m/s), but normally causes only small amplitude vibrations. Significant vortex-induced vibrations have been reported on eight short cable-stayed bridges in Japan, and wind tunnel tests showed that they are inhibited when S_c>1.6 (Miyata 1991), although earlier tests by Scruton & Walshe (1957) suggest the criterion S_c>5.

ii) Galloping (§2.6.5.4)

Although circular cylinders are not prone to galloping in winds normal to the axis, for inclined cables in a horizontal wind, the effective cross-section is elliptical, which could be unstable. Skarecky (1975) suggests that the longitudinal component of the wind has very little effect, so galloping of circular cables is unlikely, but Matsumoto et al. (1992) showed that the axial flow can be significant in some cases. Narita & Yokoyama (1991) suggested that galloping is suppressed by a minimum cable damping ratio of 0.8%. As an alternative, Irwin (1997) proposed the criterion for galloping to occur, based on wind tunnel experiments by Saito et al. (1994), as:

$$\frac{U}{fD} > c\sqrt{S_c} \qquad (2\text{-}28)$$

where: c is a constant, approximately 35-40.

However, Stubler et al. (1999) cite two examples where the wind speed exceeded the critical value according to this formula, but no vibrations were observed.

Cable vibrations on only one bridge have been attributed to galloping (Miyata 1991), although there are other cases where the excitation mechanism has been unclear, so galloping could have been the cause.

iii) *Wake galloping*

This has occurred on four Japanese cable-stayed bridges, with closely-spaced pairs of cables (Narita & Yokoyama 1991). The wake from one cable causes excitation of the other, for wind reduced velocity (=U/fD) above 25, and direction 0-45° from normal to the bridge axis. Vibrations are inhibited by the installation of spacers between the cables or damping greater than 0.8% (Miyata 1991).

2.8.3 Full-scale observations of cable vibrations, prevention measures and damping

Cable vibrations have been observed on many cable-stayed bridges. Some of the most significant examples are now presented, along with actions taken to prevent the vibrations, and measurements of damping.

In Japan, rain-wind vibrations occurred on the Meiko Nishi, Hitsuishi-jima and Iwaguro-jima, Yobuko and Rokko Bridges, all of which had secondary cables added, which prevented further vibrations (Burden 1990, Narita & Yokoyama 1991). Similar vibrations occurred on the Aratsu Bridge, on which oil dampers were fitted at the cable anchorages, increasing the typical damping from 0.13% to 1.4% (Yoshimura et al. 1989). On the Tenpozan Bridge, the cable damping decreased by approximately 50% upon grouting, to values of 0.08-0.13%, with a tendency for higher damping of shorter cables (Narita & Yokoyama 1991). From several bridges, Yamaguchi & Fujino (1998) report typical cable damping of approximately 0.16% for the first cable mode, decreasing for higher frequency modes.

Lilien & Pinto da Costa (1994) report rain-wind cable vibrations on the Ben-Ahin Bridge during construction, which were no longer observed after injecting the cable sheaths with epoxy resin, implying an increase in damping.

On both the Faroe Bridge (Langsoe & Larsen 1987) and the Helgeland Bridge (Svensson & Jordet 1996), vibrations were observed in the presence of rain, but also without rain in different wind conditions (§2.9.3). On the Faroe Bridge, the typical cable damping was estimated as 0.5%.

Stiemer et al. (1988) measured damping values of 0.27-0.42% for 14 cables on the Annacis Bridge, generally with lower damping for the longer cables. The damping was increased by approximately 10% when neoprene rings were added at the cable anchorages.

Virlogeux (1998) quotes values of damping measured on several bridges, from 0.01% to 0.2%, excluding values for the SSC from initial studies (Macdonald 1995a,b). Stubler et al. (1999) list estimated values for different cable types, from 0.08-0.13% for grouted parallel strand cables to 0.15-0.3% for locked coil cables.

For such low damping, the aerodynamic damping could be significant, even in light winds. However, apparently it was not considered in any of the above studies, so significant errors may exist in the quoted structural damping estimates. For the Cochrane Bridge, which had suffered rain-wind cable vibrations, Irwin et al. (1999) estimated theoretical aerodynamic damping, but based only on the component of wind velocity normal to the cable in its vertical plane. The estimates were subtracted from the measured damping, yielding structural damping values of 0.1-1.5%, with a trend for

lower values on longer cables. It appears that the aerodynamic damping caused by a general wind velocity has not been considered previously.

2.9 Cable-deck interaction

A particular feature of cable-stayed bridges is the possibility of dynamic cable-deck interaction†. The natural frequencies of bridge cables ('cable vibrations') are in the same range as natural frequencies of the structure as a whole ('global vibrations'), so vibrations of the two types can interact.

2.9.1 Cable excitation by deck or pylon movement

A simplified form of cable-deck interaction considers the response of a cable to movement of one or both ends due to the global behaviour, but without the deck and pylon vibrations being affected. Several authors have addressed the response of a sagging cable to a sinusoidal displacement at one end, theoretically or with numerical simulations (Uhrig 1993, Lilen & Pinto da Costa 1994), and with physical model tests (Perkins 1992, Pinto da Costa et al. 1996). Essentially there are two types of response:

i) Vibration of the cable at the excitation frequency, particularly for support motion perpendicular to the cable. For small amplitude vibrations the relationship between end excitation and cable response is approximately linear, although cable non-linearities become important for large vibrations. This is referred to as 'linear' interaction in this thesis.

ii) Vibration of the cable at half the excitation frequency, particularly for support motion along the cable axis, related to changes in cable tension. This is termed 'parametric' (or 'autoparametric') excitation. Increased damping inhibits the onset of this behaviour, requiring a larger support displacement amplitude for it to occur, but if initiated, the amplitude of vibrations is affected little by the damping.

Thus, for a given cable mode, there are two principal frequencies of support excitation which can cause an instability - one at the cable's natural frequency and another at double this frequency. Other instabilities theoretically exist for excitation frequencies of $2f_n/k$, for k = any integer (Uhrig 1993, Lilen & Pinto da Costa 1994), but for $k>2$ they are generally not considered to be of practical significance.

The response is mainly in the vertical plane of the cables, but out-of-plane vibrations and coupling of modes can occur (Perkins 1992).

---

† The term 'cable-deck interaction' is taken to include cable-pylon interaction.

2.9.2 Full interaction

Cable vibrations can also affect the global structure, leading to full interaction. Vibrations of either the deck or cables can excite the other, while non-linear effects, such as parametric excitation of the cable, can lead to energy transfer between modes. For longer bridges the cable mass is more significant, so the effects of the cable vibrations are more important.

It has been suggested that the interaction leads to additional damping of global modes, termed 'system damping', whereby the cable vibrations remove energy from the deck vibrations (Gimsing 1997, Virlogeux 1998). However there is little evidence of this in practice. The effect of cable-deck interaction was assessed using a physical model of a cable-stayed bridge with added masses on the cables, which were found to have little effect on the damping (Garevski 1990, Garevski & Severn 1993). However, Yamaguchi & Fujino (1998) suggest that cable damping can contribute significantly to the global damping.

For FE modelling of cable-deck interaction, Causevic & Sreckovic (1987) used equivalent lumped masses to represent the first mode of cable vibrations in a full bridge model. Interaction in the general case was addressed by Abdel-Ghaffar & Khalifa (1991), who modelled each cable as a series of truss elements - the Multiple Element Cable System (MECS) - in contrast with the normal One Element Cable System (OECS). Many additional modes were predicted by the MECS model, most of which were predominantly local cable modes, but some of which were coupled cable-global modes. For each mode of the equivalent OECS model, the MECS model predicted several closely-spaced modes with similar shapes for the deck and pylon, but with different cables participating.

Taladhar et al. (1995) considered the MECS further, and found that 2-4 elements per cable, depending on cable length, were sufficient to model the interaction. The results of an MECS FE analysis of a dynamic, rather than aeroelastic, scale model of the Jindo Bridge showed reasonable agreement with the measured modes (Caetano et al. 1996). A limitation of estimating mode shapes by the MECS method is that only linear dynamic behaviour is considered, so the parametric effect is not modelled.

Cable-deck interaction was studied experimentally on a simple cantilever beam with a single cable by Fujino et al. (1993). Both linear and parametric interactions were observed, in close agreement with a mathematical model, but the critical frequency bands for the excitation were narrow.

2.9.3 Evidence of cable-deck interaction at full scale

Analysis of the Helgeland Bridge with an MECS FE model, with wind loading applied to the deck alone, predicted significant cable motion (Kovacs et al. 1992, Svensson & Jordet 1996). However, site observations indicated that the greatest cable vibrations were due to rain-wind excitation, so the significance of cable-deck interaction was unclear. Some cable vibrations on the Faroe Bridge (Langsoe & Larsen 1987) and the Annacis Bridge (Stiemer et al. 1988) were attributed to cable-deck interaction, but with little evidence.

There has been some clearer evidence of cable-deck interaction. When vortex-induced vibrations of the Kessock Bridge deck occurred (§2.6.5.3), the longest cables were also observed to vibrate (Cullen Wallace 1985). Irwin et al. (1999) report deck vibrations felt during rain-wind cable vibrations on the Cochrane Bridge. Deger et al. (1996) detected the cable natural frequencies on the deck of a cable-stayed footbridge, while de Smet et al. (1996) found that cable vibrations had an influence on the global response of a curved asymmetric cable-stayed bridge. On the Polcevera Creek Viaduct, with single prestressed concrete stays, Gentile et al. (1997) identified some modes incorporating cable and deck vibrations, matching their MECS FE model. Finally, Yamaguchi & Fujino (1998) report cable vibrations during relatively large amplitude forced vibrations of bridge decks, including some evidence of parametric excitation.

There remains a need for more specific measurements of cable-deck interaction at full scale, to complement the analytical work and physical modelling which has been undertaken on this subject, and to determine its significance in practice.

2.10 Construction stages

Long-span bridges are potentially most vulnerable to large vibrations during construction. For suspension bridges, classical flutter during construction has been considered (Brancaleoni 1992), since the vertical and torsional frequencies are generally closer than for the final bridge. However, the issue is seen as less critical for cable-stayed bridges.

Buffeting of cable-stayed cantilevers has been considered more. For example, lateral buffeting was recognised as a potential problem in the erection of the Normandy Bridge (Virlogeux 1992). Buffeting analysis and wind tunnel tests of the Baytown Bridge estimated the maximum response during construction to be up to 50% higher than for the finished bridge (Scanlan & Jones 1990). Irwin (1987) proposed a buffeting analysis method for a cable-stayed balanced cantilever, achieving good agreement with an aeroelastic model of the Annacis Bridge, while a simplified buffeting analysis for different construction stages is presented by Zan & Wardlaw (1987). Khalil & Bush (1987)

considered buffeting and also flutter for the Skytrain Bridge, which needed temporary cables to stabilise the top of the pylon during construction.

Wind normal to the bridge axis is usually considered the worst case, but during construction skew winds can be more serious (Tanaka et al. 1998). Xie et al. (1991) proposed a buffeting analysis method for skew winds, but ignoring the free end of the cantilever, achieving good agreement with wind tunnel tests. Scanlan (1993) provides an alternative method, based on variable force coefficients, depending on the wind direction.

For design, full aeroelastic models of the critical construction stages are often tested to estimate the buffeting response, but these do not allow for errors in the relative torsional and vertical natural frequencies, which could be important for flutter.

For free-standing pylons, vortex shedding and galloping can be problematic, for which tuned mass dampers and wind deflectors have been installed for the construction of several bridges (§2.6.5.3&2.6.5.4).

2.10.1 Full-scale tests during construction

Very few full-scale dynamic tests have been performed on cable-stayed bridges during construction. In forced vibration tests, Yoshimura et al. (1989) measured the damping of a free-standing pylon of the Aratsu Bridge as 0.14%, increasing to 1.9% after the installation of a tuned mass damper. Narita & Yokoyama (1991) report values of 0.21%-0.51% for four other free-standing pylons in similar tests, but they stress the need for long-term monitoring of the wind and response.

Vortex-induced vibrations were measured on a completed cantilever of the Ewijk Bridge (§2.6.5.3). Also five modes were identified, confirming the natural frequencies from an FE model, and exhibiting damping ratios of 0.25-0.8% (Persoon 1981, van Nunen & Persoon 1982). Ostenfeld & Langsoe (1987) report the monitoring of a completed cantilever of the Faroe Bridge, for which the amplitudes of vertical vibrations agreed well with the results of a buffeting analysis, for wind speeds up to 15m/s.

Despite the increasing popularity of cable-stayed bridges and the common use of the balanced cantilever construction method, no more comprehensive dynamic measurements during construction have been reported.

2.11 Conclusions

The principal issues and methods of analysis of cable-stayed bridge dynamics have been reviewed, with a particular emphasis on wind loading. Observations and key results from previous full-scale tests have been

demonstrated. Tests over long periods and during construction would be of particular value. The main needs for full-scale testing are:

i) Identifying the significance of non-linear behaviour;

ii) Validating methods of FE modelling and model updating;

iii) Obtaining measurements of global and cable damping, particularly identifying the contribution of aerodynamic damping (for comparison with theory), and the residual contribution from structural damping;

iv) Identifying any aerodynamic or aeroelastic instabilities and the conditions causing them, particularly in comparison with wind tunnel test results;

v) Determining the amplitude of vibrations in relation to wind conditions, for comparison with buffeting analyses, particularly considering the expression for aerodynamic admittance and the validity of multi-mode analysis methods;

vi) Assessing the significance of the effects of traffic and of wind barriers;

vii) Identifying cable vibration mechanisms, and evidence of cable-deck interaction - both 'linear' and 'parametric';

viii) Measuring the response during construction, for comparison with theory, and to assess the amplitude of response relative to the finished bridge.

Testing during construction allows a number of variations of the structure to be monitored, allowing changes in the response to be measured, and giving greater opportunity for different effects to be observed. Long-term monitoring enables the response in different conditions to be measured, can reveal variations in parameters, and allows the accuracy of results to be improved by averaging.

The monitoring programme described in Chapter 4 aims to provide data for the above purposes. The results presented in Chapters 8-10 address each of these issues.

CHAPTER 3 BACKGROUND TO MONITORING OF THE SECOND SEVERN CROSSING

3.1 Introduction

The previous chapter demonstrated the need for full-scale test results from cable-stayed bridges, to improve the understanding of their dynamic behaviour. To address this need, the work described in this thesis focussed on the dynamic monitoring of the Second Severn Crossing (SSC) cable-stayed bridge, and subsequent analysis of the data. Chapter 4 deals with the site monitoring, Chapters 5-7 with the methods of data analysis and some initial results, and Chapters 8-10 with the detailed dynamic behaviour of the bridge. Firstly, this chapter provides some background information on the bridge, including a description of the structure and its construction, details of the Finite Element (FE) models developed in relation to this study, and an outline of the wind tunnel tests undertaken at the design stage.

The SSC is typical of cable-stayed bridges of 400-500m span, so it can be expected that other such bridges would exhibit similar dynamic behaviour. It was chosen for this study because of its proximity to Bristol, allowing frequent site visits, and since it was under construction at the beginning of the study, providing a unique opportunity to monitor it at different construction stages.

The dynamic response of the prototype bridge is of interest for the present study, but much of the value of the results will be in their use for the validation of methods of analysis and modelling. These methods have received much attention by others (Chapter 2) and are largely beyond the scope of this thesis. However, the FE models and wind tunnel tests described in this chapter provide a basis for comparison with the measured dynamic response.

The FE models presented here are for the partially constructed SSC. The One Element Cable System (OECS) models (§3.3) were created at the University of Bristol by Dobinson, under the supervision of the author (Dobinson & Macnamara 1996). The subsequent development to form the Multiple Element Cable System (MECS) model (§3.4) was performed by Caetano of the University of Porto, Portugal, as part of a joint research project (Caetano et al. 1998). Some results of an FE model by the bridge designers, Halcrow-SEEE, were also made available for the buffeting analysis of the finished bridge (§8.6.1). The wind tunnel tests (§3.5) were performed during the design period by RWDI in Toronto, Canada (Xie et al. 1994).

3.2 Description of the Second Severn Crossing

3.2.1 Background

The SSC crosses the Severn Estuary between England and South Wales near Bristol, 5km downstream of the original Severn Bridge (Fig. 3-1). The need for additional traffic capacity, the benefit of an alternative route in case of disruptions, and the problems of restrictions to high-sided vehicles in strong winds on the Severn Bridge led to the decision to construct a second crossing. Following a study by WS Atkins and Maunsell (SSCG 1986), a 5km long crossing with a central cable-stayed bridge was recommended, with shielding to protect vehicles from the wind.

The bridge was constructed over a four year period from 1992-1996 by Laing-GTM, a joint venture of John Laing of the UK and GTM of France. The design was carried out by Halcrow-SEEE, another British-French joint venture.

The design was strongly influenced by construction methods, particularly considering the vast tidal range of the Severn Estuary (up to 14.5m). Bridge sections were prefabricated on land as far as possible, to minimise the work required in the tidal area (Kitchener & Mizon 1997). The adopted design comprised two concrete viaducts, each over 2km long, and a symmetrical cable-stayed bridge of 948m with a main span of 456m over The Shoots, the main channel in the centre of the estuary (Fig. 3-2). It is this cable-stayed bridge which is the subject of this study (Fig. 3-3). A brief description follows, but further details are provided by Mizon et al. (1997).

3.2.2 Definitions

For clarity of later descriptions the following terms are defined (Fig. 3-3):

Pylon: The complete H-shaped structure at either end of the main span;

M1: The pylon to the west (Welsh side) of the main span and the section of deck supported by it;

M2: The pylon to the east (English side) of the main span and the section of deck supported by it;

Tower: The vertical part of one of these pylons on one side of the deck only;

Backspan: The section of the cable-stayed deck to the east of Pylon M2 (or west of M1), extending over the two intermediate piers;

Completed cantilever (construction stage): The completed M2 half of the cable-stayed section, before connection to the viaduct or M1, and without the wind barriers, deck surfacing and other finishes;

Longitudinal: In relation to the structure (including the pylons): the direction along the axis of the bridge deck;

In relation to the wind: the direction of the mean wind velocity;

South normal: The direction normal to the axis of the bridge on the south side (bearing 203° from true north, Fig. 3-1). Wind directions in this thesis are measured clockwise from this direction. The centreline of the estuary downstream is approximately 30° from south normal.

3.2.3 Structural details

The bridge deck is of composite construction, comprising two longitudinal steel girders of varying section along the length, transverse steel trusses at 3.65m spacing and a reinforced concrete slab of between 225mm and 400mm depth (Fig. 3-3(b)). It was prefabricated in units of 7.3m length. It is 35m wide and carries three lanes of traffic and a hard shoulder in each direction.

The cables are connected on either side of the deck in the centre of each deck unit, between alternate transverse trusses, except for a few special units at the ends and adjacent to the pylons. There are 30 cables on either side of each of the four towers, arranged in a semi-fan configuration (Fig. 3-3(a)). They comprise between 19 and 75 parallel steel strands, enclosed in high density polyethylene (HDPE) sheaths. Each strand is in turn wound from seven wires. The strands are individually anchored below the deck, transferring the load onto intermittent steel edge beams between adjacent solid steel cantilevers from the transverse trusses.

The two pylons are 137m high from the top of the caissons, with the deck being approximately 40m above this level (Fig. 3-3(c)). They comprise hollow reinforced and post-tensioned concrete sections with a wall thickness of between 0.5m and 1.5m, with internal reinforced concrete tension beams to transfer the forces between opposite cables. Reinforced and post-tensioned concrete cross-beams link the two towers of each pylon just below deck level and at approximately three-quarters' height.

In each backspan there are two 'intermediate' concrete piers, which provide additional restraint to the superstructure (Fig. 3-3(a)). For some loading combinations they carry uplift, so the deck is tied down to them with cables.

The restraints of the deck are symmetrical. The deck bearings do not fix the cable-stayed section longitudinally, but the cables provide a restoring force for any longitudinal

displacement of the deck from the central position. Spring dampers at the pylons also contribute to the restoring force and heavily damp any longitudinal relative movement at these points. The effect is that long-term movements from temperature changes are permitted, whereas short-term movements from vehicular breaking loads are restrained. Therefore, for the dynamic case, longitudinal movements of the deck relative to the pylons are effectively restrained. During construction, the spring dampers were locked in position since there were temporary out-of-balance longitudinal forces from the cables, which otherwise would have caused large displacements.

At the piers and at the joints with the concrete viaducts at the ends of the cable-stayed deck, the bearings allow longitudinal movement, although friction has to be overcome (§6.2.6). Vertical and lateral movements are restrained at the ends and at each pier and pylon.

3.2.4 Construction

The cable-stayed section was constructed as a balanced cantilever from each pylon (Fig. 3-4). Prefabricated sections were lifted onto each end of the deck alternately, the steel girders were bolted, the cables fixed to each side of the deck and tensioned, and a short section of concrete cast in situ to form a continuous slab. The construction programme was governed by the time required to construct the 2km long concrete viaducts from each bank, so there was sufficient time available to construct the two cable-stayed cantilevers sequentially using the same equipment. This is relatively unusual, since for most cable-stayed bridges the main span is on the critical path of the programme, so the two cantilevers are constructed simultaneously. The result was that the M2 cantilever was completed and then little work was undertaken on it for five months while the M1 cantilever was constructed. This gave an ideal opportunity to monitor the cantilever in this potentially vulnerable state in various wind conditions, with little change to the structure.

3.2.5 Wind barriers

One unique feature of the SSC is the use of continuous wind barriers to protect vehicles. These were adopted so that the crossing could remain open to all traffic in all weather conditions, in contrast with the Severn Bridge which is often closed to high-sided vehicles. 3m high barriers with 50% porosity have been found to reduce the overturning moments on 4m high vehicles by over 50% (Wyatt 1992), which was considered sufficient protection. A series of full-scale tests of the effects on vehicles of different barrier arrangements was conducted for the SSC (Head et al. 1997), and extensive wind tunnel sectional model tests were carried out to ensure the aerodynamic stability of the

bridge deck with the barriers (SSCG 1986, §3.5). From the pre-tender investigations it was considered that a streamlined underside to the bridge was necessary, either in the form of a streamlined boxed girder deck or a wind enclosure of the same external shape. The Contractor opted for a composite deck, with two longitudinal steel plate girders, and commissioned further wind tunnel tests which eventually obtained a cross-section which met the specification without the use of the enclosure, thus making a considerable saving in construction costs (Irwin et al. 1994).

3.3 One Element Cable System (OECS) Finite Element (FE) models

At an early stage of this study, three FE models (§2.4.3) of the SSC cantilever were created. Although the focus of this study was the analysis of the site data (Chapters 4-10), it was of value to create models for comparison with the some of the measured results to validate both the method of modelling and the site data processing techniques, and as a basis for further studies.

The completed M2 cantilever was the construction stage most monitored (§4.2). Also, it was not connected to the approach viaducts, avoiding the issue of accurately modelling the associated boundary conditions. For these reasons it was chosen as the basic structure for FE modelling in this study. Two-dimensional (2-D) and three-dimensional (3-D) One Element Cable System (OECS) models were created (Dobinson & Macnamara 1996), in which each cable (or pair, for the 2-D model) was represented by a single truss element. These models can only predict 'global' modes, involving the deck and pylon, and ignore any local cable vibration effects (§2.9).

These models could be developed to form variations, such as the Multiple Element Cable System (MECS) model in §3.4. Other possibilities include models of the finished bridge or other construction stages. Alternative methods of FE modelling of the structure, particularly the deck, could be investigated to improve and validate the methods, or the models could be updated to match the measured response (§2.4.4). The site measurements from the different construction stages (§4.5) could be used for comparison with variations of the models, for example to validate an updating method, by extension of an updated model to a later construction stage.

3.3.1 General description of the models

The structure was modelled using the general FE software package Solvia (Solvia 1989), based on construction drawings and material properties supplied by the Contractor (Table 3-1). In order to model the torsional and lateral modes of vibration, a 3-D model was required, but a 2-D vertical plane model was also created for comparison with the 3-D model and to allow the development of a 2-D MECS model (§3.4). The

details below refer to the 3-D model except where stated. For the 2-D model, the pylon, piers and cables were modelled in the same ways, except that the element parameters had double the values, to account for the structural members on both sides of the deck.

The results of interest for this study were the mode shapes and natural frequencies, which, for dynamic wind loading of long-span bridges, are the principal outputs sought from FE models (§2.4.3). These were to be compared with the results from site measurements for low amplitude vibrations (§8.3.2), so linear dynamic behaviour could be assumed. For the static loading, a geometric non-linear analysis was performed, to define the equilibrium state for the starting point of the dynamic analysis (§2.4.1&2.4.3). This was particularly important for the following MECS model (§3.4).

Table 3-1 Material properties for FE models

Material	Dynamic modulus (kN/mm^2)	Poisson's ratio	Density (kg/m^3)
Deck steel	200	0.29	7800
Deck and pylon concrete (compressive strength $60N/mm^2$)	44	0.20	2450
Cable steel	195	-	*

* Specified as mass per unit length - varies from 33.5kg/m to 123.2 kg/m for different cables

3.3.2 Details of pylon and piers

Each tower was modelled using 62 beam elements, with section properties varying with height due to the taper. The cross-beams beneath the deck and near the top of the pylon were modelled as a series of beam elements, with section properties varying for the top beam, which was also tapered. For the 2-D model, the cross-beams were treated as lumped masses at the appropriate levels of the pylon.

The intermediate piers were each modelled as four beam elements. The density for the model elements was adjusted to take account of the non-structural mass concrete infill to the lower 7.7m of each pier.

The bases of the pylon and piers, at top of caisson level, were assumed to be fully fixed supports (§6.2.5). For the cantilever construction stage, the two ends of the deck were free, so the bases provided the only external restraints.

The deck bearings were modelled as fixed for all translations, following preliminary tests which indicated this is how they performed for low amplitude vibrations (§6.2.6).

3.3.3 Details of cables

Each cable was represented as a single truss element, which could therefore only carry axial loads. The total mass per unit length, including the HDPE sheath and wax filling, was specified, whereas the stiffness was based on only the area of the steel strands. The Young's Modulus for each cable was modified to take account of the difference in lengths between the actual and idealised cables, due to the thicknesses of the deck and the pylon, and to allow for the effect of cable sag (§2.4.1). For the 2-D model, it was also modified to allow for the slight inclination of the cables out of the vertical plane of the model.

The cable prestress was modelled by defining the initial strain of each cable element. With the high degree of redundancy, the actual force in each cable could not be determined. However the initial strain could be estimated as:

$$\varepsilon_{init} = \frac{T - T_{dead}}{AE} \tag{3-1}$$

where: T = cable tension for the construction stage and loading state of interest

T_{dead} = component of cable tension due to the dead load

A = cross-sectional area of cable steel

E = Young's Modulus of cable steel (modified as described above)

The actual cable tensions for the completed cantilever were unknown, but they were estimated by the Contractor to be approximately 85% of the final design tensions. For each cable, T_{dead} was estimated as the axial cable force with a vertical component equal to half the weight of a single deck section (7.3m length). Thus, when the static load was applied, the resulting total cable tensions in the model approximated to the Contractor's estimated tensions.

3.3.4 Details of deck

The various modelling techniques outlined in §2.4.3 were considered for the deck. It was decided to use a model which closely resembled the actual bridge geometry, rather than equivalent spine or plate elements, thus avoiding complex calculations of equivalent section properties.

The main girders were modelled as beam elements, with the section properties varying according to the girder size. The transverse trusses were represented by equivalent single beam elements at their neutral axes, to model their overall axial and bending stiffnesses.

The tapered cantilever girders at the ends of each truss were taken as inclined beam elements. The concrete slab was modelled as four shell elements across the deck width for each length between transverse trusses. These elements allowed in-plane stresses, which are important for longitudinal compression and overall bending of the deck. The girders and the centre of the truss were connected to the slab with rigid links to preserve the correct spacing between them for composite action to develop.

The cable anchorages, at the edge of the deck in alternate bays between transverse trusses, were modelled by beam elements at the level of the shell elements. They spanned parallel to the bridge axis between the tapered cantilever girders, with the cables connected at the centres of each span.

Using this modelling approach, a total of 2209 elements was used to model the cantilever structure, 1941 being for the deck. The cross-sections of the actual bridge deck and of the model are shown in Fig. 3-5.

For the 2-D model, the deck was represented by a single line of beam elements, with the equivalent overall axial and vertical bending stiffnesses of the composite section, varying along the deck according to the size of the main steel girders. The masses of the beam elements included the contribution from the transverse trusses and cantilevers, although these did not contribute to the stiffnesses. The total number of elements in the 2-D model was 253.

The 2-D and 3-D FE models of SSC cantilever are shown in Fig. 3-6, along with the co-ordinate axes adopted.

3.3.5 Results of the OECS FE models

30 modes were computed for the 2-D model, up to approximately 10Hz, and 39 for the 3-D model, up to about 4Hz. The shapes of the first four vertical plane modes from the 2-D model are shown in Fig. 3-7. The natural frequencies and mode shapes of more modes (from both models) are presented in §8.3.2, where they are compared with the results from site measurements (§4.5.3).

The first 17 vertical plane modes were identified by both OECS FE models, with excellent agreement of the mode shapes. The natural frequencies agreed within 5%, except for three modes, which were the only ones with dominant longitudinal motion of the pylon or deck. Thus, for the modes dominated by vertical bending of the deck, the agreement was very good, indicating that the composite bending behaviour of the concrete slab and steel girders was accurately modelled in the 3-D model.

One explanation for the larger discrepancies for the pylon-dominated modes, and indeed the small differences in natural frequencies for all modes, is that the 3-D model

indicated a component of motion of the pylon in the lateral (y) direction, which was not permitted for the 2-D model. The north and south towers of the pylon would symmetrically bend inwards and outwards, or 'breath', due to the slight inclination of the cables out of the vertical x-z plane.

The first mode, from the 3-D model, was a lateral sway mode of the cantilever with a small torsional component, at a natural frequency of 0.351Hz. The second mode was the first vertical bending mode of the deck with a component of longitudinal pylon motion, at 0.384Hz. The 39th (highest calculated) 3-D mode had a natural frequency of 4.248 Hz. Results of preliminary tests indicated that higher frequency modes could not be clearly identified from the site measurements (§6.2.3), so the frequency range of interest for the main tests was up to 5Hz (§4.3.2), covering all of the modes from the 3-D FE model.

The majority of modes from the 3-D model, other than the vertical plane modes, involved components of torsional and lateral motion of the deck and pylon. These always appeared together, due to the offset between the mass and torsion centres of the deck (Irwin 1979a). There were two modes (13th, 1.427Hz and 38th, 3.995Hz) dominated by 'breathing' of the pylon, and one (39th, 4.248Hz) with the major component being longitudinal extension and contraction of the deck. From the 2-D model, the first mode involving significant vertical extension and contraction of the pylon was at 7.333Hz. Therefore, it was expected that all modes up to 4Hz could be detected by measuring accelerations vertically on either side of the deck, longitudinally in each tower of the pylon and laterally on one side of the deck and in one tower (§4.5.3).

3.4 Multiple Element Cable System (MECS) Finite Element (FE) model

As discussed in §2.9, cable-deck interaction is likely on cable-stayed bridges, due to the similar natural frequencies of cable and 'global' vibrations. To investigate this interaction, an MECS FE model (§2.9.2) was created (Caetano et al. 1998), allowing local cable vibrations.

3.4.1 Details of the MECS model

The MECS model was based on the 2-D OECS model. This was used in preference to the 3-D version to limit the model size. A large number of additional elements was required for the discretisation of the cables and many additional modes arose, so many more modes had to be computed, adding to the computation time. The 2-D MECS model was still manageable, but gave an indication of the resulting behaviour.

Each cable was split into a series of 12 truss elements, which was considered adequate to model their first few modes of vibration. A non-linear static analysis was performed

prior to calculating the natural frequencies and mode shapes, to define the equilibrium state. This was particularly important for the MECS model, since it determined the cable sag due to self-weight, which is a source of significant non-linearity in cable-stayed bridges (§2.4.1). The resulting geometry was slightly different than for the OECS model, for which the cables were assumed straight. Also the correction to Young's Modulus for the effect of cable sag did not need to be applied as for the OECS model.

The equilibrium cable tensions were of more importance than for the OECS model because of their effect on the cable natural frequencies. Cable prestress was modelled in the same way as for the OECS model, but several iterations of the non-linear static analysis were performed to achieve reasonable agreement with the estimated tensions, taken as 85% of the final design tensions (§3.3.3). A state was achieved with 80% of the cable tensions within 20% of the estimated values, which was comparable with the accuracy of the estimates themselves (§10.4.2). The differences from the actual cable tensions meant that the cable natural frequencies, and hence the cable-deck interaction, would not be accurately modelled. However, the general effect of the cable behaviour could be represented.

3.4.2 Results of the MECS FE model

The MECS model produced many more modes in a given frequency range than the OECS model. For example, below 1Hz there were 63 MECS modes compared with only four OECS modes. The majority of these additional modes were essentially local vibrations of individual cables. To identify modes with significant cable-deck interaction, the ratio of the maximum cable displacement to the maximum deck (or pylon) displacement was calculated for each mode shape. Large values represented local cable vibrations, whereas lower values indicated interaction. The minimum ratio for the first 100 MECS modes (up to 1.386Hz) was 1.79, showing that the cables participate to a significant extent in all modes of the deck and pylon in this range.

For the modes with relatively low ratios (<50), the deck and pylon displacements generally resembled those of mode shapes from the OECS model. Typically several MECS modes, with closely-spaced natural frequencies, had deck and pylon mode shapes similar to a single OECS mode shape. Table 3-2 lists the MECS modes with cable/deck displacement ratios less than 50, along with their associated OECS modes. Mode O1 had only one equivalent MECS mode, but its natural frequency was below the lowest cable natural frequency (0.406Hz, §10.4). However, Modes O2 and O3 in particular had multiple equivalent MECS modes, since their natural frequencies were in the range of the first natural frequencies of the cables.

Table 3-2 Summary of MECS model modes with cable/deck ratios <50

MECS mode no.	MECS natural frequency (Hz)	Ratio max. cable/deck displacements	Associated OECS mode no.	OECS natural frequency (Hz)
M1	0.361	2.86	O1	0.384
M2	0.415	28.4	O3	
M3	0.427	23.1	O2	
M7	0.440	27.7	O2	
M12	0.471	30.4	O2	
M13	0.479	47.2	O2/O3	
M16	0.493	42.2	O2	
M18	0.511	1.79	O2	0.545
M27	0.624	45.1	O3	
M29	0.647	41.4	O3	
M30	0.669	17.3	O3	
M31	0.671	49.6	O3	
M32	0.672	30.0	O3	
M33	0.690	10.1	O3	0.654
M35	0.697	43.9	O3	
M55	0.922	46.0	O4	
M58	0.940	11.4	O4	0.941
M65	1.06	8.73	O5	1.115
M68	1.08	24.5	O5	
M73	1.14	3.41	O6	1.153

Fig. 3-8 shows the three most significant (lowest ratio) MECS modes associated with Mode O2. Since the cable displacements were much greater than the deck displacements, the deformed shapes of the cables and the remaining structure (deck, pylon and piers) are shown separately at different scales, to enable the deck mode shapes to be seen. Different cables participate in each mode, but the deck shapes are similar. The mode with the lowest cable/deck displacement ratio (Mode M18, ratio 1.79) most closely resembles the corresponding OECS mode (Mode O2, Fig. 3-7).

The MECS model indicates that cable-deck interaction is important for cable-stayed bridges, resulting in groups of closely-spaced modes with similar behaviour of the deck and pylon but different cable vibrations. However, the amplitudes of the modal responses depend on the generalised loads of the modes (§2.4.2), so if the loading on the deck is dominant, modes with high cable/deck displacement ratios may not be evident.

3.5 Wind tunnel testing

During the design period, wind tunnel tests were performed by RWDI. The final report of these tests (Xie et al. 1994) is referred to extensively in this thesis, for comparison with the results from the site monitoring. Thus the accuracy and shortcomings of wind tunnel testing could to some extent be evaluated. The design tests for the SSC are now outlined.

Sectional models of a 120m length of the bridge deck, at a scale of 1:50, were tested to ensure aerodynamic stability of the deck for flutter (§2.6.5.1) and vortex shedding (§2.6.5.3). The cross-section was finalised after 123 tests of different configurations. The final design was tested in smooth flow and in turbulent flow with a longitudinal turbulence intensity of 6%, equivalent to 13% at full scale (§9.5.3), and with vertical angles of attack from -5° to +5°. Four variations of the basic cross-section were tested, with traffic on each and both carriageways, and with the wind barriers enlarged to simulate ice accretion. The structural damping ratio of the model was 0.7%. Vortex-induced vibrations were predicted, but with an acceptably low amplitude, so the cross-section was accepted. The results are compared with the vortex-induced behaviour monitored on site in §9.5.

Static force coefficients and their derivatives with respect to vertical angle of attack were measured in the sectional model tests. These were used in the estimation of aerodynamic damping, which is compared with values derived from the site measurements in §8.4.2.

A buffeting analysis for the finished bridge was also performed by Xie et al. (1994), based on the force coefficients from the sectional model tests and natural frequencies and mode shapes from an FE model by the bridge designers, Halcrow-SEEE. The results of the buffeting analysis are compared with the amplitudes measured on site in §8.6.3.

Full aeroelastic models at 1:125 scale were tested for the finished bridge and five construction stages, including the completed cantilever. The structural damping ratios of the first three modes of the finished bridge model were measured as 0.65%, 0.4% and 1.2%. The performance of the model was found to meet the design specifications for aerodynamic stability and amplitude of buffeting vibrations, which compared well with the results of the buffeting analysis (§8.6.4).

The design 120 year wind speeds were 37m/s one-hour mean, 46.3m/s gust, and 60.2m/s for the onset of flutter. These were considerably in excess of the maximum wind speeds recorded on site (§6.4.1) over a total monitoring period of approximately 24 months, so the range of wind tunnel results that could be directly validated was limited.

3.6 Conclusions

This chapter has provided background information on the SSC cable-stayed bridge, including a brief description of the structure and its construction. The next chapter will deal with the site monitoring of the bridge, both during construction and after completion.

The three FE models of the cantilever structure developed for this study have been described, and results of the natural frequencies and mode shapes have been presented. The 2-D and 3-D OECS models were in good agreement for the vertical plane modes, indicating that the method of representing the deck for the 3-D model adequately models the composite behaviour for bending. From the 3-D model, 39 modes, with frequencies ranging from 0.351Hz to 4.248Hz, were identified. Thus, together with results of the preliminary tests on site (§6.2.3), the frequency range of interest for the main tests was identified as up to 5Hz (§4.3.2). It was also determined that the global modes of the structure could all be monitored by six accelerometers (§4.5.3). The modes from the OECS models are compared with those measured on site in §8.3.2.

An MECS model was developed, based on the 2-D OECS model, to investigate the possibility of cable-deck interaction on the SSC (§2.9). Many more modes were computed than for the OECS model, most of which were dominated by local vibrations of individual cables. However, for most of the OECS modes, several closely-spaced modes with similar deformations of the deck and pylon were identified, with different cables participating. This indicates that cable-deck interaction was likely to occur for this bridge and that it could be important in the dynamic response. Evidence of this from the measured behaviour is addressed in §10.7, and implications for larger amplitude vibrations are discussed in §10.8.

Finally, the design wind tunnel tests conducted for the SSC have been outlined, results of which are compared with the measured response for vortex-induced vibrations in §9.5. The force coefficients from the tests were used to estimate the aerodynamic damping, according to quasi-static theory (§2.6.3). Results of this are compared with values from the measured data in §8.4.2, while the accuracy of the design buffeting analysis, also based on the force coefficients from the model tests, is addressed in §8.6.

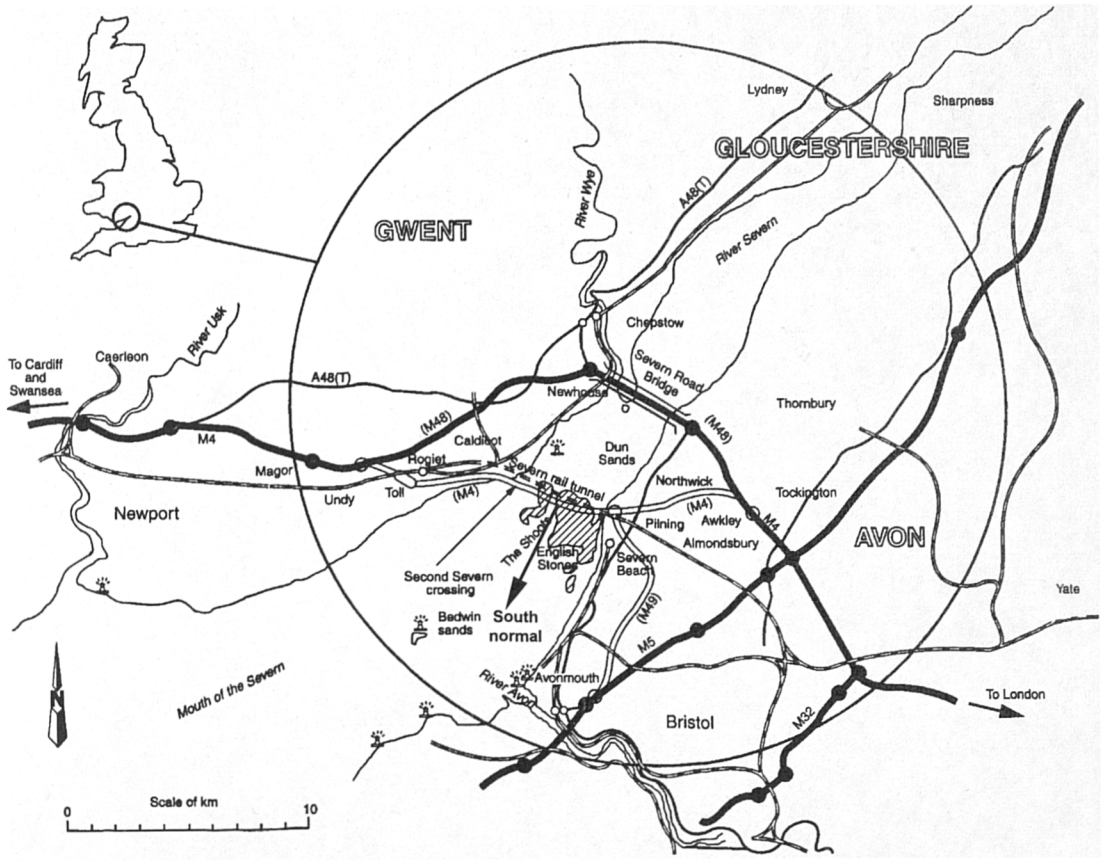

Fig. 3-1 Location map of Second Severn Crossing†

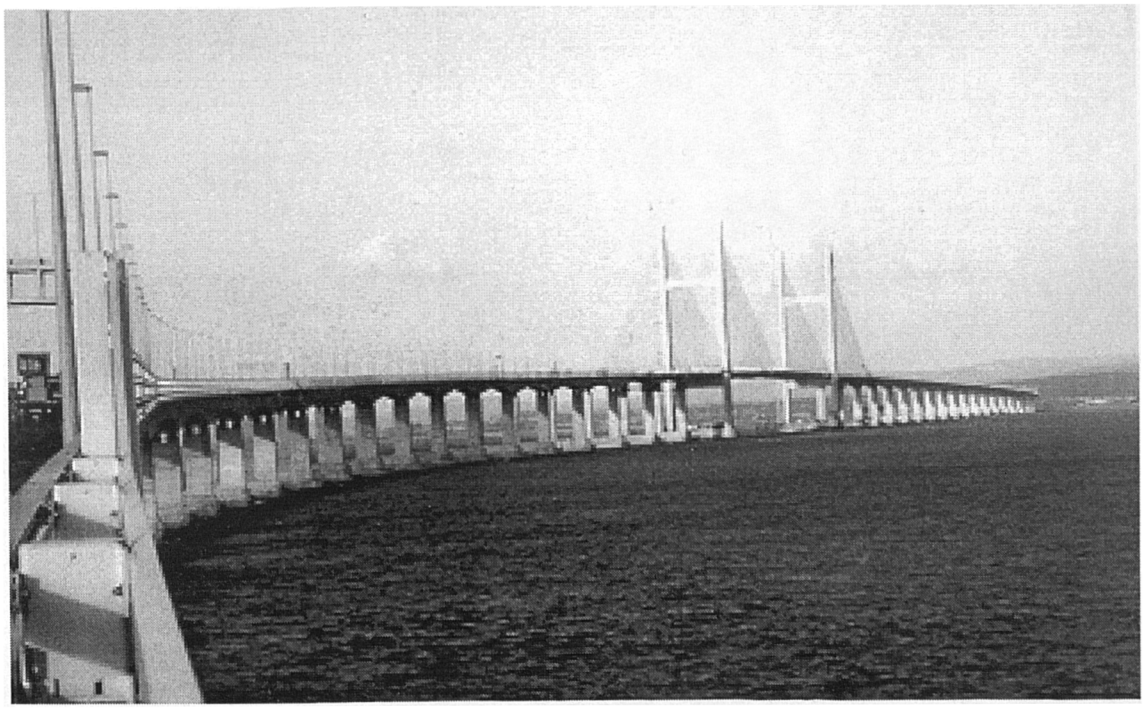

Fig. 3-2 Second Severn Crossing: full bridge

† After Head et al. (1997), with permission from Thomas Telford (Publishing) Ltd.

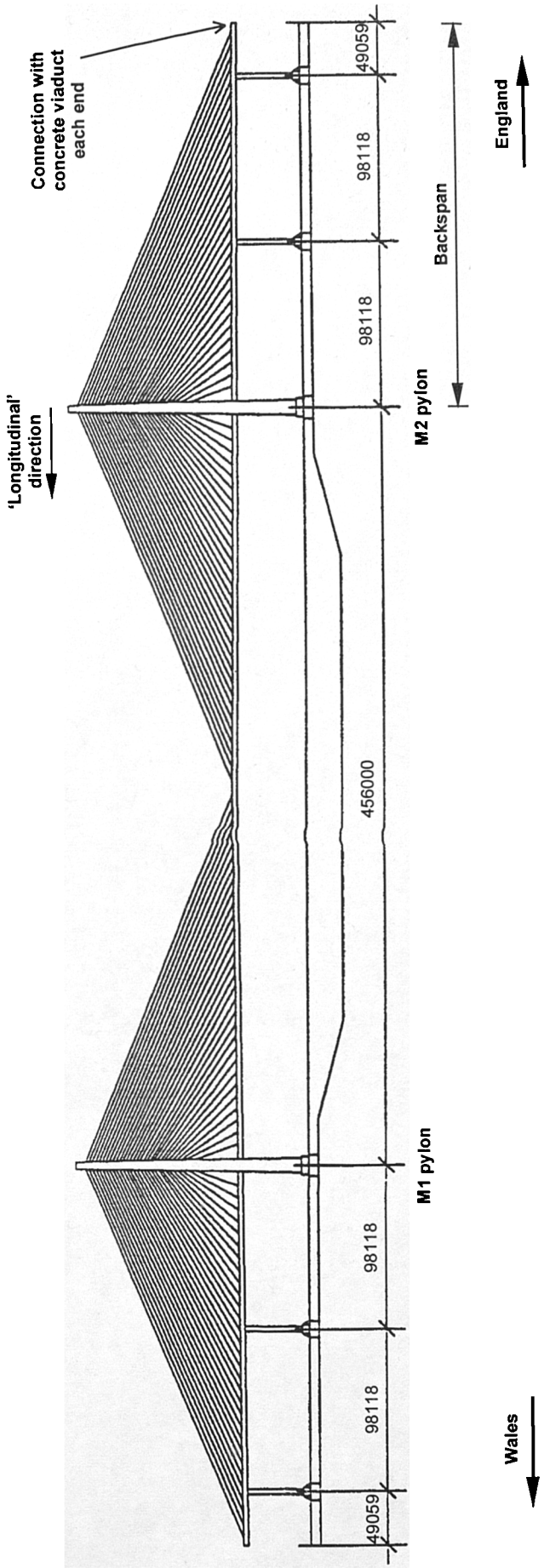

Fig. 3-3(a) Second Severn Crossing cable-stayed bridge: South elevation (dimensions in mm)

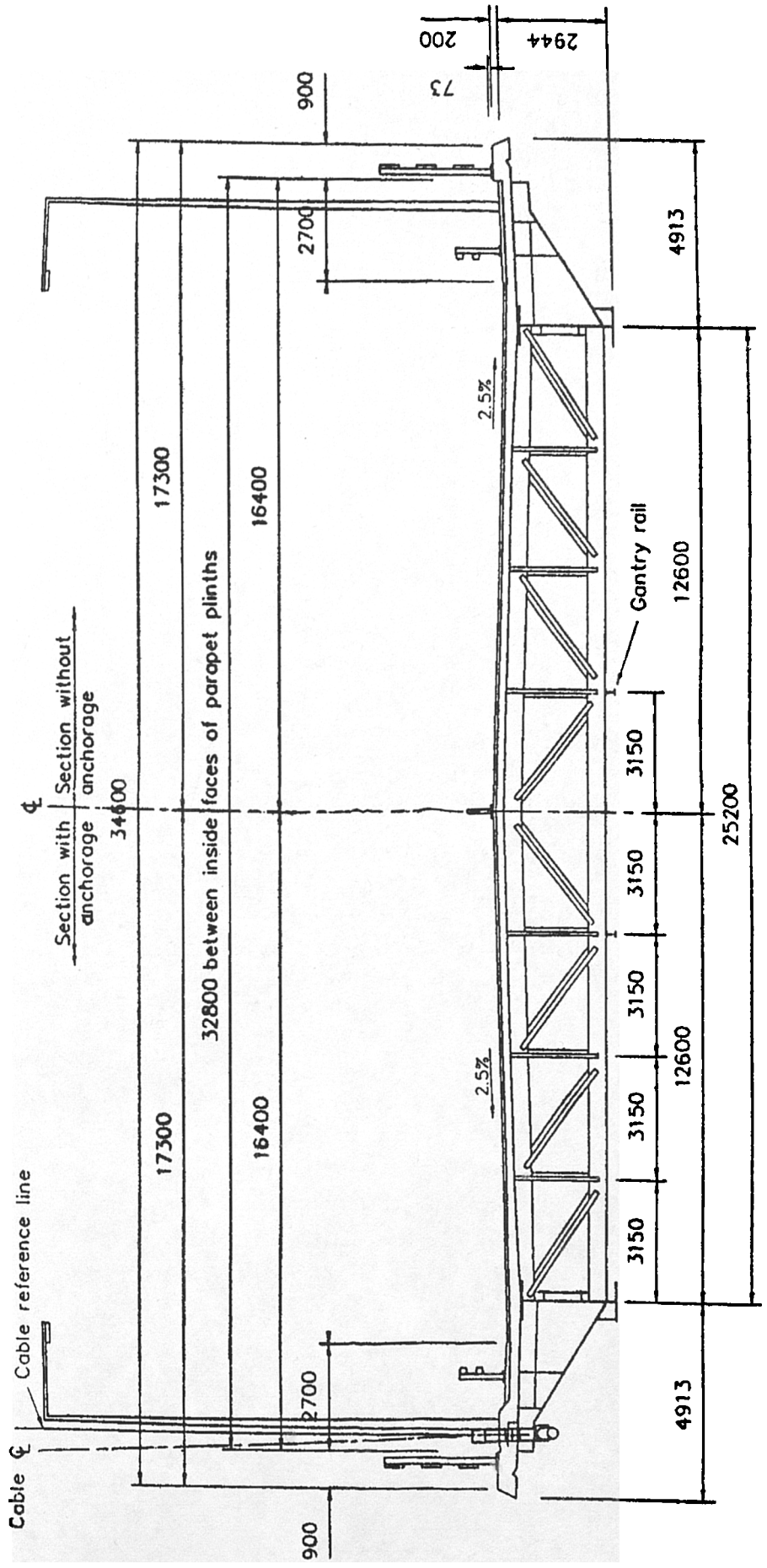

Fig. 3-3(b) Second Severn Crossing cable-stayed bridge: Deck cross-section (dimensions in mm)

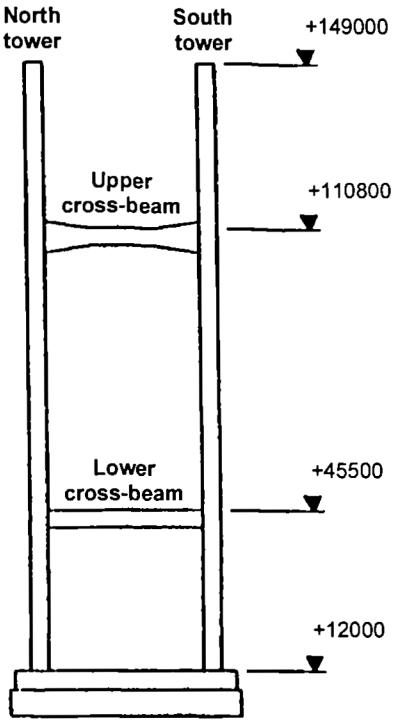

Fig. 3-3(c) Second Severn Crossing cable-stayed bridge: West elevation of pylon (dimensions in mm)

Fig. 3-4 Second Severn Crossing cable-stayed section during construction

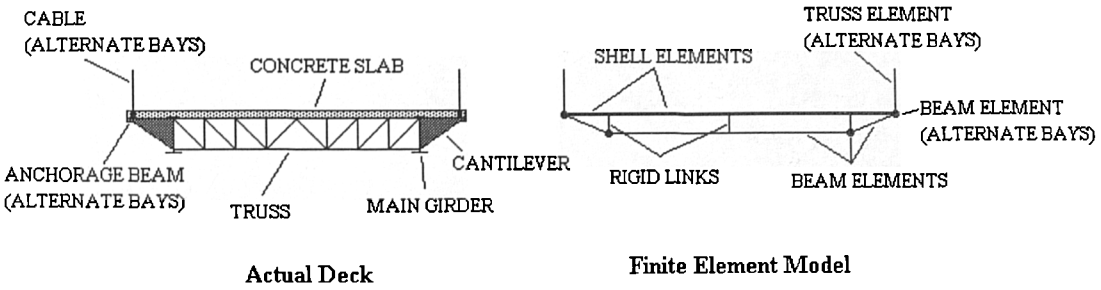

Fig. 3-5 Cross-sections of actual and FE model bridge decks

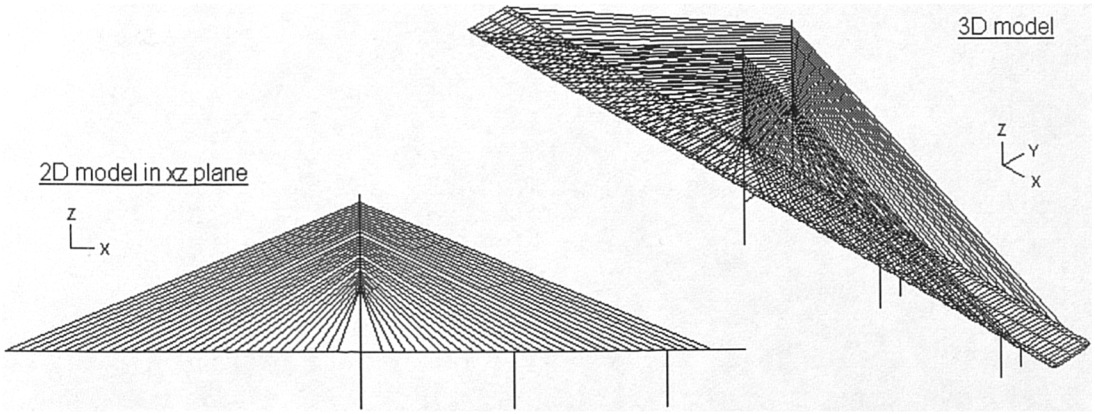

Fig. 3-6 2-D and 3-D FE models of SSC cantilever

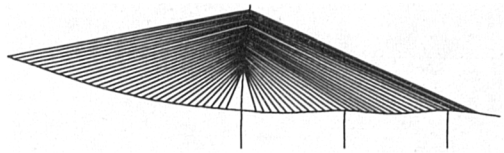

Mode O1, 0.390Hz

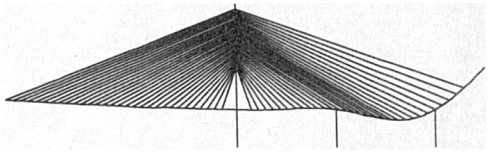

Mode O2, 0.513Hz

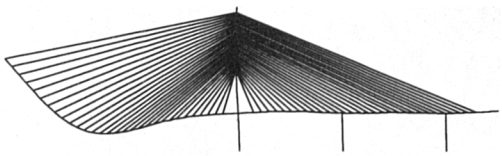

Mode O3, 0.680Hz

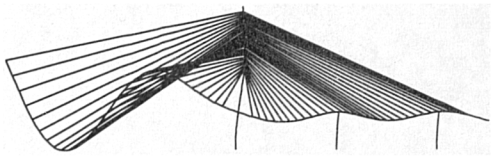

Mode O4, 0.932Hz

Fig. 3-7 First four mode shapes from 2-D OECS model

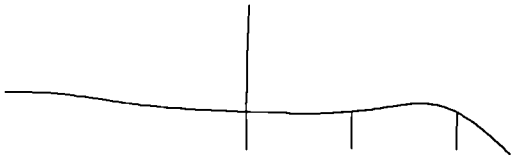

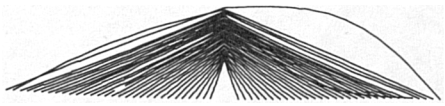

Mode M3, 0.427Hz, cable/deck ratio 23.1

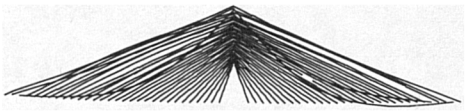

Mode M7, 0.440Hz, cable/deck ratio 27.7

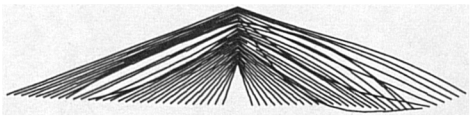

Mode M18, 0.511Hz, cable/deck ratio 1.79

Fig. 3-8 Selected mode shapes from MECS model associated with OECS Mode O2 (deck/pylon and cables shown separately at different scales for clarity)

CHAPTER 4 MONITORING OF THE SECOND SEVERN CROSSING

4.1 Introduction

It was shown in Chapter 2 that there is a need for vibration data from full-scale cable-stayed bridges. This provided the motivation for this research, which concentrated on the dynamic monitoring of the Second Severn Crossing (SSC) cable-stayed bridge and subsequent analysis of the data.

The SSC was particularly suitable for monitoring during erection since the construction programme involved one cantilever being complete but isolated for a considerable period of time. Due to the proximity of the bridge to Bristol, frequent site visits were possible throughout construction of the cable-stayed section (January 1995 – June 1996) and after completion. An extensive instrumentation system was installed to monitor vibrations, along with wind and temperature conditions. Although dynamic tests have been performed on many long-span bridges, it is believed that this series of tests is the most comprehensive to have been undertaken on a cable-stayed bridge during construction (§2.10.1).

During bridge erection, the emphasis was on acquiring as many measurements as possible whilst the opportunity existed. The data are intended for future research, as well as the present study, so full analysis of them is beyond the scope of this thesis. However, a description of all of the site testing is provided for reference, and to identify appropriate methods of site testing for future full-scale monitoring activities.

This chapter describes the monitoring equipment and the various tests undertaken at the different construction stages. Following an overview of the tests, instrumentation details are provided, including the signal conditioning and data acquisition parameters adopted. Thus, the type and format of the data are defined, which are of importance for the following data analysis (Chapters 5&7).

An innovative remote displacement monitoring system, the Computer Vision System (CVS), is described. Although few of the site recordings for it have yet been processed, it will provide unique displacement data for future analysis, and it has been used to confirm measurements from accelerometers, particularly for large amplitude vortex-induced vibrations (§9.3).

The objectives and methods for each type of test are described, which provide the basis for the results presented in Chapters 6,8,9&10, and the data available for further analysis.

Finally the practical difficulties of the site monitoring are described, and the limitations of the data discussed, which limit the accuracy of the results which could be obtained.

4.2 Overview of Monitoring

The SSC was described in §3.2, along with the method of construction (§3.2.4) and definitions of parts of the structure, which are used here (§3.2.2).

The bridge was monitored at various stages of construction commencing in March 1995, when the first cantilever (M2) was half built. Fig. 4-1 shows the construction and testing programme until shortly after bridge completion. After it was opened to traffic in June 1996, further monitoring was conducted until May 1999 (Macdonald 1997,1998,1999).

Over the monitoring period, several different types of test were performed. 'Preliminary tests' (§4.5.1) used a simple monitoring system (§4.3.3) and included brief modal surveys of the M2 cantilever when half built, and the free-standing M1 pylon. They also addressed some particular details, such as the movement of the deck bearings and the rigidity of the foundations. Additional 'brief modal surveys' (§4.5.2), using the same equipment, were conducted at different construction stages of the cantilevers. The bridge is symmetrical, so results from the two cantilevers are comparable.

A more extensive monitoring system (§4.3.1) was installed for the 'main tests', comprising detailed modal surveys, long-term tests, and cable damping tests (§4.5.3-4.5.5) on the completed M2 cantilever and later stages, including the finished bridge.

The majority of the results in later chapters are from the main tests on the M2 completed cantilever (Fig. 4-2) and the finished bridge, since these were the stages for which the most data were acquired. However the key results of the preliminary tests are also presented (§6.2), and the response of the finished structure without the wind barriers is considered (§8.6.5).

Dynamic excitation was purely ambient, from wind, construction operations and traffic, except for the cable damping tests, for which manual excitation was employed.

4.3 Instrumentation

4.3.1 Full monitoring system and instruments

For the main tests, the equipment shown in Fig. 4-3 was installed, comprising a 16-channel data acquisition system and the CVS, which was under development at the time (§4.4). Accelerometers, anemometers, temperature sensors and, occasionally, displacement transducers were employed as described below, along with video cameras for the CVS.

i) *Accelerometers - Sundstrand QA-700 servo-accelerometers*

These are accurate for low accelerations and at low frequencies, down to approximately 0.1Hz, and have been found to perform well in field testing of other long-span bridges and dams (Owen 1994, Daniell & Taylor 1999). They were operated in conjunction with custom-built combined power supplies, amplifiers and filters, which had a facility to remove the DC component of the signal for any instrument orientation (Brownjohn et al. 1986).

The accelerometers were chain calibrated with their respective signal conditioning units by a certified calibration laboratory, before and towards the end of the testing period. Also, between these times, they were calibrated against a reference Setra accelerometer on the Earthquake Shaking Table at Bristol, at which time the gain of the amplifiers was also calibrated.

Up to eight accelerometers were used simultaneously. For deck and pylon measurements they were mounted on steel blocks of sufficient weight to hold them down, supported on three points to eliminate rocking. During the last series of tests they were bolted down into position to prevent any movement in very strong winds.

ii) *Anemometers - Gill Instruments 1012S ultrasonic anemometers*

These give outputs of wind speed, direction and vertical wind speed, updated at 0.96s intervals. One was used throughout the tests, positioned at various locations on the bridge deck at different stages of construction. It was held typically 10m above the deck, to minimise the effect of the deck on the wind at the measurement location. During construction it was usually on the centreline of the bridge, approximately 2/3 of the way along the main span of the completed M2 cantilever, or occasionally on the north side of the deck. After completion of the bridge, it was moved to the top of a lamp post on the north side of the deck just west of midspan, approximately 12m above the road surface (Fig. 4-4). Another anemometer was installed during the winter of 1997-98, on

the south side of the deck, just east of midspan. This was considered necessary since it was more often the windward side of the deck. Thus comparisons could be made between the measured wind on the north and south sides (§6.4.6).

The anemometers were calibrated by the manufacturer and they were installed on site as new. In their final positions on the lamp posts their orientations were surveyed, and corrections were applied to the direction and vertical component measurements to obtain the values relative to the bridge itself.

iii) *Temperature sensors - Analog Devices AD590 two-terminal IC temperature transducers*

These produce a current output proportional to absolute temperature. Five sensors were employed, monitoring the temperature of the air, the main steel girder on the north side, the core concrete of the deck and pylon, and a mock-up section of a typical cable. Before installation on site they were chain calibrated with their respective signal conditioning units, at freezing and boiling points.

iv) *Displacement transducers - Celesco displacement transducers*

These were used for the cable damping tests, to measure the displacement of the cables relative to the deck in the vertical plane. Normally only one cable was monitored at a time, but occasionally a second transducer measured displacements of another cable simultaneously. These instruments are essentially precision potentiometers, which had been calibrated in the laboratory. The input voltage on site was measured with a precision voltmeter and manually recorded for each test.

4.3.2 Signal conditioning and data acquisition

The central measurement station, for signal conditioning and data acquisition, was located in a site office on the bridge deck in the early stages of construction, and in the lower cross-beam of the M2 pylon later (Fig. 4-5).

Instrument cables up to 250m long were used between the measurement instruments, distributed around the bridge, and the central measurement station. Occasionally two cables were linked in series. Care was needed to ensure that there was the minimum deterioration of the signals over these long cable lengths. The types of instruments, signal processing hardware and cabling were chosen to achieve this. For example, shielding of all cables was required, earth loops had to be avoided, and separate wires were needed for power supply and voltage measurement to avoid signal voltage drops. Also all cables and connections had to be fully waterproof, to withstand the hostile environment of the estuary.

Each of the instruments was connected to its respective power supply and/or signal conditioning unit and was set to give an output in the range ±5V. The signals were all passed through identical low-pass filters to prevent aliasing when digitised (Bendat & Piersol 1986). During the early tests, custom-built 2nd order (12dB/octave) Butterworth filters were used, based on Barr & Stroud EF40 universal filters. Because of the relatively gradual cut-off rate, the accelerometer signals were passed through two filters in series, so they acted as 4th order (24dB/octave) filters. Later these were substituted by individual Fern Instruments EF6 8th order (48dB/octave) Butterworth filters.

For the main tests, the standard sampling frequency was 25Hz, to relate to the video camera frame rate for the CVS and to adequately record signals in the frequency range of interest, up to 5Hz (§3.3.5&6.2.3). The filter cut-off frequency was set at 7.23Hz for the EF40 filters and 7Hz for the EF6 filters. They had a constant magnitude FRF, within 2%, up to 2Hz for the EF40 filters and up to 5Hz for the EF6 filters, while at the Nyquist frequency of 12.5Hz, the magnitudes were respectively 10% and 0.86% of the pass band magnitudes. Each filter channel (or pair, when used in series) was calibrated before use on site with a multi-sine signal from an Advantest R2911C spectrum analyser (Fig. 4-6).

An identical spectrum analyser was occasionally used on site to observe the frequency content of the signals and to check the correct operation of the other equipment. However, normally the raw time histories of each channel were recorded. Although this produced a very large quantity of data and did not give immediate results on site, it allowed the maximum flexibility in processing the data at a later stage.

Generally the signals were digitised with a Computer Boards CIO-DAS16/330i (CIO) Analogue to Digital Converter (ADC) board, in conjunction with a CIO-SSH16 simultaneous sample and hold board, to ensure that signals from all of the instruments were captured simultaneously. For some earlier tests, a Data Translation DT2821 ADC board was used, which did not have the simultaneous sample and hold capability, so there were short time delays between the channels, which had to be corrected by subsequent data processing (§5.5).

The zero volts level for the CIO ADC board was variable, so before installation on site each channel was adjusted to minimise the error. For the accelerometer and displacement transducer readings, any remaining error was unimportant since they had an arbitrary DC output which was removed by subsequent data processing. However, for the anemometers and temperature sensors the DC component of output was significant, so a calibration file was recorded periodically. Data were recorded by the acquisition system while the output of each temperature sensor was measured with a precision voltmeter and the anemometers' calibration routine was run, producing a series of

known output voltages. The measurement data from both types of instrument could then be adjusted accordingly when they were processed.

Digitised signals were recorded on a Colossus portable computer using Asyst software (Macmillan 1987). There were several variations of the data acquisition program, for short tests, long duration tests using multiple data files, and for synchronisation with the CVS (§4.4.3).

For the long-term tests, data acquisition was often set to be triggered by a certain wind speed. Data were collected in clusters of 1024 samples (i.e. 2.56s, 64 samples per channel for 16 channels). When using the trigger option, the average wind speed over these clusters was calculated. If it exceeded the threshold value, data recording was triggered, otherwise another cluster of data was collected for comparison with the threshold. Data were saved in multiple small files for convenience of subsequent processing and to prevent significant data loss in the event of equipment failure or power loss. The standard file length was 4096 (i.e. 2^{12}) samples per channel, corresponding to 163.84s, but for processing they could be sub-divided or concatenated if required. Data for the later long-term tests were stored on high capacity optical disks, which were changed periodically. A tape streamer was also available for backing up data. For 16 channels each at 25Hz, the total rate of data acquisition was 2.8MB/hr, which would fill an optical disk in 9.5 days if continuous.

Detailed records were kept of the instrument configuration for each test, including reference numbers of each instrument, signal conditioning channel and cable, for calibration and to assist with troubleshooting.

All of the equipment at the measurement station was powered through an uninterruptible power supply, to provide a stable supply and an estimated half-hour of power during disruptions. This was particularly important during construction, when there were regular changes in electricity supply between generators and frequent power surges or cuts.

4.3.3 Simple monitoring system

For the preliminary tests and brief modal surveys (§4.5.1&4.5.2), the simple monitoring system in Fig. 4-7 was used. It comprised two accelerometers and a spectrum analyser, and often a portable computer for data backup. The advantages of this system were its portability, simplicity and speed to set up. It was ideal when there was little time available or no space to store equipment, at early construction stages.

The accelerometers and signal conditioning units were identical to those for the main tests (§4.3.1). The spectrum analyser was a Diagnostic Instruments DI2200 portable

instrument, with built-in anti-aliasing filters. The data were recorded in its internal memory and on an external memory card as a backup.

For each test, Power Spectral Densities (PSDs) of both acceleration channels, and the 'pseudo-Frequency Response Function'† (FRF) and coherence relating them, were recorded. They were calculated by the spectrum analyser from an average of 32 time records, each of 32s, with the Hanning window applied (§5.6.1). This gave a frequency resolution of 1/32 Hz (i.e. 0.03125Hz), while the sampling rate was 64Hz, with frequencies up to 25Hz recorded. For each test, time histories of both channels for a single 32s record were also saved, which gave a useful visual representation of the vibrations.

4.4 Computer Vision System (CVS)

4.4.1 General description of the system

In parallel with the monitoring programme, the CVS was developed, to enable remote displacement measurement on site. Conventional displacement transducers often cannot be used on large flexible structures since there is seldom a local fixed point relative to which measurements can be taken. Accelerometers can give accurate dynamic measurements, but for very low frequencies (<0.1Hz) they become inaccurate due to instrument limitations and integration errors in determining displacements. The CVS was therefore developed to measure displacements directly, from a remote reference point. Details of the system are given by Macdonald et al. (1998), but a brief description is provided here.

Targets are fixed to the structure at points of interest for displacements, and standard video cameras are trained on them. The system itself digitises the images and tracks the co-ordinates of the targets.

The current system is based on an earlier system developed for use on the Humber Bridge (Stephen et al. 1991,1993, Brownjohn et al. 1993). The new system has improved performance for the basic tracking tasks and new features, including sub-pixel interpolation of target position, multiple camera and multiple target capabilities, and 3-D tracking by stereoscopic viewing of a target by two cameras. The image processing side of the system was developed by the Advanced Computing Research Centre at the University of Bristol.

† This is not strictly a Frequency Response Function, since it is comparing two outputs rather than an output with an input, however the comparison is still useful for determining mode shapes.

4.4.2 Evaluation of the system

Tests were performed on the system using controlled dynamic displacements on the Earthquake Simulator at the University of Bristol, independently monitored by Celesco displacement transducers with 0.2mm accuracy. Fig. 4-8 shows the very good agreement between the measurements, for a two-dimensional earthquake motion. The maximum error was ±5.5mm (<1 pixel) horizontally and ±3.7mm (0.3 pixels) vertically, each corresponding to approximately 0.1% of the field of view. Improved accuracy was obtained for sinusoidal vibrations and for larger targets. In the horizontal direction the limiting factor was the resolution of the camera rather than of the digitiser.

Fig. 4-9 shows the FRF and coherence between the Celesco and CVS measurements, indicating good agreement below 7Hz, above which the errors increased as the displacements decreased. This was also approaching the Nyquist frequency of the CVS, so it can be considered as the practical limit of the system.

4.4.3 Site monitoring

Video cameras for the system were installed on the SSC, with up to three used simultaneously. Since the system was under development at the time, and to allow reprocessing of the video data with different tracking parameters, the camera outputs were recorded onto three-hour Super-VHS video tapes, and processed with the CVS itself in the laboratory. The three camera views and one blank image were multiplexed onto one tape, each at 12.5Hz, which was adequate to detect the significant displacements, which occurred below 1Hz.

A single unit generated the synchronisation signals for all of the cameras and a rectangular 25Hz pulse to trigger the ADC. It also produced the blank video image and multiplexed the four video images. To relate reference times on the video tape and the data acquisition system, the data acquisition computer gave a series of digital pulses at the beginning of each file, which were converted to high frequency tone bursts, which were recorded on an audio track of the video tape. A 12.5Hz square wave was recorded on the other audio track in the same way, to help distinguish the four multiplexed images.

For automatic monitoring, the video recorder was controlled by the data acquisition computer through an RS232 link. Recording was triggered by the wind speed exceeding a specified threshold value. Once the video tape was full, it was rewound and the threshold raised, to permit re-recording if the wind speed increased. The relationship of the CVS site equipment to the conventional data acquisition system is shown schematically in Fig. 4-3.

Black target boards with circles or rings of reflective material were mounted on the north and south sides of the bridge deck near midspan (Fig. 4-10) and at the top of the north tower of the M2 pylon. Thus vertical, torsional and lateral displacements of the deck and longitudinal and lateral displacements of the tower could be monitored, although often just the two deck targets were tracked. The targets were illuminated to permit monitoring at night and to reduce the adverse effects of variation in image brightness.

The cameras, with 800mm focal length lenses, were installed at the base of the M2 pylon (Fig. 4-11), which experiences very little movement (§6.2.5). Purpose-made brackets allowed accurate adjustment of horizontal and vertical angles, and could be locked in place, while plywood boxes protected the cameras and lenses from wind buffeting. Each camera had a local power supply unit, but received synchronisation signals from the central unit and sent back video signals. A portable monitor was used for camera alignment and for adjusting the focus and aperture. When possible, the 1/1000s electronic camera shutters were utilised, to minimise blur of the targets, but in low light the standard video 1/50s was used.

The system was calibrated by comparing the actual size of the target board and its size in pixels in the digitised image.

The output of the CVS was compared with integrated accelerometer measurements from the target locations. Comparisons of typical vertical displacements of one side of the deck are shown in Fig. 4-12. For periods up to approximately 10s (Fig. 4-12(a)) the agreement is very good, with the discrepancy being less than 0.5mm, corresponding to 0.11 pixels, or 0.045% of the field of view. This was obtained with the camera more than 200m from the target, with a vertical field of view of approximately 1.1m.

Over longer periods (Fig. 4-12(b)) there was significant drift between the measurements, believed to be due to errors on the displacements from the accelerometer (§4.4.1), with the CVS remaining stable. The CVS enables the long-period displacements from passing vehicles to be measured accurately, which could enable an influence line to be measured if a single vehicle of known weight passed. It could also be used, for example, to assess the effects of temperature on displacements or to estimate the lift and drag coefficients of the deck from the quasi-static components of displacements due to the wind. These effects are difficult to monitor on site by any other means.

Unfortunately, hardware problems with the system, which was under development, limited the number of video tapes that it was possible to process for the present study. However, processing of the tapes will be possible in the future with new hardware, to produce unique displacement data for a cable-stayed bridge near midspan.

4.4.4 Further developments of the system

The system has been further developed recently, and has been found to be useful for a variety of other applications at vastly different scales, down to strain measurements of specimens less than a millimetre long (Towse et al. 1999).

Developments include the use of faster hardware to improve both reliability and accuracy. More rugged hardware will also make it more portable and suitable for use on site for real-time monitoring of civil engineering structures. There are applications in the laboratory also, with several points being able to be tracked simultaneously, without the needs for cabling or for fixing instruments to the specimen.

4.5 Description of Tests

Having described the equipment that was used for the monitoring, the details of each type of test are now provided.

4.5.1 Preliminary tests

The preliminary tests were conducted, using the simple monitoring system (§4.3.3), when approximately half of the M2 cantilever had been constructed, i.e. approximately 120m on either side of the pylon, shortly past the first intermediate pier in the backspan. Also the M1 pylon was complete, except for fixing the top cross-beam in place (Fig. 4-13). The objectives of these tests were to determine the modal behaviour of the cantilever and pylon, to assess the effectiveness of structural restraints, and to assist in the planning of the later main tests.

These tests principally measured the relative movements of different parts of the structure. Generally, one accelerometer was kept in a fixed position as a reference, and the other was moved to different locations to determine the mode shapes. Tests were carried out in two orthogonal directions for each instrument location, and additional tests measured the relative movements in each direction at the reference locations, and between reference locations when more than one was used. For the M2 tests, the reference locations were the end of the main span cantilever and the top of the north tower, which were expected to be anti-nodes for the majority of modes. A total of 47 tests were carried out, with the accelerometers positioned at the locations shown in Fig. 4-14. Five similar tests were conducted on the M1 north tower on one day, with the equipment and a generator being taken to the top of the tower, which was used as the reference location.

Particular tests aimed to establish the fixity of the bridge deck bearings in each direction for dynamic movements, using accelerometers placed on either side of the bearings, on

the pier and the pylon. Also tests were conducted with the accelerometers on the caisson at the base of the M2 pylon to determine its rigidity, and longitudinally on the deck to establish the significance of this motion. Measurements were also taken for one typical bridge cable, approximately half way along the main span cantilever.

The average wind speed and direction, from the ultrasonic anemometer, were recorded manually for each test. The temperature of the cables and the concrete deck were also noted periodically, as measured by thermocouples embedded in them by the Contractor during construction.

Results of the preliminary tests are presented in §6.2.

4.5.2 Brief modal surveys

In addition to the preliminary tests, similar tests were performed at particular construction stages using the same equipment, to measure the natural frequencies and mode shapes. The main construction stages of interest were just before connection of the cantilever to each pier in the backspan, since these were potentially the most vulnerable states and they related to wind tunnel full aeroelastic models (Xie et al. 1994). The structure was also tested just after connection to each of the piers to determine the difference in response. This information could be used for comparison with Finite Element (FE) models to validate modelling of the piers and connections.

Each modal survey was carried out over a maximum of three days, since the structure was changing rapidly. They were mainly performed on the M1 cantilever, although one other intermediate stage was tested on the M2 cantilever.

Average wind speed and direction during the tests were obtained from the Contractor's instruments, to provide an indication of the wind loading.

Although it was considered important to measure the response of the structure at these intermediate construction stages while the opportunity existed, detailed processing of these data is beyond the scope of this thesis.

4.5.3 Detailed modal surveys

For the completed cantilever and the finished bridge, detailed modal surveys were conducted using the full monitoring system (§4.3.1). The objective was to obtain more accurate and detailed mode shapes of the structure at these important construction stages, for comparison with FE model results (§3.3&8.3.2).

For the cantilever tests, the instruments were located as shown in Fig. 4-15. Six accelerometers were used in two sets of three at various cross-sections of the deck and pylon. Two accelerometers measured the deck vertical (or pylon longitudinal) motion on

either side, from which pure bending and torsional components could be distinguished from the sum and difference, while the third monitored the lateral movement. From the results of the One Element Cable System (OECS) FE models (§3.3.5), instruments arranged thus were expected to detect all of the global modes of the structure up to 4Hz. One set was kept at a reference cross-section, either at the tip of the cantilever (or near midspan for the finished bridge) or at the top of the pylon, both expected to be anti-nodes for the majority of modes. The second set was moved to a series of different cross-sections, coinciding with nodes of the FE models (§3.3), to measure the relative amplitudes. For each cross-section a half-hour record was acquired, and several tests, often of longer duration, were performed to relate the two reference cross-sections. The simultaneous measurement of all of the principal components of motion enabled the relationships between them to be defined (e.g. lateral deck motion combined with torsional pylon motion). Temperatures and wind velocity were recorded simultaneously to enable correlation with the measured response, and for some tests video recordings were made for the CVS. A partial modal survey of the completed structure was carried out in the same way.

Results of the detailed modal survey of the cantilever are presented and compared with the results of the OECS FE models in §8.3. Detailed processing of the equivalent data for the finished bridge is beyond the scope of this thesis.

4.5.4 Long-term tests

The full monitoring system was also used for long-term tests, to obtain data on the response of the bridge in various wind conditions. Also, from the longer records, more accurate estimates could be made of the modal parameters, particularly damping ratios (§5.6.2, 7.5.4&8.4.1). During construction, records were generally made over night or at weekends, while there were no dynamic construction loads. There were occasional tests for longer periods of up to two weeks.

After completion of the bridge, the equipment was operated from autumn to springtime for the following three years (1996-1999), with only short breaks each week to download recorded data. For the majority of these tests, data were only recorded when the wind speed exceeded a trigger level, although on some occasions continuous records were acquired. After the detailed modal survey of the finished bridge, the accelerometers were kept in fixed positions. One set of three was positioned 23.42m to the east of midspan of the main span, where both symmetric and anti-symmetric modes could be monitored. Another set of three was kept at the top of the M2 pylon.

Two more accelerometers were fixed to Cable 61N - the longest main span cable from the M2 north tower. However, corrosion of the connections and difficulty of access once the bridge was open meant that few records were obtained from these instruments.

Wind velocities from the first anemometer were recorded throughout the long-term tests, with the second one, on the south side of the deck, being added later. Temperature data were also acquired, and for some early tests CVS video recordings, triggered automatically in strong winds (§4.4.3).

During the winter of 1997-98, baffles were added to the bridge deck to limit vortex-induced vibrations (§9.6). Thereafter, monitoring was concerned with the effectiveness of this measure. A consistent approach to the monitoring was used to ensure comparability of the data before and after the modifications.

The long-term tests provide the basis for many of the results presented in Chapters 6,8,9&10. Following preliminary analysis of all of the data sets (§6.3), periods of interest for the present research, in terms of wind conditions or bridge response, were identified for further processing. Less than 10% of the data have been analysed in detail to date, so they provide a valuable resource for much future work.

4.5.5 Cable damping tests

Short series of tests were performed to investigate the damping of cable vibrations in the first mode, for a representative sample of four cables. The tests were performed before and after injection of the corrosion protection wax into the cable sheaths to determine its effect on the damping.

The cables were excited manually, using a rope tied around each cable approximately 10m above the bridge deck. Each cable was excited in the vertical plane, in time with vibrations in its fundamental mode, for up to five minutes. The free decay of vibrations was monitored to enable the damping to be calculated by the Logarithmic Decrement Method (§10.3.1). The full monitoring system was used (§4.3.1), with accelerometers measuring in-plane and out-of-plane cable vibrations at the excitation location (Fig. 4-16, §10.3). A displacement transducer monitored the movement of the same point relative to the bridge deck in the vertical plane, perpendicular to the cable. Temperatures and wind velocity were also recorded. For some tests, the motion of the deck and the opposite cable were also measured, using accelerometers, the CVS and a displacement transducer.

At the time of the tests, all of the bridge cables were tied down to the deck with ropes (§10.2). The majority of the tests after waxing of the cables were performed with and

without the equivalent cable on the opposite side of the deck released, to determine whether there was any significant interaction between the two cables.

Results of the cable damping tests are presented in Chapter 10.

4.6 Practical difficulties and limitations of the site monitoring

Many practical difficulties were encountered on site, which dictated which tests were possible, and affected the reliability and usefulness of the results. Working on a bridge during construction had several consequences, including limited access to the site, security of equipment, unreliable power supplies, unquantifiable excitation due to construction work, and frequent damage to instruments and signal cables. The data acquisition software and some items of hardware were several years old, providing limited data storage for the earlier tests, allowing limited flexibility of usage, and sometimes proving unreliable.

The weather proved problematic, with high winds preventing access, or light winds providing little excitation at particular construction stages of interest. Also there were problems with water ingress to electrical connections and equipment, and repairs on site were difficult.

The modal surveys were carried out with a maximum of six accelerometers frequently moved between measurement locations. Due to construction proceeding concurrently, data from successive tests often did not relate to precisely the same stage of construction. Also, factors such as cable tensions and the condition of structural connections, which would affect the dynamic behaviour, could not be determined accurately. Therefore differences, which are difficult to quantify, were present between different data sets and between the actual bridge and the FE models.

For the tests using the simple monitoring system, with only two accelerometers, vertical (or longitudinal) bending and torsional modes could not always be distinguished, particularly if the natural frequencies were closely-spaced.

Ambient excitation has several limitations. It cannot be controlled, in contrast with wind tunnel or forced dynamic testing, so the effects of different parameters could not easily be distinguished. Also, limited data were acquired in higher wind speeds. Many signal processing methods could not be applied since the loading was unknown, and assumptions were required regarding its characteristics (§5.3.1&6.5). Also the loading and response would not necessarily be stationary, which is a usual assumption for random data analysis (§5.2.2).

The wind conditions were only measured by one or, latterly, two anemometers, but there would be significant variation of the wind loading over the structure (§2.6.4.2). The

response was only measured simultaneously at a few locations, which was particularly a limitation for monitoring cable vibrations and cable-deck interaction (Chapter 10). The CVS enabled the direct measurement of displacements, but again only at a limited number of locations, and only for periods of up to three hours.

Despite the above difficulties and limitations, a valuable set of data was collected from the monitoring exercise. Measurement errors and the accuracy of the spectra which could be obtained from the data are addressed in §5.5&5.6, Chapter 6 deals with characteristics of the ambient loading, and Chapter 7 describes an improved method of ambient vibration data processing to minimise the resulting errors in modal parameter estimates.

4.7 Conclusions

The construction of the SSC gave a rare opportunity for monitoring the dynamic behaviour of a cable-stayed bridge in detail at several stages of construction. The monitoring of such structures at full scale is vital in understanding their dynamic behaviour (§2.11). The monitoring programme described here is believed to be the most comprehensive set of dynamic tests undertaken on a cable-stayed bridge during construction.

The monitoring equipment and the signal conditioning and data acquisition parameters have been described, which determined the type and format of the data available for processing. The methods of analysis of these data are discussed in Chapters 5 and 7.

The CVS was developed and was shown to be a viable means of monitoring displacements remotely. A measurement accuracy of 0.5mm was achieved at a distance of over 200m. Although little processing has been performed to date on the video data from site, it gave confirmation of the accelerometer measurements, and additional uses of the data have been identified. The system has since been developed further, so it could now be applied more fully to similar applications.

The various types of dynamic test on the SSC have been described, which define the range of data available for analysis. The results of the preliminary tests are presented in §6.2, and the measured wind characteristics from the long-term tests are discussed in §6.4. The detailed modal survey of the completed cantilever yielded mode shapes, which are compared with the OECS FE model output (§3.3.5) in §8.3, while the cable damping test data form the basis of Chapter 10. The remaining results discussed in Chapters 8-10 are largely findings of the long-term tests.

The practical difficulties of the site monitoring and the limitations of the resulting data have been highlighted. The accuracy of the measurements and of the results which can be extracted are discussed in Chapters 5&7. Despite the limitations, ambient excitation

proved very effective for monitoring the structure, identifying many aspects of the dynamic behaviour (Chapters 8-10).

The tests outlined in this chapter aimed to gather as much information as possible at particular construction stages, given the limitations of time and available equipment. Although the principal aspects of the dynamic behaviour of the bridge are addressed in this thesis, many of the data records are yet to be processed in detail. The formation of this database was of significance in itself, providing the opportunity for much further research into particular aspects of the behaviour and validation of analysis and modelling techniques (§11.6.2).

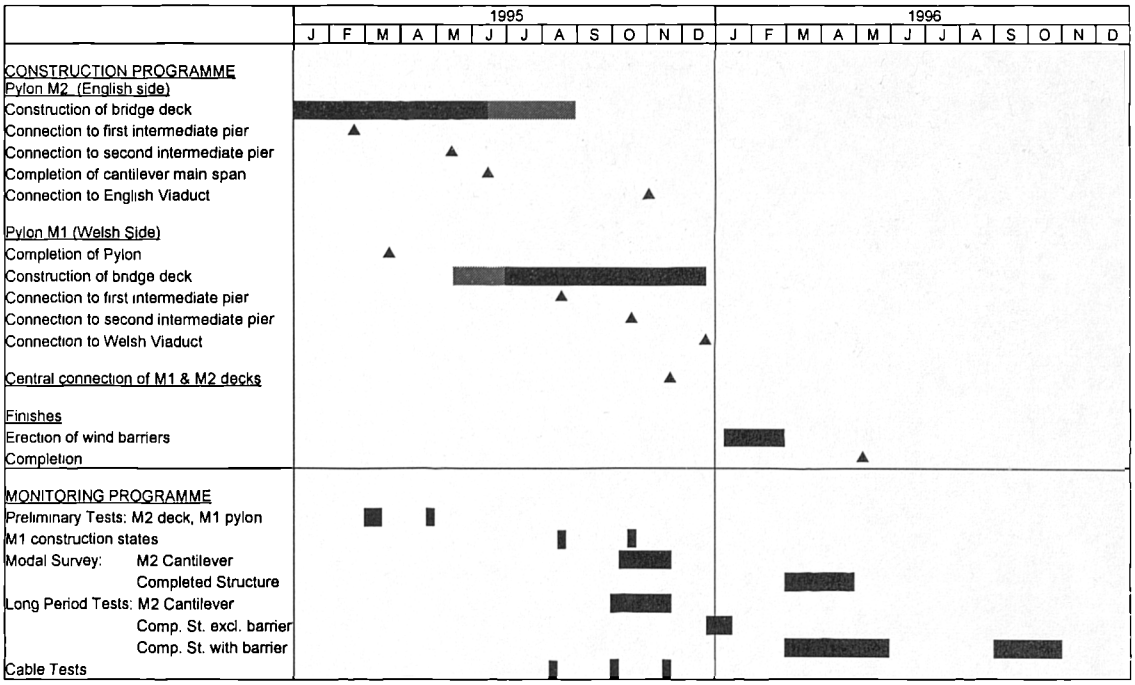

Fig. 4-1 Construction and testing programme

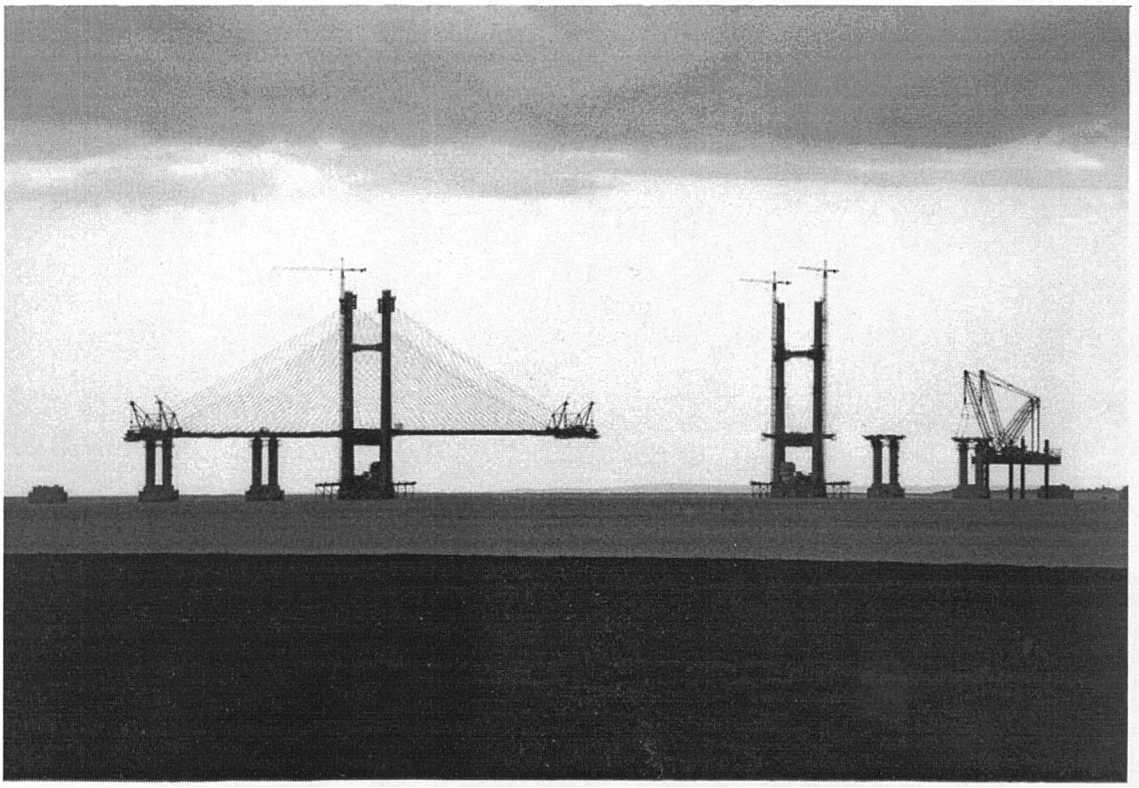

Fig. 4-2 M2 cantilever near completion (viewed from north)

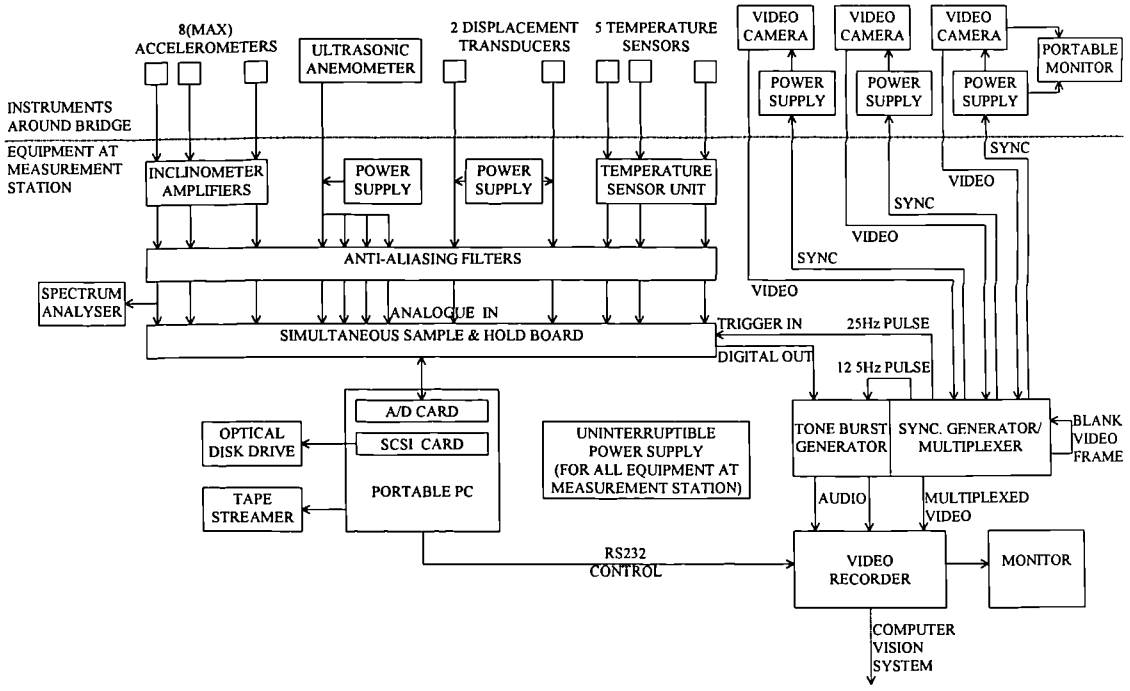

Fig. 4-3 Full measurement system

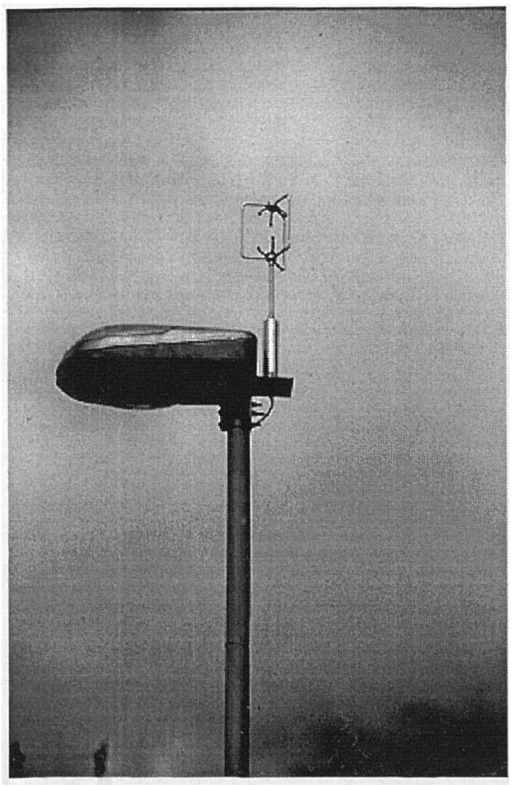

Fig. 4-4 Ultrasonic anemometer on lamp post

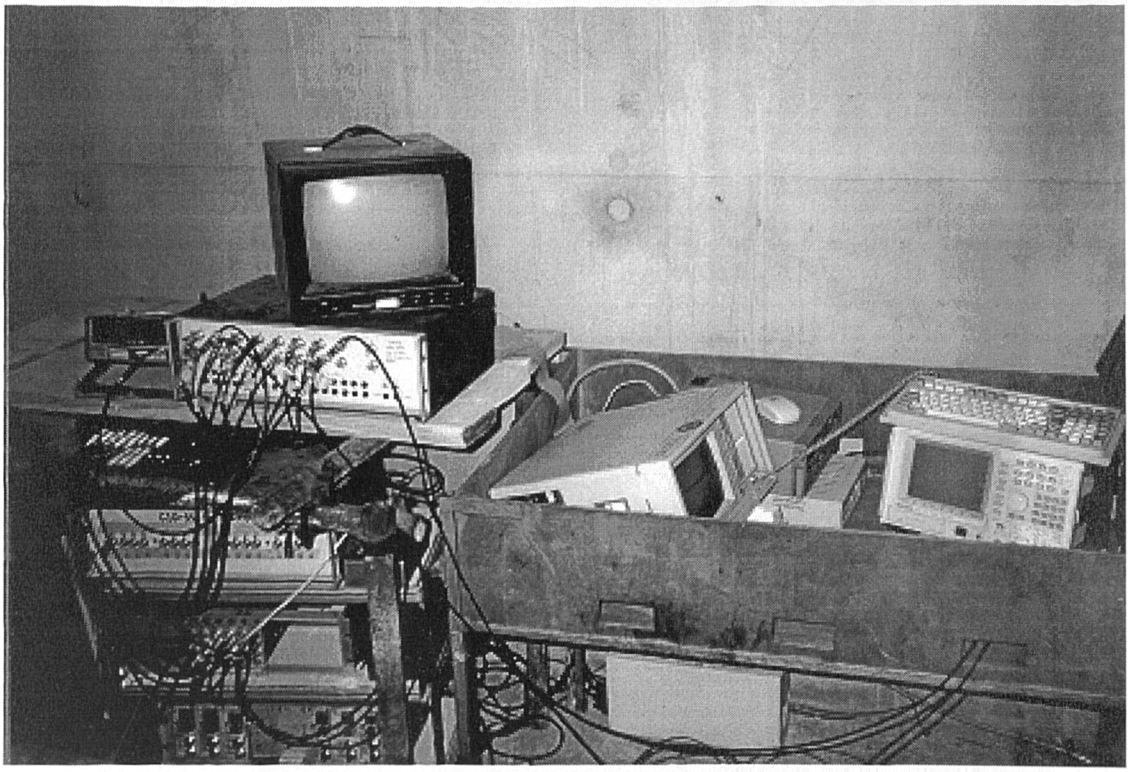

Fig. 4-5 Equipment at the central measurement station in the M2 lower cross-beam

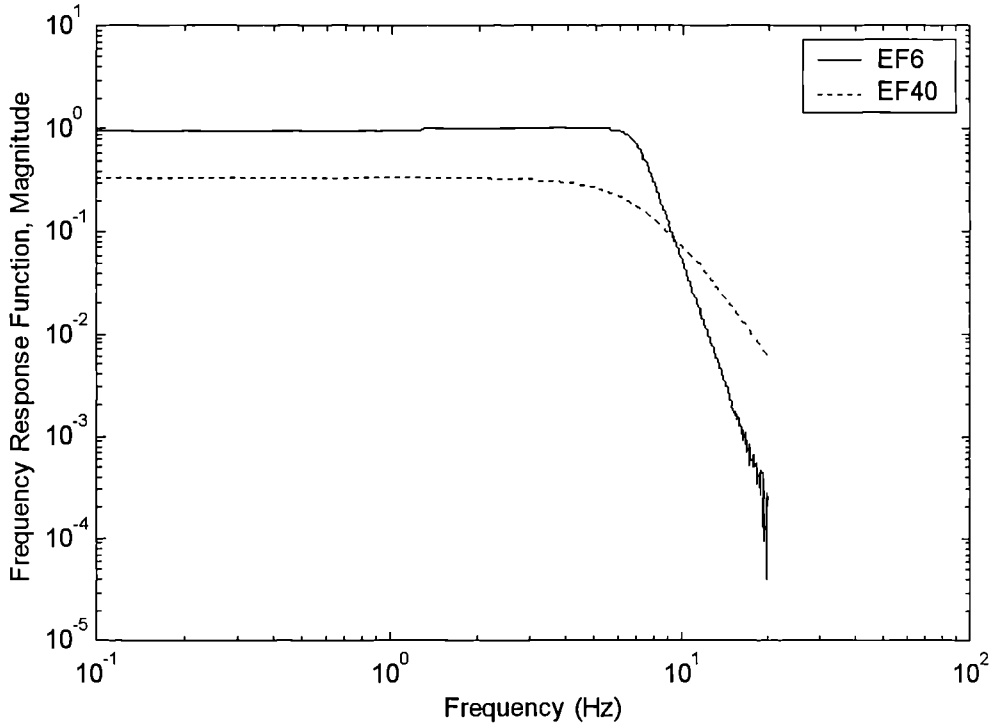

(a) Frequency Response Function, Magnitude

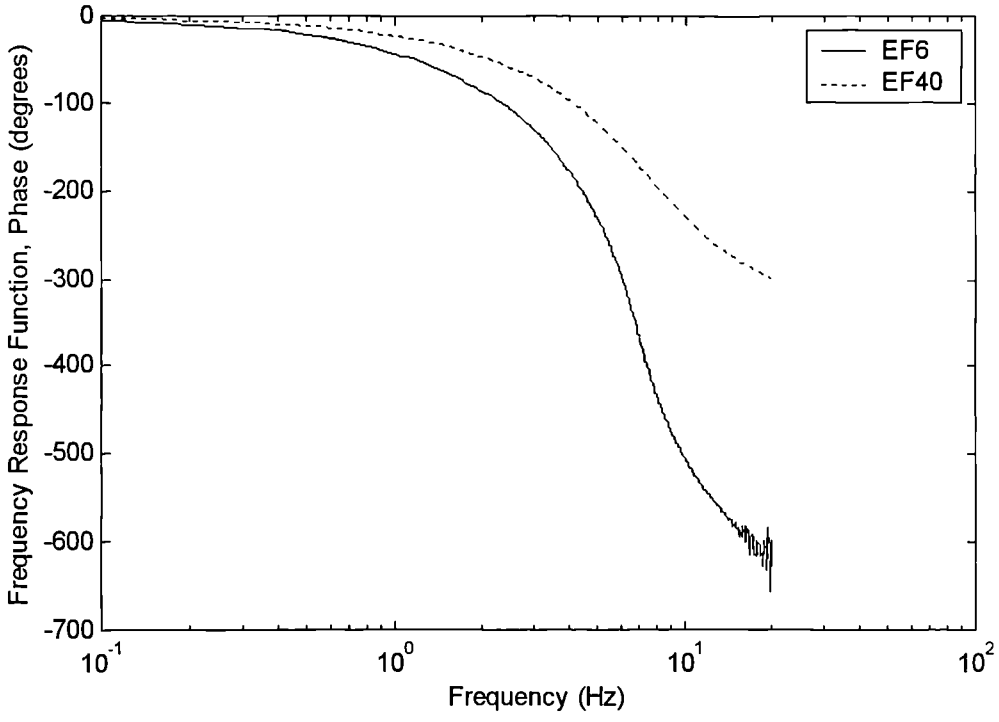

(b) Frequency Response Function, Phase

Fig. 4-6 Measured characteristics of typical channels of anti-aliasing filters

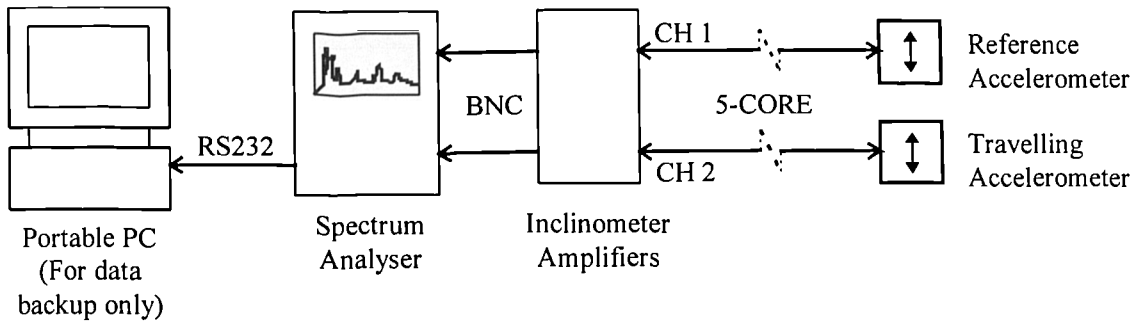

Fig. 4-7 Simple measurement system

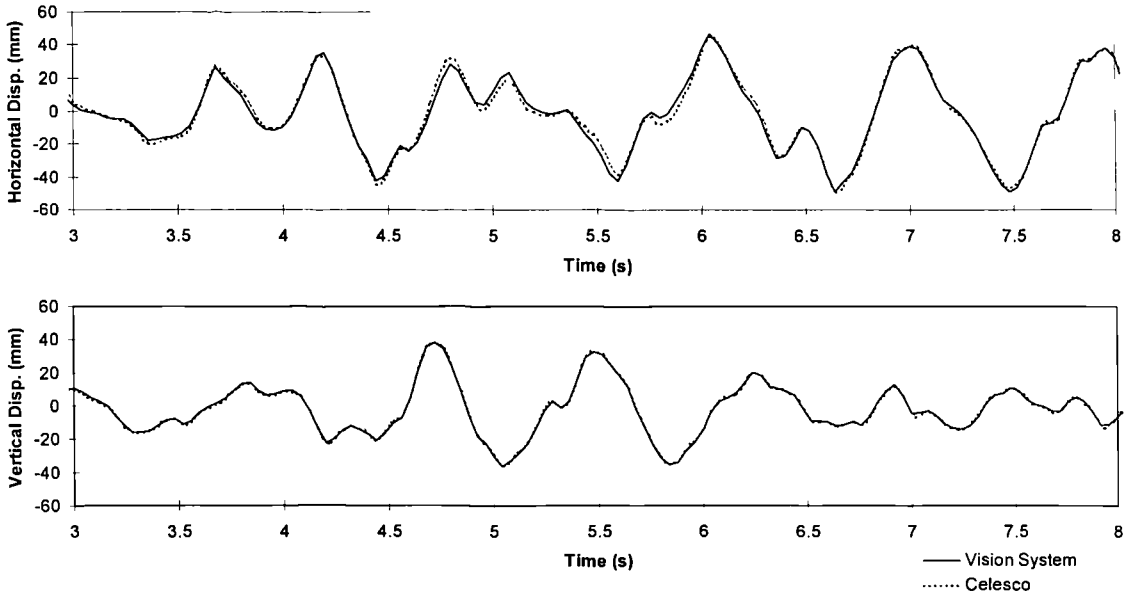

Fig. 4-8 Comparison of CVS and Celesco measurements of shaking table displacement for 2-D earthquake

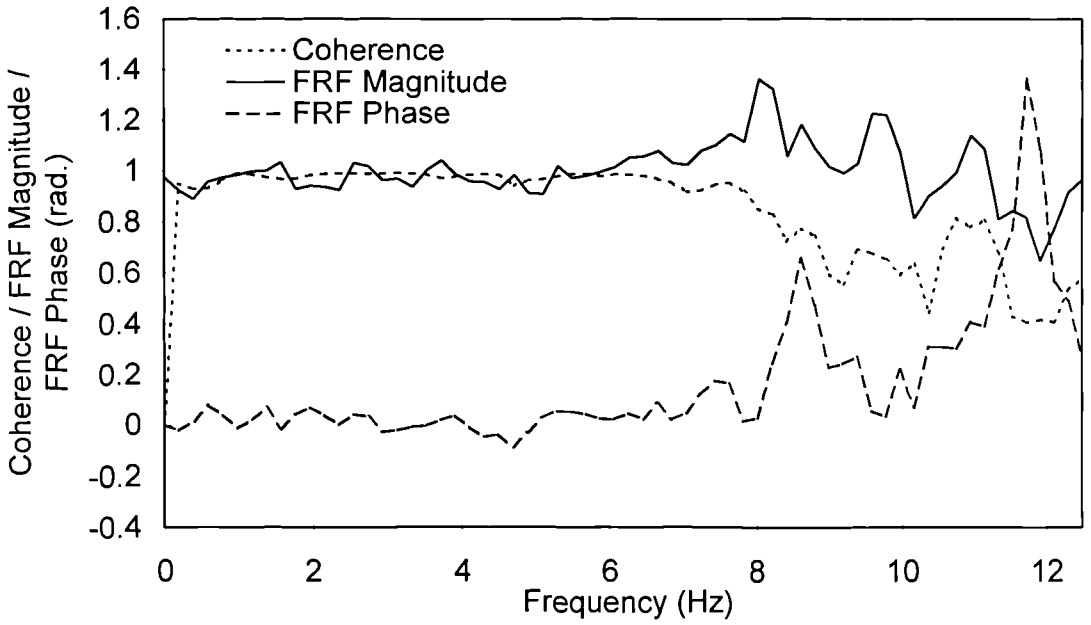

Fig. 4-9 Frequency domain comparison of CVS output with Celesco measurements for horizontal component of 2-D earthquake

Fig. 4-10 CVS target on SSC near midspan

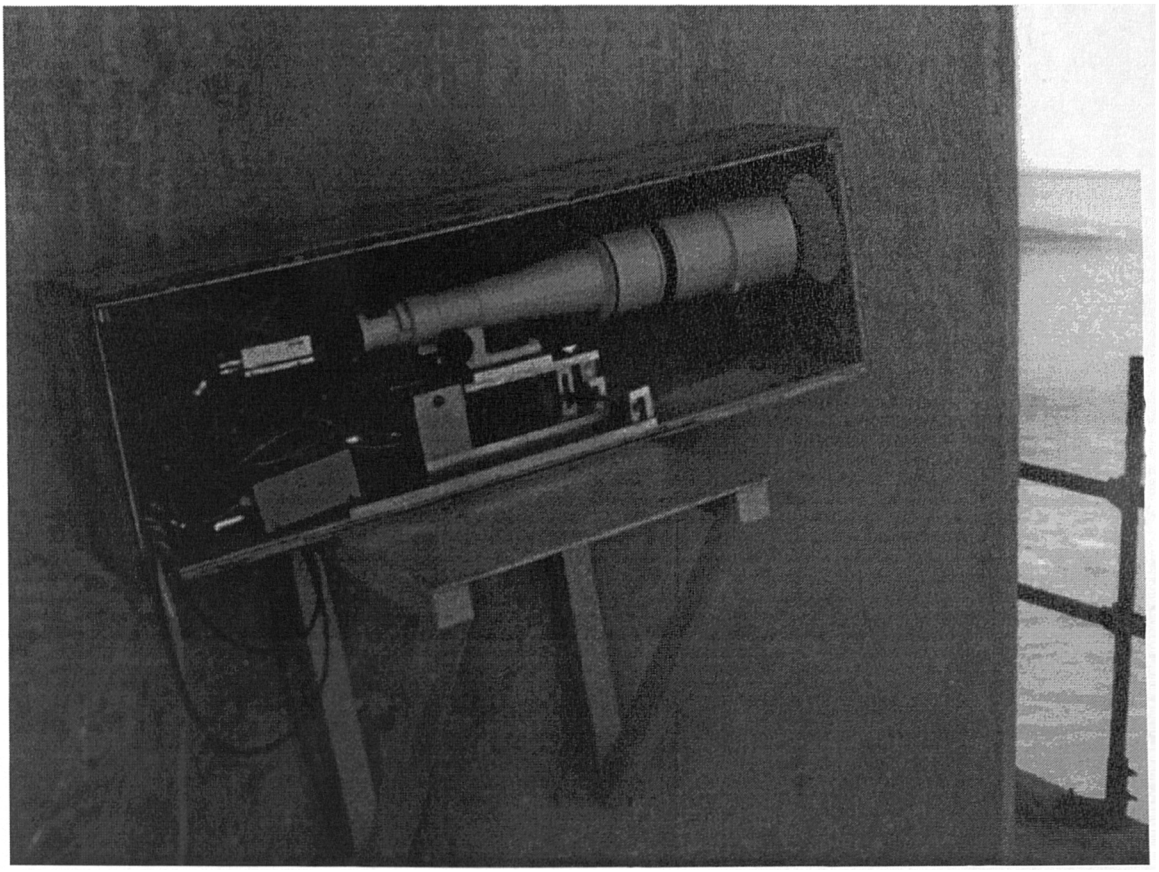

Fig. 4-11 CVS camera on SSC at base of pylon

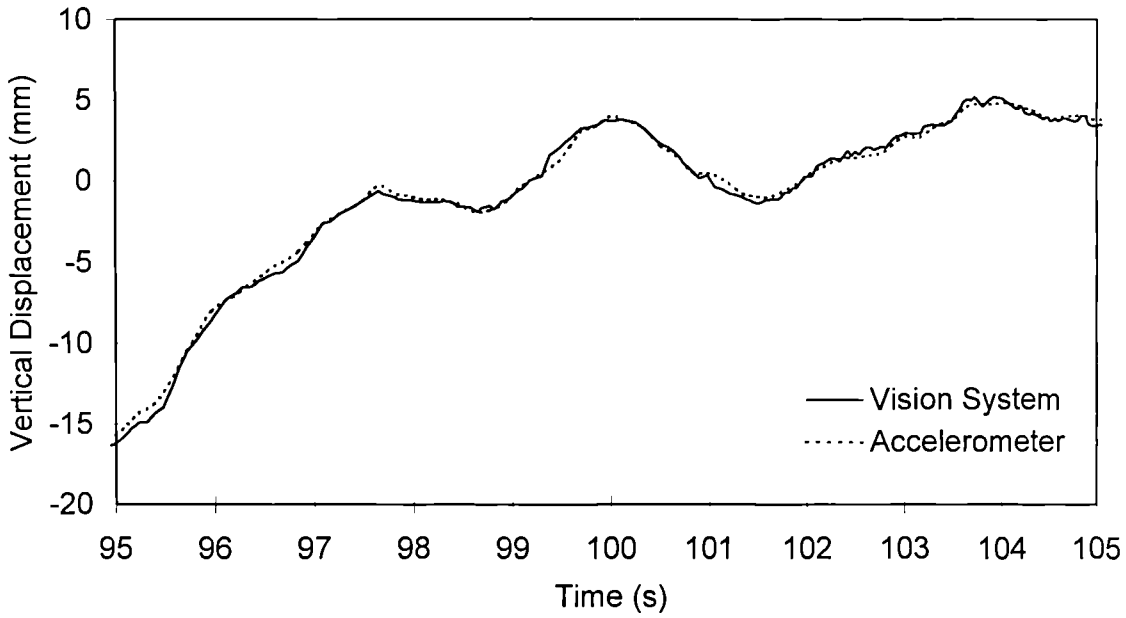

(a) Detailed view of 10s record

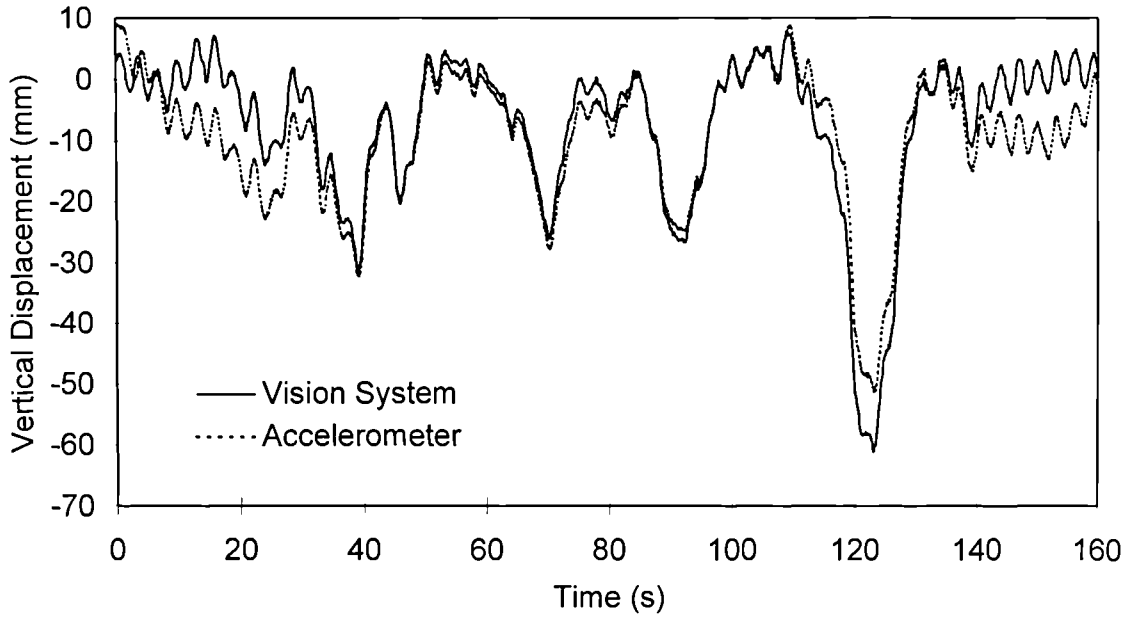

(b) Longer record showing relative drift

Fig. 4-12 Comparison between typical vertical deck displacements measured by CVS and calculated from accelerometer data

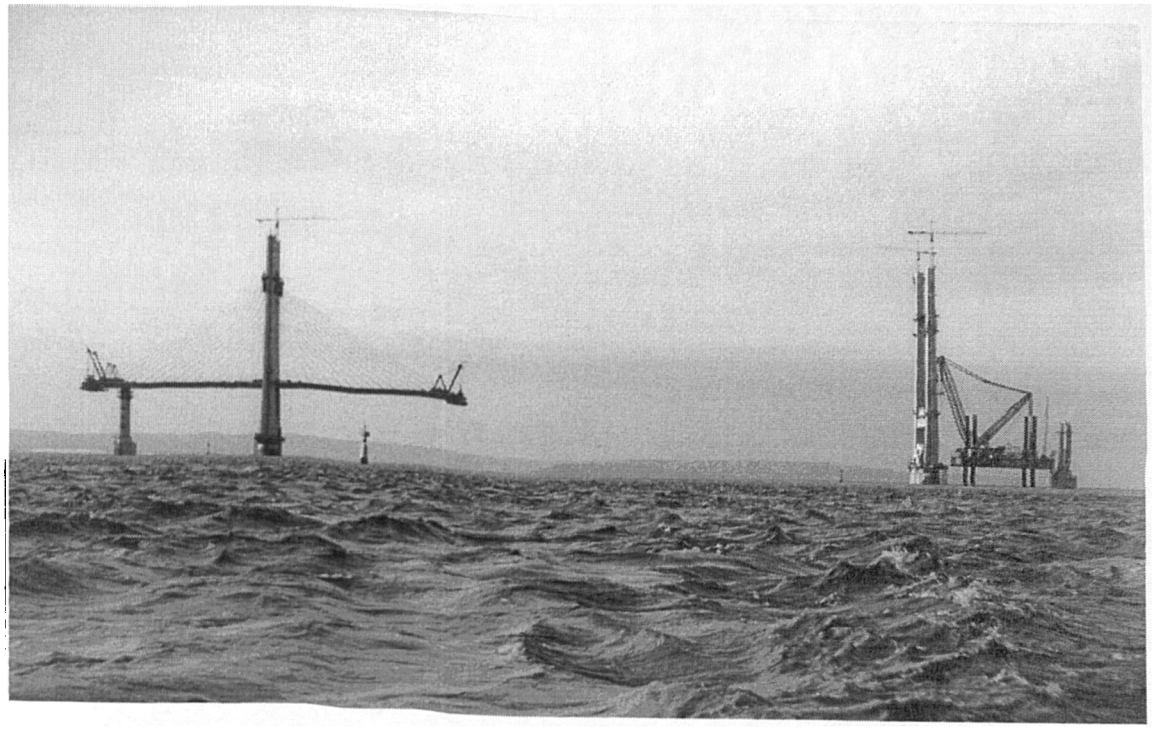

Fig. 4-13 State of construction for preliminary tests (north elevation)

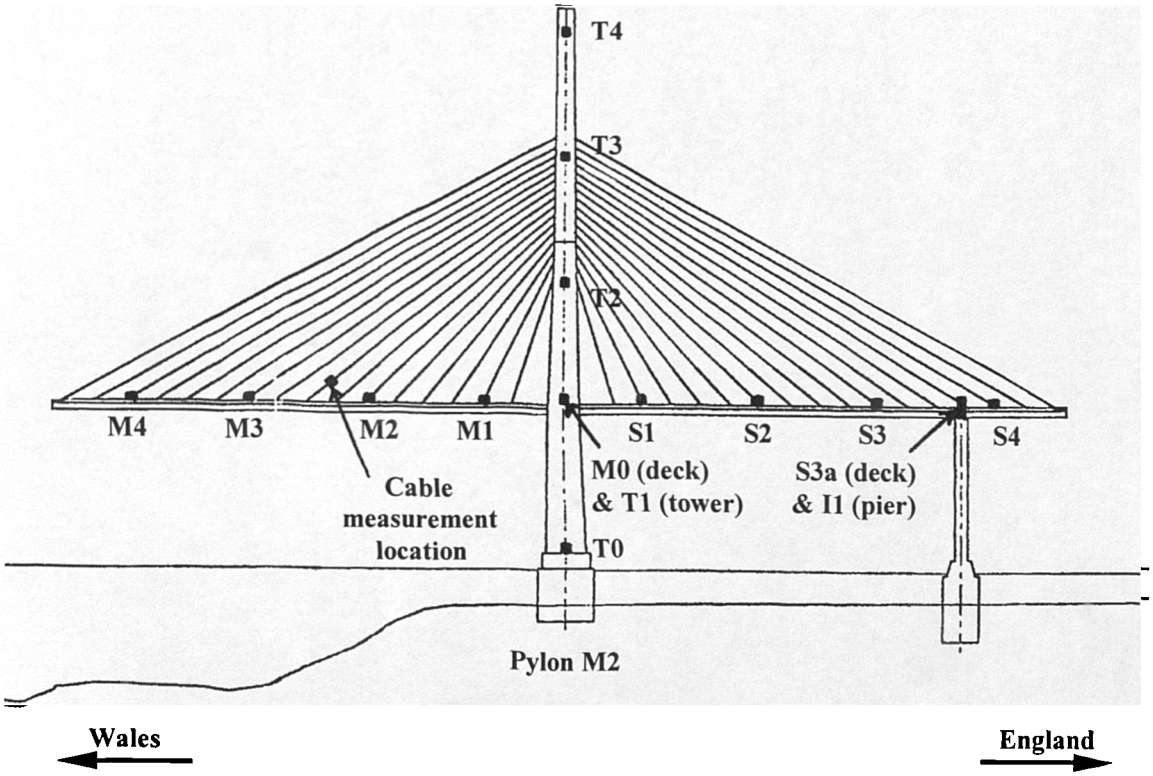

Fig. 4-14 Instrument locations for M2 preliminary tests (south elevation)

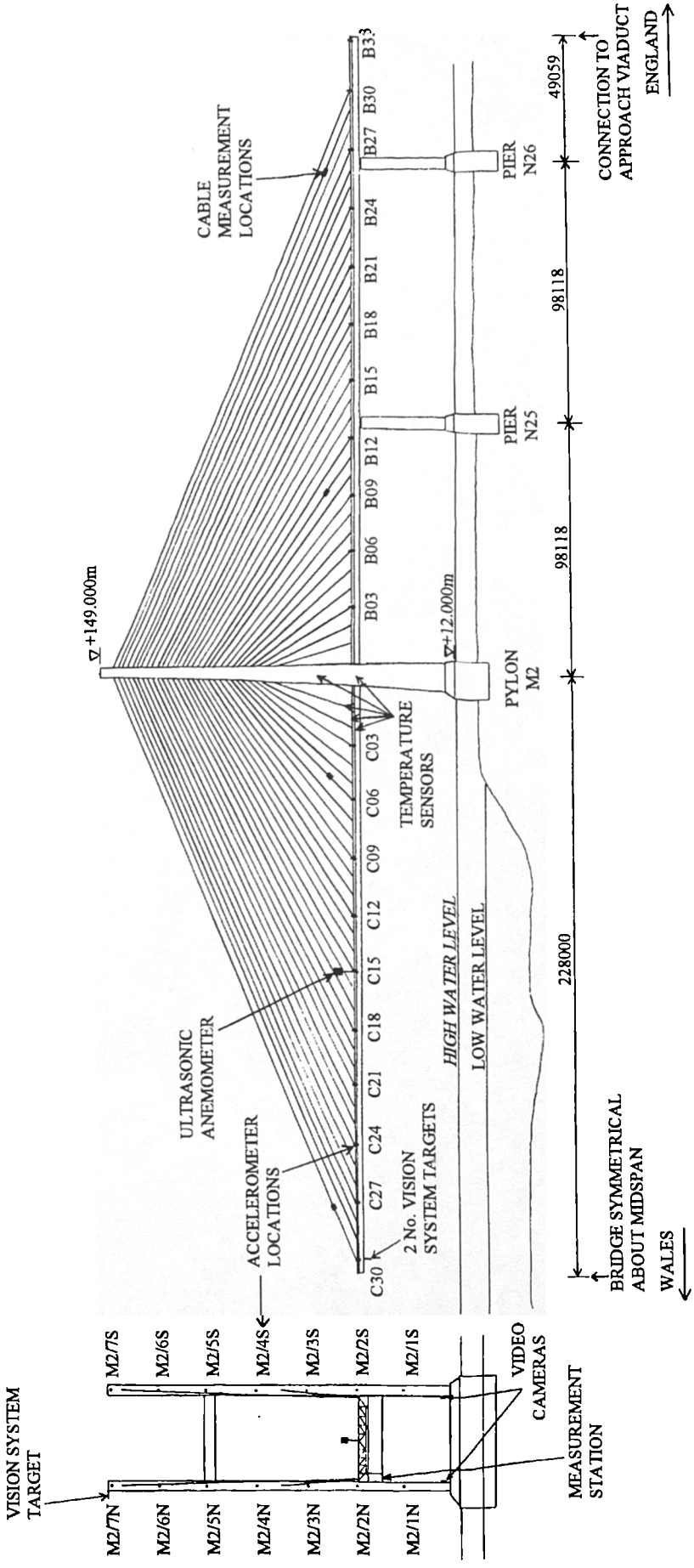

Fig. 4-15 Instrument locations on M2 completed cantilever

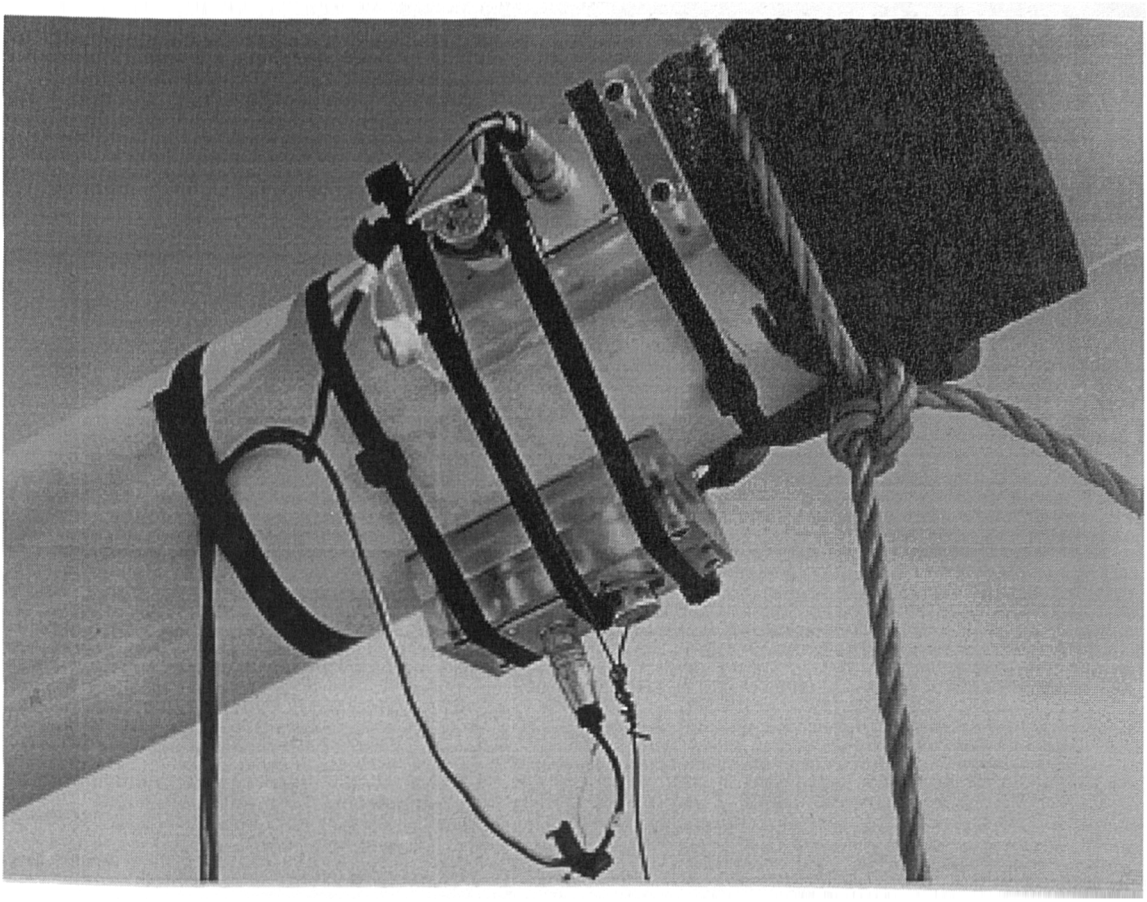

Fig. 4-16 Accelerometers mounted on cable to measure in-plane and out-of-plane vibrations

CHAPTER 5 SYSTEM IDENTIFICATION FROM AMBIENT VIBRATION DATA AND ESTIMATION OF ERRORS

5.1 Introduction

The vibration and wind data collected from the Second Severn Crossing (SSC) site (Chapter 4) required processing to extract the desired results. The primary parameters of interest in dynamic testing are the natural frequencies, damping ratios and mode shapes of vibration, the most difficult of which to extract accurately are the damping ratios. This chapter reviews the methods available for the analysis of ambient vibration data and introduces the basic method adopted for the SSC data processing. Developments of the method, to overcome deficiencies of standard techniques, are presented in Chapter 7.

The sources of errors in the measurement of site data and in the estimation of Power Spectral Densities (PSDs) are also discussed in this chapter, along with a method for testing the stationarity of the data for spectral analysis. The errors are quantified for the SSC data, giving an indication of the accuracy of estimated spectra used to obtain the results that are presented in Chapter 8.

5.2 Background to data processing

Before discussing methods of data analysis, it is necessary to give an outline of the modal analysis approach, to identify the parameters being sought, and to define some of the terms used in this thesis relating to spectral analysis.

5.2.1 Modal analysis

The basic theory of structural dynamics is covered in the standard texts (e.g. Clough & Penzien 1993, Craig 1981). For a linear system, the total response can be described by the superposition of modal responses, through the well-established field of modal analysis (Ewins 1984).

The response in each mode is characterised by its modal parameters, namely the natural frequency, damping, mode shape and amplitude (§2.4.2). 'System Identification' aims to estimate these parameters, based on measured data, for the modes that provide a significant contribution within the frequency range of interest. This can be used simply to describe the dynamic behaviour, or to validate or update analytical models describing the system (§2.4.3&2.4.4).

5.2.2 Spectral analysis and stationarity

For random signals, such as wind loading or bridge response, the average frequency content is described by the Power Spectral Density (PSD) (also known as the autopower spectral density), and the relationship between two signals, including the relative phase, is given by the Cross Spectral Density (CSD). These are most efficiently estimated from recorded time histories via the Fast Fourier Transform (FFT).

The output (response) PSD of a Single-Degree-Of-Freedom (SDOF) system subject to random excitation is given by:

$$S_{yy}(f) = |H(f)|^2 S_{xx}(f) \tag{5-1}$$

where: f = frequency

$S_{xx}(f)$ = PSD of input (excitation)

$H(f)$ = Frequency Response Function (FRF) of the system

For the r^{th} mode of a structure, represented by a viscously damped SDOF oscillator (§2.4.2), the FRF relating generalised force input to generalised modal displacement output is given by:

$$\mathrm{H}_r(f) = \frac{1}{M_r(2\pi f_r)^2\{1-(f/f_r)^2 + 2\zeta_r(f/f_r)i\}} \tag{5-2}$$

where: $f_r = \omega_r/2\pi$ = natural frequency of the mode

ζ_r = modal damping ratio

M_r = generalised mass (equation (2-3))

$i = \sqrt{-1}$

The strength of a relationship between two random signals, either an input and an output or, in the case of ambient vibration tests, two outputs measured at different locations, is measured by the coherence, given by:

$$\gamma_{xy}^2(f) = \frac{|S_{xy}(f)|^2}{S_{xx}(f)S_{yy}(f)} \tag{5-3}$$

where: $S_{xy}(f)$ = CSD between signals x and y

The coherence is real and can have values in the range zero (uncorrelated) to one (fully correlated).

In spectral analysis it is assumed that the statistical properties of the signals do not vary from one block of data to another. This property is known as stationarity (or strictly, ergodicity, if the records are from different times). Clearly site measurements on a bridge are not stationary, since the wind and other loads vary significantly, but for periods of up to a few hours the loading is often treated as stationary. This issue is revisited in §5.6.4, where the stationarity test used for this study is described.

5.3 Review of system identification methods

There are many system identification methods available for the estimation of modal parameters from measured data. However, for ambient vibration data the choice is more limited and assumptions need to be made about the loading. This section reviews the available methods and their shortcomings, leading towards the development of a new method to overcome some of the limitations (Chapter 7).

5.3.1 Limitations of ambient vibration data for system identification

The normal experimental approach to the system identification problem is to excite the structure with known loads and to measure the responses at certain locations. Thus the modal parameters can be extracted from the resulting FRFs, or by equivalent techniques in the time domain. An extensive review of system identification methods is given by Maia et al. (1997). However, the majority of these methods requires the input as well as the output to be known, from which the true FRF, including its phase information, can be ascertained. For example, one of the most commonly used techniques involves fitting a circle to the FRF in the argand plane (Ewins 1984).

For full-scale dynamic testing, ambient loading is often relied upon for the excitation (§2.3), as was the case for the SSC main tests (Chapter 4). For such tests, since the loading is not measured, the true FRF cannot be found, so only limited techniques are available for the analysis of the data. In addition, some assumption of the loading characteristics must be made. Usually a white noise loading spectrum is assumed, which may be reasonable over a narrow frequency range, but it can give significant errors if the total response over a wider range is considered (§7.6). Also, since the loading is random, it is not always possible to distinguish between effects of variations in the loading and characteristics of the structural behaviour. Only by considering the average characteristics of the response over a significant period can reasonable estimates of the modal parameters be obtained.

Generally, for cable-stayed bridges the natural frequencies are well spaced and the damping is low, so the natural frequencies are clearly defined. They can be estimated from records of only a few minutes duration, although longer records lead to higher accuracy. However, the damping is more difficult to determine accurately, so records at least an hour long are required. Other problems become apparent for long records, such as non-stationarity of the loading or variations of other parameters, such as temperature.

Although this discussion refers to frequency domain data, the same limitations apply whichever system identification method is used, since they are due to fundamental properties of the measured data.

5.3.2 System identification methods for ambient vibration data

Although the number of methods available for system identification from ambient vibration data is relatively limited, several techniques have been proposed over the last two decades. They can be classified as frequency domain or time domain methods, which are now considered separately.

5.3.2.1 Frequency domain methods

Frequency domain system identification methods can also be classified as Single-Degree-Of-Freedom (SDOF), in which the resonance around each natural frequency is treated in isolation, or Multiple-Degree-Of-Freedom (MDOF), in which case all of the modes are considered simultaneously. SDOF methods are addressed first.

The simplest method for extracting modal parameters is the Peak Picking (or Peak Amplitude) and Half Power Bandwidth (HPB) Method (Bishop & Gladwell 1963). The estimated natural frequencies are simply the frequencies in the response PSD at which maximum responses occur. The mode shapes can be estimated from the relative amplitudes of response at different points on the structure. The damping ratio is obtained from the HPB Method, based on the width of the resonant peak:

$$\zeta \approx \frac{(f_2 - f_1)}{2f_n} \tag{5-4}$$

where: f_n = natural frequency

f_2 and f_1 = frequencies above and below f_n at which the PSD is half the peak value, assuming the loading spectrum to be white noise over the HPB.

This it is the most commonly used method for ambient vibration analysis due to its simplicity, and since other common methods, for which the force must be known, are not

applicable. A disadvantage is that it is based on spectral values at only three discrete frequencies (or five if interpolation of the half power points is used), each of which is subject to a variance error (5.6.2).

An improved method is to fit a curve corresponding to the response of an SDOF system, assuming white noise loading, to the measured PSD in the vicinity of each peak. This uses more spectral points, so more accurate results can be obtained. The method is well established and has been used for several ambient vibration studies of bridges (e.g. Brownjohn 1988, Owen & Blakeborough 1993, Gentile et al. 1997). An iterative numerical procedure is usually needed for the curve-fitting, but a variation of the method, approximating the square root of the PSD to a parabola in the vicinity of each peak, was adopted by Jones & Spartz (1990), enabling direct calculation of parameters for the best fit.

These SDOF methods assume each mode can be treated in isolation, ignoring the contributions of other modes, generally leading to an overestimation of the damping.

An MDOF method applicable to ambient vibration data is the Frequency Domain Prony Method (Brittingham et al. 1980), based on the fact that the theoretical response PSD can be expressed as the ratio of two polynomials in $(i\omega)^2$ ($\omega = 2\pi f$ = circular natural frequency), assuming a white noise input. The modal parameters are obtained from the coefficients of the polynomials for the best fit to the measured PSD. Another similar MDOF method is the Transfer Function Real Condensation Method (Chatelet & Piranda 1995).

As MDOF methods, these require an estimate of the number of modes present. The results are sensitive to this estimate, and true modes can be missed or the results can include erroneous additional modes. Another problem with MDOF methods is that the assumption of white noise loading becomes less valid as a wider frequency range is considered, particularly for wind loading (§7.6).

A variation on using individual PSDs from measurements at different locations on a structure is the use of the Averaged Normalised Power Spectral Density (ANPSD) introduced by Felber & Ventura (1996). The ANPSD contains information from all of the measurement points, but if the measurements are not taken simultaneously, as is often the case for modal surveys of large structures, no account is taken for differences in loading spectra or modal parameters.

Jones et al. (1995) proposed an alternative method, based on the iterative application of a Kalman filter to the PSD, and tested it on simulated data of an SDOF system. It is also potentially able to estimate the parameters of the loading spectrum based on an assumed model, but it is yet to be applied to site data.

The major problem with all frequency domain methods based on the FFT is that the damping ratios tend to be overestimated due to bias errors (§5.6.1), with the results being sensitive to the frequency resolution of the PSD.

An alternative to the FFT for estimating the PSD is the Maximum Entropy Method. This can give smoothed spectral estimates at any frequency resolution, with reduced bias errors (Campbell & Vandiver 1982). It was used, along with the Peak Picking and HPB Method, by Rodrigues & Campos-Costa (1998) for the ambient vibration analysis of two bridges. It is effectively based on a time domain method similar to the ARMA method (§5.3.2.2), so has the same shortcomings.

5.3.2.2 Time domain methods

Time domain system identification methods are generally MDOF methods, although, if the modes are well separated, the time history can be filtered and treated as an SDOF response. This is the basis of the Logarithmic Decrement Method (§10.3.1), for which the damping is given by the rate of decay of free vibrations of a single mode, after the termination of excitation.

In the normal MDOF case, an estimate of the number of modes is required, as for frequency domain MDOF methods. The results are dependent on the estimate, so this is one of the main drawbacks of these methods.

Gersch et al. (1973) developed the Auto-Regressive Moving-Average (ARMA) method, which has been applied to bridge vibration data (Giorcelli et al. 1996, Jensen et al. 1999). It is a time series model in which the present output is a linear combination of its own past and that of the input. The modal parameters are given indirectly by the coefficients of the model. Non-stationary data can give erroneous results, but a method for dealing with mildly non-stationary data, by splitting the record into a series of short records each assumed stationary, was developed by Gersch & Martinelli (1979). Peeters & De Roeck (1998) used a related method, but using state space parameters, for the system identification of a telecommunications mast.

Another similar method, based on a series describing the autocorrelation function, is the time domain Maximum Entropy Method, applied by Campbell & Vandiver (1982) to the analysis of offshore structures. Estimation of damping by this method is equivalent to the HPB method.

The Random Decrement (RDD) Method (Cole 1968), has also been applied to ambient vibrations of bridges (Asmussen et al. 1998). This is based on averaging sections of the time histories, triggered, for example, by crossings of a threshold value, to obtain an estimate of the free decay response. Standard time domain techniques, such as the Ibrahim Time Domain Method (Ibrahim & Mikulcik 1977) or the Polyreference Complex

Exponential (PCE) Method (Vold & Rocklin 1982) can then be used. A difficulty of the RDD Method is the optimum selection of the trigger.

James et al. (1996) developed the Natural Excitation Technique and applied it to data from various structures, including a bridge (Farrar & James 1997). It is based on the calculation of auto and cross-correlation functions of measured responses, equivalent to free vibration responses. The parameters can therefore be extracted by free decay methods, as for the RDD Method. The PCE Method and the Eigensystem Realisation Algorithm (Juang & Pappa 1985) have been used in this case.

All of the above MDOF time domain methods assume a white noise input, which is not a good model of wind loading (§7.6). A development of the ARMA and RDD Methods by Ibrahim et al. (1996) has considered filtered white noise loading, but it has yet to be applied to site data.

5.3.2.3 General comments on system identification from ambient vibration data

A different system identification approach, to estimate values in the stiffness matrix directly, was used by Torkamani & Ahmadi (1988) on ambient vibration data from a tall building during construction. However, the use of direct methods for ambient vibration tests are limited to structures which can be represented by Finite Element (FE) models with few degrees of freedom, so they could not be reliably applied to a cable-stayed bridge.

Despite the large number of methods available, there have been few comparisons between them, particularly for ambient vibration data. One study of three methods (Brincker et al. 1996) found estimated natural frequency to be in close agreement, but the difficulty of accurately estimating damping was highlighted, as were problems due to non-stationarity and erroneous computational modes for MDOF methods.

In summary, the principal shortcomings of system identification methods for ambient vibration data are:

i) For frequency domain methods based on the FFT, overestimation of damping ratios due to bias errors (§5.6.1).

ii) Inappropriateness of the assumption of white noise for wind loading, particularly important for MDOF methods.

iii) For SDOF methods, neglect of the contributions of other modes.

iv) For MDOF methods, estimation of the number of modes, leading to the omission of modes or the identification of erroneous additional modes.

The need to overcome these deficiencies led to the development of an improved method, based on curve-fitting of PSDs (Chapter 7), overcoming bias errors (§7.4), allowing for a specific assumed loading spectrum (§7.6), and dealing with the combined response of several modes (§7.7).

5.4 System identification approach for main Second Severn Crossing tests

The approach to the system identification of the SSC was the two-stage process of estimation of PSDs from the measured time histories, followed by application of the improved curve-fitting method (Chapter 7). The advantages of the conventional PSD curve-fitting method (§5.3.2.1), maintained for the improved method, include:

i) Its proven track record.

ii) User control over initial estimates of natural frequencies.

iii) Well defined estimation of errors on PSDs.

iv) The ability to overlay fitted and measured spectra to visually check the quality of the match and to identify discrepancies.

v) The ability to selectively eliminate non-stationary sections of data.

The curve-fitting method was suitable for the developments described in Chapter 7, since a realistic loading spectrum could be defined in the frequency domain (§7.6), and the effects of bias errors and the combination of modal responses could be determined.

Before curve-fitting can be performed, the PSD of the response needs to be found. The estimation of this and other spectral properties of random data are covered in the standard texts (Bendat & Piersol 1986, Newland 1975).

The following sections focus on the sources and minimisation of errors, both in the measurements (§5.5) and the spectral calculations (§5.6). The discussion here is specific to the analysis of the SSC data, so initial estimates of its modal parameters are used to quantify errors, and values of signal processing parameters suitable for this application are determined. The estimation of PSDs is of primary interest here, but similar processes and errors are involved in the calculation of CSDs.

The measured vertical (or longitudinal) accelerations on each side of the deck and pylon were first added and subtracted, to separate the pure bending and torsional responses

5.4.1 Typical spectra of measured vibrations

Typical PSDs of the ambient vertical accelerations of the SSC deck, for both the completed M2 cantilever (§3.2.2) and finished bridge, are shown in Fig. 5-1. These are provided to give an indication of the typical response for the sake of the following

discussion on errors. The wind conditions for the two records were similar, but the finished bridge also experienced traffic loading (§6.6). The first natural frequencies in the two cases were very close, at approximately 0.33Hz, while the frequency range of interest, covering more than 40 global modes (§3.3.5&6.2.3), was up to 5Hz. Clear peaks are evident in the spectra, indicating well-defined modes with low damping. Therefore, as a first approximation, most modes can be considered independently. Initial curve-fitting (§7.3) indicated that the damping ratios were typically around 0.5%. For the cantilever, the ratio between successive natural frequencies of modes of a particular type (e.g. deck vertical) was typically 1.4:1, but for the finished bridge they were generally closer together, at around 1.2:1.

5.5 Measurement errors

Various errors can occur during data acquisition, some of which may be eliminated at the signal processing stage, but others may not. Care in the selection of equipment and experimental techniques (Chapter 4) is required to minimise these errors. This section deals principally with accelerometer measurement errors on the SSC, but some issues also relate to other instruments.

The first point in the measurement chain at which errors may occur is at the measurement instrument. Accelerometers have a resonant frequency which dictates an upper limit to their useable frequency range, but for the accelerometers used on the SSC (§4.3.1(i)) this was above 300Hz, so the errors at the low frequencies measured were negligible. At the low frequency end, which is of more importance, accelerometers are limited by their measurement resolution since the accelerations are so low. The instruments used had a measurement resolution threshold of 1μg, approximately 0.05% of the typical accelerations of the deck in light winds.

The accelerometers were calibrated with an accuracy of ±2.5% at a series of frequencies, but the variation over the range 1-5Hz was less than 3%, while the gain of the accelerometer amplifiers was found to be accurate to within 1%. The signals from each channel were multiplied by their appropriate calibration factors (at 1Hz) at the signal processing stage. The other instruments were also calibrated, or referred back to the manufacturer's calibration with known tolerance (§4.3.1).

Noise could be picked up on the long signal cables to each instrument, so it was minimised by using shielded cables and appropriate electrical signals (§4.3.2). Filters eliminated high frequency noise and any aliasing of frequencies above the Nyquist frequency (§4.3.2). The EF40 filters attenuated the signals (Fig. 4-6), so a correction was made at the signal processing stage, but the EF6 filters had built-in amplifiers, so they did not cause any attenuation in the frequency range of interest.

Both Analogue to Digital Converter (ADC) boards (§4.3.2) had a resolution of 12 bits, i.e. $2^{12} = 4096$ distinct levels. Therefore, if the full range was used the quantisation error would be 1/2/4096 = 0.012%. However, to try to ensure that the maximum signals did not exceed the range of the board, a smaller range was used in practice. This was particularly important for the long-term tests, since the amplitude of signals could vary significantly over the data acquisition period, so sometimes the active range was only about ±0.1V, compared with the full range of ±5V. Thus the quantisation error was increased to 1/2/4096x5/0.1 = 0.6%.

Occasionally the range of the ADC board was exceeded, so, before further processing, blocks of data during which the signal reached the upper or lower limit were discarded.

Slight differences between the accelerometer signal conditioning units introduced relative time lags between the signals, which would give apparent phase differences. The phase difference of each channel relative to a reference Setra accelerometer was recorded in the calibration tests (4.3.1(i)). In all cases it was found to be linear with frequency, indicating a constant time delay. The maximum delay between any two channels was 0.0035s, corresponding to a phase lag of 1.24°/Hz. Therefore, for the range of frequencies of interest (0-5Hz), the phase difference was a maximum of 6.2°. Below 2Hz, or comparing any other pair of channels, the phase difference would be significantly less (typically 1.5°), so no correction was deemed necessary. The anti-aliasing filters of each type had very similar phase responses to each other, so again no correction was necessary.

When the DT2821 ADC board was used, sampling was not simultaneous, so again there would be an apparent phase difference between acquired data channels. The channels were sampled at equal intervals within the 0.04s (i.e. 1/25Hz, §4.3.2) for a full set of samples. Since 16 channels were recorded, the time delay between successive channels was 0.04/16 = 0.0025s. The channels to be compared with each other were up to 4 channels apart, so the maximum time delay was 0.01s, corresponding to a phase difference of 7.2° at 2Hz. Where necessary, this phase difference was removed when considering the phase between channels (§7.8&10.7.2).

Another source of error of the measured signals was low frequency drift of the DC component of accelerometer signals, due to electrical instability of the offset compensation circuit, particularly affected by temperature and humidity. Usually this effect was not perceptible, but potentially it could appear as a low frequency component in the spectral estimates. To reduce the effect of this, the linear trend was removed from each accelerometer time history for each block of data, leaving only the dynamic components. This also removed the remaining arbitrary DC level due to the orientation of the instrument, after only approximate elimination on site by the offset compensation circuit (§4.3.1).

Since the accelerometers were sensitive to the component of gravity acting in their direction of measurement, rotation of the instruments in a vertical plane would give an apparent acceleration. This would occur with torsional vibrations of the deck, for which the error in the vertical acceleration reading at the edge of the deck can be shown to be approximately:

$$\varepsilon = \frac{g\alpha_{\max}}{\omega_n^2 B} = \frac{2ga_{\max}}{\omega_n^2 B^2} \tag{5-5}$$

where: g = acceleration due to gravity

α_{max} = maximum torsional rotation of the deck

a_{max} = maximum vertical displacement of the edge of the deck due to torsion

ω_n = circular natural frequency

B = deck width.

For the worst case likely to be experienced on site for this bridge, $a_{max} \approx 0.1$m, $\omega_n = 2\pi$ x $0.33s^{-1}$ and $B = 35$m, giving $\varepsilon = 0.037\%$. Therefore the effect of rotation for vertical accelerometers on the deck can be disregarded.

For lateral accelerometers on the deck, torsional deck motion would give an erroneous reading of an acceleration of approximately:

$$\ddot{x}_{err} = g\alpha = \frac{2ga}{B} \tag{5-6}$$

where: α = torsional rotation of the deck

a = vertical displacement of the edge of the deck due to torsion

Thus, torsional vibrations of circular frequency ω_n and acceleration amplitude $\ddot{a}_{\max}$ at the edge of the deck, would give an apparent lateral acceleration amplitude of:

$$\ddot{x}_{err,\max} = \frac{2g\ddot{a}_{\max}}{\omega_n^2 B} \tag{5-7}$$

In the worst case of the lowest natural frequency (0.33Hz), this gives the erroneous impression of lateral vibrations of 13% of the amplitude of the torsional vibrations. Therefore, when considering the response of the lateral accelerometers this error was taken into account.

For the pylon accelerometers, which were orientated horizontally, rotations in the vertical planes would give similar errors. Since the rotations were not measured, the readings were taken to be only due to the horizontal accelerations, resulting in slight errors in the mode shapes at these points, particularly for low frequency modes. However, other estimated modal parameters would not be affected.

For the accelerometers mounted on the cables, tilting would cause errors in the measured accelerations of in-plane modes. For a typical cable, based on a half sine assumed mode shape for the first mode, with the instrument mounted approximately 10m above the deck, the error is approximately 2%. For a given measurement location and vibration mode, the error is constant in percentage terms, so measurements of natural frequencies and damping parameters would not be affected.

Finally, misalignment of the accelerometers would cause a component of acceleration in an orthogonal direction to be measured. Estimating the alignment to be accurate to within 2° of the desired orientation, the maximum erroneous measurement would be 3.5% of the orthogonal acceleration. This was most significant for the lateral accelerometers, since the vertical acceleration was generally greater (§8.6.5). The error for other accelerations would be significantly lower.

5.5.1 Estimation of signal to noise ratio for accelerometer signals

The significance of noise on the measured accelerations was estimated by considering the signals from two accelerometers placed on the bridge deck immediately adjacent to each other, in typical conditions of moderate wind. The actual acceleration could be considered to be identical for the two instruments, so the difference between the signals gave a measure of the noise. This would include errors from the instruments, signal conditioning units and filters, noise picked up on the instrument cables, and quantisation errors from the digitisation of the signals.

The Root Mean Square (RMS) values of the two signals agreed within 1%, which was consistent with the calibration tests on the accelerometer amplifiers. The coherence between them is plotted in Fig. 5-2. Only one file, of 164s duration, was recorded with the two accelerometers adjacent, so there is considerable variance of the frequency-dependent results due to limited spectral averaging (§5.6.2). However, below 6Hz the coherence was consistently above 0.9, with it often being above 0.99. This gives a measure of the maximum level of coherence that could be expected between any two accelerometer signals on site when considering the relative responses of different parts of the structure. At higher frequencies the coherence drops, largely due to the reduction in the signal amplitude.

Assuming that the noise on the two signals was uncorrelated and had equal variance, an estimate of the noise on one signal is given by $1/\sqrt{2}$ of the difference between the two measured signals. On this basis, the PSD of the noise was calculated, along with the PSD of the actual acceleration, estimated as the mean of the two signals (Fig. 5-3). The noise showed no great difference in amplitude with frequency, in contrast with the acceleration itself. At higher frequencies, the drop in measured acceleration amplitude, in part due to the filtering, increased the significance of the noise.

The amplitude of the noise relative to the signal can be expressed as the ratio of their RMS values. On this basis the noise is 7.3% of the signal (i.e. Signal to Noise (S/N) ratio of 23dB), however this does not take into consideration the reduced significance of the noise at lower frequencies, which are of greater interest.

Another measure of the amplitude of the noise in relation to the signal is given by the magnitude of the 'pseudo-FRF' between them (Fig. 5-4). The increased significance of the noise at higher frequencies is clear. Below 5Hz the average noise is 4.0% (S/N ratio 28dB), whereas below 2Hz it is 1.9% (S/N ratio 34dB).

For the data file considered, the maximum signal amplitude was ±0.35V (7% of the ADC board range), giving a quantisation error of 0.17%, which would be typical. The S/N ratio would also be influenced by the amplitude of accelerations and instrument cable lengths.

The acceleration measurement errors for the SSC tests are summarised in Table 5-1. Since the noise was measured on site using the full instrumentation chain, it includes other errors from this chain, so it gives a realistic estimate of the total of these errors for typical measurements. Corrections for the errors from other sources could be made, if necessary.

5.6 Estimation and limitation of errors in spectral estimates

The PSDs of the random vibrations were estimated from the measured SSC time histories. Bendat & Piersol (1986) provide details of the calculations, and of the origin and estimation of errors. This section discusses the errors as related to the SSC data, and the values of processing parameters required to obtain accurate estimates of the PSDs for subsequent curve-fitting.

Table 5-1 Summary of acceleration measurement errors for SSC tests

Source of error	Estimated error	Comments
Accelerometer measurement resolution	0.05%	Max. for typical accelerations
Accelerometer calibration	2.5%	Max.
Accelerometer amplifier gain	1%	Max.
Quantisation	0.6%	Max. in practice
'Noise' (including above errors)	4.0% below 5Hz 1.9% below 2Hz	Typical
Filter phase lag	1.24°/Hz	Max.
DT2821 ADC phase lag	3.6°/Hz	Max. between accelerometers. Corrected when necessary
Vertical deck accelerometer rotation	0.037%	For torsional vibrations
Lateral deck accelerometer rotation	13% of torsional amplitude at edge of deck	Max. at 1st torsional frequency. Decreases with frequency
Cable accelerometer rotation	2%	Typical for in-plane vibrations
Accelerometer misalignment	3.5% of acceleration in orthogonal direction	Max. expected. Significant for lateral deck accelerations

There are two types of errors in spectral analysis:

i) Bias errors, which are systematic errors from the method of signal processing.

ii) Variance errors, which result from the random nature of the vibrations and finite length of the measured signals.

For clarity of the following discussion, the following terms are defined:

Record — The recorded time history of the signal for which the PSD, and subsequently modal parameters, are to be calculated.

Block — Sub-divisions of the record for individual processing.

File length — The standard length of files recorded in the long-term tests on the SSC, equal to 4096 ($=2^{12}$) samples at 25Hz, i.e. 163.84s (§4.3.2).

The PSDs were calculated via the FFT, for which the blocks need to be 2^m samples long, where m is an integer. For this process the recorded files could be sub-divided or concatenated into blocks of various lengths.

5.6.1 Bias errors

Bias errors occur at spectral peaks, due to the discretisation of the spectrum. Each discrete value is representative of the PSD over a certain frequency range, resulting in a reduced peak value (Fig. 5-5). The error at a peak, relative to the actual spectral value, is given by:

$$\varepsilon_b \approx \frac{B_e^2 S_{yy}''(f)}{24 S_{yy}(f)} \approx -\frac{1}{3}\left(\frac{B_e}{B_r}\right)^2 \qquad (5\text{-}8)$$

where: $S_{yy}(f)$ = true PSD

$S_{yy}''(f)$ = second derivative of $S_{yy}(f)$ with respect to frequency

B_e = frequency resolution = $1/T_e$, where T_e = length of each block

B_r = HPB of the resonant peak

the second approximation only holds for $B_e/B_r << 1$

For an SDOF system, B_r is given approximately by $2f_n\zeta$, so, for a given damping ratio, the error is greater for lower frequency modes. It can be reduced by improving the frequency resolution, i.e. by using longer blocks.

Bias errors are increased by leakage - the phenomenon of spreading of the spectral content for frequency components which do not fit precisely into the finite length of the block. The effect can be reduced by multiplying the time history by a 'window' weighting function, which reduces the signal to zero (or near zero) at the ends. However, the window leads to a certain amount of leakage, even for the frequencies which are periodic within the record length. The application of windows and the characteristics of a range of alternative window functions are discussed by Harris (1978).

The Hanning window is the most commonly used window function, and was employed in the estimation of the measured spectra for the SSC. Its effect in the frequency domain is discussed in §7.4.2.

Bias errors spread peaks in the PSD, leading to overestimation of the damping. This can be particularly important for the lowest natural frequencies of long-span bridges (Littler 1992).

5.6.2 Variance errors, spectral averaging and overlapping of blocks

Variance errors arise from the random nature of the data. The long-term average statistical properties of a signal are defined by its PSD. However, the PSD estimated

from a finite length record differs from the true PSD, with the standard error on each spectral value given by:

$$\varepsilon_r = \frac{1}{\sqrt{B_e T}} \tag{5-9}$$

where: T = length of the record

For FFT analysis of a single block, $B_e = 1/T$ so the standard error is unity. It can be reduced, although at a loss of frequency resolution, by spectral averaging by:

i) Frequency smoothing, which is performed by averaging several adjacent spectral values, thus increasing B_e, or;

ii) Segment averaging, which involves splitting the original record into a series of blocks, calculating the PSD of each, and averaging them. Thus B_e is then based on the individual block length whereas T is still the original record length. The error then becomes:

$$\varepsilon_r = \frac{1}{\sqrt{n}} \tag{5-10}$$

where: n = number of blocks into which the original record is split

The effect of segment averaging is shown in Fig. 5-6.

Segment averaging is preferable for ambient vibration data, since the blocks need not necessarily be contiguous. Thus, individual blocks containing non-stationary data can be eliminated (§5.6.4). Also, the shape of the window function in the frequency domain (§7.4.2) is not affected, and overlapping of blocks can be used.

Overlapping of blocks, for continuous data, creates more blocks for a given record length, so reduces variance errors (Welch 1967, Carter & Nuttall 1980). This is particularly beneficial for 50% overlapping when using the Hanning window. There is little additional benefit in greater overlapping.

Harris (1978) gives a formula, based on the work of Welch (1967), to estimate the variance errors of spectral estimates using overlapped blocks and various window functions. For 50% overlapped blocks and the Hanning window, this reduces to:

$$\varepsilon_r \approx \frac{1.028}{\sqrt{n}} \tag{5-11}$$

where: n = total number of blocks

Comparing this with equation (5-10), the additional overlapped blocks are almost as beneficial as additional independent blocks. For a given record length, since n is almost doubled, the error is reduced by a factor of approximately 1.4.

5.6.3 Total error on estimated spectra

The total standard error for each spectral value of the estimated PSD is given by:

$$\varepsilon^2 \approx \varepsilon_b^2 + \varepsilon_r^2 \tag{5-12}$$

where: ε_b = bias error, including the contribution from leakage

ε_r = variance error, after spectral averaging and overlapping

The variance error is proportional to $1/\sqrt{n}$ (equation (5-11)), whereas the peak bias error is proportional to $B_e^2 = 1/T_e^2 = n^2/T^2$ (equation (5-8)). Therefore, for a given total record length, T, the variance error is reduced by sub-dividing it into a greater number of blocks, whereas the bias error is increased. Therefore, for conventional spectral processing, a compromise has to be reached for the number of blocks to minimise the total error (Daniell & Taylor 1999).

Table 5-2 shows the estimated errors for SSC data, for a record length of just under three hours (64 consecutive files). The variance errors are calculated based purely on the number of blocks, whereas the bias errors are also based on estimated parameters of the first mode of the structure (0.33Hz, damping 0.5%). For higher frequency modes with similar damping values, the bias errors will be lower. For this example, the optimum block length is equal to four concatenated files (10min 55s), giving a total error in the spectral values of 19%. This error is still relatively large, but based on conventional processing, it can only be reduced by increasing the record length. For practical cases this runs into difficulty since the loading may cease to be stationary and other parameters, such as temperature, may vary over the longer period.

The trade-off between bias and variance errors can be avoided using the improved curve-fitting method developed in §7.4, which eliminates the effect of bias errors, leaving only the variance errors. Thus, shorter blocks can be used to obtain more accurate estimates, although a longer total record length is always beneficial.

Table 5-2 Estimates of errors in PSD for 175min record for mode with natural frequency 0.33Hz and damping 0.5%

No. of files concatenated per block	Block length, T_e (min:s)	Variance error (overlapping blocks) (%)	Bias error (excluding leakage error) (%)	Total error (excluding leakage error) (%)
1	2:44	9.1	-114*	114
2	5:28	13	-29*	32
4	10:55	18	-7.1	19
8	21:51	27	-1.8	27
16	43:41	39	-0.45	39

* Estimates of bias errors become inaccurate for large errors

When considering the relative response of two parts of the structure, bias errors are present in both PSDs. However, near peaks, usually one mode is dominant and the shapes of the two PSDs are similar. Therefore, the bias errors (including those from leakage) will be similar, so the relative magnitudes of the spectra will not be significantly affected. Thus, for a given record length, shorter blocks again give more accurate results. Furthermore, the variance errors will to some extent be cancelled out since they are due to the same random load. Therefore, for comparison of the response amplitude of two points, shorter records are required than for the accurate estimation of natural frequencies and damping from a single PSD.

5.6.4 Elimination of non-stationary records – Run Test

The calculation of the PSD assumes that the signal is stationary (§5.2.2). Ambient vibration data are often considered to be stationary, but this should be checked. Errors can occur if non-stationary data is processed. For example, variations in the natural frequency of a mode from one block to another would cause broadening of the peak of the averaged spectrum, leading to an overestimate of the damping (Brownjohn 1994).

Stationarity of the SSC data was tested by a Run Test (Kendall & Stuart 1973) of the mean square values of consecutive data blocks (Bendat & Piersol 1986). A significance level of 5% was chosen to give a meaningful test, but without rejecting a significant amount of stationary data unnecessarily.

The Run Test was preferably used at two different levels. It was applied to each block, divided into sub-blocks for the calculation, to confirm the validity of the PSD for the block. Hereafter this is referred to as the 'self-stationarity test'. If a block was found to be non-stationary, it was eliminated from further processing, following the approach of Daniell & Taylor (1999). Then, for the remaining blocks, the Run Test was used again to check the stationarity of the overall record, to confirm that the blocks represented signals

from the same stationary process, so that averaging of the spectra was valid. This is termed the 'overall stationarity test'.

Stationarity tests on SSC accelerometer records found that the results depended on the length of blocks and number of sub-blocks, as well as the significance level chosen. The sub-blocks had to be sufficiently long to contain several periods of the fundamental frequency so that the mean square values would not vary significantly due to these vibrations. It was found that sub-blocks of at least 40s (i.e. approx. 13 times the fundamental period) gave more consistent results. For the self-stationarity test to be meaningful at a 5% level of significance, a minimum of 16 sub-blocks were required (using only powers of two), since for eight sub-blocks no blocks would be rejected. If more than 16 sub-blocks were used, a greater proportion of blocks was rejected. This showed that the results of the Run Test were not particularly consistent. However, it could be assumed that the blocks that were rejected in all cases were those which exhibited the most non-stationary characteristics. Also, it was desirable to use short blocks to reduce variance errors by segment averaging. Therefore, the preferred blocks were equivalent to four files long (i.e. 16384 samples, 655.36s) divided into 16 sub-blocks (each 1024 samples, 40.96s), to give a meaningful stationarity test with the shortest reasonable block length. In this case typically 75% of the blocks passed the self-stationarity test at a 5% level of significance.

For the overall stationarity test, again a minimum of 16 blocks were required for a meaningful check, giving a total record length of almost three hours. It was found that the Run Test was normally passed at the 5% level of significance using continuous records of this duration. For longer periods, the loading conditions would change, so the records ceased to be stationary. To attempt to overcome this, blocks were grouped together from different periods, but with the wind speed and direction within narrow ranges (2m/s, 30°), as performed by Littler (1992). However, in most cases the resulting ensemble of blocks was found to be non-stationary, presumably due to differences in the wind turbulence, traffic loading, temperature or other factors. Therefore, it was preferable to process single three-hour records to achieve stationarity.

Shorter records, for example from the half-hour modal survey tests, were insufficiently long to be able to perform meaningful stationarity tests at both levels. Therefore, only the overall stationarity test was performed and, if passed, it was taken to indicate stationarity of the whole record.

5.7 Conclusions

Methods of system identification from ambient vibration data have been reviewed. Fewer methods are available than for forced vibration data, and an assumption of the loading

spectrum is required. Shortcomings of the methods previously used include overestimation of damping due to bias errors, inappropriate assumption of a white noise loading spectrum, and difficulties of correctly identifying or accounting for multiple modes. An improved method is developed in Chapter 7 to address these issues. It is then applied to the data recorded on the SSC in Chapter 8.

The first stage of the improved method is conventional estimation of PSDs. The errors in PSD estimates have been discussed, with particular reference to the SSC data. Both measurement errors (Table 5-1) and spectral estimation errors (Table 5-2) have been quantified. A method for the elimination of non-stationary data has also been described, to ensure that the estimation of PSDs is valid. The overall procedure for calculating the PSDs of measured data is shown schematically in Fig. 5-7.

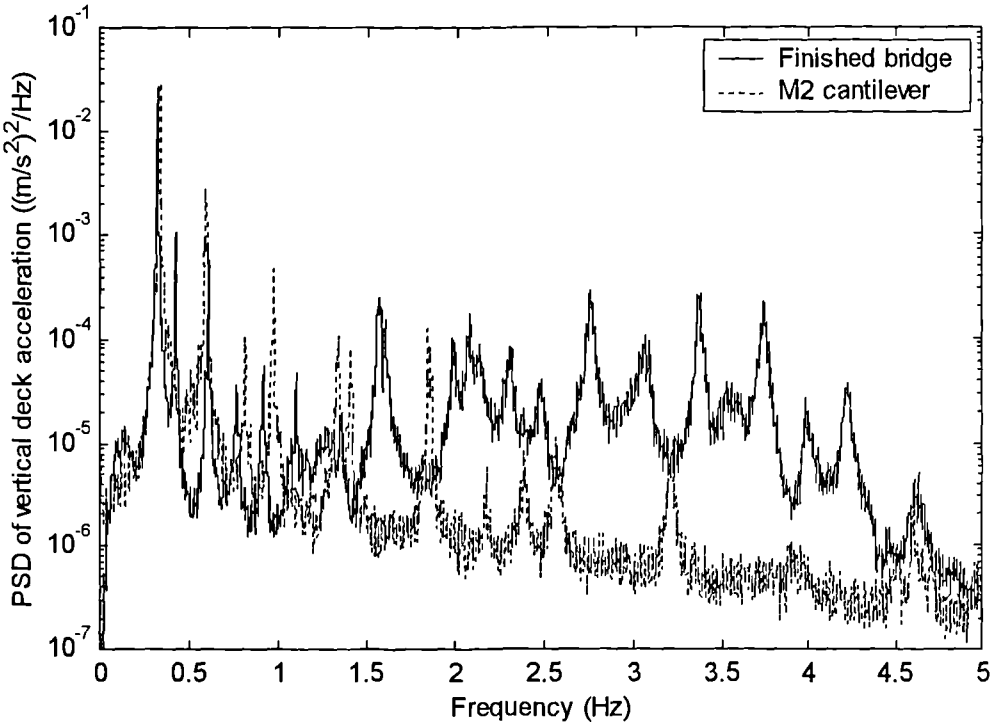

Fig. 5-1 Typical PSDs of vertical acceleration of deck near midspan for completed M2 cantilever and finished bridge (wind approx. 13m/s normal to bridge)

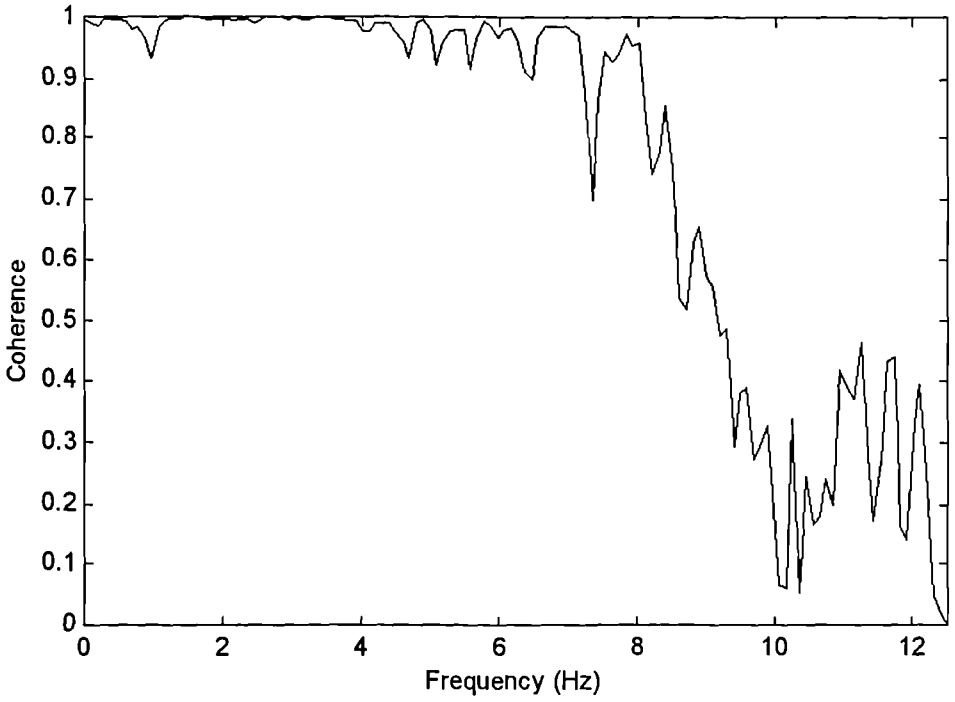

Fig. 5-2 Coherence between accelerometer signals from two instruments immediately adjacent on bridge deck

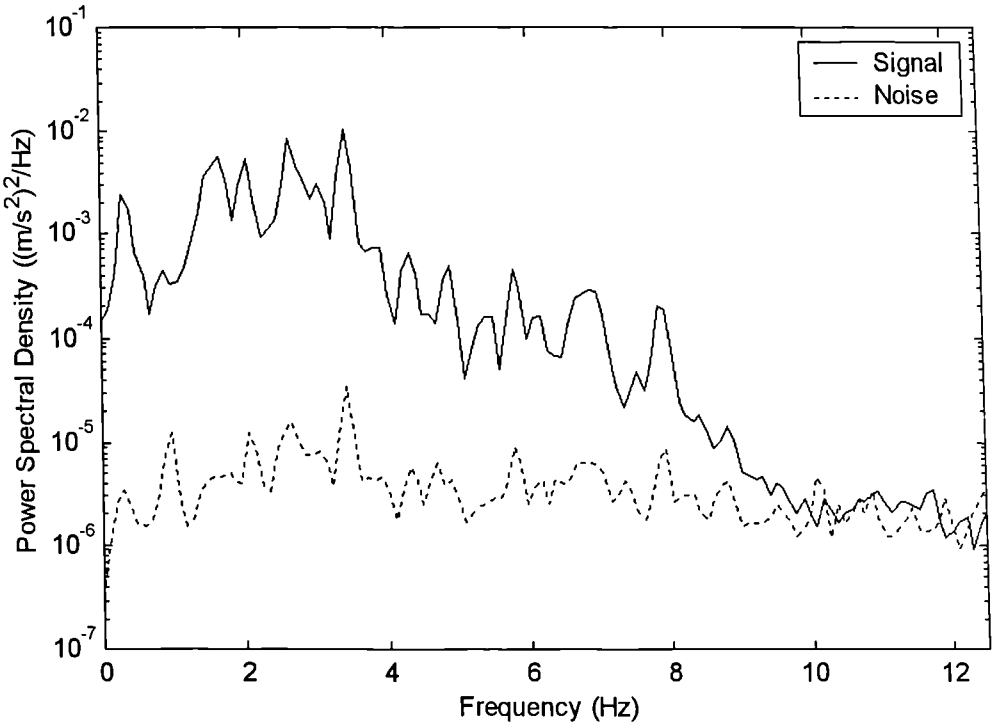

Fig. 5-3 PSDs of typical deck vertical acceleration and accelerometer noise

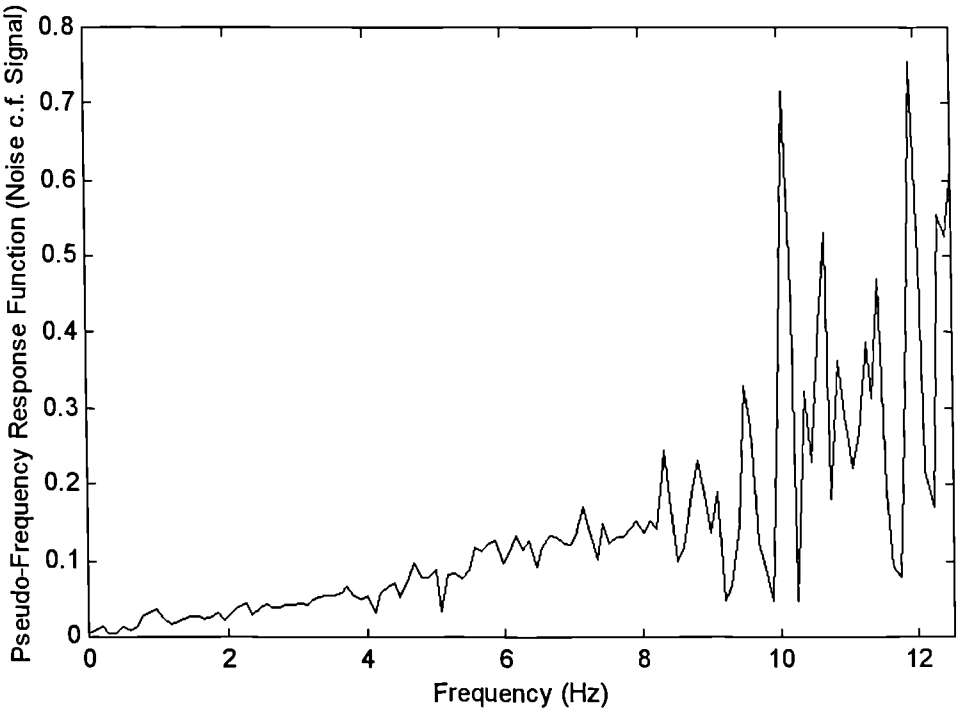

Fig. 5-4 Magnitude of pseudo-FRF of accelerometer noise relative to typical deck vertical acceleration

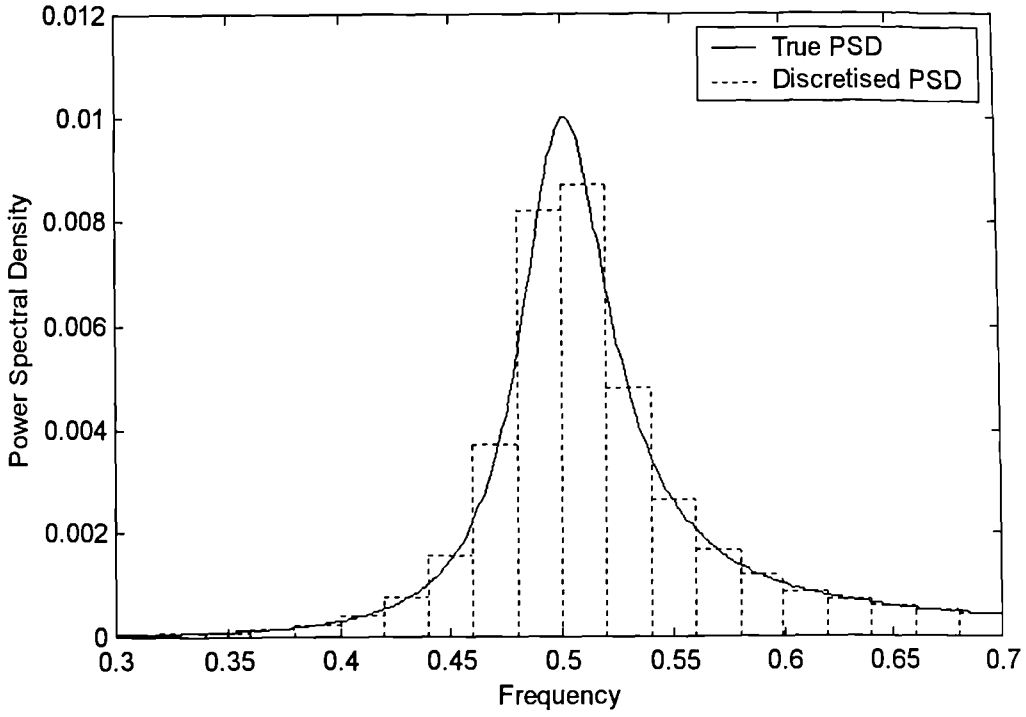

Fig. 5-5 Schematic representation of bias error at peak in PSD

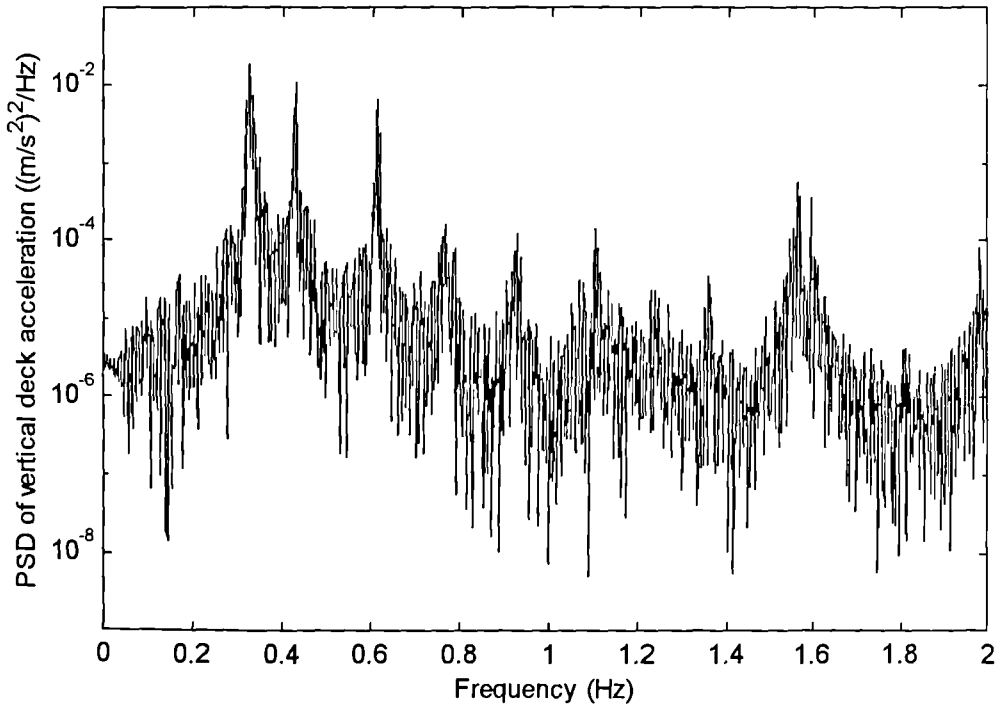

(a) Record processed as single block

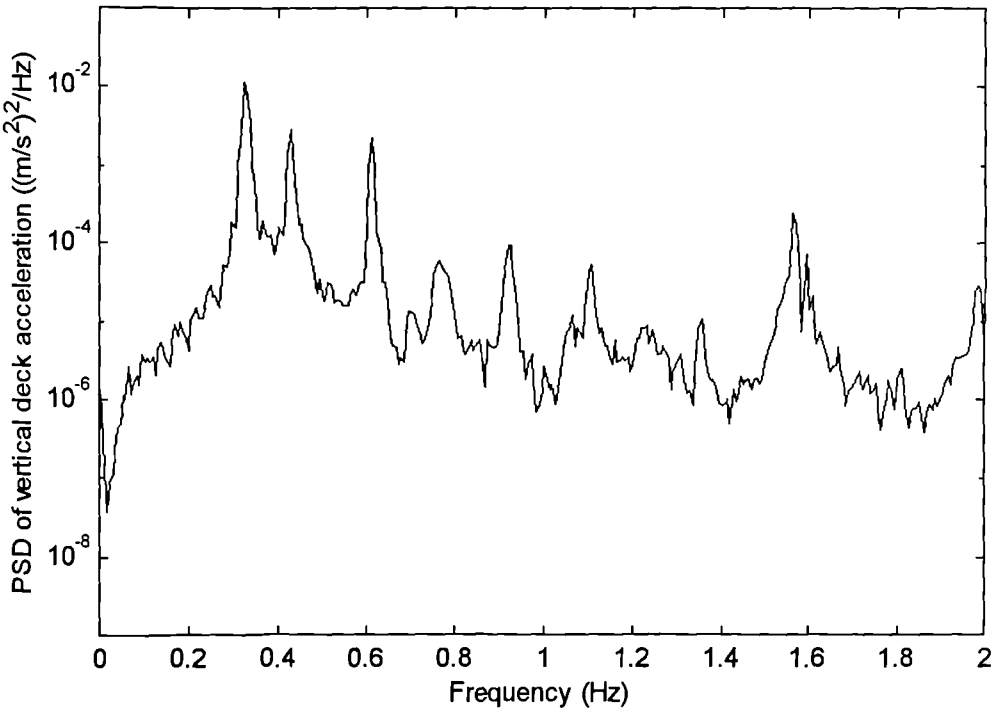

(b) Record divided into 8 blocks

Fig. 5-6 Reduction of variance errors by segment averaging

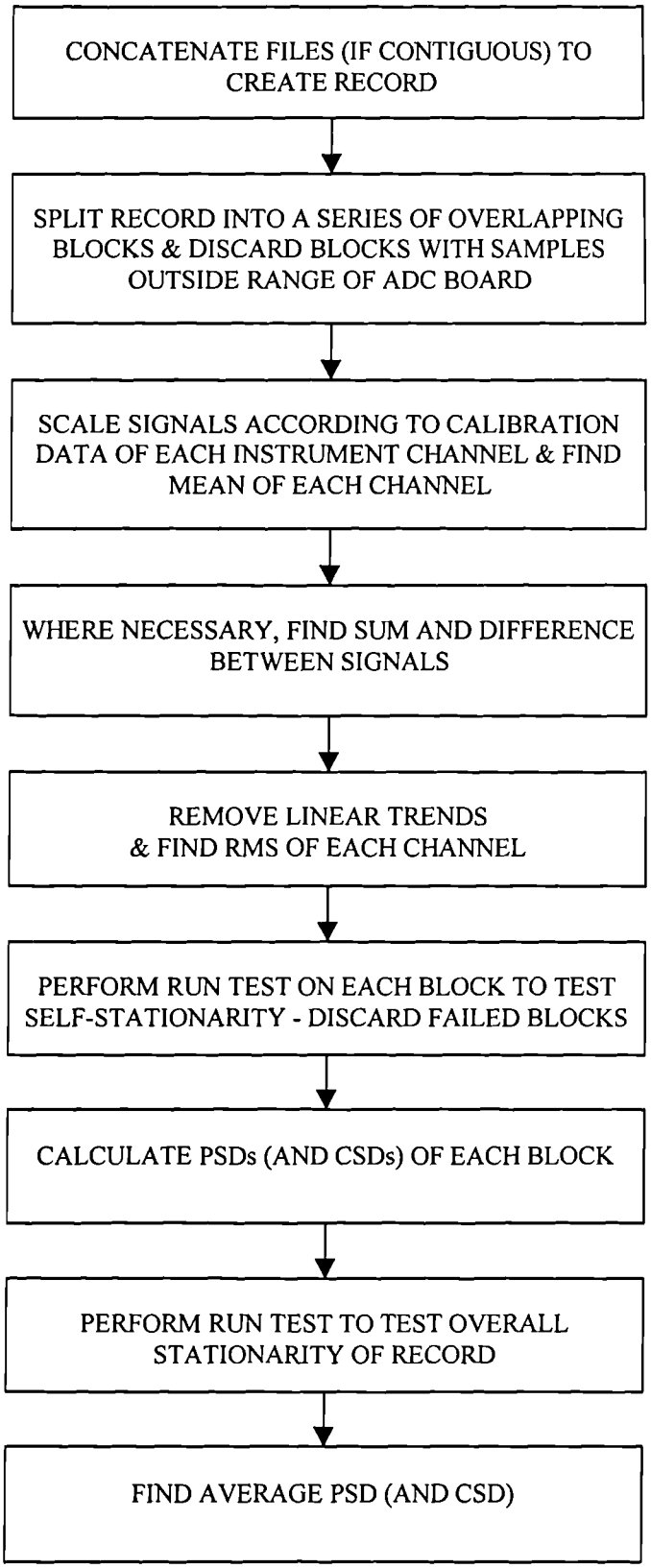

Fig. 5-7 Schematic representation of calculation of Power Spectral Densities (PSDs) and Cross Spectral Densities (CSDs) from measured data

CHAPTER 6 INITIAL CONSIDERATIONS IN THE DYNAMIC LOADING AND RESPONSE OF THE SECOND SEVERN CROSSING

6.1 Introduction

This chapter presents the results of the preliminary tests and wind measurements from the monitoring of the Second Severn Crossing (SSC) (Chapter 4). The preliminary tests identified several features of the dynamic behaviour. These were of interest for the planning of the main tests (§4.5.3-4.5.5), and they justify certain assumptions used in the Finite Element (FE) modelling (Chapter 3) and in the later more detailed analysis of the main test data (Chapters 8-10).

From the wind measurements, assumptions of the stationarity of the wind velocity and the spatial variation of loading are validated, which are required for the methods of analysis applied to the SSC main data (Chapters 5&7).

Measured wind velocity spectra are compared with a theoretical model, and measured turbulence parameters with values used in design (§2.6.4). Considering these, along with further theory of the spatial variation of wind loading on long-span bridges, an estimated spectrum of wind loading is derived.

Traffic loading is also addressed, including its importance for the finished bridge relative to wind loading.

The estimated wind and traffic loading spectra are later used in the development of an improved system identification method for ambient vibration data (Chapter 7), to enable more accurate estimates of modal parameters than normally possible.

6.2 Results of preliminary tests

6.2.1 General description of tests

The preliminary tests were performed as described in §4.5.1. The majority of the tests were carried out on the M2 cantilever (§3.2.2). At the start of testing, there were 16 deck sections on each side of the pylon (Fig. 4-13) and by the end of the tests, there was one additional section on each end. On one day a series of tests was performed on the north tower of the free-standing M1 pylon.

The wind speed during the tests was in the range 3-14m/s, but typically about 10m/s, while the wind direction varied considerably.

6.2.2 Signal processing

The data for the preliminary tests were recorded by the simple monitoring system (§4.3.3). With the exception of some 32s time histories, they were stored as averaged frequency domain data. A typical Power Spectral Density (PSD) of vertical deck acceleration is shown in Fig. 6-1.

The most noticeable vibrations of the bridge deck occurred when a fork lift truck, with solid tyres, was in operation, causing a non-stationary excitation. Since the spectra were calculated directly on site using the spectrum analyser, the non-stationary data were not eliminated, so the PSDs would strictly be invalid (§5.2.2). However, they were adequate for preliminary purposes. Blocks of data in which the accelerations exceeded the input range of the analyser were eliminated.

Natural frequencies were extracted from the PSDs by the Peak Picking Method (§5.3.2.1). Only peaks which occurred consistently for several tests were considered. Peaks occurring only occasionally were assumed to be due to variance errors (§5.3.1&5.6.2).

Mode shapes were estimated from the magnitude of the 'pseudo-Frequency Response Functions' (FRFs) of the acceleration at each measurement station relative to the acceleration at a reference location, at each natural frequency (§4.3.3&4.5.1). It was assumed that there was no vertical motion of the deck at the bearings on the pylon or at the intermediate pier in the back span.

6.2.3 Modal behaviour of cantilever

For most records there was no significant response of the bridge above 10Hz, although some spectra did show relatively large accelerations, particularly in the 11-16Hz frequency range (Fig. 6-1). It is thought that these were due to greater excitation in this frequency range from construction work in progress (e.g. cable tensioning or fork lift truck). It was not possible to identify any frequencies which occurred consistently, from which modes could be identified, above approximately 4Hz. Therefore, for the main tests, the frequency range of interest was restricted to below 5Hz (§4.3.2).

There were essentially six types of 'component mode' of the SSC, namely vertical, torsional and lateral deck modes, and longitudinal (with respect to the bridge deck), torsional and lateral pylon modes. The vertical and torsional deck modes were both detected by the vertical motion of the edge of the deck, and similarly longitudinal and

torsional pylon modes by the longitudinal motion of the tower on one side. For lateral modes, both sides of the deck and pylon were assumed to move together. Therefore, all six types of component mode were monitored by the vertical and lateral motion of one side of the deck and the longitudinal and lateral motion of one tower. Since only two accelerometers were used for the preliminary tests, only for a few particular tests were they placed on opposite sides, allowing vertical and torsional modes to be distinguished by sum and difference of the accelerometer signals (Fig. 6-2). For the other tests, vertical and torsional modes could not be distinguished directly, but for well separated modes, they could be identified by the natural frequencies. Modes occurring at close natural frequencies could not always be distinguished.

A total of 34 modes, up to 4.1Hz, were identified in the preliminary tests, most of which were a combination of two or more component modes. This is consistent with the results of the FE models of the completed cantilever (§3.3.5). At least ten component modes of each type were identified. The first ten modes are summarised in Table 6-1, showing the component modes comprising each. The measured shapes of the first two modes are shown in Fig. 6-3.

Table 6-1 Measured modes of M2 cantilever in preliminary tests

Mode no.	Frequency (Hz)	Deck modes			Pylon modes			Average coherence
		Vertical	Tors.	Lateral	Long.	Tors.	Lateral	
1	0.39	**✓**			✓			>0.9
2	0.50			✓		✓	**✓**	>0.9
3	0.63		**✓**			✓		>0.8
4	0.73	**✓**			✓			>0.9
5	0.73			**✓**			✓	>0.9
6	1.09	✓			**✓**			>0.8
7	1.09		✓	✓		**✓**	✓	>0.8
8	1.18						**✓**	<0.6
9	1.40		**✓**	✓		✓		<0.6
10	1.45				**✓**			>0.8

Notes: Ticks represent measured components
Principal component in bold

The coherences between responses at different points on the structure at the natural frequencies were typically above 0.6 (Table 6-1), indicting response in the same mode of vibration. Exceptions included Mode 8, which was localised at the top of the pylon, with very little motion elsewhere, and Mode 9, which was a backspan mode with very little response at the reference location. Modes 4&5 and 6&7 were paired at the same frequencies, within the resolution of the measurements, but they were identified as

separate modes by the very low coherence between some component modes. Separation of the mode shapes was, however, more difficult in these cases.

The frequency resolution used was very coarse in relation to the width of the peaks, with typically only two divisions covering the Half Power Bandwidth (HPB). Therefore the HPB method (§5.3.2.1) gave overestimates of the damping, with a value as high as 5% for the first mode. Above 3Hz, for which the poor resolution was becoming less important, values were typically 1%, which were closer to later estimates using longer records and a more accurate method (§8.4.3).

6.2.4 Amplitude of vibrations

Integration of the accelerations found the Root Mean Square (RMS) displacement at the end of the cantilever deck to be approximately 3mm in a wind of 13m/s at 30° to south normal (§3.2.2), while at the top of the pylon it was less than 1mm.

6.2.5 Rigidity of pylon base

A comparison of the longitudinal acceleration PSDs on the caisson and at the top of the pylon is presented in Fig. 6-4. The caisson acceleration was approximately 1% of the top of pylon acceleration at the natural frequencies. In the lateral direction, the accelerations of the caisson gave a flat PSD at approximately $1x10^{-10}(m/s^2)^2/Hz$, with no noticeable response at the natural frequencies of the pylon. The caisson could therefore be considered rigid in this direction, and the measured PSD could be taken as the noise level.

The pylon mode shapes for the lowest frequency modes showed that there was negligible rotation at caisson level. For the analysis of the bridge it would seem reasonable to treat the pylon bases as rigidly built into the foundation (§3.3.2), although in reality the slight caisson movement in the longitudinal direction gives reduced modal stiffnesses, slightly reducing the natural frequencies.

6.2.6 Fixity of bearings

Fig. 6-5 shows the PSD of longitudinal acceleration at locations on either side of the bearings on the backspan pier. The spectra are similar, particularly at lower frequencies, although the bearings were nominally free in this direction. Also the FRF magnitude is approximately unity, the phase zero, and the coherence unity. Similar results were obtained in the lateral direction and at the pylon bearings. It was presumed that the differences at higher frequencies were due to local variations in mode shapes of the higher modes, since the accelerometers were in practice a significant distance apart.

Based on these results, for the purposes of this study, the bearings were assumed to be fixed for dynamic effects (§3.3.2), although it should be noted that the experiments were undertaken at low vibration levels, so at high levels this assumption may not hold.

6.2.7 Significance of longitudinal deck motion

Fig. 6-6 shows the spectra of the vertical, lateral and longitudinal accelerations of the north side of the end of the deck. Generally, peaks in the longitudinal PSD only occur at frequencies of peaks in the PSD of either of the other components, typically with acceleration amplitudes of less than 20% of the main component. The one notable exception is at 1.4Hz which corresponds to Mode 9, which was predominantly a back span mode, so it had a small vertical component at the end of the deck. It appears that there are no modes below 4Hz with a dominant longitudinal deck component. The longitudinal response is believed to be mainly rigid body motion, since the pylon at deck level showed a similar response in the same direction. It appears that longitudinal vibrations of the deck are not significant in their own right at low frequencies, so no further measurement of them was made.

6.2.8 Cable vibrations

The one cable monitored was the eighth from the pylon on the north side of the main span (Cable 83N), approximately half way along the cantilever, chosen as a typical cable. Both the in-plane and out-of plane cable vibrations were measured by accelerometers 5.6m from the elastomeric guide at the deck end. The spectra for the two cable planes are shown in Fig. 6-7. The vibrations occurred mainly at harmonics of the fundamental frequency (1.18Hz), as expected for a taut cable with fixed ends.

The peak cable accelerations in the two planes occurred at the same frequencies, with relative phases close to 0° or 180°, indicating that the vibrations were planar, rather than elliptical. The amplitude of in-plane vibrations was typically 1.4 times the out-of-plane amplitude, but this varied for each natural frequency, indicating that each mode occurred in a different plane. It seems likely that each mode may occur in any plane, depending on the excitation.

The amplitude of the cable acceleration was of the order of ten times the amplitude at the end of the cantilever deck. The coherence between deck and cable vibrations was low, but there were small peaks in the cable spectra coinciding with deck natural frequencies, particularly at low frequencies, indicating some degree of interaction.

6.2.9 Free-standing pylon

Fig. 6-8 shows the spectra of the accelerations at the top of the M1 pylon, before deck construction. The natural frequencies and mode types are summarised in Table 6-2. The vibrations in the two horizontal orthogonal directions was independent, and for each direction there were a few modes at different frequencies with similar shapes (Fig. 6-9). For longitudinal motion, some of these modes would be pure bending modes and others would be torsional modes. Other repeated mode shapes could be due to the influence of the cross-beams, particularly as the upper one was not yet fully connected. Above 10Hz no clear peaks could be identified in the acceleration PSDs.

Table 6-2 Measured modes of free-standing M1 pylon

Mode no.	Frequency (Hz)	Lateral mode	Longitudinal mode	No. of nodes
M1/La1	0.23	✓		0
M1/Lo1	0.36		✓	0
M1/La2	0.84	✓		0
M1/La3	1.44	✓		1
M1/La4	1.75	✓		1
M1/Lo2	1.82		✓	1
M1/Lo3	2.03		✓	1
M1/La5	2.47	✓		2
M1/La6	2.70	✓		2
M1/La7	3.81	✓		2
M1/Lo4	4.06		✓	2
M1/Lo5	4.39		✓	2
M1/Lo6	4.64		✓	2
M1/La8	4.70	✓		2
M1/La9	5.30	✓		3
M1/La10	5.41	✓		3
M1/La11	5.89	✓		3
M1/Lo7	8.38		✓	3
M1/La12	8.52	✓		3
M1/La13	9.48	✓		3

In each direction the first mode was dominant, the amplitude being several times as great as for any other mode. Relative to M2 with the deck sections, the amplitudes were approximately 30% as great for similar wind conditions, showing that the principal

excitation for M2 was the wind load on the deck. For the later construction stages and the finished bridge it is therefore reasonable to consider only the loading on the deck (§2.6.4.2&6.5).

6.3 Preliminary analysis of data from main tests

For the main long-term data (§4.5.4), the first stage in the processing was to calculate average wind conditions and response amplitudes, to identify periods for subsequent detailed processing. The averages were taken over the recorded file lengths of 163.84s (4096 samples, §4.3.2), for ease of calculations.

Average values of wind speed, direction, vertical angle of attack and horizontal and vertical turbulence intensities were calculated, corrected for the orientation of the anemometers. For the accelerometer records, the mean value of each channel was subtracted for each file length, and the RMS acceleration calculated. Plots could then be produced of each averaged parameter against time (e.g. Fig. 6-10 & Fig. 6-11) and of the relationships between them, for example RMS vertical acceleration of the deck against average wind speed (Fig. 6-12). A clearer relationship was apparent between the RMS vertical acceleration and the average component of the wind normal to the bridge axis (Fig. 6-13, §6.5.5). The amplitudes of vibrations and their relationship to the wind conditions are considered further in §8.6 and §9.3&9.4.

6.4 Characteristics of the wind

Measurements of the wind characteristics on the SSC are now considered, in order to:

i) Compare them with characteristics assumed in design;

ii) Justify the assumption of stationarity, required for spectral analysis (§5.2.2);

iii) Derive an estimated wind loading spectrum for the bridge (§6.5), which is used for the improved system identification method (§7.6).

Wind velocities were measured by the ultrasonic anemometers (§4.3.1(ii)).

6.4.1 Wind direction and speed

Long-term tests, after completion of the bridge, were set to record data triggered by a wind speed exceeding 14.3m/s. Over two six month periods (October-April 1997-98 and 1998-99), data were recorded for a total of 50 days (15% of the time). The mean wind velocity over these records was from 30° to the west of south normal, which also corresponds with the direction of the centreline of the estuary downstream (Fig. 3-1). Only 14% of the records were for wind from the north side of the bridge.

The maximum recorded one-hour mean wind speed was 28.2m/s at 24° to the west of south normal, on 4/1/98, with a peak 10s gust of 35.5m/s, while the maximum one-hour mean wind speed from the north side was 15.4m/s. These compare with a design 120 year one-hour mean wind speed of 37m/s, 46.3m/s gust, and a flutter design wind speed of 60.2m/s (Xie et al. 1994). The most extreme conditions monitored were therefore well within the design serviceability range for the structure, and far from flutter.

6.4.2 Turbulence intensity

Longitudinal (with respect to wind direction) and vertical turbulence intensities (§2.6.4.1) were calculated directly from the RMSs and mean values of wind velocity time histories, over the 163.84s file lengths. Records of this length would not capture long period wind variations, but their contribution to the turbulence intensity is small (approx. 5% of total), as confirmed by calculating some averages over one-hour periods.

The average turbulence intensities over the 50 days of records are given in Table 6-3, based on measurements on the windward side of the deck. The values given by the Engineering Sciences Data Unit (ESDU 1993) for design are also shown, based on a height of 60m (anemometer level) above open water, and a reference wind speed (10m above the water) of 20m/s.

Differences in turbulence intensity with wind direction were expected, due to the local topography. Therefore, averages for wind from the north and south sides of the bridge were separated, and a narrower range within ±30° from south normal was also selected (Table 6-3). This showed slightly higher levels of turbulence for north winds, over the shorter stretch of water, and lower values for the narrow range from the south.

Table 6-3 Average turbulence intensities (windward side of deck)

Description	Longitudinal (%)	Vertical (%)
ESDU (60m above open water, at 20m/s)	9.5	5.2
Average measured -all records	6.8	4.0
-from north side	7.8	5.2
-from south side	6.7	3.8
-from south, within ±30° of bridge normal	6.2	3 5

Similar values of longitudinal turbulence were measured in a study of the Wye Bridge just upstream of the SSC (Smith 1980), with an average of approximately 7% for winds predominantly from the south-west, over the open water of the estuary.

The average measured turbulence intensities were considerably lower than predicted by ESDU, except for the vertical turbulence for wind from the north, for which a greater ground surface roughness would apply. For the wind from the narrow range to the south, which would have a roughness height most comparable with the assumed value for open water, ESDU overestimates the turbulence intensities by approximately 50%. However, in stronger winds the sea roughness would increase, so the turbulence would increase. Therefore the ESDU values, which vary little with wind speed, may be reasonable for maximum design wind speeds. The consequences of lower turbulence for typical wind speeds, as measured, are that the buffeting loading would be lower than expected, but there could be adverse effects for aerodynamic and aeroelastic instabilities (§2.6.5), in particular for vortex shedding (§2.6.5.3, Chapter 9).

Although there was considerable variation in the turbulence intensities between individual records, there was no apparent relationship with the wind speed, except for very low wind speeds (<5m/s), which sometimes exhibited greater turbulence (up to approximately 20% longitudinal and 10% vertical).

6.4.3 Stationarity of wind velocity

Run Tests (§5.6.4) on the records of wind speed, direction and vertical wind speed found that approximately 70% of blocks of length 11 or 22 minutes passed the self-stationarity test for all three measurements, at a 5% level of significance. Virtually all records of length one or three hours passed the overall stationarity test, with the number failing being below 5%, i.e. within the percentage which statistically would be expected to fail the check for truly stationary data.

Despite the failure of some blocks, considering the high proportion that passed, and the results of the overall stationarity tests, it is seems reasonable to take the wind loading to be approximately stationary, for up to one hour, as is generally assumed (Simiu & Scanlan 1986). From the measurements on the SSC there seemed to be no significant reduction in the stationarity for periods of up to three hours, so wind records of this length were also assumed to be stationary for this study.

Any lack of stationarity in the actual loading for a particular record was effectively taken into account by the stationarity tests of the vibration response of the structure, which found that a similar proportion of blocks and records passed (§5.6.4).

6.4.4 Integral length scales of turbulence

The integral length scales ${}^{x}L_u$ and ${}^{x}L_w$ (§2.6.4.1), giving the average size of turbulent eddies, were calculated from the measured wind velocities, for comparison with the

values from ESDU (1993) used in design. Based on Taylor's hypothesis of 'frozen turbulence' (Simiu & Scanlan 1986), the integral length scales are given by:

$$^{x}L_i = \frac{1}{\sigma_i^2}\int_0^\infty R_{i_1 i_2}(x)dx = \frac{U}{\sigma_i^2}\int_0^\infty R_{i_1 i_2}(\tau)d\tau \qquad (6\text{-}1)$$

where: U = mean wind velocity

σ_i = RMS of i

$i = u$ (longitudinal) or w (vertical) varying component of velocity

$R_{i_1 i_2}(x)$ = cross-correlation function of i at zero time lag with respect to along-wind position

$R_{i_1 i_2}(\tau)$ = autocorrelation function of i at one position with respect to time

The autocorrelation functions, $R_{i_1 i_2}(\tau)$, were found from the inverse Fast Fourier Transforms (FFTs) of the PSDs of measured wind velocities at a point, while U and σ_i were found by averaging over the time histories. Three-hour records were used for the calculations, divided into blocks of 11min (2^{14} samples) for the calculation of the PSDs, to allow enough blocks for a meaningful stationarity test, and for each one to be long enough to capture the majority of the long period turbulence. Wind velocities were taken from the anemometer on the windward side of the deck, to obtain an estimate of the free stream turbulence.

The values of $^{x}L_u$ were found to vary significantly within the range 60-350m, with an average of approximately 220m and a trend for longer lengths in higher wind speeds. This agrees well with ESDU (1993), which gives a similar trend and a value of 230m for this site (anemometer 60m above open water) for a 20m/s wind. Measured values of $^{x}L_w$ were in the range 25-80m, with an average of approximately 50m, whereas ESDU (1993) gives a value of 20m. However, the SSC site measurements of the vertical component of wind were significantly affected by the presence of the deck (§6.4.6).

6.4.5 Spectra of wind turbulence

Spectra of longitudinal and vertical turbulence were calculated from three-hour records from the windward side of the deck in various wind conditions. The maximum frequency for which they were valid was 0.52Hz, due to the sampling frequency of the ultrasonic anemometers (§4.3.1(ii)), while the minimum frequency considered was $1.5\text{x}10^{-3}$Hz, based on the 11min block length. Although the mean wind speed, turbulence intensities and integral length scales varied considerably between the records, the spectra could be compared using the non-dimensional 'reduced PSD' ($= Sf\sigma_i^2$, where f = frequency) and

'reduced frequency' ($= {}^{x}L_j f/U$). These are plotted against each other on log scales for the longitudinal component of velocity in Fig. 6-14, for three different wind speeds, along with the von Kármán reduced spectrum (§2.6.4.1). In this form the measured spectra are similar and agree well with the von Kármán spectrum (equation (2-14)). The agreement even holds for low wind speeds, although ESDU (1993) takes it only to be applicable for 'strong winds', defined as wind speeds above 10m/s at 10m height, equivalent to approximately 12m/s at the anemometer height. Therefore, although the turbulence intensity given by ESDU (1993) appears to be overestimated for light to moderate winds on the SSC (§6.4.2), the form of the spectral formula can be taken to be a good model for the conditions measured.

Reduced PSDs of the vertical component of velocity are shown for the same three records in Fig. 6-15, with the corresponding von Kármán spectrum (equation (2-15)). Again the reduced wind spectra measured in different conditions are similar, and the agreement with the von Kármán spectrum is reasonable, although not as good as for the longitudinal spectrum. The discrepancies may be due to the effects of the bridge deck on the vertical wind component (§6.4.6), and the tendency for the von Kármán model to overestimate the magnitude of measured spectra (ESDU 1993).

Wind velocity spectra of the von Kármán form seem to provide a reasonable model of the measured spectra, so they are used for the derivation of the estimated wind loading spectrum (§6.5).

The coherence between vertical and longitudinal velocities at a point was in all cases low, at all frequencies, with an average value of less than 0.1. The vertical and longitudinal velocity spectra can therefore be assumed to be uncorrelated and the Cross Spectral Density (CSD) between them is of considerably lower magnitude than the PSDs.

6.4.6 Comparison of measured wind on windward and leeward sides of the deck

Outputs from the two anemometers, on either side of the deck of the finished bridge, were compared. The spacing of the anemometers was approximately 32m across and 33m along the bridge, with the south one being to the east of midspan and the north one to the west.

The 164s average wind speed from the two anemometers differed by less than 1m/s, and the direction by less than 3°, in virtually all cases. This is in agreement with the assumption that the averages of these parameters are approximately constant over the extent of the bridge deck, so they can be measured at a single point.

The average vertical angle of attack for the finished bridge was found to be +5.9° (positive upwards) on the windward side and +0.3° on the leeward side. The average in

the free stream would be expected to be 0°. This shows that, 12m above the deck surface, the vertical direction of the wind is significantly affected by the presence of the deck, particularly due to upwards deflection on the windward side. Therefore the absolute values of the vertical angle of attack, as recorded, are not an accurate measure of the free stream values. However, they would be expected to experience similar variations.

Comparison of turbulence intensities found that, on average, the longitudinal turbulence was 4% higher on the leeward side, whereas the vertical turbulence was 22% lower. The spectra of longitudinal turbulence were very similar (Fig. 6-16). The slight increase in turbulence intensity on the leeward side is reflected by the marginally higher values of the spectrum at higher frequencies, due to small scale turbulence from the deck and traffic. In contrast, there was a significant difference between the vertical wind velocity spectra on the two sides of the deck (Fig. 6-17). The low frequency (large scale) vertical components are greatly reduced on the leeward side by the presence of the deck, accounting for the reduction in vertical turbulence intensity.

Fig. 6-16 and Fig. 6-17 are both plotted as PSD, normalised with respect to $f U^2$, against actual frequency, rather than as 'reduced' PSD and frequency, so that the frequencies are clear and the longitudinal and vertical spectra can be directly compared. Above approximately 0.2Hz they are similar, whereas at lower frequencies the longitudinal spectra are considerably greater, on both sides of the deck.

The coherence between longitudinal velocities measured by the two anemometers, approximately 46m apart, was high (approximately 0.9) at very low frequencies (large scale turbulence), but above 0.1Hz the mean was less than 0.1 (Fig. 6-18). Therefore some large eddies would have a coherent effect over a sizeable area at very low frequencies, but in the frequency range of modes of the SSC (above 0.3Hz, §5.4.1) the correlation of loading over the bridge surface would be very low. The coherence for vertical wind velocity was considerably lower, with an average of approximately 0.2 below 0.1Hz, due to the smaller average size of vertical eddies and the effect of the deck on the larger ones for measurements on the leeward side. From the low coherences above 0.1Hz, the short correlation length assumption can be justified (§2.6.4.2).

6.4.7 Relationship to bridge response

The coherence of bridge deck acceleration in relation to wind velocity from a single anemometer was always very low at all frequencies, with an average below 0.1. This shows that wind measurements at a single location cannot be taken to be directly related to the response, and hence to the total dynamic loading, of the structure. This is further evidence of the lack of correlation of the wind loading over the structure. Therefore, the

measurements of the wind obtained can only be taken to give reasonable estimates of the mean wind and the statistical properties of the turbulence, which from the limited data available have been shown to be consistent at different locations, except when affected by the presence of the bridge deck itself.

6.5 Wind loading

Having discussed the measured wind velocity parameters, the resulting loading spectrum is now considered. A simplified expression for the form of the spectrum is derived, which is used subsequently for the improved system identification method (§7.6). It is based on the buffeting theory described in §2.6.4, with certain simplifications, which are justified below for parameters relating to the SSC measurements. Only the variation of the loading spectrum with frequency is of interest for the system identification method, rather than the absolute magnitude of the spectrum.

In this study, only the completed M2 cantilever and the finished bridge are considered in detail. The preliminary tests showed that wind loading on the pylon is much lower than on the deck (§6.2.9), so the only the loading on the deck is considered here.

6.5.1 Spectrum of point wind loading

As discussed in §2.6.4.1, the wind loading at a point on a structure is proportional to a linear combination of the longitudinal and vertical PSDs of wind velocity and their CSD. The von Kármán spectra for longitudinal and vertical velocity have been shown to provide a good model of the measured spectra (§6.4.5), although with lower turbulence than estimated by ESDU (1993). The theoretical CSD is of considerably lower magnitude than the PSDs, so it is often ignored in design (§2.6.4.1) The very low measured coherence between vertical and longitudinal velocities confirmed the insignificance of the CSD (§6.4.5), so it is disregarded here.

The von Kármán longitudinal and vertical (un-reduced) spectra, and indeed all other proposed wind spectra (§2.6.4.1), at high frequencies are approximately proportional to $f^{-5/3}$ (equations (2-14)&(2-15)). According to ESDU (1993), this becomes a good approximation for $fz/U > 0.1$, where z is the height above the ground (or water). For the SSC deck (50m above water), in a mean wind speed of 30m/s, this is satisfied for frequencies above 0.06Hz. In the lower wind speeds measured on site (§6.4.1), this lower limit is reduced. Since the first natural frequency of the bridge was approximately 0.33Hz (§5.4.1), the wind velocity spectra, and hence the point loading spectrum can be taken to be proportional to $f^{-5/3}$ in the range of all of the natural frequencies of the structure, for the measured wind speeds.

6.5.2 Effect of spatial variation of wind loading along bridge length

The treatment of the spatial variation of wind loading in buffeting theory, based on the joint acceptance, is discussed in §2.6.4.2. The very low coherence of wind velocities above 0.1Hz, as measured at the two anemometers (§6.4.6), confirms that on the SSC the correlation length is short in comparison with the bridge dimensions. Therefore the short correlation length assumption (§2.6.4.2) can be used, for which the wind correlation and mode shape factors of the joint acceptance can be separated. The mode shape factor is a constant for each mode, whilst the wind correlation factor is frequency dependent. Irwin (1977) provides two expressions for wind correlation factors, for the longitudinal and vertical components of wind velocity separately:

$$\overline{C}_{luu} = \frac{3.774\left({}^{y}L_u/L\right)}{\left\{1+70.8\left(2{}^{y}\tilde{f}_u\right)^2\right\}^{1\,2}} \tag{6-2}$$

$$\overline{C}_{lww} = \frac{1425\left({}^{y}L_w/L\right)\left(2{}^{y}\tilde{f}_w\right)^2}{\left\{1+70.8\left(2{}^{y}\tilde{f}_w\right)^2\right\}^{1\,2}\left\{1+189\left(2{}^{y}\tilde{f}_w\right)^2\right\}} \tag{6-3}$$

where: L = bridge deck length (= 473m for each full SSC cantilever)

$${}^{y}\tilde{f}_u = \frac{f\,{}^{y}L_u}{U}$$

$${}^{y}\tilde{f}_w = \frac{f\,{}^{y}L_w}{U}$$

These two factors are each approximately proportional to f^{-1} at high frequencies. Using ESDU (1991) length scales (${}^{y}L_u$ = 92m, ${}^{y}L_w$ = 15m), for a 30m/s wind these become good approximations above 0.03Hz for the longitudinal factor and 0.3Hz for the vertical factor, as shown in Fig. 6-19. Again, for lower wind speeds, the approximations hold for lower frequencies.

Scanlan & Gade (1977) provide an alternative formulation, using the approximate overall wind correlation factor:

$$\overline{C}_{ls} = \frac{2(C-1)}{C^2} \tag{6-4}$$

where: $C = \dfrac{AfL}{U}$

A is a constant, conservatively taken as 7, although possibly as high as 20

This factor also tends to a line of slope f^{-1}, in this case above approximately 0.05Hz for a 30m/s wind (Fig. 6-19).

Therefore, from either formulation, in the range of the natural frequencies of the SSC (above 0.3Hz), the spatial variation of the loading along the bridge deck effectively modifies the loading spectrum by a factor proportional to f^{-1}.

6.5.3 Aerodynamic admittance

The effect of the variation in wind velocity over the cross-section is described by the aerodynamic admittance (§2.6.4.3), which can significantly reduce the loading compared with a uniform velocity. The most commonly used expression for it is the approximation to Sears' function (equation (2-17)). Irwin (1977) provides an alternative expression, which was used for the design buffeting analysis of the SSC (§8.6.1), in the following slightly modified form (Xie et al. 1994):

$$\chi^2 = \frac{4}{\eta_1^2 \eta_3^2}\left(\eta_1 - 1 + e^{-\eta_1}\right)\left(\eta_3 - 1 + e^{-\eta_3}\right) \qquad (6\text{-}5)$$

where: $\eta_1 = 0.95\frac{B}{{}^{x}L_u}\sqrt{1 + 70.8\left(\frac{f\,{}^{x}L_u}{U}\right)^2}$

$$\eta_3 = 0.475\frac{D}{{}^{z}L_u}\sqrt{1 + 70.8\left(\frac{2f\,{}^{z}L_u}{U}\right)^2}$$

B = width of deck (but see §6.5.5 for skew winds)

D = depth of deck

Sears' and Irwin's functions are plotted against frequency for the SSC deck in Fig. 6-20, for a wind speed of 30m/s. For Irwin's expression, the ESDU (1991,1993) length scales (${}^{x}L_u$ = 320m, ${}^{z}L_u$ = 59m) and the depth of the deck excluding the wind barriers were used. The addition of the wind barriers on the finished bridge would cause a slight reduction in the values.

The two expressions give very different values, particularly in the range of the first few natural frequencies of the bridge (0.33-1Hz), for which they differ by up to a factor of three.

Sears' function strictly applies to an aerofoil and it can underestimate the aerodynamic admittance for bridge decks (§2.6.4.3), so for the bluff cross-section of the SSC (Fig.

3-3(b)) it may not be appropriate. However, the design buffeting analysis, based on Irwin's expression, gave reasonable agreement with the full aeroelastic model (Xie et al. 1994). Therefore, in this study, it was decided to use Irwin's formulation for the assumed loading.

Unfortunately the aerodynamic admittance calculated on this basis does not reduce to a simple power relationship with frequency in the frequency range of interest, as for the wind velocity spectra and wind correlation factor. Therefore the full expression was retained in the calculation of the total wind loading. Since it is dependent on wind speed (and direction §6.5.5), it was evaluated for each record, based on the measured mean wind velocity.

6.5.4 Spectrum of generalised wind loading

The spectrum of generalised wind loading for each mode is given by the wind velocity spectra modified by the aerodynamic admittance and the joint acceptance (§2.6.4). Above 0.3Hz for the SSC, based on the approximations discussed in §6.5.1&6.5.2, it reduces to:

$$S_{wind}(f) = R_r S_w f^{-8/3} \chi^2(f,U) \qquad (6\text{-}6)$$

where: R_r is a mode shape factor, constant for given mode

S_w is a function of the wind parameters, but constant for a given record

6.5.5 Effect of wind direction

The above discussion assumes the wind is normal to the bridge axis, which is generally taken to be the worst case in design. However, the measured response on site could be due to wind from any direction.

Buffeting in skew winds was discussed in §2.10. Xie et al. (1991) found only slight modification of a conventional buffeting analysis gave good agreement with measurements on a full aeroelastic model subject to skew winds. The main differences in the analysis were the use of an effective wind speed equal to the normal component of the actual wind, and an effective deck width equal to the distance across the deck in the direction of the wind. The normal component of the wind determines the magnitude of the loading, and hence response, as confirmed in the preliminary analysis of the SSC data (§6.3). However, it would not affect the form of the loading spectrum in the frequency range of interest. Therefore, the only correction made to the estimated loading spectrum for the SSC was to consider the effective deck width, taken as:

$$B_{eff} = \frac{B}{|\cos\theta|} \tag{6-7}$$

where: θ = direction of wind from south normal

This only affected the aerodynamic admittance, for which B in equation (6-5) was replaced by B_{eff}. Thus, for a given record, the aerodynamic admittance was calculated based on the average wind speed and direction, which, substituted into equation (6-6), gave the estimated wind loading spectrum.

6.6 Traffic loading

The effects of traffic loading on bridges are discussed in §2.7. Here the effects for the SSC are addressed, particularly to justify an assumed traffic loading spectrum.

Quasi-static deflections due to the passage of heavy vehicles were evident in the displacement measurements from the Computer Vision System (CVS) (Fig. 4-12(b)). Typical deflections were of the order of 50mm at mid-span, but the actual weights of the vehicles were unknown. Measurements of the quasi-static displacements for a known load could be used for validation of the FE model for static loads, but this was not pursued in this study, since the dynamic response was of more interest.

No measurements of the dynamic loading of traffic were possible, and records of traffic flows were not kept. However, other than in strong winds, a clear daily cycle of the amplitude of the RMS deck accelerations was evident (Fig. 6-21). In light winds (e.g. 26 April), the total RMS response was approximately three times greater during week days than at night. The response, and therefore the loading, was clearly non-stationary over full days, but it could be stationarity for periods of a few hours and the Run Test was utilised before the calculation of PSDs (§5.6.4).

Since the traffic loading was not measured, its characteristics could only be inferred from the bridge response in different conditions, for example from acceleration PSDs at different times of day (Fig. 6-22). From equation (5-1), for a given system Frequency Response Function (FRF), $H(f)$, the response PSD is proportional to the loading PSD. Therefore, if the response spectra in different conditions are compared, a relationship between the input spectra can be determined. The 'relative spectrum' is defined here as:

$$|H_{rel}(f)|^2 = \frac{S_{x_2x_2}(f)}{S_{x_1x_1}(f)} = \frac{S_{y_2y_2}(f)}{S_{y_1y_1}(f)} \tag{6-8}$$

where: $S_{x_1x_1}(f)$ and $S_{x_2x_2}(f)$ are the loading PSDs for two different records

$S_{y_1y_1}(f)$ and $S_{y_2y_2}(f)$ are the measured response PSDs for the two records

Although this definition is based on a Single-Degree-Of-Freedom (SDOF) system, for uncoupled modes and generalised loads, the relative spectra of all modes would be identical. The same relative spectrum is therefore obtained from the measured PSDs of the total response.

For the SSC, the relative spectra comparing PSDs from a variety of times of day (i.e. different traffic conditions), in low wind speeds, were found to be constant across the full frequency range. Therefore, traffic loading could be assumed to be dominant and to have a spectrum of a consistent shape. For wind speeds above approximately 9m/s with little traffic (at night), or 12m/s in heavy traffic (day), compared with periods of light wind and similar traffic conditions, the relative spectra showed an increase in the frequency range 0.1-2Hz (Fig. 6-23). This indicated dominant wind loading in this range. This is consistent with measurements on the Kessock Bridge, where wind became dominant over traffic loading for wind speeds above approximately 10m/s (Owen 1994). The form of the wind loading spectrum has already been established (§6.5.4), so the relative spectra gave evidence of the form of the traffic loading spectrum since:

$$|H_{rel}(f)|^2 = \frac{S_{x_2x_2}(f)}{S_{x_1x_1}(f)} = \frac{S_{wind}(f) + S_{traf}(f)}{S_{traf}(f)} \qquad (6\text{-}9)$$

where: $S_{wind}(f)$ and $S_{traf}(f)$ are the wind and traffic loading PSDs respectively

If the traffic loading were to have a white noise spectrum, and the wind loading is approximated by equation (6-6) (ignoring the mode shape factor, which cancels in the division for the relative spectrum of each mode), above approximately 0.3Hz this would become:

$$|H_{rel}(f)|^2 = \frac{S_w f^{-8/3}\chi^2(f,U) + S_t}{S_t} = \frac{S_w}{S_t} f^{-8/3}\chi^2(f,U) + 1 \qquad (6\text{-}10)$$

where: S_w and S_t are constants related to the wind and traffic loading respectively

Using equation (6-5) to estimate the aerodynamic admittance, based on the measured mean wind speed and direction, and choosing appropriate values for S_w/S_t, relative spectra of this form are plotted in Fig. 6-23 as bold lines. The average slope of the relative spectra from the measured data, and the trend towards unity at higher frequencies are in good agreement with the theoretical curves, which supports the hypothesis of a white noise spectrum of traffic loading in this frequency range.

At very low frequencies the traffic loading is dominant, giving a relative spectral value of unity, even in light traffic with strong winds. This is believed to be due to the quasi-static deflections caused by vehicles, which were particularly evident from the CVS measurements (§4.4.3, Fig. 4-12). This effect is believed to have been responsible for the increase in the PSD of deck vertical acceleration below 0.2Hz (Fig. 6-22), well below the first natural frequency (0.33Hz). This 'hump' in the PSD was not evident for records during construction (i.e. with no traffic). Although of importance to quasi-static displacements, this effect is of little direct significance to the dynamic response of the bridge, except for the erroneous measurement of low frequency lateral acceleration due to quasi-static rotation (§5.5&8.3.4).

6.7 Conclusions

The preliminary tests (§4.5.1) enabled several features of the dynamic behaviour of the SSC to be established, showing the value of ambient vibration data. The principal findings were as follows:

i) 34 natural frequencies and mode shapes of the M2 cantilever were identified, from 0.39Hz up to 4Hz. There was little consistent response above 10Hz. The identification of so many modes, with clearly defined natural frequencies and mode shapes, shows that the Peak Picking Method (§5.3.2.1) gives reasonable results for these parameters for the lightly damped well-spaced modes of cable-stayed bridges.

ii) Estimation of the damping ratios by the Half Power Bandwidth Method (§5.3.2.1) gave high values for the lowest frequency modes, decreasing for higher modes. This is indicative of the inaccuracy of this method due to bias errors (§5.6.1), giving greater errors for short records and low frequency modes.

iii) The base of the pylon can be treated as rigidly built into the foundation, and the deck bearings on both the pylon and the intermediate supports are effectively rigid in all directions for low amplitude vibrations.

iv) Longitudinal vibrations of the deck are not significant below 4Hz. Generally it moves with the pylon at that level.

v) The cables vibrate at harmonics of a fundamental frequency in any plane, but typically with an in-plane component approximately 1.4 times the out-of-plane component. Less than 10% of the way along the cable from the deck its acceleration amplitude was approximately 10 times that of the deck.

vi) 7 longitudinal and 13 lateral natural frequencies and modes were identified for the free-standing M1 pylon, up to 10Hz. The first natural frequency was at 0.23Hz.

There appeared to be several very similar mode shapes but with different natural frequencies, believed to be due to the influence of the pylon cross-beams.

vii) The wind loading on the deck of the cantilever structure is dominant over the loading on the pylon, as assumed for conventional buffeting analyses (§2.6.4).

For the main long-term test data (§4.5.4), preliminary analysis enabled periods for subsequent detailed processing to be identified. The results of the detailed processing are presented in Chapters 8-10. The component of the wind normal to the bridge axis was shown to give better correlation with the amplitude of response than the wind speed.

The measured wind velocity was found to be approximately stationary for periods of up to three hours. Also the form of the von Kármán spectra (§2.6.4.1) provides a good model of the turbulence, even in light winds. The measured turbulence intensities were lower than the ESDU (1993) values used for design, but this may have been due to the relatively low wind speeds experienced. The presence of the bridge deck significantly affected the vertical component of wind velocity at the measurement locations, 12m above the deck, on both the windward and leeward edges.

The short correlation length assumption of wind loading (§2.6.4.2) was validated for the SSC, by very low measurements of coherence between wind velocities at different locations on the structure, and between the wind velocity at one point and the bridge response.

An estimated spectrum of the generalised wind loading of each mode of vibration was derived, considering the wind velocity spectra and the spatial variation of the loading.

For the finished bridge, traffic loading was found to be dominant for wind speeds below approximately 9m/s for light traffic, or 12m/s for heavy traffic. The spectrum of traffic loading was shown to approximate to white noise, at least in range 0.3-2Hz. In strong winds (above approximately 15m/s), wind loading can be taken to be dominant in the frequency range 0.3-1.5Hz.

The derived wind and traffic loading spectra are used by the improved system identification method (Chapter 7), to enable more accurate estimates of modal parameters, particularly damping, than normally possible from ambient vibration data. This method is then applied to the SSC data in Chapter 8.

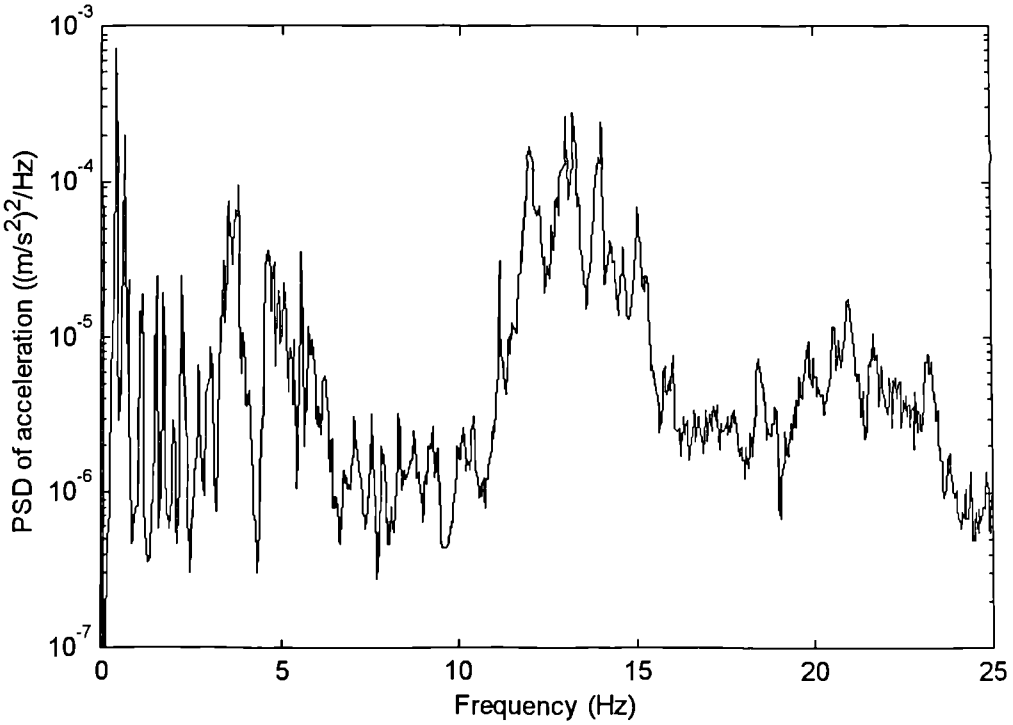

Fig. 6-1 Typical PSD of vertical acceleration of the end of the M2 cantilever deck in preliminary tests, full frequency range (wind 13m/s, 30° to west of south normal (§3.2.2))

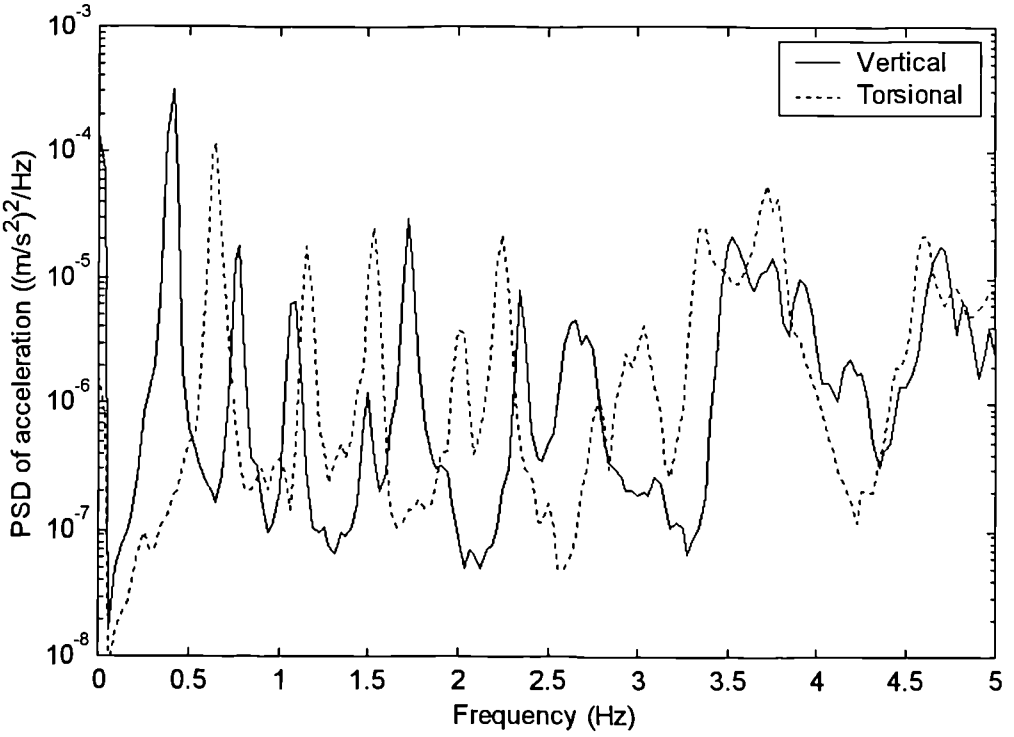

Fig. 6-2 Typical PSD of acceleration of the end of the deck in preliminary tests, up to 5Hz, vertical bending and torsional components separated (wind 13m/s, 30° to west of south normal)

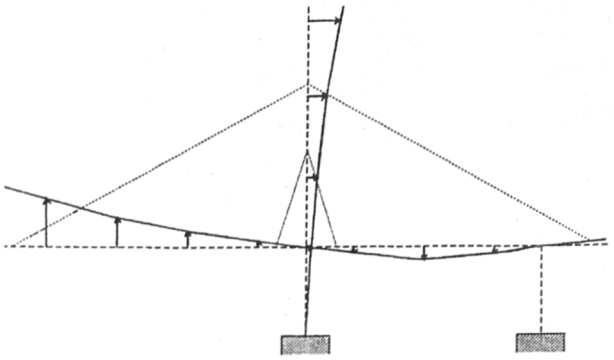

South elevation

Mode 1, 0.39Hz

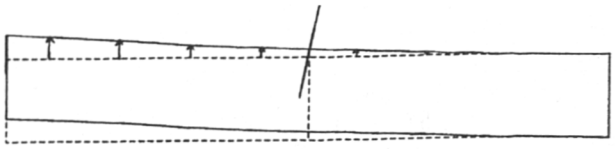

Plan

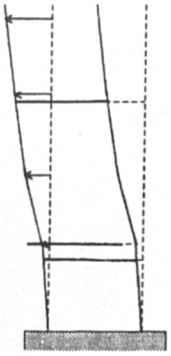

West elevation

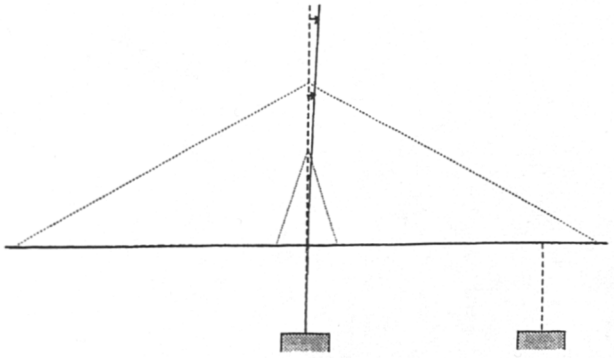

South elevation

Mode 2, 0.50Hz

Fig. 6-3 First two measured mode shapes of M2 cantilever from preliminary tests

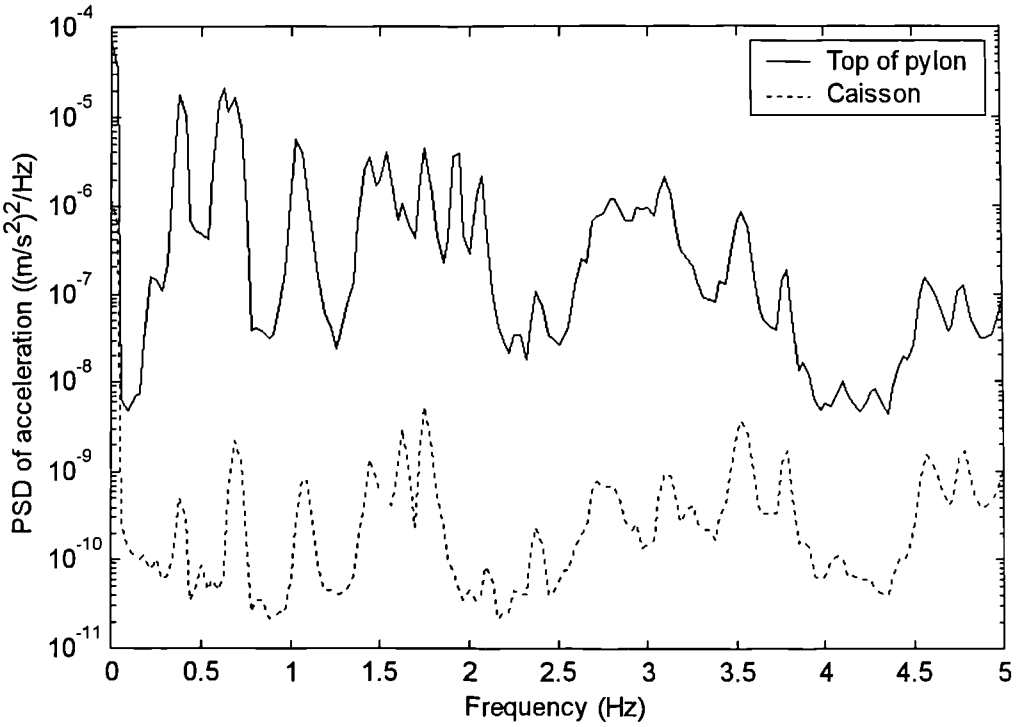

Fig. 6-4 Comparison of PSDs of longitudinal acceleration at top of pylon and on caisson

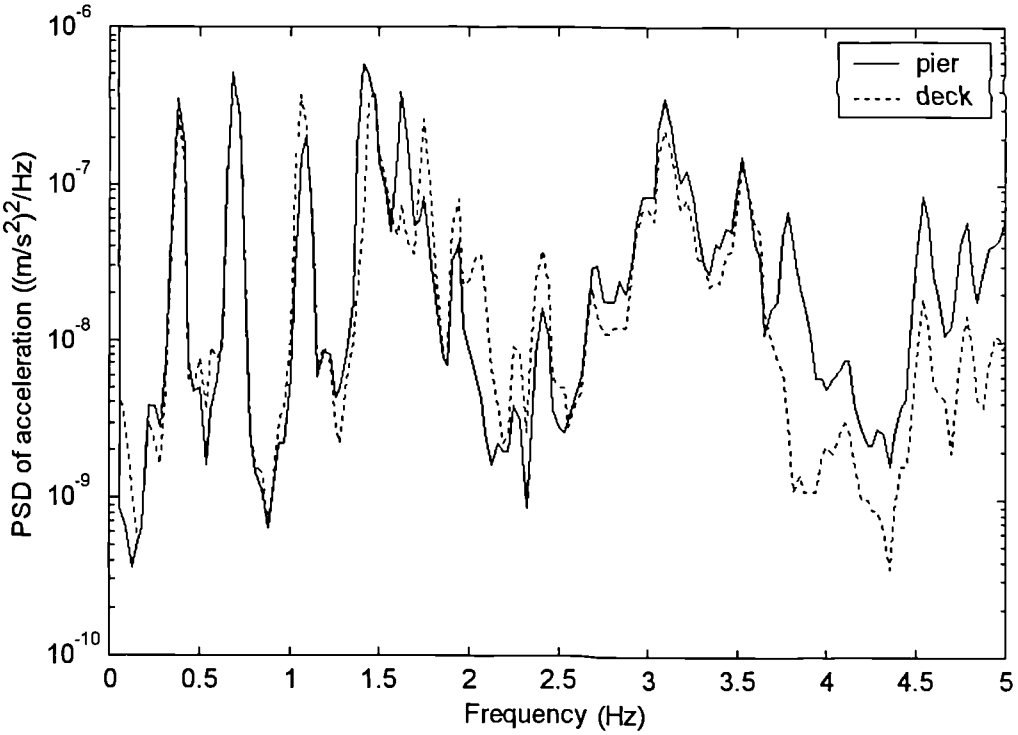

Fig. 6-5 PSDs of longitudinal accelerations either side of bearing

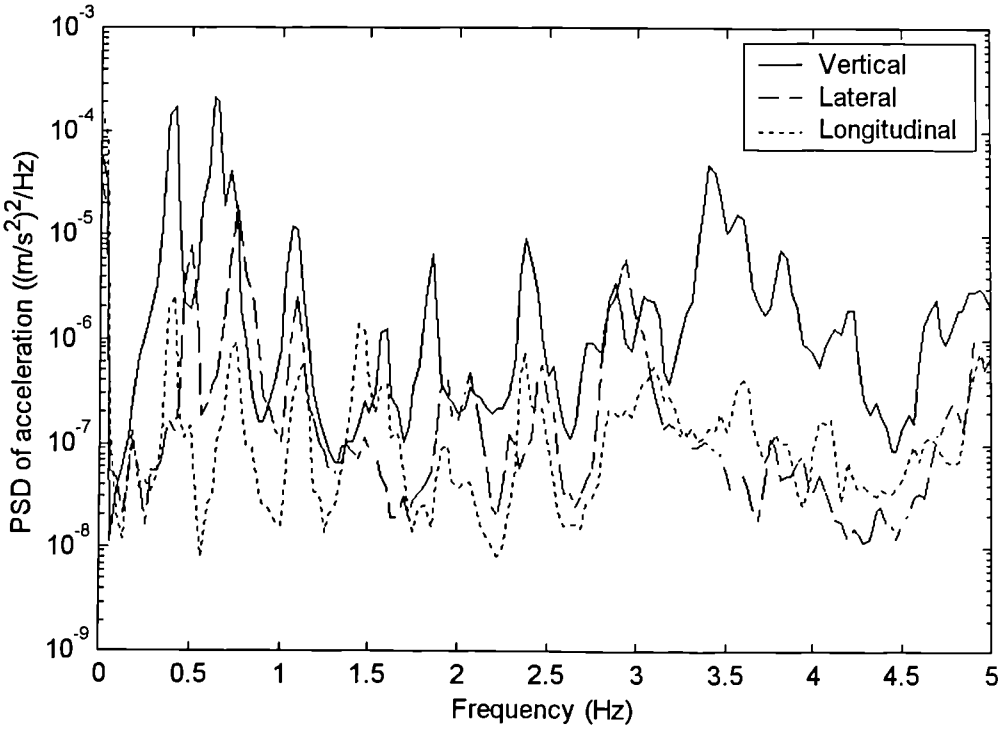

Fig. 6-6 PSDs of vertical, lateral and longitudinal accelerations of north side of the end of the deck in preliminary tests

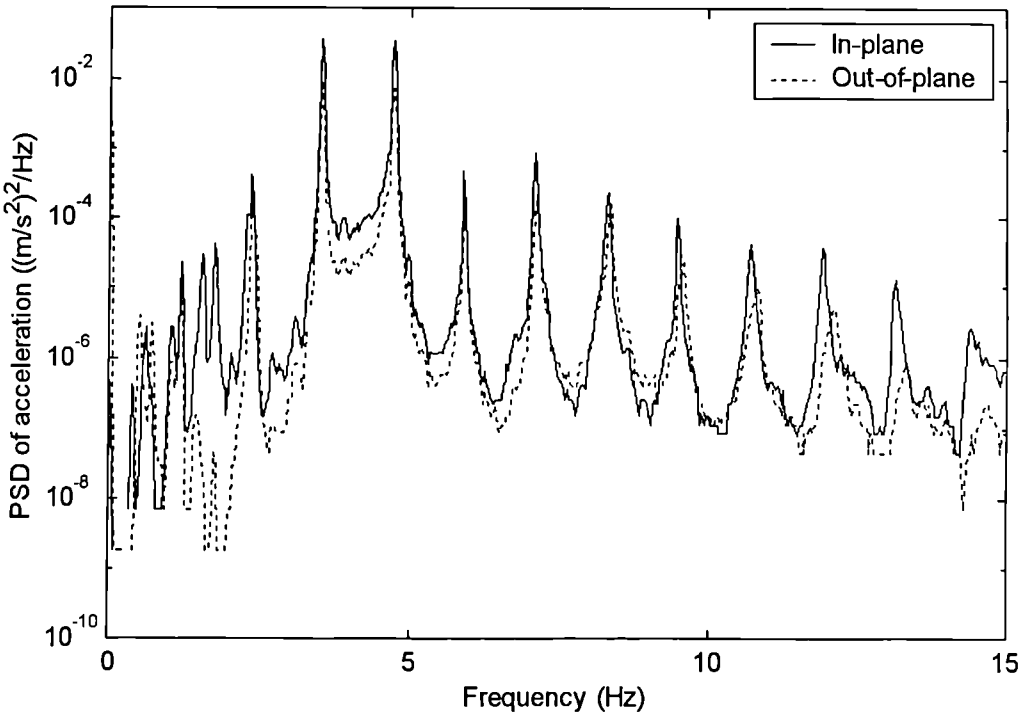

Fig. 6-7 PSDs of cable accelerations 5.6m from deck end in orthogonal directions in preliminary tests

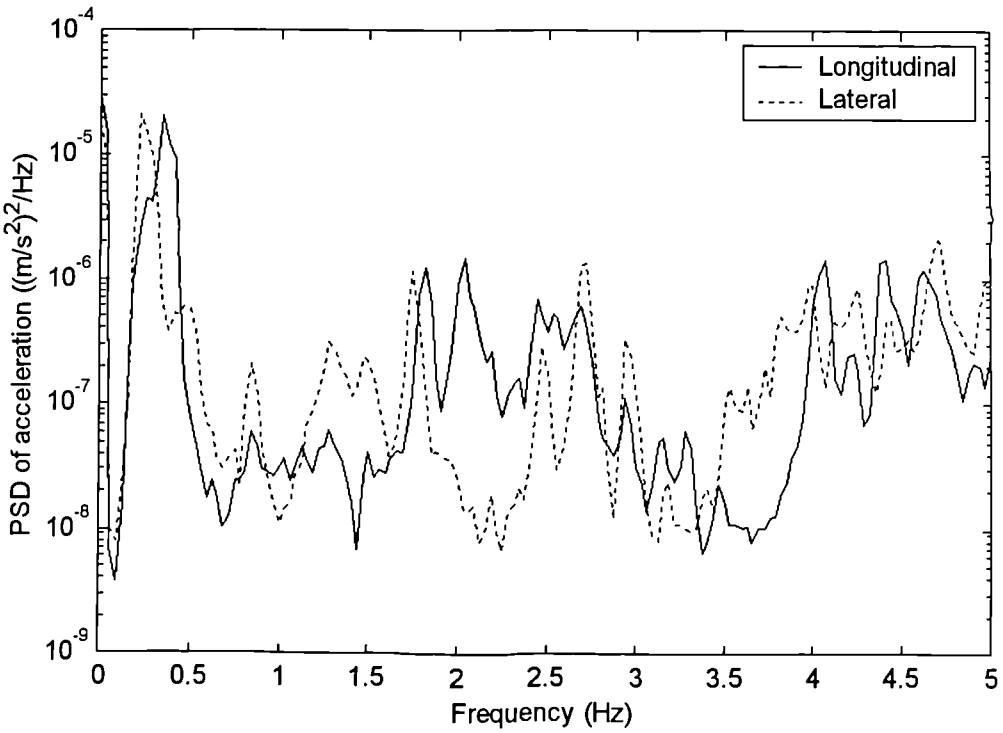

Fig. 6-8 PSDs of accelerations at top of free-standing M1 pylon (wind 9m/s, 20° from south normal)

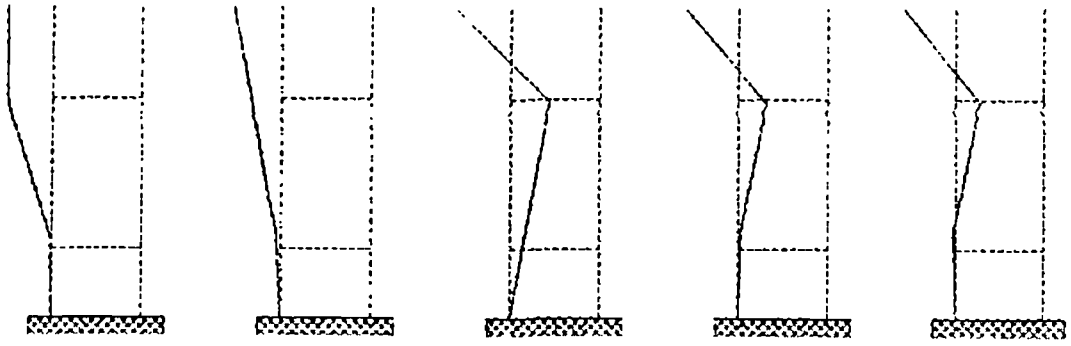

Fig. 6-9 First five measured lateral mode shapes of free-standing M1 pylon

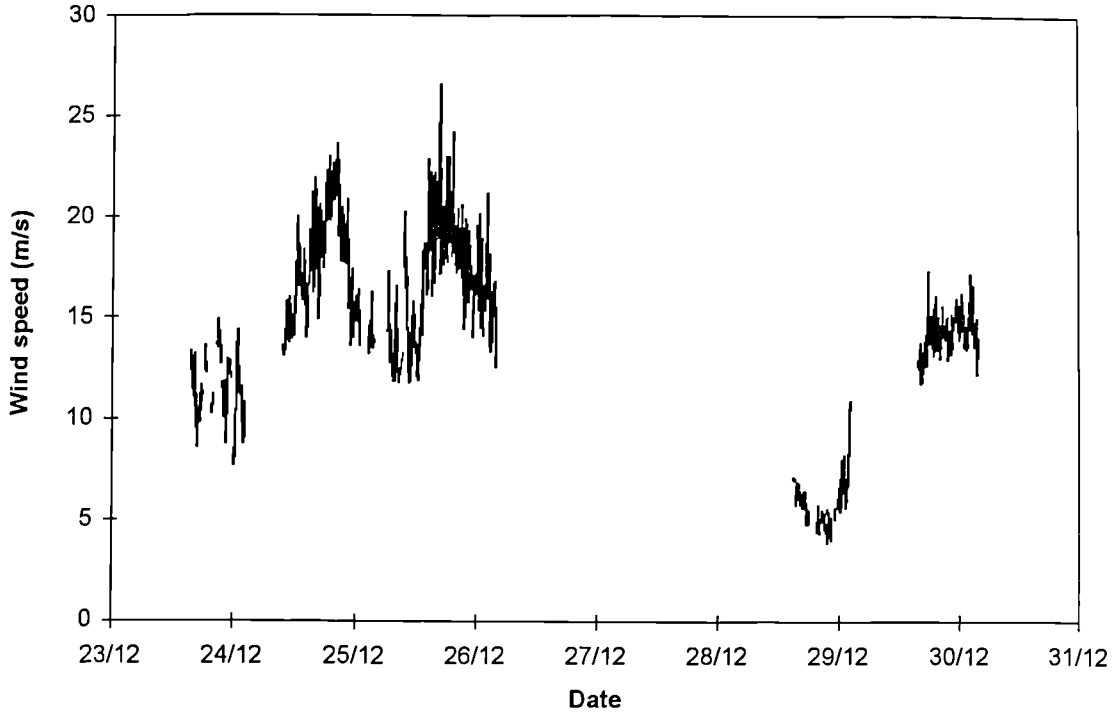

Fig. 6-10 Typical plot of wind speed against time for finished bridge (gaps occur when recording not triggered)

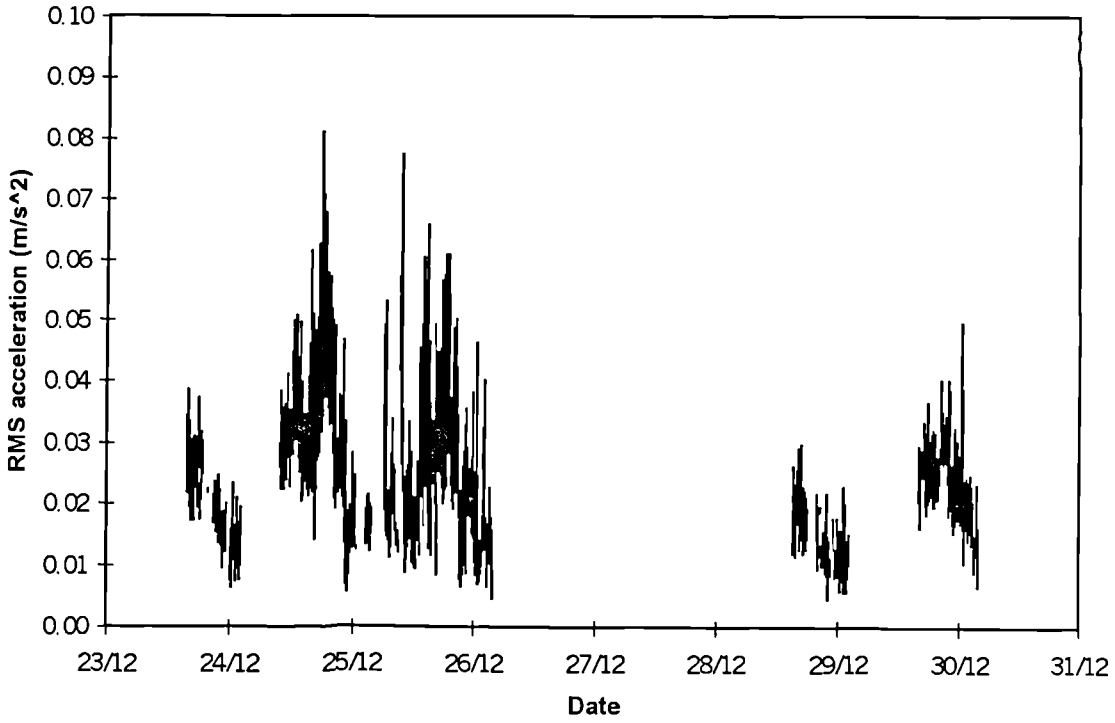

Fig. 6-11 Typical plot of RMS vertical acceleration of the deck against time for finished bridge (gaps occur when recording not triggered)

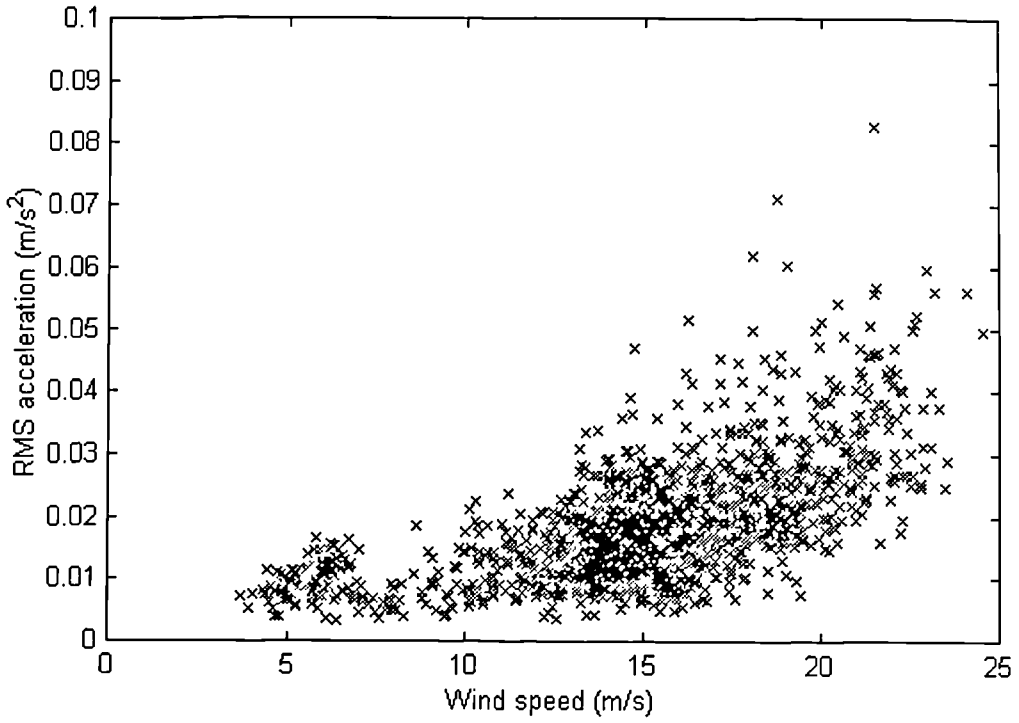

Fig. 6-12 Typical plot of RMS vertical acceleration of the deck against wind speed for finished bridge

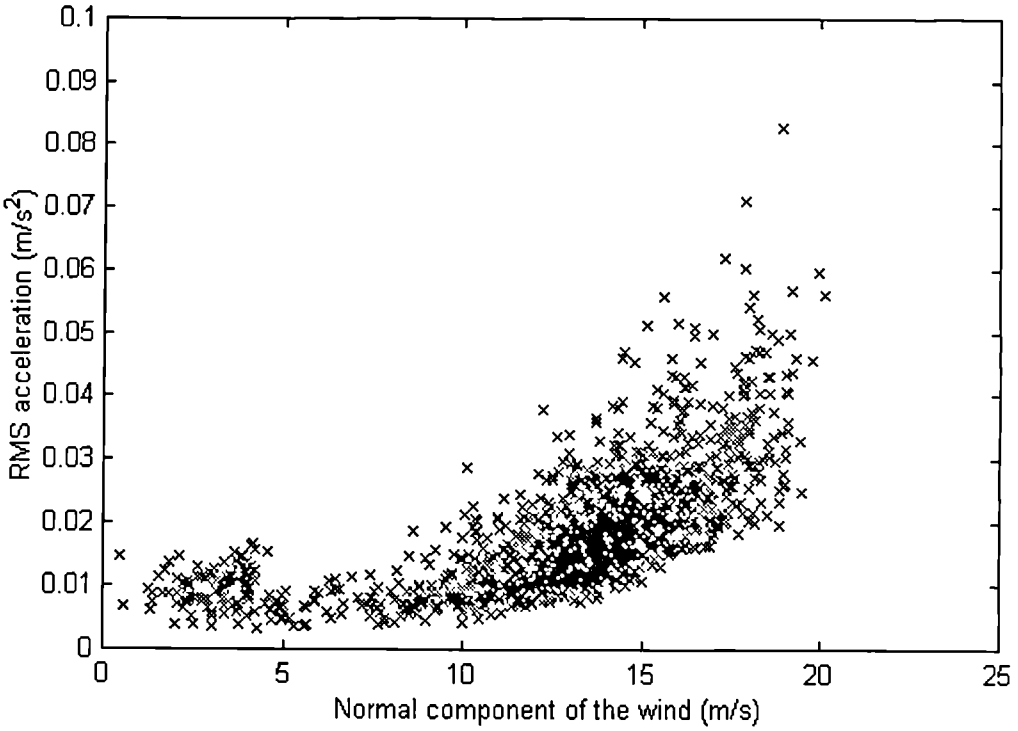

Fig. 6-13 Typical plot of RMS vertical acceleration of the deck against normal component of wind speed for finished bridge

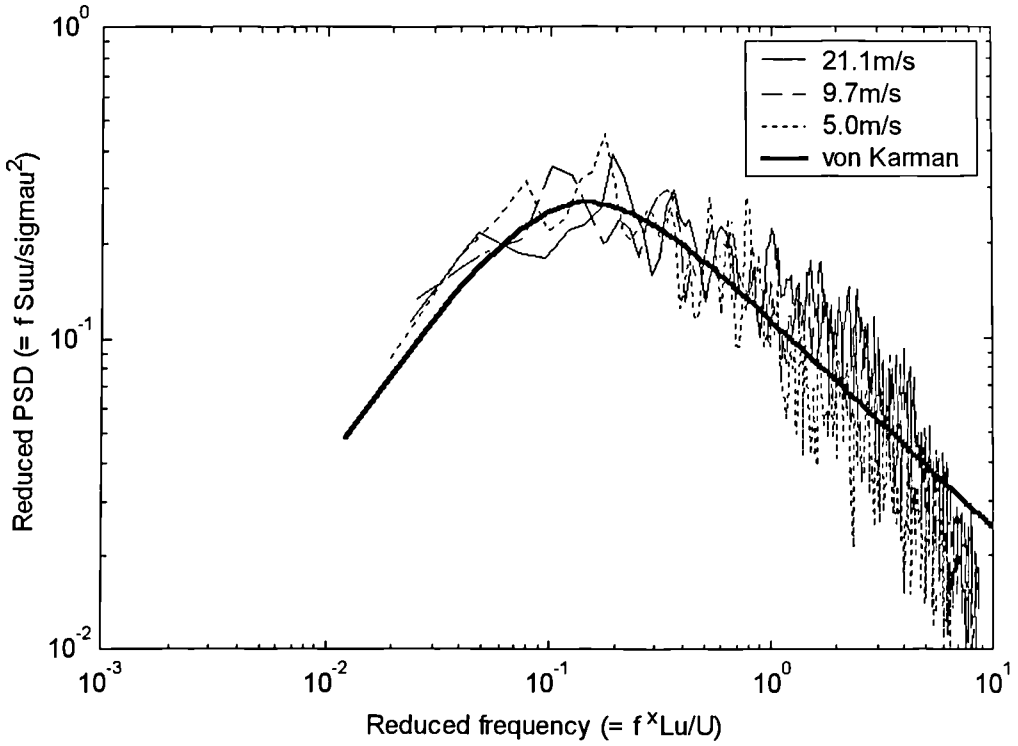

Fig. 6-14 Measured PSDs of longitudinal wind velocity on windward side of SSC deck at various wind speeds, compared with von Kármán spectrum (equation (2-14))

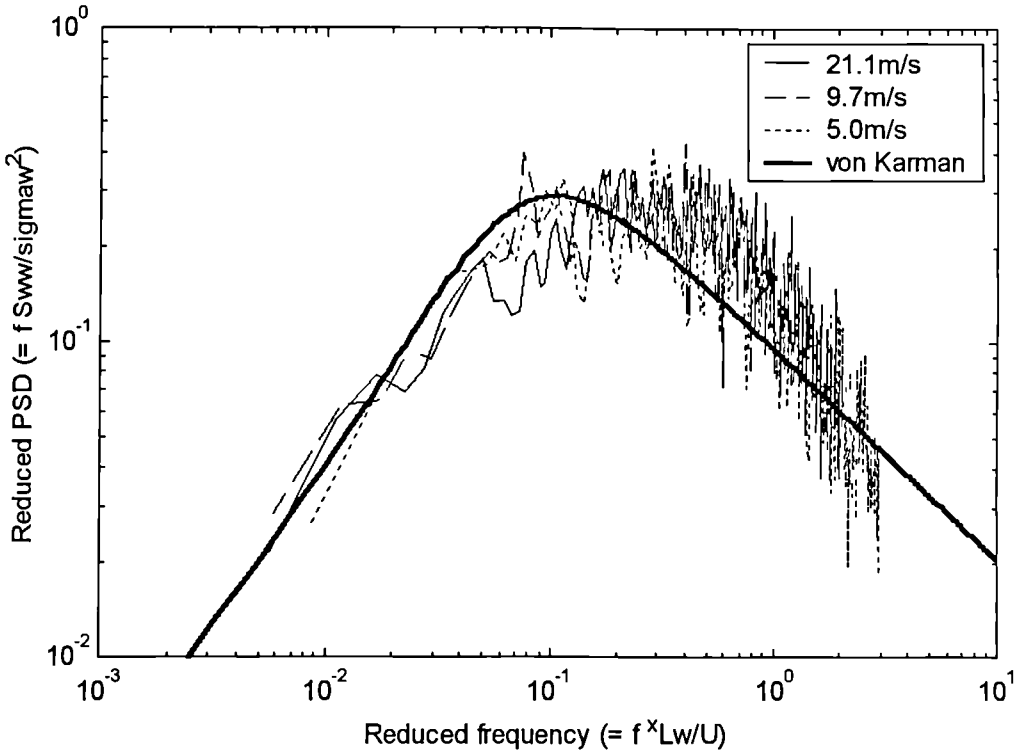

Fig. 6-15 Measured PSDs of vertical wind velocity on windward side of SSC deck at various wind speeds, compared with von Kármán spectrum (equation (2-15))

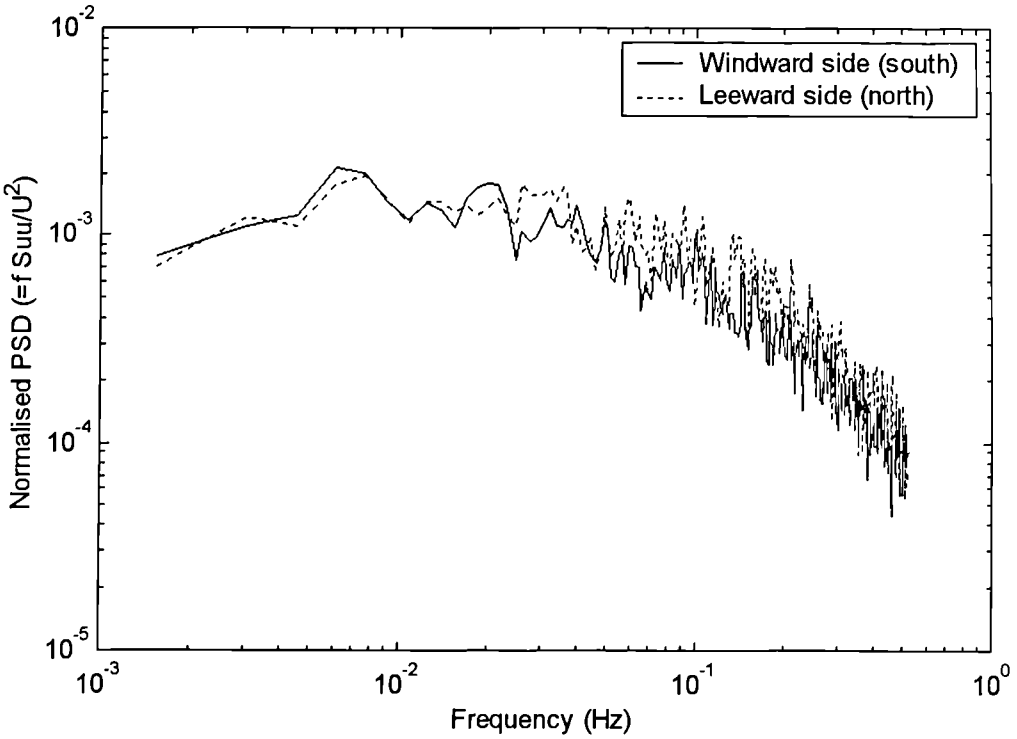

Fig. 6-16 Comparison of measured longitudinal wind velocity spectra on windward and leeward sides of SSC deck (wind 9.7m/s, 28° east of south normal)

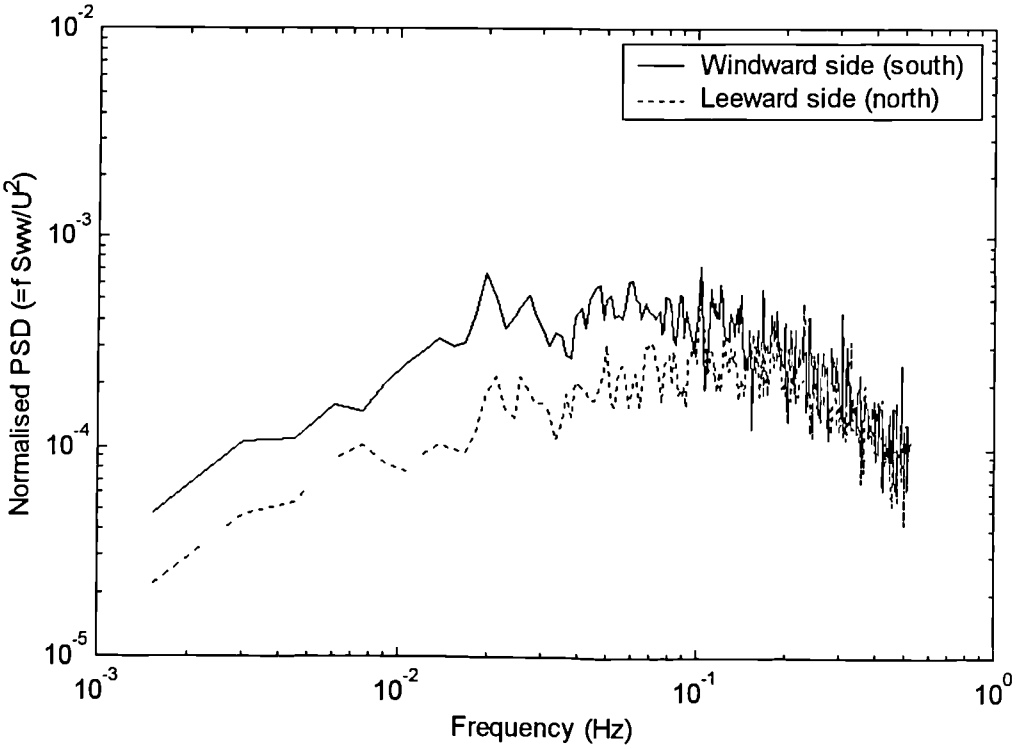

Fig. 6-17 Comparison of measured vertical wind velocity spectra on windward and leeward sides of SSC deck (wind 9.7m/s, 28° east of south normal)

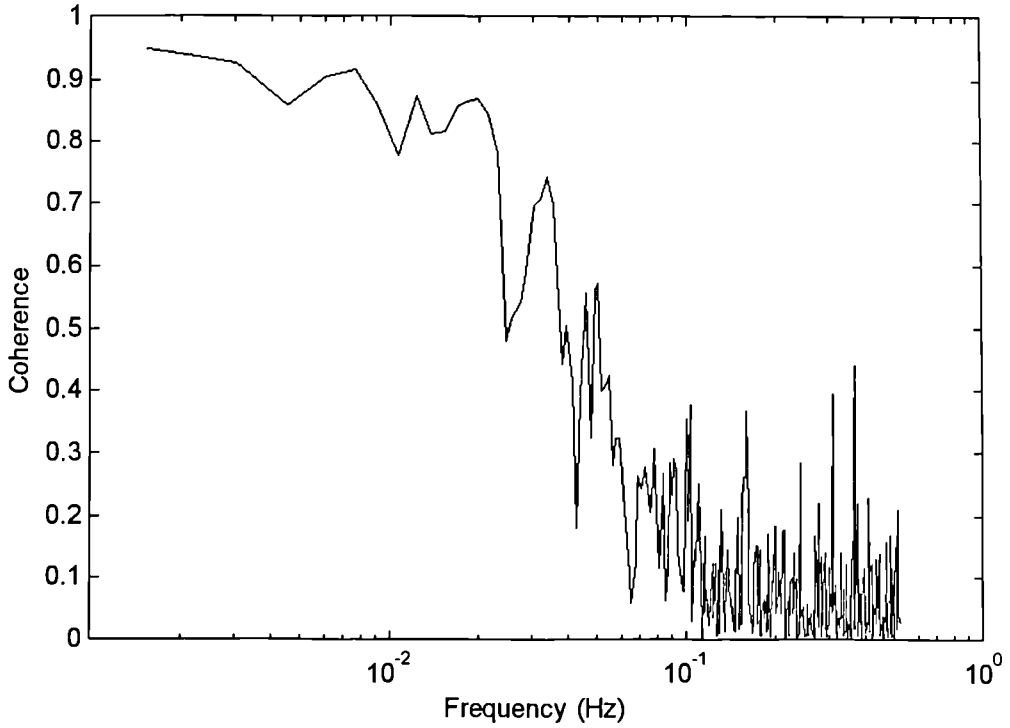

Fig. 6-18 Coherence between measured longitudinal wind velocities on windward and leeward sides of SSC deck (wind 9.7m/s, 28° east of south normal)

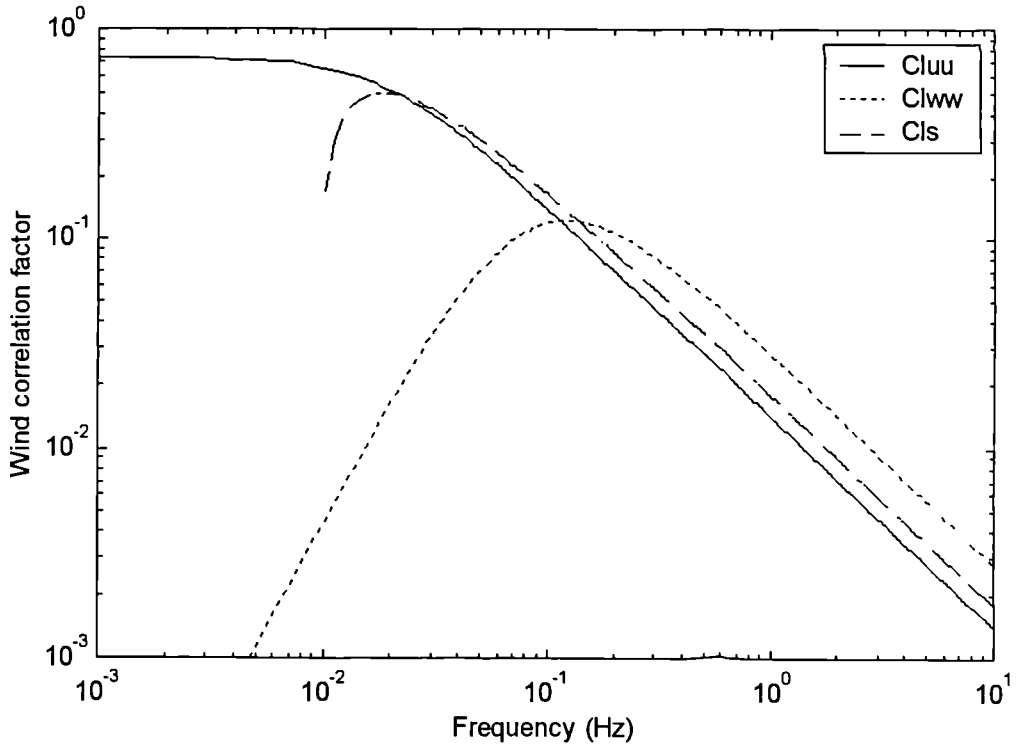

Fig. 6-19 Wind correlation factors (equations (6-2)-(6-4)) for completed SSC cantilever in 30m/s wind

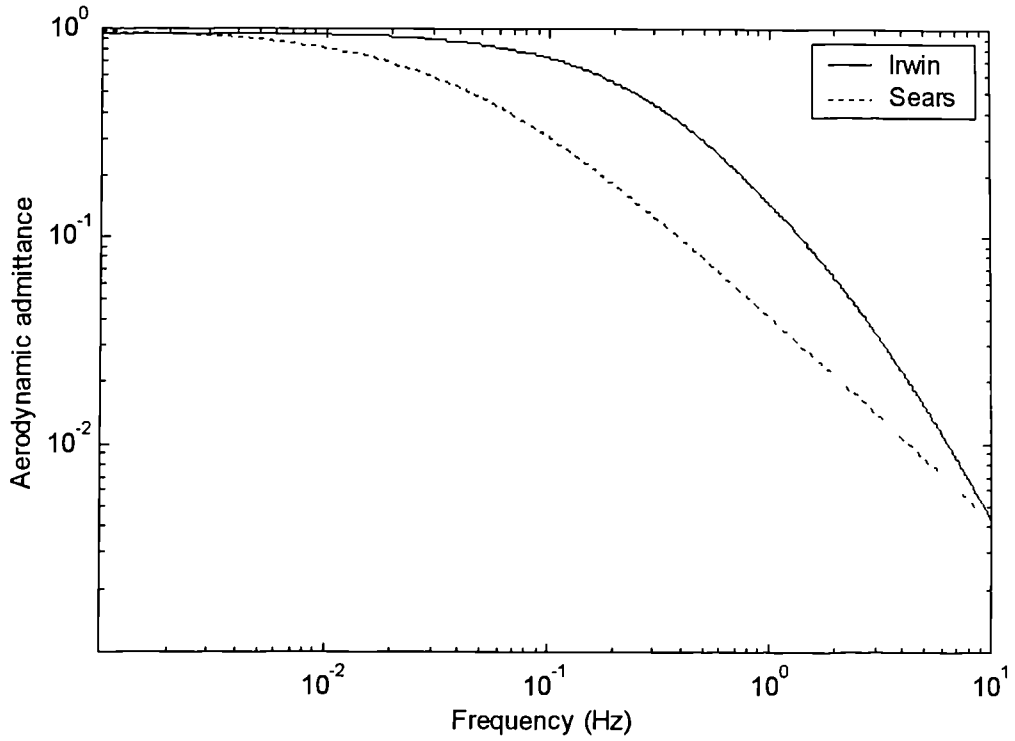

Fig. 6-20 Estimated aerodynamic admittance of SSC bridge deck (without wind barriers) for 30m/s wind, normal to bridge

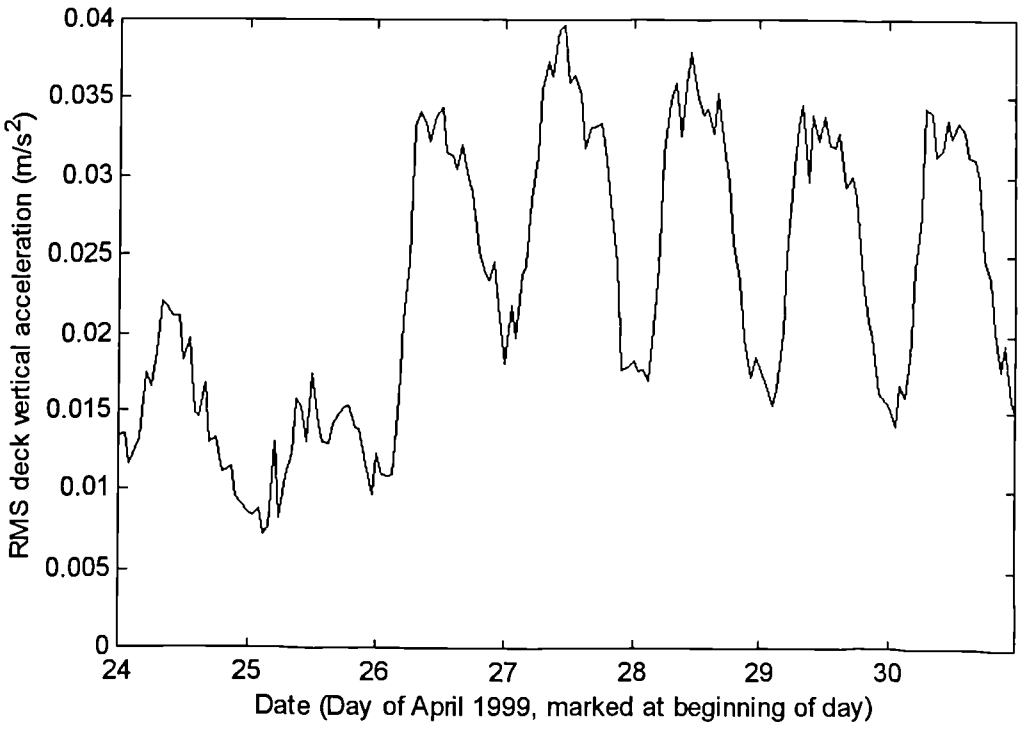

Fig. 6-21 Hourly RMS deck vertical accelerations for finished bridge, showing daily variation with traffic loading, Sat. 24 – Fri. 30 April 1999 (wind speed up to 15m/s)

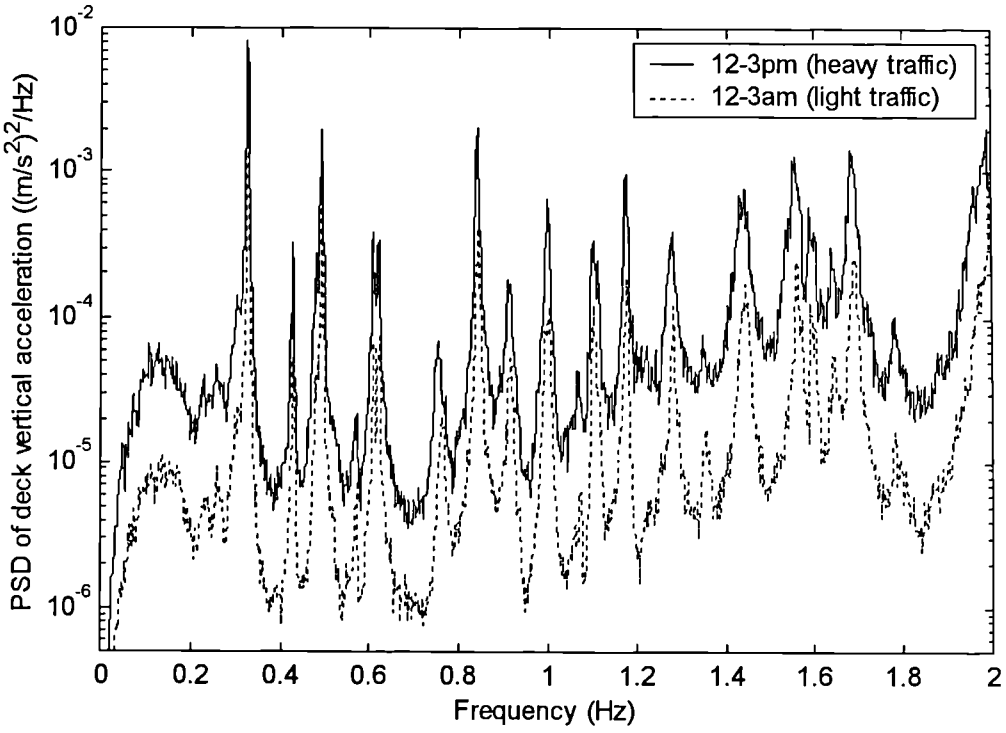

Fig. 6-22 PSDs of deck vertical acceleration of finished bridge in different traffic conditions in light winds (<3m/s)

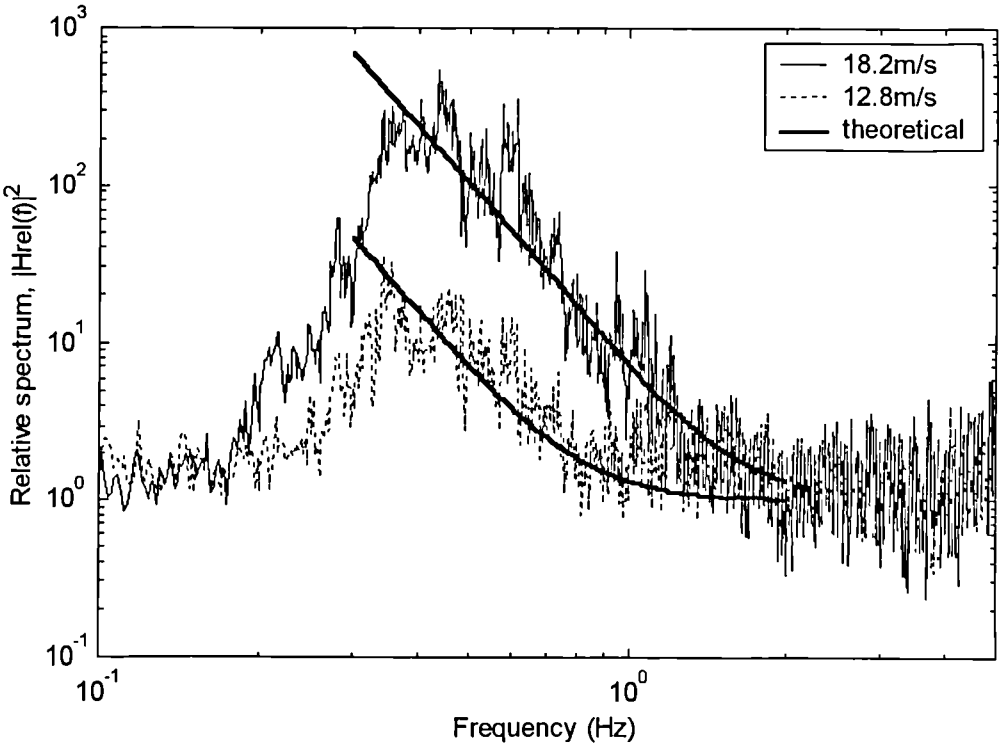

Fig. 6-23 Relative spectra of deck vertical accelerations in different wind conditions compared with response in light wind (2.8m/s), for finished bridge with light traffic (night-time)

CHAPTER 7 IMPROVED SYSTEM IDENTIFICATION FROM ESTIMATED SPECTRA

7.1 Introduction

This chapter describes the Iterative Windowed Curve-fitting Method (IWCM), a new method of system identification from ambient vibration data, based on the frequency domain curve-fitting method (§5.3.2.1).

In §5.3.2 it was shown that, for system identification from ambient vibration data:

i) Frequency domain methods based on the Fast Fourier Transform (FFT) are subject to bias errors (§5.6.1), leading to overestimates of damping.

ii) Methods for ambient vibration data generally assume a white noise loading spectrum, which is inappropriate for wind loading (§6.5).

iii) Single-Degree-Of-Freedom (SDOF) methods neglect the contributions of other modes.

iv) Multiple-Degree-Of-Freedom (MDOF) methods require an estimate of the number of modes, which affects the results and can lead to errors.

The IWCM overcomes bias errors (§7.4) and allows for a specific assumed loading spectrum (§7.6). It is essentially an SDOF method, but an iterative procedure deals with the combined response of several modes (§7.7). The new developments are assessed and the accuracy of the results are estimated. The method is also extended for the estimation of mode shapes (§7.8).

As an example, the method is applied to data from the Second Severn Crossing (SSC) (Chapter 4), converted to estimated response Power Spectral Densities (PSDs) (Chapter 5). This enables justification of the assumptions for the SSC and for values of processing parameters to be defined. The estimated wind and traffic loading spectra derived in Chapter 6 are used in the analysis. Results from the SSC data, using the IWCM, are presented in Chapter 8.

The IWCM is based on the comparison of estimated response PSDs, from measured data or theory. The terms used in this thesis to describe the different PSDs, some of which are subject to bias and/or variance errors, are defined in Table 7-1. The terms 'PSD' and 'spectrum' are used interchangeably. All of the response spectra used in this chapter refer to acceleration responses.

Table 7-1 Definitions of various response spectra discussed in Chapters 7&8

Name	Definition	Subject to errors:	
		Bias	Variance
Measured	Spectrum estimated from (windowed) measured response data (§5.6)	✓	✓
Simulated measured	Spectrum estimated from (windowed) simulated response data	✓	✓
Expected measured	Expected measured spectrum	✓	
True	Spectrum of the (theoretically infinitely long) un-windowed response data		
Model	Theoretical spectrum, based on estimated modal parameters		
Windowed model	Model spectrum, modified by the window function in the frequency domain	✓	
Fitted	Final best fit to measured spectrum of the sum of several windowed model spectra	✓	

7.2 Assumption of linear superposition of modal responses

In this analysis, the total response PSD is assumed to be equal to the sum of the response PSDs of several modes, each represented by an SDOF oscillator (§2.4.2&5.2.1). This in turn is based on the following assumptions:

i) *The system is linear*

Although cable-stayed bridges can exhibit significant non-linearities for static loading, the low amplitude dynamic behaviour is approximately linear (§2.4.1 &2.4.3).

ii) *The modes are uncoupled*

The modes can be coupled by damping, but when it is low, as for cable-stayed bridges (§2.5.1), the coupling can be neglected with little loss of accuracy (Maia et al. 1997). The modes can also be coupled aeroelastically by the flutter derivatives (§2.6.5.1), but for conventional buffeting analyses this is ignored (§2.6.4). Multi-mode combined buffeting and flutter analyses do consider this effect (§2.6.6), but Jain et al. (1996) found that the difference from the assumption of uncoupled modes only becomes significant at wind speeds approaching the flutter speed. Therefore, for the wind speeds monitored on the SSC (§6.4.1), the coupling can be neglected.

iii) *The generalised loads are uncorrelated*

The generalised load for each mode is given by equation (2-4) (§2.4.2). The generalised loads would be correlated if two modes were of similar shape, or if the spatially distributed loads were correlated. However, since mode shapes are orthogonal with respect to mass (Ewins 1984), and the majority of the mass of cable-stayed bridges is in the deck, the global modes have distinct shapes. On long-span bridges, the correlation length of wind loading is generally assumed sufficiently short for the generalised loads to be considered uncorrelated (§2.6.4.2). This was supported for the SSC by measurements of very low coherence between wind velocities at two locations, and between the wind velocity at one location and the bridge response (§6.4.6&6.4.7).

When considering the results for the SSC, variations in modal parameters and discrepancies between the measured and fitted spectra are investigated as evidence of departures from the above assumptions (§8.5).

7.3 Conventional curve-fitting of Power Spectral Densities

Before introducing the new developments of the IWCM, details of the conventional curve-fitting method (§5.3.2.1) are provided here.

The PSD of the output of a Single Input Single Output (SISO) system subject to random excitation is given by (Bendat & Piersol 1986):

$$S_{yy}(f) = |H(f)|^2 S_{xx}(f) \tag{7-1}$$

where: f = frequency

$S_{xx}(f)$ = PSD of input

$H(f)$ = Frequency Response Function (FRF) of the system

For a given mode of a structure, equivalent to an SDOF oscillator with viscous damping, the FRF relating force input to acceleration output ('accelerance') is (Maia et al. 1997):

$$H(f) = \frac{-(f/f_n)^2}{M\{1-(f/f_n)^2 + 2\zeta(f/f_n)i\}} \tag{7-2}$$

where: f_n = undamped natural frequency

ζ = damping ratio

M = generalised mass (equation (2-3))

$i = \sqrt{-1}$

Thus, combining equations (7-1) and (7-2), the 'model' acceleration PSD, for a force input, is given by:

$$S_{yy}(f) = \frac{S_{xx}(f)}{M^2} \frac{(f/f_n)^4}{[\{1-(f/f_n)^2\}^2 + (2\zeta f/f_n)^2]} \tag{7-3}$$

Therefore, if it is assumed that near the natural frequency the effect of other modes is negligible and that $S_{xx}(f)$ is constant (i.e. white noise input), the above expression can be fitted to the 'measured' acceleration PSD over a limited frequency range. This yields estimates for the three unknown parameters - natural frequency (f_n), damping ratio (ζ) and amplitude ($\sqrt{(S_{xx}/M^2)}$). This is usually performed by a numerical method to find the least-squares best fit between the discrete measured and model spectra.

7.4 Dealing with bias errors – the Windowed Curve-fitting Method (WCM)

For measured spectra, the existence of bias errors at peaks is unavoidable for random data of finite length (§5.6.1). However, it is a systematic error, with a clearly defined origin. The following procedure, the Windowed Curve-fitting Method (WCM) was therefore developed to compensate for this error when extracting modal parameters for individual modes from measured spectra. The case of multiple modes is addressed in §7.7 by the IWCM.

For FFT spectral estimates, the window function defines the bias errors, including the effects of both the discretisation of the spectrum and leakage (§5.6.1). The WCM is based on consideration of the effect of the window on the PSDs.

7.4.1 Theoretical basis of the method

It can be shown that the expected measured spectrum, estimated from measured data using a series of windowed blocks (§5.6.1&5.6.2), is equal to (Therrien 1992):

$$E[\hat{S}_{yy}(f)] = \frac{\int_{-\infty}^{\infty} S_{yy}(f) W^2(\phi - f) d\phi}{\int_{\infty}^{\infty} W^2(f) df} \tag{7-4}$$

where: $W(f)$ = Fourier transform of the time domain window function, $w(t)$

$S_{yy}(f)$ = true spectrum

Strictly this only applies to two-sided spectra, since the convolution integral of the numerator includes negative frequency components. However, in practice it is only very close to zero frequency that there is any significant overlap of the negative and positive frequency components. Therefore, for the present study the equation was taken to apply to single-sided spectra, with negligible error in the frequency range of interest.

The normalising factor in the denominator of equation (7-4) is to scale the magnitude of the expected measured spectrum to match the total power of the true spectrum, to compensate for the attenuation from the window. It is normally evaluated in the time domain for the calculation of measured spectra:

$$\int_{\infty}^{\infty} W^2(f)df \equiv \int_{\infty}^{\infty} w^2(t)dt \qquad (7\text{-}5)$$

For conventional curve-fitting (§7.3), and other standard frequency domain methods (§5.3.2.1), the measured spectrum is taken to be a direct estimate of the true spectrum. However the convolution smoothes it, thus introducing bias errors. The WCM, in contrast, takes into consideration the difference between the spectra.

7.4.2 Window functions

If no window is deliberately employed in the calculation of measured spectra, a rectangular (or 'boxcar') window is effectively applied. This is equal to unity for the period of the record (taken as $-T/2$ to $T/2$) and zero at other times, giving a frequency domain window function of:

$$W_r(f) = \frac{\sin(\pi f T)}{\pi f} \qquad (7\text{-}6)$$

This has 'side lobes' of significant magnitude (Fig. 7-1), indicating considerable leakage.

The most commonly used window, which was used for the processing of the SSC data, is the Hanning window, defined in the time domain as (Bendat & Piersol 1986):

$$w_h(t) = \frac{1}{2}\left\{1 + \cos\left(\frac{2\pi t}{T}\right)\right\} \qquad -T\ 2 < t < T\ 2$$
$$= 0 \qquad \text{otherwise} \qquad (7\text{-}7)$$

giving a frequency domain window function of:

$$W_h(f) = \frac{\sin(\pi f T)}{2\pi f(1 - f^2 T^2)} \tag{7-8}$$

This has a broader central lobe but the side lobes are significantly reduced in amplitude (Fig. 7-2). Therefore, although there is greater leakage to the adjacent discrete spectral values, the leakage to frequencies beyond that is greatly reduced.

The result of the Hanning window on measured spectra is generally to give a more accurate estimate of the true spectrum than arises from the rectangular window, but to broaden peaks in the PSD. This increases the bias errors at the peaks, particularly for coarse frequency resolutions, tending to produce more exaggerated damping estimates from conventional system identification methods. However, this error is effectively eliminated with the WCM.

7.4.3 Description of the Windowed Curve-fitting Method

The conventional curve-fitting method aims to minimise the sum of the square errors between the discrete values of the measured and model spectra (§7.3). The measured spectrum is subject to bias errors, whereas the model spectrum is not. However, applying the frequency domain convolution of equation (7-4) to the model spectrum, the windowed model spectrum can be found. For the WCM, the least-square error minimisation is performed between this spectrum and the measured spectrum. The measured spectrum is thus based on the measured response signal with the window applied in the time domain before spectral estimation, and the windowed model spectrum has been modified by the same window function in the frequency domain. Both spectra are therefore subject to the same bias errors, so the effects of the errors are eliminated.

Using this approach, the choice of window is arbitrary. However, the Hanning window is still beneficial compared with the rectangular window, since it reduces the frequency range that needs to be considered for the convolution. The window function exists over an infinite frequency range, so it has to be truncated. However, it rapidly tends to zero (Fig. 7-2), and its square decays even more rapidly, so only a limited number of side lobes need be included to achieve the desired accuracy.

7.4.4 Implementation of the method

The IWCM was implemented as follows. The windowed model spectrum, based on estimated modal parameters, was found by calculating discrete values of the model spectrum (equation (7-3)) at sub-divisions of the frequency interval of the measured

spectrum, followed by a numerical convolution with the square of the frequency domain window function (equation (7-4)). The discrete values at the same frequency intervals as for the measured spectrum were then selected. The objective was to find the optimum values of the modal parameters to minimise the error of this spectrum from the measured spectrum within the frequency range of dominance of the mode. Due to the complexity of the calculation of the windowed model spectrum, an explicit evaluation of the modal parameters for the best fit was not possible, so a numerical iterative procedure was implemented to find a least-squares solution.

Considering a typical PSD from the SSC (Fig. 5-1), the peak values were approximately 100 times greater than the intervening minima. Therefore, minimising the sum of the square errors for the PSD itself would give high weighting to the few points around the maximum and very low weighting to the remaining points. Although the points around the maximum are of most importance, for the measured spectrum they are still subject to variance errors, so a more even weighting of the error function is desirable. For equal standard errors on the spectral estimates at all frequencies, as would arise from variance errors alone (§5.6.2), fitting the function $\log(S_{yy}(f))$ would give equal weighting to all points. However, for the points further from the peaks, noise and the effects of other modes are more significant so their uncertainty is greater. It was therefore decided to base the fit on the compromise of $\sqrt{S_{yy}(f)}$, which maintained a higher weighting for the points around the peak but not to the extreme of $S_{yy}(f)$.

Therefore the sum of the square errors between the square roots of the measured and windowed model spectra was calculated. This was minimised, and the three modal parameters estimated, using the Matlab function 'fminsearch' (Mathworks 1999), which employs the Nelder-Mead simplex method (Nelder & Mead 1965). The termination tolerance on the value of the error function was set to $1\text{x}10^{-15}$ to ensure convergence. With this tolerance, the results were found to be insensitive to the initial estimates and, by visual inspection, in all cases the spectra agreed well. Therefore the results were accepted as the true least-squares solution.

7.5 Test of Windowed Curve-fitting Method with simulated data

The WCM was tested using simulated data to validate the method, and to determine the number of side lobes of the window function and the number of sub-divisions of the frequency resolution necessary to obtain accurate results.

Simulated data were created by time domain convolution of a gaussian white noise input with the displacement impulse response function of an SDOF oscillator, followed by double numerical differentiation. The parameters of the SDOF system were chosen to be representative of a typical mode of vibration of the SSC (§5.4.1). A frequency of 0.6Hz

and damping ratio of 0.5% were selected, along with an arbitrary amplitude. Since the data were created from a random input, the spectra derived from them were subject to variance, as for measured site data, so its effect could also be investigated. The equivalent of 1600 files† of site data (i.e. approx. 73 hours) were created to give sufficient independent records to calculate the variances of the results obtained.

PSDs were calculated from sections of these data, as for site data (§5.4), and then the WCM was applied to attempt to re-extract the modal parameters. The curve-fit was generally performed over the frequency range 0.55-0.65Hz, typical of the range of frequencies available for fitting individual peaks in the site measured spectra.

7.5.1 Comparison of windowed model spectra and simulated measured spectra

To confirm that the windowed model spectra from equation (7-4) were compatible with the simulated measured spectra, their shapes were compared visually. Fig. 7-3 shows the model spectrum, calculated directly from the defined modal parameters, along with windowed model spectra and typical simulated measured spectra, for both the rectangular window and the Hanning window. In both cases the shapes of the simulated measured and windowed model spectra agree very well, giving confidence in the calculation of the windowed model spectra. The slight differences are due to variance in the simulated measured spectra, from the random nature of the simulated data. The differences in the spectra resulting from the different windows (§7.4.2) are also clear.

7.5.2 Bias errors

Fig. 7-4 shows the bias errors at the peaks of the windowed model spectra compared with the model spectrum, along with the estimated bias errors from equation (5-8). The bias errors are shown for varying block length, corresponding to varying frequency resolution. A block length equal to one file length (163.84s, 4096 samples) yields a frequency resolution of 6.1×10^{-3} Hz. This gives a ratio of frequency resolution to Half Power Bandwidth (HPB) (B_e/B_r) of 1.02. Therefore, the ratio is virtually equivalent to the inverse of the number of files per block. It can be seen in Fig. 7-4 that the Hanning window gives increased bias errors over the rectangular window and that, in the range considered, for all but the shortest records, equation (5-8) underestimates the errors. This emphasises that the equation is only a reasonable estimate of the error for high frequency resolution, and that for ambient vibrations of large structures the bias errors at resonances can be considerable.

† Each file represents 163.84s (4096 samples) of data (§4.3.2).

7.5.3 Damping ratio estimates

The bias errors cause overestimates of damping for conventional frequency domain system identification methods. Fig. 7-5 shows the mean errors of the damping estimates from the conventional curve-fitting method and the WCM, applied to the simulated measured spectra calculated using the Hanning window. For the shorter block lengths (coarser frequency resolution), the conventional curve-fitting method gives gross overestimates, but the WCM consistently gives virtually no error. The small errors present are believed to be due to statistical variations in the results. This demonstrates that the method effectively eliminates the errors due to bias, even for very coarse frequency resolutions. The remaining errors are due to variance alone.

For a given total record length, the variance errors on the spectra are reduced by averaging over a larger number of blocks, at the expense of reduced frequency resolution (§5.6.2). Therefore, although with averaging the spectral values are more accurately defined, there are then less points in the frequency range for curve-fitting, so the results are more sensitive to errors in each point.

To optimise the block length for a given total record length, a series of tests were performed using the simulated data. Damping estimates were calculated by the WCM from simulated measured spectra obtained from many simulated records split into blocks of varying lengths. The variance, and hence the normalised error, of the damping estimate for each block length was calculated, relative to the known actual damping ratio (0.5%).

The results are plotted in Fig. 7-6 for different total record lengths. It can be seen that there is little variation in the normalised damping error with block length, although there is a slight trend towards higher errors for longer blocks and in all cases there is a minimum for blocks 0.5 files long (81.92s, 2048 samples). This corresponds to a frequency resolution of 12.2×10^{-3} Hz, approximately twice the HPB of the peak and with only eight points in the 0.1Hz frequency range used for the curve-fitting. For the site spectra, the frequency range between some minima in the spectra was as little as half of this, so the calculation was repeated, fitting the curve in the frequency range 0.575-0.625Hz, for a total record length of 50 files. The results are also shown in Fig. 7-6, with only a marginal increase (typically 8%) in the error, and the minimum still occurring for blocks 0.5 files long. However, for the 0.25 file length test, there were insufficient points in the frequency range to obtain a reasonable fit so the errors were very large.

7.5.4 Accuracy of modal parameter estimates

Although blocks 0.5 files long gave the minimum error for a given total record length, the error was not very sensitive to block length. For the SSC data, blocks 4 files long

(approx. 11 min) were the optimum for the stationarity test (§5.6.4), so this was chosen as the preferred block length for the main analysis of the site data. This also had the advantage of giving a relatively high frequency resolution, to enable the initial identification of close modes, which could be blurred together using a coarser resolution. For records shorter than three hours, meaningful self-stationarity and overall stationarity tests could not both be performed (§5.6.4), so for such records the optimum block length of 0.5 files was used, and only the overall stationarity test was carried out.

For blocks 4 files long, Fig. 7-7 shows the effect of variance errors (based on the number of blocks) on the normalised error of the damping estimate. The damping estimates were calculated from simulated measured spectra based on the fixed block length, for records of between 6 and 100 blocks. The variance errors of the spectrum were obtained from equation (5-10). It can be seen that there is a linear relationship between the errors and, if overlapped blocks are not used, the error on the damping estimate is approximately equal to half the variance error on the spectrum. Also shown are the damping errors with 50% overlapped blocks included, but still plotted against the spectral errors based on the original number of blocks. The overlapping gives a significant reduction in the damping errors, which approximately fit the empirical equation:

$$\varepsilon_d = \frac{0.38}{\sqrt{n}} \tag{7-9}$$

where: n is the number of original (non-overlapped) blocks.

Assuming that the damping error is normally distributed, 95% of the estimates can be expected to be within 1.96 times the normalised error from the actual value. For SSC site records of three hours duration, with 75% of blocks passing the self-stationarity test (§5.6.4), there would typically be 13 blocks plus 12 overlapped blocks, so the 95% confidence limits of the damping estimate would be ±21%. To halve the error, a four-fold increase in total record length would be required.

The errors in natural frequency estimates are shown in Fig. 7-8, calculated simultaneously with the damping estimates by the WCM. The errors are of much smaller magnitude, being of the order of 0.1%, even for averaging over only 6 blocks. Again, the addition of the overlapping blocks gives a significant reduction in the error. Using overlapped blocks 4 files long, the error in natural frequency is given approximately by:

$$\varepsilon_f = \frac{2.2\text{x}10^{-3}}{\sqrt{n}} \tag{7-10}$$

Therefore, for 13 blocks plus 12 overlapped blocks (3hr record with stationarity test), the 95% confidence limits of the natural frequency estimate would be ±0.12%.

The above error bounds are based on simulated data, so the errors for site data, with noise and other external influences, would be expected to be greater. Noise would have the effect of increasing the measured PSDs, which would be most significant in the ranges of low response between resonances, causing overestimation of damping. It would also increase the variance of the spectrum, and hence the error of the damping estimate. However, for the SSC accelerometer measurements, the noise amplitude below 5Hz was approximately 4% of the signal amplitude (§5.5.1), so the noise PSD magnitude was $0.04^2 = 1.6\text{x}10^{-3}$ of the acceleration PSD, which was small compared with the variance errors. Other reasons for increased errors in estimates from site data are discussed in §8.4.1.

7.5.5 Processing parameters for SSC analysis

The WCM was tested with varying numbers of side lobes of the frequency domain Hanning window and different sub-divisions of the frequency resolution, for the preferred block length of 4 files. The estimates of modal parameters converged to within 0.1% for just one side lobe on each side of the central lobe, due to the rapid decay of the Hanning window in the frequency domain, and only two sub-divisions of the frequency resolution, because of the relatively high resolution. For analysing the measured SSC data, two side lobes and four frequency sub-divisions were used for added confidence.

For the 0.5 file long blocks, it was found that the modal parameter estimates converged to within 0.05% for one side lobe of the window function, and eight sub-divisions of the frequency resolution. For added confidence, two side lobes and 16 frequency sub-divisions were employed for the analysis.

7.6 Assumed loading spectra

For ambient vibration measurements, the load is not measured so its characteristics need to be assumed for system identification. The conventional assumption is that its has a white noise spectrum (§5.3&7.3).

If the damping of a particular mode is low, the bandwidth of the resonant peak in the spectrum is narrow, so this would seem a reasonable assumption considering only the narrow frequency range around the individual peak, as for conventional curve-fitting. However, such SDOF system identification methods also assume that the PSD around each peak represents the response of only one mode, which may give significant errors, particularly for closely-spaced or low amplitude modes, for which other modes provide a considerable contribution to the PSD. Therefore, for more accurate results, the response

of each mode should be considered over a wider frequency range covering other spectral peaks, as for MDOF methods. However, the form of the loading spectrum then becomes more important.

For the SSC in its finished state, in wind speeds below approximately 12m/s, the dominant loading was from traffic (§6.6). It was shown that this had a loading spectrum approximating to white noise, at least in the frequency range 0.3-2Hz, so the conventional assumption was acceptable. However, during construction (i.e. no traffic), or in strong winds, the wind loading was dominant, so the loading spectrum was quite different (§6.5.4).

Fig. 7-9 shows the results of fitting individual curves to several peaks in a typical construction state PSD, using the WCM assuming white noise loading, and summing the resulting windowed model spectra. Although the fitted curves match the individual peaks well, the total response is overestimated, particularly between peaks and at low amplitude peaks. In some cases, using this method, the contribution of higher frequency modes was swamped by the response in the first few modes. It is therefore necessary to use a more realistic loading spectrum when considering the combined response of several modes.

An estimated spectrum for wind loading for each mode was derived in §6.5:

$$S_{wind}(f) = R_r S_w f^{-8/3} \chi^2(f, U, \theta) \qquad (7\text{-}11)$$

where: R_r is a function of the mode shape

S_w is a function of the wind parameters, but constant for a given record

$\chi^2(f,U,\theta)$ = aerodynamic admittance, from equation (6-5), modified for wind direction, θ (§6.5.5)

This loading spectrum exhibits a rapid decay of magnitude with increasing frequency, so the contribution of the lower modes to the response at higher frequencies is attenuated.

For a damping ratio of 0.5%, typical for the SSC (§5.4.1), the difference in magnitude of the above loading spectrum over the HPB of a resonant peak in the response spectrum is typically 4%. Therefore, over this frequency range, the improvement in accuracy of the damping estimate compared with the white noise loading assumption is marginal. However, the ratio of consecutive natural frequencies of the first few modes was typically 1.2:1 or more (§5.4.1), so over the full width of each peak, between intermediate minima, the magnitude of the loading spectrum could vary by as much as 50%. If this greater frequency range is used for the curve-fitting, there could be a

significant difference in the damping values obtained. The discrepancies become even greater considering a frequency range covering several spectral peaks.

The wind loading was dominant during construction, and also for the finished bridge in the frequency range 0.1-2Hz for strong winds, so in these cases the above wind loading spectrum would be a reasonable approximation to the total loading (§6.6). For the more general case of the finished bridge with both wind and traffic loading, the loading spectrum could be estimated by the above spectrum plus a component of white noise. The relative amplitudes of the wind and traffic loading would need to be considered, for example by estimating their absolute values or by curve-fitting relative spectra (§6.6). For this study, the estimation of damping for the finished bridge was restricted to occasions with light winds (§8.4.1), so the intermediate case was avoided.

7.6.1 Curve-fitting with wind loading spectrum

The WCM was modified to deal with a loading spectrum other than white noise. Two alternative approaches were considered:

i) Dividing the measured response spectrum by the assumed loading spectrum (based on equation (7-1)), then fitting a curve as for white noise loading.

ii) Modifying the form of the model spectrum (equation (7-3)) before windowing and fitting to the measured spectrum.

The first method could be implemented simply, using any assumed loading spectrum, but it would distort the effects of the bias errors in the measured spectrum, which would cause errors in the application of the WCM (§7.4). The second method would be more precise, but would require additional computations within the iteration loop of the WCM, greatly increasing the calculation time. The chosen method, for the wind loading spectrum of equation (7-11), was a combination of the two. A factor of $f\chi^2(f,U,\theta)$, which does not vary rapidly with frequency in the range 0.1-2Hz, was allowed for by the first method, and the factor $f^{-11/3}$ was included in the equation of the model spectrum (equation (7-3)). Thus, the more involved calculations were kept outside the iteration loop, but without significantly distorting the spectrum.

The factor $R_r S_w$ in the loading spectrum for each mode (equation (7-11)) was included in the estimate of the modal amplitude, since the absolute loading spectrum was of little interest for this study.

The peaks in the measured spectrum of Fig. 7-9 were re-fitted using the WCM with the assumed wind loading spectrum. Fig. 7-10 shows that the fitted spectrum calculated on this basis is clearly a better fit to the measured spectrum.

There remains some doubt over the accuracy of the assumed wind loading spectrum, particularly over the estimate of the aerodynamic admittance (§2.6.4.3&6.5.3). Therefore, the WCM curve-fitting was repeated using loading spectra proportional to $f^{-8/3}$ and $f^{-14/3}$, corresponding to the extremes of the aerodynamic admittance function, to determine the sensitivity of the results to the form of the loading spectrum. For the frequency range considered, there was little variation in the estimated natural frequencies and damping. The reason for this is that the response in each mode decays rapidly away from the natural frequency, so each mode only influences the total response over a modest frequency range, over which the error in the loading spectrum would be limited. Therefore, significant error in the form of the assumed loading spectrum is possible before the errors in the resulting modal parameters become appreciable. However, the assumed wind loading spectrum (equation (7-11)) does give a marked improvement in the accuracy of the fitted spectrum, and significant differences in modal parameters, compared with a white noise loading spectrum (i.e. proportional to f^0).

7.7 Dealing with contributions from other modes – the Iterative Windowed Curve-fitting Method (IWCM)

Fig. 7-10 shows that, simply summing the results from individual SDOF curves fitted to each peak, the total fitted spectrum overestimates the measured spectrum, even with the loading spectrum taken into account. This is because of the contributions from other modes around each peak in the measured PSD, so the assumption that it can be represented by an SDOF curve overestimates the damping.

The Iterative Windowed Curve-fitting Method (IWCM) was therefore developed, as follows, to take account of the effect of other modes and thus extract the parameters of individual modes more precisely.

If the assumption of linear superposition of modal responses is maintained (§7.2), the total PSD of the response is given by:

$$S_{yy}(f) = \sum_i {}_iS_{yy}(f) = \sum |H_i(f)|^2 S_{x_i x_i}(f) \qquad (7\text{-}12)$$

where: ${}_iS_{yy}(f)$ = contribution to the response PSD of mode i

$S_{x_i x_i}(f)$ = PSD of the generalised load of mode i

$H_i(f)$ = FRF of mode i.

If, near a peak, the contributions of the other modes are not significant, the above equation reduces to the SDOF system normally considered for curve-fitting (equation

(7-1)). However, more accurate results can be obtained by considering the full equation. The contribution of a single mode, r, to the response PSD is then given by:

$$|H_r(f)|^2 S_{x_r x_r}(f) = S_{yy}(f) - \sum_{i \neq r} |H_i(f)|^2 S_{x_i x_i}(f) \qquad (7\text{-}13)$$

Based on this equation, the technique adopted was as follows:

i) Fit curves to the individual peaks in the measured PSD, using the WCM, to obtain initial estimates of the parameters of each mode.

ii) For each mode in turn, calculate the contributions of the other modes, based on the estimated parameters from (i), and subtract these from the measured PSD.

iii) Fit a curve to the remainder, using the WCM, to obtain improved estimates for the parameters of the mode in question.

The procedure was performed iteratively until the estimated parameters converged for all modes.

In principle, this technique could be used with a different assumed loading spectrum for each mode. However, for the SSC analysis the assumed loading spectra (equation (7-11)) only differed in magnitude (dependent on R_r), which was included in the modal amplitude term.

To eliminate the effect of leakage from adjacent modes, their contribution in (ii) above was calculated as the windowed model spectrum, based on their estimated modal parameters.

The IWCM is summarised in Fig. 7-11.

7.7.1 Effectiveness of the IWCM, as applied to SSC data

Considering the results of the IWCM applied to SSC data, the estimated natural frequencies varied very little with the iteration. Generally the difference in natural frequency estimates was less than 0.1%, rising to 0.3% for closely-spaced or low amplitude modes. However, significant differences were obtained for the damping estimates.

In some cases, the initial estimate of damping was over three times the value obtained after several iterations. The error was greatest for the modes with low amplitude, as would be expected. However, even for well defined modes, such as the second torsional deck mode (Mode TL2, Table 8-1), the damping was initially overestimated by as much as 30%. After the second iteration the errors were reduced to typically 10%, and each

subsequent iteration reduced the error in all values by approximately an order of magnitude. For the main data processing, five iterations were used, to reduce the error to the order of 0.01%, which would be insignificant compared with the errors from other sources.

The effectiveness of the technique can be seen by comparing Fig. 7-10 and Fig. 7-12. The summation of the SDOF response PSDs found using the IWCM (Fig. 7-12) gives an improved fit to the measured total response spectrum. The total curve now fits very well, both at the peaks and, more significantly, in the intervening frequency ranges. This indicates that the method gives a reasonable estimate of the contribution of all of the modes and suggests that the assumptions made were reasonable. Furthermore, by considering the shape of the curve between peaks, any distortion of the fitted curve relative to the measured curve may be evidence of inaccurate damping estimates or that other modes may be present (e.g. Modes TL3&TL6, §8.3.4).

The IWCM was applied to the SSC spectra over a limited frequency range, up to a maximum of 5Hz. The higher frequency modes, which would have a contribution to the response below 5Hz, were therefore not identified. However, the contribution of each mode decreases rapidly below its natural frequency, so in general the errors would not be significant, except in the frequency range of the highest few modes identified.

7.8 Estimation of mode shapes

The mode shapes are defined by the relative amplitudes (and phases) of the vibrations at different locations on the structure in each mode. For ambient vibration tests, to obtain reasonably detailed mode shapes with a limited number of instruments, one or more instruments are kept at reference locations and others are moved around to measure the relative responses at a series of different positions. 'Modal surveys' were conducted in this manner on the SSC (§4.5.2&4.5.3).

Conventionally, the relative amplitudes are obtained from the 'pseudo-FRF' of the vibrations at each location relative to a reference location, at each natural frequency (Owen & Blakeborough 1993). It is generally assumed that the modes of lightly damped structures are uncoupled (§2.4.2), so the modes are normal. This can be confirmed by considering the phase of the pseudo-FRF, or Cross Spectral Density (CSD) from which it is derived. For normal modes the phase is close to 0° or 180°.

Estimates of mode shapes by the conventional method are based on only the spectral estimates at the natural frequencies, or, rather, the nearest discrete values of the spectra. They are therefore subject to errors from bias, variance and the contributions of other modes. Although these effects may be similar for the spectra from the two locations, so they may to some extent cancel out, they could still be significant for low amplitude

measurements, for example near nodes. Therefore, a new method was developed, considering the relative modal amplitudes calculated by the IWCM. This allows for bias errors and the effects of other modes, and by curve-fitting over several spectral values it reduces the effect of variance errors.

By the new method, to find the relative amplitudes at two measurement locations, firstly the IWCM is applied to the two measured PSDs, yielding estimates of the modal parameters, including modal amplitudes, at each location. However, for the modal amplitudes at two locations to be comparable, they need to be based on the same natural frequencies and damping ratios. For a given mode, these are theoretically the same wherever they are measured on the structure, but in practice the estimates differ. Best estimates can be obtained from averages of the values from the two measurement locations, weighted according to the peak values of the PSDs to give lower weight to the less accurate estimates from locations of small amplitude. The natural frequencies and damping for all modes are then fixed at these best estimates, and the IWCM curve-fitting is repeated to obtain compatible estimates of the modal amplitudes, and hence the relative amplitudes at the two locations.

This method does not provide the signs of the relative amplitudes, since modal amplitudes are related to the square root of the PSD. However, the signs can be obtained from the CSD at the nearest discrete frequency to each natural frequency, taking the nearer of 0° or 180° measured phase, assuming the modes to be normal.

The mode shapes are simply built up from the relative amplitudes at each measurement location compared with the reference location. Different loading conditions, or variations in natural frequencies or damping between the individual tests, are taken into account by the method, since only the relative response of the two points is of interest.

The estimation of mode shapes for the SSC (§8.3.1) was based on the relatively short records (30 min) of the modal survey (§4.5.3). Therefore, the errors in natural frequency and damping estimates were higher than for the long-term tests, but again, since only the relative response was sought, this was of little importance.

7.9 Summary of data processing procedure for main SSC tests

The procedure for estimating the natural frequencies and damping ratios from the SSC long-term acceleration data was a two stage process. Firstly the PSDs were calculated (Fig. 5-7), and then the parameters were estimated using the IWCM (Fig. 7-11). The wind loading spectrum used in the procedure (§7.6) was calculated from the aerodynamic admittance, based on the mean wind speed and direction over the record length.

The preferred record length of three hours (66 files), and block length of 655.2s (4 files), were dictated by the stationarity test (§5.6.4). The frequency resolution was therefore 1.53×10^{-3}Hz, giving typically 60 spectral points over the full width of each resonant peak in the PSD. Of the 33 overlapping blocks, typically 25 would pass the self-stationarity test at the 5% level, hence, from equations (7-9) and (7-10), the 95% confidence limits of the estimated damping and natural frequency, for well-defined modes, were approximately ±21% and ±0.12% respectively. For the WCM, four sub-divisions of the frequency resolution and two side lobes of the frequency domain Hanning window function were used in the convolution, which were adequate to eliminate the effects of bias.

For the 30min modal survey tests, the records were split into blocks of 81.92s (0.5 files), being the length which gave the minimum errors in modal parameter estimates from the tests on simulated data (§7.5.3). For these, 16 sub-divisions of the frequency resolution and two side lobes of the frequency domain Hanning window function were used with the WCM.

Average wind parameters and temperature were also found for each record, to enable the causes of variations in the modal parameters to be investigated (§8.4&8.5).

All of the above processing was performed using Matlab (Mathworks 1999) routines written specifically for this study, but applicable to the analysis of ambient vibration data from any structure, providing the same assumptions can be made (§7.2) and that an appropriate loading spectrum can be estimated.

7.10 Conclusions

The Iterative Windowed Curve-fitting Method (IWCM) has been developed, for the extraction of modal parameter estimates from ambient vibration data. This was achieved through three improvements to the conventional curve-fitting method:

i) Development of the Windowed Curve-fitting Method (WCM) to overcome bias errors (§7.4).

ii) Consideration of a realistic loading spectrum, for example for wind loading, rather than white noise (§7.6).

iii) Consideration of the combined response of multiple modes, rather than each mode being treated in isolation (§7.7).

Bias errors are often quoted as a disadvantage of frequency domain system identification methods (§5.3.2.1), but their effects have been eliminated by the WCM, as validated by the tests on simulated data (§7.5). The remaining errors in the modal parameter estimates

are largely due to variance errors, which are inherent in any analysis of random vibration data. The remaining errors have been estimated for the SSC processing.

The frequency domain approach has enabled the estimated wind loading spectrum (§6.5) to be included in the analysis, to further reduce errors. This has enabled the combined contributions of all modes over a wide frequency range to be considered, achieving a much better fit to the measured response spectra than the conventional method. This is particularly important for closely-spaced or low amplitude modes, for which the effects of other modes around the spectral peaks are significant. It also enables the complete frequency range, including areas between identified natural frequencies, to be inspected for discrepancies between the measured and fitted spectra, thus revealing other aspects of the dynamic behaviour of the structure (§8.5).

A method for estimating mode shapes, based on the IWCM, has been developed. This should yield more accurate mode shapes than the conventional method of considering the pseudo-FRFs at discrete frequencies.

The above methods are applied to the extraction of modal parameters from the SSC data in the following chapter.

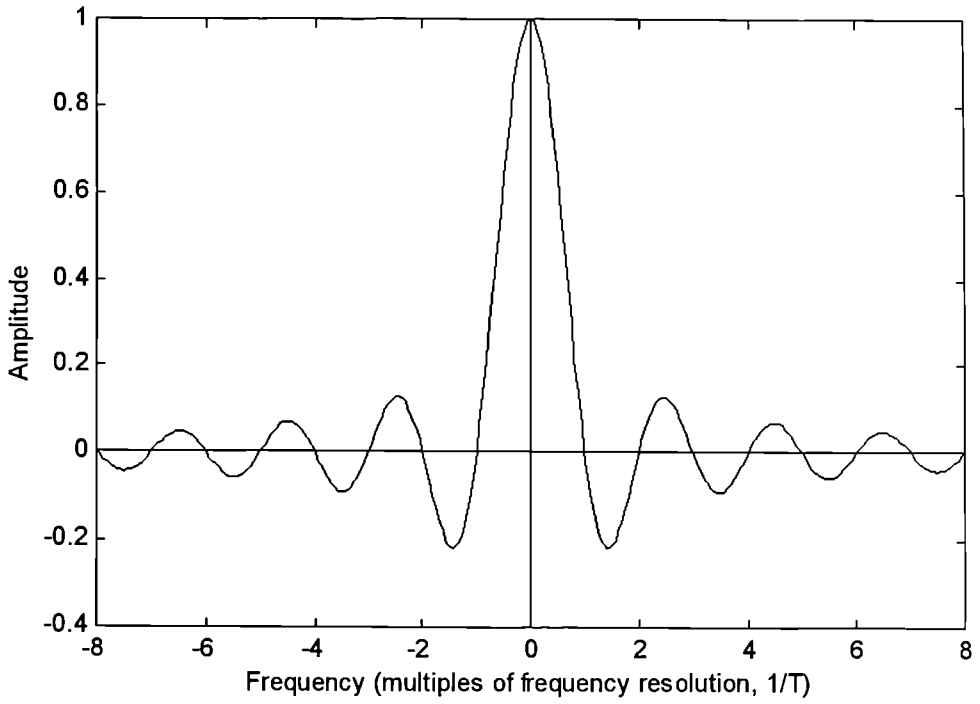

Fig. 7-1 Fourier Transform of rectangular (boxcar) window

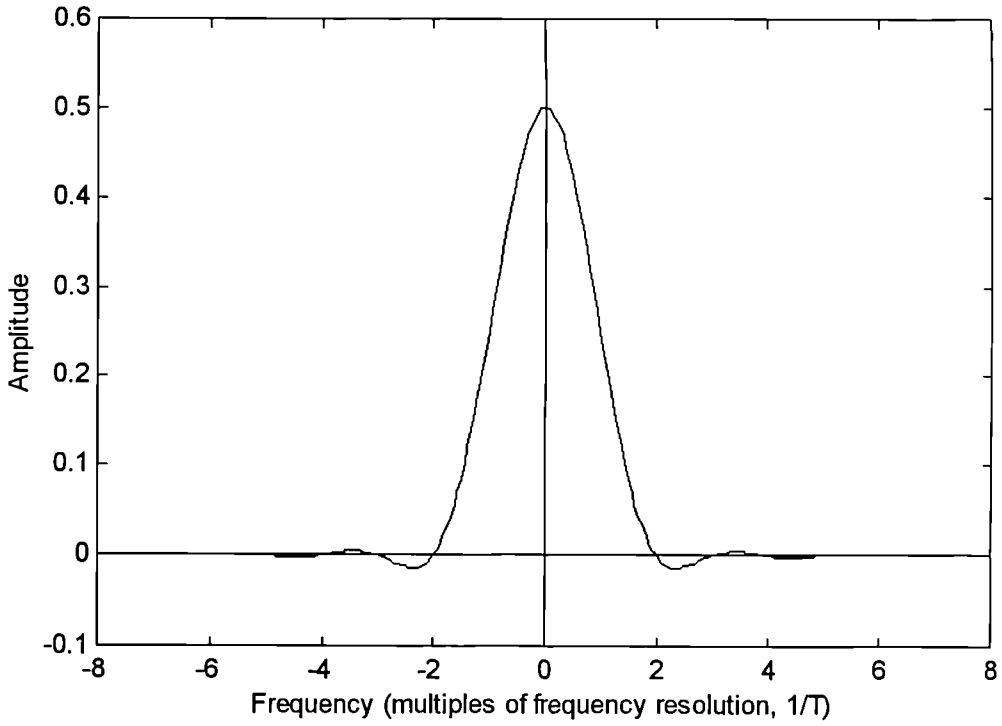

Fig. 7-2 Fourier Transform of Hanning window

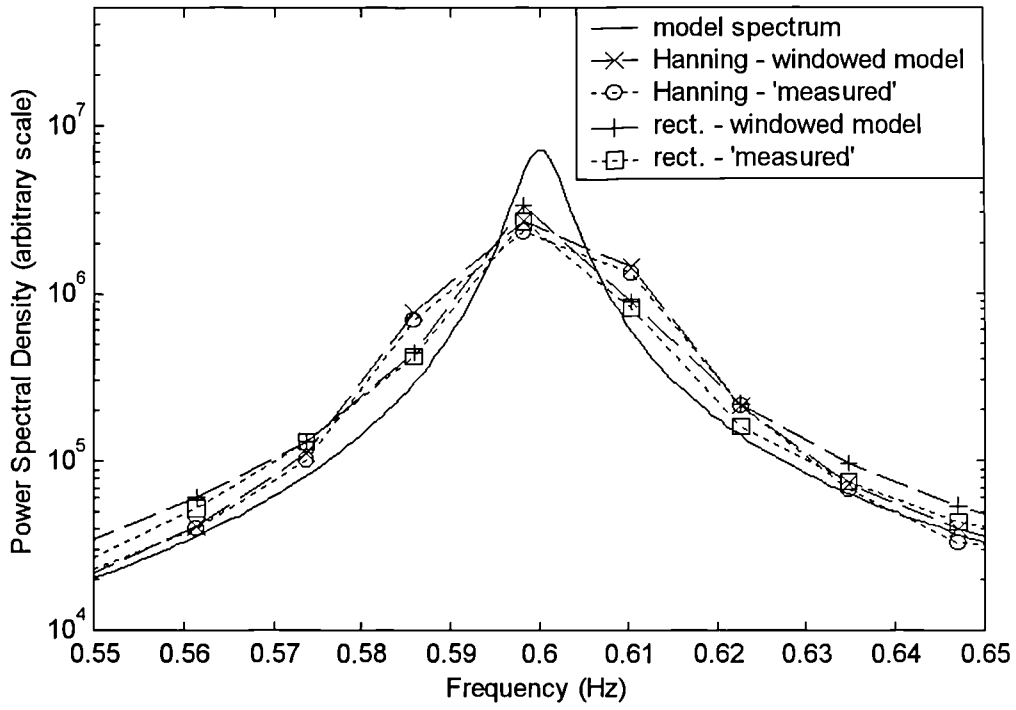

Fig. 7-3 Comparison of model spectrum (based on defined modal parameters), windowed model spectra and typical simulated measured spectra (block length 0.5 files, 81.92s, frequency resolution 12.2x10^{-3} Hz)

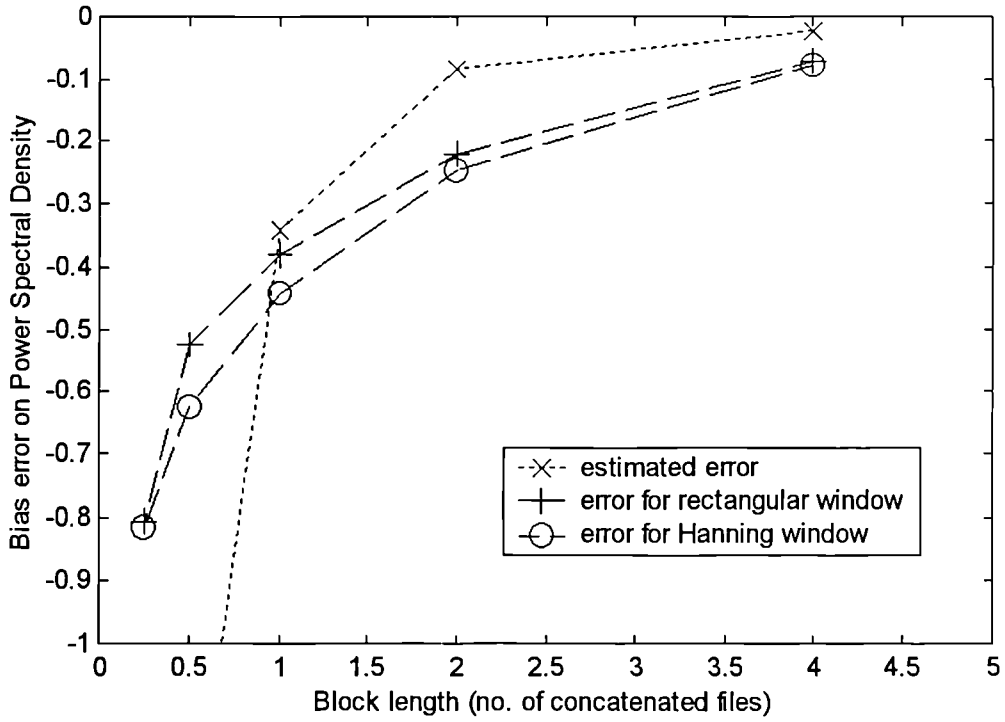

Fig. 7-4 Bias errors of windowed spectra at natural frequency for simulated data, for varying block length (i.e. varying frequency resolution)

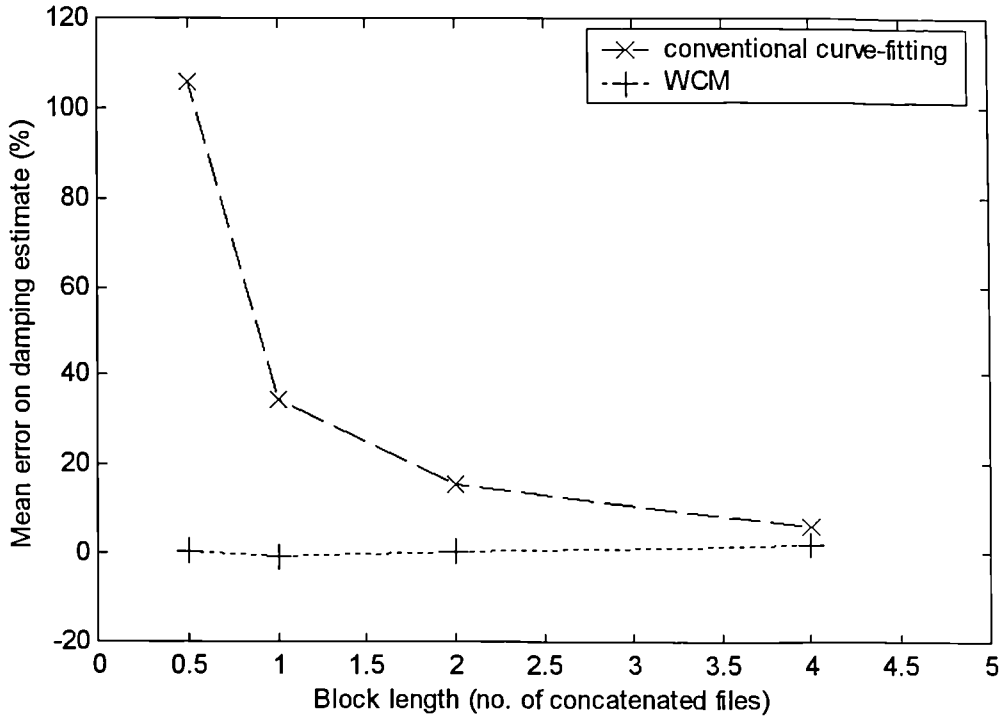

Fig. 7-5 Mean error on damping estimate for simulated data using conventional curve-fitting method and WCM (individual file length = 163.84s)

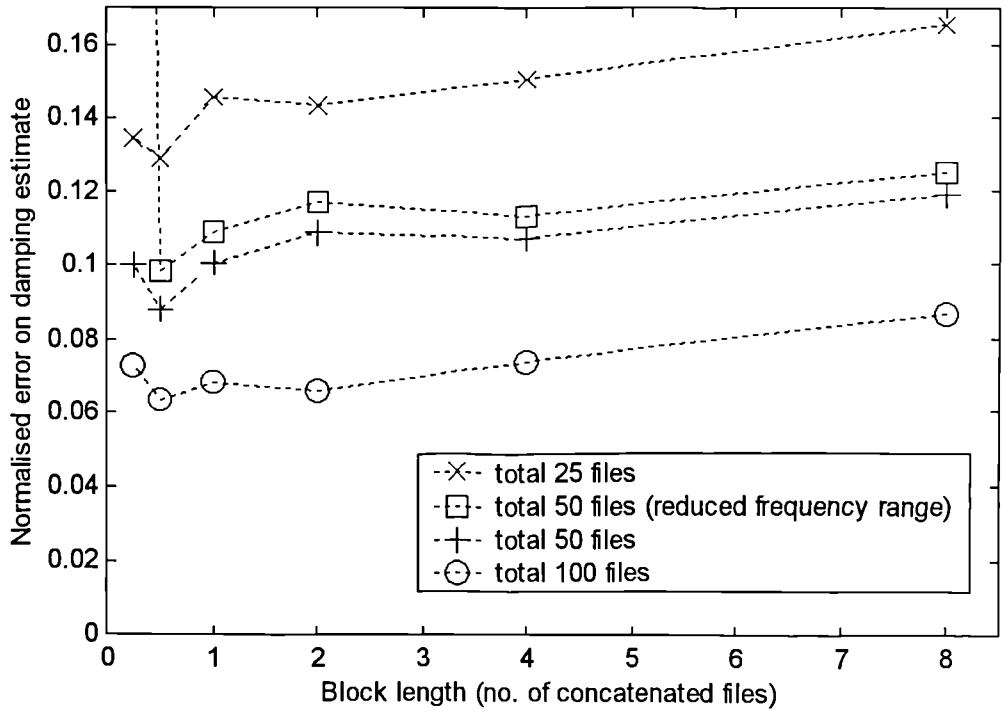

Fig. 7-6 Normalised error on damping estimates, using WCM, from simulated data for given total record length, against individual block length

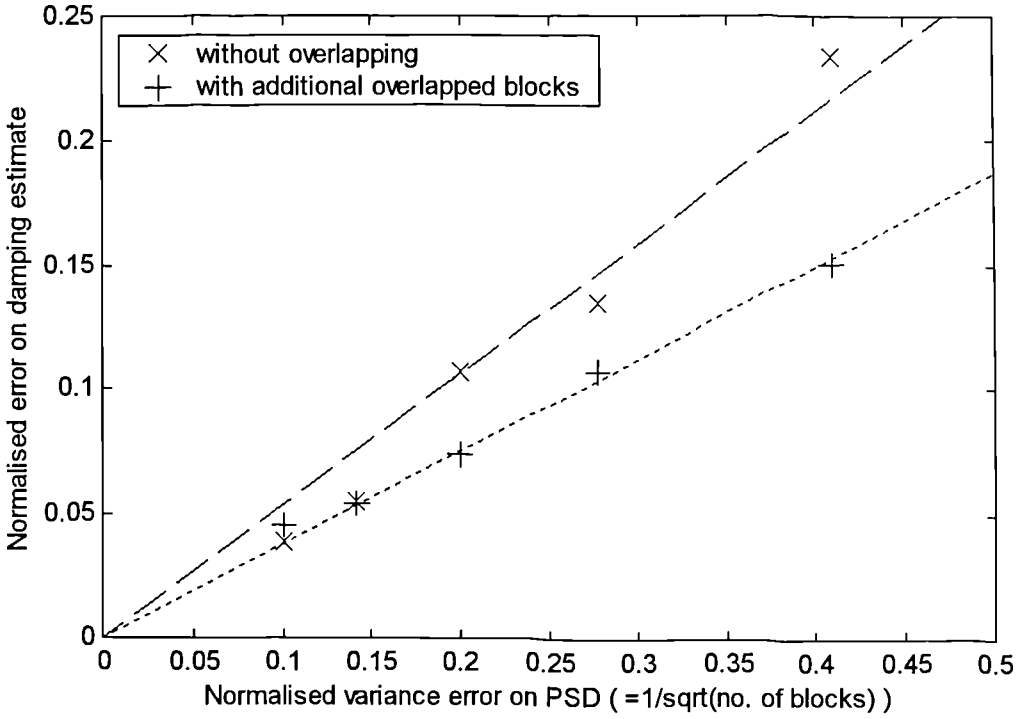

Fig. 7-7 Normalised error on damping estimates, using WCM, from simulated data for given block length, against variance error of spectrum (based on no. of blocks for averaging, each block 4 files long)

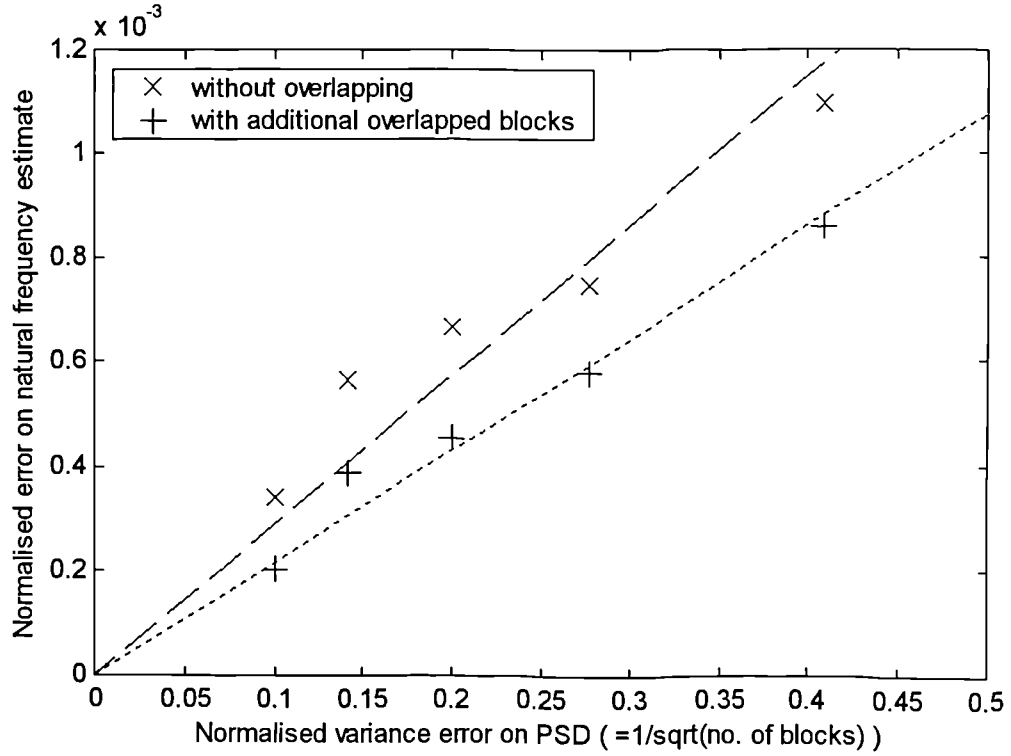

Fig. 7-8 Normalised error on natural frequency estimates, using WCM, from simulated data for given individual block length, against variance error of spectrum (based on no. of blocks for averaging, each block 4 files long)

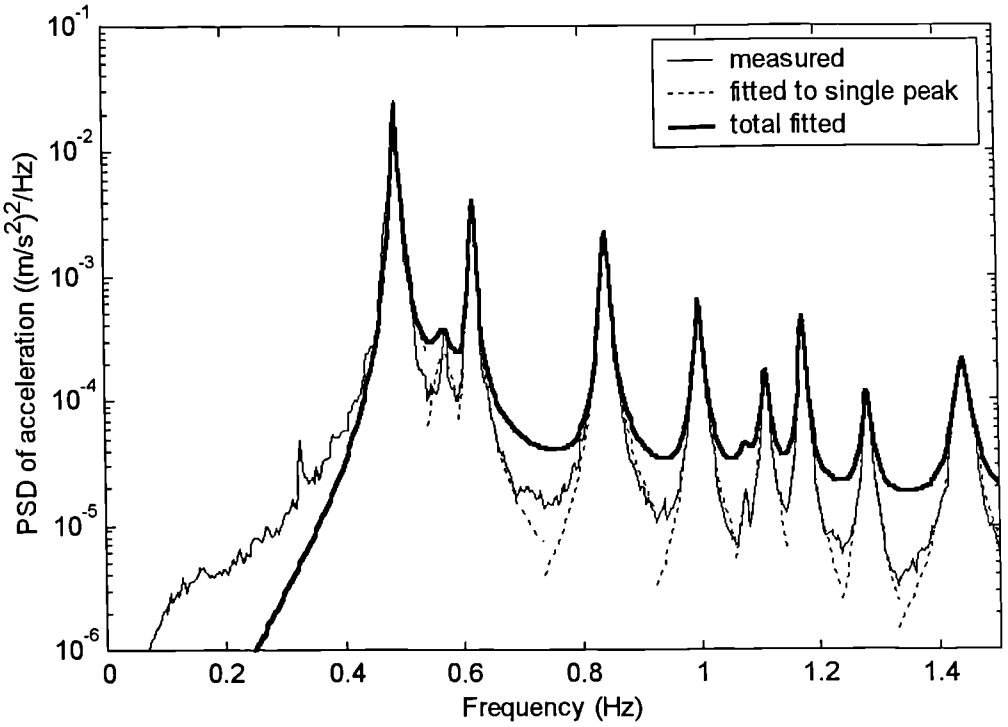

Fig. 7-9 Results of curve-fitting individual peaks (with WCM) and summing resulting estimated spectra, based on white noise loading spectrum

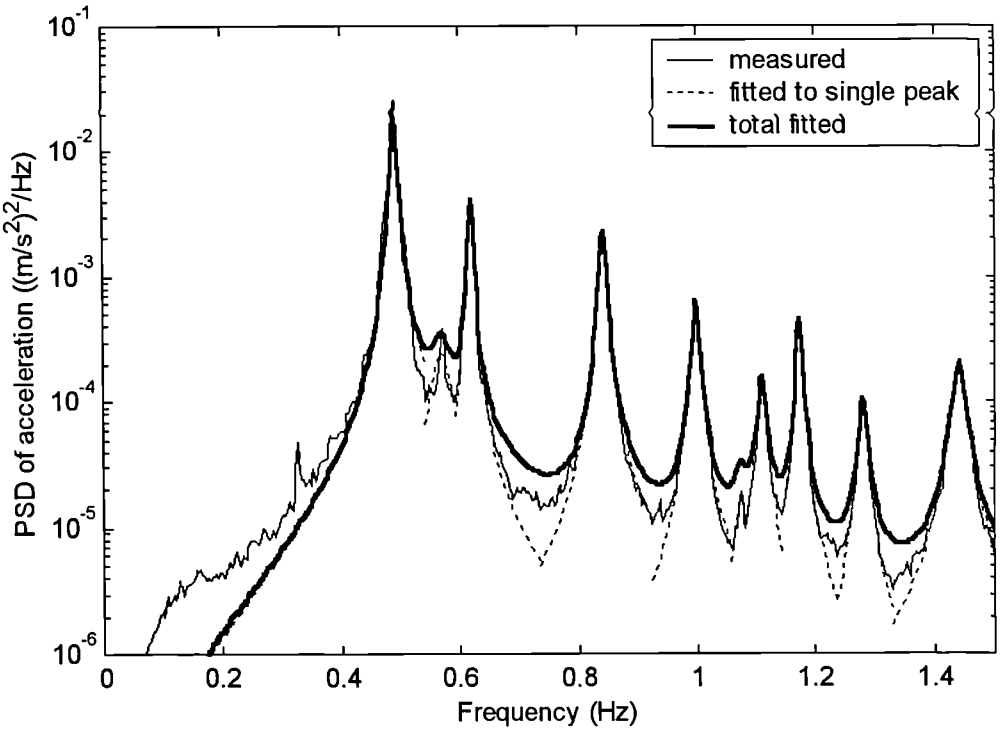

Fig. 7-10 Results of curve-fitting individual peaks (with WCM) and summing resulting estimated spectra, based on wind loading spectrum (equation (7-11))

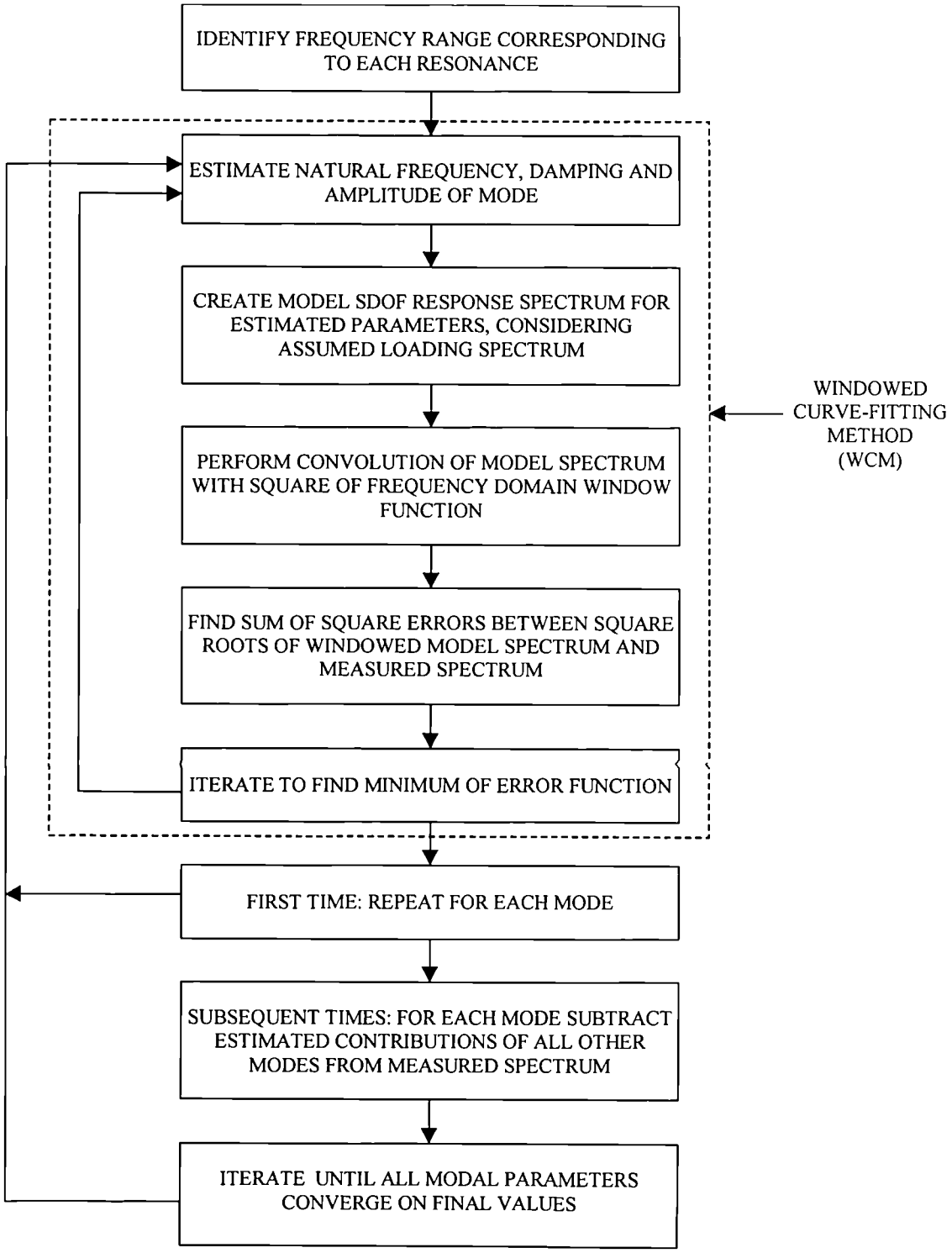

Fig. 7-11 Schematic representation of the IWCM, for calculation of modal parameters from PSDs

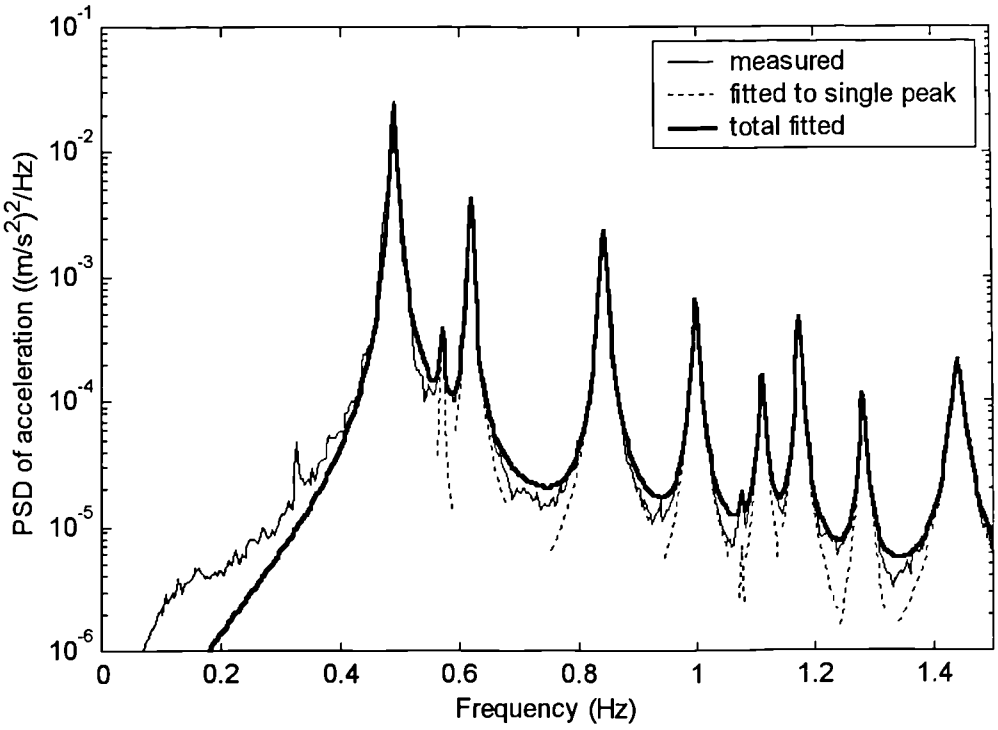

Fig. 7-12 Results of curve-fitting with the IWCM, taking into consideration contributions from other modes and wind loading spectrum

CHAPTER 8 MODAL BEHAVIOUR AND BUFFETING VIBRATIONS OF THE SECOND SEVERN CROSSING

8.1 Introduction

In this chapter, the Iterative Windowed Curve-fitting Method (IWCM), developed in Chapter 7, is applied to the Second Severn Crossing (SSC) data (Chapter 4), to study the modal behaviour of the structure, defining its basic dynamic characteristics. Also the amplitude of vibrations due to buffeting are considered, especially in relation to the design predictions.

Natural frequencies and mode shapes of the cantilever structure were identified from the modal survey data (§4.5.3), and compared with results of the Finite Element (FE) models (§3.3). Thus the validity of the FE modelling method, site measurements and system identification method could be assessed. Natural frequencies and components of the modes of the finished bridge were also identified. The data provide a valuable resource for validating and updating FE models (§2.4.3&2.4.4).

The damping of each mode was estimated by application of the IWCM to long-term records (§4.5.4), allowing more accurate estimates to be made than otherwise possible from ambient vibration data (§7.10). Many damping estimates for each mode were made, for different wind conditions, from which the contributions of aerodynamic (§2.6.3) and structural damping could be separated. Comparisons were then made with quasi-static aerodynamic damping theory, and between the estimated structural damping ratios for the cantilever and the finished bridge.

Other variations in modal parameters were considered, including the effect of traffic mass on natural frequencies and the possibility of identifying temperature effects or structural non-linearities from the recorded data. Discrepancies between measured spectra and those fitted by the IWCM were taken as evidence of departures from the assumptions of the method (§7.2).

In addition, amplitudes of buffeting vibrations were compared with those predicted from the design buffeting analysis, and the relative amplitudes for the cantilever and the finished structure, with and without the wind barriers, were considered.

Throughout this chapter the mechanism of excitation of the bridge is generally assumed to be buffeting from the wind (§2.6.4&6.5). Cases of suspected vortex shedding were excluded from these results and are covered separately in Chapter 9. Also only 'global

modes', of the deck and pylon, are considered here. Cable vibrations and cable-deck interaction are addressed in Chapter 10.

Definitions of parts of the structure from §3.2.2, and of types of spectra from Table 7-1, are used throughout this chapter.

8.2 Curve-fitting of Power Spectral Densities

The IWCM system identification method was applied to the Power Spectral Densities (PSDs) calculated from the SSC data (§5.4). The natural frequencies were initially estimated by visual identification of the peaks appearing consistently in several PSDs. Based on these initial estimates, the IWCM was applied, extracting the natural frequencies, damping ratios and mode shapes.

In Fig. 8-1 to Fig. 8-3, typical fitted spectra from the IWCM, based on the assumed wind loading spectrum (§6.5.4), are compared with measured spectra for the three main components of motion at the end of the cantilever deck. For vertical and torsional vibrations the curves were fitted up to 5Hz, and for lateral vibrations up to 3.2Hz. Above these frequencies the measured spectra became less clear, so the natural frequencies could not be so well defined. In the ranges considered, the measured and fitted spectra agreed well in most cases.

For the finished bridge, the natural frequencies were generally closer together and the spectra became less clear at lower frequencies than for the cantilever, so the frequency range for curve-fitting was limited to below 1.5Hz. Generally the average wind speed was below 12m/s for the analysed records, so traffic loading was taken to be dominant and a white noise loading spectrum was assumed (§6.6). Again the measured and fitted spectra generally agreed well (e.g. Fig. 8-4).

The good agreement of the spectra suggests that the IWCM assumptions of modal superposition (§7.2) and of the loading spectra (§7.6) were reasonable, and that the identified modes describe the dynamic behaviour of the structure well. However, occasionally discrepancies between the measured and fitted spectra were apparent, as discussed in §8.5.

8.3 Natural frequencies and mode shapes

Natural frequencies and mode shapes are normally calculated for design by FE analysis (§2.4.3). It is important that they are determined accurately, so that the response to dynamic loads can be predicted. The site monitoring allowed the natural frequencies and mode shapes of the SSC cantilever to be determined, for validation of the results of the FE models (§3.3).

For design, normally only the first few modes are considered, since these contribute most to the total response, although multi-mode analyses often consider a larger number of modes (§2.4.3&2.6.6). For model updating, it is also desirable to define more modes, to provide additional information for matching the FE model to the measured data (§2.4.4). Thus, parameters can be adjusted to obtain an accurate model of the measured modes, or alternative FE modelling methods can be investigated. Also, changes to the dynamic behaviour for structural health monitoring are more likely to be accurately identified using a larger number of modes (§2.4.4).

There were essentially six types of 'component mode' of the SSC (excluding cable vibrations), namely vertical, torsional and lateral deck modes, and longitudinal (with respect to the bridge axis), torsional and lateral pylon modes. Vertical deck and longitudinal pylon vibrations occurred together in two-dimensional modes, while the other four components normally existed together, due to the offset between the centres of stiffness and mass of the deck (Irwin 1979a).

8.3.1 Measured natural frequencies and mode shapes of cantilever

Mode shapes of the completed cantilever were estimated from the half-hour records of the detailed modal survey (§4.5.3), as described in §7.8. The natural frequencies were taken as the average of the estimates from all of the measurement locations, weighted by the amplitudes, since the natural frequencies were more accurately defined for large spectral peaks. At this stage, damping ratios were not considered, except as required by the method (§7.8), since the short record lengths would result in low accuracy.

The coherence at each natural frequency, between accelerations measured simultaneously at different locations, was noted, to determine whether the vibrations were related to the same mode. In most cases the coherence for identified modes, other than near nodes, was above 0.8, with it often exceeding 0.95.

The assumption of normal modes was supported by the phase of the Cross Spectral Densities (CSDs) between the accelerations, at the natural frequencies, generally being within 15° of 0° or 180°. The exceptions occurred in cases of low coherence (<0.6), usually when one accelerometer was near an antinode.

For the cantilever deck, the natural frequencies and mode shapes of 21 vertical and 19 torsional modes below 5Hz, and 15 lateral modes below 3.2Hz, were identified by the IWCM.

For the pylon, the fitted spectra did not match the measured spectra very well (§8.5.3). Therefore the relative amplitudes, and hence the mode shapes, were estimated on the basis of the square root of the ratio between measured PSDs at the frequencies of the

spectral peaks. 22 longitudinal, 31 lateral and 25 torsional pylon modes were identified below 5Hz.

The relationships between the component modes of different types were determined from the coherences and relative amplitudes between the accelerations measured simultaneously at the reference locations. The natural frequencies and component modes are summarised in Table 8-1 for the first 32 global modes, up to 2.6Hz, with the principal component shown in bold. The global modes are categorised as vertical plane or torsional/lateral modes.

8.3.2 Comparison of measured cantilever modes with FE model results

The measured natural frequencies and mode shapes of the cantilever were compared with those obtained from the One Element Cable System (OECS) FE models (§3.3). The FE model natural frequencies and the errors from the measured natural frequencies are shown in Table 8-1 also. There is almost a one-to-one correspondence between the measured and FE model modes, which were paired by visually comparing the mode shapes. The first 10 vertical plane mode shapes are plotted in Fig. 8-5, and the first 15 torsional/lateral mode shapes in Fig. 8-6. The FE modes are shown as lines and the measured modes as crosses at the measurement locations, while the chain dotted lines represent the static equilibrium position. The cables are omitted for clarity. For the torsional/lateral modes (Fig. 8-6) three orthogonal views are shown. The south elevation and plan show the measured displacement of the south side of the deck (north side from FE model dotted in elevation), while the west elevation of the pylon shows the measured lateral displacement of the north tower and the FE model displacement of the end of the deck. Measured points are not shown where there was no discernible peak in the relevant PSD.

Most of the FE model and measured mode shapes match very well, giving confidence in the methods of FE modelling, site measurement and system identification. The vertical plane modes were also compared by the Modal Assurance Criteria (MACs) between each possible pairing of measured and FE model mode shapes (Fig. 8-7). The relatively high values (>0.65) on the diagonal of the plot indicate good agreement of those mode shapes, again with almost a one-to-one correspondence.

Table 8-1 Comparison of measured and FE model modes for cantilever

Mode no.	Meas. freq. (Hz)	FE mode no.	FE freq. (Hz)	Freq. error (%)	Deck modes			Pylon modes		
					V	T	La	Lo	T	La
TL1	0.332	1	0.351	5.7		✓	**✓**		✓	✓
V1	0.338	2 (O1)	0.384	13.7	**✓**			✓		
TL2	0.458	3	0.523	14.3		✓	✓		✓	**✓**
V2	0.491	4 (O2)	0.545	11.1	**✓**			✓		
TL2a	0.513	-	-	-			✓		✓	✓
TL3	0.547	5	0.599	9.4		**✓**	✓		✓	✓
V3	0.596	6 (O3)	0.654	9.6	**✓**			✓		
TL3a	0.698	-	-	-		**✓**			✓	
V4	0.818	7 (O4)	0.941	15.1	**✓**			✓		
TL4	0.847	8	1.041	22.9		**✓**			✓	✓
V5	0.977	11 (O6)	1.153	18.0	**✓**			✓		
TL5	1.005	9	1.059	5.4						**✓**
V6	1.015	10 (O5)	1.115	9.8	**✓**			✓		
TL6	1.105	12	1.377	24.6					**✓**	
TL7	1.197	14	1.453	21.5		**✓**	✓		✓	
TL8	1.215	13	1.427	17.5						**✓**
TL9	1.272	16	1.526	20.0		**✓**			✓	✓
V7	1.336	15 (O7)	1.470	10.0	**✓**			✓		
V8	1.404	17 (O8)	1.592	13.4	**✓**			✓		
TL10	1.542	18	1.734	12.4			**✓**			✓
TL11	1.646	19	1.903	15.6		**✓**	✓		✓	✓
V9	1.846	20 (O9)	2.000	8.4	**✓**			✓		
TL12	1.815	22	2.086	14.9		**✓**	✓		✓	✓
TL13	1.983	21	2.029	2.3		✓	**✓**		✓	
V10	2.096	25 (O10)	2.345	11.9				**✓**		
TL14	2.115	24	2.340	10.6		✓	**✓**		✓	✓
TL15	2.177	30	3.067	40.9			✓		**✓**	✓
V11	2.179	26 (O11)	2.455	12.7	**✓**			✓		
TL16	2.236	23	2.237	0.0						**✓**
TL17	2.332	27	2.686	15.2		**✓**	✓		✓	✓
V12	2.379	28 (O12)	2.688	13.0	**✓**			✓		
V13	2.568	29 (O13)	2.931	14.1	**✓**			✓		

Notes: Mode numbers: Vx – Vertical plane modes, TLx – Torsional/Lateral modes
Numbers in brackets indicate 2-D FE model mode numbers
'Frequency error' gives error of FE frequency relative to measured frequency
Component modes: V – Vertical, T – Torsional, La – Lateral, Lo – Longitudinal
Ticks represent measured components. Principal component in bold

Some modes are worthy of particular comment:

- Modes V2 and V6 (2-D FE 2&6, Fig. 8-5) were predominantly backspan modes, with very little motion at the end of the cantilever, used as the reference location. Therefore, although peaks were often identified in the PSDs at the natural frequency, it was not possible to define the measured mode shapes. Consequently the MACs for the FE mode shapes (2-D FE 2&6, Fig. 8-7), compared with all of the measured shapes, are very low. Similarly, Mode TL6 (3-D FE 12, Fig. 8-6(b)) is predominantly a backspan mode according to the FE model, so it was not well defined by the measured data. For future monitoring exercises, to ensure that all modes could be measured, another reference location in the deck backspan would be required. However, this would significantly increase the number of tests needed, unless more accelerometers were available.
- Modes V5 and V6 (2-D FE 6&5, Fig. 8-5) are close in frequency (measured 3.9% difference). V5 is predominantly a main span mode, while V6 is a backspan mode. As measured, they are reversed in order from the FE model. This indicates an error in the relative stiffnesses (or masses) of the main and back spans in the FE model. The stiffness of the intermediate piers may be significant for this, since they vibrate longitudinally in 2-D FE Mode 6 (Mode V5, Fig. 8-5).
- Modes V7 and V8 (2-D FE 7&8, Fig. 8-5) are close in frequency (measured 5.1% difference) and have similarities in their shapes. Although the measured and FE model mode shapes agree well for the main span of V7 and backspan of V8, the relative amplitudes of the main and back spans are not well predicted by the model. Again this indicates an error in relative stiffnesses (or masses).
- Modes TL2a and TL3a (Table 8-1) were apparent in the measured spectra for some records. However, they were not consistently present, reasonable mode shapes could not be identified, and they were not predicted by the OECS FE models. It is possible that these were additional modes resulting from cable-deck interaction (§2.9&10.7.2.1), as predicted by the Multiple Element Cable System (MECS) FE model (§3.4.2). Although it was a 2-D model, not permitting torsional/lateral motion, it predicted multiple modes with similar deck and pylon deformations, particularly associated with modes O2 and O3 of the OECS model (§3.4.2), which had comparable frequencies to the additional measured modes. Further analysis of the data is required to investigate this in detail.

The discrepancies between the measured and FE model modes were often greater for torsional/lateral modes than for vertical plane modes. This was often a result of low measured amplitudes of some components. Also, as 3-D modes, they were more susceptible to errors in relative stiffnesses in the FE model. However, 17 torsional/lateral

modes were matched with measured modes with reasonable to good agreement (Table 8-1 & Fig. 8-6).

Generally, the agreement of mode shapes deteriorated at higher frequencies (Fig. 8-6(e)). Above 2.6Hz, although several more modes were identified from the site data, it was often difficult to match them to specific FE modes, generally due to differing relative responses of parts of the structure. However, for modes dominated by the main span in vertical bending or torsion, good agreement could still be obtained.

The measured and FE model natural frequencies (Table 8-1) are compared graphically in Fig. 8-8. On average, the FE model overestimated the natural frequencies by 13%. This could to be due to errors in the material properties (Table 3-1), particularly the Young's Modulus of concrete, for which the dynamic value used (44kN/mm^2) is 22% higher than the static value for the same grade of concrete (BSI 1990). Gentile & Martinez y Cabrera (1999) found that Young's Moduli differing by 13% were required in FE models of two nominally identical bridges to match the measured natural frequencies. The discrepancies could alternatively be from errors in the equilibrium state following the static analysis (§3.3.1), leading to inaccurate contributions of geometric stiffness, or from some flexibility of the foundations (§6.2.5). Deger et al. (1996) and Link et al. (1996) reduced errors between measured and FE model natural frequencies for two bridges by adjusting the model foundation stiffnesses. Updating the FE model is beyond the scope of this study, since many different strategies could be adopted, and at present there is no particular evidence of which would be most appropriate. However, the large number of modes identified would be useful for further study on this subject. Any model updating should address the apparent error in relative stiffnesses of the main and back spans, as well as the errors in natural frequencies.

Notwithstanding the overestimation of the natural frequencies, Fig. 8-8 shows reasonably consistent errors for all of the modes, for both vertical plane and torsional/lateral modes. Modelling of the deck in three dimensions is of particular importance to obtain the correct properties for torsion (§2.4.3), but the modelling method adopted (§3.3.4) appears to provide good results. The errors become more significant at the higher frequencies, with more complex shapes, for which the relative stiffnesses of components of the bridge become more important.

8.3.3 Effectiveness of IWCM in determining mode shapes

The mode shapes of the deck obtained from the IWCM (§7.8), as presented, were compared with the shapes estimated more simply from the square roots of the ratios of the measured PSDs at the natural frequencies. The values of relative amplitudes at each measurement location were typically within 5% from the two methods. The differences

were apparently random, with neither method consistently giving smoother shapes or better matches to the FE model modes. The MACs comparing these mode shapes with the FE model results were very similar (typically within 2%), again with neither method being consistently better.

The IWCM has been shown to yield realistic mode shapes, but, for the SSC data, with negligible improvement over the simpler more conventional method, based on the ratios of PSDs. However, for structures with higher damping or more closely-spaced modes, for which the components of other modes near resonant peaks in the spectra are more significant, the new method would be expected to provide better estimates. Damping estimates (§8.4.1) are more sensitive to the contributions of other modes, so for these the IWCM is very beneficial (§7.7.1).

8.3.4 Measured natural frequencies of finished bridge

Further processing of the detailed modal survey data for the finished bridge (§4.5.3) was beyond the scope of this thesis. However, data from the reference locations, near to midspan of the main span and at the top of the M2 pylon, were processed. Fig. 8-9 & Fig. 8-10 show typical acceleration PSDs from these locations. The spectral peaks were often clearer than for the cantilever, although the natural frequencies were generally closer together.

For the deck, the lateral component of acceleration was considerably less than the vertical and torsional components, except at very low frequencies (<0.1Hz), for which there was a marked increase in the apparent lateral response, compared with a decrease for the vertical and torsional responses. This was due to deck rotation causing an apparent lateral acceleration, from the component of gravity in the direction of the lateral accelerometer, which is more pronounced at low frequencies (§5.5). It was more significant for the finished bridge than for the cantilever due to the greater torsional response (§8.6.5), partly caused by quasi-static rotations from asymmetric traffic loads. The error in the measured lateral acceleration was estimated from the measured deck torsional acceleration using equation (5-7), yielding a spectrum that was similar to the measured lateral acceleration spectrum at low frequencies (Fig. 8-11). The discrepancies in the values would be due to other measurement errors and electrical drift of the instruments at these very low frequencies. At the natural frequencies, the error in the measured lateral component from the torsional component can also be seen. For the modes at 0.490Hz and 0.842Hz, the error is significant relative to the measured spectrum, which would affect the apparent amplitude of the lateral component of these modes.

The IWCM was applied to the measured spectra, estimated from three-hour records (Fig. 8-4), yielding natural frequencies and damping estimates simultaneously. The relationships between the component modes were determined by considering the natural frequencies and the coherences of the accelerations at the reference locations. The average natural frequencies and measured component modes are summarised in Table 8-2, for the first 33 global modes, up to 1.5Hz. Comments on particular modes follow:

- Mode V1 was detected by the deck lateral accelerometer, although it was believed to be a vertical plane mode. The apparent amplitude of lateral vibrations was 1.6% of the vertical amplitude, which would arise from a vertical misalignment of the lateral accelerometer of 0.9° (§5.5). At other frequencies, although the vertical acceleration was greater than the lateral acceleration, an error of this magnitude would not appear as a clear peak in the lateral acceleration spectrum, so other erroneous modes due to this cause were not identified.
- Modes V2 and TL1 were found to have the same natural frequency, but very low coherence between the component modes at this frequency indicated that they were not related. Mode TL1 was predominantly a lateral pylon mode. It would be expected to have a torsional deck component, but this was not detected. Although flutter can occur for vertical and torsional modes with close natural frequencies, it is believed, from the Halcrow-SEEE design FE model (§8.6.1), that Mode V2 was anti-symmetrical and Mode TL1 symmetrical. This, together with the low amplitude of deck torsion would mean that flutter would be unlikely to occur (§2.6.5.1). There was no evidence of coupling from the site measurements, with the coherence between the modes always being low (<0.2).
- Modes TL3 and TL6 were not identified initially, the response close to their natural frequencies being dominated by Modes TL4 and TL7 respectively. However, without them there were discrepancies between the measured and fitted spectra in these frequency ranges. The discrepancies were greatly reduced by the introduction of the two additional modes for the curve-fitting. The low amplitude of these modes at both the deck and pylon reference locations suggest that they may not be important global modes of the structure. They could be additional modes due to cable-deck interaction (§2.9, 8.5.2&10.7). Further analysis of the data, particularly of the mode shapes, is required to explore this possibility. The identification of these additional modes demonstrates a benefit of the IWCM, allowing comparison of the fitted and measured spectra over the full frequency range (§7.7).

Table 8-2 Measured modes of finished bridge

Mode no.	Frequency (Hz)	Deck modes			Pylon modes		
		Vertical	Tors.	Lateral	Long.	Tors.	Lateral
V1	0.326	✓		✓*	✓		
V2	0.427	✓			✓		
TL1	0.427			✓			✓
TL2	0.461						✓
TL3	0.477			(✓)			(✓)
TL4	0.490		✓	✓		✓	✓
TL5	0.515						✓
TL6	0.552			(✓)		(✓)	✓
TL7	0.569		✓	✓		(✓)	✓
V3	0.608	✓			✓		
TL8	0.620		✓	(✓)		✓	✓
TL9	0.708				(✓)		
V4	0.760	✓			✓		
TL10	0.842		✓	✓		✓	✓
V5	0.914	✓			✓		
TL11	0.943						✓
TL12	0.998		✓	✓		✓	(✓)
V6	1.066	(✓)			✓		
TL13	1.074		(✓)	(✓)		✓	✓
V7	1.100	✓			(✓)		
TL14	1.110		✓	(✓)		✓	
V8	1.161	(✓)					
TL15	1.173		✓	✓		(✓)	
V9	1.222	(✓)			✓		
V10	1.279	(✓)					
TL16	1.280		✓	✓		✓	✓
V11	1.351	✓			(✓)		
TL17	1.375						✓
TL18	1.400						✓
TL19	1.422						✓
TL20	1.441		✓	✓		✓	(✓)
TL21	1.472						✓
TL22	1.488						✓

Notes: Ticks represent measured components.
Principal component in bold, minor and unclear components in brackets
* Apparent deck lateral mode measured, due to misalignment of accelerometer

FE modelling of the full bridge was beyond the scope of this study, so comparisons of the natural frequencies and mode shapes were not be made. However, the availability of the site data for both the cantilever and the finished bridge could be useful for studying different FE modelling and model updating methods (§2.4.3&2.4.4). For example, the FE model of the cantilever could be updated to match the measured modal behaviour, and then, with the updated parameters, be extended to model the finished bridge. The accuracy of the agreement with the measured modes on the finished bridge would then give an indication of the usefulness of the updating method adopted. Data from the earlier construction stages of the cantilever (§4.5.1&4.5.2) could also be used for this purpose.

8.4 Damping

In addition to the natural frequencies and mode shapes, the damping ratios of the modes are required to characterise the modal behaviour of the structure fully. These are the most difficult modal parameters to determine accurately, particularly for ambient vibration tests (§5.3.1), although they are of vital importance in determining the amplitude of the response to given loading (§2.5). Also, there is little analytical basis for estimating the damping in design, so measurements from existing structures are of particular interest (§2.5.1).

The contribution of aerodynamic damping (§2.6.3) means that the total measured damping varies with wind speed. Therefore, a large number of estimates, for different wind conditions, is desirable to enable the estimation of the aerodynamic and structural damping components. The long-term records recorded on the SSC (§4.5.4) enabled such estimates to be made, whilst the use of the IWCM minimised the error on each estimate. It is believed that the components of aerodynamic and structural damping have not previously been separated in full-scale tests on a long-span bridge with a bluff cross-section (§2.6.3.1).

8.4.1 Estimation and accuracy of damping values

The IWCM was applied to three-hour records (§7.9) to extract the damping ratios, along with the natural frequencies, for both the cantilever and the finished bridge. Both the self-stationarity and overall stationarity tests were performed, and blocks or records which failed were eliminated from further processing (§5.6.4). For the cantilever records, the wind loading spectrum was assumed (equation (7-11)), whereas for the finished bridge, traffic was found to provide the dominant dynamic loading for wind speeds below approximately 12m/s, so the loading spectrum was taken to be white noise (§7.6).

For higher wind speeds, the records were often of limited length, since data acquisition was triggered only when a threshold wind speed was exceeded. Also the response was often found to be non-stationary, so few results were calculated. Longer records and more stationary data existed for lower wind speeds, from continuous recordings.

For the cantilever, there were few occasions of strong winds with the equipment in operation, so an attempt was made to process records of only one hour duration. However, the self-stationarity test was not performed, since it was not valid for the short blocks that were required, and many records failed the overall stationarity test, believed to be because individual non-stationary blocks had not been excluded. Also, due to the shorter record length, the accuracy of modal estimates was lower. Therefore, three-hour records were used in preference, although this limited the total number available.

A much larger quantity of data was available for the finished bridge, due to the longer monitoring period and the greater disk capacity which became available on site. The results presented here are based on a two-week continuous monitoring period, covering a range of wind conditions, with a maximum wind speed of approximately 15m/s. Increased accuracy of results and further comparison of different cases will be possible with the recorded data, but the extent of processing was necessarily limited within the time-scale of the present study.

The 95% confidence limits for damping estimates from the IWCM, from simulated three-hour records, were estimated as ±21% (§7.5.4). In practice the accuracy is reduced due to measurement errors (§5.5), reduced frequency ranges for curve-fitting of closely-spaced modes, and the uncertainty in the modal parameter estimates of other modes (§7.7). Further errors would result from the presence of additional modes not specifically identified (§8.5.2), or from coupling of modal responses (§2.6.6). Although the errors are considerable, they have been minimised as far as possible for ambient vibration data passing the stationarity test, by the methods developed in Chapter 7.

The accuracy of the results was limited, to some extent, by the stationarity requirement. Typically 25% of blocks in a given three-hour record were rejected, so the variance errors were greater than would be obtained from three-hour stationary records. Also some records, particularly for strong winds, were rejected by the overall stationarity test. For this study, data failing the Run Test was rejected (§5.6.4), but it would be worthwhile for further study to consider alternative approaches. For example, more refined stationarity tests could be employed, the non-stationary data could be included (if shown not to be detrimental), blocks from different times for similar loading conditions could be grouped together, or methods for processing non-stationary data could be investigated.

The IWCM assumes the loading is due to buffeting, described by the spectrum developed in §6.5.4. Therefore records including suspected vortex-induced vibrations (Chapter 9) were not processed by this method. This was ensured, for the finished bridge, by only considering records from after the installation of the baffles (§9.6).

8.4.2 Aerodynamic damping

Damping estimates for each mode, from each three-hour record, were plotted against mean wind speed and normal component of the wind, to identify the components of aerodynamic and structural damping. Clearer trends of damping were apparent for the normal component of the wind than for the wind speed, in agreement with wind tunnel tests by Kimura & Tanaka (1992). The scatter of the results was considerable, due to the inaccuracies in the damping estimates, and possibly variations from the effects of wind direction, vibration amplitude or temperature. However, for most modes a linear trend was evident (e.g. Fig. 8-12), so straight lines were fitted to the data. The variance of the measured points relative to the best-fit line was used to calculate 95% confidence limits for the gradient and intercept of the damping axis.

The gradients were compared with the aerodynamic damping gradients (ζ_{aero}/U_{norm}) anticipated from quasi-static theory (§2.6.3), using values derived from the construction drawings and force coefficients and their derivatives from the wind tunnel sectional model tests (Xie et al. 1994) (Table 8-3). For the finished bridge, different configurations had been tested in the wind tunnel, including various traffic cases and iced-up wind barriers. Since the traffic loading varied and was not monitored, the maximum and minimum values, excluding the iced-up case, were considered.

The estimated aerodynamic damping gradients and their 95% confidence limits are shown for each deck mode for the cantilever and finished bridge in Fig. 8-13 to Fig. 8-18, each plotted at the natural frequency. The expected values from quasi-static theory are inversely proportional to natural frequency (equations (2-9)-(2-11)), so are shown as continuous curves. For the finished bridge, the extreme theoretical values are both plotted, to indicate the expected range.

In some cases, the measured aerodynamic damping appears to be negative. However, often this is associated with large error bounds on the estimates, and in all such cases the value at the upper 95% confidence limit is positive. Therefore it is not possible to conclude whether negative aerodynamic damping was actually experienced.

Table 8-3 Values of parameters for aerodynamic damping estimates from quasi-static theory

Parameter	Cantilever (no wind barriers, surfacing, etc.)	Finished bridge
Deck width, B (m)	35.026	35.026
Mass / unit length, m (kg/m)	29×10^3	32×10^3
Polar second moment of mass / unit length, I (kgm)	3.7×10^6	4.0×10^6
Drag coefficient, C_D	0.0897	min: 0.1516 (smooth flow) max: 0.1612 (turbulent flow)
Lift coefficient derivative, $\frac{dC_L}{d\alpha}$	4.7965	min: 2.0311 (full traffic load) max: 3.8057 (turbulent flow)
Moment coefficient derivative, $\frac{dC_M}{d\alpha}$	0.6738	min: 0.3415 (smooth flow) max: 0.6631 (full traffic load)

Notes: 'Smooth flow' and 'turbulent flow' refer to basic configuration, without any traffic
'Full traffic load' indicates both carriageways full (in turbulent wind)
The level of turbulence was I_u = 6%, equivalent to 13% at full scale (§9.5.3)

For vertical bending modes (Fig. 8-13 & Fig. 8-16), the correlation between the values estimated from the measurements and the theoretical values is poor, even considering the large error bounds on many of the results. It can be concluded that quasi-static theory is inadequate to estimate the aerodynamic damping for these modes. For the majority of the low frequency (<2Hz) vertical bending modes, the theory overestimates the measured values, in agreement with previous wind tunnel studies (Holmes 1975, Zan & Wardlaw 1987). If relied upon in design, this would lead to larger vibrations being experienced than anticipated. For the first vertical bending modes of both the cantilever and the finished bridge, which give the greatest response to wind loading, the measured gradient is less than half of the mean theoretical value. For the higher frequency (>3Hz) vertical bending modes of the cantilever (Fig. 8-13), the confidence limits are generally larger, but the aerodynamic damping often appears to be greater than estimated by the theory. The mode just below 3Hz with the large error bounds is predominantly a pylon mode, for which the loading and aerodynamic damping mechanisms would be different than assumed. For the finished bridge (Fig. 8-16), the two modes with apparently negative

aerodynamic damping (Modes V6, 1.066Hz, and V8, 1.161Hz) were both unclear at the deck measurement location (Table 8-2), so the errors in damping estimates are considerable.

For torsional modes (Fig. 8-14 & Fig. 8-17), the agreement between the measured and theoretical values is better, with no particular tendency for errors in either direction. However, for some particular modes the errors are still considerable. For the cantilever (Fig. 8-14), the large error bounds on the two modes near 0.5Hz (Modes TL2 and TL3) could be due to the existence of Mode TL2a at an intermediate frequency, which was not directly identified in the deck torsional spectra (Table 8-1). For the finished bridge (Fig. 8-17), the two modes with apparently negative aerodynamic damping (Modes TL7, 0.569Hz, and TL13, 1.074Hz) are both predominantly pylon modes (Table 8-2). For the remaining modes, the quasi-static theory generally gives reasonable estimates of the measured values.

For lateral modes (Fig. 8-15 & Fig. 8-18) the measured aerodynamic damping was considerably greater than predicted by quasi-static theory. However, lateral deck motion was only dominant for four identified modes of the cantilever (Table 8-1), and none of the finished bridge (Table 8-2). For the remaining modes, the lateral amplitudes were relatively low and the error bounds on the estimated aerodynamic damping are often greater. For coupled torsional/lateral modes the contribution to aerodynamic damping from the torsional component is generally dominant, since the amplitude is greater and the aerodynamic damping term larger. For the finished bridge, the measured aerodynamic damping for lateral modes agrees well with the theoretical values for torsional vibrations (Fig. 8-18). However, even for Mode TL1 of the cantilever, with a dominant lateral deck component (Fig. 8-6(a)), the measured aerodynamic damping is considerably underestimated by quasi-static theory for lateral vibrations (Fig. 8-15). This is consistent with the results of Katsuchi et al. (1999), who found their analysis to overestimate the lateral response of a full aeroelastic model by factor of approximately two, attributed to errors from the estimation of lateral flutter derivatives from quasi-static theory.

Aerodynamic damping can alternatively be estimated from measured flutter derivatives from sectional model tests (§2.6.3). The flutter derivatives are non-linear functions of reduced velocity ($=UfB$), so they may give more accurate estimates of the variation of aerodynamic damping with wind speed and natural frequency.

For the first vertical bending mode of the cantilever (Fig. 8-19) and the first torsional mode of the finished bridge (Fig. 8-20), the relationship of damping with normal component of the wind gave some indication that it may have been non-linear, as predicted from flutter derivatives and similar approaches (Scanlan 1987, Katsuchi et al. 1998). For both modes, the relatively low number of damping estimates and their high variance meant that the relationships were not clear, and it would not be unreasonable to

fit straight lines to the measured points. However, parabolas gave reasonable fits to the data (Fig. 8-19 & Fig. 8-20). Processing of the additional data available for the finished bridge, and comparison with predictions of aerodynamic damping from flutter derivatives would be worthy of further study.

From limited measured data for vertical and torsional modes of the Höga Kusten Suspension Bridge, Tanaka et al. (1998) found reasonable agreement with the aerodynamic damping estimated from flutter derivatives, whereas quasi-static theory overestimated the aerodynamic damping by up to factor of two. However, in contrast with the results here, they found the least accurate estimates were for the torsional modes. The difference in structural form between the bridges, particularly of the deck cross-section (streamlined box girder c.f. SSC bluff composite deck, Fig. 3-3(b)), could explain the difference in behaviour.

8.4.3 Structural damping

The fitting of straight lines to the plots of measured damping against normal component of the wind (e.g. Fig. 8-12) also yielded estimates of the structural damping, from the intercept with the damping axis. Structural damping ratios of the identified modes and their 95% confidence limits were thus calculated for the cantilever and the finished bridge. They are plotted against natural frequency in Fig. 8-21 to Fig. 8-26.

The structural damping of the majority of modes, for the bridge in both conditions, was found to be of the order of 0.5%. All values exceeding 1% were associated with large error bounds. There were large errors on the estimates for some particular modes for the reasons given in the discussion of aerodynamic damping values above.

For the finished bridge, the estimated structural damping of the first mode (V1) was 0.29% (95% confidence limits 0.15-0.43%), which was lower than anticipated in design, and significant in the development of large amplitude vortex-induced vibrations (§9.5.3). The decay of those vibrations led to a similar damping estimate (§9.3.1), increasing confidence in the estimates from the present method. The first dominant torsional mode (TL4) was found to have structural damping of 0.25% (limits 0.05-0.44%).

There are no clear trends in the estimated structural damping ratios, but the very low values are of note. They are considerably less than the value of 0.64% for composite bridges from the British design rules for aerodynamic effects on bridges (DETR 1993), and they are at the lower end of the range of values reported from other full-scale tests on cable-stayed bridges (§2.5.1). The low values for the SSC are believed to be partly due to the subtraction of the contribution of aerodynamic damping from the measured damping, in contrast with previous estimates.

The first mode of each type, except lateral modes of the finished bridge, had one of the lowest damping ratios. This is of particular importance since generally the lowest frequency mode is excited most by the wind, and its displacement response is dominant. For the cantilever, the values were particularly low, estimated as 0.11% (95% confidence limits 0-0.34%) for Mode V1, and, for Mode TL1, 0.17% (limits 0-0.57%) from the torsional component and 0.34% (limits 0.19-0.49%) from the lateral component. One possible explanation of the lower damping of these modes is that the natural frequencies were below the lowest natural frequencies of any of the cables, so there would be no contribution from 'system damping', associated with cable-deck interaction (§2.9.2). However, there was no great change in the damping ratios between the cantilever and the finished bridge, after the addition of the secondary cables (§10.9), suggesting that system damping was not significant. It also suggests that values measured during construction of similar bridges can be taken as approximate estimates of the values that can be expected for the finished structures, which could be valuable for confirming or refining the design predictions for the finished state.

Comparison with the damping of suspension bridges brings out an interesting distinction. Damping estimates from a total of 13 suspension bridges were collected by Brownjohn (1988) and Jensen et al. (1999), all of which show a trend for larger damping for the lower frequency modes. In many cases the measured values may have been overestimated due to bias errors or aerodynamic damping, both of which cause larger errors for lower frequency modes, as emphasised by Littler (1992). However, values calculated by Jensen et al. (1999) for the Great Belt Bridge, using the ARMA system identification method (§5.3.2.2) and compensating for aerodynamic damping, still exhibited a similar trend. The results presented here for a cable-stayed bridge, after the removal of bias effects and aerodynamic damping, show no similar decrease in damping with frequency, possibly due to a different distribution of damping for the different structural forms (Raggett 1975).

8.5 Variations in modal behaviour

In addition to the variation in measured damping due to aerodynamic damping, other changes in modal parameters were considered. Effects including the additional mass of traffic, changes in temperature, and structural non-linearities each theoretically cause changes in natural frequencies and/or damping, so it was of interest whether these changes could be detected from the recorded data.

Also, identification of discrepancies between measured spectra and those fitted by the IWCM could give evidence of further aspects of the dynamic behaviour. These could include the existence of additional modes, not initially identified, or departures from the

assumptions of the method, such as the loading spectrum or that modal responses are uncoupled. Therefore the significance of any consistent discrepancies was investigated.

8.5.1 Variations in modal parameters

The natural frequencies were found to vary by up to approximately 1% with time. The variation for the first mode of the finished bridge over one week is shown in Fig. 8-27. This is the same week as for Fig. 6-21, which shows the daily variation of vibration amplitude due to traffic loading. The similar patterns suggest that the variation in natural frequency is primarily due to the presence of the traffic. For wind speeds below approximately 12m/s the traffic loading is dominant (§6.6), so the amplitude of vibrations can be assumed to be approximately proportional to the volume of traffic. Fig. 8-28 shows the Root Mean Square (RMS) acceleration plotted against natural frequency of the first mode (estimated for each three-hour record), distinguishing between records with mean wind speeds above and below 12m/s. For the lower wind speeds, there is a clear trend for decreasing natural frequency with increasing amplitude, consistent with an increase in traffic excitation and mass.

A drop in natural frequency with increasing amplitude could alternatively be due to a decrease in stiffness, for example due to cable non-linearity (§2.4.1). However, the points for wind speeds above 12m/s in Fig. 8-28 show no significant variation in natural frequency, indicating that it was the addition of traffic mass, rather than the increased amplitude itself that caused the change. There is therefore no evidence of non-linear behaviour from these observations. However, the amplitudes were low (estimated displacement less than 20mm RMS), for which the non-linearities of the structure would not be expected to be significant.

For a given mode, a decrease in natural frequency of 1% would result from an increase in generalised mass of approximately 2% (since $f_r \propto 1/\sqrt{M_r}$). If the generalised mass is concentrated in the deck, this would be equivalent to an increase in deck mass of 640kg/m, or approximately 10 heavy goods vehicles in the length of the main span (456m). This seems reasonable for the maximum traffic density, further supporting the hypothesis of the changes being due to the traffic mass. Similar changes in natural frequencies were observed for all of the vertical and torsional modes identified on the deck, except for Mode V6. This mode showed no particular trend of natural frequency with amplitude, but it was a pylon-dominated mode (Table 8-2), for which the mass of the deck and traffic would have little effect on the generalised mass.

No other consistent changes in modal parameters have been identified from the analysis of the data in this study. The temperature of the structure, or differential temperature of different parts (e.g. cables and deck), may have some influence on the natural

frequencies, but from initial observations of the measured data, the dependency is not strong and, if present, it appears to be masked by other effects. Brownjohn (1994) found from an FE analysis of the Bosporus suspension bridge that a 10°C change in temperature would cause maximum changes in natural frequencies of approximately 0.22%. For the SSC, such a change would be difficult to distinguish in the presence of changes due to traffic.

Temperature changes could also affect the damping, as could non-linear amplitude-dependent effects. However, the inaccuracy of the damping estimates and the effect of aerodynamic damping mean than it has not been possible to identify any such effects from the present study.

Further analysis of the data, accounting for the estimated effects of traffic mass and aerodynamic damping, is required to attempt to identify other causes of variations of modal parameters. The construction stages would be of particular interest for such a study, since traffic was not present.

8.5.2 Additional modes

For some measured spectra, there appeared to be additional peaks, which may have been due to additional modes, for example in Fig. 8-2 at approximately 3Hz and 4Hz. They did not occur consistently, so they were not identified as principal modes and were not fitted by the IWCM. In some cases they may have been due to a particular load (e.g. construction plant) or variance errors (§5.3.1&5.6.2). However, in others they may have been due to genuine additional modes.

For some spectra, particularly for low wind speeds, a large number of additional modes was apparent (Fig. 8-29). It is believed that this is evidence of cable-deck interaction (§2.9) causing multiple closely-spaced modes, as predicted by the MECS FE model (§3.4.2). This is considered in more detail in §10.7.2.1. The additional modes were most apparent in the cantilever spectra, i.e. before the installation of the secondary cables, which reduced the cable vibrations and thus the effect of cable-deck interaction (§10.9).

For the results of the IWCM presented in this chapter, the additional modes would cause increased errors in the estimated modal parameters, particularly damping ratios, since they would affect the spectra in the frequency ranges of curve-fitting for the identified modes. This would help explain the greater variance of the damping estimates than anticipated from the error estimation (§8.4.1). However, from inspection of a random sample of the measured spectra, the additional peaks appeared to be noticeable in less than 10% of the spectra, so the majority of the estimated modal parameters would be reasonable.

8.5.3 Discrepancies in measured and fitted spectra for pylon response

A particular occurrence of additional modes was identified in the response of the pylon, for the cantilever structure. From the measured spectra, for both longitudinal and torsional modes, the vibrations were consistently of relatively large amplitude in the 1.6-2.4Hz range. Initially four longitudinal modes were identified in this range (Modes V9-V12, Table 8-1) , which corresponded with the FE model modes. However, curve-fitting to the four dominant spectral peaks in this range led to overestimation of the response in the ranges 1.0-1.6Hz and 2.4-2.8Hz, for which the measured spectrum was of significantly lower magnitude (Fig. 8-30). This was indicative of an inadequacy of the identified modes or assumptions to accurately describe the behaviour. This discrepancy was only apparent from the direct comparison of the measured and fitted spectra, which naturally follows from the use of the IWCM. The discrepancy occurred in low amplitude parts of the spectrum, so would not have been apparent using many other system identification methods, including all time domain methods, which would only match the dominant responses.

A possible explanation of the discrepancy is that the large amplitude response in the 1.6-2.4Hz range was due to a larger number of modes than had been initially estimated for the curve-fitting. There did appear to be several closely-spaced peaks in the spectra, which could, for example, be due to cable-deck interaction (§2.9, 3.4.2&10.7). Several closely-spaced modes with low damping would give a more rapid decay of the response spectrum away from the compound peak than a smaller number of modes with higher damping.

In order to investigate this possibility, an attempt was made to fit curves to a larger number of narrow peaks within the 1.6-2.4Hz frequency range. Results for a typical spectrum are shown in Fig. 8-31, fitted with nine estimated modes, rather than the four fitted previously. Although the fitted and measured spectra are in closer agreement than for the original curve-fit (Fig. 8-30), the drop in magnitude at 1.0-1.6Hz is still not very well represented. Similar fitting of multiple modes was attempted for several measured spectra, and the discrepancy appeared consistently, indicating that is was not merely due to inaccurate curve-fitting as a result of variance on the measured spectra. It was concluded that the hypothesis of multiple close modes, assumed uncoupled, did not completely explain the discrepancy between the measured and fitted spectra.

The remaining discrepancy could be due to a breakdown of the loading assumptions for the system identification method (§6.5&7.6), as follows. The measured mode shapes indicate dominant pylon motion for modes V10 (longitudinal, 2.096Hz, Fig. 8-5) and TL15 (torsional, 2.177Hz, Fig. 8-6(e)). Also the additional modes in the 1.6-2.4Hz frequency range were not apparent in the deck spectra, so would be dominated by pylon

or cable motion. Therefore, for these modes, the loading on the pylon or cables would contribute a significant proportion of the generalised loads of the modes (equation (2-4)), so the assumption of dominant loading on the deck would cease to hold. The loading spectra for these modes would be different from that assumed (§7.6), for example from the variation in wind velocity with height above water, from the different aerodynamic admittance, or from buffeting of one tower in the wake of the other.

Furthermore, if the additional modes were due to cable-deck interaction (§2.9&10.7), the shapes of the pylon deflections in these modes would be likely to be similar to the shapes for the global modes (V10 and TL15), as demonstrated by the MECS FE model (§3.4.2). For modes of similar shapes, the generalised loads would be correlated (§7.2(iii)), resulting in coupling of the modal responses. The total response would then not be given by the sum of the responses of uncoupled modes, as assumed, but may tend to be greater within a certain frequency range, as observed in Fig. 8-31. This is supported by observation of time histories of the pylon acceleration (e.g. Fig. 8-32), which display periods of relatively large vibrations in a narrow frequency range, equivalent to the large magnitude of the spectra in the 1.6-2.4Hz range. Also apparent is the intermittent nature of these vibrations, which is not evident from the spectra. Correlation of generalised loads would be expected to produce this behaviour, since a certain pattern of loading, occurring randomly, would simultaneously excite the similar modes, causing a large total response.

These departures from the assumptions of dominant loading on the deck and uncoupled generalised loads are not considered by conventional buffeting analyses (§2.6.4), so for accurate predictions of pylon vibrations more thorough methods are required. These would need to consider closely-spaced modes of the pylon, for example following an MECS FE analysis (§2.9.2&3.4).

8.5.4 Evidence of coupling of higher frequency vertical bending modes

Another discrepancy between the measured and fitted spectra was observed in the cantilever deck vertical response at approximately 4.5Hz. Fig. 8-1 shows that there were two close modes (natural frequencies 4.500Hz and 4.626Hz) which were fitted, between which there was a marked drop in the magnitude of the response. This drop appeared consistently for all of the measured spectra, but it was not well fitted by the IWCM. This suggests that again the assumptions were not entirely valid. The drop in the response often appeared to resemble an anti-resonance in a Frequency Response Function (FRF), with a quite definite downwards spike (Ewins 1984). This could be indicative of correlated loads, which could result in the responses of the two modes being in antiphase at that frequency at the measurement location. Although both modes appeared to be dominated by deck motion, their mode shapes were not well defined, so it was not

possible to determine whether the shapes were similar, which would lead to correlation of the loads.

8.5.5 Evidence of coupling of vertical and torsional modes of cantilever

It was noted, for the cantilever, that the pairs of modes TL1 & V1, TL2 & V2 and TL3 & V3 each had very close natural frequencies (Table 8-1). In particular, Mode TL1 had a deck torsional component of a similar form to the vertical component of Mode V1 (Fig. 8-5 & Fig. 8-6(a)), so there may have been a potential for classical flutter or other coupling of these two modes (§2.6.5.1&2.6.6). From the wind tunnel study (Xie et al. 1994), the V1 frequency was expected to be 19% above the TL1 frequency, and from the 3-D FE model in this study (§3.3) a difference of 9% was expected, but from the site measurements the difference was actually only 2%. This could be due to some foundation flexibility, which would lower the natural frequency of Mode V1 more, since it had a longitudinal pylon component. The first mode for which torsional deck motion was dominant (Mode TL3) had a natural frequency 62% higher than Mode V1, compared with 37% in the wind tunnel study, and 56% for the FE model, so interaction of these modes would be less likely.

Evidence of coupling of modes was investigated from the measured data, concentrating on the vertical and torsional responses in the vicinity of the natural frequencies of Modes TL1 (0.332Hz) and V1 (0.338Hz). PSDs of the vertical and torsional accelerations are shown in Fig. 8-33 for two different wind speeds, with the wind direction approximately 15° to the east of south normal (§3.2.2) in each case. For the lower wind speed (8.9m/s), the peaks in the vertical and torsional accelerations are at distinct frequencies, implying the existence of two separate modes, but for the higher wind speed (12.2m/s), the PSD of torsional acceleration shows a second peak at the same frequency as the maximum vertical response. This suggests that there was indeed some coupling of the modes.

Considering the coherence between the vertical and torsional accelerations for the same records (Fig. 8-34), there is a peak at 0.337Hz, which was greater (maximum 0.82) for the higher wind speed, which again suggests modal coupling. However, there was no noticeable coupling of the vertical response with the lateral component of Mode TL1, and the increase in the amplitude of vibrations was not great, as would be expected for flutter. Unfortunately there were no three-hour records for the cantilever with a higher mean wind speed for which all of the monitoring equipment was in operation. However, data do exist for a variety of wind conditions for lower speeds, so the behaviour could be investigated further.

The full aeroelastic model of the bridge for this construction stage was stable up to at least 65m/s, but for the actual natural frequencies the structure may have been less stable

Therefore, in design, the possibility of errors in the predicted natural frequencies and the resulting potential for flutter should be investigated, including for construction stages. The British design rules for aerodynamic effects on bridges (DETR 1993) allow for an error in the predicted ratio of bending and torsional natural frequencies of 5%, but the error of 17% for this bridge suggests that a more conservative approach should be taken.

Coupling of modal responses has been considered by multi-mode analyses, but with no validation of the methods at full scale (§2.6.6). Usually the vertical and torsional modes of long-span bridges are well separated so any coupling only becomes significant at very high wind speeds (Jain et al. 1996, Katsuchi et al. 1999), which would be expected very rarely. However, the close spacing of the modes for the cantilever construction stage of the SSC appears to have initiated coupling at a moderate wind speed, providing data which could be valuable for validation of the analysis methods. The lateral component of Mode TL1 would also be of interest, since multi-mode analyses can include for the effects of lateral components on the total coupled response, and there is some evidence that they may be significant (Singh et al. 1996, Katsuchi et al. 1999). Also, the measured natural frequencies and mode shapes would be useful as input to the analyses.

8.6 Amplitudes of buffeting vibrations

The amplitudes of buffeting vibrations are of importance, since the maximum displacements and resulting force resultants are significant design considerations. However, few full-scale measurements of vibration amplitudes of long-span bridges have been made in varying wind conditions, for comparison with theoretical analyses (§2.6.4.4). The long-term tests on the SSC (§4.5.4) enabled such data to be obtained, which were compared with the results of the design buffeting analysis, to assess the adequacy of the analysis method. Also the response amplitudes at different construction stages were of interest, for which again there were few previous measurements at full scale (§2.10).

8.6.1 Design buffeting analysis

A buffeting analysis (§2.6.4) was performed by RWDI at the design stage of the SSC (*Xie et al. 1994*), based on the methods of Irwin (1977). The predicted responses presented here are based on the results of this design buffeting analysis.

According to Irwin's (1977) formulation, the variance of generalised vertical displacement in each mode is given approximately by:

$$\sigma_y^2 = \frac{B^2}{16\pi^4}\left(\frac{\rho B^2}{m}\right)^2\left(\frac{U}{f_n B}\right)^4 \frac{\pi}{4\zeta}\left\{I_u^2 C_L^2 \bar{S}_{uu}\bar{C}_{Iuu}F_{Juu} + \tfrac{1}{4}I_w^2\left[\frac{dC_L}{d\alpha}\right]_{\alpha=0}^2 \bar{S}_{ww}\bar{C}_{Iww}F_{Jww}\right\}\chi^2 \quad (8\text{-}1)$$

where all of the frequency-dependent terms are evaluated at f_n.

Similar expressions provide estimates of the torsional and lateral responses. The definitions of the parameters, and the basis of the values used for the SSC analysis are as follows. The bridge dimensions and the mass distribution were as designed by Halcrow-SEEE, the bridge designers.

ρ	Density of air
B	Deck width
m	Deck mass per unit length
U	Mean wind speed, assumed normal to the bridge
f_n	Natural frequency of the mode, from Halcrow-SEEE FE model (Table 8-4), which also provided the mode shapes
ζ	Total damping. Structural damping assumed to be 0.5% (or 1%) for all modes and aerodynamic damping estimated from quasi-static theory *(equations (2-9)-(2-11))*
C_L, $\frac{dC_L}{d\alpha}$	Lift coefficient and its derivative with respect to the vertical angle of attack of the wind, from wind tunnel sectional model tests (see below)
I_u, I_w	Longitudinal and vertical turbulence intensities, taken as 11% and 6% respectively
$\bar{S}_{uu}, \bar{S}_{ww}$	Reduced wind velocity spectra, from von Kármán's (1948) model of turbulence (equations (2-14)&(2-15))
$\bar{C}_{Iuu}, \bar{C}_{Iww}$	Wind correlation factors, from equations (6-2)&(6-3)
F_{Juu}, F_{Jww}	Correlation correction factors, both taken to be unity (i.e. short correlation length assumed, §2.6.4.2)
χ^2	Aerodynamic admittance, from equation (6-5)

For the sectional model tests, the empty bridge deck (the 'basic configuration') and three different traffic configurations were considered, giving a range of values of the static force coefficients and derivatives.

On the above basis, Xie et al. (1994) provide tables of the expected generalised displacement amplitudes of each of seven modes at a series of wind speeds, for structural

damping ratios of 0.5% and 1%, for the four deck configurations. The mode shapes, from the Halcrow-SEEE FE model, are also provided. The seven modes are listed in Table 8-4, along with the measured frequencies of the assumed equivalent modes on site, for comparison. These modes were assumed by RWDI to cause the majority of the deck displacement from buffeting.

Table 8-4 Modes of finished bridge included in design buffeting analysis

Mode no.	Measured frequency (Hz)	Halcrow-SEEE frequency (Hz)	Frequency error* (%)	Description
V1	0.326	0.3300	+1.2	1st symmetrical vertical
TL1	0.427	0.4037	-5.5	1st symmetrical lateral
V2	0.427	0.4269	0	1st anti-symmetrical vertical
TL4	0.490	0.4620	-5.7	1st symmetrical torsional
TL8	0.620	0.5157	-16.8	2nd symmetrical torsional
V3	0.608	0.6095	+0.2	2nd symmetrical vertical
TL10	0.842	0.6914	-17.9	1st anti-symmetrical torsional

* Error of Halcrow-SEEE frequency relative to measured frequency

From the data provided by Xie et al. (1994), the RMS total acceleration at the measurement location (23.42m from midspan) was estimated, assuming linear superposition of modal responses (§7.2), as:

$$\sigma_{\ddot{y}} = \sqrt{\sum_i \left\{\Phi_i \sigma_{y_i} (2\pi f_i)^2\right\}^2} \qquad (8\text{-}2)$$

where: i = mode number

Φ_i = magnitude of i^{th} mode shape at measurement location, relative to magnitude at reference location

σ_{y_i} = RMS generalised displacement of mode i

f_i = natural frequency of mode i

The factor $(2\pi f_i)^2$ is included to convert the displacements, from the RWDI analysis, to accelerations, for direct comparison with the measured response, assuming the response in each mode is dominated by a narrow frequency range centred at the natural frequency. The factor increases for higher frequencies, so the total acceleration response may be underestimated due to the omission of higher frequency modes in the buffeting analysis.

It was found that, for vertical vibrations, the maximum response occurred for the basic configuration and the minimum for traffic on both carriageways, whereas for torsional and lateral vibrations the maxima were for traffic on only the leeward carriageway, and the minima for the basic configuration.

8.6.2 Measured responses and wind conditions

The measured amplitudes of response to wind buffeting were considered for the finished bridge, for a data set from 23/12/97 to 5/1/98, covering the strongest winds recorded on site (§6.4.1). Recording was triggered by the 2s gust wind speed exceeding 14.3m/s, with a total of 123 hours of data recorded.

The RMS accelerations of the deck over periods of 163.84s (standard file length, §4.3.2) were calculated from the measured data, along with the mean wind parameters from the anemometer on the south (windward) side. The responses showed stronger relationships with the component of wind velocity normal to the bridge than with the wind speed (§6.3). This was confirmed by fitting straight lines on log-log plots, which found lower correlation coefficients when considering wind speed, even when selecting only those records for which the wind direction was within 45° or 30° of normal to the bridge axis. In contrast, Hay (1984) suggested that, for wind within 45° of normal to the Erskine and Wye Bridges, the wind speed was the critical parameter. These other bridges have streamlined box girder cross-sections, whereas the SSC has a bluff cross-section (Fig. 3-3(b)), which could be of significance.

8.6.3 Comparison between measured response and design buffeting analysis

The response amplitudes from the SSC site measurements and from the design buffeting analysis (§8.6.1) were compared, to assess the adequacy of the analysis method. In the comparison, the following differences should be noted:

- For the measured response, traffic loading causes background vibrations, particularly significant at low wind speeds (§6.6).
- The lateral measured response includes an erroneous component from quasi-static torsional displacements (§5.5&8.3.4).
- The mean measured turbulence intensities were 6.5% longitudinal and 3.5% vertical, compared with 11% and 6% assumed in the buffeting analysis. i.e. the measured turbulence was only 59% of that assumed, which should give a corresponding reduction in the response.

- The analysis included only seven modes (Table 8-4). Higher frequency modes were considered insignificant for the displacement response, but they could be significant for acceleration.
- The analysis assumed the wind was normal to the bridge axis, whereas the measured response is plotted relative to the normal component of the wind velocity. The longitudinal component of wind velocity may contribute to the scatter of the measured points.
- The analysis assumed 0.5% structural damping for all modes, but the measured damping was often lower (§8.4.3).
- The analysis assumed the aerodynamic damping predicted by quasi-static theory, but the measured aerodynamic damping was generally lower (§8.4.2).
- There were differences in the natural frequencies used in the analysis and measured on site (Table 8-4).

These differences mean that the results cannot be expected to match accurately. However, the most significant differences are likely to be the lower turbulence and lower damping measured on site, the effects of which would to some extent cancel each other out.

For the vertical response, comparison of the predicted and measured RMS accelerations showed good agreement (Fig. 8-35). For the torsional response, the measured response was slightly lower than predicted, but the agreement was still reasonable (Fig. 8-36). However, for the lateral response, the design analysis overestimated the measured accelerations by a factor of approximately two (Fig. 8-37). This was believed to be due to the greater aerodynamic damping for lateral modes than predicted by quasi-static theory (§8.4.2).

Notwithstanding the differences listed above, the long-term site measurements have shown the design analysis to give reasonable predictions of the response to wind buffeting, although they are somewhat conservative for lateral vibrations. Further work is required to allow more direct comparisons, accounting for some of the differences, to give a more precise assessment of the accuracy of the method of analysis. Alternative buffeting analyses could also be investigated.

8.6.4 Comparison with results of wind tunnel tests

The wind tunnel tests on the full aeroelastic model (Xie et al. 1994) gave deck responses in the form of RMS displacements, whereas the site measurements yielded RMS accelerations, so direct comparison of the results is not possible. However Xie et al. (1994) give a comparison of displacement responses at midspan from the aeroelastic

model and the buffeting analysis at 40m/s. These show reasonable agreement, with the model giving 17% lower vertical response, 49% higher torsion, and 21% lower lateral response. On this basis, the model would be expected to give a good prediction of the full-scale bridge vertical response and overestimates of the torsional and lateral responses by approximately 80%.

Integration of the measured accelerations, or analysis of the displacements measured directly by the Computer Vision System (CVS) (§4.4) are required to allow better comparison with the aeroelastic model displacements.

8.6.5 Amplitude of vibrations at different construction stages

It was also of interest to consider the relative vibration amplitudes at three particular construction stages - the completed M2 cantilever, the finished structure but without the wind barriers, and the finished bridge with the wind barriers (§3.2.5). Thus the greater vulnerability of the cantilever compared with the completed structure could be evaluated (§2.10), as could the effect of the wind barriers in increasing the loading, and hence response, of the structure (§2.7.3).

The RMS accelerations of the deck at the three construction stages are plotted against normal component of the wind velocity in Fig. 8-38 to Fig. 8-40, for the vertical, torsional and lateral responses respectively. For clarity, the responses, measured over individual file lengths, have been averaged for each 1m/s velocity range. For the cantilever the responses were measured at the end of the deck, but for the completed structure they were measured 23.42m from midspan. In each case these would be close to the maximum responses on any part of the deck, so they are comparable.

Comparing the behaviour of the cantilever with that of the completed structure without the wind barriers, for wind speeds above 10m/s the vertical response was typically 70% greater. The torsional response was very similar, but the lateral response was greater by almost a factor of three, although still smaller than the vertical and torsional components. These results highlight the susceptibility of cantilever structures to relatively large displacements, requiring specific buffeting analyses or wind tunnel tests for design (§2.10).

For the finished bridge with the wind barriers, traffic was present during the tests, causing noticeable background vibrations for normal components of wind velocity up to approximately 12m/s (§6.6). For higher velocities, compared with the finished structure without wind barriers, the vertical response was increased by approximately 50%, the torsional component by up to 100%, and the lateral response by up to 150%. Thus very significant increases in the loading and response of the structure occurred due to the introduction of the wind barriers.

Further work is required to compare the measured responses at the construction stages with results from the wind tunnel study and buffeting analyses, to assess the accuracy of these methods for predicting full-scale responses.

8.7 Conclusions

8.7.1 Modal behaviour

The modal behaviour of the SSC has been analysed for both the cantilever structure, during construction, and the finished bridge. Natural frequencies and detailed mode shapes of over 30 global modes of the cantilever were determined, which agreed well with the results of the 3-D FE analysis (§3.3). This shows that ambient vibration tests and data analysis with the IWCM can yield reasonable estimates of natural frequencies and mode shapes. Also the FE modelling approach was validated for calculating modal parameters, including for torsional/lateral modes. The natural frequencies and principal components of over 30 modes of the finished bridge were also identified, which could be used for testing model updating strategies, applied initially to the cantilever model.

The long-term records from site (§4.5.4) and the application of the IWCM (Chapter 7), enabled estimates to be made of the modal damping ratios, more accurately than normally possible from ambient vibration data. Thus, from a large number of estimates for different wind conditions, estimates of the aerodynamic and structural damping components for each mode were obtained. It is believed that this is the first time these components have been separated in full-scale tests for a long-span bridge with a bluff cross-section.

It was found, for the first few vertical modes, that the aerodynamic damping was approximately half of the value predicted by quasi-static theory. Therefore, if this theory is used in design, the amplitudes of vibrations could be significantly underestimated. For torsional vibrations, the agreement between the theoretical and measured results was better. For lateral vibrations, the aerodynamic damping was found to be significantly greater than estimated by the theory, often due to the dominance of aerodynamic damping from the torsional components of the modes. The discrepancies between estimates from quasi-static theory and the measured values, particularly for vertical modes, suggest that a more refined approach of estimating aerodynamic damping should be considered in preference, for example based on flutter derivatives. There was some evidence of non-linear or negative aerodynamic damping for some modes, but the scatter of the results meant this could not be confirmed.

The structural damping was found to be of the order of 0.5% for all modes. The values were at the lower end of the range reported from other full-scale tests, believed to be due

to the subtraction of the component of aerodynamic damping from the measured values, in contrast with previous estimates. There was no increase in damping for the lower frequency modes, as observed on suspension bridges, indicating a different distribution of damping. Values of structural damping for the cantilever and the finished bridge were found to be comparable, suggesting that estimates made during construction could be used to improve predictions of the behaviour of a completed structure.

Variations in natural frequencies of the finished bridge due to the mass of traffic were detected, with a maximum change of approximately 1%. This variation, along with the aerodynamic damping, appeared to mask any changes in modal parameters due to temperature variations, structural non-linearities or other effects. Further analysis of the data, compensating for these defined variations, may enable more subtle variations to be detected.

Discrepancies between the measured spectra and those fitted by the IWCM enabled other variations in the modal behaviour to be identified. These included the intermittent existence of some additional modes, possibly due to cable-deck interaction (§10.7.2.1), and apparent coupling of some modes, believed to be due to correlation of the generalised loads, which is not accounted for by conventional buffeting analyses.

For the cantilever, the measured natural frequencies of the first two modes (lateral, with a torsional component, and vertical) were only 2% apart - significantly closer than anticipated. In moderate winds there appeared to be some coupling between these modes. This type of behaviour is predicted by recent multi-mode analysis methods (§2.6.6), but it has not been previously observed at full scale. The data from the SSC tests could therefore be of value for validating these methods.

8.7.2 Amplitudes of buffeting vibrations

The amplitudes of vibrations of the deck of the finished bridge were compared with the results of the design buffeting analysis. Although there were several known differences between the assumed and actual behaviour, the results compared favourably, particularly for the vertical and torsional responses. Thus, the method of analysis used for design, based on the methods of Irwin (1977), including his expression for aerodynamic admittance (§6.5.3), appears to provide reasonable predictions of the actual behaviour.

The amplitudes of vibrations at three construction stages were also compared, indicating the increased susceptibility to vibrations of a single cantilever compared with the completed structure, and the significant increase in amplitudes due to the addition of traffic wind barriers.

There is much scope for more detailed evaluation of the buffeting analysis, utilising the collected site data. Results of the design analysis were calculated in terms of RMS

displacements for each mode, whereas on site the total acceleration was measured. However, results of the IWCM, in conjunction with the assumed loading spectrum (§7.6), would allow integration of the estimated displacement PSD of each mode, to obtain RMS displacements of each mode from the measurements. Alternatively, displacements measured directly by the CVS (§4.4) could be used for the comparison. Other discrepancies between the basis of the buffeting analysis and the measured data could be overcome by re-running the analysis using measured values of wind turbulence, natural frequencies and structural and aerodynamic damping. Also, the mode shapes used for the analysis could be validated against measured shapes. Thus, the accuracy of the method itself, rather than effects of the assumed input parameters, could be more precisely evaluated.

Alternative buffeting analyses could also be assessed, for example including the full integral of wind loading over the structure, rather than assuming a short correlation length (§2.6.4.2). Comparison with the results of coupled multi-mode analyses (§2.6.6) could also be considered, although the differences from the normal assumption of the superposition of uncoupled modes may not be significant for the relatively low wind speeds experienced on site.

A further possibility for the comparison would be to create estimated response spectra from the results of the buffeting analysis, and to compare these with the measured and fitted spectra. Discrepancies could be used to identify any shortcomings in the analysis.

The measured response also gives the opportunity for evaluation of the accuracy of the results of the full aeroelastic model tests. Conversion of the measured responses to RMS displacements would enable a direct comparison of the results.

The data collected from the different construction stages provide opportunities for further study of the buffeting behaviour, since the analyses can be validated against the measurements for the different stages, using different input parameters. Thus more thorough validation of the methods is possible than for the response of a single stage.

8.7.3 Concluding remarks

This chapter has defined the global modal behaviour of the SSC, and discussed its response to wind buffeting. The following chapter deals with the particular phenomenon of vortex-induced vibrations, after which Chapter 10 discusses the local vibrations of cables and evidence of cable-deck interaction on the bridge.

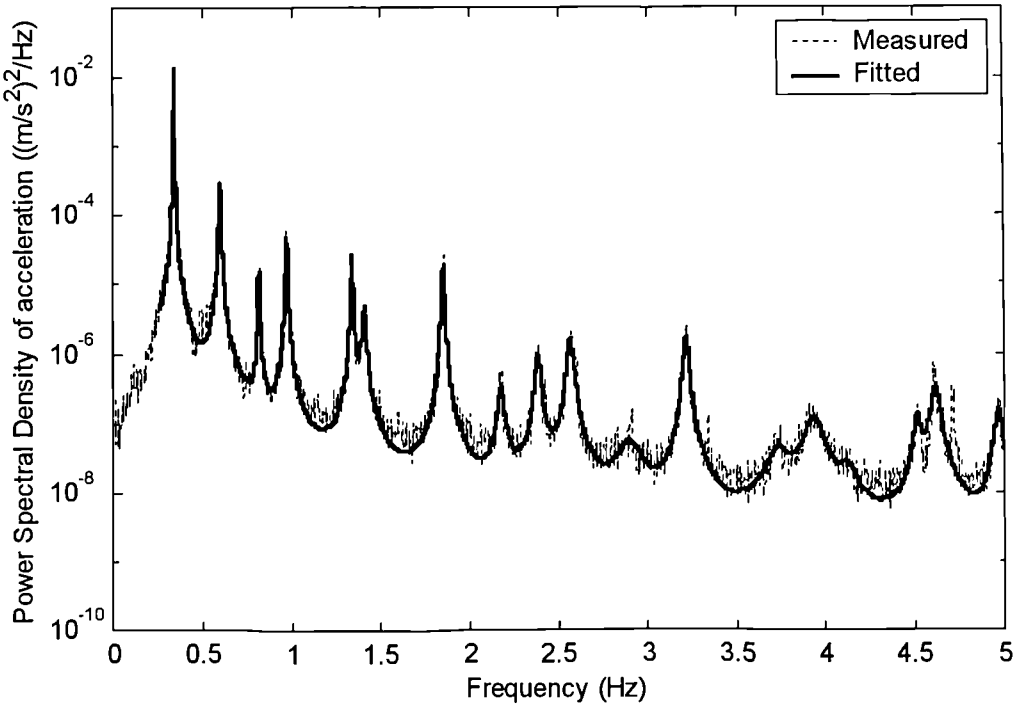

Fig. 8-1 Typical curve-fit of PSD of vertical deck acceleration of the cantilever (wind 9.0m/s, 18° to east of south normal (§3.2.2))

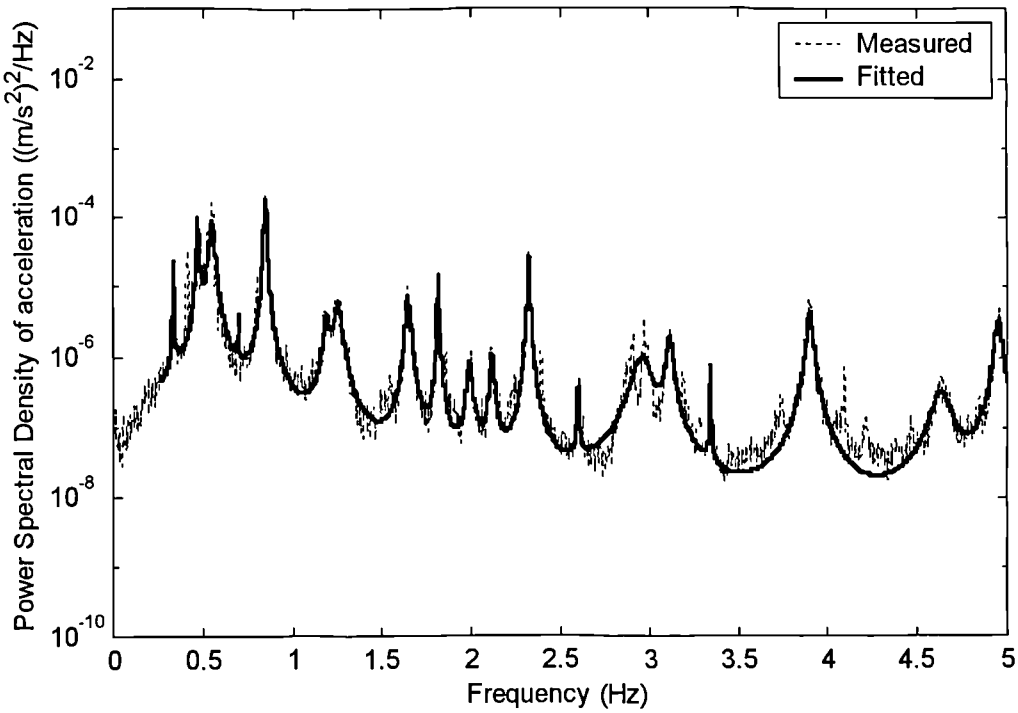

Fig. 8-2 Typical curve-fit of PSD of torsional deck acceleration of the cantilever (wind 9.0m/s, 18° to east of south normal)

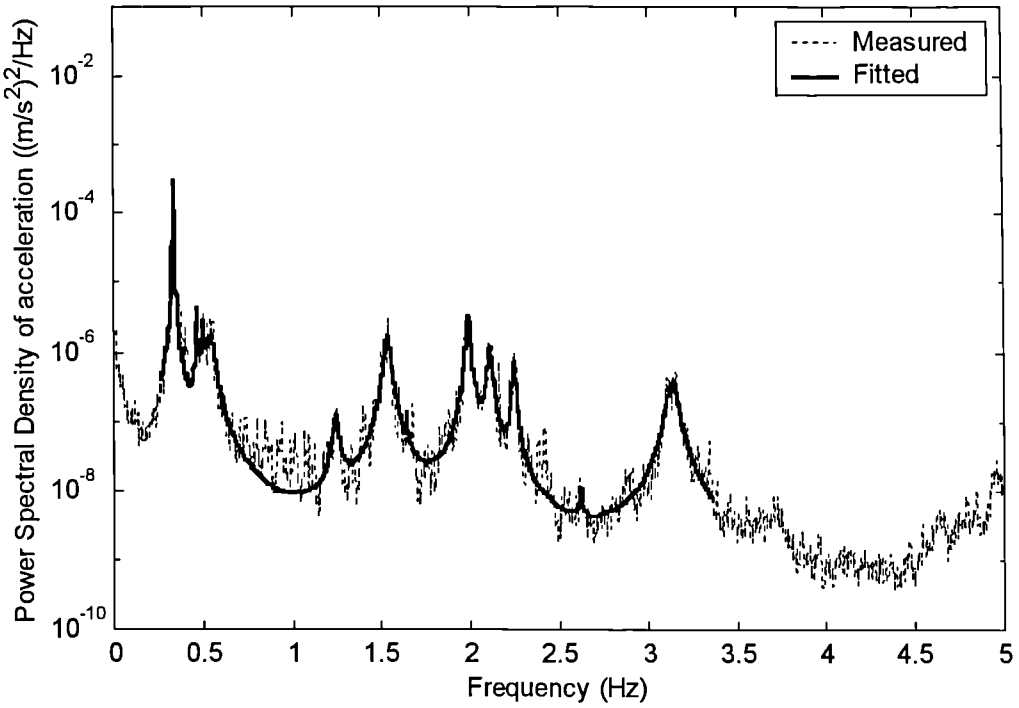

Fig. 8-3 Typical curve-fit of PSD of lateral deck acceleration of the cantilever (wind 9.0m/s, 18° to east of south normal)

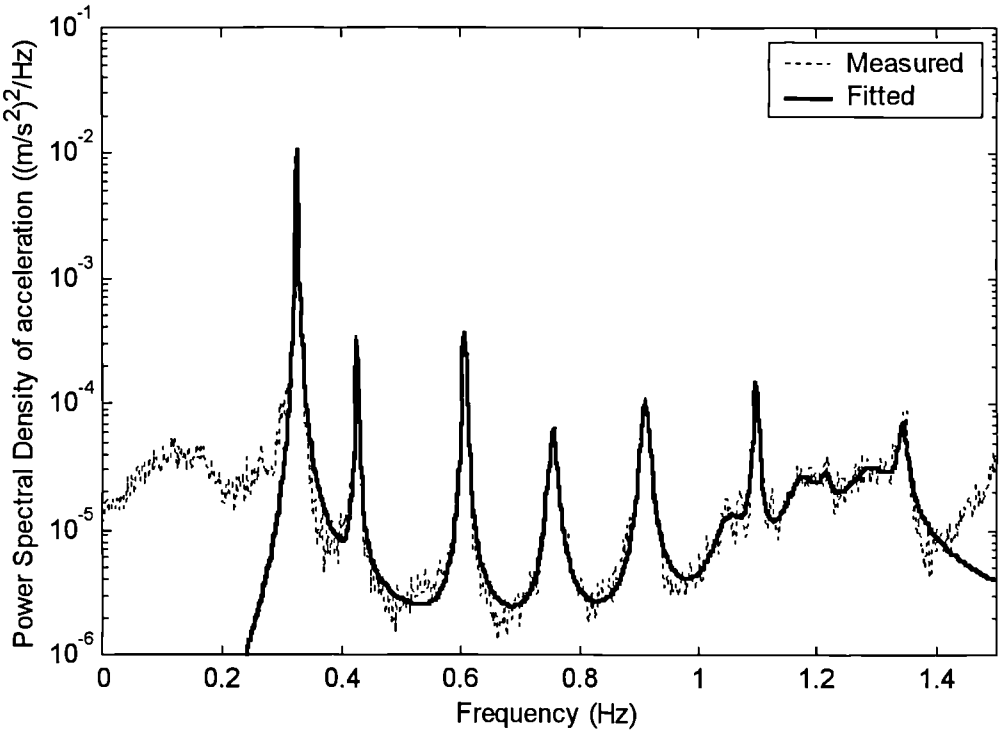

Fig. 8-4 Typical curve-fit of PSD of vertical deck acceleration of the finished bridge (with traffic loading and low wind speed)

Mode V1, 0.338Hz

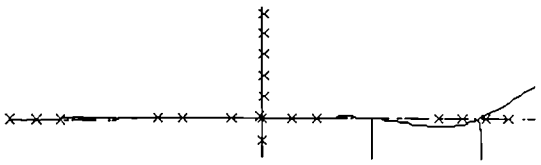

Mode V2, 0.491Hz

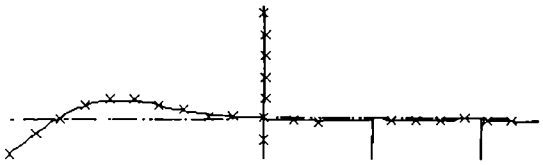

Mode V3, 0.596Hz

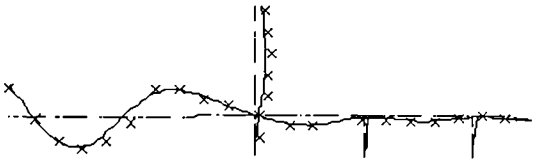

Mode V4, 0.818Hz

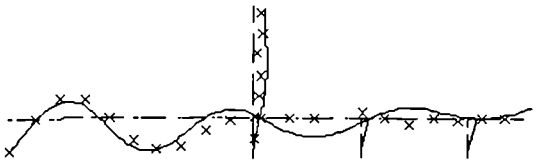

Mode V5, 0.977Hz

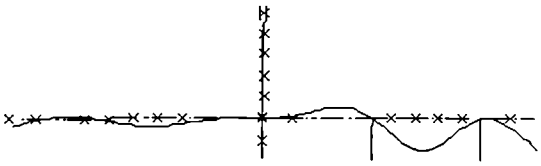

Mode V6, 1.015Hz

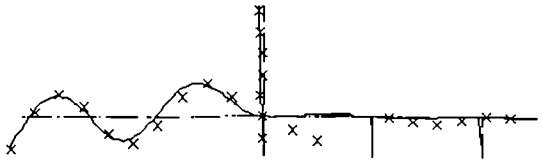

Mode V7, 1.336Hz

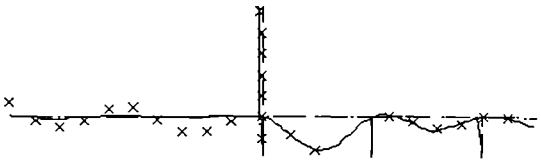

Mode V8, 1.404Hz

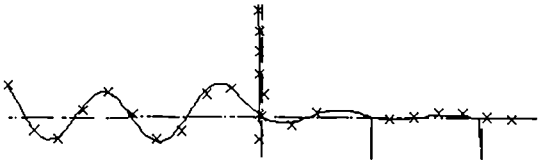

Mode V9, 1.846Hz

Mode V10, 2.096Hz

Fig. 8-5 Comparison of vertical plane mode shapes from FE model (lines) and from site data (crosses)

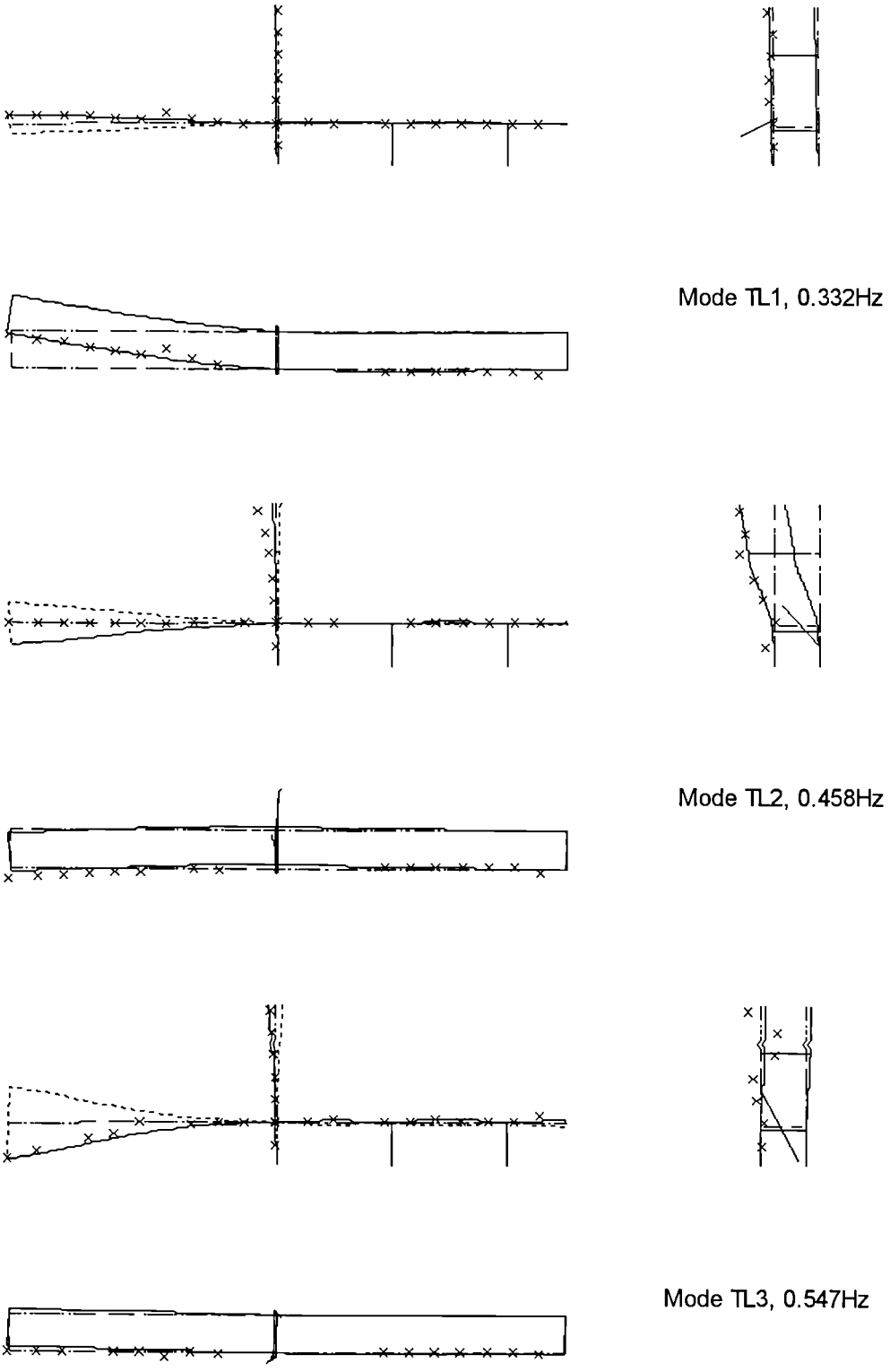

Fig. 8-6(a) Comparison of torsional/lateral mode shapes from FE model (lines) and from site data (crosses)

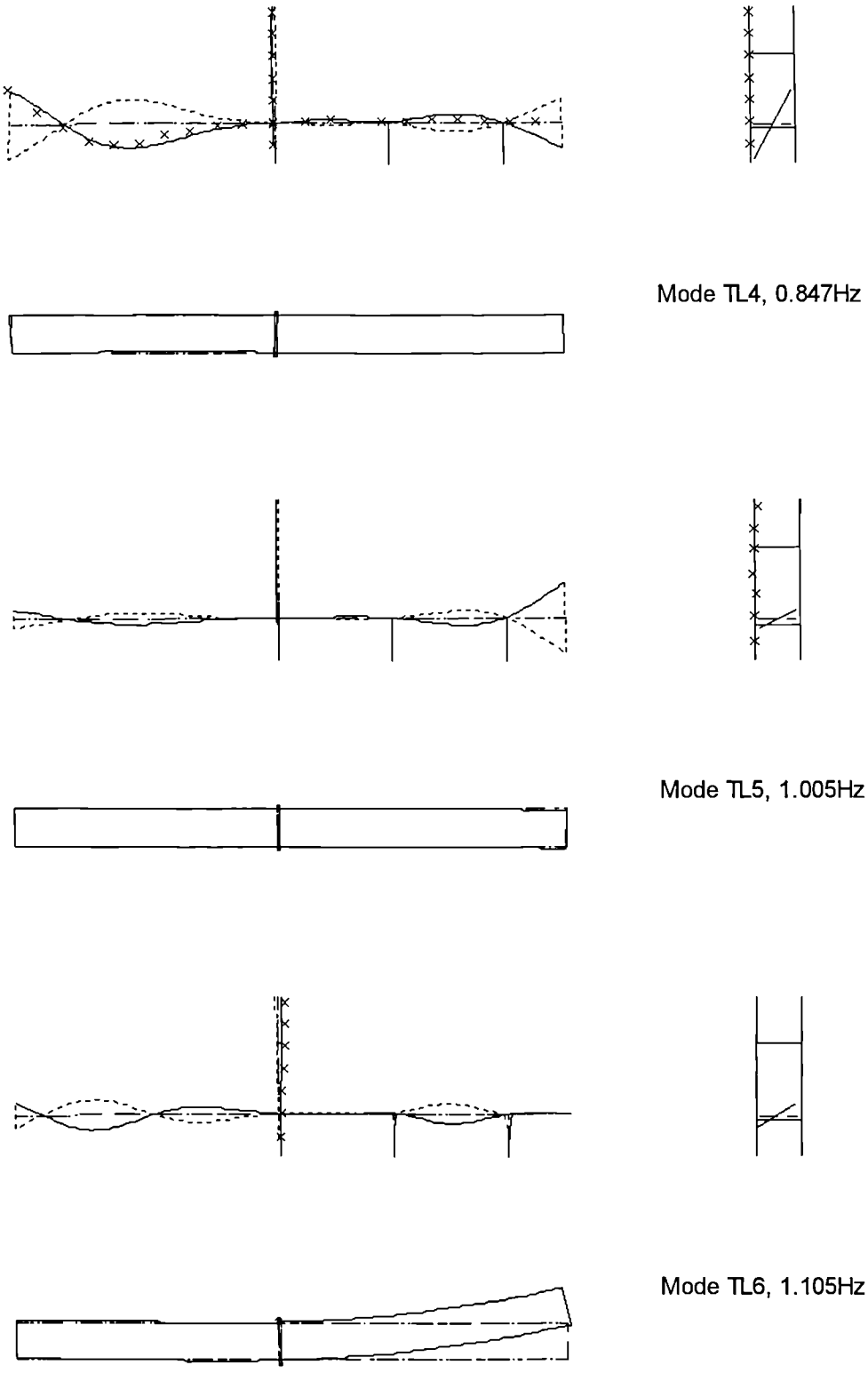

Fig. 8-6(b) Comparison of torsional/lateral mode shapes from FE model (lines) and from site data (crosses)

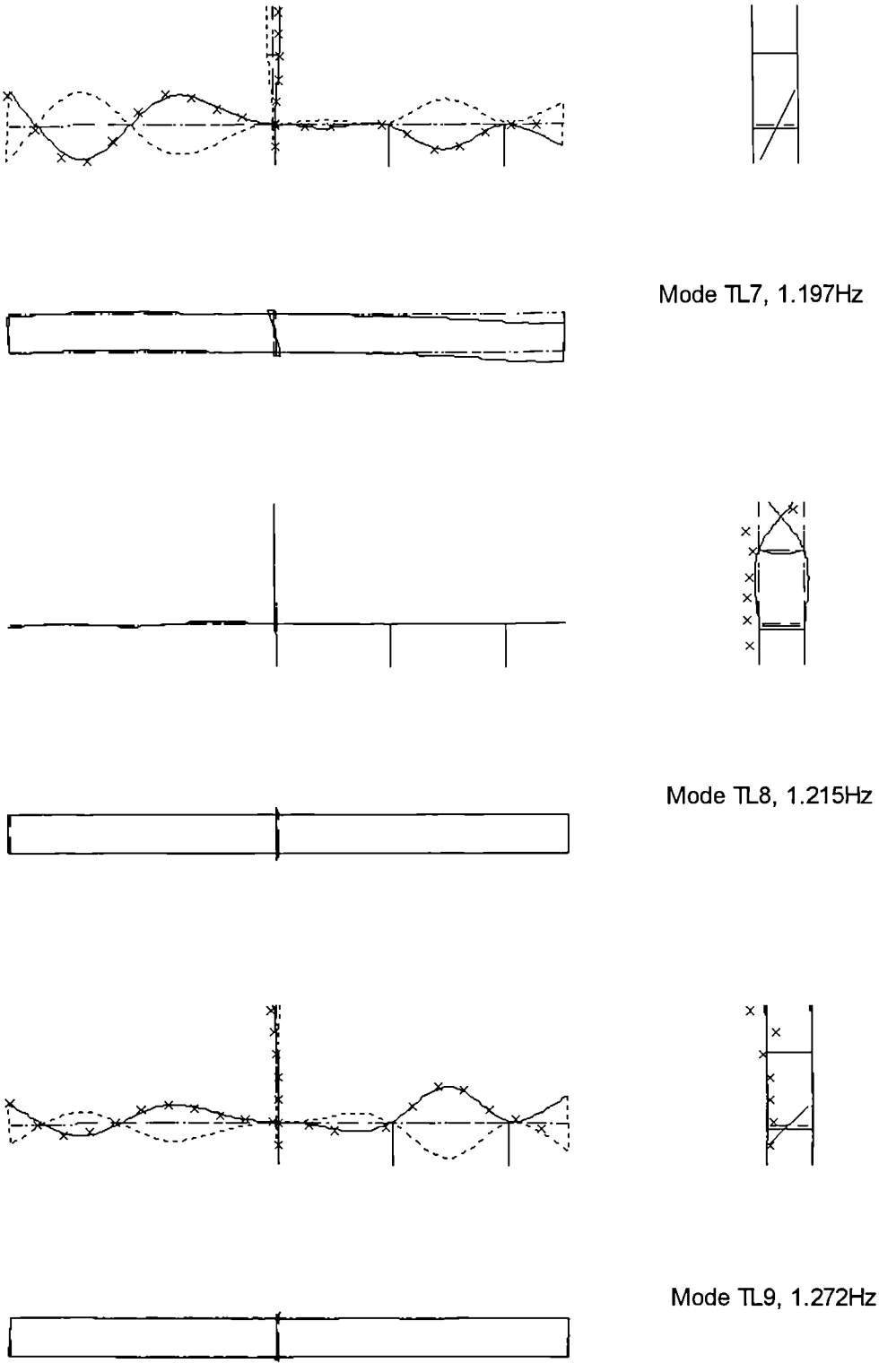

Fig. 8-6(c) Comparison of torsional/lateral mode shapes from FE model (lines) and from site data (crosses)

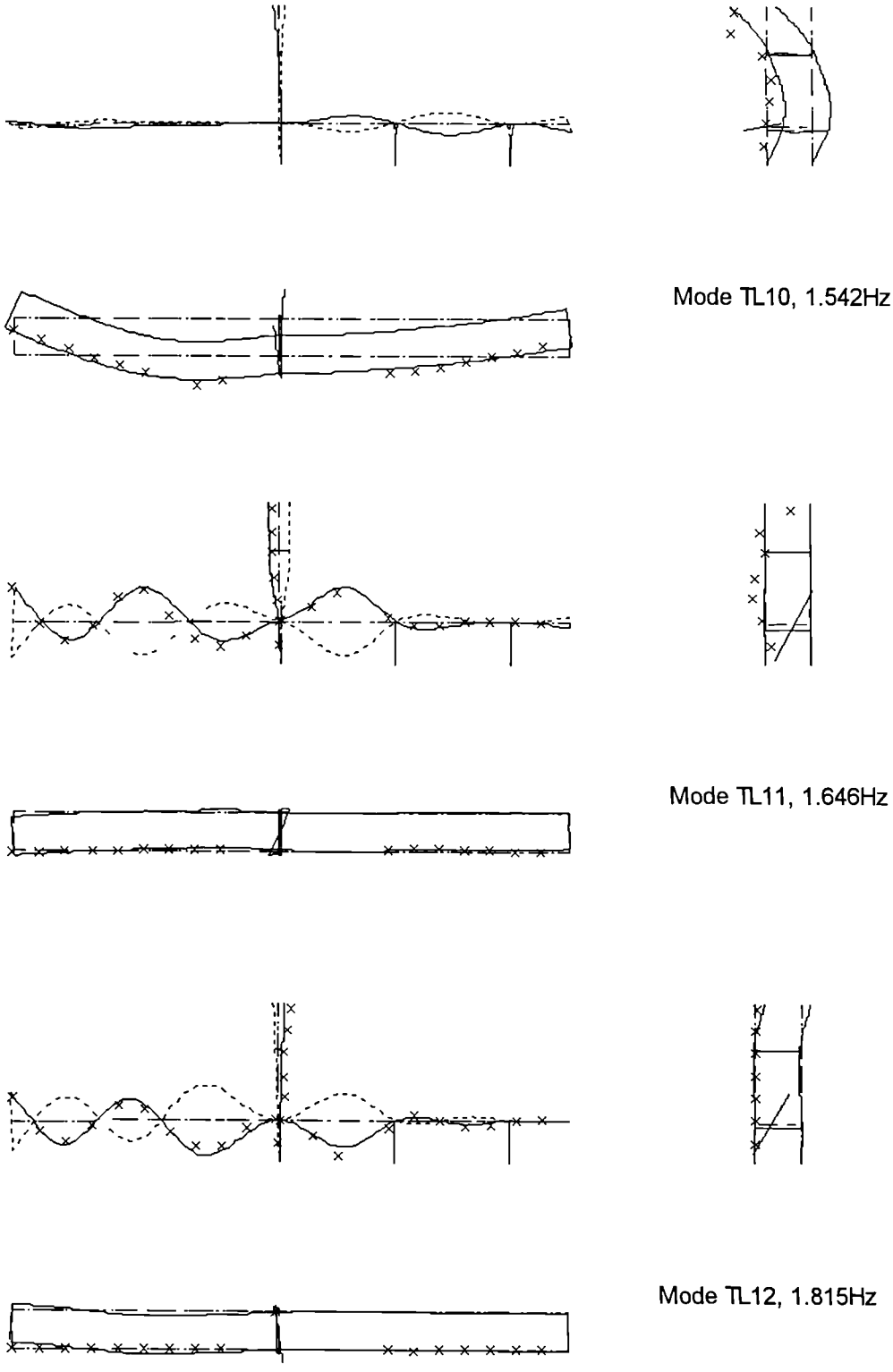

Fig. 8-6(d) Comparison of torsional/lateral mode shapes from FE model (lines) and from site data (crosses)

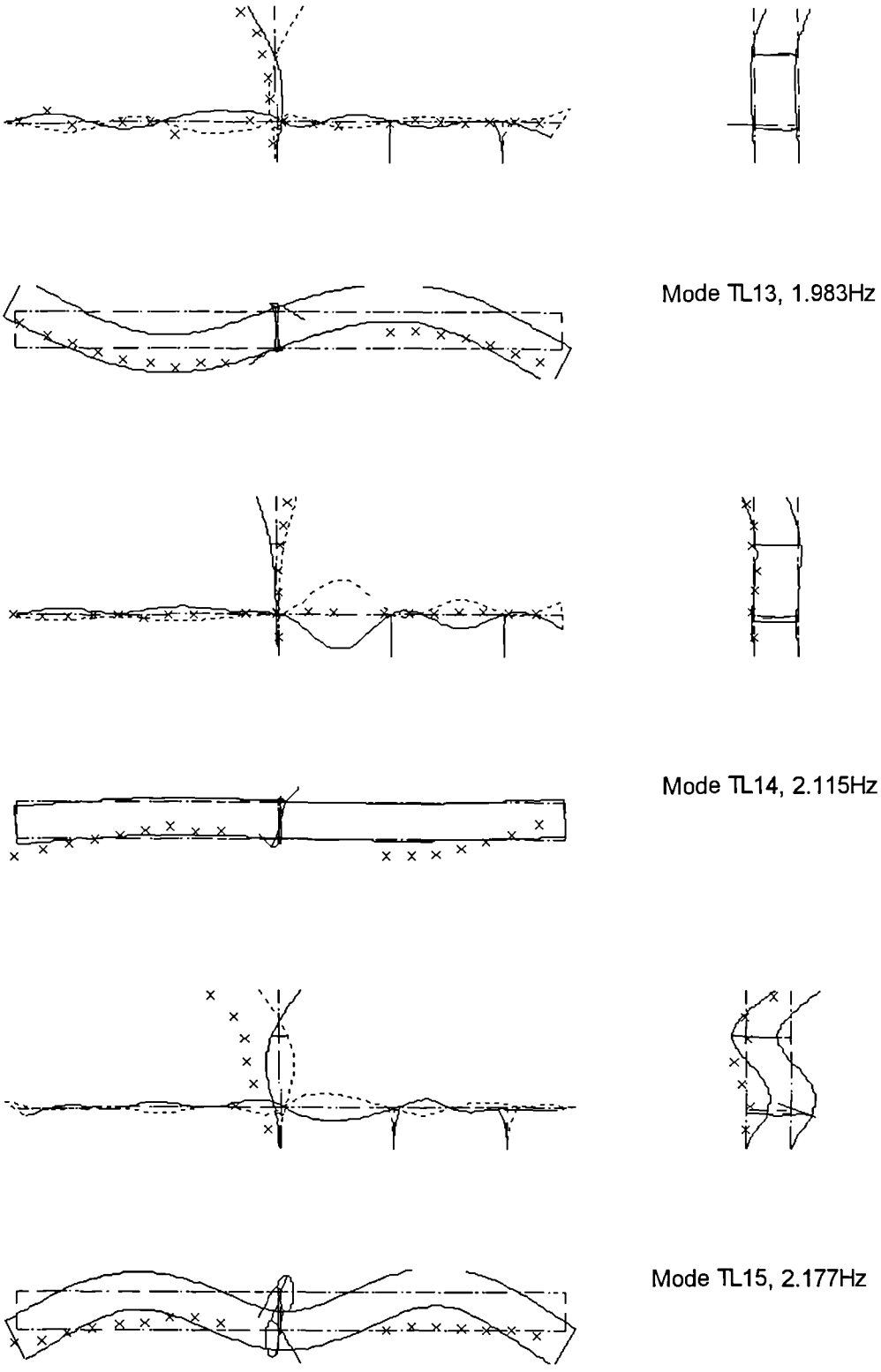

Fig. 8-6(e) Comparison of torsional/lateral mode shapes from FE model (lines) and from site data (crosses)

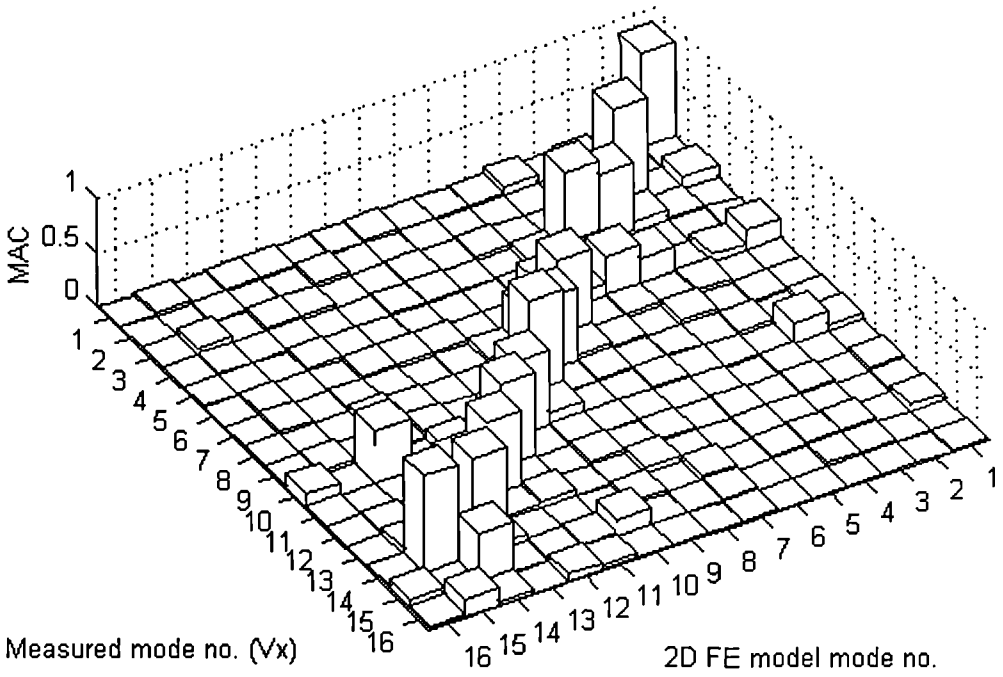

Fig. 8-7 Modal Assurance Criteria for vertical plane modes of cantilever

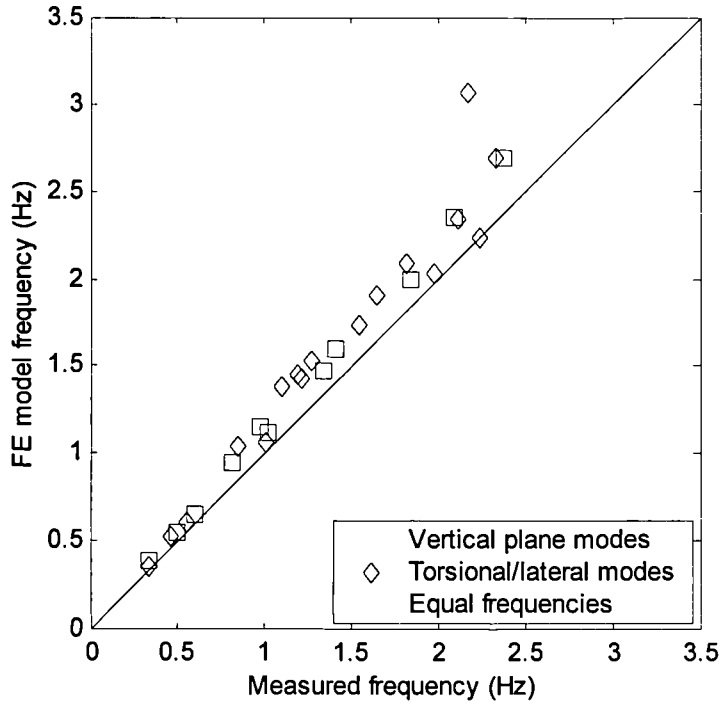

Fig. 8-8 Comparison of natural frequencies from FE model and from site data

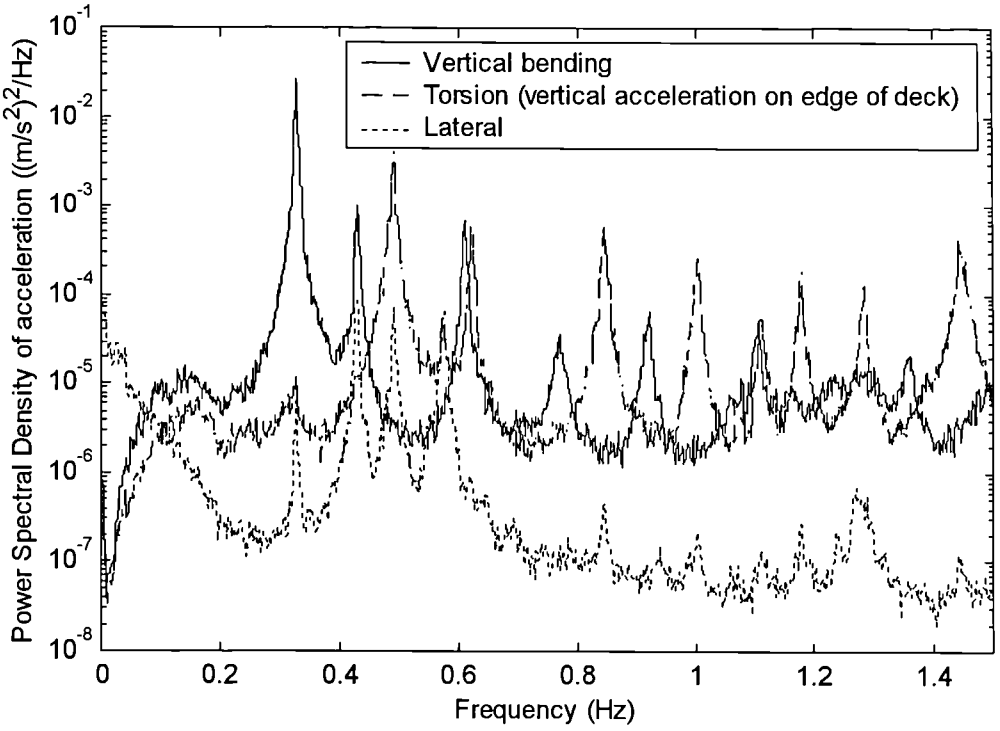

Fig. 8-9 PSDs of typical deck accelerations of finished bridge

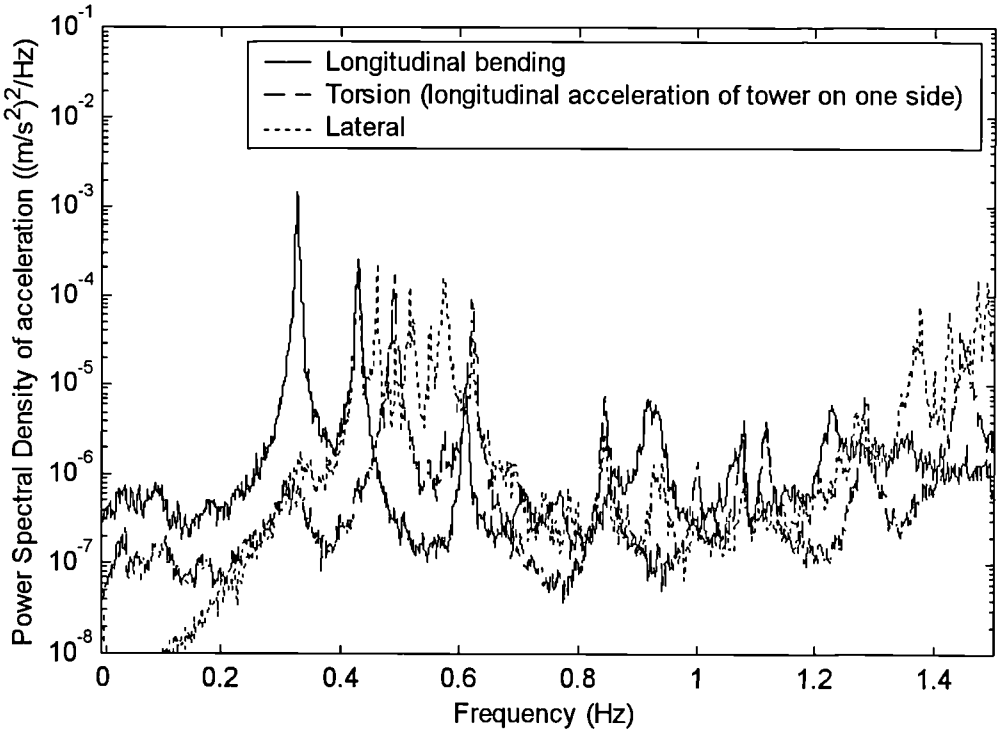

Fig. 8-10 PSDs of typical pylon accelerations of finished bridge

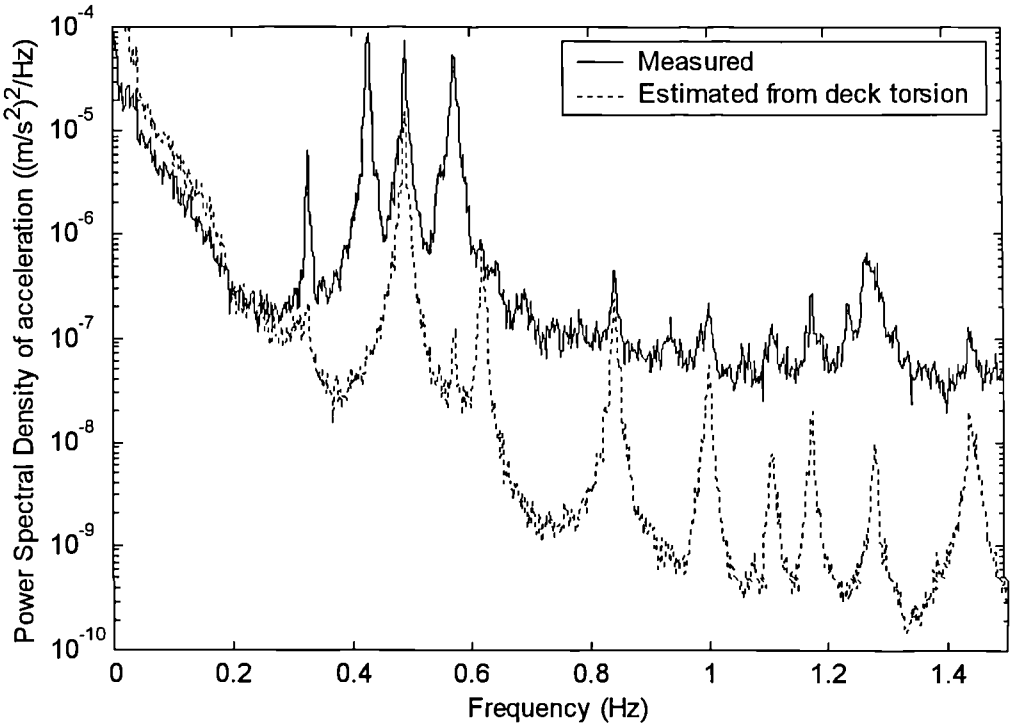

Fig. 8-11 PSDs of measured acceleration from lateral deck accelerometer and estimated apparent component due to deck torsion for finished bridge

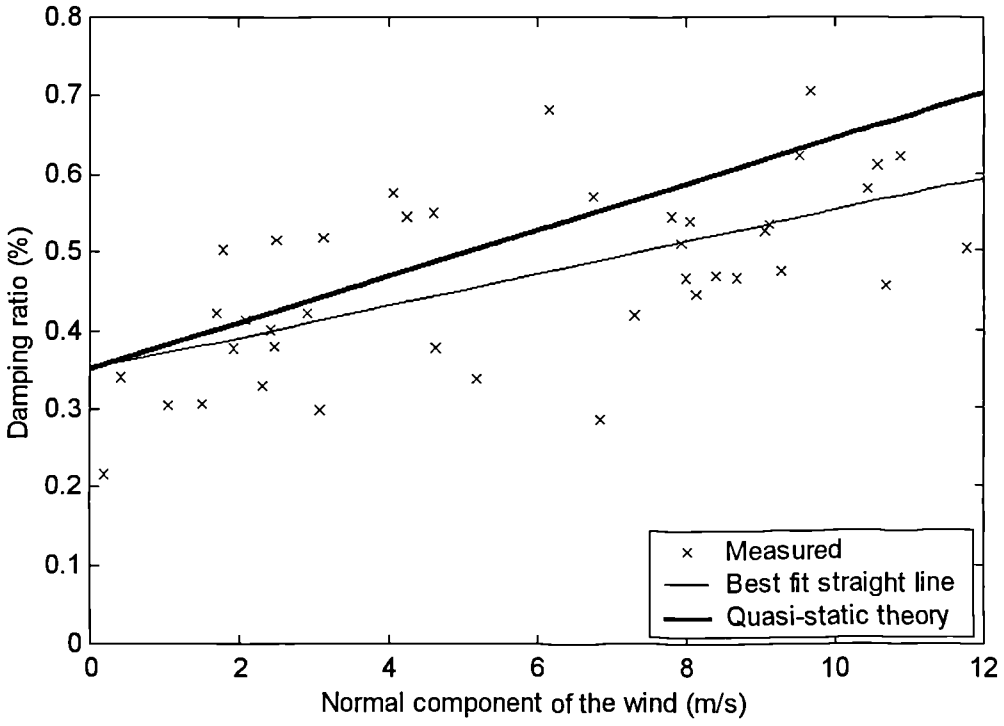

Fig. 8-12 Damping ratios for fourth vertical bending mode of cantilever

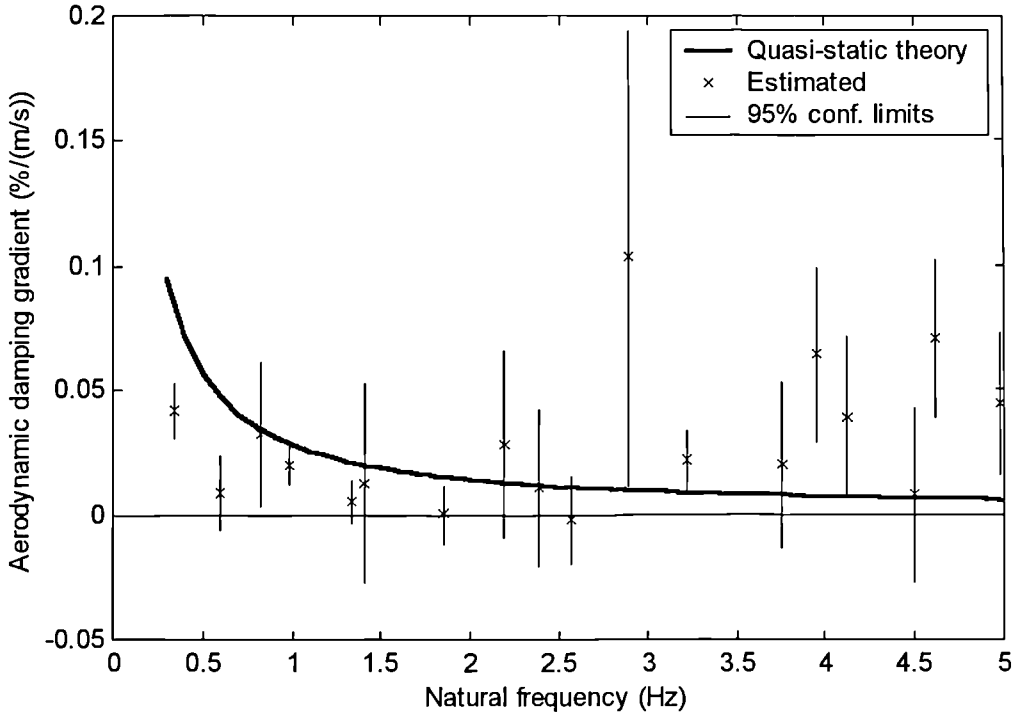

Fig. 8-13 Estimated aerodynamic damping gradients of vertical bending modes of the cantilever up to 5Hz

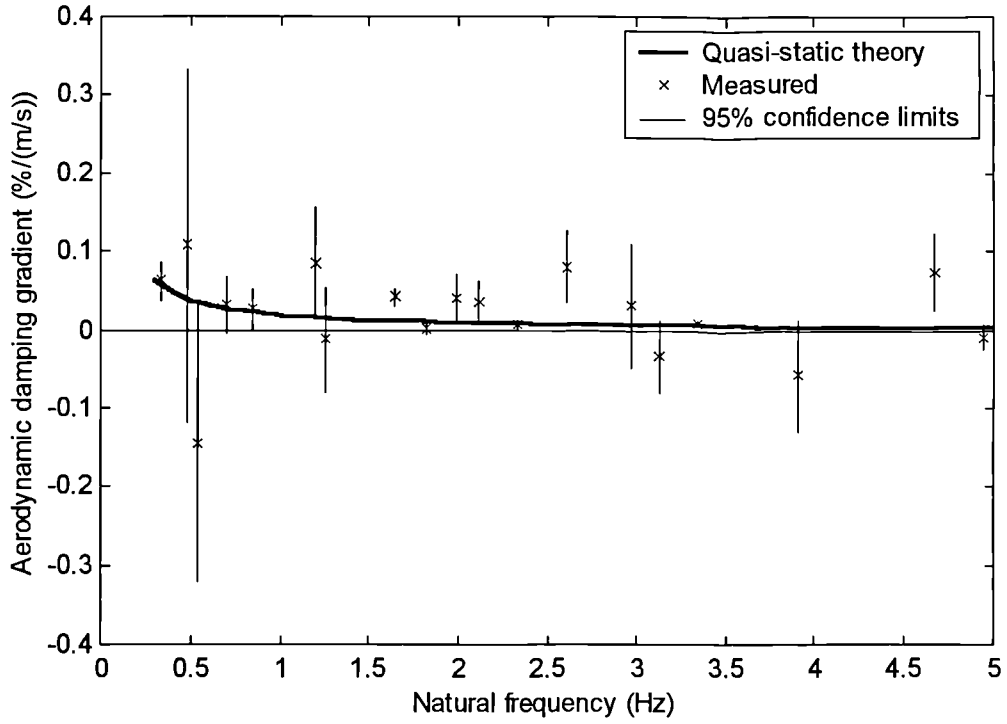

Fig. 8-14 Estimated aerodynamic damping gradients of torsional modes of the cantilever up to 5Hz

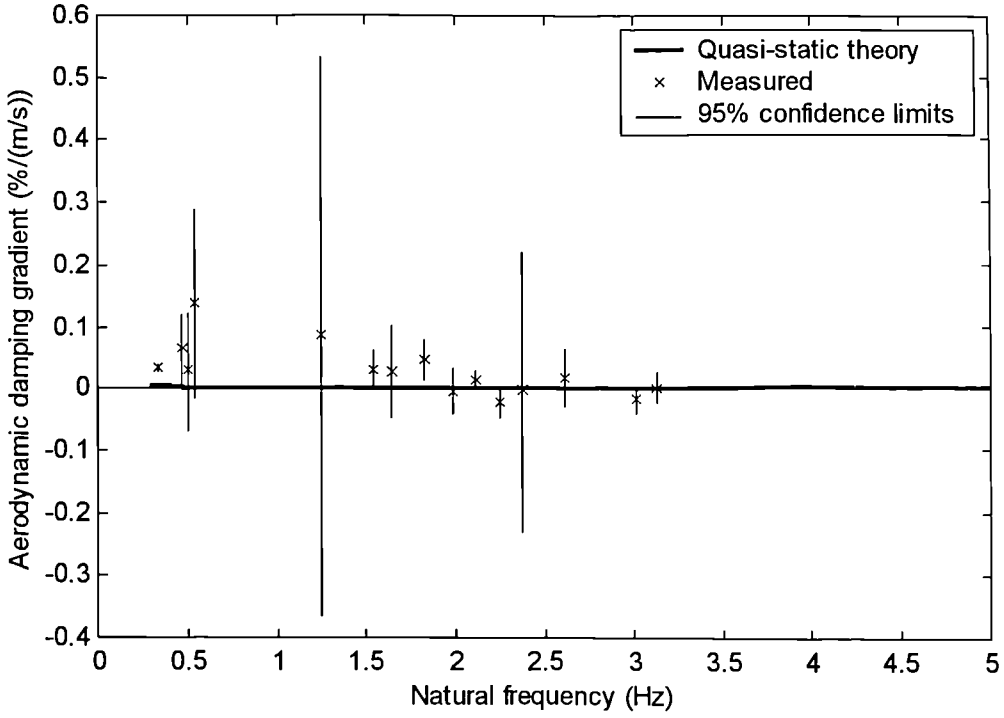

Fig. 8-15 Estimated aerodynamic damping gradients of lateral modes of the cantilever up to 3.2Hz

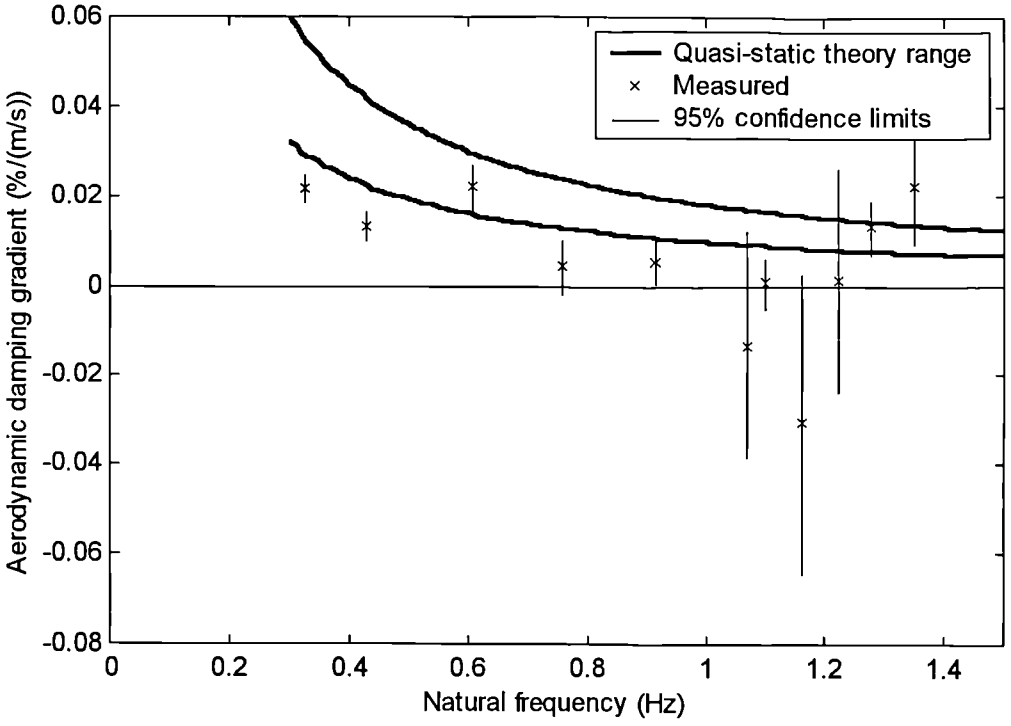

Fig. 8-16 Estimated aerodynamic damping gradients of vertical bending modes of the finished bridge up to 1.5Hz

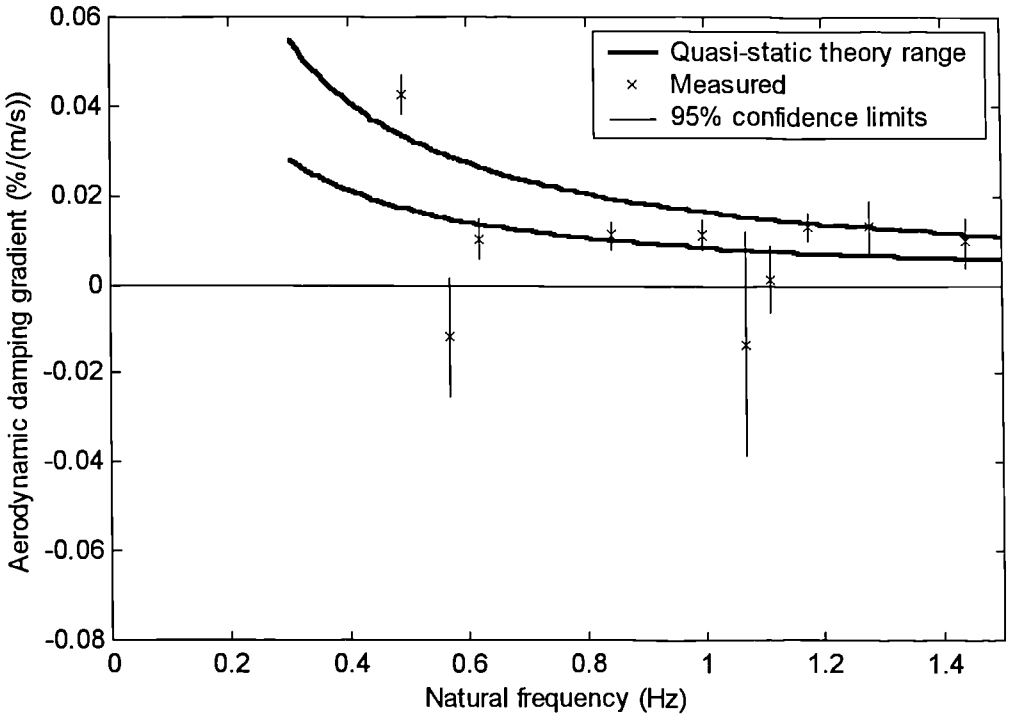

Fig. 8-17 Estimated aerodynamic damping gradients of torsional modes of the finished bridge up to 1.5Hz

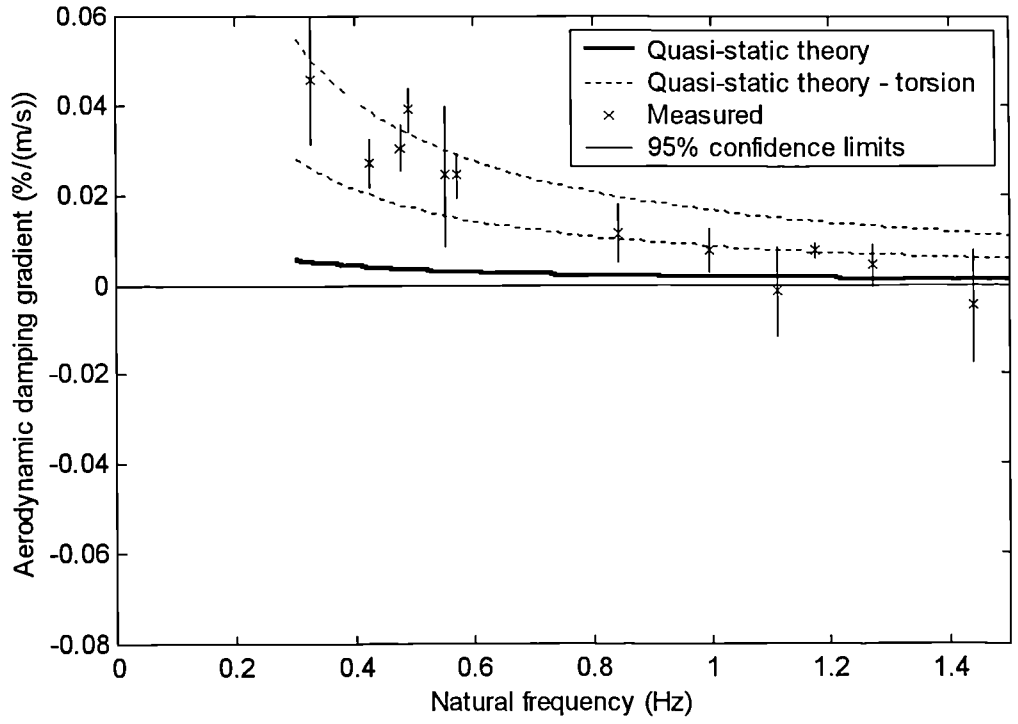

Fig. 8-18 Estimated aerodynamic damping gradients of lateral modes of the finished bridge up to 1.5Hz

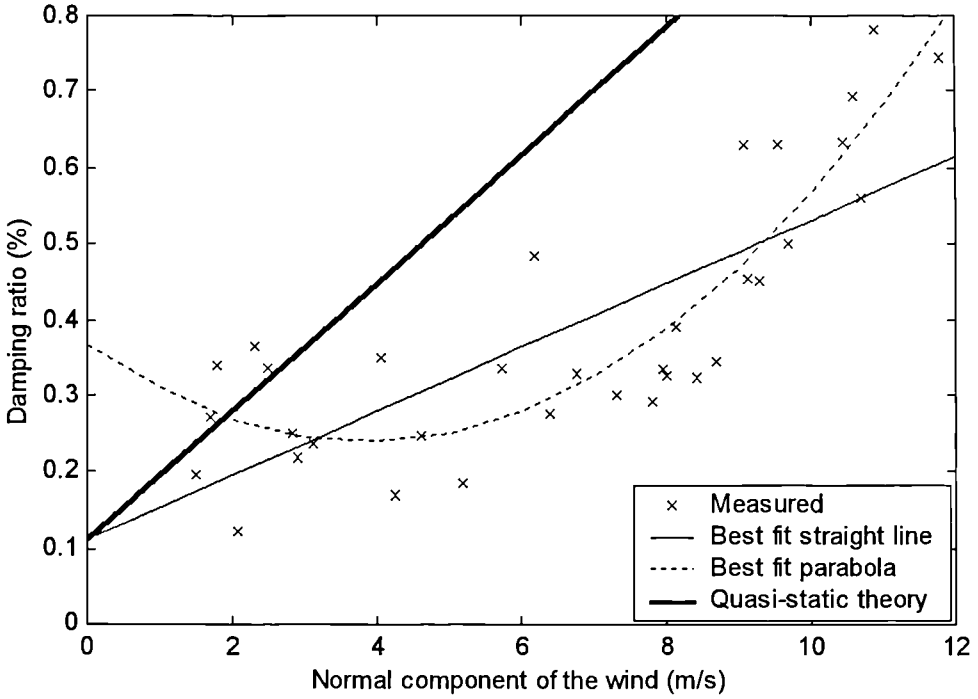

Fig. 8-19 Damping ratios for first vertical bending mode of cantilever

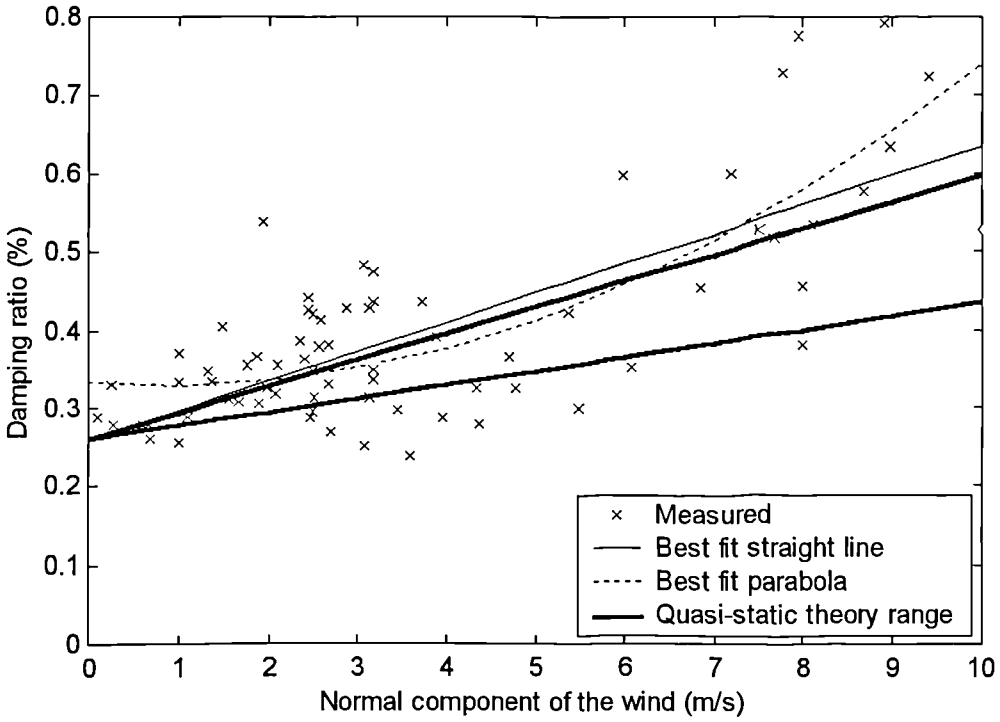

Fig. 8-20 Damping ratios for first torsional mode of finished bridge

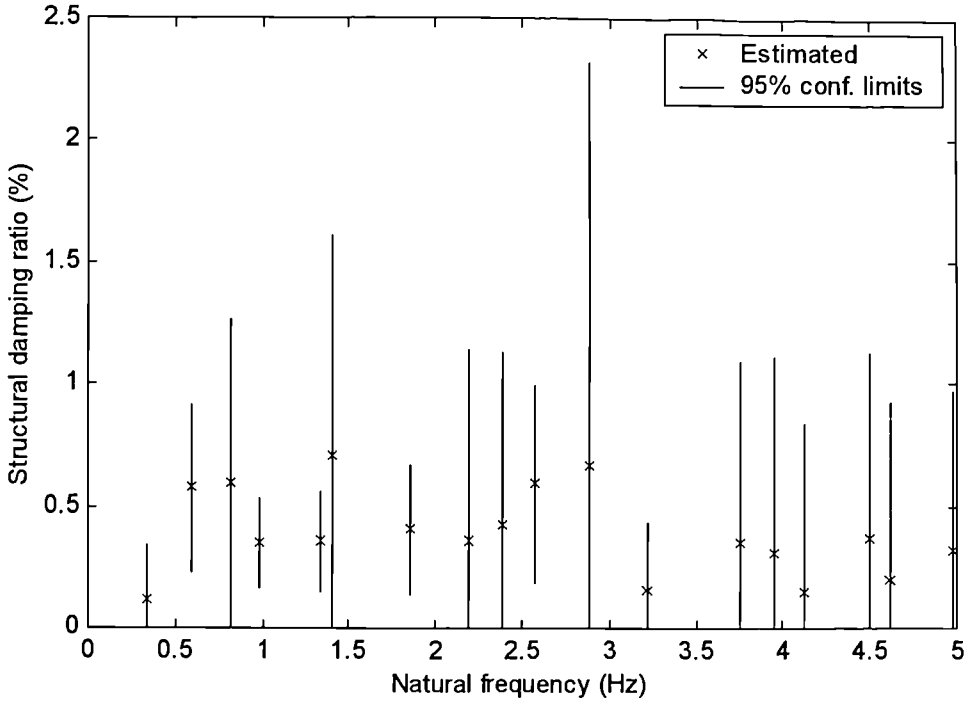

Fig. 8-21 Estimated structural damping ratios of vertical bending modes of the cantilever up to 5Hz

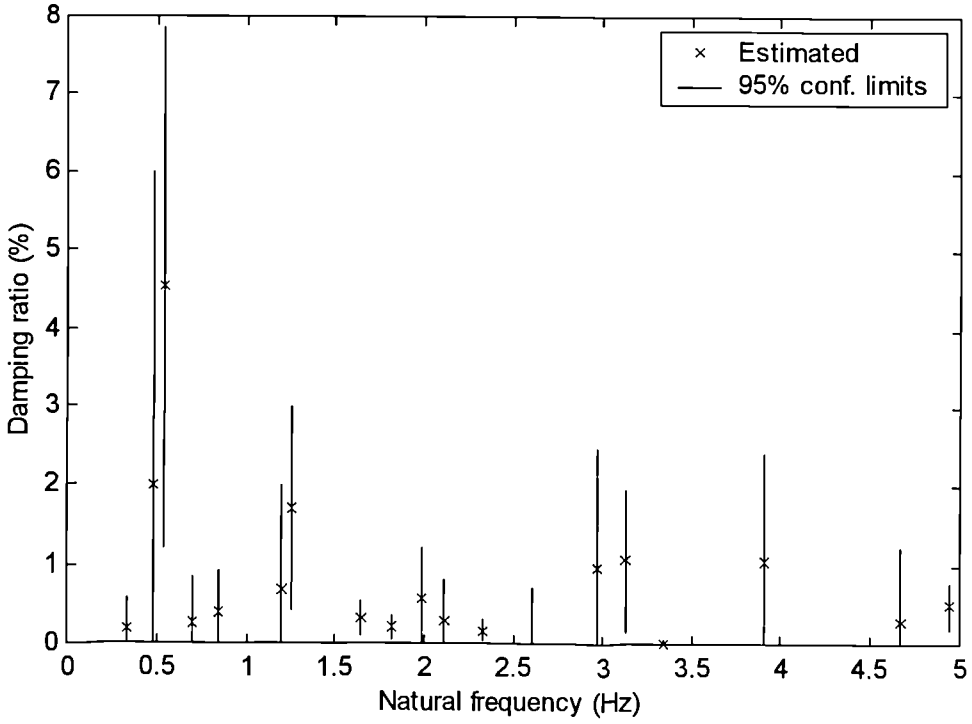

Fig. 8-22 Estimated structural damping ratios of torsional modes of the cantilever up to 5Hz

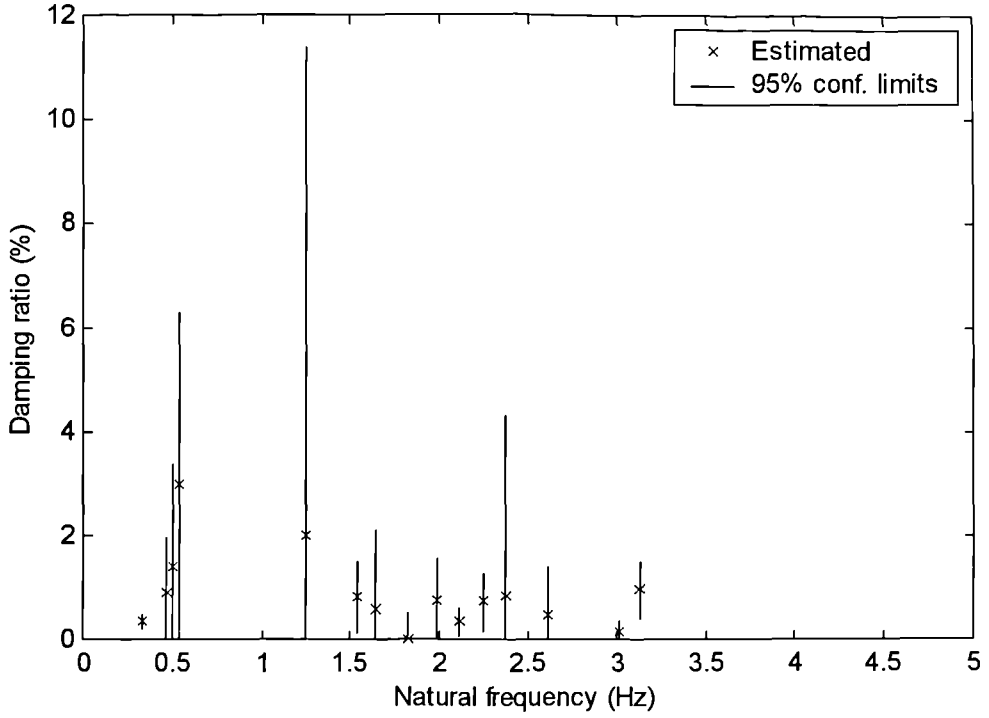

Fig. 8-23 Estimated structural damping ratios of lateral modes of the cantilever up to 3.2Hz

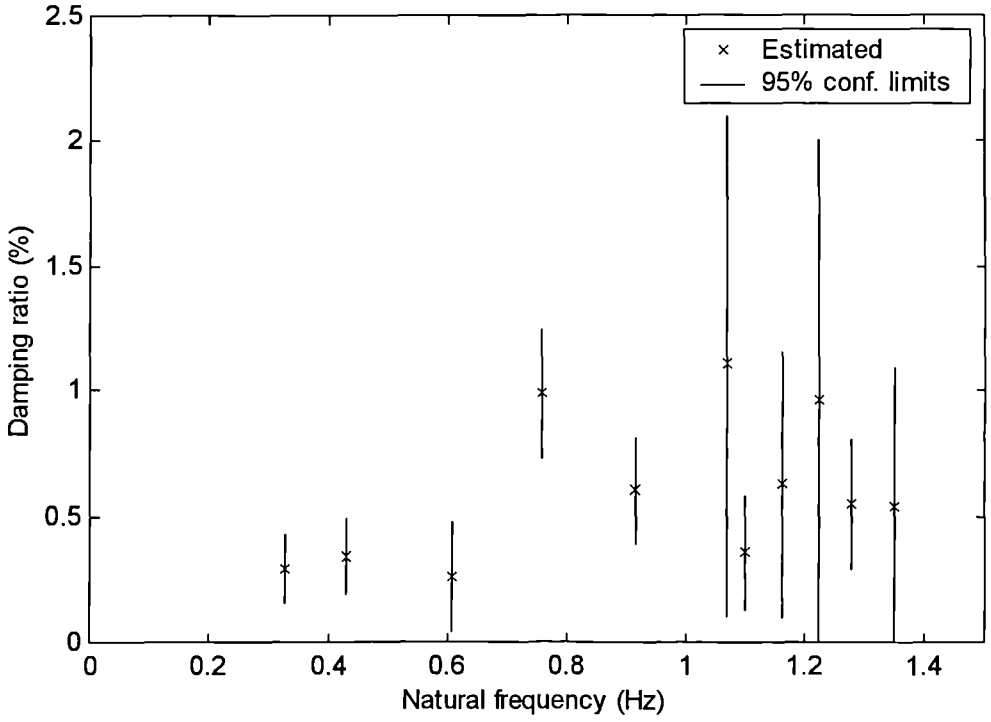

Fig. 8-24 Estimated structural damping ratios of vertical bending modes of the finished bridge up to 1.5Hz

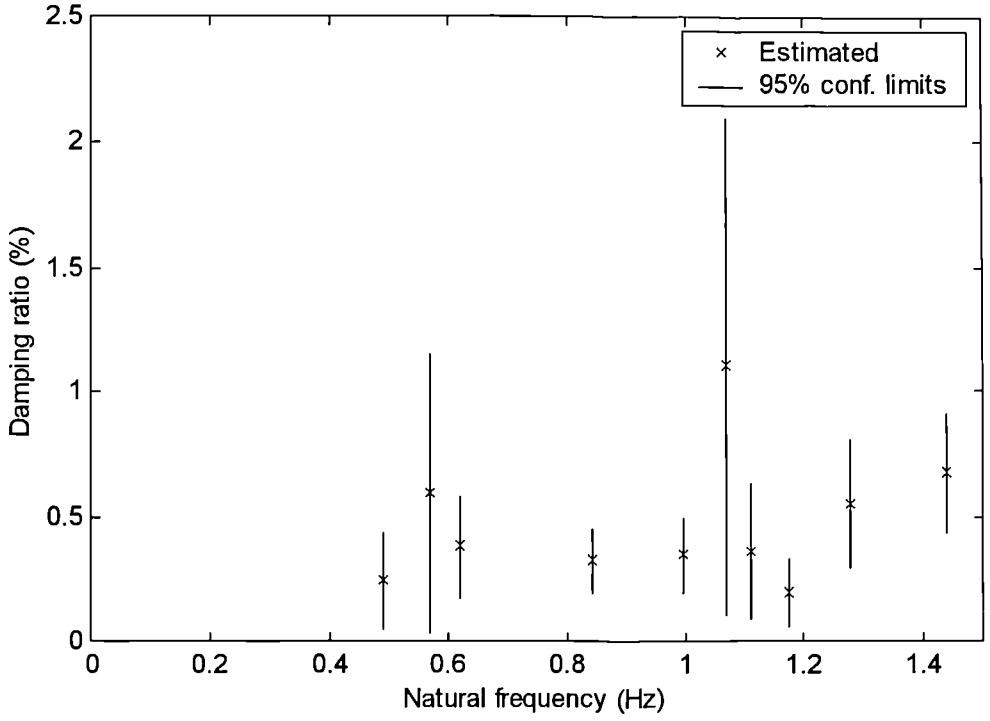

Fig. 8-25 Estimated structural damping ratios of torsional modes of the finished bridge up to 1.5Hz

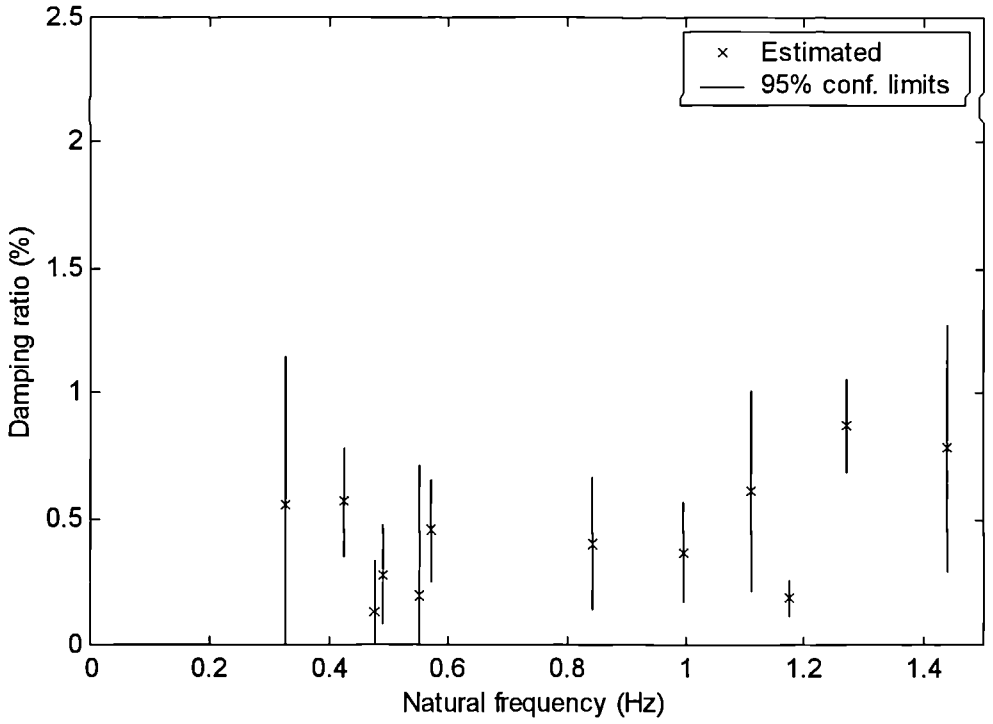

Fig. 8-26 Estimated structural damping ratios of lateral modes of the finished bridge up to 1.5Hz

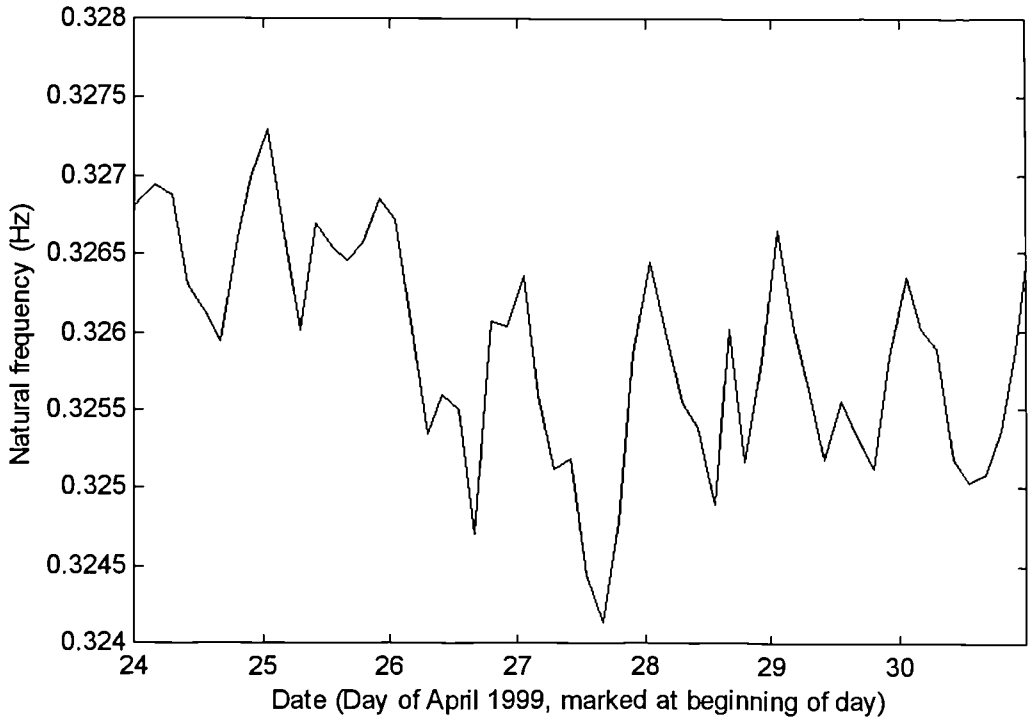

Fig. 8-27 Variation of natural frequency for first mode of finished bridge, Sat. 24 – Fri. 30 April 1999

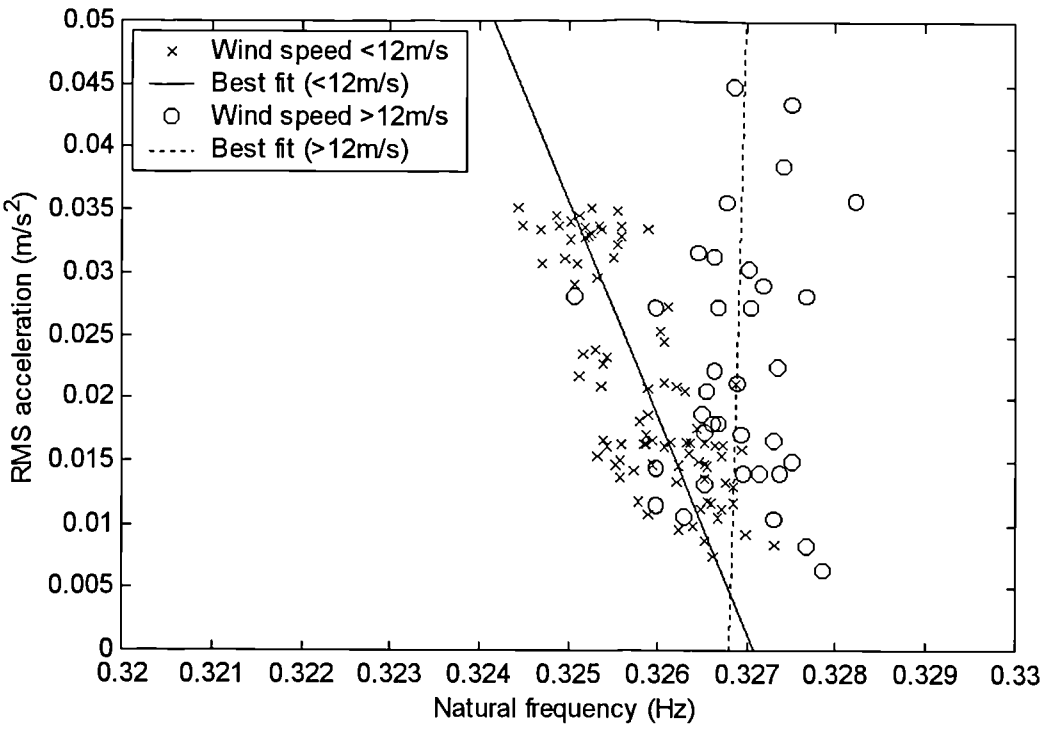

Fig. 8-28 Variation in natural frequency with amplitude of vibrations for first mode of finished bridge

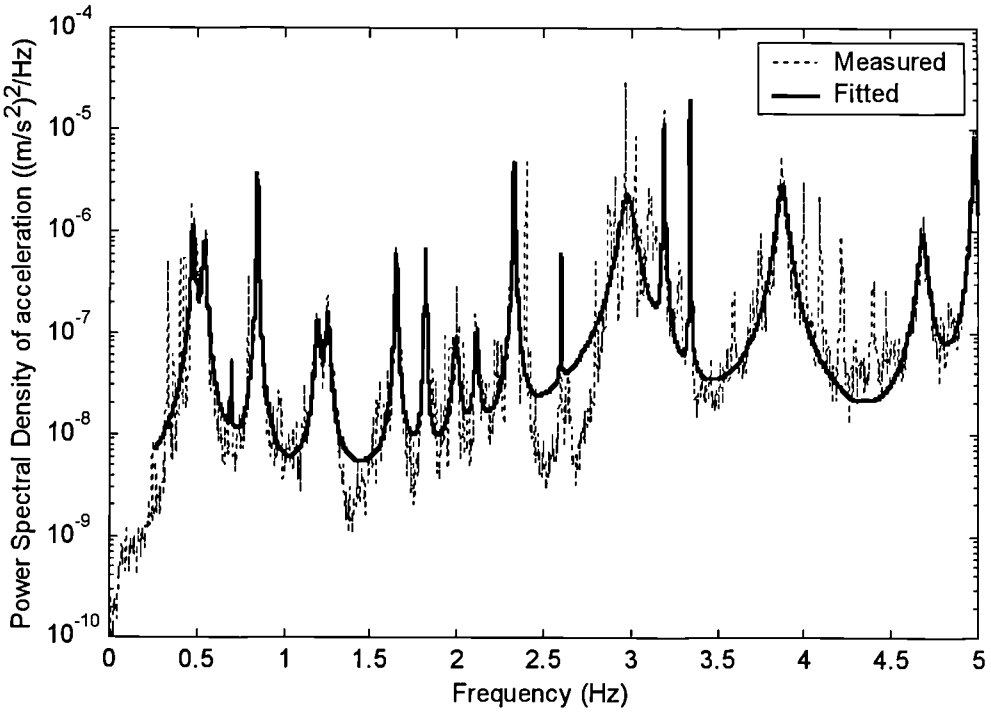

Fig. 8-29 Curve-fit of PSD of torsional deck acceleration of the cantilever, with many additional unfitted modes (wind 5.3m/s, 65° to east of south normal)

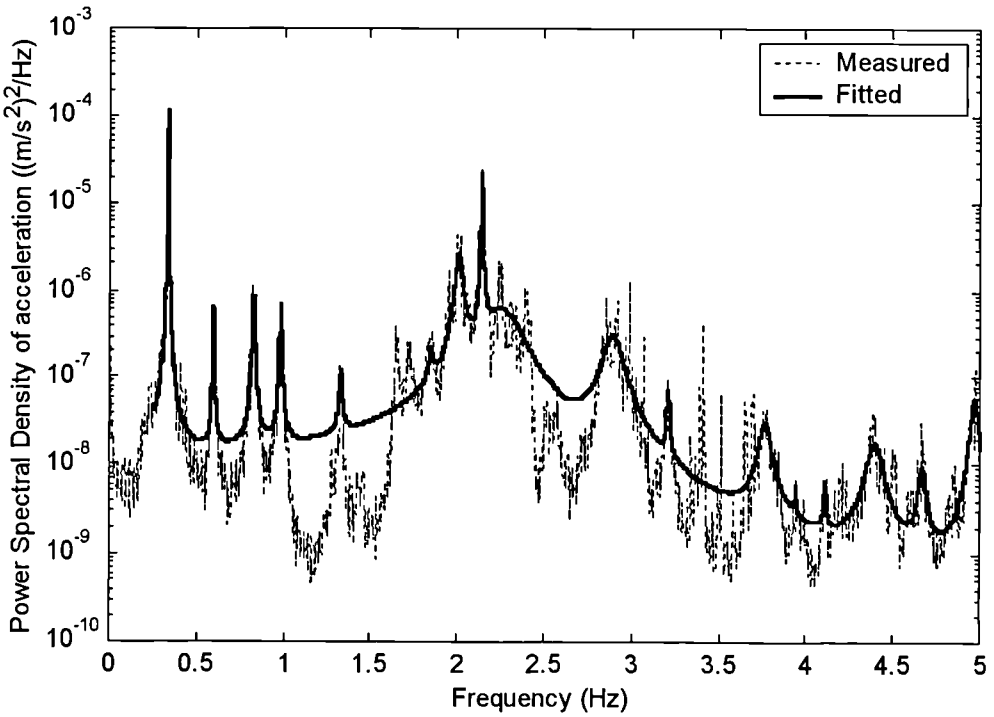

Fig. 8-30 Attempted curve-fit of PSD of measured pylon longitudinal acceleration for cantilever, with 4 estimated modes in 1.6-2.4Hz frequency range

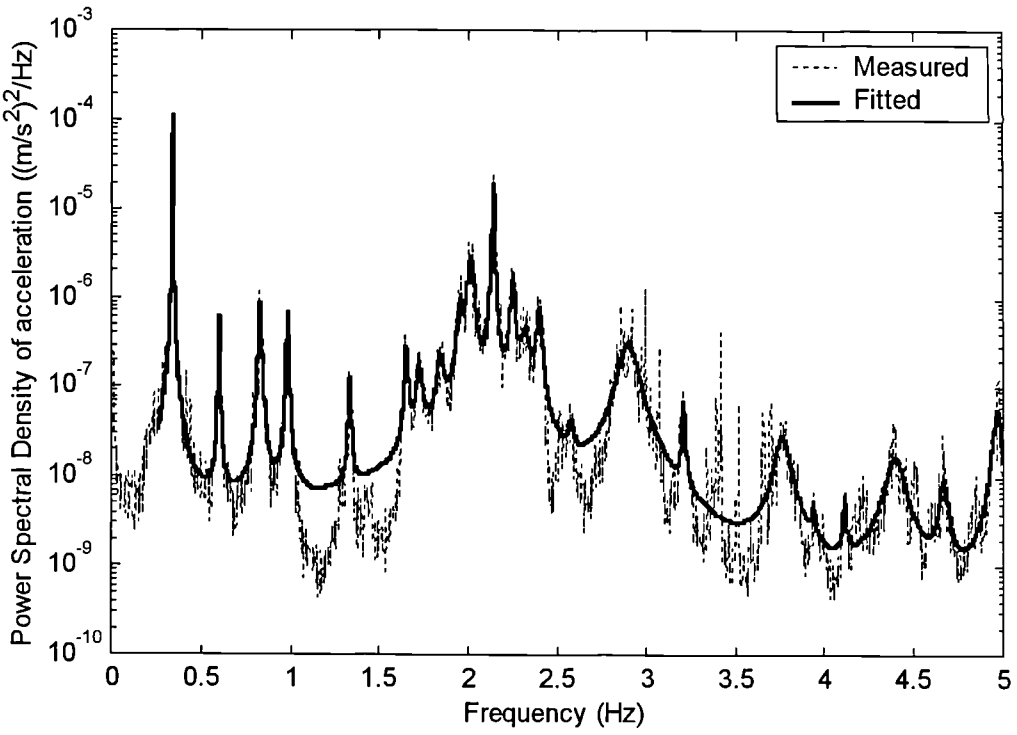

Fig. 8-31 Attempted curve-fit of PSD of measured pylon longitudinal acceleration for cantilever, with 9 estimated modes in 1.6-2.4Hz frequency range

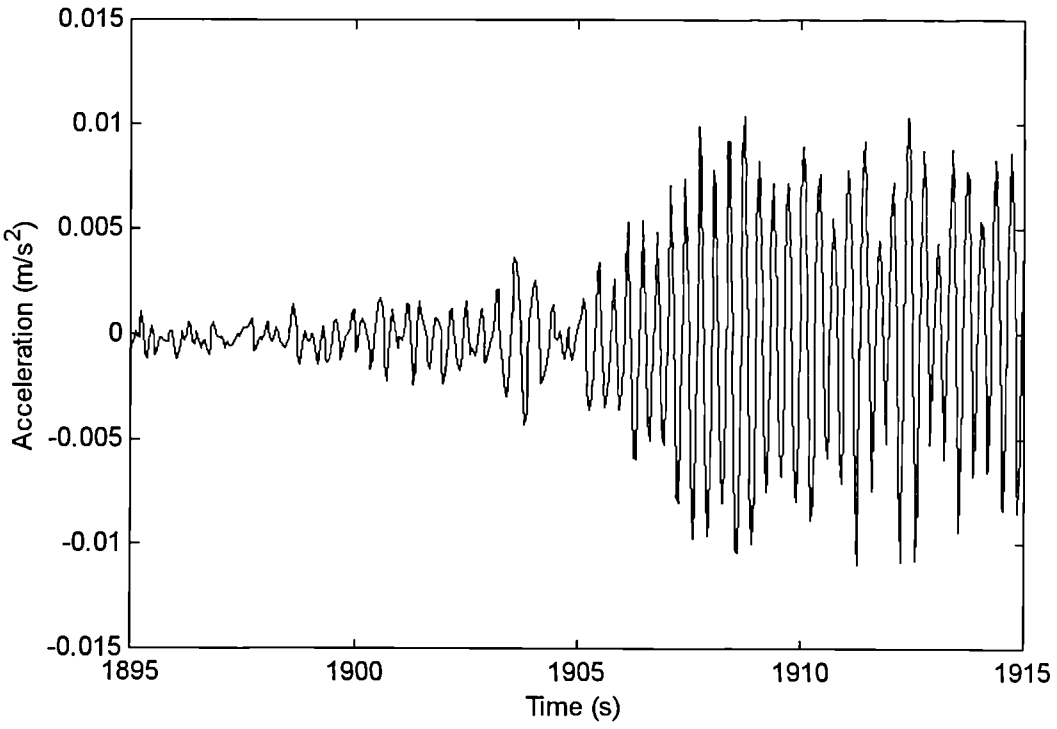

Fig. 8-32 Time history of pylon longitudinal acceleration for the cantilever, displaying period of relatively large vibrations in a narrow frequency range

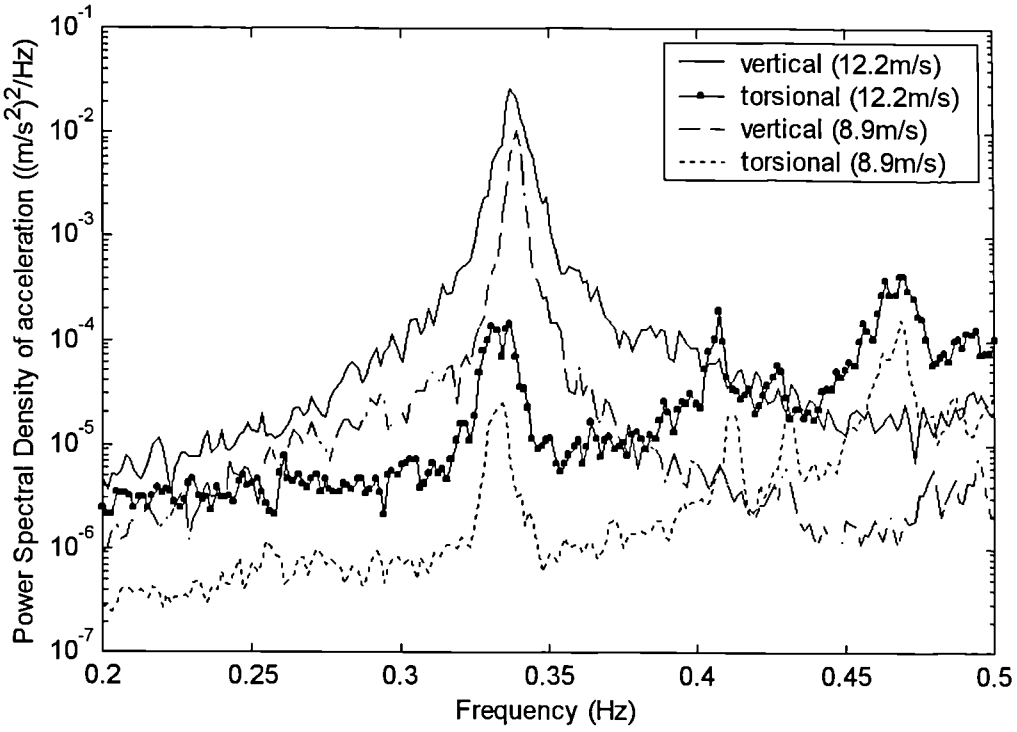

Fig. 8-33 PSDs of vertical and torsion accelerations of cantilever deck in different wind speeds, showing apparent coupling of vertical and torsional modes

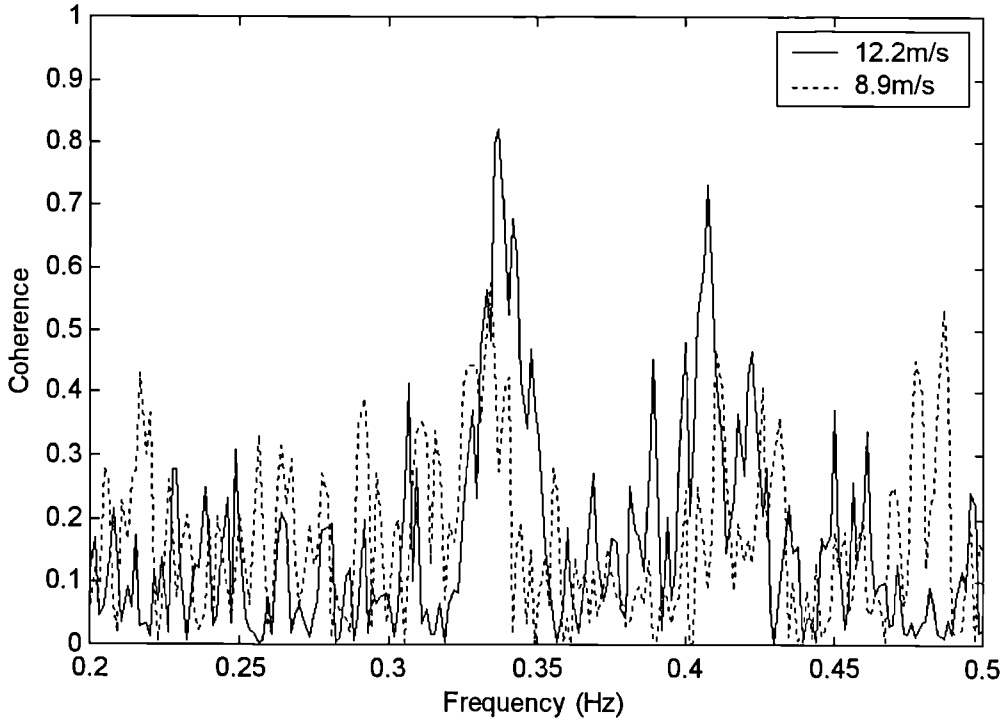

Fig. 8-34 Coherence between vertical and torsion accelerations of cantilever deck in different wind speeds, showing apparent coupling of vertical and torsional modes

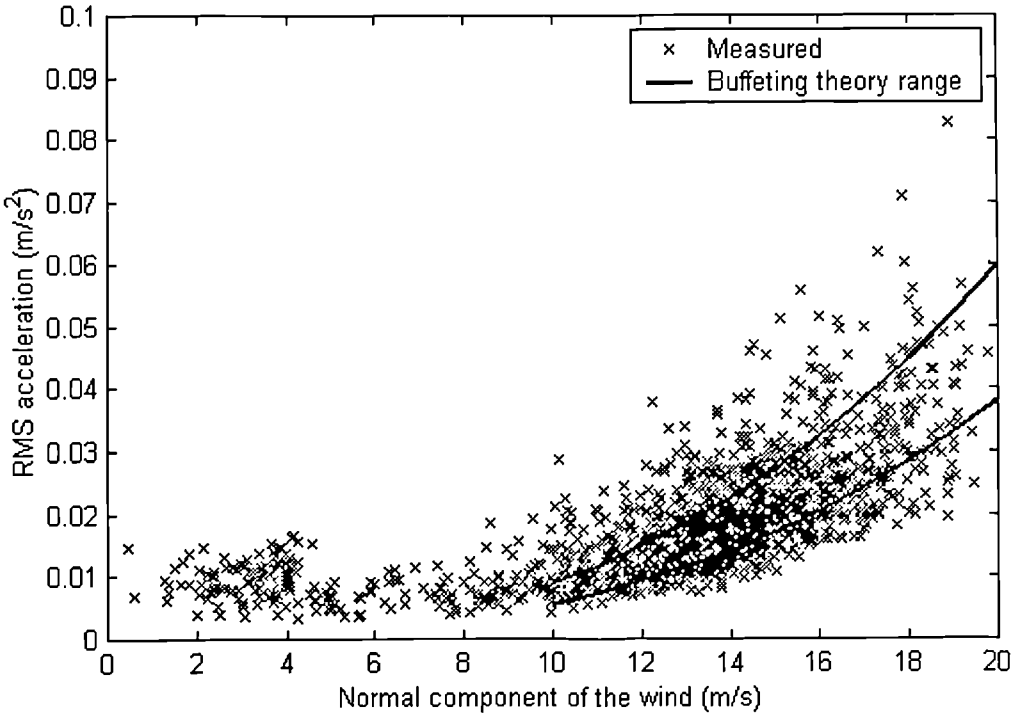

Fig. 8-35 RMS vertical bending response of finished bridge deck near midspan

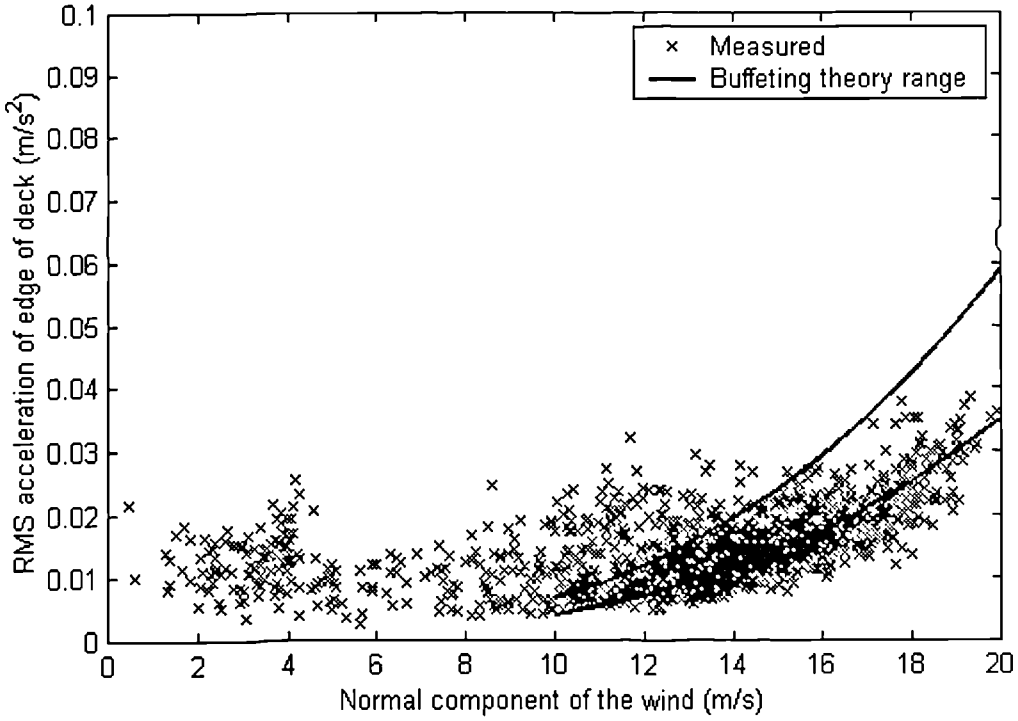

Fig. 8-36 RMS torsional response of finished bridge deck near midspan

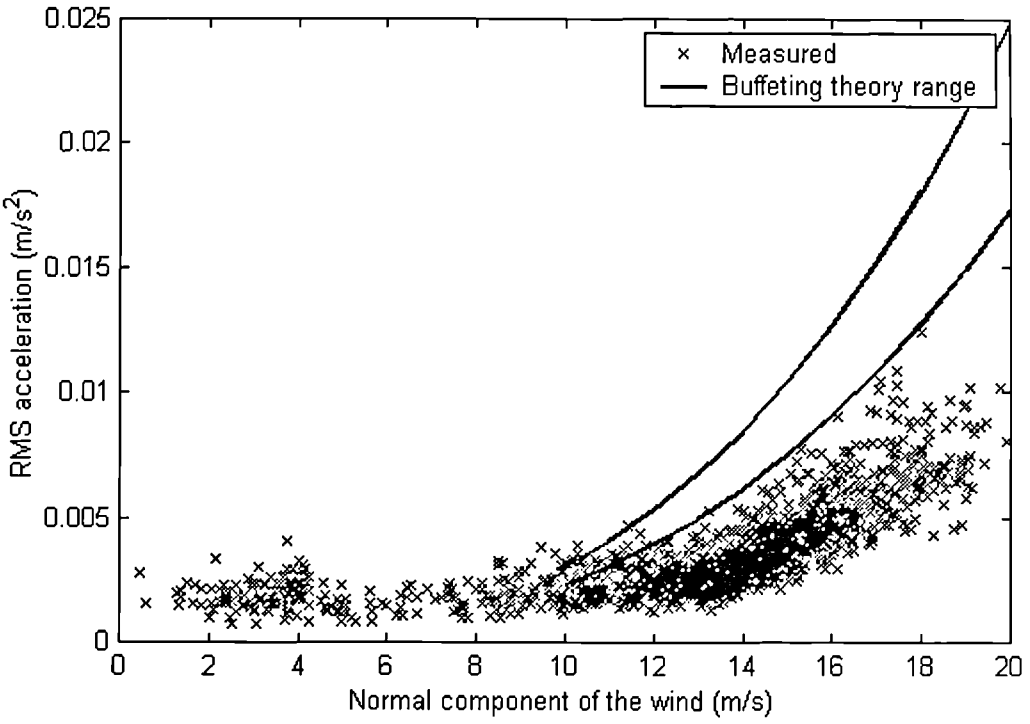

Fig. 8-37 RMS lateral response of finished bridge deck near midspan

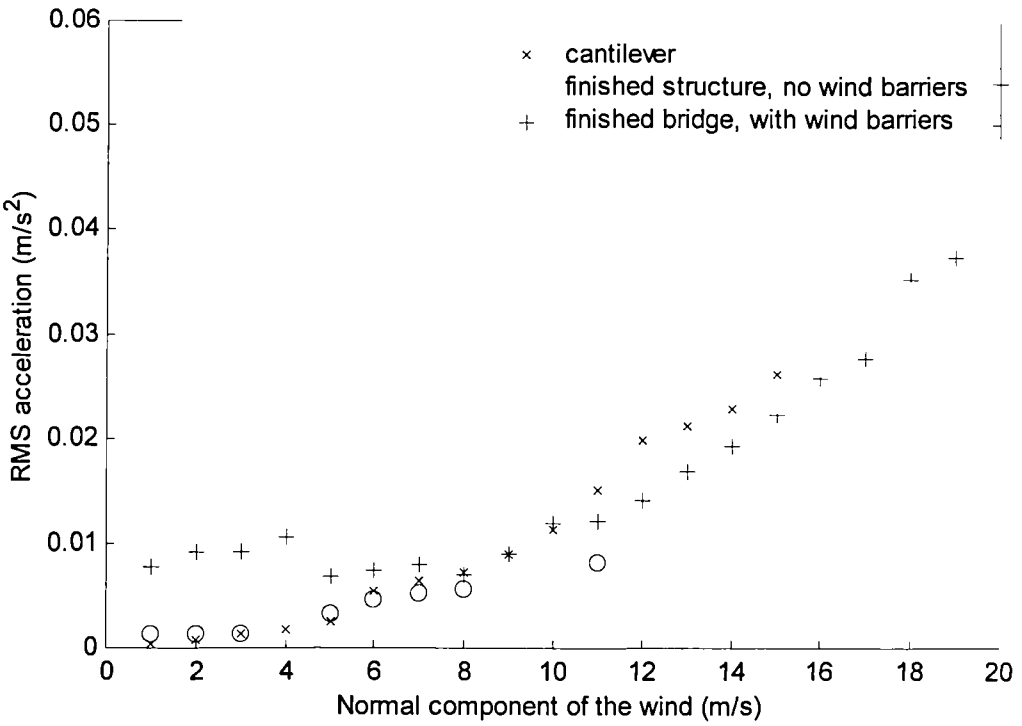

Fig. 8-38 RMS vertical response of bridge deck at different construction stages (average for each 1m/s range)

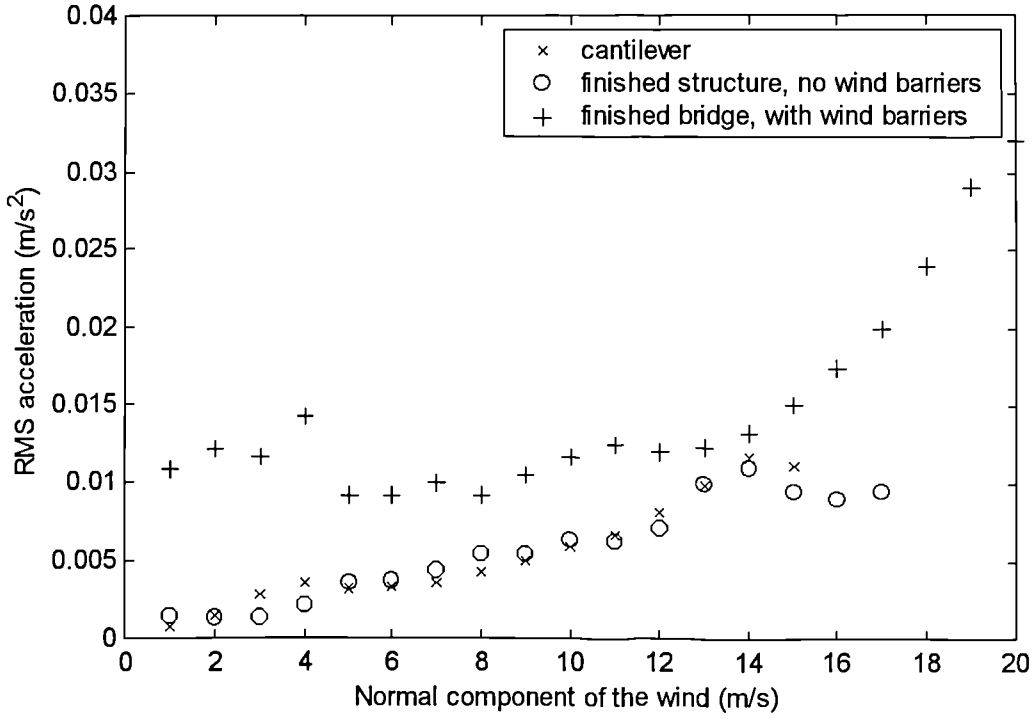

Fig. 8-39 RMS torsional response of bridge deck at different construction stages (average for each 1m/s range)

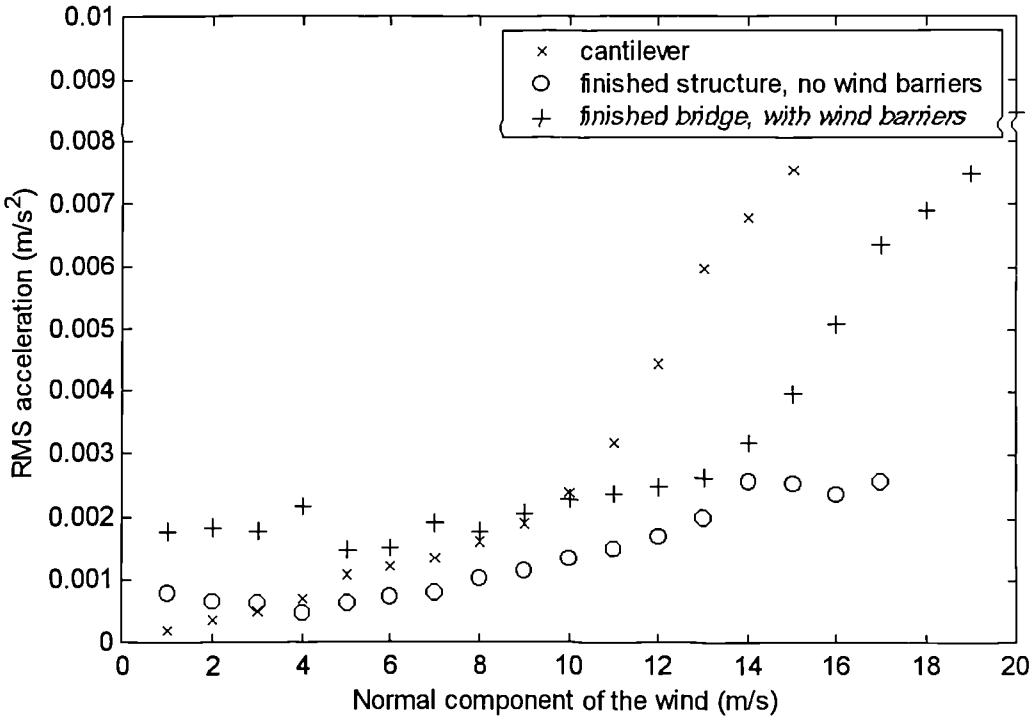

Fig. 8-40 RMS lateral response of bridge deck at different construction stages (average for each 1m/s range)

CHAPTER 9 VORTEX-INDUCED VIBRATIONS OF THE SECOND SEVERN CROSSING

9.1 Introduction

This chapter discusses the measurements of vortex-induced vibrations and associated wind conditions on the Second Severn Crossing (SSC). The phenomenon of vortex shedding is well known (§2.6.5.3), but it continues to be a problem for long-span bridges since the critical wind speed for bridge decks is generally within the expected range, there is no accurate analytical model of the behaviour, and there can be significant uncertainty in the estimated values of some of the parameters involved.

Vortex-induced vibrations were observed on the SSC once the bridge had been completed. The long-term tests (§4.5.4) recorded several instances of large amplitude vibrations and enabled the critical wind conditions to be identified. From the decay of the vibrations, the damping was estimated, for comparison with the estimates using the Iterative Windowed Curve-fitting Method (IWCM) from buffeting vibrations (§7.9 &8.4.3).

Although vortex-induced vibrations were expected from the wind tunnel study results, on site they were of significantly larger amplitude than anticipated. The principal factors leading to the discrepancies were determined as the low structural damping and low wind turbulence. Also, allowing for these factors, the accuracy of the wind tunnel results were assessed. This is of importance, not only to future wind tunnel investigations for vortex shedding, but for other applications, since the increasingly advanced methods of analysis of cable-stayed bridge aerodynamic behaviour (§2.6.6) rely on parameters obtained from such tests.

Finally, the effectiveness of the baffles, added to the bridge to inhibit vortex shedding, was assessed.

9.2 Measurement of vortex-induced vibrations and associated wind conditions

Large deck vibrations were first observed on the SSC on 3 December 1996, during a routine site visit. Subsequently long-term tests were conducted until March 1997 (§4.5.4), in which several similar large vibration 'events' were recorded. At the end of 1997, baffles were installed under the main span and a dummy fire main was added under the wind barrier on the south side of the deck to alter the aerodynamic characteristics of the bridge (§9.6). Further monitoring continued over the winters of

1997-98 and 1998-99 to determine its subsequent behaviour. The monitoring equipment was in operation almost continually during each of these periods, with recording triggered by the wind speed exceeding a threshold value, normally set at between 7.2m/s and 13.8m/s.

For all of these tests, a set of three accelerometers was positioned 23.42m to the east of midspan of the bridge (§4.5.4), allowing asymmetric as well as symmetric modes to be monitored. Wind measurements were taken throughout by the anemometer on the north side of the deck (§4.3.1(ii)). The anemometer on the south side was installed in early 1997, but no large amplitude vibrations occurred after this, so for consistency only the measurements from the north side are used in this chapter.

9.3 Characteristics of measured vibrations

Fig. 9-1 shows a spectrogram of vertical acceleration on the north side of the deck, indicating the Power Spectral Density (PSD) for a series of short data blocks (each 163.84s) for a typical four hour period including the large amplitude vibrations. The frequency resolution is relatively coarse and the variance high, since the blocks are short and there is no spectral averaging (§5.6.2). Also the vibrations were clearly non-stationary, so spectral analysis was not strictly valid. However, the spectrogram still gives an indication of the frequency content, showing a large increase in the response at 0.326Hz for a limited period, but little change in the PSD otherwise. This indicates that the vibrations were dominated by the response in the first vertical mode (Mode V1, Table 8-2), which appeared to be the case for all such events.

To obtain displacement amplitudes, the recorded accelerations were first digitally low-pass filtered at 0.38Hz to isolate the component of the first mode, then the Root Mean Square (RMS) acceleration was calculated over data blocks of 163.84s (i.e. standard file length of 4096 samples, §4.3.2), to smooth out short-term variations in the amplitude due to variations in the loading. The displacement amplitude in the first mode was then estimated by the RMS acceleration multiplied by $\sqrt{2}/(2\pi f_n)^2$, where f_n = 0.326Hz, as measured. This was based on the assumption that the vibrations were dominated by a sinusoidal component at the one frequency, which appeared to be a reasonable approximation to the response.

All amplitudes in this chapter refer to displacements at the measurement location. From the Halcrow-SEEE Finite Element (FE) model (§8.6.1), the maximum displacement in the first mode, at mid span, was expected to be 6% greater.

Several large vibration events were recorded, as tabulated in Table 9-1, all shortly after the bridge had been completed and opened to traffic. For comparison, the British design rules for aerodynamic effects on bridges (DETR 1993) give amplitude ranges for motion

discomfort of 'tolerable' up to 94mm and 'unpleasant' up to 282mm, based on the measured natural frequency.

During the first event, the accelerations exceeded the input range of the equipment as set up at the time, so recording was halted for the input ranges to be adjusted. Unfortunately the maximum amplitude ever observed occurred in the intervening period, so it was not recorded.

For the first event, the Computer Vision System (CVS) (§4.4) was also in operation briefly. A short period of the displacements measured directly by it, on the north side of the deck in line with the accelerometers, is shown in Fig. 9-2. The dominance of the first natural frequency of 0.326Hz again is apparent. The variation in the mean displacement is believed to be due to quasi-static displacements from the passage of vehicles (§4.4.3). Although no simultaneous measurements with the accelerometers and CVS were recorded, the amplitudes obtained from the two systems a few minutes apart were comparable. This gave increased confidence in the method of estimating displacement amplitudes from the accelerations, which was used for all subsequent recordings.

Table 9-1 Large amplitude vibration events

Date	Start time	Duration > 80mm (min)	Maximum amplitude (mm)
3/12/96	07:32	64	320[1] 233[2]
10/2/97	04:50 07:03	66 143	193 266
12/2/97	09:44	39	235
17/2/97	12:09 17:43 19:53	92 90 35	212 208 148
23/2/97	16:53	61	192
28/2/97	02:38 06:07	25 6	154 89
1-2/3/97	19:20 00:22 04:09 05:01	54 12 23 35	133 100 129 121

[1] Estimated from video monitor (equipment not in operation at time of maximum)
[2] Maximum measured

For each event, the vibrations built up to a large amplitude in approximately 15 minutes (Fig. 9-3), in contrast with the normal buffeting vibrations, which rarely exceeded 20mm and did not exhibit such rapid changes in amplitude. The termination of the large vibrations was also in each case quite abrupt.

The observations of large vibrations are all are consistent with vortex excitation. They were dominated by a single mode, and built up and decayed rapidly, which would coincide with the presence or absence of critical wind conditions, causing vortex shedding and lock-in (§2.6.5.3).

During construction, there were no significant vibrations of the deck exhibiting similar characteristics. The principal difference was the absence of the wind barriers. They were shown to greatly increase the loading on the deck for buffeting vibrations (§8.6.5), and they would also markedly change the flow around the cross-section, altering the vortex shedding behaviour.

9.3.1 Damping

The damping of the first mode was estimated from the decay of the large vibrations, for comparison with the value from the IWCM for buffeting vibrations (§8.4.3). The Logarithmic Decrement Method was applied to the acceleration records, as for the decay of forced cable vibrations (§10.3.1), assuming that the loading had terminated abruptly. The resulting estimates of total damping varied from 0.05% to 0.27%, with no apparent pattern.

In the absence of vortex shedding, significant aerodynamic damping would be expected, estimated as 0.33% for a 15m/s normal component of wind velocity, from the results of the IWCM (§8.4.2). However, some continuation of vortex shedding during decay of the vibrations would provide loading equivalent to negative damping. The uncertainty of these effects during the decay of the large vibrations meant that the structural damping could not be determined accurately. However, it seems likely that some vortex shedding would continue, due to lock-in to the deck vibrations, and that in such circumstances the normal mechanism of aerodynamic damping would not occur. Therefore, the maximum value of 0.27% would be expected to be the most reasonable estimate of structural damping, which agrees very well with the value of 0.29% from the IWCM for buffeting vibrations (§8.4.3), giving increased confidence in the results from the IWCM.

9.4 Conditions causing vortex-induced vibrations

Vortex-induced vibrations are caused by the wind entering a critical range (§2.6.5.3). Generally this is defined by a narrow range of wind speeds and is most critical for the wind normal to the bridge. Turbulence tends to inhibit vortex shedding, and the vertical angle of attack of the wind can also be of significance. It was of interest to determine the critical conditions for the occurrence of the large vibrations on the SSC, considering the significance of these parameters. The response and related wind conditions could then be compared with the results of the wind tunnel study (§9.5).

Plots of wind speed and direction corresponding to the displacement record of Fig. 9-3 are shown in Fig. 9-4 and Fig. 9-5 respectively, which are typical of the conditions which caused the large vibrations. The vertical angle of attack and turbulence intensities were also calculated from the anemometer measurements.

The displacements are plotted against wind speed in Fig. 9-6, while Fig. 9-7 shows the relationship of amplitudes to both wind speed and direction, for a limited number of data blocks for clarity. From these plots, the general conditions for large vibrations are apparent, corresponding to wind speed in the range 15-20m/s and direction within 15° of normal to the bridge. However, it is also clear that there are many data blocks for which these conditions existed but the vibrations were still of small amplitude. Indeed, the wind was measured within this range for a total of 77.5 hours for the bridge in this state, but the large vibrations only occurred for a total of 12.4 hours. Therefore, additional conditions must be required for large vortex-induced vibrations to occur.

For some data blocks, the wind may have been within the critical range for only a short period so the vibrations may not have had time to build up to a significant level. Also, when the wind conditions left the critical range the vibrations would take some time to die down, giving some data blocks with significant amplitude, but with the wind outside the critical range. Therefore, to consider the conditions giving rise to the measured amplitudes, the wind parameters were averaged over varying periods leading up to the time at the mid point of each data block used for the amplitude calculations. Using this method, more consistent results were obtained (Fig. 9-8 c.f. Fig. 9-7), with a narrower range of critical conditions becoming evident. The optimum period for averaging the wind parameters was found to be six data file lengths (16.4 minutes), which is consistent with the typical period for the build up of vibrations to the maximum from the normal background level (§9.3). Also, the longer averaging period would mean that the wind parameters measured at one location would be more representative of the wind conditions over the length of the bridge, since local variations in turbulence would be averaged out.

Comparisons of all the measured wind parameters with the responses were made on this basis. It was found that the component of the wind velocity normal to the bridge was more significant than the wind speed in causing large vibrations. Thus, using the revised basis of the wind calculations and the normal component of the wind, Fig. 9-9 shows a more clearly defined critical range than Fig. 9-6. The other wind conditions measured, leading up to the large amplitude vibrations, can be identified in Fig. 9-10 to Fig. 9-14, and are summarised in Table 9-2.

It should be noted that for all of the large vibrations recorded, the wind was from the south side of the bridge. Unfortunately, on no occasion, before the baffles were fitted (§9.6), was the wind recorded within the equivalent range of normal component and

direction from the north side. Therefore, the anemometer was on the leeward side and the measurements, particularly of vertical turbulence, would have been affected by the presence of the deck itself (§6.4.6). Also, the average level of turbulence for north winds was higher than for south winds (§6.4.2), which may have assisted in defining the turbulence criteria for large vibrations if wind within the critical normal component and direction range from the north had occurred.

Table 9-2 Critical wind conditions for vortex-induced vibrations (measured at leeward side of deck)

Wind parameter	Critical range
Normal component of velocity	16 – 19m/s
Direction (clockwise from south normal (§3.2.2))	-5 – 15°
Vertical angle of attack	-1 – 2°
Longitudinal turbulence intensity	< 8%
Vertical turbulence intensity	< 3.5%
Transverse turbulence intensity	< 8%

With the criteria for vortex-induced vibrations defined (Table 9-2), it was possible to consider the effect of each wind parameter individually, by selecting only the data blocks which satisfied all of the other criteria. Fig. 9-15 thus represents a plot specific to the effect of the normal component of the wind. Compared with Fig. 9-9, there are less points within the critical range but not causing large amplitude vibrations, since the other data blocks did not meet other criteria and have been eliminated. However, there is still a large number of points within the critical wind range but with relatively low amplitude vibrations. This indicates that all of the criteria of Table 9-2 combined are not sufficient to define when large amplitude vibrations would necessarily occur, although the majority of data blocks satisfying all of the criteria do show some increase in amplitude above the buffeting response. This suggests that wind measurements at a single point are inadequate to define the critical conditions for such a long bridge. The spatial variation of the wind velocity is believed to be of importance, so future monitoring exercises to study this behaviour should use an array of anemometers along the length of the bridge.

Fig. 9-16 clarifies the turbulence criterion for the SSC, by showing only points which satisfy the criteria of normal component of the wind, direction and vertical angle of attack. The points with low turbulence and low amplitude response in Fig. 9-12 mainly represented readings in low wind speeds. From the revised plot, the tendency for larger response with lower turbulence is clear. Indeed, it indicates that for longitudinal turbulence below 6%, along with the other conditions identified, large vibrations are

almost certain to occur. Also, the line of points at 4% turbulence represent the line at 13° wind direction in Fig. 9-10 and +1.3° vertical angle of attack in Fig. 9-11, showing that the particularly low turbulence increased the ranges of these other parameters for which large vibrations occurred. This could explain the asymmetry in the wind direction criterion (Table 9-2), since the centreline of the estuary, and hence the direction for the lowest average turbulence, is at approximately +30° from south normal (Fig. 3-1).

Another criterion identified in a study on the Wye Bridge (Hay 1984) was that vortex-induced vibrations only built up to large amplitudes in periods of low traffic flow. The explanation given was that large vehicles caused additional turbulence and interrupted the formation of vortices. Although no records of traffic flows were made on the SSC, the times of the events in Table 9-1 cover normal periods of both maximum and minimum traffic flows, with no apparent relationship between maximum amplitude and time of day. Therefore, the presence of vehicles did not appear to have a significant influence on the vortex-induced response. This is believed to be due to the wind barriers (§3.2.5) reducing the effect of vehicles on the wind flow.

9.5 Comparison with results of wind tunnel study

The results of the wind tunnel study (Xie et al. 1994, §3.5), and their comparison with the full-scale behaviour are now addressed, enabling the accuracy of wind tunnel testing for the prediction of vortex-induced vibrations to be assessed. The model tests did predict the vortex-induced vibrations of the SSC, although at a significantly lower amplitude than experienced on the actual bridge.

9.5.1 Sectional model tests

The sectional model tests showed clear vortex-induced responses, particularly in smooth flow and at positive vertical angles of attack (upwards wind). The maximum response amplitude was 370mm in smooth flow at a +5° vertical angle of attack. In turbulent flow (6% longitudinal, 4.7% vertical) the maximum response was 220mm, also at the +5° angle. For a horizontal wind the maxima were 100mm in smooth flow and 60mm in turbulent flow. Negative angles of attack tended to stabilise the section further. Tests on a similar cross-section in 3% longitudinal turbulence gave similar reductions in the response, compared with smooth flow, as 6% turbulence.

There was little difference in vortex shedding behaviour of the model between the different configurations of traffic and iced-up barriers. The large responses occurred for wind speeds in the range 17-22m/s in all cases, except for smooth flow with zero or negative angles of attack, for which the critical wind speed dropped to 14-16m/s. Virtually all of the model tests were performed with the wind normal to the bridge deck,

which was confirmed on site to be the critical condition, with little tolerance (Table 9-2). The few model tests with the wind from different directions showed no vortex-induced instabilities.

All of the above displacements of the model occurred in the vertical vibration mode set at the equivalent of 0.3Hz at full scale, compared with the frequency measured on site of 0.326Hz (Table 8-2). The main significance of the difference would be that the critical velocities of the real bridge would be expected to be 9% higher than those found in the wind tunnel tests (i.e. 19-24m/s on real bridge), but the amplitudes should not have been significantly affected. The structural damping of the model for the above displacements was 0.7%, compared with the estimate for the real bridge of 0.29% (§8.4.3).

9.5.2 Full aeroelastic model tests

The full aeroelastic model exhibited vortex-induced vibrations in the first mode (0.341Hz, 0.65% damping) only in smooth flow with a positive vertical angle of attack (+2.5°), for the iced-up barrier and one specific traffic case. For horizontal and turbulent winds (11% longitudinal, 6.9% vertical) there was no noticeable vortex excitation. However, full aeroelastic models are not as reliable as sectional models for evaluating vortex-induced response due to the smaller scale, making fine details more difficult to represent accurately, and because of the very low wind speeds used, for which Reynolds number (R_e)† scaling can cause errors (Irwin 1998).

9.5.3 Comparison of model test results with full-scale measured response

The low probability of smooth flow and positive vertical angles of attack occurring for any significant amount of time on site suggested that vortex-induced vibrations of the real bridge would not build up to unacceptable levels. However, responses were measured on site with amplitudes approximately five times greater than predicted by the sectional model test that was expected to be most comparable. This raises questions about the reasons for the discrepancies.

An important difference between the wind tunnel models and the actual bridge was the level of damping. The steady-state amplitude of vortex-induced vibrations is inversely proportional to the total damping. The structural damping was greatly overestimated, at 0.7% and 0.65% for the two models, compared with 0.29% estimated from site measurements of buffeting vibrations (§8.4.3). Ignoring the contribution of aerodynamic damping, which is unlikely to be significant during vortex excitation, this would account for the amplitude more than doubling.

---

† $R_e=UD/\nu$, where U = wind speed, D = representative dimension of the body, ν = kinematic viscosity.

Another significant factor was the level of turbulence. It is well know that turbulence in the incident wind inhibits the regular formation of vortices and hence reduces response levels compared with smooth flow (§2.6.5.3). The turbulence of real wind is used as a justification for using model responses in turbulent flow for predicting full-scale response, rather than the larger responses in smooth flow.

It should be noted that for sectional models the large-scale turbulence cannot be replicated, so the wind velocity spectrum is affected. Irwin (1998) suggests that, to match the higher frequency turbulence, the equivalent turbulence intensity for the model should be typically 0.46 of the full-scale value. Therefore, the 6% longitudinal turbulence used for most of the SSC sectional model tests was equivalent to 13% at full scale (c.f. 11% for the full aeroelastic model), approximately twice the average value measured on site for winds within ±30° of south normal (6.2%, §6.4.2), and above the range identified for the large vortex-induced vibrations to occur (Table 9-2).

The overestimation of wind turbulence may be because the ESDU (1993) values, commonly used for design, are for strong winds. They may be reasonable for estimating the maximum buffeting response, but for the moderate winds for vortex excitation, the sea roughness is lower, so the turbulence is lower (§6.4.2). This suggests that, for wind tunnel modelling of bridges with an upwind expanse of water, lower levels of turbulence, or indeed smooth flow, should be used for determining the susceptibility to vortex-induced vibrations.

The measured response on site was greater than that predicted from any of the wind tunnel tests for horizontal wind, even in smooth flow and taking account of the lower damping. It is estimated that, had the SSC sectional model tests been conducted in smooth horizontal flow with structural damping 0.29%, as measured on site, the amplitude of vibrations would still have been underestimated by approximately 25%. This suggests that a more conservative approach to wind tunnel test results should be taken.

The critical wind speed was overestimated by the sectional model tests with turbulent flow by approximately 20%. This would affect the return period of the critical wind speed, but this is not as important for design as the maximum amplitude. However, again this shows the level of uncertainty of the wind tunnel test results. The sectional model tests for smooth horizontal flow indicated a slightly lower critical wind speed, which was more consistent with the measurements on site, again suggesting that smooth flow is more appropriate for wind tunnel testing for vortex-induced vibrations.

The real bridge did not appear to be as sensitive to the vertical angle of attack as the model. However, since on site the wind was measured on the leeward side of the deck,

there is some uncertainty in the measured values. The sectional model and site observations were in agreement over the insensitivity to the presence of traffic.

Tests on aeroelastic models of the bridge at different construction stages revealed only small increases in vibration amplitudes, presumed to be due to vortex shedding, in very few cases in smooth flow. This is consistent with the lack of large deck vibrations observed on site before the installation of the wind barriers.

9.6 Effect of baffles in reducing vortex-induced vibrations

Baffles were installed beneath the deck, as shown in Fig. 9-17, to inhibit the formation of vortices and reduce the resulting vibrations. They were simply vertical profiled steel sheets, and were attached to the existing steelwork over a length of 251.7m (c.f. main span length 456m) in the middle of the main span. A dummy fire main was also added, beneath the wind barrier on the south side of the deck, to replicate a detail on the wind tunnel models. Monitoring then continued over two further winter periods to assess the effectiveness of these measures. The wind was recorded within the previously critical ranges of direction and normal component for a total of 95 hours. The response of the deck relative to the normal component of the wind, with all of the other criteria satisfied, is shown in Fig. 9-18, which is directly comparable with the earlier results in Fig. 9-15. Although in a few cases there was still a slight increase in the response for normal components of the wind of 17-20m/s, the maximum response was less than 10% of the maximum without the baffles. Greater amplitudes were recorded on some occasions, up to a maximum of 69mm, but these were in stronger winds from different directions, so they are believed to have been due to buffeting rather than vortex excitation.

Further sectional model tests by RWDI had demonstrated the effectiveness of the baffles and had shown them not to significantly affect the flutter behaviour of the cross-section. The full-scale measurements were consistent with these model tests, and no adverse effects of the baffles were detected on site.

9.7 Conclusions

Vibrations of up to 320mm amplitude were measured on the SSC, exhibiting characteristics of vortex-induced vibrations. They were dominated by the first vertical mode (0.326Hz, §8.3.4) and were excited by the wind in a narrow critical range.

Decay of the large vibrations enabled estimates of the damping to be made. Although there was some uncertainty of the effect of aeroelastic forces, the damping estimate believed to be most accurate agreed well with the value of structural damping for

buffeting vibrations from the IWCM (§8.4.3). This increases confidence in the accuracy of the IWCM for the analysis of ambient vibration data.

The wind criteria for the large vibrations to occur were established from the long-term site measurements (§4.5.4). Considering the average wind parameters over a period of 16.4 minutes, comparable with the time for the vibrations to build up to their maximum level, enabled the critical conditions to be more clearly defined. The turbulence intensities and vertical angle of attack were found to be significant parameters in defining the criteria for large vibrations, as well as the normal component of the wind (rather than the wind speed) and wind direction. In low turbulence (below 6% longitudinal), if the other wind parameters were in the critical region, large vibrations would almost certainly occur, but for slightly higher levels of turbulence there was still some uncertainty whether or not they would develop. Thus, although the measurements at one location could identify a narrow range of critical conditions, measurements at other positions along the bridge length, preferably on the windward side of the deck, would be required to define the criteria more precisely.

Traffic was not found to have a significant effect on the vortex-induced response of the SSC, believed to be due to the presence of the wind barriers.

The vortex-induced vibrations were significantly greater than predicted from the wind tunnel study. The sectional model test that was expected to be most comparable with the site measurements underestimated the response by a factor of five, while the equivalent aeroelastic model test predicted virtually no vortex-induced vibrations. There were two principal factors causing these discrepancies; the structural damping of the models was more than twice that estimated from site measurements for the real bridge (§8.4.3), and the turbulence of the real wind was relatively low (§6.4.2) and had much less influence on reducing the amplitude than anticipated. Both damping ratios and turbulence intensities are known to be difficult to predict, but this study emphasises their importance and suggests that the values used for design should be chosen conservatively. The wind tunnel tests for smooth flow gave more accurate predictions of the maximum amplitude than the tests for turbulent wind, so turbulence should not be relied upon too heavily to reduce the vortex-induced response.

Even taking into consideration these reasons for discrepancies, it is estimated that the wind tunnel tests would still have underestimated the response by approximately 25%, while the critical wind speed was overestimated by approximately 20%. These errors give an indication of the accuracy of the results obtainable from wind tunnel tests. State-of-the-art techniques for the analysis of cable-stayed bridges (§2.6.6) rely on the use of many aerodynamic parameters (e.g. flutter derivatives) derived from wind tunnel tests. Caution should be exercised in taking the level of refinement of analysis too far based

on parameters with the above inaccuracies. The sensitivity of the results of such analyses to these potential errors should be considered.

Finally the effectiveness of the baffles, added to reduce the vortex-induced vibrations, has been demonstrated.

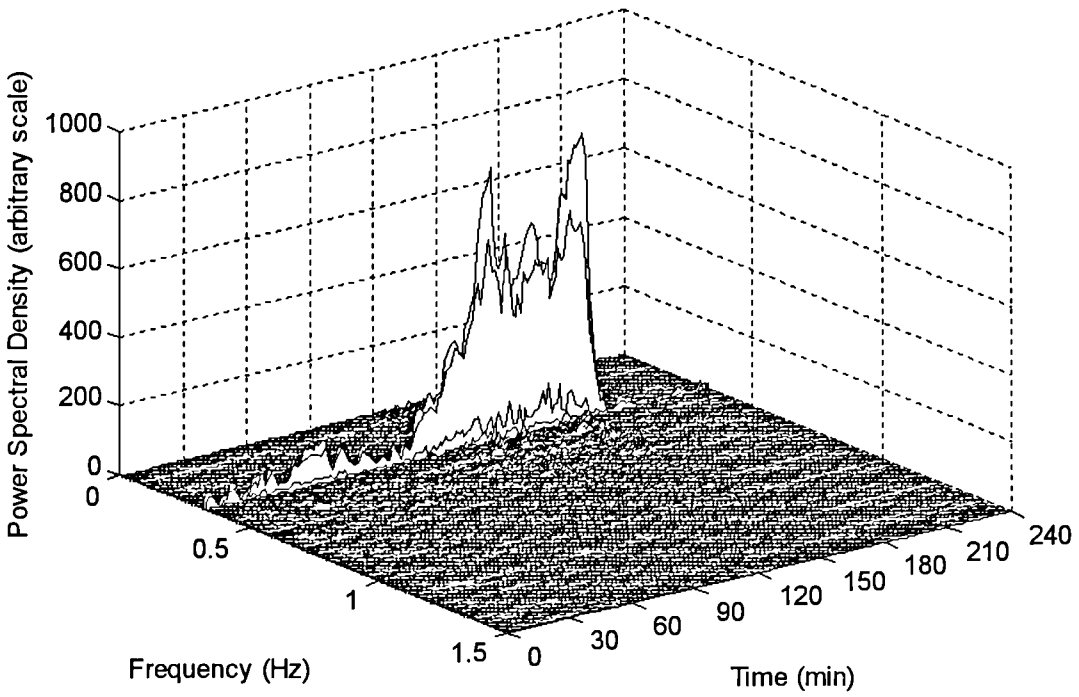

Fig. 9-1 Typical spectrogram of deck north vertical acceleration for vortex-induced vibrations

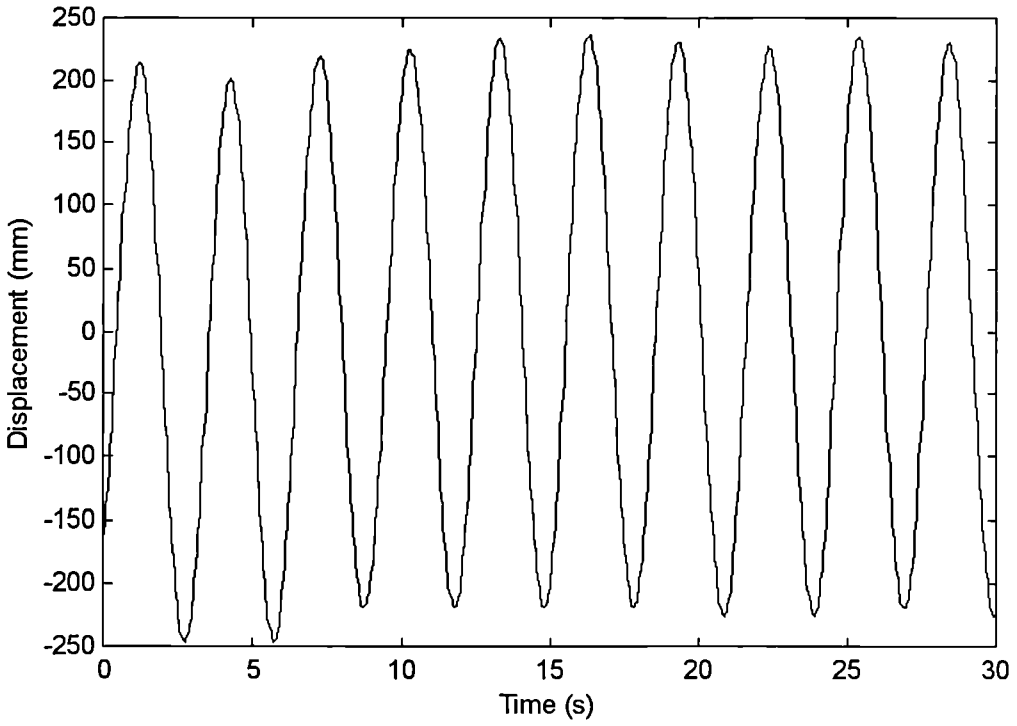

Fig. 9-2 Vertical displacement of the north side of the deck, measured directly with the Computer Vision System (08:11 on 3/12/96)

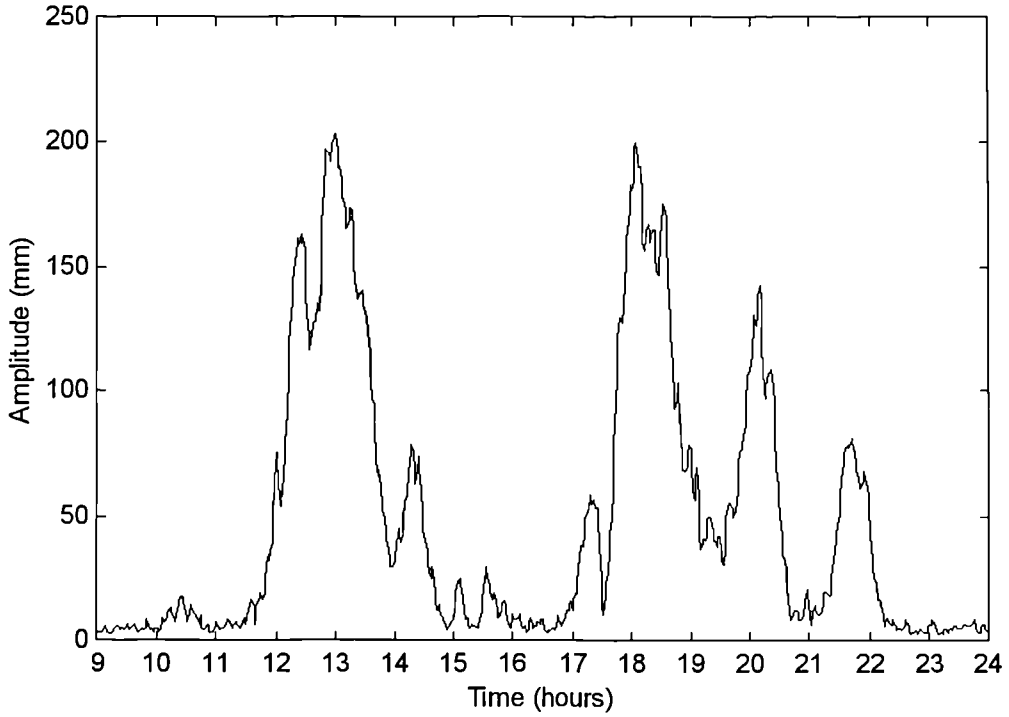

Fig. 9-3 Deck displacement amplitude on 17 February 1997, showing large amplitude vibrations

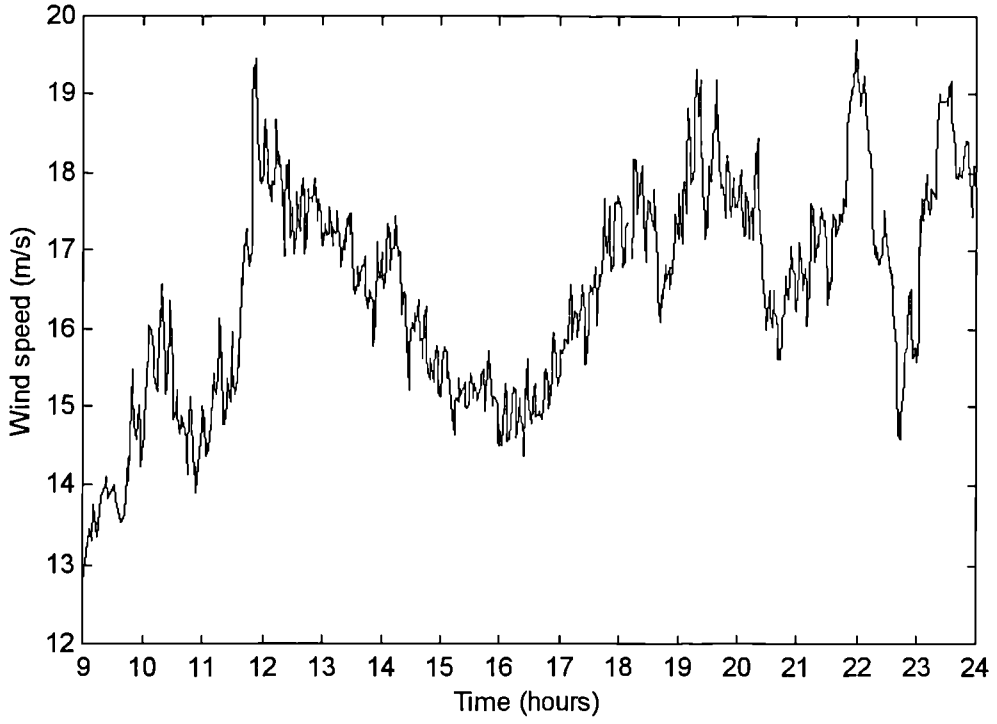

Fig. 9-4 Wind speed on 17 February 1997

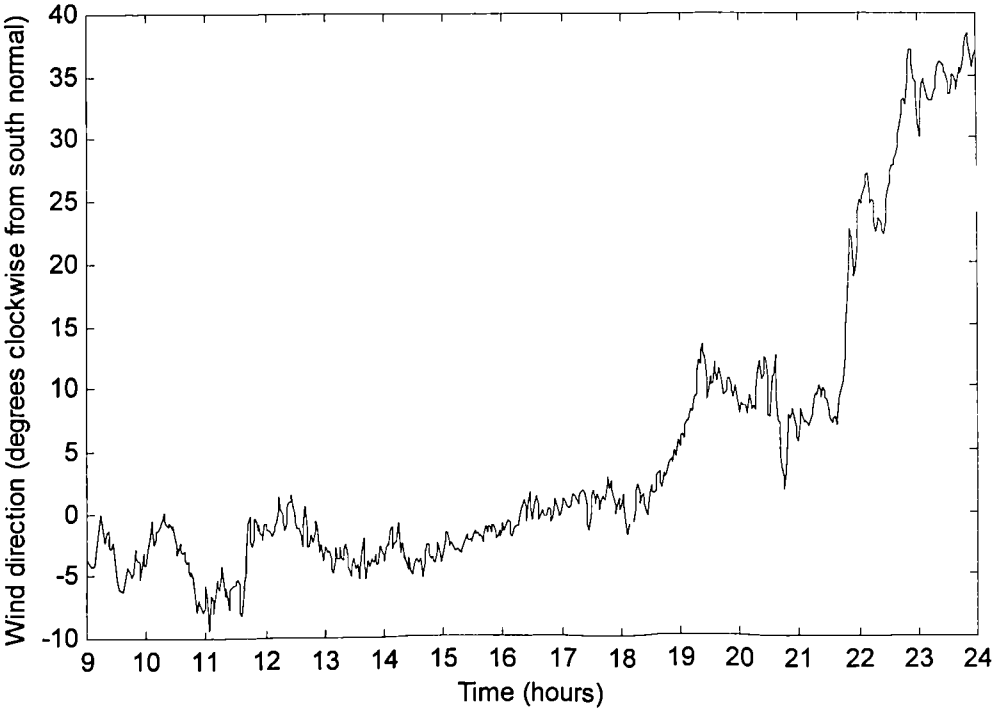

Fig. 9-5 Wind direction on 17 February 1997

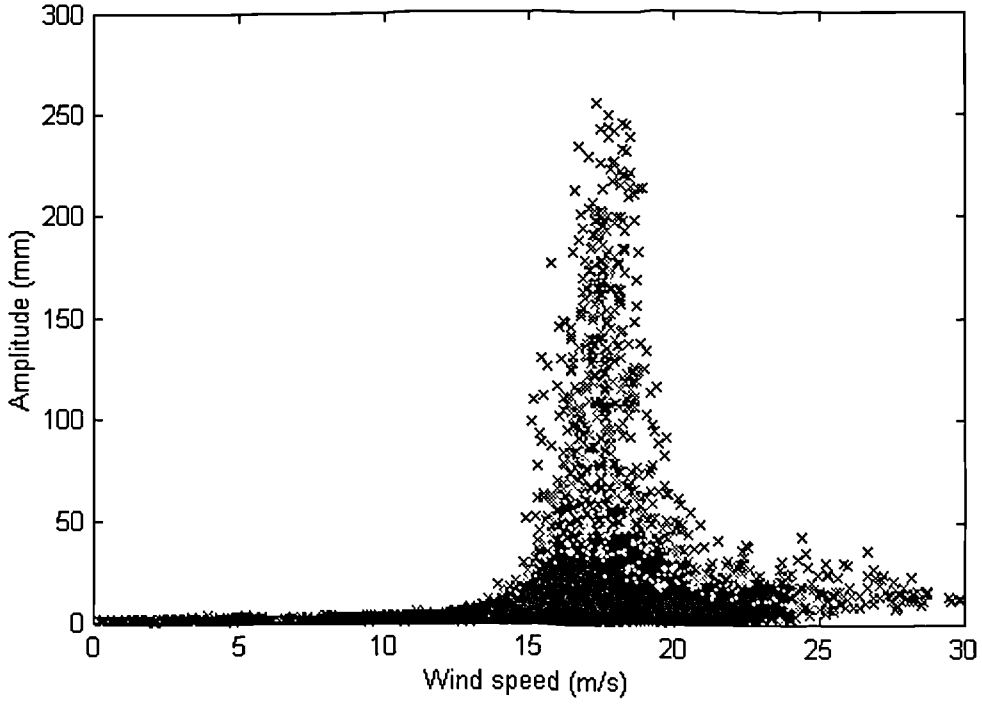

Fig. 9-6 Deck displacement amplitude against wind speed, averaged over 163.84s

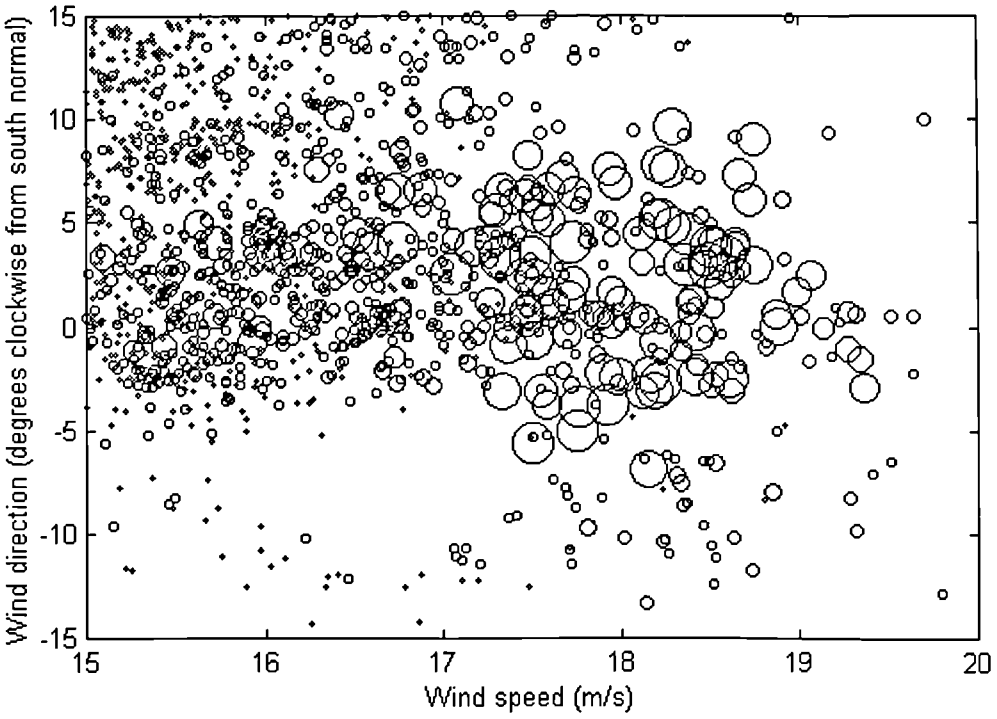

Fig. 9-7 Scatter plot of amplitude (proportional to area of circles) in relation to wind speed and direction, averaged over 163.84s (south normal defined in §3.2.2)

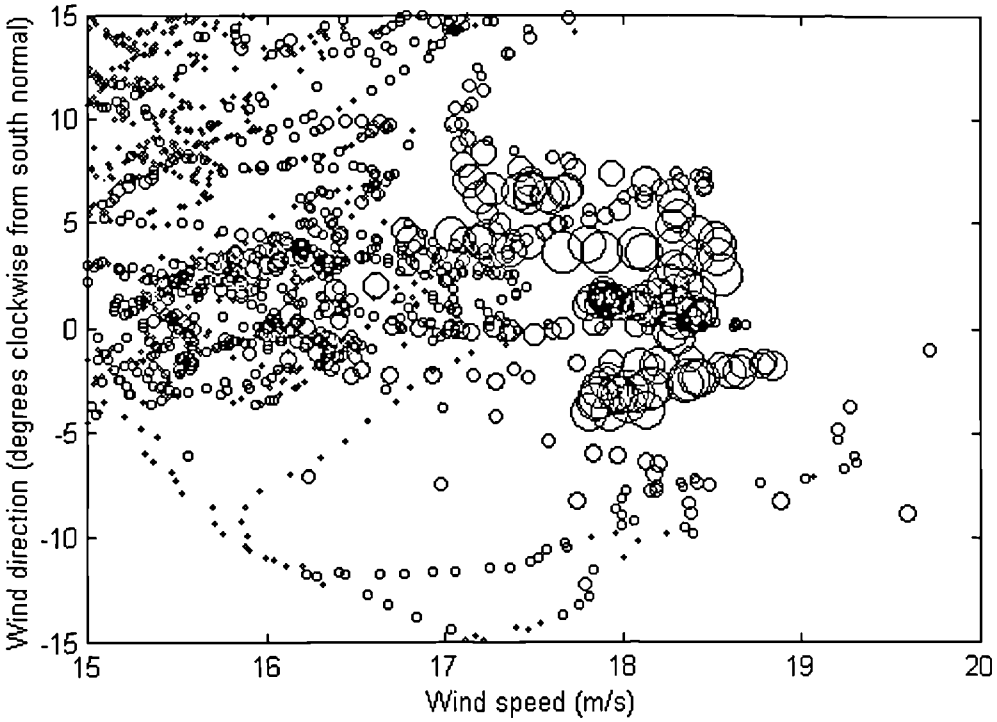

Fig. 9-8 Scatter plot of amplitude (proportional to area of circles), averaged over 163.84s, in relation to wind speed and direction, averaged over previous 16.4 minutes

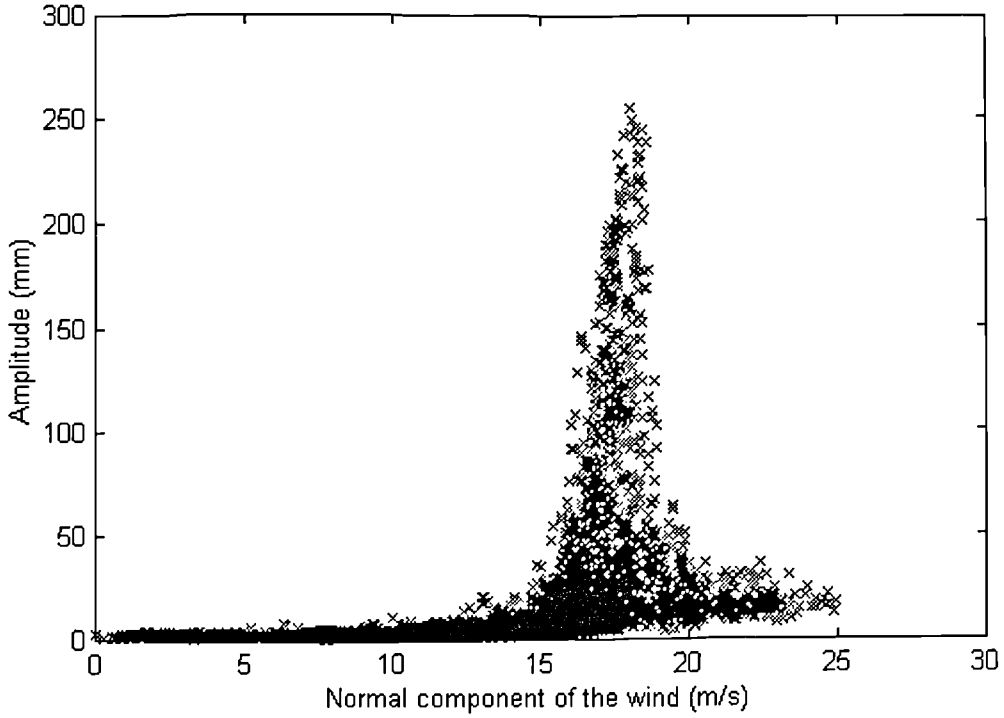

Fig. 9-9 Deck displacement amplitude against normal component of the wind (wind averaged over previous 16.4 minutes)

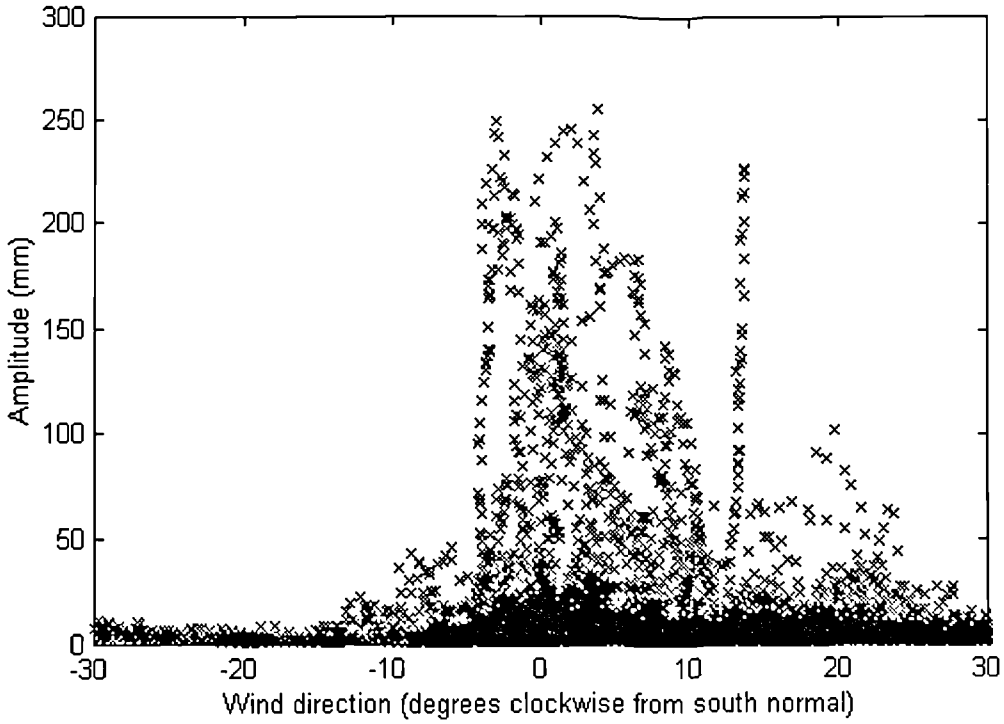

Fig. 9-10 Deck displacement amplitude against wind direction (wind averaged over previous 16.4 minutes)

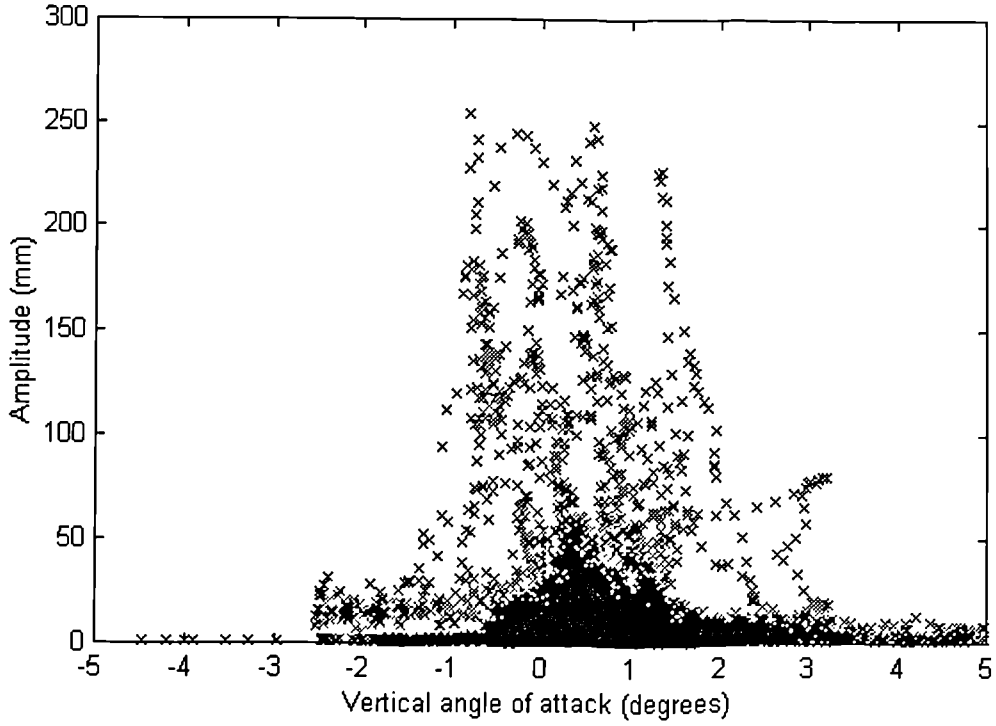

Fig. 9-11 Deck displacement amplitude against vertical angle of attack of the wind (wind averaged over previous 16.4 minutes)

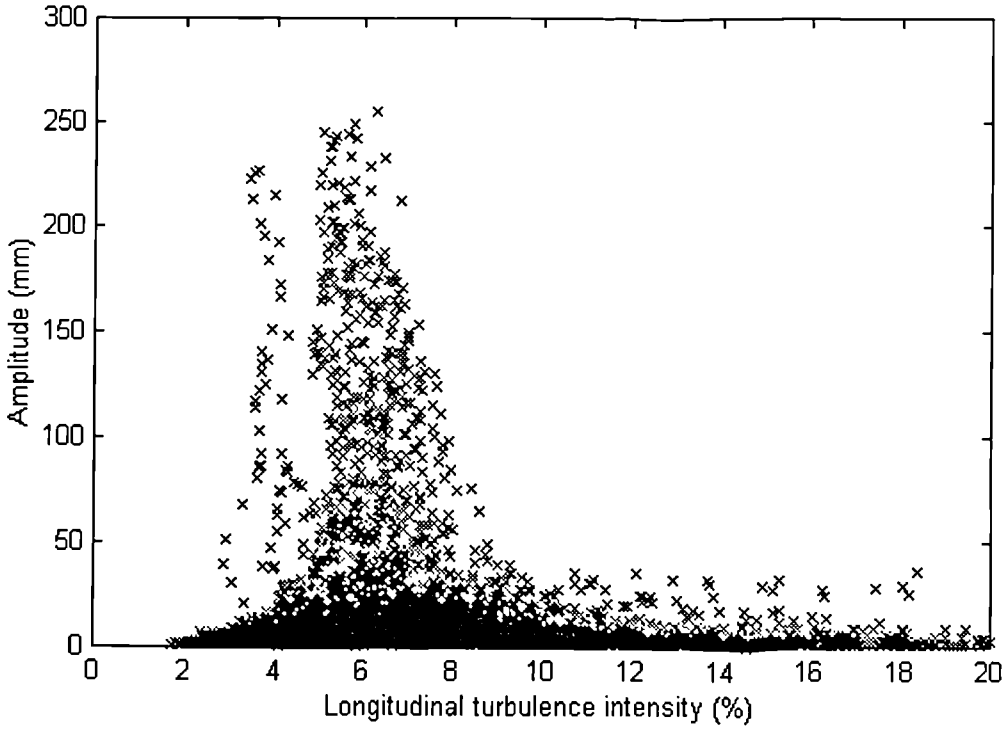

Fig. 9-12 Deck displacement amplitude against longitudinal turbulence intensity of the wind (wind averaged over previous 16.4 minutes)

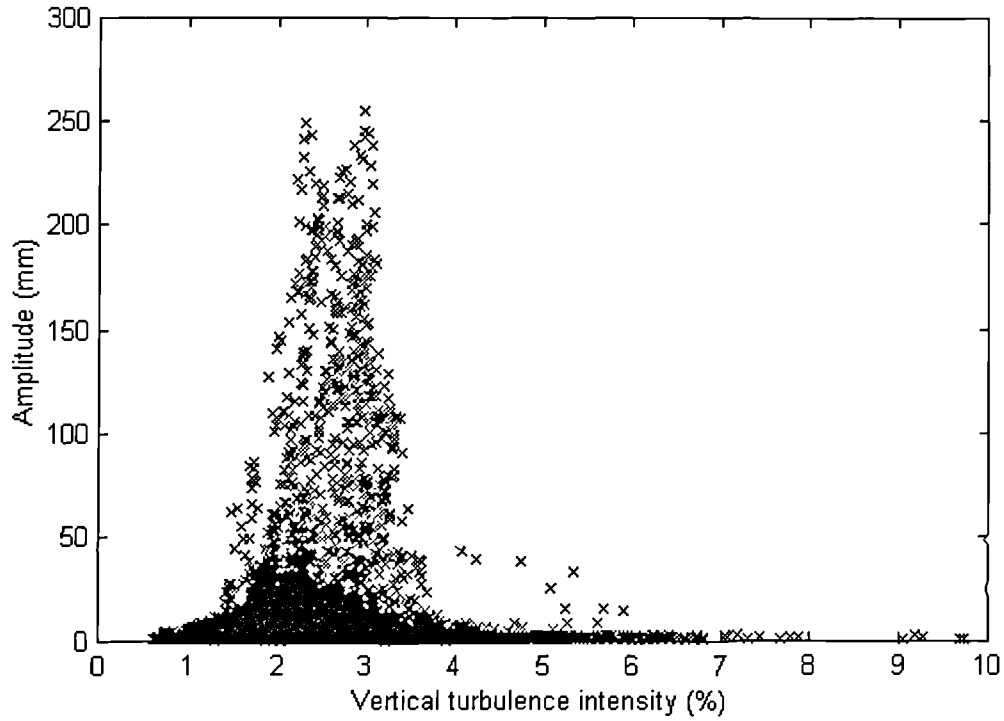

Fig. 9-13 Deck displacement amplitude against vertical turbulence intensity of the wind (wind averaged over previous 16.4 minutes)

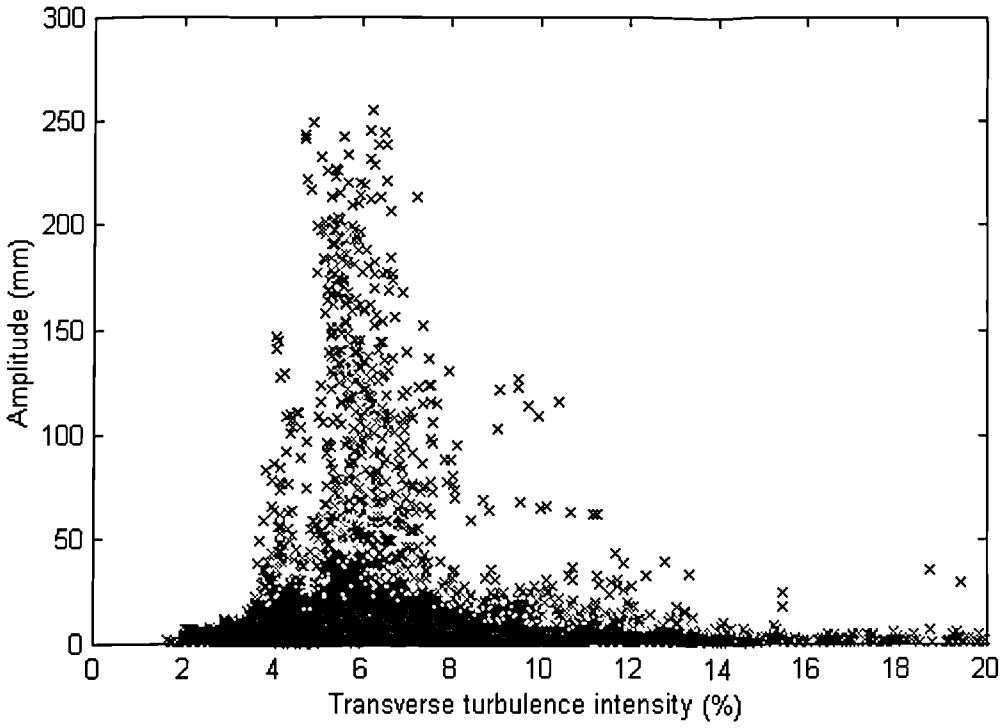

Fig. 9-14 Deck displacement amplitude against transverse turbulence intensity of the wind (wind averaged over previous 16.4 minutes)

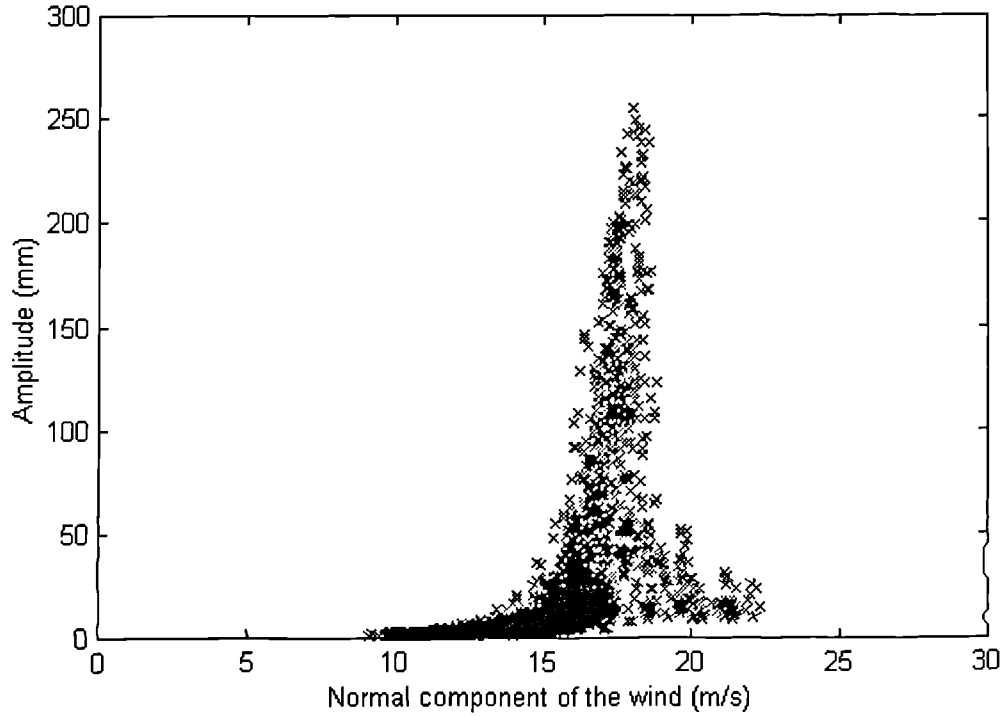

Fig. 9-15 Deck displacement amplitude against normal component of the wind - only data blocks satisfying criteria of wind direction, angle of attack and turbulence (wind averaged over previous 16.4 minutes)

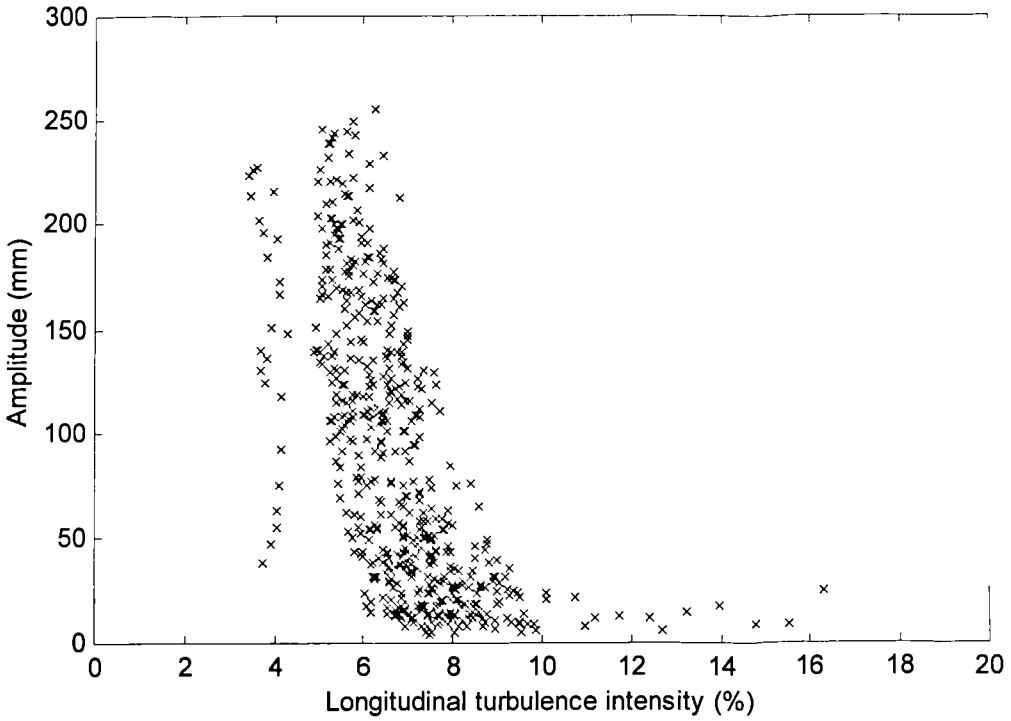

Fig. 9-16 Deck displacement amplitude against longitudinal turbulence intensity - only data blocks satisfying criteria of wind normal component, direction and angle of attack (wind averaged over previous 16.4 minutes)

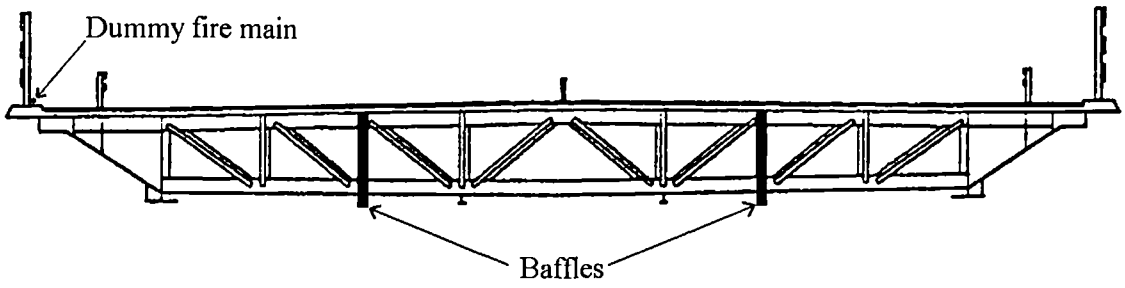

Fig. 9-17 Deck cross-section showing baffles and dummy fire main added to prevent vortex-induced vibrations

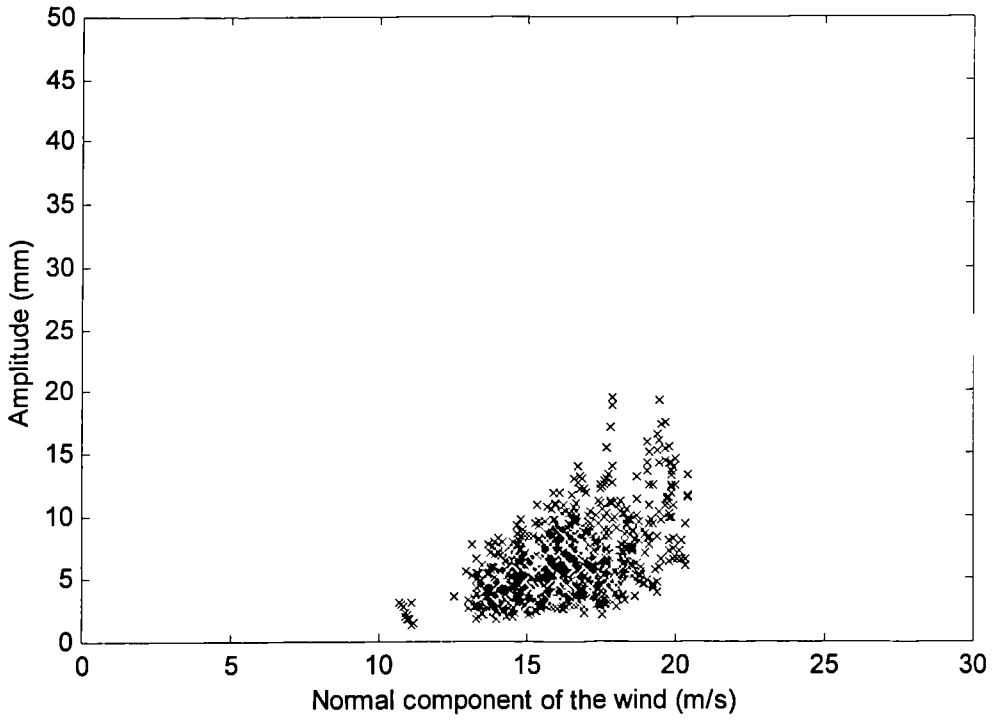

Fig. 9-18 Effect of baffles: deck displacement amplitude against normal component of the wind with baffles - only data blocks satisfying criteria of wind direction, angle of attack and turbulence (wind averaged over previous 16.4 minutes) (c.f. Fig. 9-15)

CHAPTER 10 CABLE VIBRATIONS AND CABLE-DECK INTERACTION ON THE SECOND SEVERN CROSSING

10.1 Introduction

Chapters 8&9 have discussed the 'global' vibration response (i.e. deck & pylon) of the Second Severn Crossing (SSC). This chapter addresses local vibrations of the cables, followed by the interaction of these with the global behaviour, which are important issues specific to cable-stayed bridges.

During construction of the SSC, large cable vibrations occurred. The low damping was believed to be a contributory factor, so forced vibration tests were undertaken to measure the damping of selected cables (§4.5.5). A theoretical expression for the contribution of aerodynamic damping is proposed, for the general case of an inclined cable in an arbitrary wind. This is validated by damping estimates from the vibration tests. The remaining contribution from structural damping is also determined, and the suitability of various criteria for aeroelastic instabilities are assessed.

The deck response was measured along with the cable vibrations during the forced cable vibration tests, and in ambient conditions, to detect any evidence of cable-deck interaction. Several aspects of this behaviour are identified from the measurements, including some not previously observed. The effects of cable-deck interaction for large amplitude vibrations are also discussed.

Finally, the effectiveness of the secondary cables, added to prevent the large cable vibrations, is considered.

10.2 Observations of cable vibrations

During construction of the first SSC cable-stayed cantilever (M2, §3.2.2), vibrations of the cables were observed, sometimes of large amplitude. Unfortunately, the monitoring equipment was not in operation at the time, so the details in this section are based only on records of visual observations.

The significant vibrations were observed only when it was raining, if only lightly, suggesting that they were rain-wind induced (§2.8.1). On one occasion, moderate amplitude vibrations were seen by the author, but unfortunately problems with instrument cables delayed the start of monitoring with the equipment, by which time the rain and (within 20 minutes) the vibrations had ceased. However, anemometer readings

during and after the cable vibrations showed no noticeable change in the wind speed or direction, supporting the view that the vibrations had been rain-wind induced.

The majority of the cables were seen to vibrate on some occasion. Vibrations in up to the sixth mode occurred, from visual observations by the author.

From the Contractor's records, the vibrations generally occurred in wind speeds in the range 11-25m/s, which is consistent with the results of wind tunnel tests by Verwiebe (1998). On the SSC, the larger vibrations occurred in the stronger winds. The wind direction for the vibrations was usually approximately 45° from the bridge axis, as observed on other bridges (Hikami & Shiraishi 1988, Miyata 1991) and in wind tunnel tests (Matsumoto et al. 1989). On one occasion, moderate cable vibrations occurred in a wind of 27m/s, approximately normal to the bridge. Although the mechanism may have been different in this case, the vibrations again occurred in rain, so it is likely that it exacerbated the effect, whatever the precise mechanism.

The maximum observed amplitude was estimated to be 2.5m, for the longest few cables on the main span of the M2 cantilever. These cables, spaced at approximately 2.3m centres, on occasion slapped together. During some of the most severe cable vibrations, reports indicate that the deck was also excited. Significant deck vibrations were not observed on any other occasions during construction, including in similar wind conditions but without rain, although large vortex-induced deck vibrations occurred after completion (Chapter 9). The relationships between the large amplitude deck and cable vibrations are discussed in §10.8.

In order to inhibit the cable vibrations during construction, all of the cables were restrained with ropes attached approximately 10m above the deck and tied down to other cable anchorages, at approximately 90° to the cables. This was reasonably effective in preventing large vibrations, although smaller vibrations still occurred. For the finished bridge, small diameter secondary cables were installed, tied down to the deck via rubber blocks. These proved successful in limiting the vibrations, as discussed in §10.9.

10.3 Cable vibration tests

The large cable vibrations first occurred prior to the injection of the corrosion protection wax into the cable sheaths. It was thought that this could have an influence on the damping (Narita & Yokoyama 1991, Lilien & Pinto da Costa 1994), which in turn would affect the vibration levels. Therefore, cable damping tests were performed before and after the injection of the wax to determine its effect.

Aerodynamic damping would have a contribution to the total damping measured, so another objective was to separate the components of aerodynamic and structural damping. Evidence of cable-deck interaction from the tests was also of interest.

Cable damping tests were performed on cables of the completed M2 cantilever, as described in §4.5.5, before the secondary cables were installed to limit the vibrations. Only four cables were tested, due to difficulties of access, but these were chosen to be a representative selection (Table 10-1). Manual excitation was used to cause significant vibrations (typically 100-300mm amplitude) of each cable in its first in-plane mode. The maximum attainable amplitude was reached in between one and five minutes, after which excitation was abruptly halted and the vibrations left to decay freely. The damping was then estimated by the Logarithmic Decrement Method (§10.3.1). Each test was repeated several times to obtain several damping estimates for each cable. In some cases the response of the deck and the opposite cable were measured simultaneously, to monitor any cable-deck interaction.

Table 10-1 Basic parameters of tested cables

Cable number	**61N**	**85N**	**101N**	**119S**
Location (all on M2)	Longest on main span, north side	6th shortest on main span, north side	Mid length on back span, north side	2nd longest on back span, south side
Length between elastomeric guides (m)	236.03	61.15	96.20	229.07
Angle of inclination from horizontal (degrees)	22.6	43.8	34.5	23.8
Outside diameter (mm)	180	150	160	225
No. of steel strands	53	30	37	75
Area of steel (mm^2)	7950	4500	5550	11250
Unwaxed mass / unit length (kg/m)	67.6	39.0	47.8	96.2
Waxed mass / unit length (kg/m)	79.0	47.9	57.5	115.5
Distance of measurement location from deck end (m)	26.5	16.0	21.1	29.3

Cable vibrations were also recorded in ambient conditions at various stages of construction, including for the finished bridge, after the installation of the secondary cables (§10.9). However, these data were limited due to the number of instruments and acquisition channels available (§4.3). Unfortunately, after completion of the bridge, the

instrument cables to the accelerometers on the bridge cables corroded. Access to replace them was not possible, so no further cable vibration measurements could be taken.

10.3.1 Logarithmic decrement of vibrations

The damping for the first mode of each cable (and for the decay of large vortex-induced deck vibrations, §9.3.1) was calculated from the free decay of vibrations as follows. The recorded signals were filtered in the time domain with a digital low-pass 16-pole Butterworth filter with a cut-off frequency equal to twice the fundamental frequency, to isolate the response of the first mode. The raw and filtered acceleration signals from a typical cable damping test are shown in Fig. 10-1. The filtered signal was assumed to represent the free decay response of a Single-Degree-Of-Freedom (SDOF) oscillator, for which the Logarithmic Decrement Method could be used. The theory behind this method, as applied here, is given in Appendix A, from which the damping ratio is given by:

$$\zeta = \frac{-b}{2\pi f_n} \tag{10-1}$$

where: f_n = natural frequency

b = gradient of $\ln(y_{peak})$ plotted against time

y_{peak} = amplitude of each cycle

Strictly this applies to displacement amplitudes, but, for low damping, acceleration amplitudes can be used with little error.

This variation of the method is more accurate than the basic Logarithmic Decrement Method, which just considers the relative amplitudes at two distinct times (Clough & Penzien 1993), since random errors can be averaged out by considering the best-fit straight line of the $\ln(y_{peak})$-time plot. Also any variation in damping during the decay of vibrations can be seen by a change of gradient.

To implement the method for the SSC cable vibrations, the maxima and minima were picked out from the filtered time history, and the natural frequency estimated from the average period between maxima. Consecutive half peak-peak amplitudes were calculated, thereby eliminating any signal offset and low frequency drift. Natural logarithms of these values were plotted against time and the least squares best-fit straight line fitted to each one minute block, as shown in Fig. 10-2. The average damping ratio over the minute was then determined from the gradient and natural frequency, from equation (10-1).

The method was applied to both the measured accelerations and displacements of the cables. Generally the accelerations gave less scatter of the $\ln(y_{peak})$-time plots, due to the greater accuracy of the instruments, so only the damping estimates from them are presented. However, the damping estimates from the displacement transducers were comparable, increasing confidence in the results.

10.4 Natural frequencies of cables

Before dealing with estimates of cable damping (§10.5&10.6), it is of interest to consider the natural frequencies, which were also determined from the cable vibration tests. The relationships between natural frequencies of the cables and of the global structure are of relevance to cable-deck interaction (§10.7&10.8), while cable sag has an appreciable effect on the first natural frequency, which was useful in distinguishing 'linear' and 'parametric' interaction on the SSC (§10.7.1).

10.4.1 Theoretical expressions for natural frequencies of cables

For a taut string between fixed supports, ignoring sag, the natural frequencies are given by (Blevins 1986):

$$f_r = \frac{r}{2L}\sqrt{\frac{T}{m}} \qquad (10\text{-}2)$$

where: r = mode number

T = mean tension

L = cable length (along the chord)

m = cable mass per unit length

This relationship holds for a sagging cable for out-of-plane modes, in which the vibrations are perpendicular to the sag. It also holds for anti-symmetric (even numbered) in-plane modes, but for symmetric (odd numbered) in-plane modes the gravitational and elastic potential energy vary over the vibration cycle, giving a more complex relationship. The natural frequencies of these modes, for a cable with fixed ends, are given by the solutions of the equation (Irvine & Caughey 1974):

$$\tan(\Omega_r/2) = (\Omega_r/2) - (4/\lambda^2)(\Omega_r/2)^3 \qquad (10\text{-}3)$$

where: Ω_r = normalised natural frequency of mode r (odd only) $= 2\pi f_r L\sqrt{\frac{m}{T}}$

λ^2 = Irvine's non-dimensional sag parameter $= \left(\frac{mgL\cos\beta}{T}\right)^2 \frac{EAL}{TL_e}$

L_e = cable length along the cable centreline at rest $\approx L\left\{1+\frac{1}{8}\left(\frac{mgL\cos\beta}{T}\right)^2\right\}$

β = angle of inclination of the cable from the horizontal

E = Young's modulus of the cable (or the cable steel)

A = Cross-sectional area of the cable (or the cable steel, compatible with E)

g = acceleration due to gravity

For bridge cables, the sag is small, so for modes other than the first, the differences from the taut string natural frequencies are negligible. For short cables the difference is not noticeable, but for longer cables the sag becomes significant and the natural frequency of the first in-plane mode is higher than for the equivalent taut string.

Measured natural frequencies can be used to estimate cable tensions, but the effective lengths for vibrations are not normally known precisely. If other measurements are available, the cable tensions and effective lengths can be determined more accurately, for example by a least square error method (Casas 1994).

10.4.2 Measured natural frequencies of cables and estimated cable tensions

On the SSC, cable tensions at the time of the vibration tests were only estimated indirectly by the Contractor, and no other direct measurements were available. Therefore, to enable the tensions to be calculated, the cable lengths were taken to be the distances between the inside faces of the elastomeric guides in the anchorages (Table 10-1). Thus the tensions were calculated from equation (10-2), based on the measured natural frequency of the second mode of each cable. The results are shown in Table 10-2, along with the Contractor's estimates, where available, which agree within 10%. The discrepancies are due to the uncertainty of the effective cable lengths and errors in the Contractor's estimates. The slightly higher cable tensions for the cables when waxed were due to minor changes in construction between the tests on the unwaxed and waxed cables.

The measured natural frequencies of higher modes of each cable were found to agree with equation (10-2), within the accuracy of the frequency measurements. However, the first natural frequency in each case was slightly higher than half the second natural frequency (Table 10-2), which would be due to the sag (§10.4.1). Based on the

calculated tensions, equation (10-3) was solved by iteration to obtain theoretical values of the first natural frequencies. These are also shown in Table 10-2, for comparison with the measured frequencies. The agreement is generally good, with minor discrepancies possibly being due to the uncertainty in the cable lengths. However, for Cable 61N the differences are greater than would be caused by a reasonable error in the estimate of cable length. It is believed that the discrepancies exist because on the bridge the cable ends are not fully fixed in position as assumed in the equations, which would tend to decrease the actual natural frequencies relative to the theoretical values. This hypothesis is supported by evidence of cable-deck interaction, particularly for Cable 61N in the first mode (§10.7.1).

Table 10-2 Cable natural frequencies and tensions

Cable number	61N		85N		101N		119S	
Unwaxed / Waxed	U	W	U	W	U	W	U	W
Measured 1st natural frequency (Hz)	0.425	0.406	1.620	1.511	1.096	1.011	0.506	0.503
Measured 2nd natural frequency (Hz)	0.787	0.740	3.232	3.008	2.180	2.005	0.989	0.983
Increase of 1st nat. freq. c.f. taut string, eq. (10-2) (%)	8.0	9.7	0.2	0.5	0.6	0.8	2.3	2.3
Contractor's estimate of cable tension (kN)	2392	-	1673	-	2243	-	4681	-
Calculated tension, based on 2nd nat. freq., eq. (10-2) (kN)	2333	2410	1523	1621	2102	2139	4938	5856
Error of Contractor's tension c.f. calculated tension (%)	+2.5	-	+9.8	-	+6.7	-	-5.2	-
Calculated 1st natural frequency, eq. (10-3) (Hz)	0.433	0.415	1.621	1.510	1.097	1.116	0.509	0.504
Error of calculated c.f. measured 1st nat. freq. (%)	+1.8	+2.2	+0.04	-0.10	+0.11	+0.06	+0.55	+0.15

10.5 Aerodynamic damping of an inclined cable

Damping measurements on full-scale structures are of total damping, including a contribution from aerodynamic damping (§2.6.3). Since the damping of cables is so low (typically around 0.2%, §2.8.3) the contribution from aerodynamic damping could be significant, even in light winds, causing errors in the estimated structural damping. Simple expressions for aerodynamic damping for cable vibrations in the direction of the wind or normal to the wind have been presented by Virlogeux (1998). However, it appears to have been taken into account in only one study of full-scale cable damping (Irwin et al. 1999), for which the aerodynamic damping from the component of wind

velocity in the direction of cable vibrations was subtracted from measured values. It appears that the full aerodynamic damping of an inclined cable in a wind of arbitrary speed and direction has not previously been considered.

To address this issue, theoretical expressions for the aerodynamic damping of a cable in the general case are proposed here. The full derivation is given in Appendix B. For in-plane vibrations, the proposed expression for the aerodynamic damping ratio is:

$$\zeta_{aero} = \frac{\rho D C_D}{4\omega_n m} U \left(\sqrt{\cos^2\theta + \sin^2\theta \sin^2\beta} + \frac{\sin^2\theta \sin^2\beta}{\sqrt{\cos^2\theta + \sin^2\theta \sin^2\beta}} \right) \quad (10\text{-}4)$$

where: ρ = density of air

D = cable diameter

C_D = drag coefficient

$\omega_n = 2\pi f_n$ = circular natural frequency

U = wind speed

θ = wind direction, measured from normal to the vertical plane of the cable†

Similarly, for out-of-plane vibrations the proposed theoretical aerodynamic damping ratio is:

$$\zeta_{aero} = \frac{\rho D C_D}{4\omega_n m} U \left(\sqrt{\cos^2\theta + \sin^2\theta \sin^2\beta} + \frac{\cos^2\theta}{\sqrt{\cos^2\theta + \sin^2\theta \sin^2\beta}} \right) \quad (10\text{-}5)$$

These expressions are based on the following assumptions:

i) The forces on the cable are given by quasi-static theory (§2.6.2);

ii) The component of wind velocity along the cable causes an insignificant force on the cable compared with the normal component (Skarecky 1975);

iii) The cable velocity is small compared with the wind velocity;

iv) C_D is constant over the range of relative velocities experienced between the wind and the cable (§10.6.2).

† This reference direction is used for consistency with wind directions for the whole bridge in this thesis, although it differs from the reference direction used for cable aerodynamics by some authors.

The direction-dependent factors of equations (10-4)&(10-5) (i.e. the factors in brackets) are plotted in Fig. 10-3 and Fig. 10-4 respectively, for different angles of cable inclination. For in-plane vibrations the wind direction has relatively little effect, particularly for cables inclined at approximately 30° to the horizontal, which is typical for bridge cables. For out-of-plane vibrations the damping typically varies with direction by a factor of four. It should also be noted that, except for winds close to the direction of the bridge axis, the damping of out-of-plane vibrations is higher than for in-plane vibrations, and for winds normal to the bridge there is a difference of a factor of two. This could be a factor in determining that in-plane vibrations are typically of larger amplitude than out-of-plane vibrations (§6.2.8).

10.6 Cable damping test results

From the many measured damping estimates for each cable tested on the SSC (§10.3), the contributions of aerodynamic and structural damping could be determined experimentally. Thus equation (10-4), for the aerodynamic damping, could be validated, and the residual component of structural damping could be estimated, for cables both before and after waxing. The values could then be compared with previously proposed criteria for large amplitude cable vibrations from various mechanisms (§2.8).

10.6.1 Estimation of aerodynamic and structural contributions to measured damping

Fig. 10-5 to Fig. 10-12 show the free decay of vibrations, following the termination of excitation, for the several tests performed on each cable before and after waxing. The log of each half peak-peak amplitude is plotted against time, for the application of the Logarithmic Decrement Method (§10.3.1). The gradient is proportional to the damping, as given by equation (10-1). In some cases the gradient varied between tests or as vibrations decayed during individual tests, most noticeably for Cable 61N after waxing (Fig. 10-6). The average gradients, and hence the damping ratios, were therefore calculated over one minute periods.

The variations in measured damping for each cable were considered in relation to aerodynamic damping. The average wind speed and direction over each one minute period, corresponding to each damping estimate, were calculated. Each damping estimate was then plotted against the 'equivalent normal wind speed', given by:

$$U_{eq} = U\left(\sqrt{\cos^2\theta + \sin^2\theta\sin^2\beta} + \frac{\sin^2\theta\sin^2\beta}{\sqrt{\cos^2\theta + \sin^2\theta\sin^2\beta}}\right) \qquad (10\text{-}6)$$

This corresponds to the wind-dependent factor on the right hand side of equation (10-4), and is equal to the wind speed which would cause the same theoretical aerodynamic damping if the wind direction was normal to the plane of cable vibrations. The plots of measured damping against equivalent normal wind speed are shown in Fig. 10-13 to Fig. 10-16, in which linear relationships are apparent, showing that the form of equation (10-4) for aerodynamic damping is reasonable. The relationship is particularly clear for Cable 61N (Fig. 10-13), which was the most sensitive to variations of the wind. Least-squares best-fit lines were fitted to the measured points for each series of tests. The intercept on the damping axis gives the structural damping and the gradient represents the measured variation of aerodynamic damping with equivalent normal wind speed (the 'aerodynamic damping gradient'). The variance of the points relative to the best-fit line was used to calculate 95% confidence limits for the intercept and gradient.

The results of the line-fitting, from both before and after waxing, are also shown in Fig. 10-13 to Fig. 10-16. Generally, there was less variation in the wind speed for the tests before waxing than those after, giving greater uncertainty in the best-fit lines. In the cases of Cables 85N (Fig. 10-14) and 119S (Fig. 10-16) there was insufficient variation in the equivalent normal wind speed to fit a meaningful straight line to the measured points.

For all of the cases in which line-fitting was possible, estimates of 'measured' aerodynamic damping gradient and structural damping are given in Table 10-3, along with the 95% confidence limits.

10.6.2 Aerodynamic damping results

From equations (10-4)&(10-6), the theoretical aerodynamic damping gradient for in-plane vibrations is given by:

$$\frac{\zeta_{aero}}{U_{eq}} = \frac{\rho D C_D}{4\omega_n m} \qquad (10\text{-}7)$$

C_D is a function of Reynolds number (R_e)†, but it varies little over wide ranges of R_e. For a smooth circular cylinder it is approximately 1.2 for $R_e < 2\text{x}10^5$ (Simiu & Scanlan 1986). For the largest (most critical) cables on the SSC (225mm diameter), R_e would remain below this limit for wind speeds up to 13m/s. Therefore, for the range of wind speeds experienced during the cable damping tests (< 10m/s), C_D can be taken to be 1.2.

† $R_e = UD/\nu$, where ν = kinematic viscosity.

Table 10-3 Summary of cable damping test results

Cable number	61N		85N		101N		119S	
Unwaxed / Waxed	U	W	U	W	U	W	U	W
Measured 1st natural frequency (Hz)	0.425	0.406	1.620	1.511	1.096	1.011	0.506	0.503
Measured aerodynamic damping gradient (%/(m/s))	0.035	0.040	-	0.016	0.014	0.021	-	0.030
95% confidence limits of aerodynamic damping gradient (%/(m/s))	0.022 0.048	0.037 0.043	-	0.010 0.023	0.011 0.018	0.016 0.026	-	0.014 0.046
Theoretical aerodynamic damping gradient, eq. (10-7) (%/(m/s))	0.037	0.033	0.014	0.012	0.018	0.016	0.027	0.023
Measured structural damping (%)	0.038	0.047	0.38*	0.33	0.058	0.098	0.23*	0.10
95% confidence limits of structural damping (%)	0 0.11	0.014 0.080	-	0.26 0.40	0.031 0.085	0.060 0.14	-	0 0.22

* Calculated using theoretical aerodynamic damping

Table 10-3 shows the theoretical aerodynamic damping gradients from equation (10-7), compared with the measured values. There is reasonable agreement, with all but one of the theoretical values lying within the 95% confidence limits of the measured results. The proposed relationship of equation (10-4) therefore seems to give a reasonable estimate of the aerodynamic damping for in-plane cable vibrations.

The expression does have its limitations, since it assumes that the cable velocity is small compared with the wind velocity, and that the component of wind velocity along the cable does not have a significant effect (§10.5), although it has been shown that it can be influential for cable excitation of the rain-wind type (Matsumoto et al. 1989,1992). Also, the expression ignores the effects of wind turbulence, vortex shedding and the possibility of galloping (§2.8.2). However, notwithstanding the shortcomings of the expression, the measured results fit the straight line relationship and the predicted and measured gradients agree well, within the random scatter of the points.

The aerodynamic damping expression is based on a constant value of C_D, which is reasonable for $R_e < 2\text{x}10^5$ (sub-critical), corresponding to a wind speed of 13m/s for the largest cables and 21m/s for the smallest (140mm diameter) on the SSC. For higher wind speeds, in the critical region, the linear relationship between aerodynamic damping and equivalent normal wind speed would break down. However, in the super-critical range ($R_e > 5\text{x}10^5$), C_D is fairly constant, but with a value of approximately 0.4 (Simiu &

Scanlan 1986), so the expression would again be reasonable. For the SSC, all of the cables would be in the super-critical range for wind speeds above 54m/s, with the largest ones being super-critical above 33m/s.

Quasi-static theory was found to overestimate aerodynamic damping for the SSC bridge deck (§8.4.2), but for cables it appears that the quasi-steady approach is more accurate. This is believed to be because cables are much smaller and smoother in cross-section, so the variation in wind loading over the cross-section is likely to be less affected by the movement of a cable.

The aerodynamic damping of cables is very significant compared with the structural damping, particularly for longer cables (Fig. 10-13 & Fig. 10-16). Therefore, it is recommended that for any future measurements of cable damping, the contribution of aerodynamic damping calculated from equations (10-4)&(10-5) be subtracted from the measured values to estimate the structural damping.

10.6.3 Structural damping results

Values of structural damping for the cables tested on the SSC are given in Table 10-3, based on the least-squares fit of the damping measurements against equivalent normal wind speed. For Cables 85N (Fig. 10-14) and 119S (Fig. 10-16) before waxing, lines could not reasonably be fitted to the measured points (§10.6.1), so the theoretical aerodynamic damping gradient was used to enable the estimation of the structural damping.

There is considerable variation in the estimates of structural damping, but for all cables, both waxed and unwaxed, they are very low, although similar to measurements of cable damping on other bridges (§2.8.3). The value of 0.047% for the longest cable (61N, waxed) is particularly low, whereas 0.33% for the shortest cable tested (85N, waxed) is relatively high for a parallel strand cable. *However, these results are consistent with* previous measurements showing a trend of lower damping for longer cables (Stiemer et al. 1988, Narita & Yokoyama 1991). This has been explained by the main source of structural damping being at or near the anchorages, which becomes less significant for longer cables (Irwin et al. 1999).

With such low levels of structural damping, for all but the shortest cable tested, in wind speeds above approximately 5m/s the aerodynamic damping becomes dominant. For longer cables the aerodynamic damping is higher, and the structural damping is generally lower, so the aerodynamic damping becomes dominant at even lower wind speeds. This highlights the need to separate these contributions for site measurements, particularly for longer cables. Previous measurements may have overestimated the structural damping of longer cables by not considering the aerodynamic component (§2.8.3).

Comparing the structural damping values in Table 10-3 before and after waxing, there is no clear pattern to the changes. At the extremes, Cable 101N (Fig. 10-15) showed an increase in damping by almost a factor of two, whereas Cable 119S (Fig. 10-16) showed a decrease by a similar factor. With such low levels of damping, minor changes, such as movement of the elastomeric guide during waxing, could make significant differences. Also, shifts in natural frequencies of the cables may have altered cable-deck interaction effects, which could cause differences in the measured damping (§10.7.1.3). Although changes did occur for individual cables, the lack of a pattern leads to the conclusion that the presence of the wax itself does not have a strong influence on the damping and that other effects are of greater importance.

During the cable damping tests, normally all of the cables were tied down to the deck with temporary ropes, except where the ropes would directly interfere with the cable under test. However, in some cases after waxing, the tests were repeated with the cable of equal length on the opposite side of the deck released. This was to allow any interaction between the cables, via the deck and/or pylon, to be observed. In some cases the opposite cable was seen to respond, and it was thought that this transfer of energy may have affected the apparent damping of the cable under test (§10.7.1.3). However, after taking account of changes in the aerodynamic damping, no difference was distinguishable from the random scatter of the measurements.

Temperature was also considered as a parameter which may have affected the measured damping. Therefore, the difference between the total measured damping and the best-fit line of aerodynamic and structural damping was plotted against the cable temperature (§4.3.1(iii)). Typical results are shown in Fig. 10-17. The maximum difference in temperatures for each series of tests was only 2-3°C, and no trend of variations in damping was apparent.

Two non-linear effects in the damping were observed for particular cables:

i) For Cable 101N before waxing, Fig. 10-9 shows a consistently higher damping ratio (steeper gradient) for the first 50s of vibrations. This was believed to be due to the cable sheath rattling, which could be heard for the larger vibrations. This would dissipate additional energy, and could introduce errors in the measurements due to relative movements of the cable strands and sheath. The damping ratios for this cable were only calculated for the period after the change in gradient. The change in damping was not observed for the vibrations after waxing, although they were of similar initial amplitude.

ii) For Cable 85N after waxing (Fig. 10-8), there was generally a plateau in the decay for approximately 10s, 20-30s after the termination of excitation. This is

believed to have been due to non-linear interaction with other modes of the cable and/or deck and pylon (§10.7.1.3).

10.6.4 Susceptibility of cables to large vibrations

It is of interest to compare the estimated structural damping ratios of the SSC cables with the proposed criteria for large vibrations from previous studies (§2.8.1&2.8.2). Some of the criteria are based on the Scruton number (S_c) (§2.8), rather than the damping ratio itself, so values of S_c have been calculated for the tested cables, based on the measured structural damping ratios (Table 10-4).

Miyata (1991) and Narita & Yokoyama (1991) suggested that rain-wind excitation (§2.8.1) occurs for cable damping ratios below approximately 0.3%, which is the case for all of the measured SSC cables except Cable 85N (Table 10-4). An alternative criterion of $S_c<10$ for rain-wind excitation to occur was proposed by Irwin (1997), which is satisfied by all of the SSC measured cables. Therefore, by either criterion, it is not surprising that rain-wind vibrations did occur on site (§10.2). However, Cable 85N was observed to be excited in the rain, which suggests that the limit based on S_c may be more appropriate. The minimum values of damping required for the SSC cables to achieve $S_c \geq 10$, to prevent rain-wind vibrations, are also shown in Table 10-4. For the waxed cables (with similar average densities to each other) these values are consistently in the range 0.5-0.6%. Although this is up to 16 times the measured structural damping, it is still low compared with most structures, so modest changes to the structure could provide the additional damping required.

For vortex-induced vibrations (§2.8.2(i)), it has been suggested that large vibrations occur for $S_c<1.6$ (Miyata 1991) or $S_c<5$ (Scruton & Walshe 1957). No large amplitude vibrations were observed on site without rain, which suggests that vortex excitation did not occur to a great extent. From the measured values of S_c (Table 10-4), this implies that the criterion from Scruton & Walshe (1957), or even a higher limit, is more appropriate.

Regarding galloping vibrations (§2.8.2(ii)), Narita & Yokoyama (1991) suggested that they are suppressed by a minimum cable damping ratio of 0.8%. There was no evidence of galloping vibrations on site, with much lower damping, but the wind speeds that were experienced (§6.4.1) may not have been high enough to cause this instability. Irwin (1997) has suggested that it occurs above a critical wind speed of:

$$U_{crit} = cf_n D\sqrt{S_c} \qquad (10\text{-}8)$$

where: c is a constant, approximately 35-40

The critical wind speeds for the SSC cables, based on this formula with c=40, are given in Table 10-4. They are generally very low, and were regularly exceeded on site, but with no evidence of galloping. Therefore, this expression does not appear to be appropriate for cables on site, at best underestimating the critical wind speed.

Table 10-4 Criteria for cable instabilities, based on measured structural damping

Cable number	61N		85N		101N		119S	
Unwaxed / Waxed	U	W	U	W	U	W	U	W
Measured first natural frequency (Hz)	0.425	0.406	1.620	1.511	1.096	1.011	0.506	0.503
Measured structural damping (%)	0.038	0.047	0.38*	0.33	0.058	0.098	0.23*	0.10
Scruton no., S_c (eq. (2-27)), from measured structural damping	0.64	0.94	5.4*	5.7	0.88	1.8	3.6*	1.9
Minimum damping (%) required to achieve $S_c \geq 10$	0.59	0.50	0.71	0.58	0.66	0.55	0.64	0.54
Critical wind speed (m/s) for galloping (eq. (10-8)), from measured structural damping	2.5	2.8	23*	22	6.6	8.7	8.6*	6.3
Vertical deck amplitude (mm) required for parametric excitation (§10.8.3)	1.4	1.8	2.6*	2.2	0.8	1.4	11.1*	4.8

* Calculated using theoretical aerodynamic damping

10.7 Measured cable-deck interaction

Cable-deck interaction (§2.9) is a particular feature of cable-stayed bridge dynamics, since the natural frequencies of the global structure and of the individual cables are in the same frequency range. For the completed SSC cantilever, the first global mode (0.332Hz, Table 8-1) had a natural frequency slightly below the fundamental frequency of the longest cables (0.406Hz, Table 10-2). With many global and cable modes occurring above these frequencies it is highly likely that cable-deck interaction would occur.

There have been several reports of cable vibrations attributed to excitation from the deck on cable-stayed bridges (§2.9.3), but there have been few direct measurements to confirm this, or to study other aspects of cable-deck interaction (§2.9). It was therefore

of value to identify any evidence of cable-deck interaction from the SSC measurements, either from the forced cable vibration tests or in ambient loading conditions.

For the purposes of this discussion, 'linear' cable-deck interaction relates to vibrations of the cable and the deck or pylon at the same frequency (§2.9.1(i)&2.9.2), although in reality large amplitude cable vibrations would exhibit non-linear behaviour (§2.4.1). 'Parametric' cable-deck interaction relates to vibrations of the deck or pylon at twice the cable frequency (§2.9.1(ii)). Normally this is concerned with cable excitation by the deck or pylon, but here it is taken to include excitation of the deck or pylon by the cable.

10.7.1 Cable-deck interaction in forced vibration tests

10.7.1.1 Evidence of linear cable-deck interaction

During the forced cable vibration tests, related vibrations of other parts of the structure were sometimes observed or recorded (§4.5.5&10.3). Often the cable of equal length on the opposite side of the deck was excited in phase or in antiphase with the cable under test. The opposite cable could only have been excited by movements of the deck or pylon, which in turn must have been excited by the cable under test. This is a clear indication of the interaction between the cables and the global structure, with vibrations of either forcing vibrations of the other.

During tests on Cable 119S, vibrations of the four longest backspan cables on the north side (117-120N) were observed. The Multiple Element Cable System (MECS) Finite Element (FE) model (§3.4) showed that the equivalent four cables in the model interacted strongly with the second vertical global mode (Mode V2, §8.3.2). Unfortunately no measurements were taken simultaneously on the deck or these other cables to quantify this behaviour.

During tests on Cable 61N, Cable 61S responded at the same frequency, but in antiphase, with 20% of the amplitude of Cable 61N, as measured. Conversely, when Cable 61S was excited, Cable 61N vibrated in phase, with a relative amplitude of 23%. The first natural frequency of Cable 61S was 0.410Hz, slightly higher than that of Cable 61N (0.406Hz), presumably due to slightly different tensions.

The deck also participated in these modes, although with a much smaller amplitude. For the Cable 61N tests, the amplitude on the north side of the deck at the end of the cantilever (near Cable 61N anchorage) was 7.5% of the cable amplitude at the measurement location (Table 10-1). Assuming a half-sine mode shape for the cable, the deck amplitude was equivalent to 2.6% of the maximum cable amplitude. The south side of the deck responded with 71% of the amplitude of the north side in antiphase, indicating an asymmetric, predominantly torsional mode. The ratios of the amplitudes

remained constant throughout the decay of the vibrations. This indicates that the so-called cable modes are in fact modes of the complete structure, simply with the motion dominated by a single cable. This type of behaviour is predicted by the MECS FE model (§3.4). The slight asymmetry of the cables gives two modes with slightly different frequencies, one with the cables in phase and dominated by one cable, and the other with them in antiphase and dominated by the other cable.

The movement of the deck along with the cables would also cause a drop in the cable natural frequencies relative to the theoretical frequencies for fixed-ended cables, as measured (§10.4.2).

10.7.1.2 Evidence of parametric cable-deck interaction

The relationship between cable and deck accelerations, for a forced cable vibration test, is shown by the time histories in Fig. 10-18. The two signals have been scaled arbitrarily so that they can be viewed together. The deck can be seen to vibrate with a component at the same frequency as the cable. However, a component at twice the frequency is also apparent in the deck accelerations. This is evidence of the parametric effect of cable vibrations causing forces at the anchorages at twice the cable frequency (Virlogeux 1998). It is believed that this particular type of behaviour has not previously been recorded on a cable-stayed bridge.

The frequencies of cable and deck accelerations, during a similar forced cable vibration test, are shown by the Power Spectral Densities (PSDs) in Fig. 10-19. The cable and deck both vibrate strongly at the cable fundamental frequency of 0.406Hz. Indeed, for the deck, the vibrations forced by the cable are dominant over the usual vertical deck mode at 0.338Hz (Table 8-1). Components of cable acceleration in higher modes are also apparent at 0.742Hz, 1.114Hz and 1.483Hz (and higher harmonics also), but with virtually no response of the deck at these frequencies. However, there is significant deck response at 0.812Hz, precisely twice the frequency of the first cable mode. The increase of the first in-plane natural frequency of the cable, relative to a taut string (§10.4), separates double the first natural frequency (0.812Hz) from the second natural frequency (0.742Hz), clearly showing that the deck response (at 0.812Hz) is related to the first mode of the cable. Ambient vibration tests of the deck have shown that there is a global mode at 0.818Hz (Table 8-1). However, for the cable vibration tests the deck response (at 0.812Hz) was over 1000 times greater than for ambient vibrations in similar wind conditions, showing that the deck response was indeed due to the cable vibrations. The closeness in frequency of the global mode would mean that the deck was more susceptible to vibrations in this frequency range than elsewhere, leading to the large deck response. The cable also responded at 0.812Hz (Fig. 10-19), due to the excitation from

the deck at this frequency. Ambient vibration tests confirmed that this was not a normal vibration frequency of the cable.

The time history of Fig. 10-18 shows that the deck response at the double frequency had a phase lag relative to the fundamental response, which would be in phase with the cable. The Fast Fourier Transform (FFT) of the deck record showed that the phase difference between the double-frequency and fundamental components was approximately 90°. This indicates that the double-frequency response was a secondary response due to a force in time with the cable displacement, rather than the consequence of a direct displacement relationship.

The cable and deck PSDs for Cables 101N and 85N, during similar forced cable vibration tests, are shown in Fig. 10-20 and Fig. 10-21. They show similar patterns of behaviour to Cable 61N, although for these cables the sag is small, so the increase in the first natural frequency relative to the taut string model is less than 1% (Table 10-2). Therefore, the parametric effect cannot be distinguished, by the difference in frequency, from linear interaction with the second cable mode. However, the tests on Cable 85N (the most steeply inclined cable tested, Table 8-1) show very little response of the deck at the first and third natural frequencies of the cable, but significant response at the second and fourth. It is believed that these are due to the parametric effect associated with the first two modes of the cable. With the cable being more upright, the parametric effect is relatively more important and the linear effect less so, since they are respectively associated with longitudinal and transverse motion of the cable anchorage relative to the cable axis (§2.9.1).

10.7.1.3 Apparent cable damping from cable-deck interaction

In the cable damping tests, the deck response could affect the apparent damping of the cables (§10.6.3). Each cable has a different natural frequency and is attached to the deck and pylon at distinct positions, so each would be affected differently. Linear cable-deck interaction would involve vibrations of parts of the structure other than the cable itself, so energy would be dissipated elsewhere, as for global modes.

For parametric interaction, energy is transferred to other frequencies, so the apparent damping of an individual mode may be partially due to this transfer, rather than true energy dissipation. This is believed to have been the case for the damping tests on Cable 85N after waxing (§10.6.3(ii)). Fig. 10-22 shows the modal amplitudes of the cable during and after excitation at the first natural frequency. Although, after 20s of excitation, the amplitude of Mode 1 reaches a plateau, Mode 2 continues to increase in amplitude, possibly due to the parametric effect. Immediately after cessation of the excitation, the amplitude of Mode 1 decreases rapidly, as if highly damped, but Mode 2

increases in amplitude. A possible explanation is the transfer of the energy between the modes. The plateau in the decay of Mode 1 could similarly be due to the transfer of energy back to this mode from some other part of the structure.

The higher measured damping of the shorter cables (§10.6.3) could also be partly due to this effect. For the more upright cables the parametric effect is relatively more important, so they are more likely to loose energy to other modes.

10.7.2 Cable-deck interaction in ambient vibration tests

10.7.2.1 Additional modes

One characteristic of cable-deck interaction, evident in the results of the MECS FE model (§3.4.2), is the appearance of additional closely-spaced modes, compared with the One Element Cable System (OECS) model (§3.3.5) that does not permit local cable vibrations. If this behaviour occurs in practice, each main peak in the PSD of accelerations for the deck or pylon would be expected to comprise a series of close peaks, representing several modes. Evidence of this has been observed on a scale model of the Jindo Bridge (Caetano et al. 1996). However, from site measurements with unknown loading, it is normally difficult to distinguish this behaviour, since measured response PSDs are subject to variance errors (§5.3.1&5.6.2), so the detailed shapes of peaks are unclear. Furthermore, for the tests on the SSC, the cables were usually restrained by ropes, or later by the secondary cables (§10.9), so the response predicted by the MECS model may have been partially inhibited.

However, additional modes were sometimes apparent in the PSDs of ambient deck and pylon accelerations of the SSC, particularly for the cantilever, before the cables were restrained by the secondary cables (§10.9). Modes TL2a & TL3a of the cantilever (§8.3.2), and the many close modes in the pylon PSDs in the 1.6-2.4Hz range (§8.5.3) could be due to cable-deck interaction.

Several additional modes were found in the PSDs of vertical deck acceleration when applying the Iterative Windowed Curve-fitting Method (IWCM) (§8.5.2). They were most pronounced for very light winds. Fig. 10-23 shows two PSDs of vertical deck acceleration based on three-hour records that were acquired on the cantilever just a few hours apart, with no differences between them apart from the wind conditions. Cables 61N&S and 119S were left untied during the period, although all of the other cables were tied down with ropes. For the moderate wind (7.4m/s) only the usual global modes are apparent in the PSD, but in the very light wind (1.7m/s) many additional modes appear (Fig. 10-23). These are believed to be due to cable-deck interaction, since additional resonances appear at frequencies corresponding to the first few in-plane

natural frequencies of Cable 61N, as measured in the cable damping tests on the previous day, and by simultaneous ambient vibration measurements. These frequencies, of 0.406Hz for the first mode and integer (≥2) multiples of 0.371Hz, are shown by vertical dashed lines in Fig. 10-23. The presence of the additional peaks in the deck response, which occur for all frequencies of Cable 61N up to approximately 6Hz, is a clear indication that in these wind conditions the cable excites the deck, although in the stronger wind the effect is negligible. Further evidence of the direct relationship between the cable and deck vibrations in the light wind is given by the high coherence (>0.8) between the accelerations of the cable and deck at these frequencies (Fig. 10-24).

In the light wind, the amplitude of the north side of the deck at 0.406Hz was 2.5% of the maximum cable amplitude, and the south side amplitude was 73% of this. These agree well with the 2.6% and 71% obtained from the forced vibration tests (§10.7.1.1), indicating the same combined cable and deck mode.

Excitation of the deck at double the cable frequencies, due to the parametric effect, was not evident. The global deck mode at 0.818Hz (Table 8-1) dominated the response close to twice the fundamental natural frequency of Cable 61N (0.812Hz). The high coherence between the cable and deck accelerations at the cable natural frequencies indicates linear, rather than parametric, interaction. This is not surprising, since the cable vibration amplitude was low. The linear relationship holds for a wide range of amplitudes, but the force on the deck at twice the cable frequency is approximately proportional to the cable amplitude squared (Virlogeux 1998), so it is more important for larger vibrations.

Considering several long-term records (totalling 155 hours) from a period of three weeks at the same construction stage, additional modes up to 1.5Hz were only observed in wind speeds below 6m/s, and were most noticeable and consistent for the lowest wind speeds. Additional modes occurred at various frequencies, believed to be due to different cables, but some appeared consistently, indicating that they represented genuine modes. The inconsistent appearance of the other additional modes could be due to changes in the restraint of certain cables by the ropes. The wind direction was found to be unimportant for the presence of the additional modes.

10.7.2.2 Mechanism of excitation of additional modes

The dependence on wind speed for the occurrence of the additional modes can be explained by the excitation mechanism of the cables. During the acquisition period there was very little rain, so the potential cable excitation mechanisms would be vortex shedding, buffeting and galloping (§2.8.2). The buffeting loading on cables is very low, particularly at low wind speeds, and there was no evidence of galloping from the measurements (§10.6.4). Therefore, the principal excitation of the cables for these

records is believed to have been from vortex shedding (§2.6.5.3&2.8.2(i)). The frequency of vortex shedding, and hence loading, is given by (Simiu & Scanlan 1986):

$$f_V = \frac{SU}{D} \tag{10-9}$$

where: S = Strouhal number, approximately 0.2 for bridge cables

For the two records compared in Fig. 10-23, with average wind speeds 1.7m/s and 7.4m/s, for Cable 61N (180mm diameter) the average vortex shedding frequencies would be 1.9Hz and 8.2Hz respectively. The PSDs of the in-plane cable accelerations for the two records are shown in Fig. 10-25. The increase in the response of the cable around the vortex shedding frequencies for each wind speed can be seen. The variation in wind speed over each record accounts for the relatively broad range of frequencies over which the increase occurs. The dips in the response near 3.3Hz and 6.6Hz are due to the measurement location being near nodes of the modes with natural frequencies in these regions. For the lower wind speed, the skewed direction of the wind relative to the cable may account for the wider frequency range of excitation. In any case, the difference in frequency content of the cable vibrations for the two wind speeds is clear.

In the meantime, the direct excitation of the deck by the wind at these wind speeds is primarily due to buffeting. Vortex excitation of the deck was not observed during construction (§9.3), and flutter would not occur until very high wind speeds (§2.6.5.1 &2.6.5.2). Therefore, the form, although not the magnitude, of the wind loading spectrum on the deck would be similar for the two wind speeds (§6.5.4). Consequently, at the lower wind speed, below 5Hz the excitation of the cables is significant relative to the excitation of the deck, whereas for the higher wind speed, the cable excitation is relatively less significant at the low frequencies but more significant above 5Hz. This explains the presence of the additional modes at low frequencies in the lower wind speed only.

This hypothesis is supported by consideration of the PSDs of deck response at higher frequencies (Fig. 10-26). Although the global modes are less clear in this frequency range (5-8Hz), responses are again apparent at the natural frequencies of Cable 61N. However, they appear also for the higher wind speed, and at higher frequencies they become relatively less important in the lighter wind but more so for the stronger wind, in which the cables are excited more in this frequency range. The relationship between cable and deck vibrations in the two cases is clearly shown by the coherence plots (Fig. 10-27 & Fig. 10-28).

10.7.2.3 Higher frequency cable-deck interaction

On another occasion, in a wind of 4.1m/s at 185° (i.e. close to normal to the bridge axis on the north side), larger vibrations of the cantilever deck and pylon were recorded at the natural frequencies of Cable 61N from 6-9Hz (Fig. 10-29). The north and south sides of the deck and pylon responded with similar amplitudes to each other, but unfortunately the accelerometers on the cable were not connected at the time. The reason for the larger responses in this case is not clear, but vortex shedding was still believed to have been the principal excitation mechanism, with the wind being so close to normal to the bridge possibly having an adverse effect. However, the response enabled the relative amplitudes and phases of the deck and pylon motion to be determined.

The cable vortex shedding loading mechanism meant that the IWCM, based on an assumed loading spectrum for deck buffeting (§7.6), was not valid for this application. Therefore, the relative amplitudes were found from the ratio of PSDs at the natural frequencies. The background response in the frequency range of these modes was of the order of 0.1% of the peak values, so it would have little effect on the results. The phases were obtained from the Cross Spectral Densities (CSDs), corrected for the phase differences between channels due to the Analogue to Digital Converter (ADC) board time delay (§5.5). The findings are summarised in Table 10-5.

The very high coherences between the responses at different locations on the structure give confidence in the accuracy of the relative amplitudes and phases. Also, the vibrations continued for several hours, with coherences generally above 0.9, yielding values within 15% for amplitude and 6° for phase from the values in Table 10-5. The differences between the responses of north and south sides of the deck and pylon would be due to the slight asymmetry of the cables, including the restraints from the ropes. The larger responses on the north side of the deck imply that vibrations of the north cable were dominant, which is consistent with the frequencies measured on the deck and pylon, which match the harmonics of Cable 61N.

Of particular note are the different phases. For all other identified modes, the phase between the accelerations at any two locations on the structure was found to be close to 0° or 180°, with a difference of 15° only being exceeded in cases of low coherence (<0.6) (§8.3.1). However, for these vibrations the phases are quite different, despite the high coherence and very clear responses at all measurement locations. It is believed that this type of behaviour has not been previously observed on a cable-stayed bridge. Three possible explanations for the phase differences are:

i) Non-linear cable-deck interaction, possibly involving several cable modes, which exhibit non-linearity due to the cable dynamics.

ii) Complex modes, with the complexity arising from coupling of the modal equations of motion, caused by non-proportional damping (Ewins 1984), for example from damping occurring predominantly in certain locations, such as the cable anchorages.

iii) Response of the deck and pylon for each cable mode in a combination of two or more global normal modes, for example deck vertical bending and torsional modes. Although the responses of all parts of the structure in each mode would be in phase with each other, a phase lag between the modes would cause a different relative phase of the total response at each location.

The significant phase differences were measured for vibrations at relatively high frequencies and low amplitudes, so they were not of great importance to the total response of the structure. However, their source is not clear, so this behaviour should be investigated further to obtain a more complete understanding of the cable-deck interaction.

Table 10-5 Response of deck and pylon to vortex-induced cable vibrations, relative to deck north vertical response

Cable harmonic number	Frequency (Hz)	Relative amplitude, phase* and coherence		
		Deck south vertical	Pylon north longitudinal	Pylon south longitudinal
18	6.683	0.835 –8° 0.9997	0.104 97° 0.9984	0.0213 –27° 0.9893
19	7.055	0.224 23° 0.9913	0.0315 –70° 0.9950	0.0256 40° 0.9982
20	7.426	0.651 5° 0.9992	0.0450 146° 0.9965	0.0106 –74° 0.9835
21	7.797	0.941 7° 0.9996	0.0272 35° 0.9984	0.0480 108° 0.9991
22	8.169	0.494 121° 0.9889	0.111 –85° 0.9925	0.0981 –89° 0.9922
23	8.540	0.824 5° 0.9995	0.123 34° 0.9947	0.0932 26° 0.9946

* Zero phase for pylon taken to be motion away from the main span in phase with upwards motion of the deck reference location.
Measurement locations: deck: 850mm from tip of main span cantilever, 300mm from edges of deck; pylon: on centrelines of tower on each side, at Cable 61N anchorage level, 5.75m from very top.

10.7.2.4 Low frequency cable-deck interaction

Returning to the deck response in light winds (§10.7.2.1), two additional modes are apparent in the vertical deck acceleration PSD at 0.242Hz and 0.273Hz (Fig. 10-23), below the first vertical global frequency (0.338Hz, Table 8-1). These frequencies are also below the fundamental frequency of the longest cable (0.406Hz), so they cannot be due to excitation by a cable at one of its natural frequencies. The mechanism causing this response is not clear, but could be due to a non-linear effect of the cable vibrations. Two possible mechanisms are suggested:

i) Theoretical studies of parametric excitation (§2.9.1) have shown that instabilities exist for excitation frequencies of $2f_n/k$, for k = any integer (Uhrig 1993, Lilen & Pinto da Costa 1994). For k>2 they are generally ignored, since damping makes them less significant than 'normal' parametric excitation (k=1) or linear excitation (k=2). However, for very low damping and/or high levels of excitation, an end excitation frequency lower than the natural frequency can cause large cable vibrations in the mode. Since the instability is a non-linear effect, the reciprocal relationship does not necessarily hold, but it is possible that non-linear cable vibrations could cause forces on the deck at a frequency below the natural frequency of the cable, particularly with the cable ends not being fully fixed. The measured deck frequency of 0.273Hz is within 1% of 2/3 of the fundamental frequency of Cable 61N, so the response could be due to this effect.

ii) The non-linear interaction of two or more cable modes could cause a beating-type effect, producing a response below the fundamental natural frequency. For a general Single Input Single Output (SISO) non-linear system with an input equal to the sum of two sine waves of different frequencies (f_1 & f_2), the output has components at 'combinational' frequencies, e.g. f_1+f_2, f_1-f_2 or $2f_1-f_2$ (*Maia et al.* 1997). The measured deck response could be due to this type of non-linear effect.

Further work is required to identify the actual mechanism for these low frequency deck responses. In particular, the effect of the non-linear behaviour of the cables on the deck response needs to be addressed, in contrast with previous theoretical work on the response of the cables to motion of the deck or pylon (§2.9.1).

10.8 Cable-deck interaction for large amplitude vibrations

Evidence of cable-deck interaction, from measurements at relatively low amplitudes, has been presented, but it of interest to consider the effects of this behaviour at larger amplitudes, based on these findings.

10.8.1 Relationship between observed large amplitude deck and cable vibrations

It has been suggested by Virlogeux (1998) and Stubler et al. (1999) that the SSC large deck vibrations after completion (§9.3) may have been related to the earlier large cable vibrations (§10.2). Their argument was that originally the cables were excited by the deck, but with the addition of the secondary cables (§10.9), vibrations of the main cables were restrained, so the energy remained in the deck vibrations, which built up to larger amplitudes. However, the large cable vibrations only occurred in the presence of rain (§10.2), and the wind conditions for large deck vibrations (§9.4) and for large cable vibrations (§10.2) were quite different. Also, the frequency of large vibrations of the deck (0.326Hz) was below the first natural frequency of any of the cables (minimum 0.406Hz), so it is unlikely that large cable vibrations would have been induced by these deck vibrations (§2.9.1). Furthermore, the global structural damping was not greatly affected by the addition of the secondary cables (§8.4.3). The large deck and cable vibrations which occurred are therefore believed to have been due to independent mechanisms. The cable vibrations were rain-wind excited and were inhibited by the introduction of the secondary cables (§10.9), while at around the same time the wind barriers were installed (§3.2.5), which led to vortex excitation of the deck (§9.3).

The deck was observed to vibrate during periods of large cable vibrations (§10.2), but it is believed that this was due to excitation from the cables.

10.8.2 Deck excitation by large amplitude cable vibrations

The interaction between vibrations of Cable 61N and the deck was measured, for relatively low amplitudes, in both the forced and ambient cable vibration tests (§10.7.1.1 &10.7.2.1). For the linear interaction at 0.406Hz, the vibration amplitude at the end of the cantilever deck on the north side was found to be 2.5-2.6% of the maximum cable amplitude. If the same relationship held for the largest rain-wind excited cable vibrations that were observed (2.5m estimated amplitude, §10.2), it is estimated that the deck response amplitude would have been 64mm. However, such large cable vibrations would be highly non-linear so the deck response could be quite different.

Lilien & Pinto da Costa (1994) calculated theoretical displacements of a cable of the Ben-Ahin Bridge due to end excitation at its natural frequency, and found that the non-linearities reduced the cable amplitude from 7m, for linear theory, to 1.2m. If non-linearities had a similar effect on the relative amplitudes of the SSC cable and deck vibrations for the rain-wind cable excitation, the maximum deck amplitude would be approximately 370mm. With several cables vibrating simultaneously the maximum total displacement of the deck would be higher. Also, the force at the cable ends at twice the cable frequency is approximately proportional to the amplitude squared (Virlogeux

1998), so for the large cable vibrations observed it was likely to be significant, further increasing the deck response. This would be in keeping with the observations of significant deck vibrations along with the large amplitude cable vibrations (§10.2), and would support the view that the deck was excited by the cables.

The recent theoretical and limited experimental work on parametric cable vibrations (§2.9.1) has concentrated on the response of a cable to end excitation. However, the measurements from the SSC suggest that excitation of the deck from the cables is also important. On longer bridges, with a higher proportion of the total mass in the cables, this effect would become more significant, so further research is required into this aspect of cable-deck interaction.

10.8.3 Susceptibility of cables to parametric excitation from the deck

It has been suggested that large cable vibrations on several bridges may have been due to parametric excitation from the deck (Langsoe & Larsen 1987, Stiemer et al. 1988, Uhrig 1993, Lilien & Pinto da Costa 1994). However, there has been little clear evidence from full-scale measurements to support this view. On the SSC, the deck was found to be excited at twice the cable frequency in the forced cable vibration tests (§10.7.1.2), but there was no direct evidence of parametric excitation of the cables by the deck. However, the available data provide the opportunity to consider the susceptibility of actual bridge cables to this effect, which has only previously been investigated theoretically and on simple physical models (§2.9.1).

Lilien & Pinto da Costa (1994) provide an expression for the minimum amplitude of sinusoidal support vibrations, along the cable axis, to cause parametric excitation:

$$X_d = 2X_0\sqrt{\{1-(f_{ex}/2f_n)^2\}^2 + (f_{ex}\zeta/f_n)^2} \qquad (10\text{-}10)$$

where: X_0 = static cable extension

f_{ex} = support excitation frequency $\approx 2f_n$

Damping thus increases the minimum support amplitude required for instability, although it has little effect on the resulting amplitude if cable vibrations are initiated by this mechanism.

For a cable with low sag:

$$X_0 \approx \frac{TL}{EA} \qquad (10\text{-}11)$$

Hence, at the most critical excitation frequency ($f_{ex}=2f_n$), equation (10-10) reduces to:

$$X_d \approx \frac{4TL\zeta}{EA} \tag{10-12}$$

Thus, assuming the pylon motion not to be significant, the vertical deck amplitude to provide this component along the cable axis could be calculated for the four cables tested on the SSC. These critical amplitudes are given in Table 10-4, based on the measured structural damping ratios. The deck vibrations are required at twice the cable natural frequencies (i.e. minimum 0.812Hz).

The large amplitude vortex-induced vibrations of the SSC deck occurred at 0.326Hz (§9.3), so the excitation of the deck at the relevant frequencies would instead be due to buffeting. The site vibration amplitudes were not evaluated in terms of the displacement in each mode, and the measurements only covered a limited range of wind speeds. However, the site data confirmed that the design buffeting analysis (Xie et al. 1994) gave reasonable estimates of the vertical and torsional deck responses (§8.6.1&8.6.3), so this could be used to estimate the wind speed at which deck vibrations of the critical amplitude would occur.

The design buffeting analysis related to the finished bridge, whereas the cable natural frequencies and damping were measured on the cantilever. Also, the installation of the secondary cables (§10.9) would markedly change the behaviour. However, the available data gave an indication of the relevance of parametric excitation to real bridge cables.

From the measured global modes of the finished bridge (Table 8-2), the first mode to have a natural frequency above the minimum required for parametric cable excitation (0.812Hz), was Mode TL10 (0.842Hz). From the design buffeting analysis (Xie et al. 1994), the wind velocity, normal to the bridge, required to cause deck vibrations of the critical amplitude (1.8mm, assumed sinusoidal) in this mode would be approximately 18m/s.

This would suggest that parametric excitation of the cables was likely. However, in such a wind speed the aerodynamic damping would be dominant (§10.6.3). Fig. 10-30 shows the increase in the critical cable end amplitude with wind speed, based on the theoretical aerodynamic damping for in-plane vibrations of Cable 61N (Table 10-3). The discontinuity and subsequent lower gradient at higher wind speeds are due to the drop in drag coefficient for $R_e > 2\text{x}10^5$, causing relatively less aerodynamic damping (§10.6.2). Out-of-plane cable vibrations would have twice the aerodynamic damping, for wind normal to the bridge, so they would be less likely to be excited by this mechanism. Also shown in Fig. 10-30 is the predicted amplitude (assumed sinusoidal) of Mode TL10 from

the design buffeting analysis, for the worst traffic configuration for torsional response (§8.6.1). This indicates that above approximately 40m/s the maximum deck amplitude would be expected to be greater than required for parametric cable excitation. However, the critical deck displacement is required at the end of the cable, which is unlikely to be an antinode of the deck mode shape. Indeed, for Mode TL10, the displacement at the Cable 61N anchorage is only 5% of the maximum deck displacement (Fig. 10-30), which suggests that parametric excitation of this cable would not occur.

Another consideration is that the critical excitation frequency range is narrow. From equation (10-10), for 1% 'detuning' of the excitation, the critical amplitude is increased ten-fold for 0.1% damping, or by 42% for 1% damping.

The large contribution of aerodynamic damping, the dependence on the deck mode shape, and the narrow critical excitation frequency range for each cable makes parametric excitation unlikely. However, with the large number of cables on modern cable-stayed bridges (§2.2), an adverse combination could occur, although apparently only in high wind speeds. A number of factors in the behaviour remain uncertain, so there is a need for further work in this area, which should particularly address the following issues:

i) The cable end excitation is random, rather than sinusoidal as assumed by analytical studies to date (§2.9.1). This could significantly affect the cable response. Numerical simulations could approximate the deck vibrations to the response of an SDOF system to a broad band random input, providing a narrow band excitation to the cable.

ii) Perturbations of the cable due to direct buffeting or cable aeroelastic instabilities (§2.8) may affect the onset of parametric excitation. Also, the aerodynamic damping expression derived in this study has been validated for low wind speeds (§10.5&10.6.2), but it may not hold for higher wind speeds, as assumed.

iii) Traffic loading can excite the deck, without causing aerodynamic damping, although the displacement amplitudes of traffic vibrations are generally very low.

iv) Shorter cables have higher natural frequencies and hence lower aerodynamic damping, although they have higher structural damping and for the critical condition they require higher frequency deck vibrations, for which the displacements are lower.

10.9 Effects of the addition of secondary cables

Secondary cables were installed on the SSC shortly before it was opened, to reduce the rain-wind cable vibrations to acceptable levels. The secondary cables were fixed at

approximately 90° to the main cables (Fig. 10-31) and were tied down to the deck via rubber blocks to give additional damping. They were tensioned to ensure that the restraint was maintained for downwards cable movements.

After the bridge was opened, it was no longer possible to perform forced vibration tests on the cables, but data were collected in ambient conditions from the accelerometers mounted on Cable 61N. The PSDs of the in-plane and out-of-plane accelerations are shown in Fig. 10-32 and Fig. 10-33 respectively, compared with the equivalent spectra during construction (after waxing), with no secondary cables. Each spectrum is based on a one-hour record. The wind conditions were similar for the two records; 14.3m/s at 21° without the secondary cables, and 13.4m/s at 51° with the secondary cables.

A significant difference in loading between the records was the presence of traffic after the bridge was opened. It has been shown that traffic loading of the deck becomes dominant above approximately 2Hz, even in moderately strong winds (§6.6). Cable-deck interaction could account for the relatively large response of the cables in this frequency range, particularly in plane, for the record with the secondary cables.

Before installation of the secondary cables, significant vibrations occurred both in and out of plane, but typically with twice the amplitude in plane. With the secondary cables, the in-plane cable vibrations are greatly attenuated. The remaining acceleration is very similar to the adjacent deck acceleration, indicating that the cables are effectively held rigidly to the deck.

Out-of-plane vibrations with the secondary cables are still evident (Fig. 10-33), but there are several differences in the behaviour:

i) The natural frequencies are increased by 24%. This is believed to be principally due to the additional restoring force from the secondary cables, although there would also have been an increase due to the higher tensions in the cables, from the additional dead and imposed loads on the finished bridge.

ii) Below 2Hz the peak values of the PSD are typically reduced by a factor of ten, equivalent to a decrease in vibration amplitude of a factor of approximately three. This shows that, although the restraint provided by the secondary cables to out-of-plane vibrations is not as definite as for in-plane modes, the system is still effective in reducing these vibrations.

iii) With the secondary cables, the out-of-plane response around each main cable resonance behaves as a series of closely-spaced modes, rather than as a single clear mode as for the unrestrained cables. (The double peak for the first mode without the secondary cables was due to a strong deck mode causing cable vibrations just below its own first natural frequency). These multiple modes are an indication of interaction with the other main cables through the secondary

cables, in a similar manner to cable-deck interaction. The effect is less pronounced for the higher frequency modes, for which there is more motion of the cables between the secondary cables, decreasing the interaction.

It should be noted that these results are for the longest cable in the main span (Cable 61N), which had the secondary cables attached only to its underside. It was not possible to take measurements on other cables after completion, but it would be expected that the secondary cables would have a greater effect on the cables restrained from both sides.

10.10 Conclusions

Forced vibration tests on selected cables of the SSC determined their natural frequencies and damping ratios. For the longest cables, sag was important, increasing the first natural frequencies by up to 9.7% compared with an ideal taut string. Reasonable agreement was found with theoretical expressions for natural frequencies, but the movement of the cable ends appeared to cause a slight drop in the measured frequencies.

Theoretical expressions have been proposed for the aerodynamic damping of in-plane and out-of-plane vibrations of an inclined cable, for an arbitrary wind velocity (equations (10-4)&(10-5)). The contributions of aerodynamic and structural damping were determined experimentally from a large number of damping estimates from site measurements. Thus, the theoretical expression for in-plane vibrations was validated. It is believed that this is the first time that the contributions of aerodynamic and structural damping have been correctly separated for bridge cables. The aerodynamic damping can be very significant, so it is recommended, for future full-scale tests, that the theoretical aerodynamic damping be subtracted from measured values to estimate the structural damping.

The structural damping of the SSC cables appears to be higher for shorter cables, not strongly influenced by the presence of wax in the cable sheaths, and independent of temperature. It is therefore believed to arise mainly at the cable anchorages or possibly partly from the transfer of energy to other modes. The Scruton numbers for the cables are very low, so it is not surprising that significant rain-wind vibrations occurred on site during construction. Criteria for vortex-induced vibrations and galloping have also been evaluated.

Evidence of both linear and parametric cable-deck interaction was found from the forced cable vibration tests. It is believed that this is the first time that cable excitation of the deck at twice the cable frequency has been measured. This behaviour is consistent with the previous theoretical work and limited experimental studies of scale models on parametric excitation (§2.9.1). However, much of the previous work has concentrated on the response of the cable to moving anchorages, whereas in this case the force on the

deck from the cables was of more importance, so there is a need for further work in this area.

Small amplitude vortex-induced cable vibrations occurred at low wind speeds, causing deck vibrations in additional modes, similar to those predicted by the MECS FE model (§3.4.2). In stronger winds the buffeting of the deck became more important than the vortex-induced vibrations of the cables, so the cable-dominated modes at low frequencies became less significant. However, the possibility of the cables exciting the deck was demonstrated, as in the forced cable vibration tests. There is also evidence that the deck was excited noticeably by the large amplitude rain-wind cable vibrations.

Phase differences between the responses of different parts of the structure were identified for high frequency cable-deck interaction modes, and on other occasions the deck responded at frequencies below the fundamental cable and deck frequencies. Further work is required to understand these aspects of the behaviour.

The significance of parametric cable excitation from the deck has been considered. Aerodynamic cable damping, and the dependence of the effect on deck mode shapes and precise excitation frequencies appear to make the behaviour unlikely in practice, except possibly in high wind speeds. Further analytical and experimental work is required to consider more realistic conditions for this effect than previously addressed theoretically.

The secondary cables tying the main SSC cables together have been shown to be very effective in inhibiting the large amplitude rain-wind vibrations, which were observed during construction.

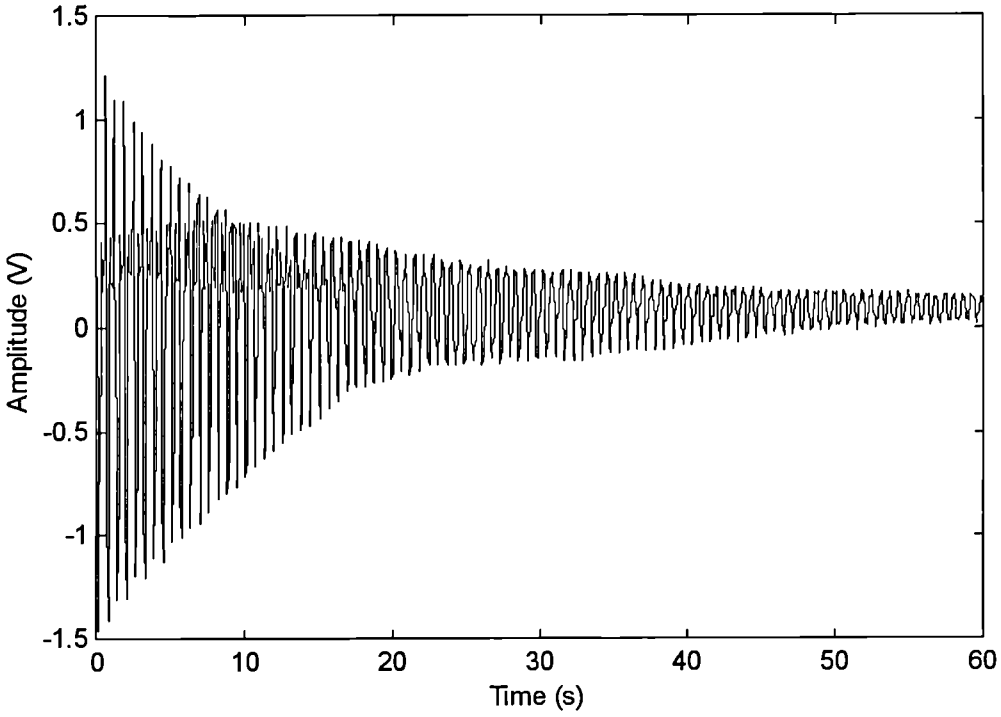

(a) Raw time history

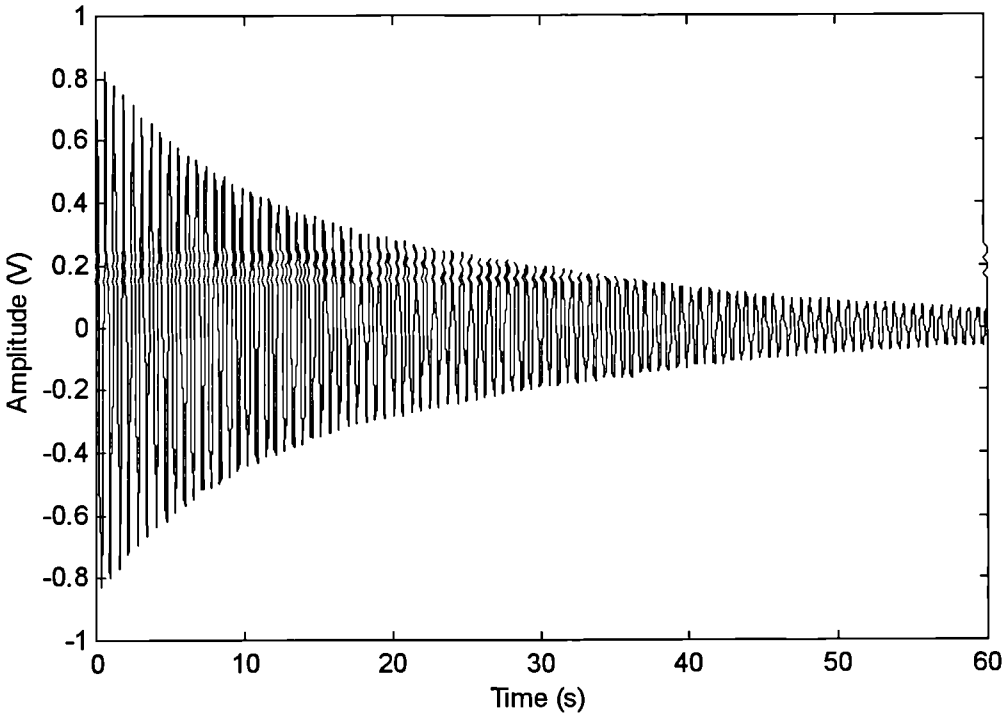

(b) Filtered time history

Fig. 10-1 Typical acceleration time history of free decay of cable vibrations

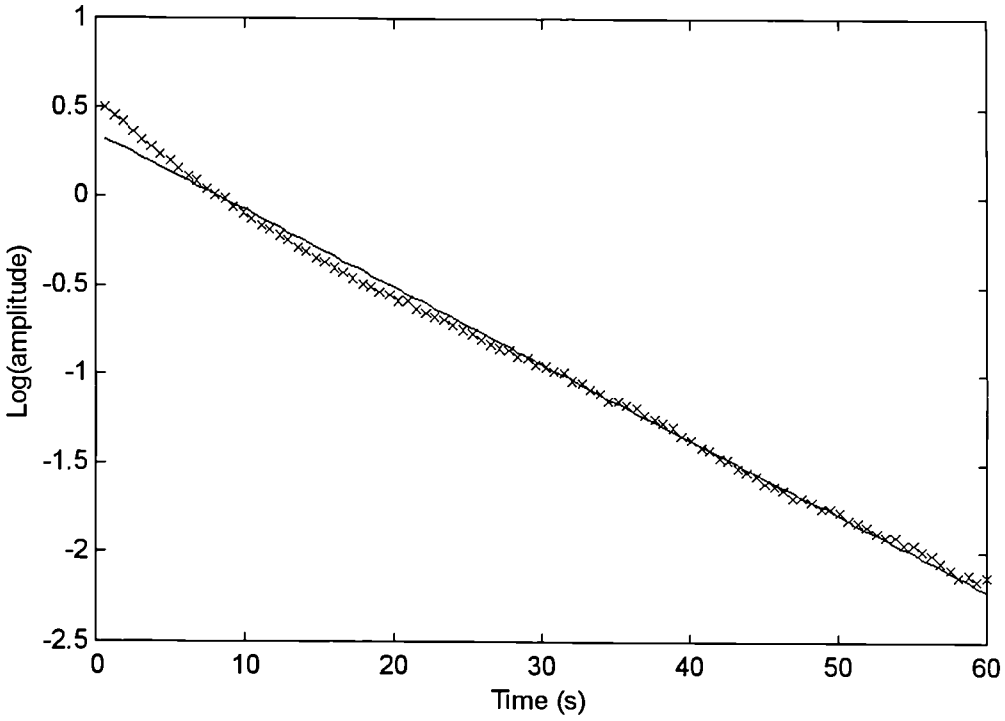

Fig. 10-2 Log(amplitude) of time history from Fig. 10-1(b), with best-fit straight line

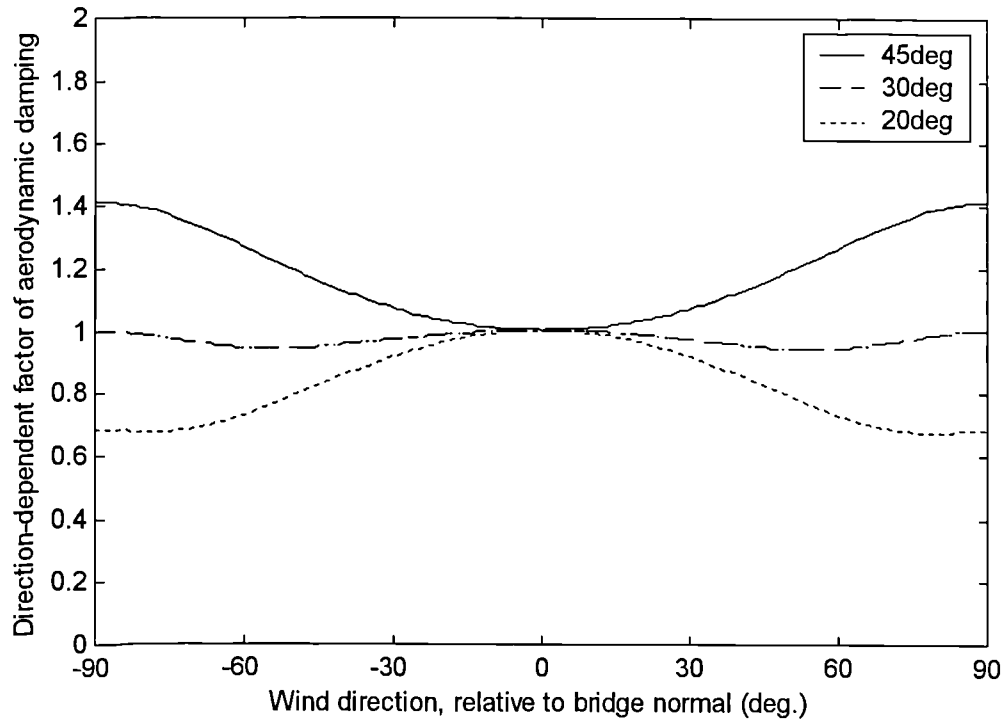

Fig. 10-3 Influence of wind direction on aerodynamic damping of in-plane cable vibrations for different angles of cable inclination

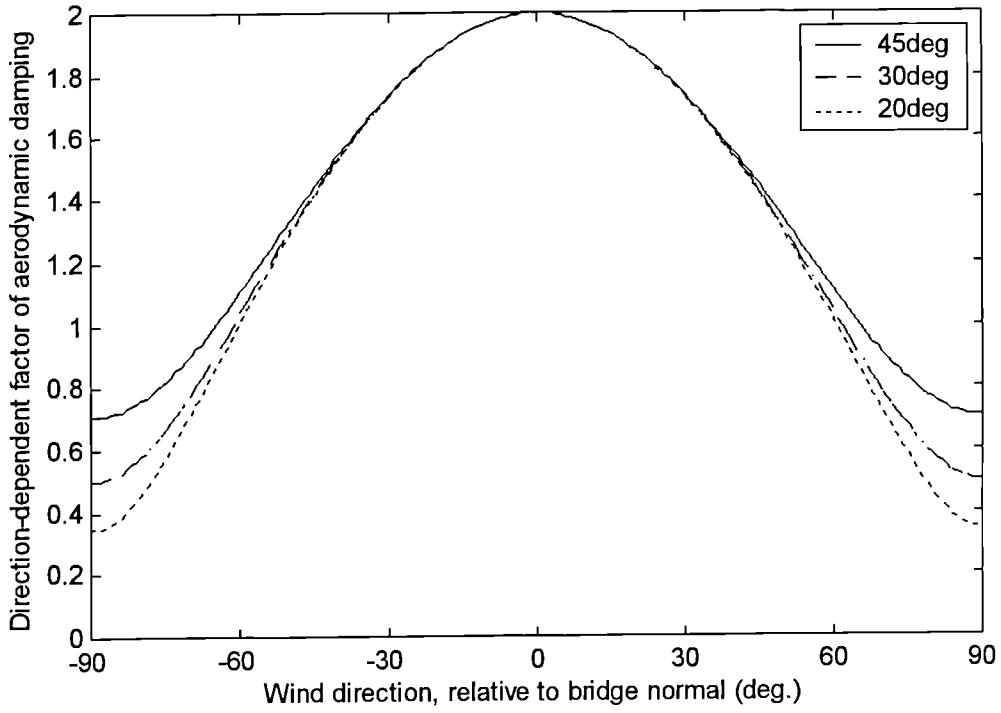

Fig. 10-4 Influence of wind direction on aerodynamic damping of out-of-plane cable vibrations for different angles of cable inclination

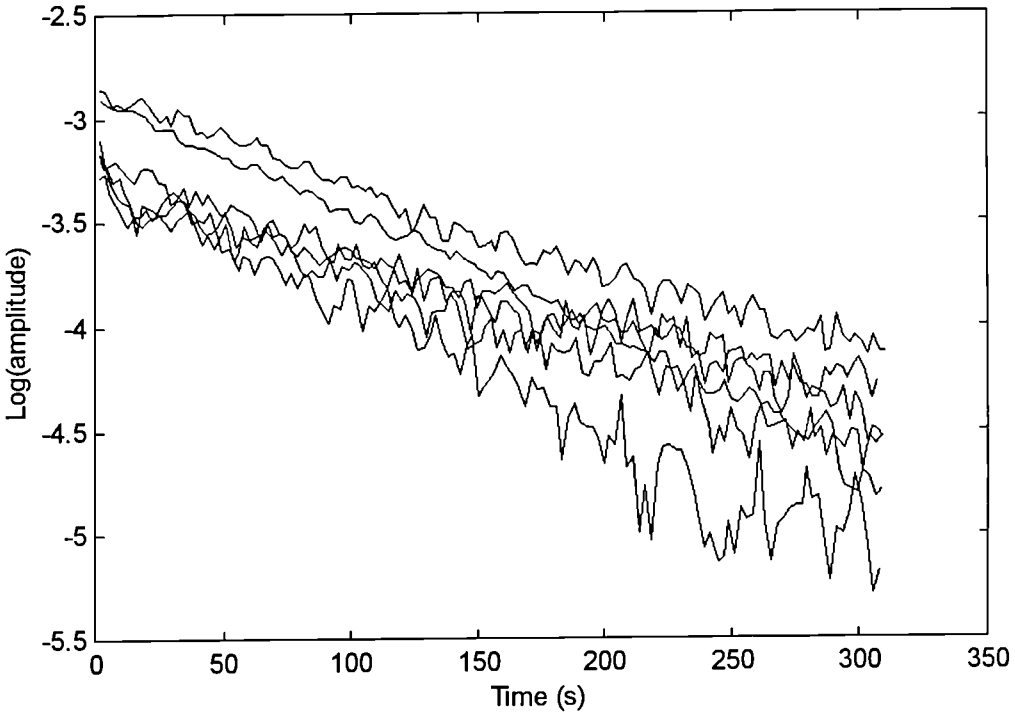

Fig. 10-5 Free decay of vibrations of Cable 61N before waxing

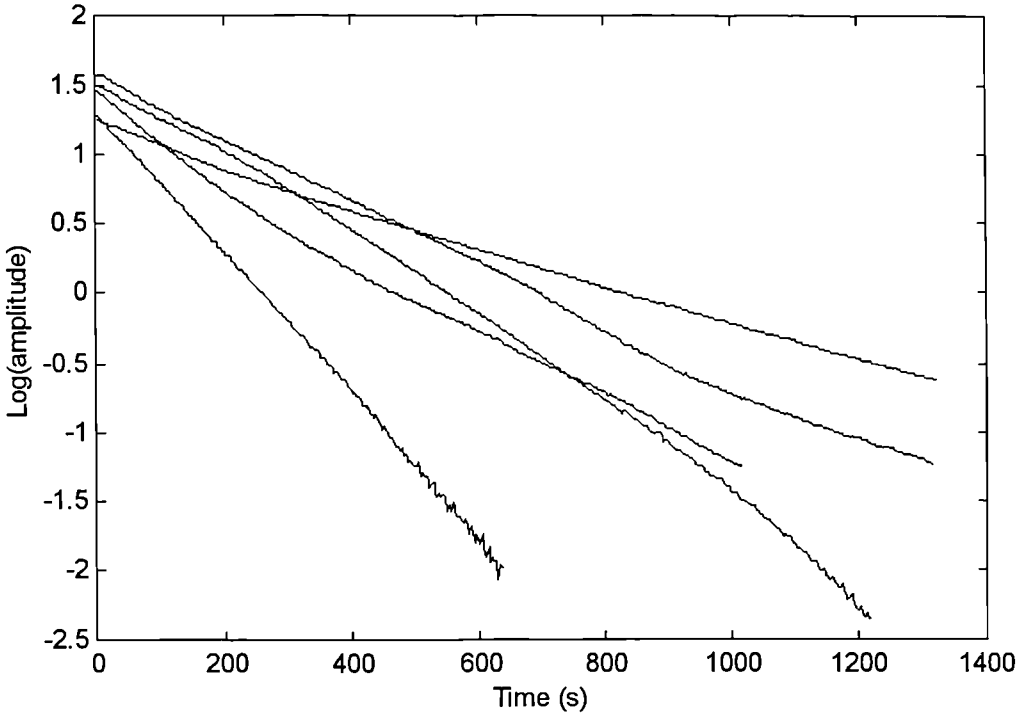

Fig. 10-6 Free decay of vibrations of Cable 61N after waxing

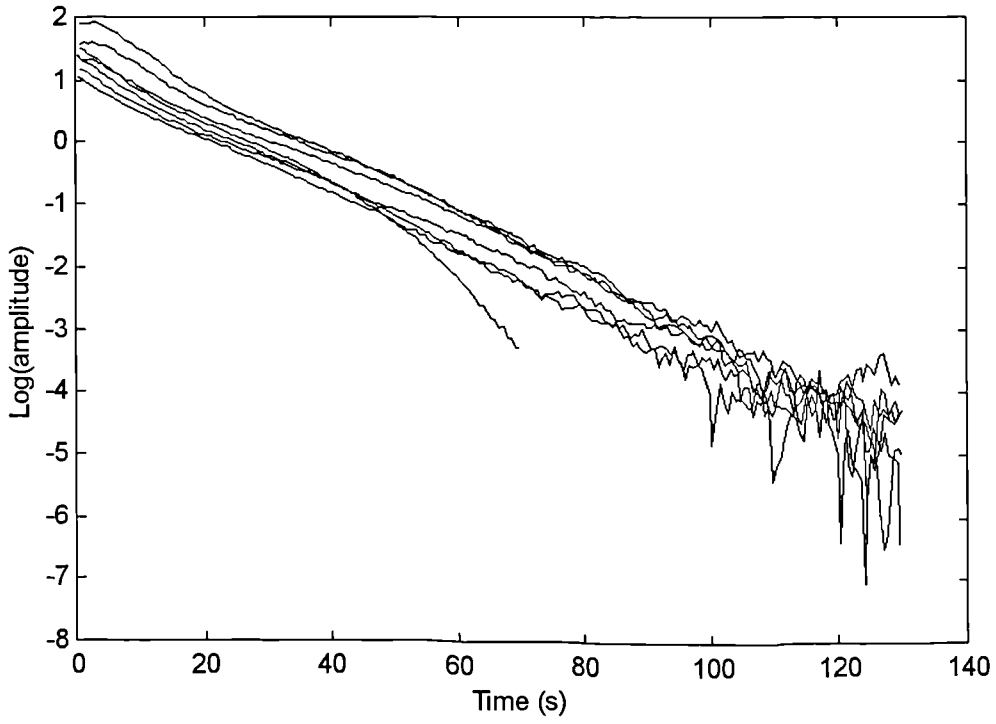

Fig. 10-7 Free decay of vibrations of Cable 85N before waxing

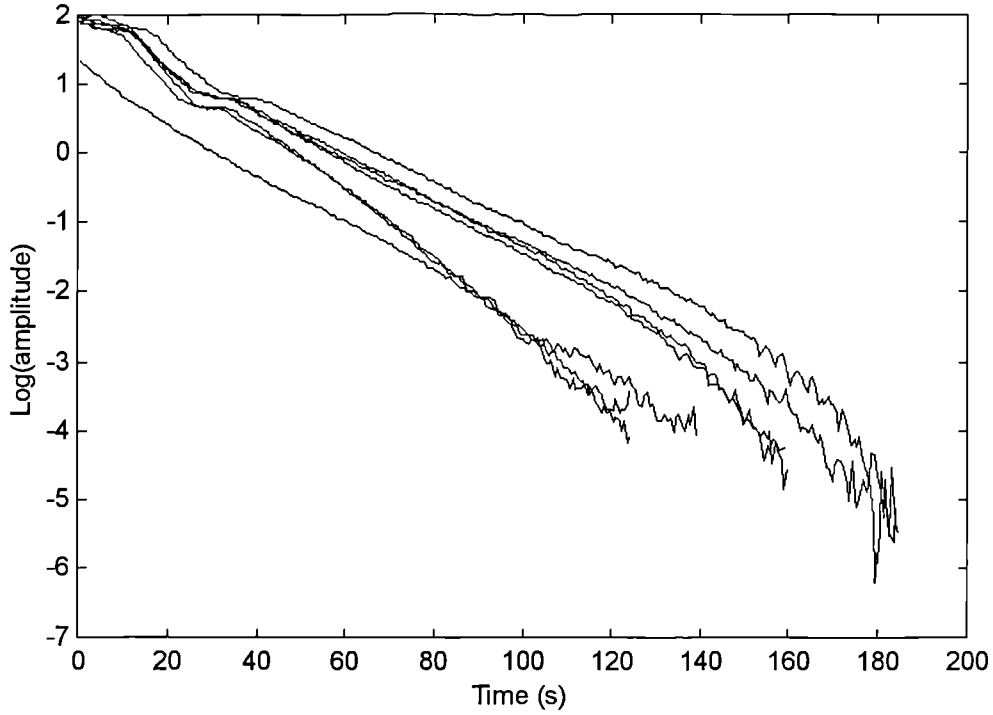

Fig. 10-8 Free decay of vibrations of Cable 85N after waxing

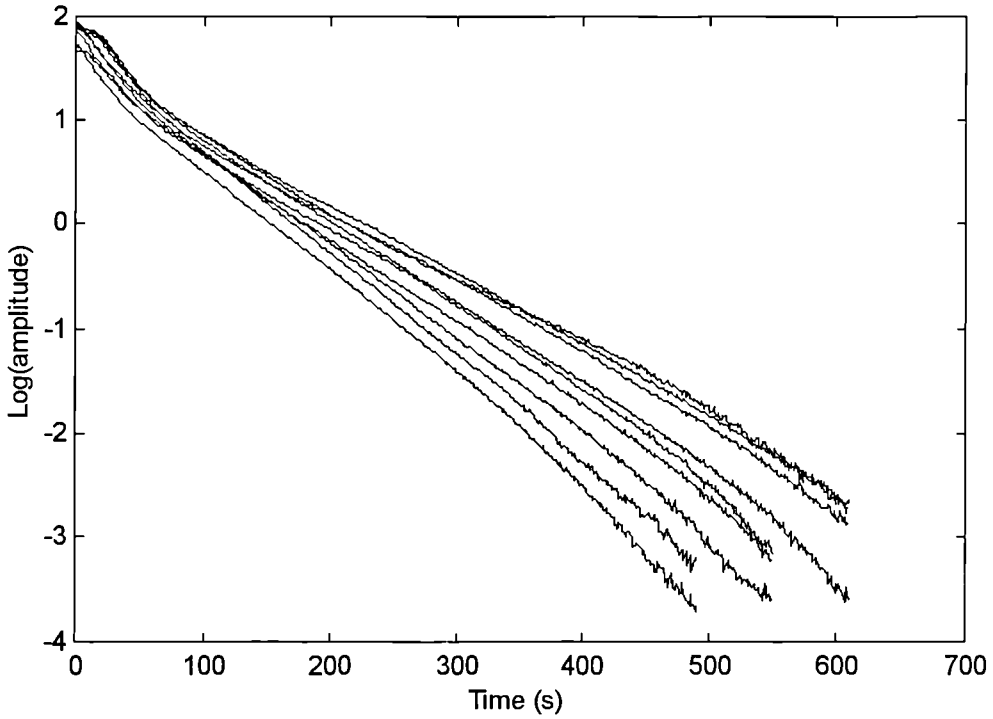

Fig. 10-9 Free decay of vibrations of Cable 101N before waxing

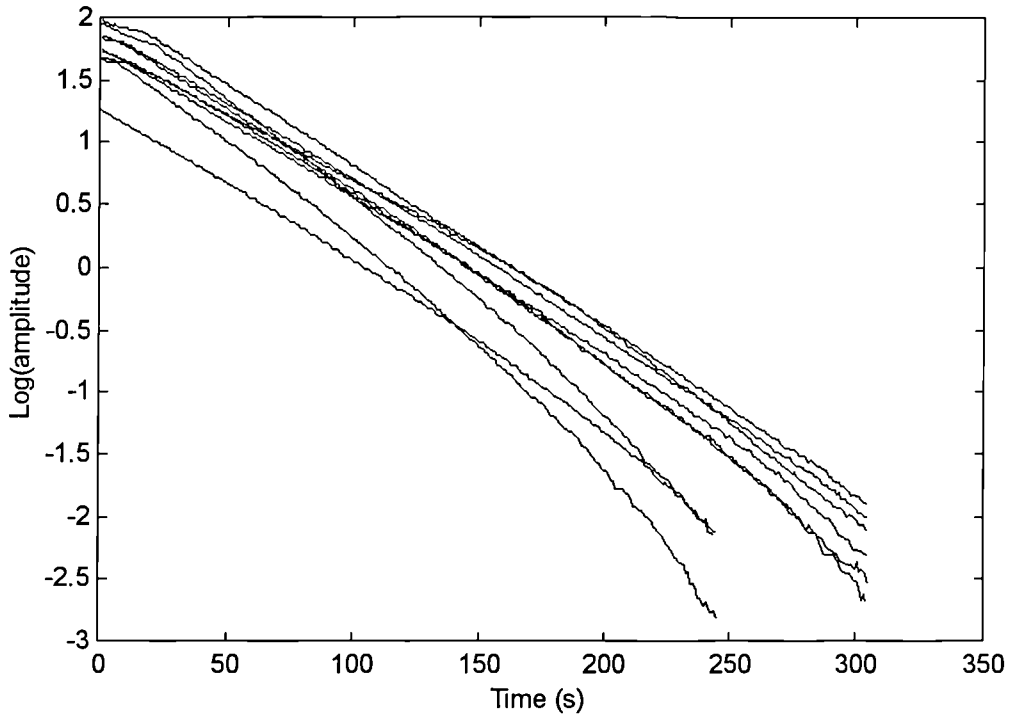

Fig. 10-10 Free decay of vibrations of Cable 101N after waxing

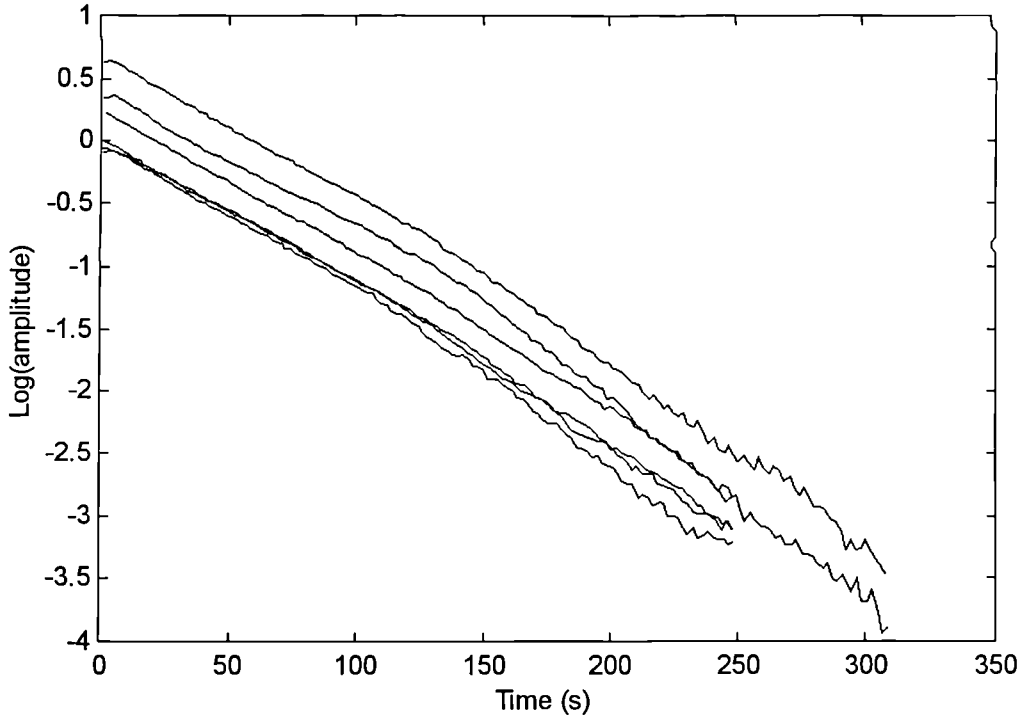

Fig. 10-11 Free decay of vibrations of Cable 119S before waxing

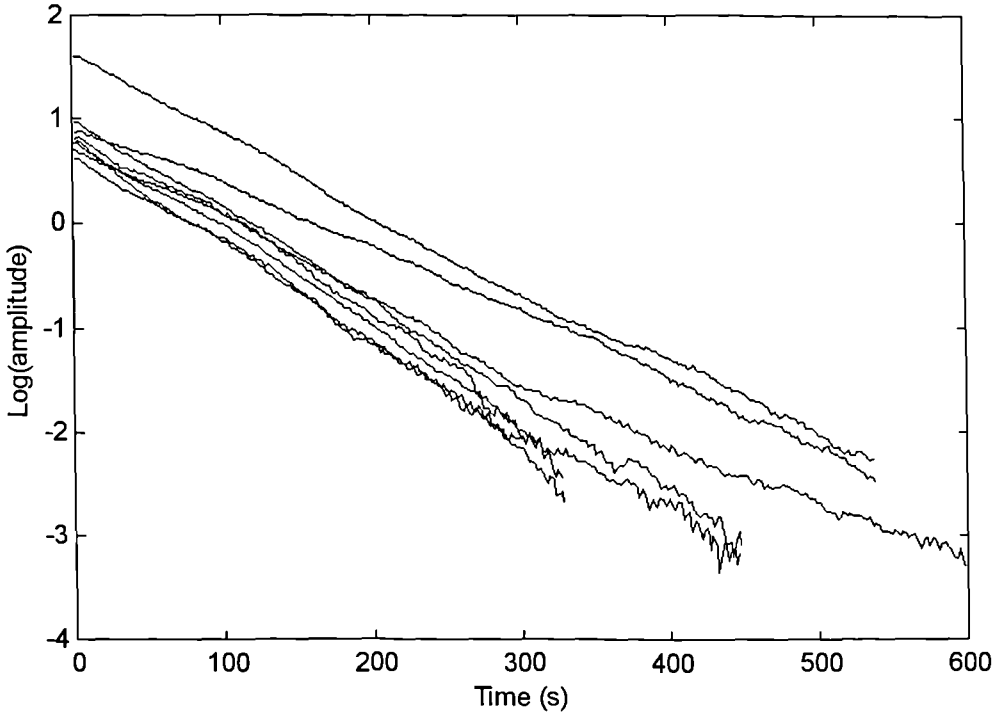

Fig. 10-12 Free decay of vibrations of Cable 119S after waxing

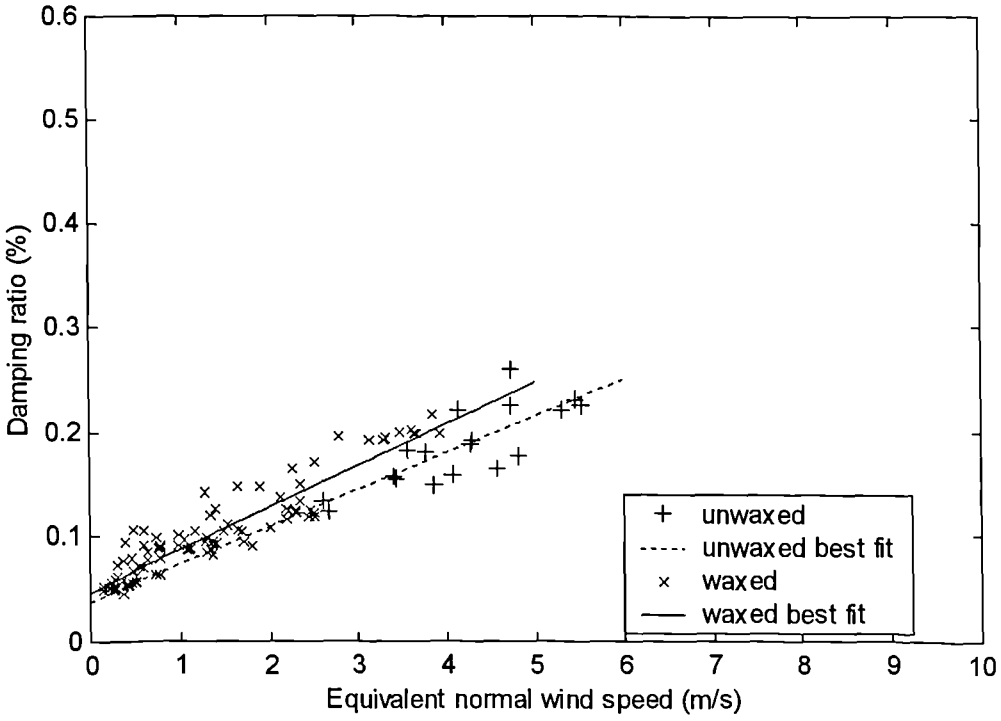

Fig. 10-13 Damping against equivalent normal wind speed (equation (10-6)) for one minute intervals of all tests on Cable 61N before and after waxing

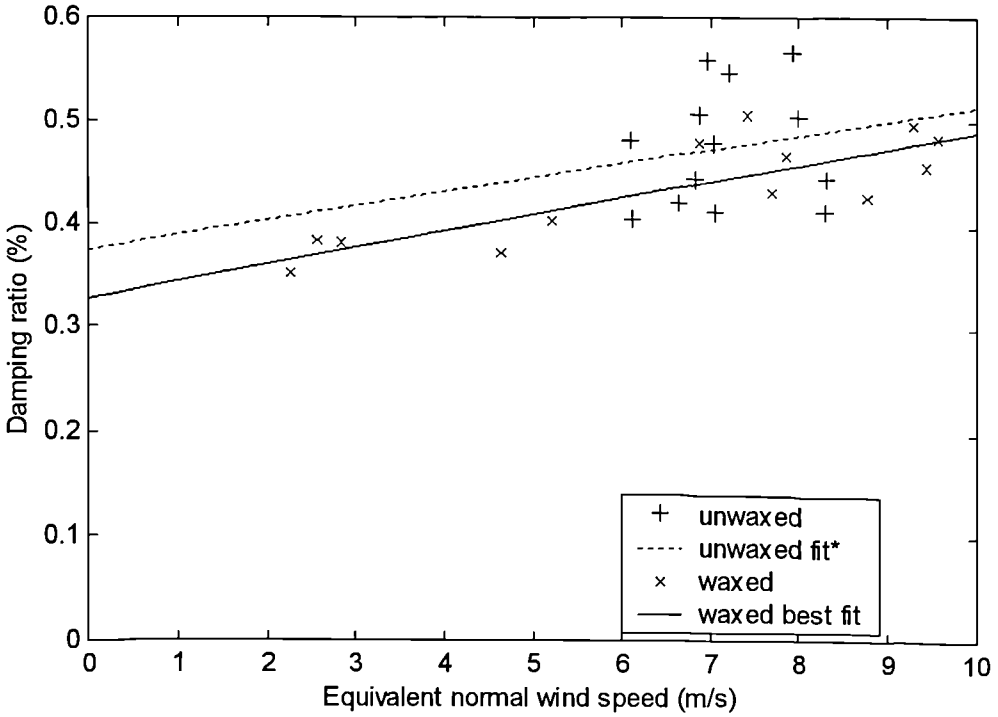

Fig. 10-14 Damping against equivalent normal wind speed (equation (10-6)) for one minute intervals of all tests on Cable 85N before and after waxing (* unwaxed line fitted using theoretical aerodynamic damping)

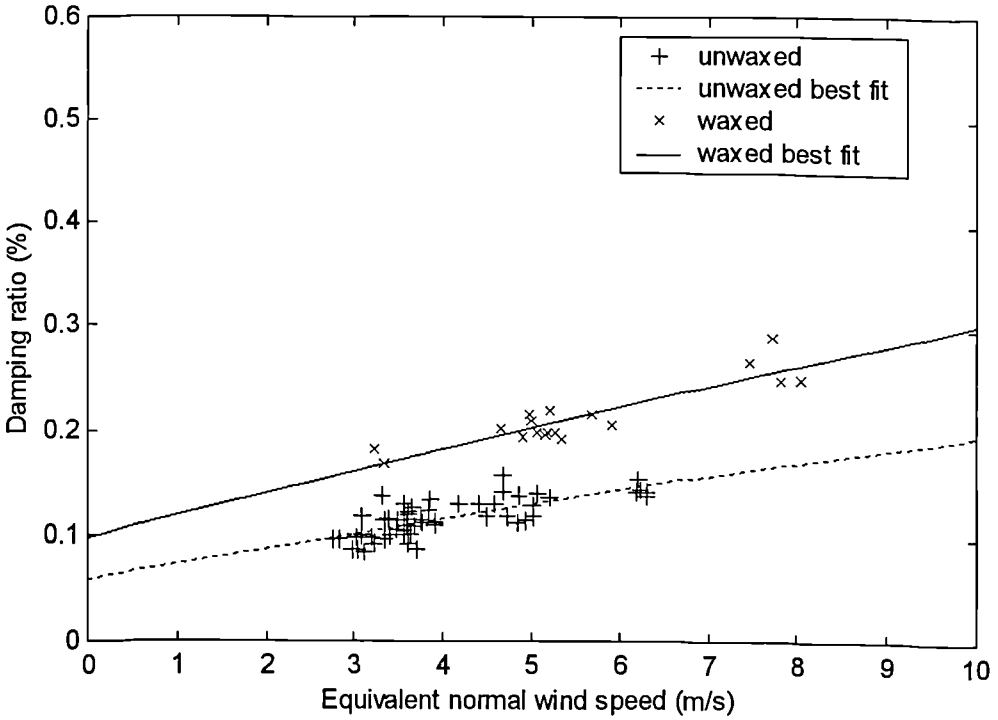

Fig. 10-15 Damping against equivalent normal wind speed (equation (10-6)) for one minute intervals of all tests on Cable 101N before and after waxing

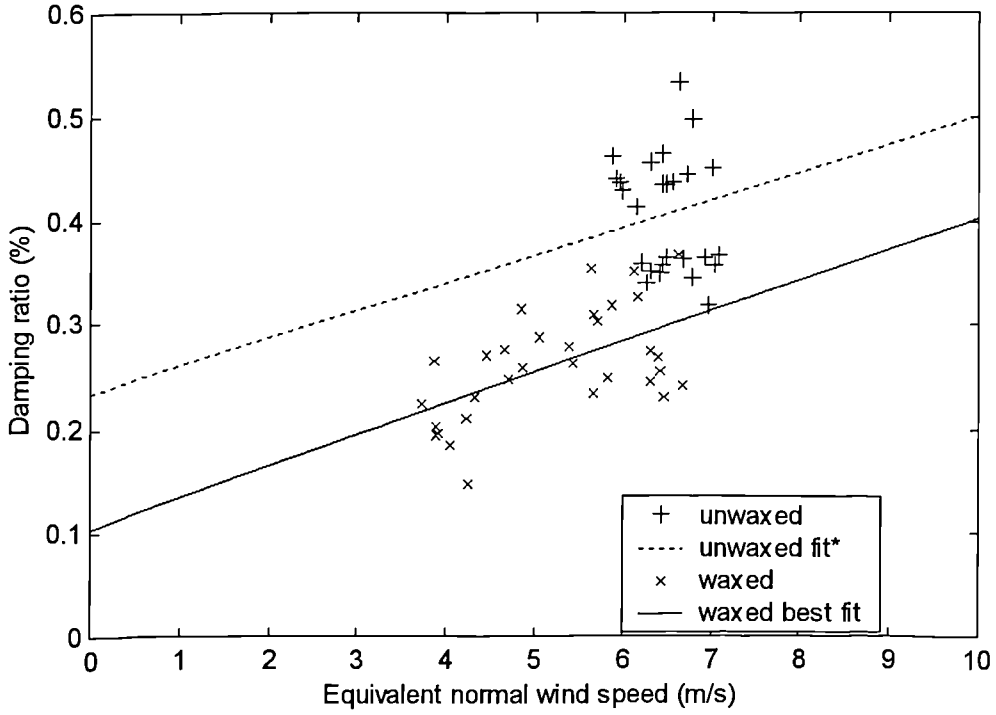

Fig. 10-16 Damping against equivalent normal wind speed (equation (10-6)) for one minute intervals of all tests on Cable 119S before and after waxing (* unwaxed line fitted using theoretical aerodynamic damping)

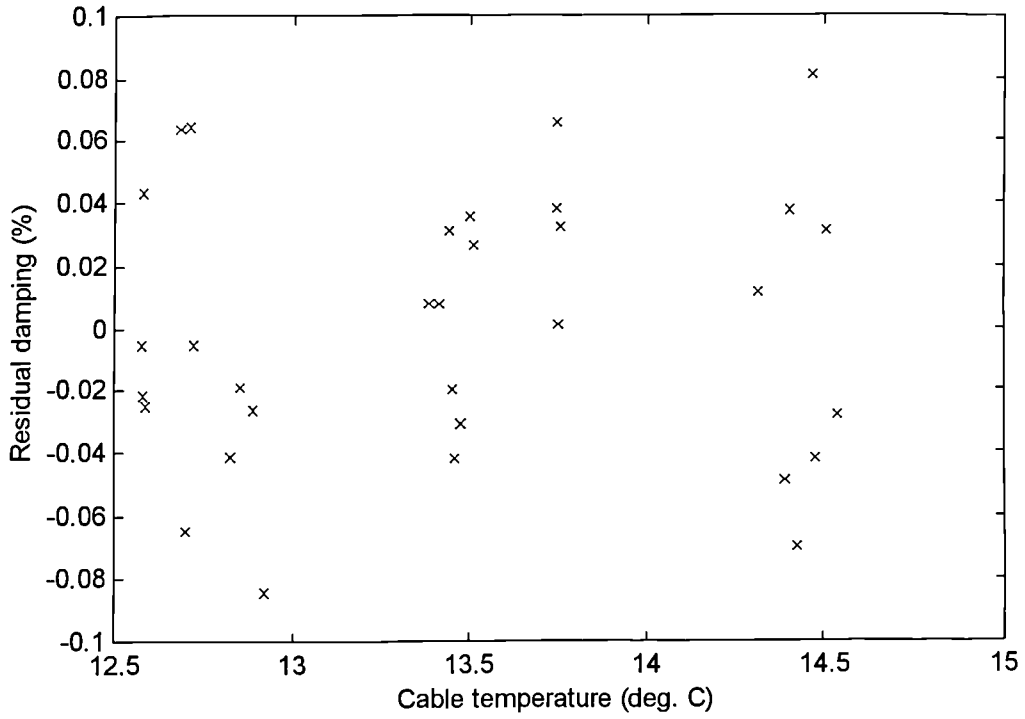

Fig. 10-17 Residual damping of cable, after subtraction of best-fit structural and aerodynamic damping estimate, against cable temperature for Cable 119S waxed

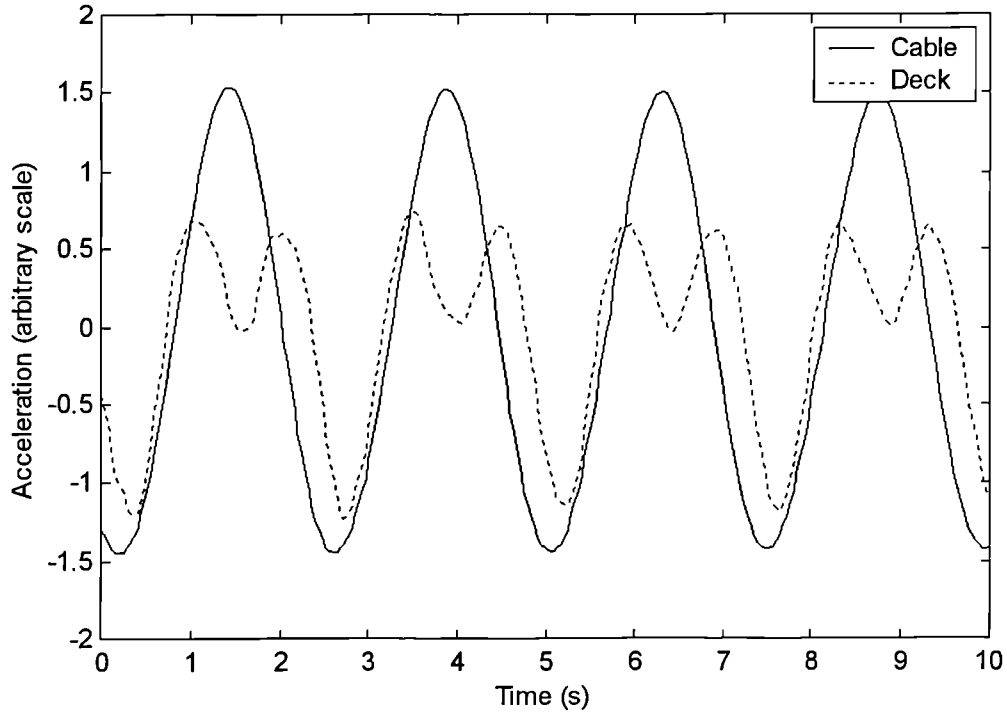

Fig. 10-18 Accelerations of Cable 61S in-plane and deck south vertical (end of cantilever) during additional test on Cable 61S (waxed) (both signals low pass filtered with cut-off frequency 1Hz)

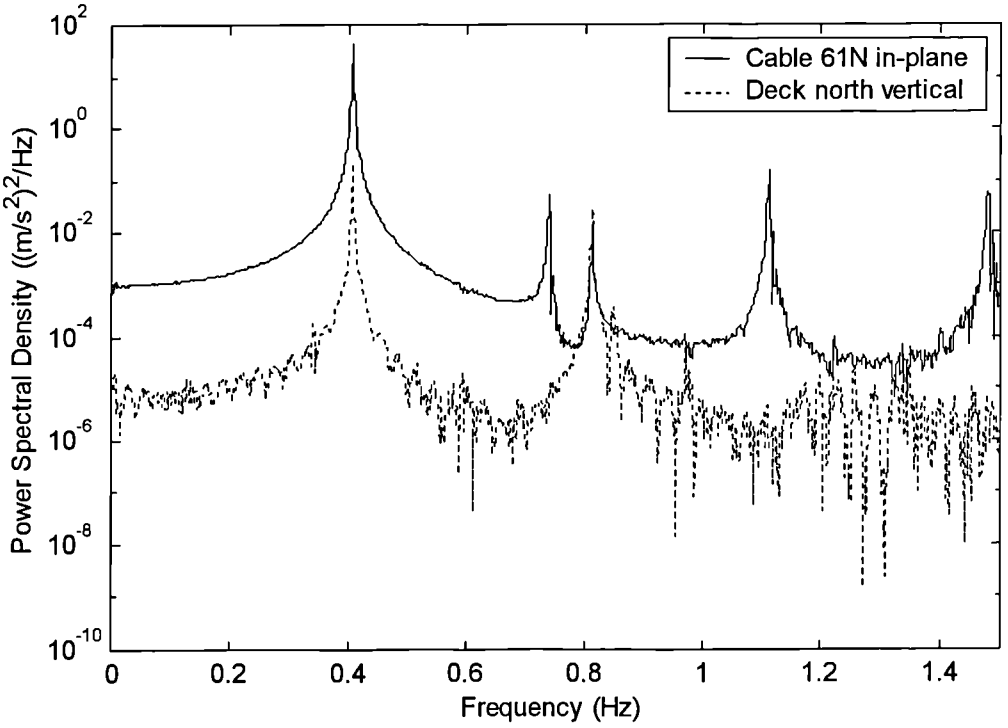

Fig. 10-19 PSDs of Cable 61N in-plane and deck north vertical (end of cantilever) accelerations during test of Cable 61N (waxed)

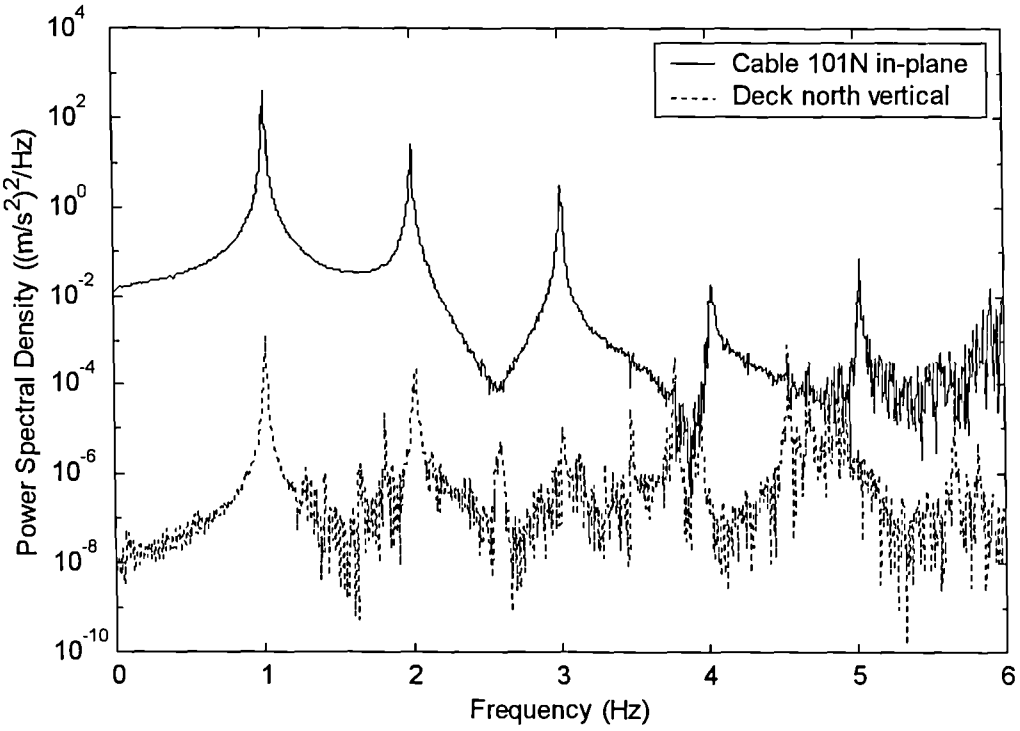

Fig. 10-20 PSDs of Cable 101N in-plane and deck north vertical (by cable) accelerations during test of Cable 101N (waxed)

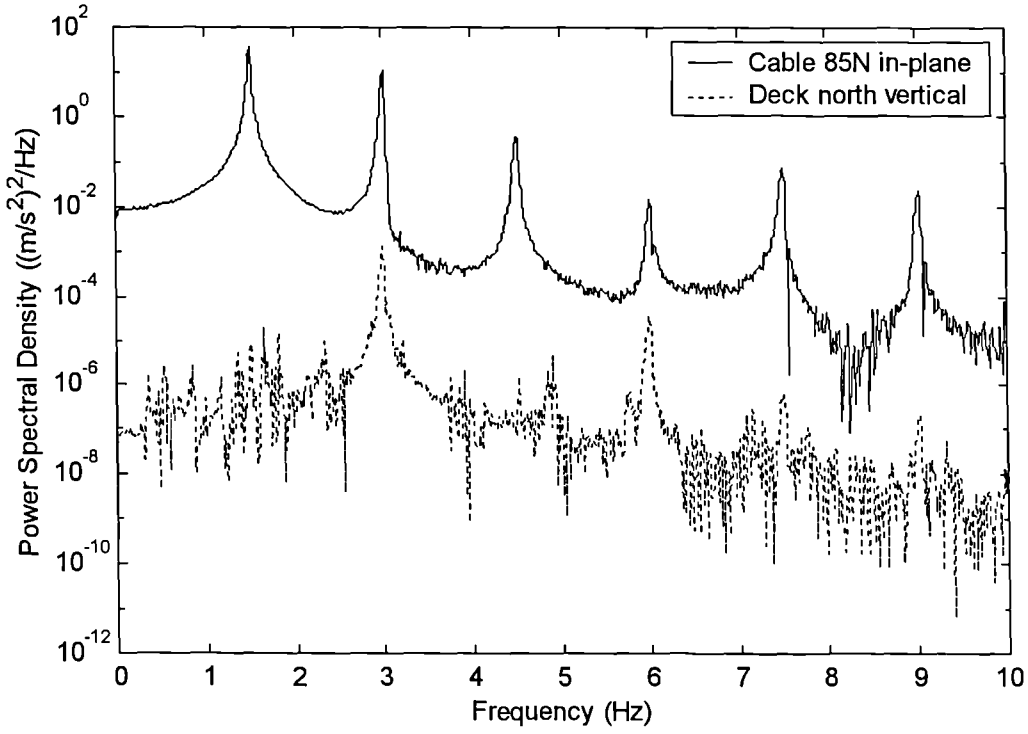

Fig. 10-21 PSDs of Cable 85N in-plane and deck north vertical (end of cantilever) accelerations during test of Cable 85N (waxed)

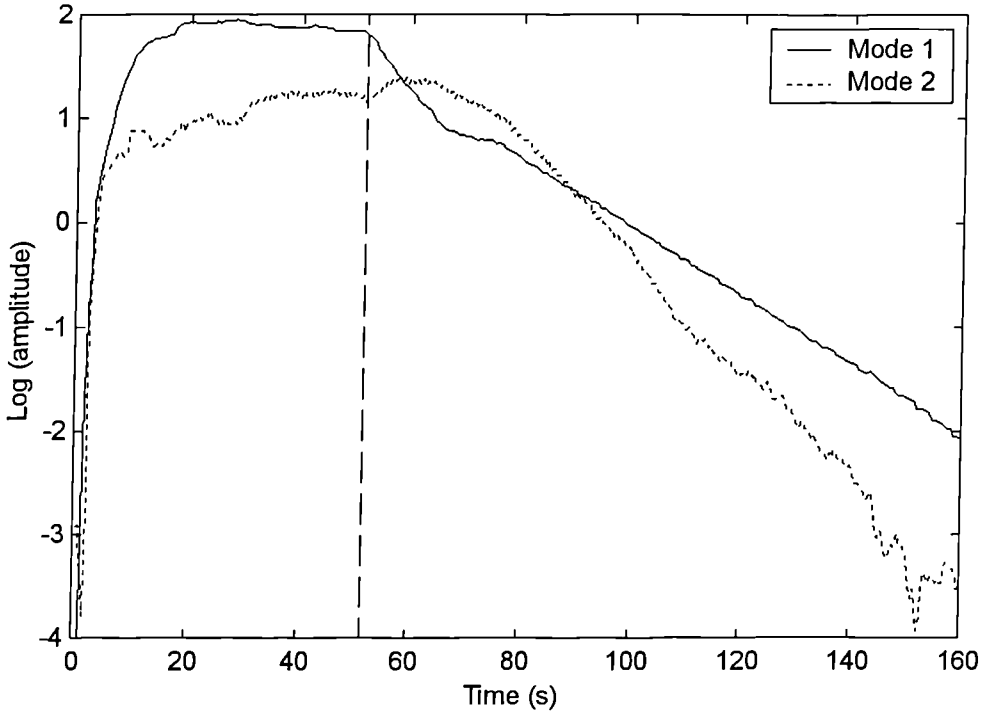

Fig. 10-22 Amplitudes of first two modes of Cable 85N (waxed) during excitation and free decay (vertical dashed line indicates time of cessation of excitation)

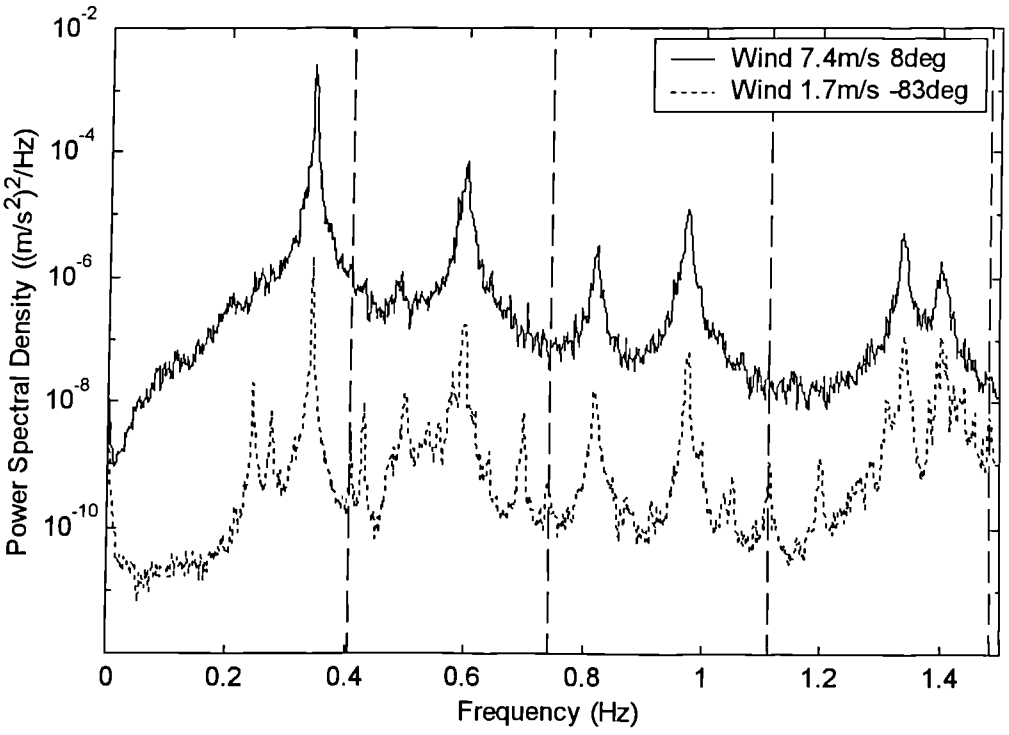

Fig. 10-23 PSDs of vertical acceleration of cantilever deck in different wind conditions (range 0-1.5Hz) (vertical dashed lines indicate in-plane natural frequencies of Cable 61N)

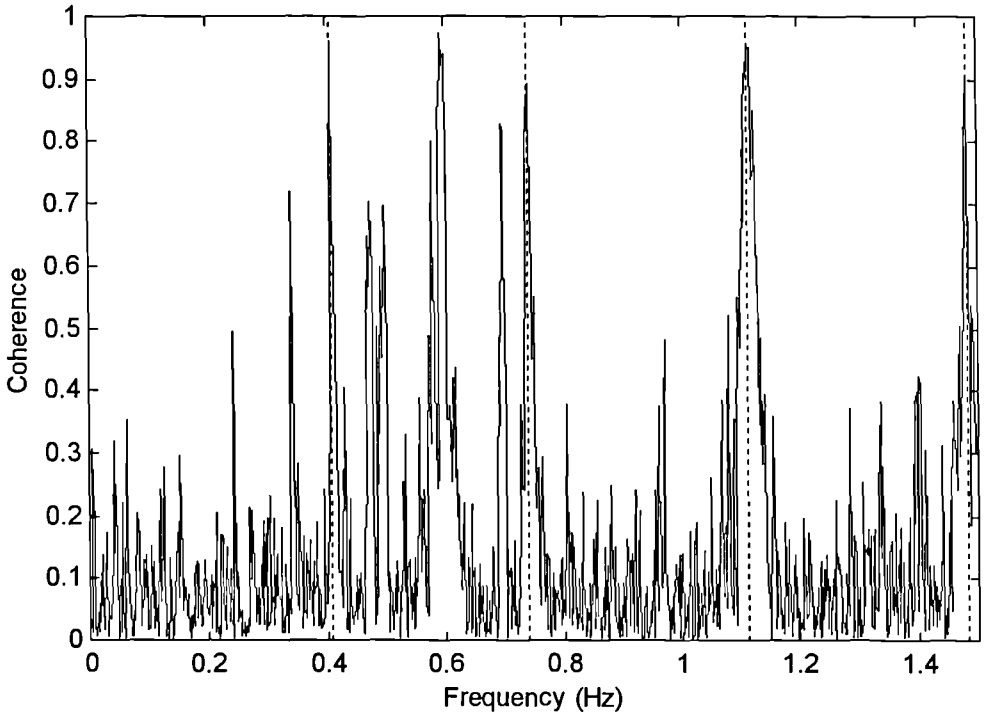

Fig. 10-24 Coherence between vertical acceleration of north side of cantilever deck and in-plane acceleration of Cable 61N, Wind 1.7m/s -83° (range 0-1.5Hz) (vertical dotted lines indicate in-plane natural frequencies of Cable 61N)

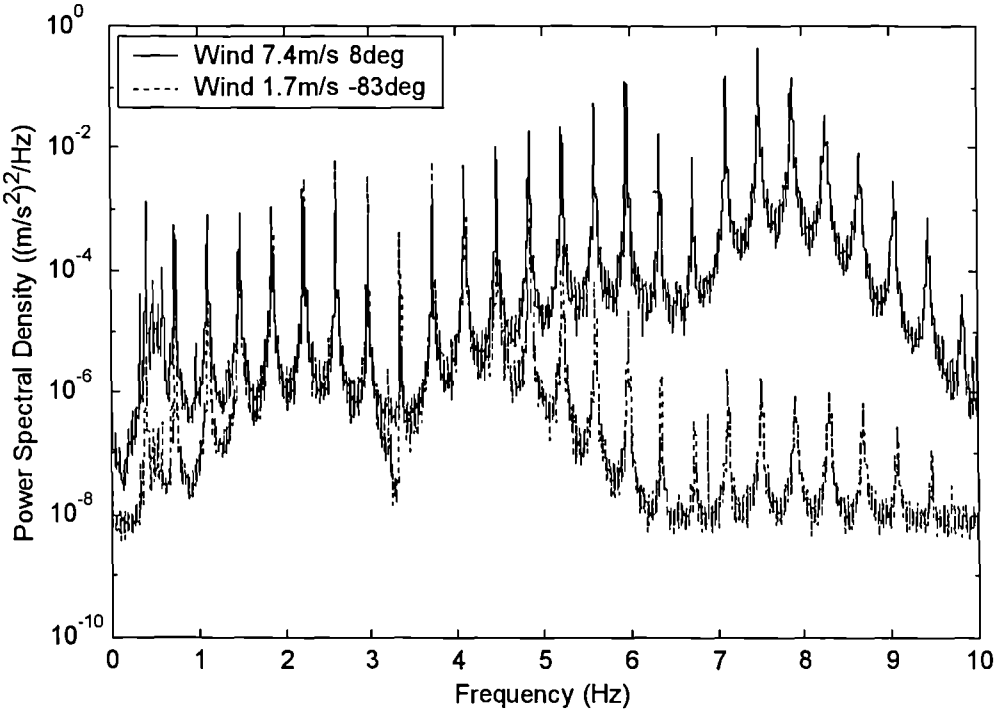

Fig. 10-25 PSDs of in-plane acceleration of Cable 61N in different wind conditions

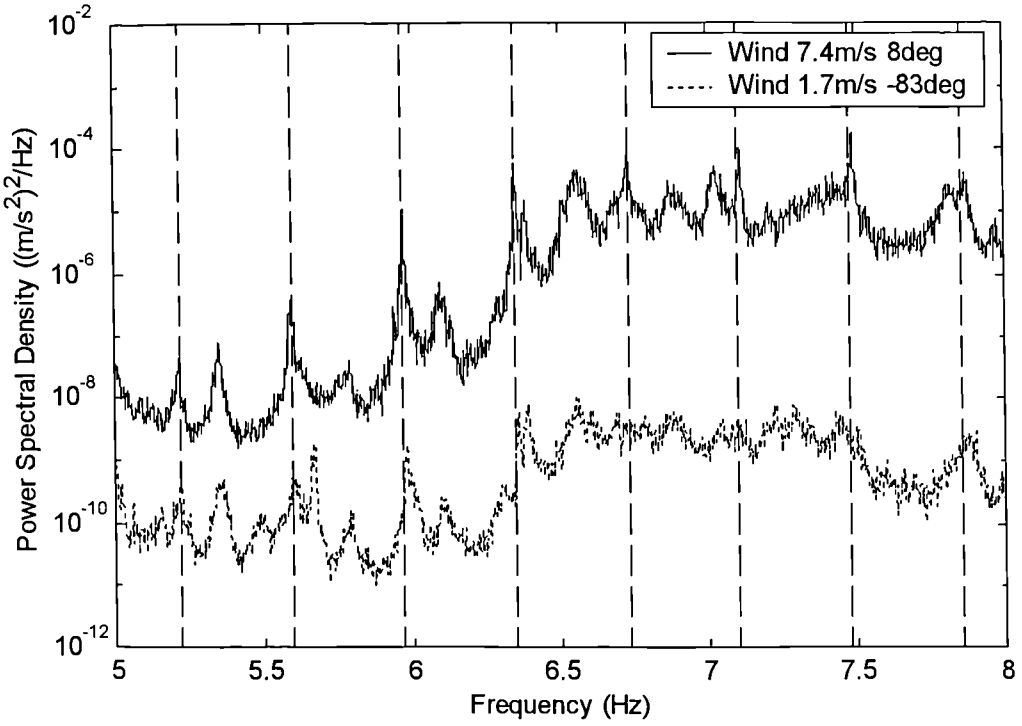

Fig. 10-26 PSDs of vertical acceleration of cantilever deck in different wind conditions (range 5-8Hz)
(vertical dashed lines indicate in-plane natural frequencies of Cable 61N)

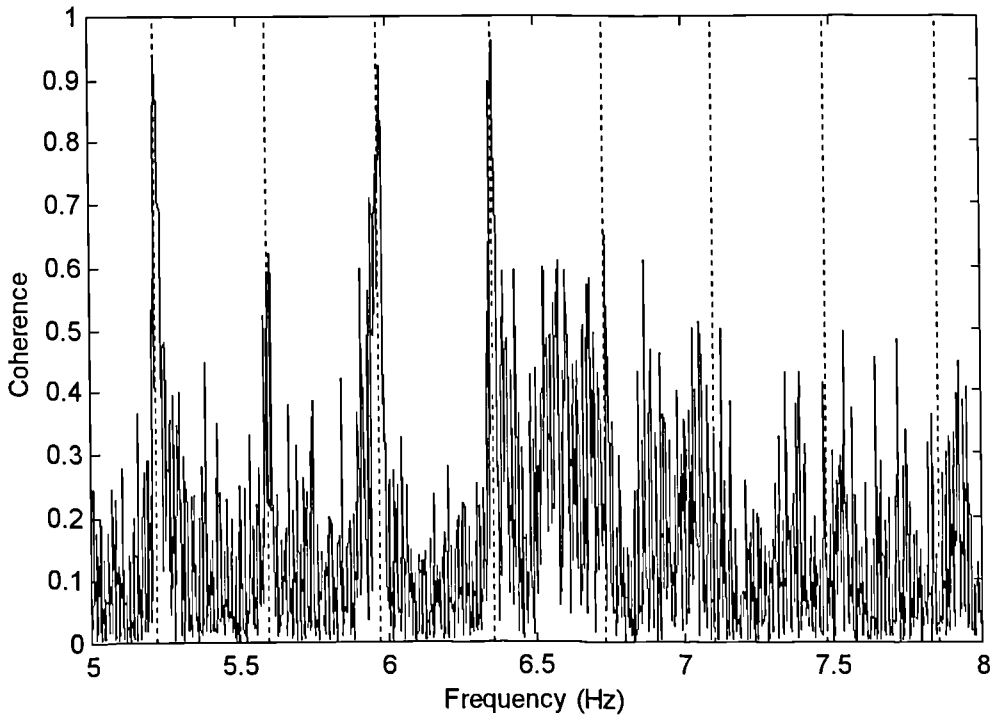

Fig. 10-27 Coherence between vertical acceleration of north side of cantilever deck and in-plane acceleration of Cable 61N, Wind 1.7m/s -83° (range 5-8Hz)
(vertical dotted lines indicate in-plane natural frequencies of Cable 61N)

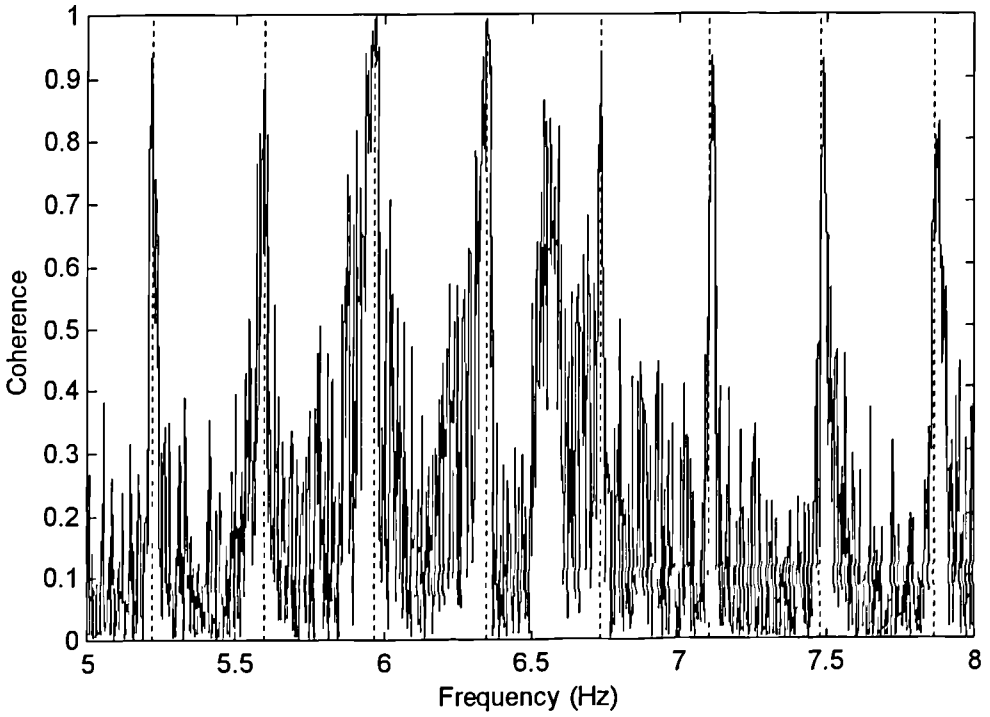

Fig. 10-28 Coherence between vertical acceleration of north side of cantilever deck and in-plane acceleration of Cable 61N, Wind 7.4m/s 8° (range 5-8Hz) (vertical dotted lines indicate in-plane natural frequencies of Cable 61N)

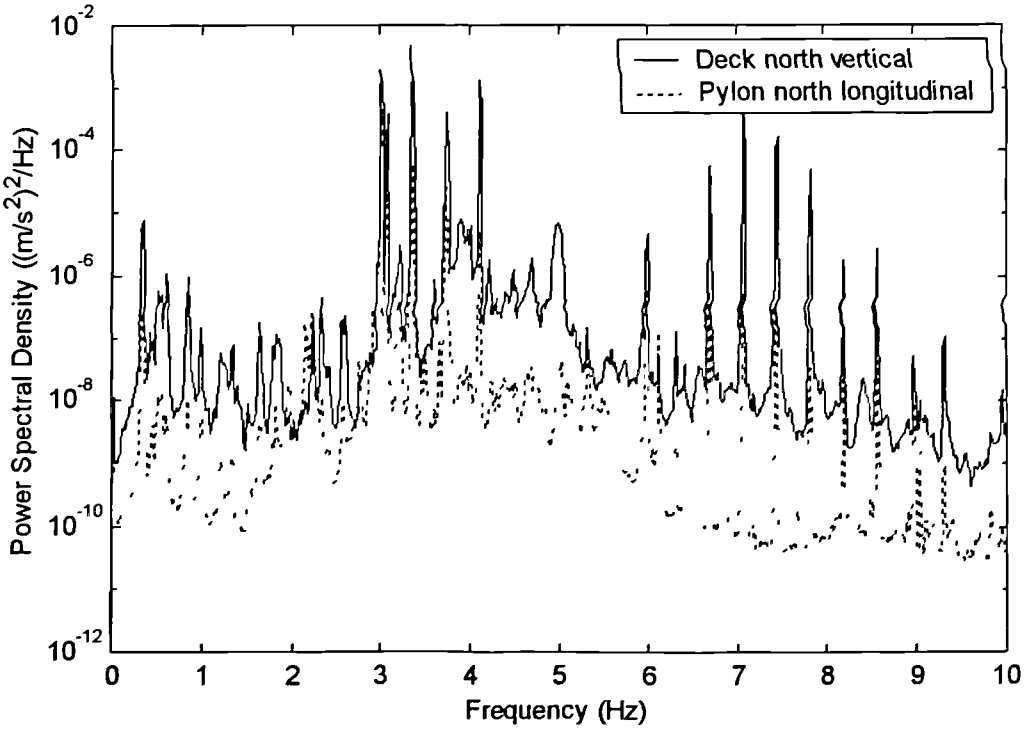

Fig. 10-29 PSDs of deck and pylon accelerations showing response at in-plane natural frequencies of Cable 61N in 6-9Hz range

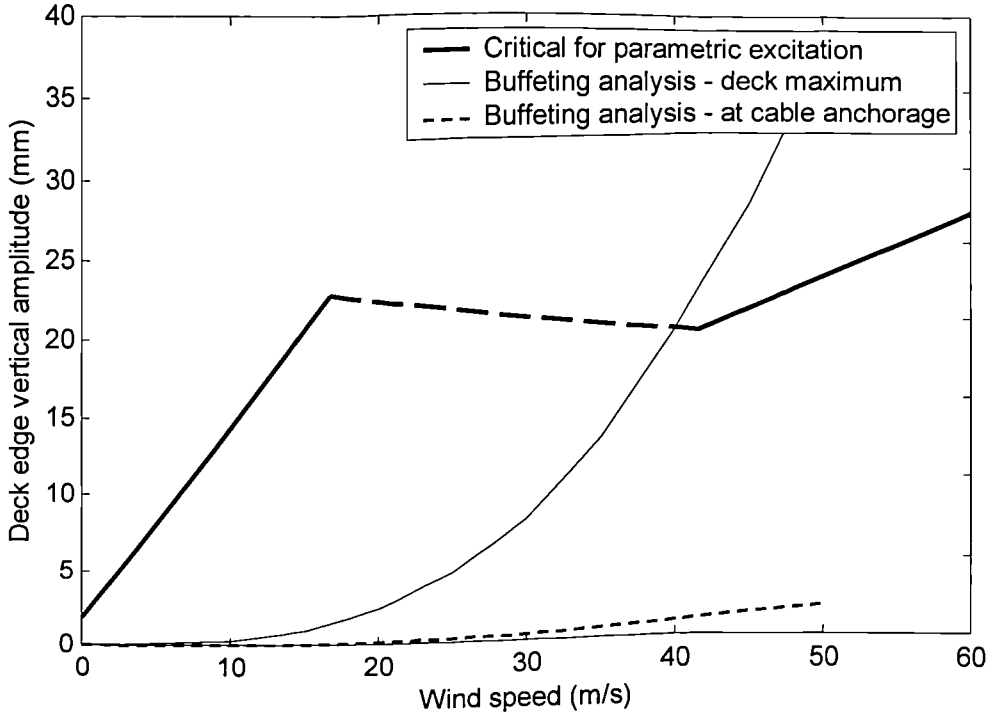

Fig. 10-30 Predicted amplitude of buffeting vibrations of Deck Mode TL10 compared with critical amplitude for parametric excitation of Cable 61N, for varying wind speed

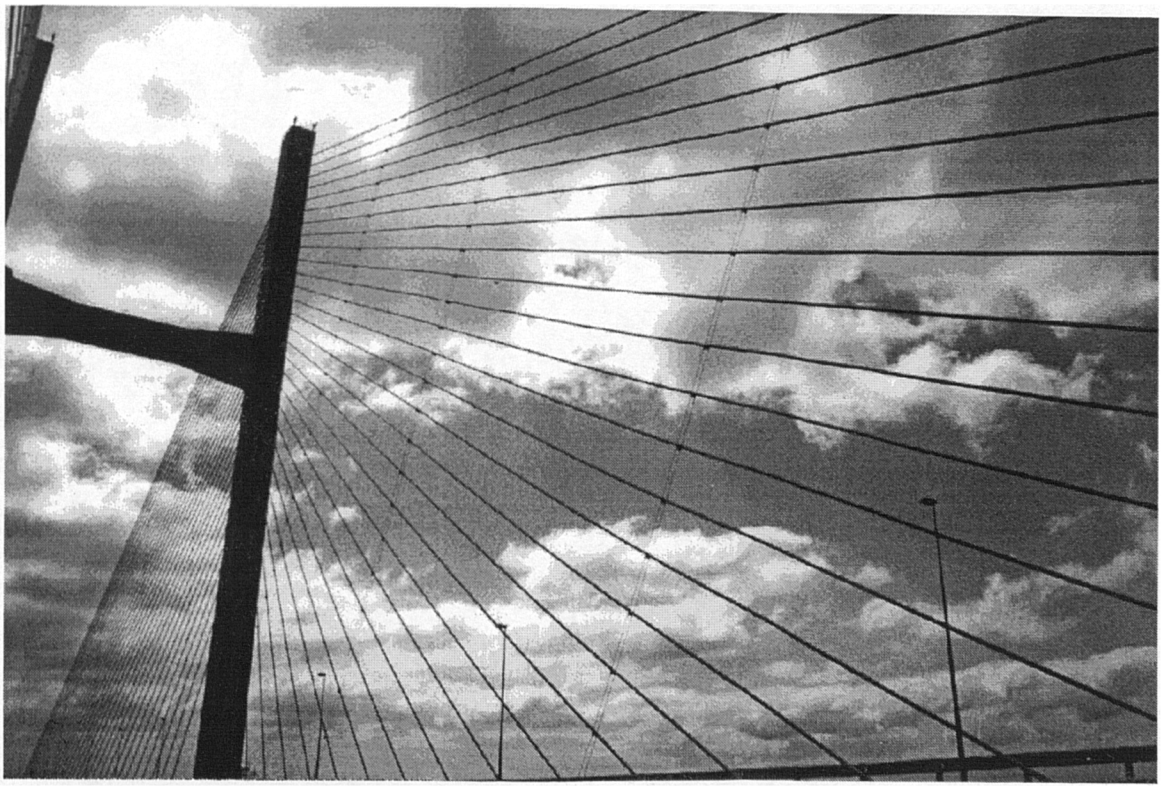

Fig. 10-31 Secondary cables installed to reduce cable vibrations

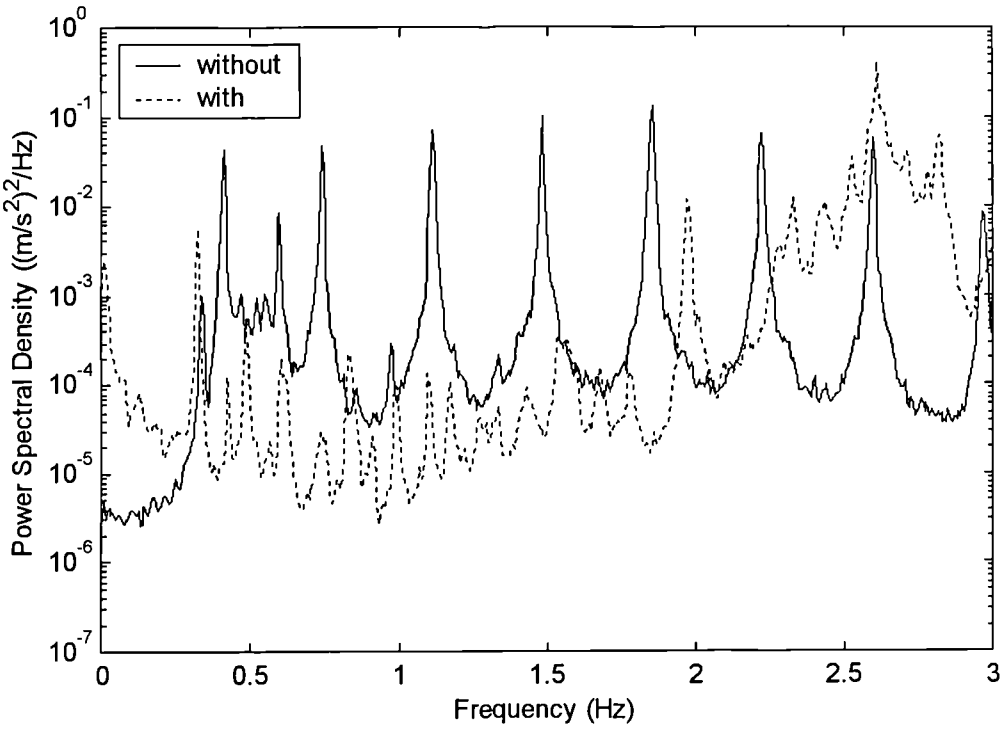

Fig. 10-32 PSDs of in-plane ambient vibrations of Cable 61N with and without secondary cables

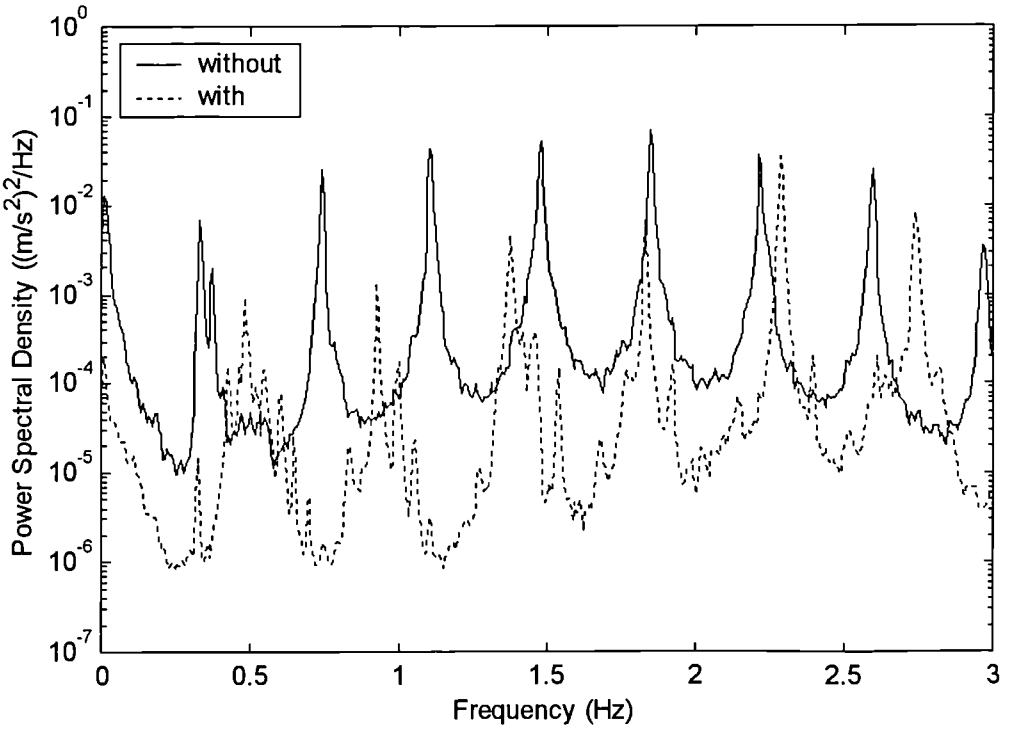

Fig. 10-33 PSDs of out-of-plane ambient vibrations of Cable 61N with and without secondary cables

CHAPTER 11 CONCLUSIONS AND RECOMMENDATIONS FOR FURTHER RESEARCH

11.1 Introduction

The objectives of the research were stated in §1.2. These have been addressed through the dynamic monitoring of the Second Severn Crossing (SSC) cable-stayed bridge, and analysis of the measured data. Although this study was based on the measurements from one particular bridge, the methods of analysis are widely applicable to ambient vibration tests on other structures, and the results can be applied generally to similar bridges. This chapter reviews the principal conclusions, particularly considering their wider application. A critical appraisal of the work is then given, and finally recommendations for further research, based on the results of this study.

11.2 Full-scale monitoring

In Chapter 2 the need for full-scale monitoring of cable-stayed bridges was demonstrated, particularly for tests over a significant period of time to capture the response in a variety of wind conditions (§2.6.4.4). The construction stage is especially vulnerable to dynamic effects, but little monitoring of it had previously been conducted (§2.10.1).

The monitoring of the SSC described in this thesis (Chapter 4) is believed to be the most comprehensive dynamic testing programme to have been undertaken on a cable-stayed bridge during construction. Monitoring was also continued for almost three years after completion of the bridge. Detailed processing of all of the data was beyond the scope of this thesis. The formation of this database provides opportunities for much further research into particular aspects of the behaviour (§11.6.2) and for the validation of analysis and modelling techniques (§11.6.1).

In parallel with the monitoring programme, the Computer Vision System (CVS) was developed, to enable the direct measurement of dynamic displacements from a remote location (§4.4). The accuracy of the system has been demonstrated and it has given increased confidence in the accelerometer measurements. Many video recordings of bridge vibrations have been made, synchronised with data acquisition from other instruments, to enable the future processing of unique dynamic displacement data, from near the centre of a cable-stayed bridge.

The monitoring programme and the data analysis in this study have given valuable insights into several aspects of the dynamic behaviour of cable-stayed bridges, including some aspects of their behaviour not previously identified at full scale (§11.4).

11.3 Improvements in ambient vibration data processing

To enable the accurate extraction of modal parameters from ambient vibration data, the Iterative Windowed Curve-fitting Method (IWCM) has been developed (Chapter 7). It has also been validated using simulated data (§7.5). The three improvements over the conventional curve-fitting method (§5.3.2.1) are:

i) Elimination of the effects of bias errors in spectral estimates (§7.4).

ii) Consideration of a realistic loading spectrum, rather than white noise (§7.6).

iii) Consideration of the combined response of multiple modes, rather than each mode being treated in isolation (§7.7).

For application to the SSC data, an estimated wind loading spectrum was derived (§6.5).

The IWCM yields more accurate modal parameters, especially damping, than previously possible from ambient vibration data. It also allows direct comparison of measured and fitted spectra, enabling discrepancies to be identified, indicating other aspects of the dynamic behaviour, for example the existence of additional modes (§8.5). The method is applicable to any ambient vibration data, particularly where a realistic loading spectrum can be estimated and the modes are reasonably well spaced.

11.4 Improved understanding of the dynamic behaviour of cable-stayed bridges

The data acquired from the SSC were processed using the IWCM and other methods to determine the detailed dynamic characteristics of the structure. Where possible, these were compared with the behaviour predicted by theoretical analyses or models to improve the understanding of the dynamic behaviour of cable-stayed bridges. This study concentrated on the response of a single complete cantilever and of the finished bridge.

11.4.1 Global natural frequencies and mode shapes of vibration

Natural frequencies and mode shapes of over 30 global modes of the SSC cantilever were determined below 2.6Hz, using the IWCM. They agreed well with the results of a 3-D Finite Element (FE) model (§8.3), thus validating the methods of monitoring, data analysis and FE modelling of the structure, particularly of the deck (§3.3). 33 modes of the finished bridge were also identified from the measurements. The natural frequencies

and mode shapes of the structure in these states, and at other construction stages, are available for assessing methods of model updating for cable-stayed bridges.

11.4.2 Global damping

The long-term site records (§4.5.4) and the application of the IWCM, enabled estimates of the modal damping ratios to be made, more accurately than otherwise possible from ambient vibration data. Thus, from a large number of estimates in different wind conditions, estimates of the components of aerodynamic and structural damping for each mode were obtained (§8.4). It is believed this is the first time that these components have been separated in full-scale tests on a long-span bridge with a bluff cross-section (§2.6.3.1).

For the first few vertical deck modes, the aerodynamic damping was approximately half of the value predicted by quasi-static theory (Davenport 1962a, §2.6.3). It is therefore recommended that the full benefit of this additional damping, according to this theory, should not be assumed in design. For torsional deck modes the theory gave more reasonable predictions, and for lateral modes it appeared to significantly underestimate the aerodynamic damping, although this was often believed to be due to a larger contribution from the torsional components of the same modes.

The structural damping, for vibrations due to traffic and light to moderate winds, was approximately 0.3% of critical for the first few modes of the finished bridge. This is considerably less than the value of 0.64% for composite bridges from the British design rules for aerodynamic effects on bridges (DETR 1993), although this higher value may be appropriate for composite bridges of other structural forms. The values measured on the SSC are at the lower end of the range of previous damping estimates from full-scale cable-stayed bridges (§2.5.1), which include values of 0.22-1.4% for the first bending modes of 22 bridges in Japan (Narita & Yokoyama 1991). The values found in this study are believed to be low partly due to the subtraction of the contribution of aerodynamic damping from the measured damping, in contrast with previous estimates. It is recommended that in design, structural damping of approximately 0.3% be assumed for composite cable-stayed bridges with a fan cable arrangement. For steel cable-stayed bridges the damping is likely to be even lower.

Values of structural damping for the cantilever and the finished bridge were comparable, suggesting that estimates made on a bridge during construction could be used to improve predictions of the behaviour of the completed structure.

11.4.3 Variations in modal behaviour

The mass of traffic on the finished bridge was found to cause changes in natural frequencies of deck-dominated modes by up to 1% with typical variations in traffic density. This, and the effect of aerodynamic damping, dominated variations in the natural frequencies and damping, so no other systematic variations in modal parameters, for example due to temperature changes or non-linearities, were detected.

Apart from some evidence of cable-deck interaction (§11.4.7), no non-linear structural behaviour was identified, indicating that for traffic and moderate wind loading linear dynamic analysis is appropriate.

There was some evidence of coupling of modal responses, which had not previously been observed on a cable-stayed bridge at full scale. There appeared to be aeroelastic coupling of the first two modes (lateral/torsional and vertical) of the cantilever, which increased in stronger winds (§8.5.5). For the buffeting response of the pylon, there were several closely-spaced modes, possibly caused by cable-deck (or rather cable-pylon) interaction, which also appeared to be coupled (§8.5.3), believed to be due to correlation of the generalised loads of the modes (§2.4.2).

Both of these forms of modal coupling are addressed by recent multi-mode analysis methods (e.g. Jain et al. 1996, Katsuchi et al. 1999, §2.6.6). The effects may become more pronounced in stronger winds or for longer bridges, so these methods should be considered further. The data from the SSC tests acquired in this study could be of value for validating these methods.

The aeroelastic coupling is believed to have occurred due to the natural frequencies being closer than expected (by 17%), possibly caused by foundation flexibility. This could lead to a significant drop in the critical wind speed for classical flutter. It is recommended that in design the effect of inaccuracies of this magnitude in the estimated natural frequencies be considered, including for construction stages.

11.4.4 Amplitudes of buffeting vibrations

For the finished bridge, dynamic traffic loading was found to be dominant for wind speeds below approximately 12m/s (or 9m/s for light traffic) (§6.6). In higher wind speeds the wind loading became dominant in the 0.3-1.5Hz frequency range, corresponding to the first few natural frequencies of the structure.

The amplitudes of deck vibrations for the finished bridge compared reasonably with the results of the design buffeting analysis (Xie et al. 1994, §8.6). This indicates that the conventional method of analysis by Irwin (1977), assuming uncoupled modal responses, is adequate for typical cable-stayed bridges in moderate winds, and that his expression

for aerodynamic admittance is reasonable for a bluff deck cross-section. On the SSC, the damping and the wind turbulence were both found to be considerably lower than anticipated in the analysis, but the effects of these errors on the response amplitude tended to cancel each other out. The design buffeting analysis was less accurate for lateral deck vibrations, overestimating the response by a factor of approximately two, possibly due to the greater aerodynamic damping than predicted for these modes.

Indirect comparison with the results of the full aeroelastic model test (Xie et al. 1994) suggest that the model gave a good prediction of the full-scale vertical response but overestimated the torsional and lateral responses by approximately 80%.

The amplitudes of vibration of the cantilever compared with the finished structure were up to three times greater, with the greatest difference occurring for lateral vibrations. The addition of the traffic wind barriers caused increases in responses of 50% vertically, 100% torsionally and 150% laterally.

11.4.5 Vortex-induced vibrations and wind tunnel testing

Vortex-induced vibrations of the SSC occurred in the first mode (0.326Hz) on several occasions, with amplitudes of up to 266mm measured and an estimated maximum of 320mm (§9.3). The wind conditions that initiated the vibrations were determined from the site measurements. They included critical ranges for the wind direction and component of wind velocity normal to the bridge axis, but the turbulence intensity and duration of the critical conditions were also significant (§9.4). Very low levels of turbulence widened the ranges of other parameters that caused large vibrations. Measurements from a single anemometer were insufficient to precisely define the criteria, so it was concluded that the spatial variation of the wind velocity is important in causing vortex-induced vibrations.

The wind tunnel study (Xie et al. 1994) underestimated the amplitude of vortex-induced vibrations by a factor of approximately five for the model test that was expected to be most comparable (§9.5). This was due to the low structural damping (§8.4.3) and low wind turbulence (§6.4.2) for the real structure, each causing underestimation of the response by approximately a factor of two. It is recommended, for bridges with a long stretch of water within 15° of normal to the bridge axis, that wind tunnel testing for vortex-induced vibrations be undertaken in smooth flow.

Allowing for these discrepancies, the error in the wind tunnel test results, compared with site measurements, was still up to 25%. This degree of error should be allowed for in the interpretation of such test results.

Baffles were added beneath the bridge deck to alter its aerodynamic profile. These were shown to be effective in inhibiting the vortex-induced vibrations (§9.6).

11.4.6 Cable damping

Theoretical expressions have been proposed for the aerodynamic damping of an inclined cable for an arbitrary wind velocity (§10.5). The expression for in-plane vibrations has been validated by site measurements (§10.6.2). It is believed this is the first time that the contributions of aerodynamic and structural damping of cable vibrations have been separated correctly. The aerodynamic damping is significant compared with the structural damping, becoming dominant for wind speeds above approximately 5m/s, or less for longer cables. It is recommended, for future tests, that values estimated from the proposed expressions be subtracted from measured damping to estimate the structural damping.

The structural damping of one of the longest SSC cables (236m long) was found to be only 0.047% of critical (§10.6.3). Again this is towards the bottom of the range of previous estimates (§2.8.3), believed to be due to the subtraction of the contribution of aerodynamic damping from the measured values. The structural damping appears to be higher for shorter cables, in agreement with previous measurements, thought to be because the damping originates primarily at the anchorages (Irwin et al. 1999) or possibly due to the transfer of energy to other modes (§10.7.1.3). The structural damping was also found to be independent of temperature and not strongly influenced by the presence of wax in the cable sheaths.

The measured cable damping ratios were used to assess various criteria that have been proposed for the onset of cable aerodynamic instabilities (§10.6.4). The measurements were in agreement with Irwin's (1997) criterion for rain-wind excitation and Scruton & Walshe's (1957) limit for vortex excitation. However, both Narita & Yokoyama's (1991) and Irwin's (1997) expressions for galloping suggest that this instability should have occurred, but there was no evidence of this from the site measurements.

Large amplitude rain-wind cable vibrations were observed on the SSC. Measurements of cable vibrations in ambient conditions before and after the addition of secondary cables showed their effectiveness in suppressing the cable response (§10.9).

11.4.7 Cable-deck interaction

Linear cable-deck interaction has been observed in the SSC measurements (§10.7.1.1 &10.7.2.1), similar to that predicted by a Multiple Element Cable System (MECS) FE model of the bridge (§3.4). Additional cable-dominated modes were identified in the cantilever deck response when cable wind loading was dominant. Non-linear

('parametric') cable-deck interaction was also found to occur, with the deck responding at twice the frequency of cable vibrations (§10.7.1.2). It is believed that this is the first time that this type of behaviour has been measured on a cable-stayed bridge. These results are consistent with the previous theoretical work and scale model tests of cable-deck interaction (e.g. Perkins 1992, Uhrig 1993, Lilen & Pinto da Costa 1994, Caetano et al. 1996, §2.9). However, much of the previous work has concentrated on the response of the cable to moving anchorages, whereas in this case the force on the deck from the cables was of more importance (§10.7.1.2). Indeed, it was shown that parametric excitation of the cables from the deck seems unlikely in practice, due to the significant aerodynamic damping and the unlikelihood of vibrations at the critical excitation frequency occurring with sufficient amplitude at the cable anchorage (§10.8.3).

Other aspects of cable-deck interaction identified for the first time at full scale were the existence of complex modes at relatively high frequencies (6-9Hz) and responses of the deck at frequencies below the normal fundamental natural frequencies of either the cables or the deck.

The significance of cable-deck interaction is likely to become greater as cable-stayed bridge spans increase, since the mass and wind loading of the cables become more significant compared with those of the deck.

11.5 Critical appraisal of the work

Although there were several positive outcomes of the research, it is appropriate to discuss its shortcomings. Suggestions for further work to address some of these issues are given in §11.6. The dynamic loading and response of cable-stayed bridges is a broad subject, and this thesis has attempted to cover the full range of issues that could be identified from the full-scale monitoring. However, this has meant that the extent of the investigation of each issue has been limited.

As this has been an essentially experimental study, comparative theoretical analysis has played a relatively minor role. It is hoped that the results presented, and the additional data collected, will be of future value in validating analytical methods. The results have identified some interesting aspects of the behaviour, but further analytical work is required to realise the full potential of the accumulated data.

Some more specific shortcomings of the work are now addressed.

11.5.1 Site monitoring

During the extensive monitoring programme, the often harsh environmental and working conditions unfortunately resulted in some notable events not being recorded, in particular the occasions of rain-wind induced cable vibrations (§10.2) and some periods of strong winds. Also, problems with equipment and damage to instrument cables resulted in the loss of some data. The data acquisition software and some items of hardware were several years old, providing limited data storage and flexibility of usage, and sometimes proving unreliable. For future monitoring exercises, more modern and robust equipment should be used to ensure continuity of operation.

Data suitable for some purposes were limited, in particular:

i) *Continuous records for the cantilever*

The strategy of only recording when a threshold wind speed was exceeded (§4.5.4) meant that relatively few records sufficiently long for estimating damping were made. Although this strategy was necessary to limit the total quantity of data, more records of several days continuous data acquisition would have been beneficial.

ii) *Simultaneous cable and deck measurements*

Relatively few recordings were made from which cable-deck interaction could be detected, due to the difficulty of access to install or move the cable accelerometers.

iii) *Data for the identification of backspan modes of the cantilever*

Although the chosen deck accelerometer reference location, at the end of the cantilever, was an antinode for the majority of modes (§4.5.3), it experienced negligible vibrations in some modes, so it was ineffective as a reference. It is suggested that two reference locations be used for similar future modal surveys.

11.5.2 Ambient loading

Reliance on ambient loading led to limitations in the system identification methods available (§5.3.1). Although the IWCM was developed, enabling more accurate estimates of the modal parameters than otherwise possible from ambient data, there remains significant uncertainty in the values extracted, particularly for damping. This is due partly to the random nature of the loading, both from wind and traffic, but it could also be affected by other uncontrolled or unmeasured parameters, such as temperature. Also, since the wind determined both the amplitude of response and the aerodynamic damping, any amplitude-dependency of the structural damping could not be assessed.

The maximum hourly wind speed recorded (28.2m/s) was less than half of the design flutter wind speed for the bridge, and there were few occasions of wind above 20m/s measured. Therefore, the extreme behaviour, including flutter and large amplitude buffeting response, was not measured. Thus only a limited range of results could be compared with the design analysis and wind tunnel tests (Xie et al. 1994), which concentrated on the response in higher wind speeds, generally of more interest in design.

There is a need for longer term monitoring of cable-stayed bridges, so that the response to extreme loading can be captured. In any case, model testing, in a controlled environment, remains the principal means for the experimental study of extreme behaviour.

11.5.3 Data processing

Although a stationarity test was employed to eliminate non-stationary blocks of data from the analysis (§5.6.4), it appeared to be quite sensitive to the values of processing parameters. A more sophisticated stationarity test would be preferable.

The IWCM assumes linear behaviour and uncoupled modes, but some results indicate that there is indeed some modal coupling (§8.5). There would therefore be some errors in the modal parameters extracted. The assumptions were necessary since the loading was not measured. They appeared reasonable in the majority of cases, but for greater coupling or non-linear behaviour the method may become unreliable. Also, the method requires the frequency range for each resonance to be defined, so modes of low amplitude or those appearing intermittently may not have been identified.

Although the accuracy of damping estimates was assessed (§7.5.4), the scatter of results showed considerably greater variation than anticipated. This has not been explained entirely, although cable-deck interaction, non-stationarity of the loading, variable mass of traffic, and other uncontrolled parameters may have been contributory factors.

The errors in all modal parameters masked subtle systematic variations, for example due to non-linear effects or temperature. The errors would also limit the potential accuracy of model updating, and could hide any changes in parameters due to structural damage or deterioration, of importance for structural health monitoring (§2.4.4).

11.5.4 Larger amplitude vibrations and non-linearities

Since recordings were not made in higher wind speeds, large amplitude vibrations were not encountered, apart from some vortex-induced vibrations. Consequently, non-linear effects other than cable-deck interaction were not detected. For larger vibrations, the changing cable sag and other non-linearities would be expected to become more

significant. Also, there may be some amplitude dependence of the structural damping, and in stronger winds the aerodynamic damping may be non-linear with wind speed.

Although detected on site, the effects of cable-deck interaction were not great at the amplitudes monitored, but they could become much more significant at higher amplitudes. This has only been considered to a limited extent (§10.8).

Non-linear effects are likely to be more important for longer bridges, as well as for larger vibrations, but this study has been unable to comment on these aspects of cable-stayed bridge behaviour.

11.6 Recommendations for further research

There are three main approaches appropriate for further research on cable-stayed bridge dynamics, based on the findings of this study; namely theoretical analyses for comparison with the measured behaviour, further analysis of the available site data, and further site monitoring.

11.6.1 Theoretical analyses

The work described in this thesis has concentrated on the collection and analysis of site data. This provides a valuable resource for validation of analytical techniques. It is therefore necessary to perform theoretical analyses specifically for the SSC, for comparison with the measured responses. This should be the main focus of further work based on this study. Particular analyses worthy of consideration are:

i) *Buffeting analyses*

The design buffeting analysis could be re-run using the measured structural and aerodynamic damping, wind turbulence, natural frequencies and mode shapes. Thus the accuracy of the method itself could be more accurately assessed. Variations on the method could be evaluated, including the full integral of wind loading over the structure, rather than assuming a short correlation length (§2.6.4.2), or considering different functions for the aerodynamic admittance (§2.6.4.3). Also, estimated spectra of responses could be generated, for a more detailed comparison with the measured responses.

ii) *Multi-mode analyses*

These have been a subject of considerable research interest in recent years (e.g. Jain et al. 1996, Katsuchi et al. 1999, §2.6.6). The apparent coupling of modal responses observed on the SSC provides an ideal opportunity for validating these

methods. Application of the methods to the many closely-spaced modes of an MECS FE model would be of particular interest.

iii) *Aerodynamic damping of global modes*

This could be estimated from flutter derivatives (§2.6.5.1), rather than quasi-static theory, to attempt to achieve better agreement with values from the site measurements.

iv) *Cable-deck interaction*

The analytical work on this to date has concentrated on the non-linear response of a cable to an imposed sinusoidal end displacement (Perkins 1992, Uhrig 1993, Lilen & Pinto da Costa 1994, §2.9.1), or linear dynamic analysis of the bridge as a whole (Abdel-Ghaffar & Khalifa 1991, Caetano et al. 1996, §2.9.2). Consideration should be given to more realistic cable end displacements and the effects of non-linear cable vibrations on the global structure. Suitable ways forward would be non-linear numerical modelling of the cable with a Single-Degree-Of-Freedom (SDOF) oscillator at one end, or a sub-structuring approach linking a physical scale model of a cable to a linear FE model of the rest of the structure.

v) *Model updating*

The existing FE model of the cantilever (§3.3) could be updated based on the measured modal parameters. Different strategies could be applied, and the resulting models could be altered to model the complete bridge or different construction stages. Comparison of the predicted modal parameters and those measured at these other stages could be used to assess the updating strategies and the possibility of updating models during construction of future bridges.

The data collected from the different construction stages provide excellent opportunities for further study of all of these areas, since parameters can be varied, allowing more thorough validation of the methods than considering only a single construction stage.

11.6.2 Further analysis of site data

There is much scope for further analysis of the site data, particularly for validation of the above analyses. The main areas worthy of consideration are:

i) *Data processing*

More refined stationarity tests, or the effects of including non-stationary data, could be explored, with a view to improving the accuracy of the modal

parameters. Also, the accuracy of the mode shapes could be considered, particularly for applications to model updating and damage detection.

ii) *Buffeting*

From the modal parameters, including modal amplitude, the contribution of each mode to the Root Mean Square (RMS) displacement could be estimated, allowing more direct comparison with the buffeting analyses. Alternatively, displacements measured directly by the Computer Vision System (§4.4) could be used for the comparison. The measured responses could also be compared more thoroughly with the results from the full aeroelastic wind tunnel model tests (Xie et al. 1994), and more detailed consideration could be given to the loading from skew winds.

iii) *Variations in modal parameters*

The effects of aerodynamic damping and traffic mass could be removed from the measured modal parameters, potentially enabling more subtle variations to be detected, for example from temperature variations or structural non-linearities.

iv) *Construction stages*

The modal parameters from the other construction stages that were monitored (§4.5.2) could be estimated. The IWCM would provide unbiased estimates of the damping, even from the spectra from short records. The results would be useful for model updating studies described above, and for investigating the variation of parameters during construction. Of particular interest would be variations in damping and in the spacing of natural frequencies, which affects the potential for classical flutter. The amplitude of the buffeting response at different stages would also be of interest, as would a more thorough evaluation of the effects of the wind barriers.

v) *Computer Vision System (CVS) displacement measurements*

The video tapes that were recorded for the CVS (§4.4.3) could be processed to obtain direct displacement measurements of the bridge. These would be particularly useful for comparison with predicted amplitudes of vibration and for determining the static force coefficients for validating values from sectional model tests.

vi) *Cable-deck interaction*

The records showing evidence of cable-deck interaction could be processed further, including by attempting to identify parameters of the additional modes of the global structure believed to be due to this effect. Also, the amplitudes and frequency spectra of deck vibrations at cable anchorages could be considered

further, in relation to theoretical work on parametric cable excitation (§2.9.1&10.8.3).

11.6.3 Further site monitoring

Given the large database formed as part of this research (§4.5), the priorities for further work should be in the above mentioned areas, to utilise the full-scale vibration data now available. However, it is recommended that further site monitoring be directed towards specific aspects of bridge behaviour not adequately covered. These would include:

i) The spatial variation of the wind loading.

ii) Further simultaneous measurements of cable and deck vibrations, for both forced and ambient vibrations, to quantify the effects of cable-deck interaction.

iii) Large amplitude response, requiring very long term monitoring to capture extreme wind loading.

iv) Direct measurement of displacements, using the updated CVS with on-site processing, to enable calculation of aerodynamic force coefficients.

v) Further estimates of damping, from very long continuous records.

This monitoring would be useful on the SSC, since its behaviour is already well understood through the present study, but measurements on other bridges would be valuable to understand the issues more generally.

REFERENCES

Abdel-Ghaffar A.M., Khalifa M.A. (1991)
Importance of cable vibration in dynamics of cable-stayed bridges
J. Engineering Mechanics Division, ASCE, Vol. 117, No. 11, pp. 2571-2589

Abdel-Ghaffar A.M., Nazmy A.S. (1991)
3-D nonlinear seismic behaviour of cable-stayed bridges
J. Structural Division, ASCE, Vol. 117, No. 11, pp. 3456-3476

Asmussen J.C., Brincker R., Ibrahim S.R. (1998)
Modal analysis based on the random decrement transform
Modal Testing and Analysis Conference, NATO Advanced Study Institute, May 3-15, Sesimbra, Portugal, pp. 389-409

Bailey A., Vincent N.D.G. (1939)
Wind-pressure experiments at the Severn Bridge
J. ICE, Vol. 11, pp. 363-380

Baker C.J. (1991)
Ground vehicles in high cross winds (three parts)
J. Fluids and Structures, Vol 5., pp. 69-90, 91-111, 221-241

Bendat J.S., Piersol A.G. (1986)
Random data: Analysis and measurement procedures (second edition)
John Wiley & Sons

Bietry J., Delaunay D., Conti E. (1994)
Comparison of full-scale measurements and computation of wind effects on a cable-stayed bridge
Proc. Int. Conf. Cable-stayed and Suspension Bridges, 12-15 Oct., Deauville, France, Vol. 2, pp. 91-100, Association Française Pour la Construction

Billington D.P., Nazmy A.S. (1990)
History and aesthetics of cable-stayed bridges
J. Structural Division, ASCE, Vol. 117, No. 10, pp. 3103-3134

Bishop R.E.D., Gladwell G.M.L. (1963)
An investigation into the theory of resonance testing
Philosophical Trans. Royal Society of London, Series A, Vol. 255, pp. 241-280

Bleich F. (1949)
Dynamic instability of truss-stiffened suspension bridges under wind action
Trans. ASCE, Vol. 114, pp. 1177-1232

Blevins R.D. (1986)
Formulas for natural frequency and mode shape
Krieger Publishing

Brancaleoni F. (1992)
The construction phase and its aerodynamic issues
Proc. Int. Symp. Aerodynamics of Large Bridges, 19-21 Feb., Copenhagen, pp. 147-158, Balkema

Brincker R., de Steffano A., Piombo B. (1996)
Ambient data to analyse the dynamic behaviour of bridges: A first comparison between different techniques
Proc. 14th Int. Modal Analysis Conf., Dearborn, Michigan, Vol. 1, pp. 477-482

Brittingham J.N., Miller E.K., Willows J.L, (1980)
Pole extraction from real-frequency information
Proc. IEEE, Vol. 68, No. 2, pp. 263-273

Brownjohn J.M.W. (1988)
Assessment of structural integrity by dynamic measurements
PhD Thesis, Department of Civil Engineering, University of Bristol

Brownjohn J.M.W. (1994)
Estimation of damping in suspension bridges
Proc. ICE: Structures and Buildings, Vol. 104, pp. 401-415

Brownjohn J.M.W., Dumanoglu A.A., Severn R.T., Taylor C.A. (1986)
Ambient vibration survey of the Humber Suspension Bridge
Research Report UBCE-EE-86-2, Department of Civil Engineering, University of Bristol

Brownjohn J.M.W., Dumanoglu A.A., Severn R.T., Taylor C.A. (1987)
Ambient vibration measurements of the Humber Suspension Bridge and comparison with calculated characteristics
Proc. ICE, Part 2, Vol. 83, pp. 561-600

Brownjohn J.M.W., Zasso A., Stephen G.A., Severn R.T. (1993)
Analysis of experimental data from wind-induced response of a long span bridge
Proc. 3rd Asia-Pacific Symp. Wind Engineering, 13-15 Dec., Hong Kong

Brownjohn J.M.W., Bocciolone M., Curami A., Falco M., Zasso A. (1994)
Humber Bridge full-scale measurement campaigns 1990-1991
J. Wind Engineering and Industrial Aerodynamics, Vol. 52, pp. 185-218

BSI (1990)
Code of practice for design of concrete bridges
British Standards Institution BS5400: Part 4

Bucher C.G., Lin Y.K. (1988)
Stochastic stability of bridges considering coupled modes
J. Engineering Mechanics Division, ASCE, Vol. 114, No. 12, pp. 2055-2071

Bucher C.G., Lin Y.K. (1989)
Stochastic stability of bridges considering coupled modes: II
J. Engineering Mechanics Division, ASCE, Vol. 115, No. 2, pp. 384-400

Burden A.R. (1990)
Japanese cable-stayed bridge design
Proc. ICE, Part 1, Vol 90, pp. 1021-1051

Caetano E., Cunha A., Taylor C.A. (1996)
Experimental analysis of coupled cable-deck motions in cable-stayed bridges
Proc. 11th World Conf. Earthquake Engineering, Acalpulco, Paper 913

Caetano E., Cunha A., Macdonald J.H.G., Taylor C.A. (1998)
Experimental analysis of the effect of cable vibrations on the dynamic behaviour of two cable-stayed bridges
Proc. 11th European Conf. Earthquake Engineering, 7-11 Sept., Paris

Campbell R.B., Vandiver J.K. (1982)
The determination of modal damping ratios from maximum entropy spectral estimates
J. Dynamic Systems, Measurement and Control, ASME, Vol. 104, pp. 78-85

Carter G.C., Nuttall A.N. (1980)
On the weighted overlapped segment averaging method for power spectral estimation
Proc. IEEE, Vol. 68, No. 10, pp. 1352-1354

Casas J.R. (1994)
A combined method for measuring cable forces: The cable-stayed Alamillo Bridge, Spain
Structural Engineering International, Vol. 4, No. 4, pp. 235-240

Casas J.R. (1995)
Full-scale dynamic testing of the Alamillo cable-stayed bridge in Sevilla (Spain)
J. Earthquake Engineering and Structural Dynamics, Vol. 24, pp. 35-51

Causevic M.S., Sreckovic G. (1987)
Modelling of cable-stayed bridge cables: Effects on bridge vibrations
Proc. Int. Conf. Cable-stayed Bridges, 18-20 Nov., Bangkok, pp. 407-420

Chatelet E., Piranda J. (1995)
Modal identification by squared amplitude fitting methods
Proc. 13th Int. Modal Analysis Conf., Nashville, Tennessee, Vol. 1, pp. 40-46

Clough R.W., Penzien J. (1993)
Dynamics of structures (second edition)
McGraw-Hill

Cole H.A. (1968)
On-the-line analysis of random vibrations
American Institute of Aeronautics and Astronautics Paper No. 68-288

Craig R.R. (1981)
Structural dynamics: An introduction to computer methods
John Wiley & Sons

Cullen Wallace A.A. (1985)
Wind influence on Kessock Bridge
Engineering Structures, Vol. 7, No. 1, pp. 18-34

Daniell W.E., Taylor C.A. (1999)
Effective ambient vibration testing for validating numerical models of concrete dams
J. Earthquake Engineering and Structural Dynamics, Vol. 28, pp. 1327-1344

Davenport A.G. (1961a)
A statistical approach to the treatment of wind loading on tall masts and suspension bridges
PhD Thesis, Department of Civil Engineering, University of Bristol

Davenport A.G. (1961b)
The spectrum of horizontal gustiness near the ground in high winds
J. Royal Meteorological Society, Vol. 87, pp. 194-211

Davenport A.G. (1961c)
The application of statistical concepts to the wind loading of structures
Proc. ICE Vol. 19, pp. 449-472

Davenport A.G. (1962a)
The response of slender, line-like structures to a gusty wind
Proc. ICE, Vol. 23, pp. 389-408

Davenport A.G. (1962b)
Buffeting of a suspension bridge by storm winds
J. Structural Division, ASCE, Vol. 88, No. ST3 pp. 233-264

Davenport A.G., King J.P.C., Larose G.L. (1992)
Taut strip model tests
Proc. Int. Symp. Aerodynamics of Large Bridges, 19-21 Feb., Copenhagen, pp. 113-124, Balkema

Deger Y., Felber A. J., Cantieni R., de Smet C.A.M. (1996)
Dynamic modeling and testing of a cable stayed pedestrian bridge
Proc. 14th Int. Modal Analysis Conference, Dearborn, Michigan, Vol. 1, pp. 211-217

DETR (1993)
Design rules for aerodynamic effects on bridges
Department of Transport et al., Design Manual for Roads and Bridges, Vol. 1, Sec. 3, BD 49/93

de Smet C.A.M., Felber A. J., Cantieni R., Krämer C. (1996)
Ambient vibration study of the new Rhein bridge for Highway N4
Proc. 14th Int. Modal Analysis Conference, Dearborn, Michigan, Vol. 1, pp. 63-69

Dobinson N.S., Macnamara H.J. (1996)
Experimental and analytical determination of the modes of vibration of the partially constructed Second Severn Crossing
MEng Major Project Report, Department of Civil Engineering, University of Bristol

Dumanoglu A.A., Severn R.T. (1985)
Asynchronous seismic analysis of modern suspension bridges. Part 1: Free vibration
Research Report UBCE-EE-85-2, Department of Civil Engineering, University of Bristol

Ehsan F., Scanlan R.H., Bosch H.R. (1990)
Modeling spanwise correlation effects in the vortex-induced response of flexible bridges
J. Wind Engineering and Industrial Aerodynamics, Vol. 36, pp. 1105-1114

Ernst M.J. (1965)
Der E-Modul von Seilen unter Berücksichtigung des Derchhanges (The E-modulus of cables taking into account their sag)
Der Bauingenieur, Vol. 40, No. 2, pp. 52-55 (in German)

ESDU (1991)
Characteristics of atmospheric turbulence near the ground: Part III: Variations in space and time for strong winds (neutral atmosphere)
Engineering Sciences Data Unit International, Item 86010, Amendment D

ESDU (1993)
Characteristics of atmospheric turbulence near the ground: Part II: Single point data for strong winds (neutral atmosphere)
Engineering Sciences Data Unit International, Item 85020, Amendment F

Ewins D.J. (1984)
Modal testing: Theory and practice
John Wiley & Sons

Eyre R., Tilly G.P. (1977)
Damping measurements on steel and composite bridges
Symp. Dynamic Behaviour of Bridges, TRRL Supplementary Report 275, pp. 22-39

Falco M., Curami A., Zasso A. (1992)
Nonlinear effects in sectional model aeroelastic parameters identification
J. Wind Engineering and Industrial Aerodynamics, Vol. 42, pp. 1321-1332

Farquharson F.B., Smith F.C., Vincent G.S. (1950-1954)
Aerodynamic stability of suspension bridges with special reference to the Tacoma Narrows Bridge (five parts)
Engineering Experiment Station, University of Washington

Farrar C.R., James G.H., (1997)
System identification from ambient vibration measurements on a bridge
J. Sound and Vibration Vol. 205, No. 1, pp. 1-18

Felber A.J., Ventura C.E. (1996)
Frequency domain analysis of the ambient vibration data of the Queensborough Bridge main span
Proc. 14th Int. Modal Analysis Conf., Dearborn, Michigan, Vol. 1, pp. 459-465

Fertis D.G. (1987)
Safety of long span highway bridges based on dynamic response
Proc. ASCE Structures Congress: Bridges and Transmission Line Structures, 17-20 Aug., Orlando, Florida, pp. 449-468

Fleming J.F. (1979)
Nonlinear static analysis of cable-stayed bridge structures
J. Computers and Structures, Vol. 10, No. 4, pp. 621-635

Fleming J.F., Egeseli E.A. (1980)
Dynamic behavior of a cable-stayed bridge
J. Earthquake Engineering and Structural Dynamics, Vol. 8, pp. 1-16

Frazer R.A., Scruton C. (1952)
A summarised account of the Severn Bridge aerodynamic investigation
Aerodynamics Division, National Physical Laboratory, Report NPL/Aero/222

Fujino Y., Warnitchai P., Pacheco B.M. (1993)
An experimental and analytical study of autoparametric resonance in a 3DOF model of a cable-stayed-beam
Nonlinear Dynamics, Vol. 4, pp. 111-138

Fung Y.C. (1993)
An introduction to the theory of aeroelasticity (Dover edition)
Dover Publications, New York

Gade R.H., Bosch H.R., Podolny W. (1976)
Recent aerodynamic studies of long-span bridges
J. Structural Division, ASCE, Vol. 102, No. ST7, pp. 1299-1315

Garevski M.A. (1990)
Dynamic analysis of cable-stayed bridges by means of analytical and physical modelling
PhD Thesis, Department of Civil Engineering, University of Bristol

Garevski M.A., Severn R.T. (1993)
Damping and response measurement on a small-scale model of a cable-stayed bridge
J. Earthquake Engineering and Structural Dynamics, Vol. 22, pp. 13-29

Gentile C., Martinez y Cabrera F. (1997)
Dynamic investigation of a repaired cable-stayed bridge
J. Earthquake Engineering and Structural Dynamics, Vol. 26, pp. 41-59

Gentile C., Martinez y Cabrera F. (1999)
Full-scale testing of twin cable-stayed bridges to compare structural behaviour
Proc. 4th European Conf. Structural Dynamics (Eurodyn '99), 7-10 June, Prague, pp. 807-812, Balkema

Gentile C., Martinez y Cabrera F., Saisi A. (1998)
Dynamic testing and seismic response of a cable-stayed bridge
Proc. 11th European Conf. Earthquake Engineering, 7-11 Sept., Paris

Gersch W., Nielsen N.N., Akaike H. (1973)
Maximum likelihood estimation of structural parameters from random vibration data
J. Sound and Vibration, Vol. 31, No. 3, pp. 295-308

Gersch W., Martinelli F. (1979)
Estimation of structural system parameters from stationary and non-stationary ambient vibrations: An exploratory-confirmatory analysis
J. Sound and Vibration, Vol. 65, No. 3, pp. 303-318

Gimsing N.J. (1997)
Cable-supported bridges: Concept and design (second edition)
John Wiley & Sons

Giorcelli E., Garibaldi L., Riva A., Fasana A. (1996)
ARMAV analysis of Queensborough Bridge ambient data
Proc. 14th Int. Modal Analysis Conf., Dearborn, Michigan, Vol. 1, pp. 466-469

Green R. (1977)
Dynamic response of bridge superstructures – Ontario observations
Symp. Dynamic Behaviour of Bridges, TRRL Supplementary Report 275, pp. 40-55

Harris F.J. (1978)
On the use of windows for harmonic analysis with the Discrete Fourier Transform
Proc. IEEE, Vol. 66, No. 1, pp. 51-83

Harris R.I., Deaves D.M. (1980)
The structure of strong winds
Proc. Conf. Wind Engineering in the Eighties, 12-13 Nov., London, Paper 4, CIRIA

Hartlen R.T., Currie I.G. (1970)
Lift-oscillator model of vortex-induced vibration
J. Engineering Mechanics Division, ASCE, Vol. 96, No. EM5, pp. 577-591

Hay J.S. (1981)
The wind induced response of the Erskine Bridge
Proc. ICE Conf. Bridge Aerodynamics, 25-26 March, London, pp. 81-90, Thomas Telford

Hay J.S. (1984)
Analyses of wind and response data from the Wye and Erskine bridges and comparison with theory
J. Wind Engineering and Industrial Aerodynamics, Vol. 17, pp. 31-49

Hay J.S. (1992)
Response of bridges to wind
Transport Research Laboratory, State of the art review 5, HMSO

Head P.R., Iley P., Bradley E.T. (1997)
Second Severn Crossing: Initial studies
Proc. ICE: Civil Engineering, Vol. 120, Special Issue 2, Second Severn Crossing, pp. 3-12

Hikami Y., Shiraishi N. (1988)
Rain-wind induced vibrations of cables in cable stayed bridges
J. Wind Engineering and Industrial Aerodynamics, Vol. 29, pp. 409-418

Holmes J.D. (1975)
Prediction of the response of a cable stayed bridge to turbulence
Proc. 4th Int. Conf. Wind Effects on Buildings and Structures, 8-12 Sept., Heathrow, pp. 187-197, Cambridge University Press

Horyna T., Ventura C.E., Foschi R.O. (1996)
Modal characteristics of timber bridges under traffic loading
Proc. 14th Int. Modal Analysis Conf., Dearborn, Michigan, Vol. 1, pp. 226-232

Ibrahim S.R., Mikulcik E.C. (1977)
A method for the direct identification of vibration parameters from the free response
Shock and Vibration Bulletin, Vol. 47, No. 4, pp. 183-198

Ibrahim S.R., Brincker R., Asmussen J.C. (1996)
Modal parameter identification from responses of general unknown random inputs
Proc. 14th Int. Modal Analysis Conf., Dearborn, Michigan, Vol. 1, pp. 446-452

Irvine H.M., Caughey T.K. (1974)
The linear theory of free vibrations of a suspended cable
Proc. Royal Society of London, Series A, Vol. 341, pp. 299-315

Irwin P.A. (1977)
Wind tunnel and analytical investigations of the response of the Lions' Gate Bridge to a turbulent wind
National Research Council of Canada, National Aeronautical Establishment, Report LTR-LA-210

Irwin P.A. (1979a)
Centre of rotation for torsional vibration of bridges
J. Industrial Aerodynamics, Vol. 4, pp. 123-132

Irwin P.A. (1979b)
Cross spectra of turbulence velocities in isotropic turbulence
Boundary-layer Meteorology, Vol. 16, pp.237-243

Irwin P.A. (1987)
Wind buffeting of cable-stayed bridges during construction
Proc. ASCE Structures Congress: Bridges and Transmission Line Structures, 17-20 Aug., Orlando, Florida, pp. 164-177

Irwin P.A. (1997)
Wind vibrations of cables on cable-stayed bridges
Proc. 15th ASCE Structures Congress, 14-16 April, Portland, Oregon, pp. 383-387

Irwin P.A. (1998)
The role of wind tunnel modelling in the prediction of wind effects on bridges
Proc. Int. Symp. Advances in Bridge Aerodynamics, 10-13 May, Copenhagen, pp. 99-117, Balkema

Irwin P.A., Mizon D.H., Maury Y., Schmitt J. (1994)
History of the aerodynamic investigations for the Second Severn Crossing
Proc. Int. Conf. Cable-stayed and Suspension Bridges, 12-15 Oct., Deauville, France, Vol. 2, pp. 143-151, Association Française Pour la Construction

Irwin P.A., Alca N., Telang N. (1999)
Wind induced stay cable vibrations – a case study
Proc. 3rd Int. Symp. Cable Dynamics, 16-18 Aug., Trondheim, Norway, pp. 171-176

Iwan W.D., Blevins R.D. (1974)
A model for vortex induced oscillation of structures
J. Applied Mechanics, ASME, Vol. 41, pp. 581-586

Jain A., Jones N.P., Scanlan R.H. (1996)
Coupled flutter and buffeting analysis of long-span bridges
J. Structural Division, ASCE, Vol. 122, No. 7, pp. 716-725

James G.H., Carne T.G., Mayes R.L. (1996)
Modal parameter extraction from large operating structures using ambient excitation
Proc. 14th Int. Modal Analysis Conf., Dearborn, Michigan, Vol. 1, pp. 77-83

Jayaraman H.B., Knudson W.C. (1981)
A curved element for the analysis of cable structures
J. Computers and Structures, Vol. 14, No. 3-4, pp. 325-334

Jensen J.L., Larsen A., Andersen J.E., Vejrum T. (1999)
Estimation of structural damping of Great Belt suspension bridge
Proc. 4th European Conf. Structural Dynamics (Eurodyn '99), 7-10 June, Prague, pp. 801-806, Balkema

Jones N.P., Spartz C.A. (1990)
Structural damping estimation for long-span bridges
J. Engineering Mechanics Division, ASCE, Vol. 116, No. 11, pp. 2414-2433

Jones N.P., Shi T., Ellis J.H., Scanlan R.H. (1995)
System-identification procedure for system and input parameters in ambient vibration surveys
J. Wind Engineering and Industrial Aerodynamics Vol. 54, pp. 91-99

Jones N.P., Scanlan R.H., Jain A., Katsuchi H. (1998)
Advances (and challenges) in the prediction of long-span bridge response
Proc. Int. Symp. Advances in Bridge Aerodynamics, 10-13 May, Copenhagen, pp. 59-85, Balkema

Juang J.N., Pappa R.S. (1985)
An Eigensystem Realisation Algorithm for modal parameter identification and model reduction
J. Guidance, Control and Dynamics, Vol. 8, No. 5, pp. 620-627

Kanok-Nukulchai W., Yiu P.K.A., Brotton D.M. (1992)
Mathematical modelling of cable-stayed bridges
Structural Engineering International, Vol. 2, No. 2, pp. 108-113

Katsuchi H., Saeki S., Miyata T., Sato H. (1998)
Analytical assessment in wind-resistant design of long-span bridges in Japan
Proc. Int. Symp. Advances in Bridge Aerodynamics, 10-13 May, Copenhagen, pp. 87-98, Balkema

Katsuchi H., Jones N.P., Scanlan R.H. (1999)
Multimode coupled flutter and buffeting analysis of the Akashi-Kaikyo Bridge
J. Structural Division, ASCE, Vol. 125, No. 1, pp. 60-70

Kawashima K., Unjoh S., Azuta Y. (1988)
Damping characteristics of cable stayed bridges
Proc. 9th World Conf. Earthquake Engineering, Tokyo, Vol VI, pp. 471-476

Kawashima K., Unjoh S., Tunomoto M. (1993)
Estimates of damping ratio of cable-stayed bridges for seismic design
J. Structural Division, ASCE, Vol. 119, No. 4, pp. 1015-1031

Kendall M.G., Stuart A. (1973)
The advanced theory of statistics, Vol. 2 (third edition)
Griffin, London

Khalil M.S., Bush L.H. (1987)
Vancouver's Skytrain cable-stayed bridge - Dynamic behaviour
Proc. ASCE Structures Congress: Bridges and Transmission Line Structures, 17-20 Aug., Orlando, Florida, pp. 357-372

Kimura K., Tanaka H. (1992)
Bridge buffeting due to wind with yaw angles
J. Wind Engineering and Industrial Aerodynamics, Vol. 42, pp. 1309-1320

Kitchener J.N., Mizon D.H. (1997)
Second Severn Crossing: Pre-construction period and design development
Proc. ICE: Civil Engineering, Vol. 120, Special Issue 2, Second Severn Crossing, pp. 13-21

Konishi I., Shiraishi N., Matsumoto M. (1975)
Aerodynamic response characteristics of bridge structures
Proc. 4th Int. Conf. Wind Effects on Buildings and Structures, 8-12 Sept., Heathrow, pp. 199-208, Cambridge University Press

Kovacs I., Svensson H.S., Jordet E. (1992)
Analytical aerodynamic investigation of cable-stayed Helgeland Bridge
J. Structural Division, ASCE, Vol. 118, No. 1, pp. 147-168

Kumarasena T., Scanlan R.H., Morris G.R. (1989)
Deer Isle Bridge: Efficacy of stiffening systems
J. Structural Division, ASCE, Vol. 115, No. 9, pp. 2297-2312

Kumarasena T., Scanlan R.H., Bosch H.R. (1990)
Wind response prediction of flexible bridges
J. Wind Engineering and Industrial Aerodynamics, Vol. 36, pp. 1365-1372

Kumarasena T., Scanlan R.H., Ehsan F. (1991)
Wind-induced motions of Deer Isle Bridge
J. Structural Division, ASCE, Vol. 117, No. 11, pp. 3356-3374

Kvamsdal T., Herfjord K., Okstad K.M. (1999)
Coupled simulation of vortex induced vibration of slender structures as suspension bridges and offshore risers
Proc. 3rd Int. Symp. Cable Dynamics, 16-18 Aug., Trondheim, Norway, pp. 117-122

Langsoe H.E., Larsen O.D. (1987)
Generating mechanisms for cable stay oscillations at the Faro Bridges
Proc. Int. Conf. Cable-stayed Bridges, 18-20 Nov., Bangkok, pp. 1023-1033

Larsen A., Walther J.H. (1997)
Aeroelastic analysis of bridge girder sections based on discrete vortex simulations
J. Wind Engineering and Industrial Aerodynamics, Vol. 67-68, pp. 253-265

Lau C.K., Wong K.Y. (1994)
Instrumentation system for Tsing Ma and Kap Shui Mun Bridges
Int. Conf. Computational Methods in Structural and Geotechnical Engineering, 12-14 Dec., Hong Kong

Lekidis V.A., Karakostas C.Z., Talaslidis D.G. (1998)
Dynamic characteristics of the cable-stayed bridge in Evripos Channel, Greece
Proc. 11th European Conf. Earthquake Engineering, 7-11 Sept., Paris

Liepmann H.W. (1952)
On the application of statistical concepts to the buffeting problem
J. Aeronautical Sciences, Vol. 19, No. 12, pp. 793-800

Lilien J.L., Pinto da Costa A. (1994)
Vibration amplitudes caused by parametric excitation of cable stayed structures
J. Sound and Vibration Vol. 174, No. 1, pp. 69-90

Lin Y.K., Ariaratnam S.T. (1980)
Stability of bridge motion in turbulent winds
J. Structural Mechanics, Vol. 8, No. 1, pp. 1-15

Lin Y.K., Yang J.N. (1983)
Multimode bridge response to wind excitations
J. Engineering Mechanics Division, ASCE, Vol. 109, No. 2, pp. 586-603

Link M., Rohrmann R.G., Pietrzko S. (1996)
Experience with automated procedures for adjusting the finite element model of a complex highway bridge to experimental modal data
Proc. 14th Int. Modal Analysis Conf., Dearborn, Michigan, Vol. 1, pp. 218-225

Littler J.D. (1992)
Ambient vibration tests on long span suspension bridges
J. Wind Engineering and Industrial Aerodynamics, Vol. 42, pp. 1359-1370

Macdonald J.H.G. (1995a)
Second Severn Crossing dynamic monitoring: Estimation of damping parameters of unwaxed cables
Earthquake Engineering Research Centre, University of Bristol, Report SSC295/REP/2

Macdonald J.H.G. (1995b)
Second Severn Crossing dynamic monitoring: Estimation of damping parameters of waxed cables
Earthquake Engineering Research Centre, University of Bristol, Report SSC295/REP/3

Macdonald J.H.G. (1997)
Second Severn Crossing dynamic monitoring: Summary of data records August 1996 – March 1997
Earthquake Engineering Research Centre, University of Bristol, Report SSC295/REP/5

Macdonald J.H.G. (1998)
Second Severn Crossing dynamic monitoring: Summary of data records October 1997 – April 1998
Earthquake Engineering Research Centre, University of Bristol, Report SSC295/REP/6

Macdonald J.H.G. (1999)
Second Severn Crossing dynamic monitoring: Summary of data records September 1998 – April 1999
Earthquake Engineering Research Centre, University of Bristol, Report SSC295/REP/7

Macdonald J.H.G., Taylor C.A., Thomas B.T., Dagless E.L. (1998)
Real-time remote monitoring of dynamic displacements by computer vision
Proc. 6th SECED Conf., Oxford, pp. 389-396

Macmillan (1987)
Asyst 2.0
Macmillan Software Company, New York

Maia N.M.M., Silva J.M.M. (editors) (1997)
Theoretical and experimental modal analysis
John Wiley & Sons

Mann J., Kristensen L., Jensen N.O. (1998)
Uncertainties of extreme winds, spectra and coherences
Proc. Int. Symp. Advances in Bridge Aerodynamics, 10-13 May, Copenhagen, pp. 49-56, Balkema

Mathworks (1999)
Matlab 5.3
The Mathworks Inc., Natick, Massachusetts, USA

Matsumoto M., Shiraishi N., Shirato H., Tsuji M. (1989)
Aerodynamic behaviour of cables of cable-stayed bridges
Proc. 2nd Asia-Pacific Symp. Wind Engineering, 26-29 June, Beijing, Vol. 2, pp. 602-609, Pergamon Press

Matsumoto M., Shiraishi N., Kitazawa M., Kniseley C., Shirato H., Kim Y., Tsujii M. (1990)
Aerodynamic behaviour of inclined circular cylinders - cable aerodynamics
J. Wind Engineering and Industrial Aerodynamics, Vol. 33, pp. 63-72

Matsumoto M., Shiraishi N., Shirato H. (1992)
Rain-wind induced vibration of cables of cable-stayed bridges
J. Wind Engineering and Industrial Aerodynamics, Vol. 43, pp. 2011-2022

Miyata T. (1991)
Design considerations for wind effects on long-span cable-stayed bridges
Proc. Seminar Cable-stayed Bridges: Recent Developments and their Future, 10-11 Dec., Yokohama, Japan, pp. 235-256, Elsevier Science

Mizon D.H., Smith N., Yeoward A.J. (1997)
Second Severn Crossing: Cable-stayed bridge
Proc. ICE: Civil Engineering, Vol. 120, Special Issue 2, Second Severn Crossing, pp. 49-63

Murià-Vila D., Gómez R., King C. (1991)
Dynamic structural properties of cable-stayed Tampico Bridge
J. Structural Division, ASCE, Vol. 117, No. 11, pp. 3396-3416

Namini A., Albrecht P., Bosch H. (1992)
Finite element-based flutter analysis of cable-suspended bridges
J. Structural Division, ASCE, Vol. 118, No. 6, pp. 1509-1526

NaritaN., Yokoyama K. (1991)
A summarized account of damping capacity and measures against wind action in cable-stayed bridges in Japan
Proc. Seminar Cable-stayed Bridges: Recent Developments and their Future, 10-11 Dec., Yokohama, Japan, pp. 257-276, Elsevier Science

Nelder J.A., Mead R. (1965)
A simplex method for function minimization
Computer Journal, Vol. 7, pp. 308-313

Newland D.E. (1975)
An introduction to random vibrations and spectral analysis
Longman

Ohlsson S.V. (1987)
Dynamic characteristics of cable-stayed bridges – nonlinearities and weakly coupled modes of vibration
Proc. Int. Conf. Cable-stayed Bridges, 18-20 Nov., Bangkok, pp. 421-431

Ostenfeld K.H., Langsoe H.E. (1987)
Full scale measurements and monitoring of major cable stayed bridge
Proc. Int. Conf. Cable-stayed Bridges, 18-20 Nov., Bangkok, pp. 997-1005

Ostenfeld-Rosenthal P., Madsen H.O., Larsen A. (1992)
Probabilistic flutter criteria for long span bridges
J. Wind Engineering and Industrial Aerodynamics, Vol. 42, pp. 1265-1276

Owen J.S. (1994)
A power spectral approach to the analysis of the dynamic response of cable-stayed bridges to spatially varying excitation
PhD Thesis, Department of Civil Engineering, University of Bristol

Owen J.S., Blakeborough A. (1993)
The prototype testing of Kessock Bridge: Modal survey
Proc. Int. Conf. Structural Dynamics Modelling, 7-9 July, Milton Keynes, pp. 129-138, NAFEMS

Owen J.S., Vann A.M., Davis J.P., Blakeborough A. (1996)
The prototype testing of Kessock Bridge: Response to vortex shedding
J. Wind Engineering and Industrial Aerodynamics, Vol. 60, pp. 91-108

Peeters B., De Roeck G. (1998)
Stochastic subspace system identification of a steel transmitter mast
Proc. 16th Int. Modal Analysis Conf., Santa Barbara, California, Vol. 1, pp. 130-136

Perkins N.C. (1992)
Modal interactions in the non-linear response of elastic cables under parametric/external excitation
J. Non-linear Mechanics, Vol. 27, No. 2, pp. 233-250

Persoon A.J. (1981)
The wind induced response of a cable-stayed bridge
Proc. ICE Conf. Bridge Aerodynamics, 25-26 March, London, pp. 91-95, Thomas Telford

Pinto da Costa A., Martins J.A.C., Branco F., Lilien J.L. (1996)
Oscillations of bridge stay cables induced by periodic motions of deck and/or towers
J. Engineering Mechanics Division, ASCE, Vol. 122, No. 7, pp. 613-622

Provis W.A. (1842)
Observations on the effects produced by wind on the suspension bridge over the Menai Stait, more especially as relates to the injuries sustained by the roadways during the storm of January, 1839; together with brief notices of various suggestions for repairing the structure
Trans. ICE, Vol. 3
Included as an appendix to Part I of Farquharson et al. (1950-1954)

Raggett J.D. (1975)
Estimating damping of real structures
J. Structural Division, ASCE, Vol. 101, No. ST9, pp. 1823-1835

Rodrigues J., Campos-Costa A. (1998)
Experimental modal analysis of bridge structures: Case studies
Proc. 11th European Conf. Earthquake Engineering, 7-11 Sept., Paris

Saito T. Matsumoto M., Kitazawa M. (1994)
Rain-wind excitation of cables on cable-stayed Higashi-Kobe Bridge and cable vibration control
Proc. Int. Conf. Cable-stayed and Suspension Bridges, 12-15 Oct., Deauville, France, Vol. 2, pp. 507-514, Association Française Pour la Construction

Sarkar P.P., Jones N.P., Scanlan R.H. (1992)
System identification for estimation of flutter derivatives
J. Wind Engineering and Industrial Aerodynamics, Vol. 42, pp. 1243-1254

Sarkar P.P., Jones N.P., Scanlan R.H. (1994)
Identification of aeroelastic parameters of flexible bridges
J. Engineering Mechanics Division, ASCE, Vol. 120, No, 8, pp. 1718-1742

Scanlan R.H. (1978a)
The action of flexible bridges under wind, I: Flutter theory
J. Sound and Vibration, Vol. 60, No. 2, pp. 187-199

Scanlan R.H. (1978b)
The action of flexible bridges under wind, II: Buffeting theory
J. Sound and Vibration, Vol. 60, No. 2, pp. 201-211

Scanlan R.H. (1987)
Interpreting aeroelastic models of cable-stayed bridges
J. Engineering Mechanics Division, ASCE, Vol. 113, No. 4, pp. 555-575

Scanlan R.H. (1993)
Bridge buffeting by skew winds in erection stages
J. Engineering Mechanics Division, ASCE, Vol. 119, No. 2, pp. 251-269

Scanlan R.H., Gade R.H. (1977)
Motion of suspended bridge spans under gusty wind
J. Structural Division, ASCE, Vol. 103, No. ST9, pp. 1867-1883

Scanlan R.H., Jones N.P. (1990)
Aeroelastic analysis of cable-stayed bridges
J. Structural Division, ASCE, Vol. 116, No.2, pp. 279-297

Scanlan R.H., Tomko J.J. (1971)
Airfoil and bridge deck flutter derivatives
J. Engineering Mechanics Division, ASCE, Vol. 97, No. EM6, pp. 1717-1737

Scott Russell J. (1841)
On the vibration of suspension bridges and other structures; and the means of preventing injury from this cause
Trans. Royal Scottish Society of Arts, Vol. 1
Included as an appendix to Part I of Farquharson et al. (1950-1954)

Scruton C., Walshe D.E.J. (1957)
A means for avoiding wind-excited oscillations of structures with circular or nearly circular cross-section
National Physical Laboratory, Aerodynamics Division, Report NPL/Aero/335

Sears W.R. (1941)
Some aspects of non-stationary airfoil theory and its practical application
J. Aeronautical Sciences, Vol. 8, No. 3, pp. 104-108

Seif S.P., Dilger W.H. (1990)
Nonlinear analysis and collapse load of P/C cable-stayed bridges
J. Structural Division, ASCE, Vol. 116, No. 3, pp. 829-849

Shiraishi N., Matsumoto M. (1983)
On classification of vortex-induced oscillation and its application for bridge structures
J. Wind Engineering and Industrial Aerodynamics, Vol. 14, pp. 419-430

Simiu E., Scanlan R.H. (1986)
Wind effects on structures (second edition)
John Wiley & Sons

Singh L., Jones N.P., Scanlan R.H., Lorendeaux O. (1996)
Identification of lateral flutter derivatives of bridge decks
J. Wind Engineering and Industrial Aerodynamics, Vol. 60, pp. 81-89

Skarecky R. (1975)
Yaw effects on galloping instability
J. Engineering Mechanics Division, ASCE, Vol. 101, No. EM6, pp. 739-754

Skrinar M., Strukelj A. (1996)
Eigenfrequency monitoring during bridge erection
Structural Engineering International Vol. 6, No. 3, pp. 191-194

Smith I.J. (1980)
Wind induced dynamic response of the Wye Bridge
Engineering Structures, Vol. 2, No. 4, pp. 202-208

Smith B.W., Barker C.P. (1998)
Design of wind screens to bridges, experience and applications on major bridges
Proc. Int. Symp. Advances in Bridge Aerodynamics, 10-13 May, Copenhagen, pp. 289-298, Balkema

Solvia (1989)
Solvia 90
Solvia Engineering AB, Västerås, Sweden

SSCG (1986)
Study of second Severn crossing, final report
Second Severn Crossing Group (WS Atkins & Maunsell), Department of Transport, HMSO

Stephen G.A., Dagless E.L., Taylor C.A. (1991)
A visual tracking system for the measurement of dynamic structural displacements
Concurrency: Practice and Experience, Vol. 3, No. 4, pp. 357-366

Stephen G.A., Brownjohn J.M.W., Taylor C.A. (1993)
Measurements of static and dynamic displacement from visual monitoring of the Humber Bridge
Engineering Structures, Vol. 15, No.3, pp. 197-208

Steinman D.B. (1950)
Aerodynamic theory of bridge oscillations
Trans. ASCE, Vol. 115, pp. 1180-1260

Stiemer S.F., Taylor P., Vincent D.H.C. (1988)
Full scale dynamic testing of the Annacis Bridge
IABSE Proceedings P-122/88

Stubler J., Ladret P., Domage J.B., Peltier M. (1999)
Bridge stay cable vibration: Phenomena, criteria and damper technology
Proc. 3rd Int. Symp. Cable Dynamics, 16-18 Aug., Trondheim, Norway, pp. 163-170

Svensson H.S., Jordet E. (1996)
The concrete cable-stayed Helgeland Bridge in Norway
Proc. ICE: Civil Engineering, Vol. 114, No.2, pp. 54-63

Taladhar R., Dilger W.H., Elbadry M.M. (1995)
Influence of cable vibration on seismic response of cable-stayed bridges
Canadian Journal of Civil Engineering, Vol. 22, pp. 1001-1020

Tanaka H., Larose G.L., Kimura K. (1998)
Aerodynamics of long-span bridges during erection
Proc. Int. Symp. Advances in Bridge Aerodynamics, 10-13 May, Copenhagen, pp. 119-127, Balkema

Teunissen H.W. (1980)
Structure of mean winds and turbulence in the planetary boundary layer over rural terrain
Boundary-layer Meteorology, Vol. 19, pp. 187-221

Therrien C.W. (1992)
Discrete random signals and statistical signal processing
Prentice-Hall

Torkamani M.A.M., Ahmadi A.K. (1988)
Stiffness identification of a tall building during construction period using ambient tests
J. Earthquake Engineering and Structural Dynamics, Vol. 16, pp. 1177-1188

Towse A., Setchell C., Potter K., Clarke A.B., Macdonald J.H.G., Wisnom M.R., Adams R.D. (1999)
Use experience with a developmental general purpose non-contacting extensometer with high resolution
American Society for Testing and Materials (ASTM) 2nd Symp. Non-traditional Methods of Sensing Stress, Strain and Damage in Materials and Structures, 17 Nov., USA

Troitsky M.S. (1988)
Cable-stayed bridges: theory and design (second edition)
BSP Professional Books

Uhrig R. (1993)
On kinetic response of cables of cable-stayed bridges due to combined parametric and forced excitation
J. Sound and Vibration Vol. 165, No. 1, pp. 185-192

van Nunen J.W.G., Persoon A.J. (1982)
Investigation on the vibrational behaviour of a cable stayed bridge under wind loads
Engineering Structures Vol. 4, pp. 99-105

Verwiebe C. (1998)
Rain-wind-induced vibrations of cables and bars
Proc. Int. Symp. Advances in Bridge Aerodynamics, 10-13 May, Copenhagen, pp. 255-263, Balkema

Virlogeux M. (1992)
Wind design and analysis for the Normandy Bridge
Proc. Int. Symp. Aerodynamics of Large Bridges, 19-21 Feb., Copenhagen, pp. 183-216, Balkema

Virlogeux M. (1998)
Cable vibrations in cable-stayed bridges
Proc. Int. Symp. Advances in Bridge Aerodynamics, 10-13 May, Copenhagen, pp. 213-233, Balkema

Vold H., Rocklin G.T. (1982)
The numerical implementation of a multi-input modal estimation method for mini-computers
Proc. 1st Int. Modal Analysis Conf., Orlando, Florida, pp. 542-548

von Kármán T. (1948)
Progress in the statistical theory of turbulence
Proc. National Academy of Sciences, Washington D.C., USA., Vol. 34, pp.530-539

Walshe D.E., Wyatt T.A. (1983)
Measurement and application of the aerodynamic admittance function for a box-girder bridge
J. Wind Engineering and Industrial Aerodynamics, Vol. 14, pp. 211-222

Walther R., Houriet B., Isler W., Moïa P. (1989)
Cable stayed bridges
Thomas Telford, London

Wang T., Huang D. (1992)
Cable-stayed bridge vibration due to road surface roughness
J. Structural Division, ASCE, Vol. 118, No.5, pp. 1354-1374

Wardlaw R.L. (1981)
Some observations on the effects of turbulence on the aerodynamic stability of bridge road decks
Proc. ICE Conf. Bridge Aerodynamics, 25-26 March, London, pp. 73-76, Thomas Telford

Wardlaw R.L. (1991)
Cable supported bridges under wind action
Proc. Seminar Cable-stayed Bridges: Recent Developments and their Future, 10-11 Dec., Yokohama, Japan, pp. 213-234, Elsevier Science

Welch P.D. (1967)
The use of fast Fourier transform for the estimation of power spectra: A method based on time averaging over short, modified periodograms
IEEE Trans. Audio Electroacoust. Vol. AU-15, pp. 70-73
Reprinted in *Digital Signal Processing*, Rabiner L.R., Rader C.M. (editors), IEEE Press, 1972, pp. 335-338

Wilson J.C., Atkins J.C. (1999)
Damping in seismic response of cable-stayed bridges
8th Canadian Conf. Earthquake Engineering, Vancouver, pp. 703-708

Wilson J.C., Gravelle W. (1991)
Modelling of a cable-stayed bridge for dynamic analysis
J. Earthquake Engineering and Structural Dynamics, Vol. 20 pp. 707-721

Wilson J.C., Liu T. (1991)
Ambient vibration measurements on a cable-stayed bridge
J. Earthquake Engineering and Structural Dynamics, Vol. 20 pp. 723-747

Wyatt T.A. (1977)
Mechanisms of damping
Symp. Dynamic Behaviour of Bridges, TRRL Supplementary Report 275, pp. 10-21

Wyatt T.A. (1980)
On the dynamic properties of cable-stayed bridges
J. Constructional Steel Research, Vol. 1, No. 1, pp. 10-17

Wyatt T.A. (1991)
The dynamic behaviour of cable-stayed bridges: Fundamentals and parametric studies
Proc. Seminar Cable-stayed Bridges: Recent Developments and their Future, 10-11 Dec., Yokohama, Japan, pp. 151-170, Elsevier Science

Wyatt T.A. (1992)
Recent British developments: Windshielding of bridges for traffic
Proc. Int. Symp. Aerodynamics of Large Bridges, 19-21 Feb., Copenhagen, pp. 159-170, Balkema

Xie J., Tanaka H., Wardlaw R.L., Savage M.G. (1991)
Buffeting analysis of long span bridges to turbulent wind with yaw angle
J. Wind Engineering and Industrial Aerodynamics, Vol. 37, pp. 65-77

Xie J., Near D., Irwin P.A. (1994)
Wind tunnel studies for the Second Severn Crossing
Rowan Williams Davies & Irwin Inc., Ontario, Canada, Final Report 91-141F-5-ARO

Yamaguchi H. (1990)
Analytical study on growth mechanism of rain vibration of cables
J. Wind Engineering and Industrial Aerodynamics, Vol. 33, pp. 73-80

Yamaguchi H., Fujino Y. (1998)
Stayed cable dynamics and its vibration control
Proc. Int. Symp. Advances in Bridge Aerodynamics, 10-13 May, Copenhagen, pp. 235-253, Balkema

Yamaguchi H., Jayawardena L. (1992)
Analytical estimation of structural damping in cable structures
J. Wind Engineering and Industrial Aerodynamics, Vol. 43, pp. 1961-1972

Yoshimura T., Inoue A., Kaj K.I., Savage M.G. (1989)
Aerodynamic stability of the Aratsu Bridge
Proc. 2nd Asia-Pacific Symp. Wind Engineering, 26-29 June, Beijing, Vol. 2, pp. 637-644, Pergamon Press

Zan S.J., Wardlaw R.L. (1987)
Wind buffeting of long span bridges with reference to erection phase behaviour
Proc. ASCE Structures Congress: Bridges and Transmission Line Structures, 17-20 Aug., Orlando, Florida, pp. 432-448

Zan S.J., Tanaka H., Yamada H., Wardlaw R.L. (1989)
Parametric investigation of wind-induced cable-stayed bridge motion using an aeroelastic model
J. Wind Engineering and Industrial Aerodynamics, Vol. 32, pp. 161-169

Zasso A. (1996)
Flutter derivatives: Advantages of a new representation convention
J. Wind Engineering and Industrial Aerodynamics, Vol. 60, pp. 35-47

Abbreviations

ASCE	American Society of Civil Engineers
ASME	American Society of Mechanical Engineers
IABSE	International Association for Bridge and Structural Engineering
ICE	Institution of Civil Engineers
IEEE	Institute of Electrical and Electronics Engineers
SECED	Society for Earthquake and Civil Engineering Dynamics
TRRL	Transport and Road Research Laboratory

Appendix A

Logarithmic Decrement Method for the estimation of damping ratios

This appendix provides the theory behind the Logarithmic Decrement Method, as applied to the estimation of cable damping (§10.3.1) and deck damping (§9.3.1), from the free decay of vibrations. This variation of the method is more accurate than the basic Logarithmic Decrement Method, which just considers the relative amplitudes at two discrete times (Clough & Penzien 1993), since it is not dependent on individual samples, but rather smoothes out the random errors.

The displacement free response of a viscously damped Single-Degree-Of-Freedom (SDOF) oscillator is given by (Clough & Penzien 1993):

$$y = Ae^{-\zeta\omega_n t}\cos(\omega_D t) \tag{A-1}$$

where: A = initial amplitude

ω_n = undamped circular natural frequency

ω_D = damped circular natural frequency

ζ = damping ratio

t = time

For low damping, the difference between the damped and undamped natural frequencies is negligible, and the acceleration free response can be considered to be of the same form.

Taking the natural logarithm of the peak values (y_{peak}), occurring at $t = 2\pi n/\omega_n$, where n is an integer:

$$\ln(y_{peak}) = \ln(A) - \zeta\omega_n t \tag{A-2}$$

Hence, the damping ratio is given by:

$$\zeta = \frac{-b}{\omega_n} = \frac{-b}{2\pi f_n} \tag{A-3}$$

where: f_n = natural frequency

b = gradient of $\ln(y_{peak})$ plotted against t

Appendix B

Aerodynamic damping of an inclined cable

This appendix provides details of the derivation of equations (10-4)&(10-5) for the in-plane and out-of-plane aerodynamic damping ratios of an inclined cable for a wind of arbitrary speed and direction (§10.5).

The drag force (i.e. along wind component of aerodynamic force) per unit length on a prismatic body is given by (Simiu & Scanlan 1986):

$$F_D = \tfrac{1}{2}\rho D C_D V^2 \qquad \text{(B-1)}$$

where: ρ = fluid density

D = reference dimension of the body (the diameter for a circular cylinder)

C_D = drag coefficient

V = velocity of the flow

C_D is a function of Reynolds number (R_e)†, but it is approximately constant over wide ranges of R_e. For a smooth circular cylinder it is approximately 1.2 in the sub-critical range of $R_e < 2\text{x}10^5$. It then drops sharply in the critical range around $2\text{x}10^5 < R_e < 5\text{x}10^5$, above which it has a value of approximately 0.4, which then rises only slowly with further increasing R_e (Simiu & Scanlan 1986). Thus outside the critical range it can be taken to be a constant.

For an inclined cable, a horizontal wind has velocity components along the cable, normal to the vertical plane of the cable and normal to the cable in its plane. The components normal to the cable exert the significant forces on it, and it is a reasonable approximation to ignore the force contribution of the component along the cable (Skarecky 1975). Therefore, the expression for aerodynamic damping ratio is initially derived for a cylinder with the wind normal to the axis. Fig. B-1 shows the geometry of the wind and cable velocities and the resulting force. The magnitude of the relative wind velocity is given by:

$$W = \sqrt{(V\cos\phi + u)^2 + (V\sin\phi)^2} \qquad \text{(B-2)}$$

where: u = cable velocity

† $R_e = VD/\nu$, where ν = kinematic viscosity.

ϕ = direction of wind velocity (Fig. B-1)

Based on quasi-static theory (§2.6.2), the component of the drag force resisting motion of the cable in the direction of u is given by:

$$\begin{aligned} F_u &= \tfrac{1}{2}\rho D C_D W^2 \cos\psi \\ &= \tfrac{1}{2}\rho D C_D \left[(V\cos\phi + u)^2 + (V\sin\phi)^2\right] \frac{(V\cos\phi + u)}{\sqrt{(V\cos\phi + u)^2 + (V\sin\phi)^2}} \\ &= \tfrac{1}{2}\rho D C_D \sqrt{(V\cos\phi + u)^2 + (V\sin\phi)^2}\,(V\cos\phi + u) \\ &= \tfrac{1}{2}\rho D C_D \sqrt{(V^2 + 2uV\cos\phi + u^2)(V\cos\phi + u)^2} \\ &= \tfrac{1}{2}\rho D C_D \sqrt{V^4\cos^2\phi + 2V^3 u\cos\phi + 2V^3 u\cos^3\phi + V^2u^2 + 5V^2u^2\cos^2\phi + 4Vu^3\cos\phi + u^4} \end{aligned} \tag{B-3}$$

For $V>>u$, the expression under the square root can be approximated by $\left[V^2\cos\phi + Vu\left(1+\cos^2\phi\right)\right]^2$, which correctly gives the first four terms, i.e. all the first order terms in u and the significant term without $\cos\phi$, which is important to give a good approximation when ϕ is close to ±90°. Thus the force is approximated by:

$$F_u \approx \tfrac{1}{2}\rho D C_D \left[V^2\cos\phi + Vu\left(1+\cos^2\phi\right)\right] \tag{B-4}$$

This comprises a quasi-static term due to the drag force on the stationary cable (i.e. the term in V^2) and a term proportional to the velocity of the cable (u), which is equivalent to a damping term in the equation of motion. Hence the aerodynamic damping ratio is:

$$\zeta_{aero} = \frac{\rho D C_D}{4\omega_n m} V\left(1+\cos^2\phi\right) \tag{B-5}$$

where: ω_n = circular natural frequency

m = cable mass per unit length

The general expression (B-5) is now transformed for the case of a cable inclined at angle β to the horizontal, experiencing a horizontal wind of speed U and direction θ, measured clockwise from normal to the vertical plane of the cable†. The components of wind velocity relative to the cable are:

† This reference direction is used for consistency with wind directions for the whole bridge in this thesis, although it differs from the reference direction used for cable aerodynamics by some authors.

Normal to the vertical plane of the cable: $U\cos\theta$

Normal to the cable in its vertical plane: $U\sin\theta\sin\beta$

Parallel to the cable: $U\sin\theta\cos\beta$

Therefore, in the plane normal to the cable the wind speed and angle relative to the direction of cable motion, for in-plane vibrations of the cable, are given by:

$$V = U\sqrt{\cos^2\theta + \sin^2\theta\sin^2\beta} \tag{B-6}$$

$$\cos\phi = \frac{\sin\theta\sin\beta}{\sqrt{\cos^2\theta + \sin^2\theta\sin^2\beta}} \tag{B-7}$$

Substituting these into (B-5) gives, for in-plane vibrations:

$$\zeta_{aero} = \frac{\rho D C_D}{4\omega_n m} U\left(\sqrt{\cos^2\theta + \sin^2\theta\sin^2\beta} + \frac{\sin^2\theta\sin^2\beta}{\sqrt{\cos^2\theta + \sin^2\theta\sin^2\beta}}\right) \tag{B-8}$$

Similarly, for out-of-plane vibrations of the cable it can be shown that:

$$\zeta_{aero} = \frac{\rho D C_D}{4\omega_n m} U\left(\sqrt{\cos^2\theta + \sin^2\theta\sin^2\beta} + \frac{\cos^2\theta}{\sqrt{\cos^2\theta + \sin^2\theta\sin^2\beta}}\right) \tag{B-9}$$

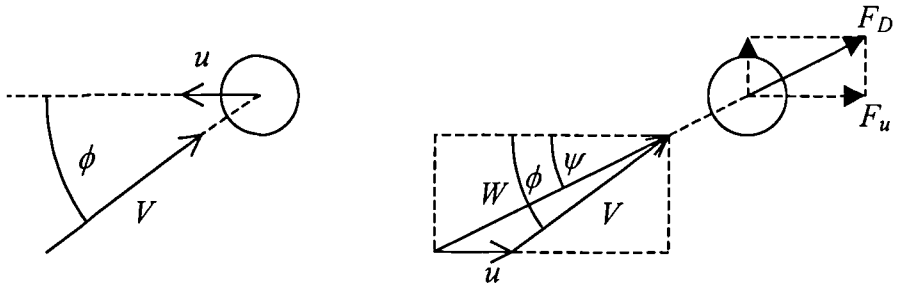

Fig. B-1 Incident wind and resulting force on a moving circular cylinder